Design and Implementation of Energy Efficient Wireless Body Area Networks over Cognitive Radio Platform

A Dissertation Submitted for the Degree of
Doctor of Philosophy (Engineering)

By

Tanumay Manna

Under the Supervision of:

Prof. (Dr.) Iti Saha Misra

Department of Electronics and
Telecommunication Engineering
Faculty Council of Engineering & Technology
Jadavpur University
Kolkata-700032, India

June 2019

INDEX NO- 89/15/E

Design and Implementation of Energy Efficient Wireless Body Area Networks over Cognitive Radio Platform

Dedicated to my parents, Tarun Manna and Mita Manna, who have always loved me unconditionally and whose good examples have taught me to work hard for the things that I aspire to achieve. This work is also dedicated to my sister, Madhurima who was there for me throughout this process and gave me lots of support.

SUPERVISOR

PROF. ITI SAHA MISRA

Professor
Department of Electronics & Telecommunication Engineering
Jadavpur University
Kolkata-700032, India
Email: iti@etce.jdvu.ac.in, itisahamisra@yahoo.co.in

LIST OF PUBLICATIONS

(*From the Contents of the Dissertation*)

SCI-INDEXED JOURNAL PUBLICATIONS

1. **Tanumay Manna** and Iti Saha Misra, "Design, Implementation and Analysis of Cognitive Radio enabled Intelligent WBAN Gateway for Cost-Efficient Remote Health Monitoring," in Press, *Physical Communication, Elsevier*, May 2019, doi: 10.1016/j.phycom.2019.100713.

2. **Tanumay Manna** and Iti Saha Misra, "Performance Analysis of Scheduled Access Mode of the IEEE 802.15.6 MAC Protocol under Non-Ideal Channel Conditions," in Press, *IEEE Transactions on Mobile Computing*, Feb. 2019, doi: 10.1109/TMC.2019.2901852.

3. **Tanumay Manna** and Iti Saha Misra, "A Prediction and Scheduling Framework in Centralized Cognitive Radio Network for Energy Efficient Non-Real Time Communication," *International Journal of Communication Systems, Wiley*, vol. 31, no. 13, e3716, Sep. 2018, doi:10.1002/dac.3716.

4. **Tanumay Manna** and Iti Saha Misra, "Implementation of Relay based Collaborative Spectrum Sensing using Coalitional Games in Wireless Cognitive Radio Networks," *Computers and Electrical Engineering Journal, Elsevier*, vol. 45, pp. 77-99, Jul. 2015, doi: 10.1016/j.compeleceng.2015.03.006.

BOOK CHAPTER (*Scopus Indexed*)

1. **Tanumay Manna** and Iti Saha Misra, "Implementation of Energy Efficient WBAN using IEEE 802.15.6 Scheduled Access MAC with Fast DWT based Backhaul Data Compression for e-Healthcare," *Communication Systems and Networks, COMSNETS 2018 Revised Selected Papers, Lecture Notes in Computer Science (LNCS), Springer*, vol. 11227, pp. 26-51, Jan. 2019, doi: 10.1007/978-3-030-10659-1_2. **(One of the 12 papers selected among 134 submissions)**

INTERNATIONAL CONFERENCES

1. **Tanumay Manna** and Iti Saha Misra, "Design of Resource/Energy-Efficient Energy Detector for Real-Time Cognitive Radio using WARP," in Proc. *5th IEEE International Conference on Opto-Electronics and Applied Optics (OPTRONIX-2019)*, Mar. 2019, Kolkata, India. (In Press)

2. **Tanumay Manna** and Iti Saha Misra, "Implementation of Energy Efficient WBAN using IEEE 802.15.6 Scheduled Access MAC for e-Healthcare," in Proc. *10th IEEE International Conference on Communication Systems & Networks (COMSNETS-2018)*, pp. 267-274, Jan. 2018, Bangalore, India. IEEE Xplore Link: http://ieeexplore.ieee.org/document/8328207/

3. **Tanumay Manna** and Iti Saha Misra, "Designing an Analytical Model for IEEE 802.15.6 Scheduled Access Mode in Non-Saturation Regime," in Proc. *IEEE Radio and Antenna Days of the Indian Ocean (IEEE RADIO-2016)*, pp. 1-2, Oct. 2016, Reunion Island, France. IEEE Xplore Link: https://ieeexplore.ieee.org/document/7772032/

4. **Tanumay Manna** and Iti Saha Misra, "A Fast Hardware based Hidden Markov Model Predictor for Cognitive Radio," in Proc. *6th IEEE International Advanced Computing Conference (IACC-2016)*, pp. 752-758, Feb. 2016, Andhra Pradesh, India. IEEE Xplore Link: https://ieeexplore.ieee.org/document/7544933/

5. **Tanumay Manna**, Iti Saha Misra, Salil Kumar Sanyal and Tamal Chakraborty, "A Framework for Implementation of Wireless Body Area Network over Software Defined Radios," in Proc. *IEEE Region-10 Technical Symposium (TENSYMP-2015)*, pp. 17-20, May 2015, Ahmedabad, India. IEEE Xplore Link: https://ieeexplore.ieee.org/document/7166227/.

LIST OF PATENTS

(*From the Contents of the Dissertation*)

1. **Tanumay Manna** and Iti Saha Misra, "Method and Apparatus for Energy Efficient Data Transmission in Cognitive Radio System," App. No.- 201731002796A, *Indian Patent Journal*, pp. 3214, 10 Feb. 2017. Patent Journal Link: http://www.ipindia.nic.in/writereaddata/Portal/IPOJournal/1_440_1/Part1.pdf (Filed and Published)

2. **Tanumay Manna** and Iti Saha Misra, "Cross-Layer Apparatus and Method for Cognitive Radio System," App. No.- 201731019587A, *Indian Patent Journal*, pp. 22550, 07 Jul. 2017. Patent Journal Link: http://www.ipindia.nic.in/writereaddata/Portal/IPOJournal/1_1499_1/Part-1.pdf (Filed and Published)

LIST OF PRESENTATIONS IN INTERNATIONAL CONFERENCES

(*Related to the Thesis*)

PRESENTATIONS HELD ABROAD

1. **Tanumay Manna** and Iti Saha Misra, "Designing an Analytical Model for IEEE 802.15.6 Scheduled Access Mode in Non-Saturation Regime," in Proc. *IEEE Radio and Antenna Days of the Indian Ocean (IEEE RADIO-2016)*, pp. 1-2, Oct. 2016, **Reunion Island, France**. IEEE Xplore Link: https://ieeexplore.ieee.org/document/7772032/ ***(Awarded in YSA Competition, Travel Grants by SERB & CICS, Govt. of India)***

PRESENTATIONS HELD WITHIN INDIA

1. **Tanumay Manna** and Iti Saha Misra, "Design of Resource/Energy-Efficient Energy Detector for Real-Time Cognitive Radio using WARP," in Proc. *5th IEEE International Conference on Opto-Electronics and Applied Optics (OPTRONIX-2019)*, Mar. 2019, **Kolkata, India**. (In Press)
2. **Tanumay Manna** and Iti Saha Misra, "Implementation of Energy Efficient WBAN using IEEE 802.15.6 Scheduled Access MAC for e-Healthcare," in Proc. *10th IEEE International Conference on Communication Systems & Networks (COMSNETS-2018)*, pp. 267-274, Jan. 2018, **Bangalore, India**. IEEE Xplore Link: http://ieeexplore.ieee.org/document/8328207/
3. **Tanumay Manna** and Iti Saha Misra, "A Fast Hardware based Hidden Markov Model Predictor for Cognitive Radio," in Proc. *6th IEEE International Advanced Computing Conference (IACC-2016)*, pp. 752-758, Feb. 2016, **Andhra Pradesh, India**. IEEE Xplore Link: https://ieeexplore.ieee.org/document/7544933/
4. **Tanumay Manna**, Iti Saha Misra, Salil Kumar Sanyal and Tamal Chakraborty, "A Framework for Implementation of Wireless Body Area Network over Software Defined Radios," in Proc. *IEEE Region-10 Technical Symposium (TENSYMP-2015)*, pp. 17-20, May 2015, **Ahmedabad, India**. IEEE Xplore Link: https://ieeexplore.ieee.org/document/7166227/

CERTIFICATE FROM THE SUPERVISOR

This is to certify that the thesis entitled "**Design and Implementation of Energy Efficient Wireless Body Area Networks over Cognitive Radio Platform**" submitted by **Shri Tanumay Manna**, who got his name registered on **17th April, 2015** for the award of Ph.D. (Engg.) degree of Jadavpur University is absolutely based upon his own work under the supervision of **Prof. (Dr.) Iti Saha Misra** and that neither his thesis nor any part of the thesis has been submitted for any degree/diploma or any other academic award anywhere before.

Signature of the Supervisor
Prof. Iti Saha Misra
Department of Electronics and
Telecommunication Engineering
Jadavpur University
Kolkata-700032, India

Email: iti@etce.jdvu.ac.in
itisahamisra@yahoo.co.in

ACKNOWLEDGEMENT

This thesis represents not only my work at the keyboard, it is a milestone in more than five years of work at JU and specifically within the Broadband Wireless Communication Laboratory, famously known as the OPNET Lab. My experience at JU has been nothing short of amazing. This thesis is a result of many such experiences I have encountered at JU from dozens of remarkable individuals who I also wish to acknowledge.

First and foremost, I wish to thank my supervisor, Prof. Iti Saha Misra, founder of JU OPNET Laboratory. She has been supportive since the days I began working on the Cognitive Radio test-bed as a postgraduate. I thank ISM Ma'am wholeheartedly, not only for her tremendous academic support, but also for giving me so many wonderful opportunities. She has taught me, both consciously and unconsciously, how good engineering is done using both mathematics and hands-on exploration. During the most difficult times when writing this thesis, she gave me the moral support and the freedom I needed to move on. Without her guidance and constant feedback this Ph.D. would not have been achievable.

Similar profound gratitude goes to Prof. Salil Kumar Sanyal, for his insightful comments and for sharing with me his tremendous experience in the communication field. His scientific inputs, personal helps and friendly nature has always made me feel at ease while working alongside him in the OPNET Lab.

Thanks are also due to the Council of Scientific and Industrial Research (CSIR), for their financial support, which helped me in pursuing my doctoral research.

My time at JU was made enjoyable in large part due to the many friends that became a part of my life. I am grateful to my seniors Dr.Budhaditya, Dr.Tamal, Ms. Anindita, Mr. Sudipta, Dr. Prasun, Dr. Chitradeep, and fellow lab mates Arijeet, Tanmoy, Sreya, Gaurav, Bodhisatwa, Aritra and many more for all the memorable moments. Talking about friends, I also have to thank a very special person, Sanjib Sarkar, whom I consider my best friend since undergraduate studies. His unconditional support has been essential all these years.

Lastly, I would like to thank my family for all their love and encouragement. For my parents who raised me with a love for science and supported me in all my pursuits. For my sister Madhurima who has always motivated me through thick and thin. Thank you.

ABSTRACT

The traditional healthcare system is primarily structured and optimized for illness management rather than wellness management. Due to this, the current healthcare scenario is facing two primary challenges: increase in life expectancy and rising healthcare costs. In addition, in recent years there has been a sudden increase in largely lifestyle-related chronic health conditions, from diabetes and dementia to coronary heart disease and cancers. Personal health systems through wearable healthcare monitoring is a key solution that will enable the transition to a more proactive, affordable, and ubiquitous healthcare. Recent advances in integration and miniaturization of physical sensors, embedded microcontrollers, wireless technologies, and radio interfaces on a single chip, have greatly expanded the ability of wireless sensor networks to closely monitor and track conditions of patients in healthcare area. Such network consisting of wireless sensors that are implantable, wearable or placed within the close proximity of the body, providing timely data is called a Wireless Body Area Network (WBAN). In a WBAN, the sensor nodes wirelessly send their data to a hub/ Body Network Controller (BNC) (e.g. smart watch, smart phone) present close to body. IEEE has recently standardized WBAN communication by releasing IEEE 802.15.6 standard that provides the Physical (PHY) and Medium Access Control (MAC) layer guidelines for efficient WBAN communication. The fundamental philosophy behind this access layer communication of a standalone WBAN is to allow a person to monitor and have more control over his health. Moreover, blessed with Internet and Communication Technologies (ICT) convergence, the ability of a standalone WBAN is enhanced manifold with its integration to an e-healthcare architecture. An e-healthcare architecture allows small amounts of WBAN captured data to be transferred in near real-time or Non Real-Time (NRT) by the BNC over a convergence or backhaul link to remote end like a database or healthcare monitoring center. Thus, by leveraging the e-healthcare architecture in general, and the convergence layer in particular, a WBAN allows a patient/citizen to be mobile and also facilitate ubiquitous remote health monitoring. However, every rose has its own thorn, and WBAN is no exception. In particular, there are specific challenges to deployment of highly energy-efficient access layer/backhaul data transmission, as well as spectrum efficient and cost-effective convergence layer com-

munication. This thesis primarily addresses these challenges through the use of Cognitive Radio (CR) technology.

One of the primary objectives of effective WBAN access layer (or simply WBAN) communication is to make it energy-efficient, thereby enhancing the sensor node battery life time. However, the non-ideal nature of WBAN channels such as varying Signal-to-Noise Ratio (SNR) affect the latency, reliability, energy-efficiency of WBAN communication. CR is a suitable technology that can allow the sensor nodes to adapt their communication parameters based on the current channel conditions with the overall objective of maximizing the energy-efficiency while still satisfying the frame delay and reliability requirements as stated in IEEE 802.15.6 standard. However, considering the significance of such a system, prior to CR based optimization, there is an immediate requirement to study the standalone WBAN performance under varied channel conditions ultimately leading to efficient test-bed implementation following the IEEE 802.15.6 standard.

Considering the challenges from convergence layer perspective, the proliferation of the wireless communication services coupled with the fixed spectrum allocation policy has led to spectrum scarcity crisis. The situation is likely to be aggravated with the exponential increase of the Internet-of-Things (IoT) devices and applications (like WBAN based e-healthcare), which are supposed to be connected to the mobile networks worldwide. In addition to the spectrum scarcity problem, the traditional licensed Wide-Area Access Network (WAN) technologies also pose cost-efficiency issues. More specifically, unlike the cable Internet connectivity which is widely spread and low cost, mobile Internet connectivity is yet to go long way for low cost solution, especially in developing countries. Subsequent studies on the search for potential solutions to the afore-mentioned spectrum scarcity and cost-efficiency issues have led to the birth of Cognitive Radio Networks (CRNs) that leverage CR technology to facilitate Dynamic Spectrum Access (DSA). CRNs use DSA to exploit different under-utilized spectrum bands in order to increase the overall spectrum utilization and subsequently reduce the issues of spectrum congestion. Moreover, the cost of DSA is expected to be much lower than the cost of purchasing a licensed band. Therefore, using CRN for backhaul communication would allow the network operators efficiently use the available spectrum and also make fundamental IoT services like healthcare monitoring affordable to public particularly in developing nations, where the cost of data transfer is still high. Hence, CR technology based DSA will act as a driving factor not only from the network operator and end user's perspective but also for the IoT and healthcare industry. Considering the enormous significance of such a system, there is an immediate requirement to explore the possibilities of implementing NRT applications like WBAN enabled remote health monitoring over CRN. The focus lies on developing device level and network level policies toward ensuring cost-efficient

and reliable backhaul communication, while maximizing the Secondary User (SU) (e.g. BNC) energy-efficiency and protecting the incumbent Primary User (PU) from interference at the same time. Thus, WBAN communication (access and backhaul) over CR Platforms is truly a challenging yet promising aspect, both for the next generation healthcare industry as well the next generation wireless communication networks.

It is evident that IEEE 802.15.6 standard plays a crucial role in the designing of efficient WBAN communications. Hence, the first objective of this thesis is to conduct in-depth studies of WBAN communication as per the IEEE 802.15.6 standard. Among the different MAC protocols of IEEE 802.15.6, we select Time Division Multiple Access (TDMA) based Scheduled Access MAC (SAM) for our work. We select SAM because it is an energy conserving protocol having reduced duty cycle, with no contention, idle listening, and overhearing problems. It also provides good solutions to high traffic correlation, which often arises in WBAN that needs to track multiple physiological signals at the same time. However, this study is hindered by the lack of a comprehensive simulation platform for IEEE 802.15.6 based WBAN in literature. Accordingly, we propose an accurate OPNET simulation model to analyze and evaluate IEEE 802.15.6 SAM performance. In this regard, models of superframe generation, packet transmission and calculation of sensor node energy consumption are established at the OPNET process layer of the sensor nodes and hub through an interrupt based design. Using the designed model, simulations are made to study the performance in terms of frame delay, throughput and energy consumption of the sensor nodes with respect to system parameters like allocation intervals and traffic loads. The results show that the OPNET model can effectively describe the behavior as per the IEEE 802.15.6 SAM, and set up a good basis for future study such as validating analytical observations and also facilitate performance analysis and optimization of designed WBANs. To achieve the latter objective, we implement a complete WBAN that is capable of monitoring multiple physiological signals of a patient by means of IEEE 802.15.6 SAM. In the WBAN setup, data from multiple sensors are sent to a BNC using low power transceivers. To this end, the BNC is designed to multiplex the data from multiple sensors and send them to a remote server over the Internet using cellular communications, thereby enabling ubiquitous remote health monitoring. The remote server is further configured to accept data from multiple patients, de-multiplex different data of a single patient and store them in a database for pervasive access. Issues related to the hardware implementation of sensor nodes and BNC, and the design of the SAM are addressed. Detailed performance analysis of the WBAN is performed in our developed OPNET simulator model to determine the optimum Allocation Intervals (AIs) for the sensor nodes that maximizes network capacity while maintaining a frame delay constraint. Further, in order to prolong the battery life of sensor nodes, we obtain the optimal Payload Sizes

(PSs) that maximize their energy-efficiency. The developed test-bed model for WBAN also provides important insight into the sensor node mechanism and resources, which we later exploit for embedding CR enabled adaptability.

To introduce CRN at the backhaul of WBAN and truly take advantage of DSA, the first step should be the proper design of a real-time CR interface (i.e. SU) that can be used for opportunistic IP enabled communication over PU channels in a CRN. To this end, we perform analytical and simulation study of the performance of energy detection based spectrum sensing under sensing uncertainties and varied PU activities particularly taking into consideration the peculiarities of a traditional Software Defined Radio (SDR) like Wireless Open Access Research Platform (WARP). In addition, we evaluate the normalized interference metric so as to keep the interference to PU channels within predetermined limit. The practical realization of Real-Time (RT) CR interface is fulfilled through the design of Energy Detection based CR MAC (ECR-MAC) at the Embedded Processor (EP) of WARP. It incorporates our proposed Practical Energy-Efficient Energy Detection (PED) method, that uses already available Field Programmable Gate Array (FPGA) resources for practical realization of energy detection. From simulation study we also infer that the PED method leads to significant reduction in energy consumption for spectrum sensing at higher detected PU SNRs. Subsequent validation in test-bed confirms the ability of ECR-MAC in facilitating opportunistic IP enabled SU communication over PU activity channels. We use the developed CR test-bed in future proof of concepts to validate the research findings and render them suitable for widespread deployment.

After the initial simulation based performance analysis and test-bed design of WBAN and backhaul CRN, the focus shifts towards a finer level of study and optimization followed by related design and implementation. To this aim, first we present an analytical model for the scheduled access mechanism of IEEE 802.15.6 based WBAN taking into account the impact of non-ideal transmission channel. We provide a thorough analysis and closed form expressions for the frame delay; reliability of data transfer; throughput; energy consumption and energy-efficiency of the sensor nodes with medium to high data rate applications. We validate our theoretical derivations through simulation results obtained from our designed OPNET model. The results show the variation in the performance indicators with respect to different system parameters, such as beacon period, data transmission rate, traffic loads, channel SNR, AIs and PSs. Our results indicate the tradeoff between average frame delay and energy-efficiency with respect to selection of AIs and PSs. Thus, through this analysis we show how a network designer can prepare a look-up table that would allow our already developed sensor nodes to leverage their CR capabilities to sense the channel SNR and

adapt their AIs and PSs to achieve maximum EE under average frame delay and reliability constraints.

After the incorporation of CR in the WBAN access layer, the next important objective is to design and implement a BNC as a gateway between WBAN and backhaul CRN. To this end, in this thesis we design and implement an intelligent WBAN gateway that uses CR to opportunistically access licensed PU channels to facilitate spectral-efficient, cost-efficient and reliable NRT backhaul transmission of WBAN data. The gateway is termed herein as BodyCog-BNC. For this, we develop and implement a cross-layer based modified protocol stack at the BodyCog-BNC comprising of BodyCog-BNC Management Entity (BME) and BodyCog-BNC CR Medium Access Control (BCR-MAC) units. The BME and BCR-MAC together exploit cross-layer message passing to facilitate the novel idea of spectrum agility. A spectral agile BodyCog-BNC in case of lack of proper PU channels or occurrence of successive handoffs in multiple PU channels is capable of intelligently switching to conventional licensed WAN technology. Furthermore, the cross-layer based modified protocol stack facilitates session management and energy-efficient backhaul CR transmission over a PU channel employing a proposed Inter-Sensing Time Optimization (ISTO) algorithm. ISTO leverages on convex optimization to select the optimum inter-sensing time for a PU channel to maximize the energy-efficiency within a PU interference constraint under sensing uncertainties. Closed form analytical expressions are also derived to estimate the average consumed energy, switching probability, switching time and the cost-efficiency of BodyCog-BNC. The cost-efficiency metric encompasses both the data transfer costs as well as the electricity costs incurred to recharge the BNC for replenishing the extra energy consumed due to cognitive actions. Exhaustive performance analysis shows that the BodyCog-BNC (WBAN gateway), provides a cost-efficient solution for varied healthcare applications under varied operating conditions and CR cost regimes. Finally, by leveraging i) our already developed WBAN BNC, ii) the real-time CR terminal created earlier and iiii) our proposed BME and BCR-MAC architectures, we implement a prototype of BodyCog-BNC and provide a proof of concept of the feasibility of BodyCog-BNC in enabling NRT remote health monitoring.

So far, we have shown the integration of the BodyCog-BNC into a basic CRN as envisioned in IEEE 802.22, where CBS allocates channels to SUs based on whitespace database, and the additional protection to incumbent PU communication needs to ensured by SUs through spectrum sensing. However, we now consider the alternate popular CRN policy where the Cognitive Base Station (CBS) performs all necessary cognitive actions for PU channel access, thereby simplifying the SU (BNC) design. It is intuitive that this method will be more energy-efficient for the SUs but at the cost of increased resource requirement at the CBS. Thus considering that resource is not a constraint for the CBS, the last phase of the thesis proposes

a framework for centralized CRN that facilitates better spectrum utilization and low-cost opportunistic NRT data transfer (e.g. BNC of WBAN) with high energy-efficiency. The novelty of this framework is to incorporate Hidden Markov Model (HMM) based prediction within the traditional CR sensing-transmission cycle. To minimize the prediction time, we design a Hardware based HMM engine (H2M2) to be used by the CBS. The CBS exploits the H2M2 engine over high PU activity channels to minimize the collisions between PUs and NRT SUs, thereby reducing the SU energy consumption. However, this is at the cost of reduced throughput. Taking this into account, we propose an Inter Sensing-Prediction Time Optimization algorithm, that identifies the predictable PU activity channels and maximizes the throughput within a PU interference threshold. Furthermore, to minimize the total battery consumption of all the SUs within CRN, a Battery Consumption Minimizing Scheduler is designed at the CBS that efficiently allocates the predictable PU channels to the NRT SUs. By exploiting the un-utilized high PU activity channels the proposed Centralized Scheduling, Sensing and Prediction (CSSP) framework improves the spectral efficiency of the CRN. Exhaustive performance studies show that CSSP outperforms traditional non-predictive sensing techniques in terms of energy-efficiency and interference management. Finally, the practical utility of the system is established with respect to WBAN based remote health monitoring by developing a prototype model of H2M2 in FPGA board and using it in association with the CRN test-bed, developed earlier, through a hardware co-simulation environment, that shows a suitable direction of use for future IoT applications.

Table of Contents

List of Figures

List of Tables

List of Abbreviations and Acronyms

AAL	Ambient Assisted Living
Acc.	Accumulator
ACCPT	Accept
ACK	Acknowledgment
ADC	Analog to Digital Converter
AI	Allocation Interval
ALGO	Algorithm
AP	Access Point
APN	Access Point Name
APP	Application Layer
ARQ	Automatic Repeat Request
B-DWT	BNC Discrete Wavelet Transform
BCH	Bose, Chaudhuri, and Hocquenghem
BCMS	Battery Consumption Minimizing Scheduler
BCR-MAC	BodyCog-BNC CR MAC
BCRD	BCR-MAC Development framework
BCU	BNC micro-Controller Unit
BEE2	Berkeley Emulation Engine 2

BER	Bit Error Rate
BLE	Bluetooth Low Energy
BME	BodyCog-BNC Management Entity
BMED	BME Development framework
BNC	Body Network Controller
BodyCog-BNC	BNC between WBAN and Cognitive Radio Network
BPSK	Binary Phase Shift Keying
BS	Base Station
BSS	Base Station based Sensing
BTCS	BME TCP/IP Client-Server framework
C-MCU	Client MCU
CAP	Contention Access Phase
CBS	Cognitive Base Station
CCA	Clear Channel Assessment
CCC	Common Control Channel
CDR	Compression Data Ratio
CE	Cost-Efficiency
CHAN	Channel
CONN	Connection
CRC	Cyclic Redundancy Check
CR	Cognitive Radio
CRN	Cognitive Radio Network
CSA	Concurrent Spectrum Access
CS	Carrier Sense

CSMA/CA	Carrier-Sense Multiple Access with Collision Avoidance
CSS	Collaborative Spectrum Sensing
CSSP	Centralized Scheduling, Sensing and Prediction
CTC	Clear Timer on Compare
CTMC	Continuous Time Markov Chain
CTRL	Control
CVD	Cardio Vascular Disease
DB	Database
DBPSK	Differential Binary Phase Shift Keying
DDNS	Dynamic DNS
DISCON	Disconnection
DNS	Domain Name Service
DQPSK	Differential Quadrature Phase Shift Keying
DSA	Dynamic Spectrum Access
DS	Data Stream
DSP	Digital Signal Processor
DUR	Duration
DWT	Discrete Wavelet Transform
EAP	Exclusive Access Phase
ECG	Electrocardiograms
ECR-MAC	Energy Detection based Cognitive Radio MAC
EE	Energy-Efficiency
EELDC	Energy-Efficient Low Duty Cycle
EFC	Electric Field Communication

EMG	Electromyogram
EP	Embedded Processor
EXP	Expiry
FCC	Federal Communications Commission
FCS	Frame Check Sequence
FEC	Forward Error Correction
FFT	Fast Fourier Transform
FIFO	First-In-First-Out
FIR	Finite Impulse Response
FM-UWB	Frequency Modulated UWB
FM	Frequency Modulation
FPGA	Field Programmable Gate Array
FRM	Frame
FS	Frame Subtype
FSM	Finite State Machine
GCM	Google Cloud Messages
GDP	Gross Domestic Product
GFSK	Gaussian Frequency Shift Keying
GMSK	Gaussian Minimum Shift Keying
GPP	General Purpose Processor
GPRS	General Packet Radio Service
GSM	Global System for Mobile
GT	Guard Time
GUI	Graphical User Interface

H-MCU	Hub MCU
H2M2	Hardware based HMM engine
HBC	Human Body Communication
HBCMS	Heuristic Battery Consumption Minimizing Scheduler
HCS	Header Check Sequence
HMM	Hidden Markov Model
I-Ack	Immediate Acknowledgment
IAI	Inter-Allocation Interval
ICI	Interface Control Information
ICT	Internet and Communication Technology
IEEE	Institute of Electrical and Electronics Engineers
IE	Information Elements
IoT	Internet-of-Things
IP	Internet Protocol
IR-UWB	Impulse Radio UWB
ISM	Industrial, Scientific, and Medical band
ISPTO	Inter Sensing-Prediction Time Optimization
ISR	Interrupt Service Routine
ISTO	Inter-Sensing Time Optimization
KKT	Karush-Kuhn-Tucker
KP	Kernel Procedure
LDC	Low Duty Cycling
LQI	Link Quality Indicator Values
LSB	Least Significant Bit

$\mathscr{L}T$	Laplace transform
LUT	Look-up Table
M-Hwcosim	MATLAB Hardware Co-simulation
M2M	Machine-to-Machine
MAC	Medium Access Control
MAP	Managed Access Phase
MCPA	Markov-based Channel Prediction Algorithm
MCU	Microcontroller Unit
MGM	Management
MICS	Medical Implant Communication Service
MPDU	MAC Protocol Data Unit
MSDU	MAC Service Data Unit
NB	Narrow Band
NFF	Non-Final Fragment
NR	Newton-Raphson
NRT	Non-Real Time
OFDM	Orthogonal Frequency Division Multiplexing
OOB	Out-Of-Band
OPT	Optimal
OSA	Opportunistic Spectrum Access
PC	Personal Computer
PED	Practical Energy-Efficient Energy Detection
PER	Packet Error Rate
PGF	Probability Generating Function

PHS	Personal Health System
PHY	Physical Layer
PKT	Packet
PLCP	Physical Layer Convergence Protocol
PPDU	Physical layer Protocol Data Unit
PRD	Percentage Root Mean Difference
PSDU	Physical layer Service Data Unit
PS	Payload Size
PU	Primary User
QoS	Quality of Service
QPSK	Quadrature Phase Shift Keying
RAP	Random Access Phase
REQ	Request
RESP	Response
RF	Radio Frequency
RHM	Remote Health Monitoring
RLSD	Released
RLS	Release request
ROC	Receiver Operating Characteristics
RR	Radio Resource
RSAP	Remote Server Application Program
RS	Remote Server
RSSI	Received Signal Strength Indicator
RT	Real-Time

Rx	Receiver
S-MCU	Sensor MCU
SAM	Scheduled Access MAC
SAP	Service Access Point
SAR	Specific Absorption Rate
SDR	Software Defined Radio
SG	Smart-Grid
SHMMP	Software based HMM Prediction
SIFS	Short Inter-Frame Spacing
SIM	Subscriber Identity Module
SI	Synchonization Interval
SMS	Short Message Service
SNR	Signal-to-Noise Ratio
SOLN	Solution
SPI	Serial Peripheral Interface
SUCS	Successful
SU	Secondary User
SYNC	Synchronization
TCP	Transmission Control Protocol
TCS	Target Channel Sequence
TDMA	Time Division Multiple Access
TMR	Timer
TRANS	Transmission
TVWS	Television Band White Space

Tx	Transmitter
UART	Universal Asynchronous Receiver/ Transmitter
UDP	User Datagram Protocol
UHF	Ultra High Frequency
UP	User Priority
USB	Universal Serial Bus
USRP	Universal Software Radio Peripheral
US	United States
UWB	Ultra Wide Band
UWC	Underwater Acoustic Communication
VHF	Very High Frequency
VoIP	Voice over Internet Protocol
WAN	Wide-Area Access Network
WARP	Wireless open Access Research Platform
WBAN	Wireless Body Area Network
WHO	World Health Organization
WHS	Wearable Health System
WLAN	Wireless Local Area Network
WMTS	Wireless Medical Telemetry Service
WPAN	Wireless Personal Area Network
WRAN	Wireless Regional Area Networks
WSN	Wireless Sensor Network

Chapter 1

Introduction

❝ *Fundamentally, the answers to our challenges in healthcare relies in engaging and empowering the individual.*❞

-Elizabeth Holmes, CEO, Theranos

A healthy nation is often regarded as a wealthy nation. In 1948, the World Health Organization (WHO) defined health as more than just the absence of illness; a state of complete physical, mental and relational well being. It's about taking care of the body and mind to prevent future illness, and being resilient enough to bounce back easily if one gets sick. However, as mankind is getting sucked into the 'doing' society, it is getting difficult to disconnect from the technologies like phones, tablets, stress, pressure which pushes everyone to be constantly 'doing'. This culture of stress, the constant need to be 'doing', compounded by the feeling of a lack of time affects every aspect of the health.

As a result, in recent years there has been a sudden increase in largely lifestyle-related chronic health conditions, from diabetes and dementia to coronary heart disease and many cancers. Millions of people die every year from cancer, Cardio Vascular Disease (CVD), asthma, Parkinson's, diabetes, obesity, and many more such chronic or fatal diseases. For example, there are roughly 30 million heart patients and about two lakh surgeries being performed every year in India. Four out of five CVD deaths are due to heart attacks and strokes. According to the latest statistics from WHO, due to the burden of CVD, India may have lost $237 billion from the loss of productivity and spending on health care over a 10-year period (2005–2015) [1]. Individuals at risk of CVD may demonstrate abnormal heart rhythm and cardiac symptoms. Identifying the patients with these symptoms indicating highest risk of CVDs and ensuring they receive appropriate treatment can prevent these premature deaths. This is also true for most of the diseases. Research has shown that most

diseases can be prevented if they are detected in their early stages. Therefore, future health care systems should provide proactive management of wellness rather than illness, and focus on prevention and early detection of disease.

The present healthcare systems which are structured and optimized for illness management are also facing two major challenges- increase in life expectancy and rising healthcare costs. According to the reports of World Health Organization (WHO), in India the overall life expectancy has increased from 66.4 years in 2010 to 68.3 years in 2015, whereas in United States (US) from 78.7 years in 2010 to 79.3 years in 2015 [2], and the global change is from 68 years in 2009 to 71.4 years in 2015. Going by the current estimates, the worldwide population over age 65 years is expected to more than double from 357 million in 1990 to 761 million in 2025. Also, according to the World Bank data [3] the overall healthcare expenditure (in % of Gross Domestic Product (GDP)) in India has increased from 4.0% in 1995 to 4.7% in 2014, whereas in US it has increased from 13.1% in 1995 to 17.1% in 2014, and the global change is from 8.5% in 1995 to 9.9% in 2014. It is projected that health care expenditures in US will reach almost 20% of the GDP in less than 10 years, threatening the well being of the entire economy [4]. Similar trends are also predicted for other countries. These statistics necessitate the need to shift towards more scalable and affordable solutions. Another major challenge is to provide better low-cost healthcare services to an increasing number of people using the limited financial and human resources.

Personal Health Systems (PHS) through wearable healthcare monitoring is considered as a key solution to all these problems enabling proactive, affordable and ubiquitous healthcare monitoring. It is considered as a possible future of healthcare services [5]. It allows monitoring of one's vital physiological signals like electrocardiograms (ECG), electromyogram (EMG), pulse oximeters, dosimeters, movement alarms and many more, while allowing them to engage in their normal activities instead of staying at a hospital or home or close to a specialized medical device. This can be achieved through a network consisting of intelligent, low-power, micro and nano-technology sensors and actuators, which can be placed on the body, or implanted in the human body (or even in the blood stream), providing timely data. Such networks are commonly referred to as Wireless Body Area Networks (WBANs). They allow citizens/patients to have more responsibility in managing their own health and interacting, whenever is necessary, with care providers. In addition to proactive healthcare, long-term use of WBANs also reduces healthcare costs by removing the need for costly in-clinic visits or in-hospital monitoring of patients.

Further, due to the remarkable progress in Internet and Communication Technologies (ICT), WBANs can be integrated with Internet by transmitting the data using long distance communication technologies comprising Wide-Area Access Networks (WANs) like cellular

communications, e.g. GSM, GPRS, 3G, 4G. This is termed as the *convergence layer or backhaul* of a WBAN. Whereas, the WBAN comprising of the sensors and hub communicating over short distance close to the body is also termed as the *access layer*. The convergence layer provides mobility to the patients allowing them to carry on their daily activities in both outdoor as well as indoor environments while still facilitating ubiquitous remote monitoring of the patient's health over the Internet. Importantly, as WBANs provide large time intervals of medical data, doctors will have a clearer view of the patient's status [6].

However, the advantages of WBANs do not come without its own challenges both at the access and convergence layer. Specifically, at the WBAN access layer most of the on-body and implanted sensor nodes are battery operated, and cannot be used indiscriminately because of the limited energy sources. Therefore, the access layer communication needs to energy-efficient so as to prolong their battery life. Furthermore, depending on different e-health applications WBAN access layer communication needs to meet different Quality of Service (QoS) requirements like low frame delay, high reliability. Such an access layer can be realized if sensor nodes have the ability to efficiently adapt their own radio resources based on the radio environment, type of applications and network parameters. This include sensor node resources such as packet size, transmission power, modulation levels or network resources like allocation intervals. This enhanced quality of information and experience for the user, with cognition and reconfigurable capabilities can be achieved by means of Cognitive Radio (CR). U.S. Federal Communications Commission (FCC) defines [7] "A Cognitive Radio (CR) is a radio that can change its transmitter parameters based on interaction with the environment in which it operates". Apart from this, WBANs also impose other constraints like the scarcity of hardware and radio communication resources which need to be taken into account.

Similarly, the convergence layer communication also faces some major challenges. More specifically, the proliferation of the wireless communication technologies has put a serious question mark on the availability of licensed spectra for admission of new services. Industry analysts predict that by 2020 about 50 billion devices are supposed to be connected to mobile networks worldwide, which include devices/sensors sending information between Machine-to-Machine (M2M), to servers, or to the cloud [8]. This will lead to severe spectrum scarcity, which will be a limiting factor to new services like WBAN based e-healthcare. However, an examination by FCC [7] revealed that the temporal and geographical variations in utilization of the fixed licensed spectrum band ranges from 15% to 85%. Consequently, there has been tremendous interest in exploiting the unoccupied wireless spectrum also known as 'white spaces' using "Dynamic Spectrum Access (DSA)" policies [9–11]. CRs through efficient implementation over Cognitive Radio Networks (CRNs) have the potential to realize DSA by

sensing and accessing the white spaces while minimizing the interference to the incumbent Primary Users (PUs).

In addition to the spectrum scarcity issue, the licensed WAN technologies also pose cost-efficiency issues. More specifically, unlike the cable Internet connectivity, which is widely spread and low cost, mobile Internet connectivity is yet to go a long way for low cost solution, especially in developing countries. CR technology that enables opportunistic DSA can make low cost long distance data transfer possible while still giving the same level of mobility and connectivity as licensed WAN. This is because the cost of DSA is expected to be much lower than the cost of purchasing a licensed band [8, 12]. This would make fundamental Internet-of-Things (IoT) services like healthcare monitoring more affordable to public particularly in developing nations, where the cost of data transfer is still high. Therefore, CR technology based DSA will act as a driving factor not only from the network operator and end user's perspective but also for the IoT and healthcare industry.

It is, therefore, imperative from these discussions that CR is a promising technology for efficient design of both WBAN access layer communication as well as WBAN backhaul transmission. The WBAN communication at access layer presents specific challenges that need to be alleviated using CR technology. For example, the WBAN access layer communication needs energy-efficient real-time capture of data with high reliability and low delay. Whereas, for backhaul transmission, incorporation of CR and WBAN brings with them additional challenges that must be fulfilled to realize the true potential of CRN as a cost effective backhaul technology. For example, for long-term remote health monitoring, WBAN backhaul transmission needs to be highly reliable and cost-efficient, while ensuring maximum energy-efficiency for longer battery life of WBAN hub. CRN on the other hand tend to disrupt this communication due to its inherent property of opportunistic channel access, leading to reduced reliability. ***Hence, the aim of this thesis is to address these challenges using CR technology for building an energy-efficient WBAN (including both access and convergence layer) and facilitate cost-efficient pervasive remote health monitoring.***

In accordance with the focus of research in this thesis, this chapter provides a brief introduction to the overall research problem as dealt with in this thesis. Thereafter, the state-of-research activities in this problem domain are discussed in detail. Based on the limitations of the existing studies in the literature, the motivation behind the proposed research in the thesis is duly established and the objectives are subsequently formulated to address the different aspects of the problem domain. Finally, a general discussion on the overall organization of the thesis is provided, followed by an outline of the flow of the thesis along with a summary of the significant outcomes.

1.1 Overview of the Research Problem

Healthcare industry is experiencing new trends of delivering healthcare across the entire range of services, from primary to tertiary care, in which the individual patient has a stronger role to play in the healthcare process. These trends arise mainly from the need to meet major socioeconomic challenges related to: citizens' expectations for high-quality care, demographic changes (the ageing population), increased prevalence of chronic diseases and rising healthcare costs [13]. To this end, the concept of Personal Health Systems (PHS) was introduced in the late 1990s. It is enabled by significant progress in sciences and technologies like biomedical sciences, micro and nano-technologies as well as ICT. PHS place the individual citizen/ patient at the center of the healthcare process. In doing so, PHS provide benefits to both the individuals as well as the authorities: first, by improving the quality of individual healthcare, and secondly, by containing the rising healthcare costs through efficient use of technology.

This need for proactive and affordable healthcare systems led to the origin of Wearable Health Systems (WHS), which are a specific category of PHS. WHS comprises of body-worn sensors in the form of wrist watch or "biomedical clothes". It provides continuous health monitoring and helps change personal habits. Further through application of ICT, if WHS is integrated into a telemedicine system, it opens possibilities for sending alarms to caregivers or emergency response teams when life-threatening changes occur. In addition, patients can benefit from long-term monitoring as a part of a diagnostic procedure, for assessing the efficacy of treatments and outcomes of clinical trials, or supervision during recovery from an acute event or surgical procedure or can achieve optimal maintenance of a chronic condition. Furthermore, the circadian and diurnal variations in physiological signals can be captured during long-term health monitoring. These variations, for example, are a very good recovery indicator in cardiac patients after myocardial infarction [14]. Some of the additional benefits of long-term health monitoring are- i) the ability to confirm the adherence to treatment guidelines (e.g., regular cardiovascular exercise), b) monitoring the effects of drug therapy, for example, the monitors can be used during stroke rehabilitation, or brain trauma rehabilitation, or physical rehabilitation after hip or knee surgeries. However, traditionally the wired WHS like Holter monitors [15] which comprise of unwieldy wires between the sensors and the monitoring system that limit the patient's activity and level of comfort and thus negatively influencing the measured results [16]. Also, the WHS discussed till now do not facilitate communication of implantable sensors to outside world, e.g. monitoring of pacemaker activities.

The recent advancement in embedded electronics and wireless sensor networks have facilitated a revolution in WHS that precisely addresses the aforementioned problems of wired

WHS. The miniaturization and integration of physical sensors, embedded microcontrollers and radio interfaces on a single chip, wireless networking and microfabrication have resulted in a shift from the traditional wired WHS to Wireless Body Area Networks (WBANs) [17]. WHS using WBANs allow patients to engage in their normal activities instead of staying at home or close to a specialized medical service. WBAN basically comprises of several miniaturized sensors attached to or implanted in the body and wirelessly sending data to a hub, also known as Body Network Controller (BNC), which is also located close to the body. A standalone WBAN can be represented as in Figure 1.1.

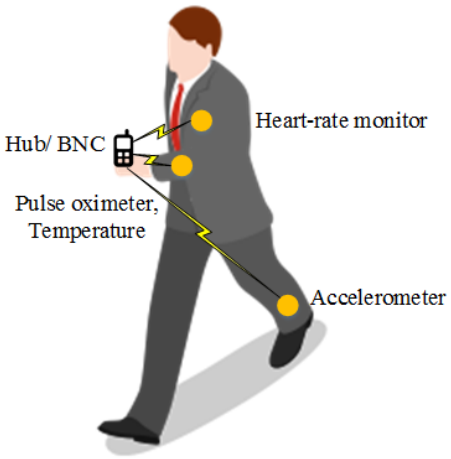

Fig. 1.1 Standalone WBAN illustrating placement of sensors and BNC.

As WHS have evolved into WBANs, similarly, advances in mobile technology have led to the transformation of a basic cellphone into a smartphone. The shift in mobile computing and applications have further transformed a smartphone into a digital hub enabling it to collect and store data from a variety of sensor-based devices [18, 19]. Therefore, with additional WBAN capabilities, a smartphone can readily serve as a BNC. Consequently, intelligent integration of WBAN with smartphone applications can provide real-time feedback to the user about the current health status [20]. Several healthcare applications are already available that leverage short distance Wireless Personal Area Network (WPAN) technologies like IEEE Bluetooth [21] or 802.15.4 (Zigbee) [22] to obtain data from sensors or smart watch and present interactive display of one's physical conditions on smartphone. However, current personal area network communication technologies such as Bluetooth or ZigBee are not meant for WBAN communications. More in detail, they do not meet the medical (closeness to human tissue) requirements. Additionally, it does not support increase in data rate, QoS and reliability needs of WBANs. To address this, IEEE 802.15.6 [23] Task group has recently

developed a short range WBAN standard. Figure 1.2 provides a comparison of the data rates and power requirements among the different technologies [24]. As shown in Figure 1.2, the current technologies meet the data rate requirements but they do not satisfy the power requirement of less than 10mW in WBANs. Moreover, IEEE 802.15.6 specifies other stringent requirements in terms of the low latency, high reliability and power requirements for different modes of channel access. Also, since the IEEE 802.15.6 is relatively new, there are no available WBAN hardware setups following this standard. Hence, there is need to study, design, implement and further optimize WBAN as per the recent IEEE 802.15.6 standard.

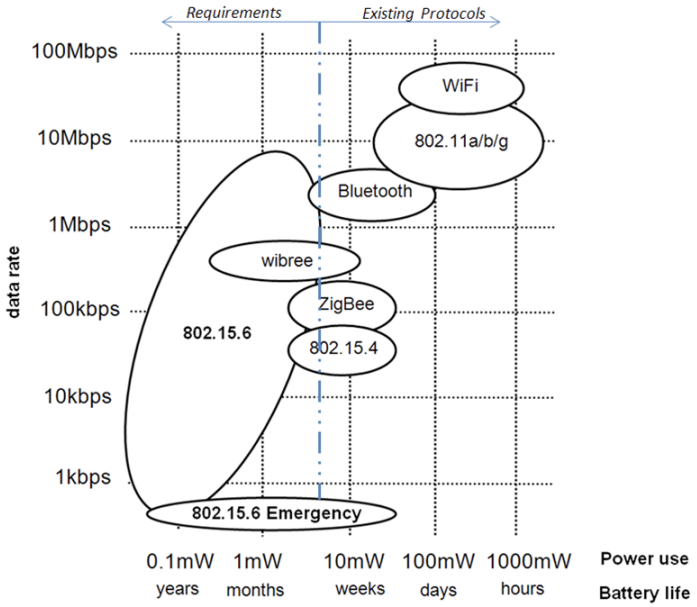

Fig. 1.2 Power requirements and data rates in WBANs [24].

Medium Access Control (MAC) protocols are one of the key enabling techniques of WBANs [25]. They play a vital role in determining the performance of WBAN in terms of the battery life of the energy constrained sensor nodes and the delay in sending a data packet to the hub. Contention free Time Division Multiple Access (TDMA) and contention based Carrier-Sense Multiple Access with Collision Avoidance (CSMA/CA) or Slotted Aloha are the two basic MAC mechanisms used in WBANs to support variety of periodic and urgent traffic [26]. Both of these access mechanisms have their own advantages and shortcomings which depend on factors like data rate and network conditions [27]. Usually, CSMA/CA is considered to be appropriate for low, urgent, adaptive, scalable traffic patterns and frequent network changes, whereas the TDMA is recommended for high correlated traffic and infrequent network changes [28–30]. In most of the cases of patient monitoring the traffic is often correlated [31]. For example, to get a clearer picture of a patient's overall

health, a physician requires a complete view of the patient's vitals namely temperature, blood pressure, ECG which have to be recorded simultaneously at periodic intervals. Similarly, for tracking the performance of an athlete, a WBAN need to continuously track high data rate applications like EMG, ECG, along with low data rate signals like temperature. Contention based MAC is not suitable in such cases of high traffic correlation [31] as they encounter heavy collisions and extra energy consumption. Schedule-based protocols such as TDMA, provide good solutions to the traffic correlation. These protocols are energy conserving protocols because the duty cycle is reduced and there are no contention, idle listening, and overhearing problems [31]. A comparison between TDMA and CSMA protocols is reported in [32]. It is shown that TDMA method is more suitable for nondynamic types of networks. Fortunately, WBAN has a nondynamic network structure (fixed network topology) [33]. To integrate their advantages, IEEE 802.15.6 provides a hybrid MAC protocol that supports both CSMA-CA, Slotted Aloha and TDMA based Scheduled Access MAC (SAM). As will be shown later in Section 1.2, in-depth study of SAM is still limited. This calls for its detailed analytical modeling, performance analysis and optimization for maximum energy-efficiency.

The goals of WBAN are to achieve (a) improved mobility, and (b) service flexibility. However, as WBANs rely on the wireless medium for communication they are affected by variations in the wireless channel Signal-to-Noise Ratio (SNR). Channel SNRs are subject to variations due to relative changes in the channel between sensors and BNC arising as a result of movements in human body, or collective movement of the entire WBAN through different environments due to mobility of the patients, or due to interference from other co-existing systems on the same channel as the WBAN. The fluctuations in channel SNR affect the latency, reliability, energy-efficiency of WBAN communication. Therefore, the MAC layer of a WBAN has to be carefully designed to adapt to the varying channel conditions. Cognitive Radio (CR), which is implemented based on Software Defined Radio (SDR) [34], is a promising technique to improve the efficiency of wireless communications by intelligently adapting to channel conditions. A CR transceiver can observe and learn the status of the operating environment, make a decision, and adapt the wireless transmission parameters accordingly. Therefore, leveraging on the adaptive and intelligent capabilities of CR, in this thesis we apply it to the WBAN communications based on scheduled access MAC to facilitate healthcare applications by taking into account the stringent constraints on latency, reliability and energy-efficiency under varied system parameters like applications, data rate, modulation levels etc.

WBANs are capable of transforming how citizens interact with and benefit from ICT and manage and think about their health. One major step towards this goal is integrating WBAN within a e-healthcare 3-tier architecture as shown in Figure 1.3. Within a WBAN based

e-healthcare system, the WBAN communication illustrated earlier in Figure 1.1 constitutes Tier-1 referred as the *WBAN access layer*. Whereas, the Tier-2 comprises the long distance *WBAN convergence layer or backhaul*. The backhaul communication is between BNC and one or more access point (APs). Tier-2 communication aims to interconnect WBANs with various networks, which can be easily accessed in daily life as well as cellular networks and the Internet [35]. The last tier/ Tier-3 is known as the *service layer* and is application specific. It can comprise of database for storing patient information, medical server for pervasive data access etc. A detailed discussion on the design and development of the service layer is beyond the scope of this thesis.

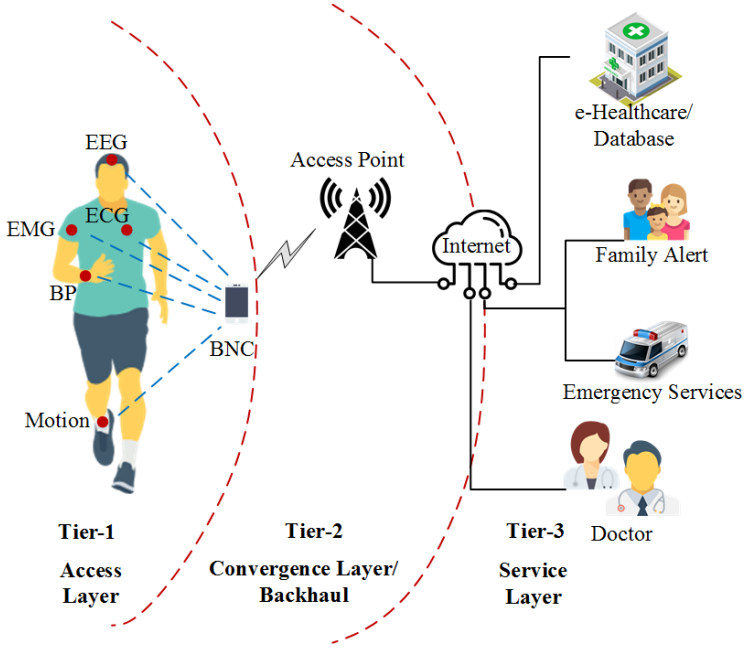

Fig. 1.3 WBAN as part of 3-tier e-healthcare architecture.

The backhaul layer facilitates transfer of WBAN data over the Internet and can provide Real-Time (RT) or near real-time (also termed as Non-Real Time (NRT)) updates to user's medical records. RT patient monitoring is mainly applicable for home and hospital environments, which have free Wireless Local Area Network (WLAN) technology [36] to provide Internet access. Though not limited by technology, RT monitoring over licensed Wide-area Access Network (WAN) technologies like 3G or 4G involves high data transfer costs and thus are impractical. The long distance licensed WAN technologies are more suited for NRT long-term periodic pervasive monitoring of patients who are not severely ill but still needs to have an extensive record of their physiological conditions, for e.g. as an alternative to regular and rather costly in-clinic follow-ups. With large time intervals of medical data, doctors will have a clearer view of the patient's status [6].

The use of licensed WAN technologies can provide guaranteed QoS [37]. Although these licensed spectra generally served well in the past, there is a phenomenal increase in their access due to increase in the wireless subscribers and the swift integration of bandwidth-intensive applications with respect to communication, gaming, social networking and other interactive multimedia services. Due to this, the problem of spectrum congestion has increased manifold in fixed spectrum assignment policy based licensed WANs [10]. Additionally, the advent of IoT is set to create an explosion of devices that also requires access to mobile networks for pervasive connectivity. This would further aggravate the issue of spectrum scarcity. This problem severely limits system capacity and degrades the transmission for ongoing users. Consequently, this has led to various studies on spectrum usage. Recent studies by FCC have pointed that large portions of spectrum are left unutilized both in frequency and time domain (for example, television broadcasting bands) [38]. Dynamic Spectrum Access (DSA) through the use of CR aims to solve the spectrum scarcity by opportunistically providing access to these unutilized frequency slots. This has led to the emergence of Cognitive Radio Network (CRN) that promises to increase the overall spectrum utilization by allowing opportunistic transmissions of different applications.

Apart from improving spectrum utilization, another vital advantage of CRN that can be a major driving factor for essential services like long-term health monitoring is the cost effectiveness of DSA. Since DSA is based on the basic ideology of opportunistic access of licensed spectrum, the cost of accessing a CRN will be lower as compared to using the same spectrum as a licensed user [8]. The cost-efficiency is particularly beneficial to people of developing nations where the cost of mobile internet is still considerably high. Furthermore, it will provide real cost incentives for basic healthcare services to penetrate rural areas which lack proper healthcare infrastructure. Moreover, the payoff from the CR users will add to the profit of the network operators and healthcare service providers. Therefore, CR is a promising technology that can be exploited in the form of CRN for cost-efficient WBAN backhaul communication to facilitate NRT remote health monitoring.

The basic idea of CRN is to allow unlicensed users, also known as Secondary Users (SUs) to opportunistically transmit in the available licensed spectrum bands that are allocated to incumbent Primary Users (PUs), when the corresponding PUs are absent or idle. The exploitation of these 'white spaces' by SUs in the absence of PUs is highlighted in Figure 1.4. It comes as a straightforward deduction that when WBAN uses CRN as backhaul, the BNC serves as the SU.

The general architecture of CRN that is deployed to exploit the unused spectrum holes in the licensed spectrum band is shown in Figure 1.5. As illustrated, the CRN coexists with the primary network at the same location and on the same spectrum band. The CRN can be

either centralized or adhoc. In case of a centralized CRN, a Cognitive Base Station (CBS) serves as the central managing unit and coordinates all the SUs which can also be a WBAN BNC attempting to send NRT data over the CRN backhaul. In case of adhoc CRN, the SUs coordinate among each other for PU channel access. Since, we are concerned with remote health monitoring using WBAN, we will focus on centralized CRN and unless specifically mentioned otherwise, the term CRN will refer to the centralized infrastructure as in Figure 1.5.

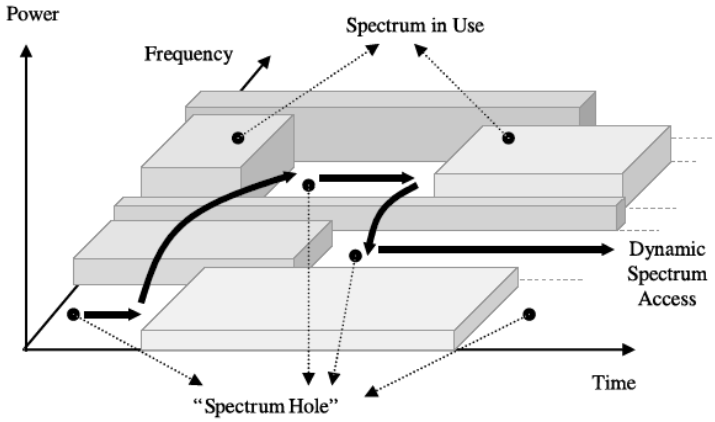

Fig. 1.4 Spectrum hole concept [10].

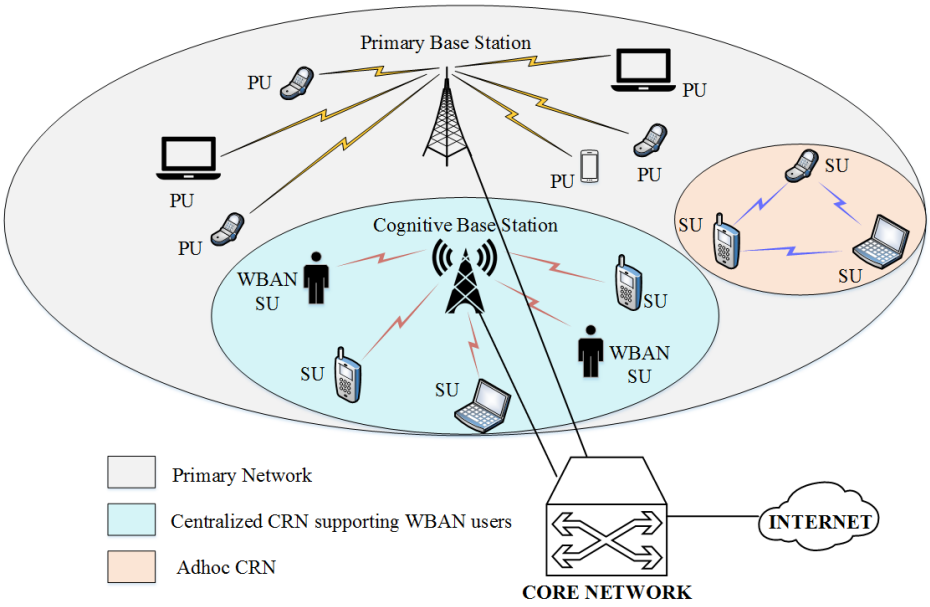

Fig. 1.5 Architecture of a CRN.

The first worldwide standard based on this CRN architecture is the IEEE 802.22 standard [39, 40] that mainly focuses on the UHF (Ultra High Frequency)/VHF (Very High Frequency) TV bands between 54-862 MHz. The project is also formally called the standard for Wireless Regional Area Networks (WRANs). However, the broad domain of CRN is not only limited to TV bands. It also extends to different licensed bands. In general, DSA based CR systems can be classified into two broad spectrum sharing scenarios [10], namely *underlay spectrum sharing*, and *overlay spectrum sharing*.

In an underlay based spectrum sharing scheme [41], SUs spread their transmission over a wide range of frequency bands while maintaining the interference with PUs below the noise floor. On the other hand, the overlay based spectrum sharing policy [42–45] supports opportunistic usage of idle channels by SUs in the absence of PUs and is considered in this thesis for further evaluation of spectral efficient and cost-efficient WBAN backhaul communication.

Taking into account the absolute priority of PU over a SU with respect to channel access in overlay based CRN, a SU must vacate itself on PU arrival and perform spectral handoff to shift to another idle channel for its transmission. In the absence of a suitable idle channel, this SU is dropped from the network. Thus arrival of a PU triggers unwanted disruptions in SU transmissions, which may affect the reliability of the sensitive applications like healthcare monitoring. Therefore, use of CRN as a backhaul needs to take into account such disruptions and the designed BNC should be intelligent enough to detect such scenarios and take suitable actions. Real-world implementation of WBAN over CRN backhaul, therefore, faces unique challenges in spectrum sensing and analysis, spectrum mobility and sharing [10], along with the appropriate tuning of wireless device parameters and regulations on spectrum usage.

In addition, to the spectrum sensing and sharing challenges, another crucial aspect that affects efficient design of backhaul CRN for WBAN is the energy-efficiency of the BNC that serves as a SU. A high energy-efficiency ensures prolonged battery life of the BNC, i.e. more time between two recharge cycles. Interestingly, implementation of WBAN over CRN in general, and achieving high energy-efficiency in particular, depends on the CRN policy. More in detail, if the CRN is designed to have a CBS that is resourceful enough in terms of higher computation capabilities it may perform spectrum sensing and resource scheduling on behalf of all the SUs, making the entire process centralized and very energy-efficient. However, if the CBS is part of a basic CRN as envisioned in IEEE 802.22 [46], where the role of the CBS is limited to assigning PU channels to the SUs based on information derived from a whitespace database. Then the spectrum sensing operations required to provide additional protection to PUs need be performed individually by the SUs while still ensuring maximum energy-efficiency of the SUs. Accordingly, in this thesis, we consider both centralized

sensing at CBS and individual SU sensing scenarios for energy-efficient WBAN deployment over backhaul CRN.

Thus it is inferred from the discussion in this section that the use of CR in- i) WBAN for health monitoring as a standalone network as per the IEEE 802.15.6 standard and/or, ii) a CRN backhaul for WBAN as part of e-healthcare architecture, can prove to be a determining factor towards ensuring energy-efficient and cost effective ubiquitous health monitoring which will ensure better quality of life and provide proactive and affordable healthcare for all. To this end, in this thesis we focus on the ***"Design and Implementation of Energy Efficient Wireless Body Area Network over Cognitive Radio Platforms"*** where the design and implementation issues are suitable addressed to maximize the energy-efficiency of communication while maintaining the QoS and reliability requirements of WBAN and ensuring that interference to PU is kept within a tolerable limit in the backhaul CRN. More specifically, the design and implementation aspects focused in this thesis as follows:

- ***Simulation, characterization and implementation of a practical energy-efficient WBAN as per IEEE 802.15.6 based Scheduled Access MAC (SAM) protocol for e-healthcare*** while satisfying the QoS requirements of physiological signals.
- ***Analytical modelling and performance evaluation of the WBAN as per IEEE 802.15.6 SAM under non-ideal channel conditions and thereby incorporating CR capability*** in WBAN sensor nodes to facilitate adaptation of parameters to achieve maximum energy-efficiency.
- ***Characterizing and developing an energy-efficient practical real-time CR system in test-bed for dynamic spectrum access*** capable of hosting IP based communication while keeping interference to PUs within acceptable limit.
- ***Cross-layer design and implementation of an intelligent BNC*** that serves as a gateway between the developed WBAN access layer and backhaul CR terminal to facilitate reliable, cost-efficient and energy-efficient NRT backhaul transmission of medical signals. In this regard, the issues related to deployment of the BNC over CRN are also addressed through individual sensing and optimization.
- ***Design of centralized framework for a CRN*** leveraging prediction and scheduling strategies at the CBS to enable energy-efficient NRT transmission of data by the BNCs.

1.2 State-of-Art of the Research

As already discussed in the previous section, the proposed research work in this thesis provides design and implementation solutions after conducting extensive study on the prospect of IEEE 802.15.6 in WBAN with added CR capability and the prospect of using CRN as backhaul for WBAN in a 3-tier healthcare architecture. This section provides a brief overview of these studies and thereby establishes the motivation for the proposed work in this thesis.

Existing wireless healthcare monitoring systems using WBANs exploit the short-range wireless systems such as ZigBee (IEEE 802.15.4) [47–49], WLANs [50, 51], GSM [52] and Bluetooth (IEEE 802.15.1) [53, 54]. In these works, mostly sensors are used to collect medical data from patient's body and then use short range technologies like Bluetooth or Zigbee to transfer it to a control unit.The control unit then connects to a gateway like a mobile device using Wi–Fi link to access Internet. Generally, to minimize the power consumption and the size of the sensor device, Zigbee has been the most popular choice. In this regard, WLAN technologies are especially avoided because of their large size and power consumption used to provide longer ranges (i.e. 100 m). For WBAN communications, in addition to unlicensed 2.4GHz ISM bands, designers have also used medical bands such as MICS (Medical Implant Communication Service) (402-405 MHz) and WMTS (Wireless Medical Telemetry Service) (608–614, 1395–1400, 1429–1432MHz) that are specifically regulated for medical monitoring by communication commissions around the world [55–57].

As highlighted above, in its initial stages, WBAN communications were primarily setup following IEEE 802.15.4 standard [22]. The standard was originally meant for Wireless Personal Area Networks (WPANs) which operate on low data rates. It was designed to facilitate efficient low-power and low-complexity, short-range radio frequency-based wireless communication with a support for node-mobility [58]. However, the performance of IEEE 802.15.4 was soon realized to be unsatisfactory as it does not support the improvement of QoS and increase of data rate. To address this, IEEE 802.15.6 Task Group was setup which provides a new set of Physical layer (PHY) and MAC layer specifications [23], particularly for wireless communications involving WBANs. IEEE 802.15.6 is a standard for short range wireless communication in the vicinity of, or inside the human body. It provides support for QoS, extremely low power, and high data rates up to 10 Mbps. Figure 1.2 shows that the current technologies meet the speed requirement of IEEE 802.15.6 in terms of data rates but not the power requirements of less than 10mW in WBANs. Furthermore, IEEE 802.15.6 is complaint with the non-interference guidelines, and takes into account the mobility of the sensor nodes and radiation pattern shaping to minimize the Specific Absorption Rate (SAR) into the human body.

IEEE 802.15.6 [23] provides PHY Layer specifications for narrowband, Ultra Wide Band (UWB) and Human Body Communications (HBC). We won't focus much on HBC as it not related to Radio Frequency (RF) communication and it uses human tissue as the medium for data transfer, that presents its own set of challenges. The narrowband PHY of IEEE 802.15.6 in addition to allowing communication over the 2.4GHz ISM, MICS and WMTS bands, also specify communication over other less congested ISM bands such as 433MHz band. While UWB PHY allow data transfer at low power and high bandwidth over 3–10 GHz band. Although UWB claimed very low power initially in the literature, its implementation in the integrated circuits have exhibited power consumption more than that of the conventional narrowband short-range wireless chips [59]. The high power consumption is mainly due to the receiver design at higher RF with high analog gains at the front-end to receive very low levels of transmit power. For an implant node in WBAN, UWB will cause high penetration loss because it operates at high frequencies (3–10GHz for medical applications) [60].

Efficient WBAN system design also requires accurate channel modelling to characterise the variations is channel conditions which would allow other processes in a node to operate accordingly. In this regard, the authors in [61, 62] conducted extensive WBAN channel modeling and show lognormal distribution to best fit the channel characteristics for on-body narrowband WBAN communications. Similar research work [63] based on UWB communication over on-body channels have reported that the small-scale fading follows lognormal distribution.

Regarding MAC layer protocols, the standard provides MAC layer specifications for CSMA/CA, slotted Aloha, scheduled, un-scheduled and polling based channel access. In this regard, significant analytical work has been carried out for performance evaluation of IEEE 802.15.6 using CSMA/CA MAC in [64–66], and slotted Aloha MAC in [67]. In [64, 65], detailed performance analysis of CSMA/CA has been carried out under saturation and non-saturation regimes respectively. While [66] provides further analysis under non-ideal channel characteristics. Chowdury et al. in [67] provided throughput performance analysis of the slotted Aloha under varied traffic loads.

As explained in [68], the term CR generally refers to a radio system that has the ability to sense its RF environment and modify its spectrum usage based on what it detects. Consequently, the benefits of incorporating CR capabilities in WBAN were realized and studied in 2012 by Santigo et al. in [69] and Mohammady et al. in [70]. In these works, the authors use CR to potentially alleviate the problems of medical communication environments like co-existence with other electronic devices and improvement in spectral efficiency.

With the advent of IoT, the problem that will be faced by next generation 5G networks is to provide access to a huge number of devices that support IoT applications. Traditionally,

the 2G-4G systems rely on the so-called orthogonal multiple access. For example- Time Division Multiple Access (TDMA) in 2G cellular communications [71]. However, such orthogonal multiple access will be difficult to support for future IoT applications. With IoT, the cell density in a cellular network will increase many folds and number of available time slots or bandwidth resources will be insufficient. Due to this, multiple orthogonal access is not suited for 5G. As a result, it is not without reason that a lot of research has gone into exploring non-orthogonal multiple access which enables putting a number of users into limited bandwidth channels [8, 72, 73]. Ideally non-orthogonal multiple access can strike a better trade-off between system throughput and user fairness. This certainly creates interference between different users, which will cause some users to experience low data rates. But interestingly in IoT, there are many devices which should be served timely with low data rates. One such example is wireless healthcare, where wearable devices (heart monitors, bio-sensors, etc), BNCs of WBANs need to send patient data timely to hospital severs, but the data rates used by these devices are not likely high. Leveraging non-orthogonal multiple access, it is possible to squeeze in a lot of IoT users/devices with different QoS requirements into the same time slot or frequency channels. In this sense, the concept of non-orthogonal approaches is very exciting and perfect for the IoT.

One way to illustrate the benefit of non-orthogonal multiple access is as a special use case of CR technologies. Dynamic Spectrum Access (DSA) through the use of CR permits admission of new opportunistic users into underutilized channels. This concept of CR was envisioned in the landmark study by J. Mitola in [74] keeping in mind the prospective growth in demand for wireless services. Of course opportunistic channel access will cause some performance degradation for the initial users, but such degradation can be controlled by maintaining an interference temperature limit or a careful power control mechanism is carried out among the users. The initial study in this regard was carried out by S. Haykin in [75], where the author took over from where Mitola had left his preliminary research on CR. This study has focused on the signal processing aspects of CR and introduced interference temperature as a metric for quantifying and managing the interference in CRN. Also this paper discusses the aspects of channel-state estimation and modeling, and describes the operations of dynamic spectrum management in coordination with the transmit-power control mechanisms. Both these works subsequently triggered a plethora of contemporary research on CR and CR based systems in relation to spectrum sensing and analysis [76–78], management [79] and mobility [80].

However, it was not until 2013-14 when the energy-spectral efficiency trade-offs in using cognitive radio in 5G were studied by Hong et al. in [8]. In this study, the reasons for using cognitive cellular network, which integrates conventional licensed cellular radio and

cognitive radio into a holistic system were highlighted. It was proposed that the CR can be used to cope with overload traffic in peak hours or provide opportunistic delay-insensitive multimedia downloads, IoT communication at low cost. Two possible system architectures, namely non-cooperative and cooperative are illustrated along with various usage scenarios, three levels of capacity analysis, and two types of capacity metrics that enable a wide range of energy-spectral efficiency trade-off analysis.

For CR to be employed for DSA by energy constrained IoT devices such as sensors and BNCs, any proposed scheme needs to be energy-efficient while ensuring high reliability. Further, they should be robust so as to overcome adverse conditions. The performance of spectrum sensing depends on detection timing to determine how long and how frequently spectrum sensing should be carried out. In this regard, periodic sensing framework is discussed in [81], in which each frame consists of a sensing block and an inter-sensing block. Subsequently, in [82], a periodic sensing timing is proposed to improve the channel utilization of CR users while limiting their interference with PUs, taking into consideration the impact of sensing uncertainties like false alarm and miss-detection [83]. While, Xu et al. in [84] maximized the channel utilization using an opportunistic spectrum access strategy for a slotted SU overlaying an un-slotted primary network under interference constraint and energy consumption constraint. Focus is also given to the design of efficient spectrum mobility/handoff techniques in [85–87] which handles the sudden arrival of PU during SU transmission, thereby making CRNs more robust. In this relation, it proposes the use of cross-layer message passing to facilitate switching of PU channels so as avoid disruption in SU communication.

Practical validation of proposed theories and mechanisms in CR test-beds comprising of Software Defined Radio (SDR) boards has mainly been focused towards non-real time offline processing [88–90]. In the afore-mentioned offline mode of operation most signal transmission, reception, signal processing and MAC layer processing, are controlled by external computer software that interact with the SDRs. This obviously does not represent the real CR test-bed setup. However, more recently a real-time CR test-bed is reported in [91] where a RECOG model is proposed that configures centrally managed Access Points (APs) with several cognitive functionalities, while bestowing the SUs with two transceivers for simultaneous sensing and transmission, and finally implements VoIP and video streaming applications in the system.

Overall, the novelty and significance of the study are established in Figure 1.6 by drawing a comparative analogy between the work that has already been achieved in literature and which aspects are still lacking and need further investigations.

Existing Works	⇒	Required
WBAN implementation [47–49]		IEEE 802.15.6 based WBAN implementation for energy-efficient health monitoring
Performance analysis of IEEE 802.15.6 MAC ptocols based on CSMA/CA and slotted Aloha [64–67]		Performance analysis of IEEE 802.15.6 based scheduled access MAC and parameter optimization using CR under non-ideal channel conditions for higher energy-efficiency
DSA envisioned as a solution for IoT services in 5G [8] and reliability issues related to DSA [85–87]		Design and implementation of highly reliable and cost-efficient remote health monitoring using WBAN over backhaul CRN
Parameter optimization in DSA to achieve high capacity [81, 82, 84]		Parameter optimization and suitable framework to achieve maximum energy-efficiency
Tools used: Mainly analytical and non-real time implementation [88–90]		Validation in simulation and real-time hardware test-bed with optimal resource utilization

Fig. 1.6 Relevance of the proposed research

Based on the outcome of Figure 1.6, the motivation for addressing the research challenges in this thesis is established in the next section.

1.3 Motivation

The primary motivation towards conducting the proposed work in this thesis is driven by two important factors that include:

i) the need to perform detailed analysis of the IEEE 802.15.6 based standalone WBAN under scheduled access mode and thereby improve the WBAN performance and energy-efficiency of sensor nodes using the intelligence and adaptability provided by CR.

ii) the ability to exploit opportunistic communication as allowed by a backhaul CRN through DSA policies for achieving spectrum efficient communication and cost-efficient remote health monitoring using the WBAN.

In view of the enormous significance of these technologies in the Wearable Health Systems (WHS) and remote health monitoring as highlighted in Section 1.2, the research community has taken due cognizance of this prospect with several works being conducted on both standalone WBAN and incorporation of DSA for efficient IoT enabled communication in future 5G networks, primarily with respect to latency, reliability, energy-efficiency and cost-efficiency as briefed in previous section. However, it is clear from Figure 1.6 that a complete performance study of IEEE 802.15.6 scheduled access MAC and the integration of WBAN over CRN backhaul for NRT remote health monitoring under different scenarios covering all aspects related to analysis, design and implementations are yet to be carried out and this drives the impetus for the proposed research work in the thesis. Accordingly, this section brings out the key areas of focus in the thesis work by discussing the shortcomings of the relevant works in literature.

To begin with, any analytical study must be suitably verified using real life-like observations either in simulation models or test-bed prototypes. It is pretty evident from the literature survey of the previous section that the current works on WBAN based on IEEE 802.15.6 have laid more focus on the analytical aspects rather than the implementation details. In general, few simulation models have been developed for Wireless Sensor Networks (WSNs) using various platforms like NS2 [92], OMNet++ [93], Castaslia [94], OPNET [95]. Castalia provides an implementation of IEEE 802.15.6 MAC. However, the lack of a proper Graphical User Interface (GUI) makes coding, realizing network environment and performing simulation a rather complicated process. OPNET on the other hand has an elaborate GUI. But OPNET does not have any built-in simulation model based on IEEE 802.15.6 standard. Fortunately, Jurcik et al. in [96] illustrated a Zigbee implementation that did not use the OPNET Modeler standard library and the corresponding results obtained were very reliable. This motivated us to use the design philosophy in [96] and extend it for IEEE 802.15.6 scheduled access MAC in OPNET. ***Therefore, due to a lack in simulation models and studies for IEEE 802.15.6 MAC protocols in general, and scheduled access MAC in particular, the initial focal point of this work is towards developing a comprehensive simulation model for IEEE 802.15.6 scheduled access MAC that will serve as a dedicated platform for conducting further studies in this discipline.*** Like simulation models, implementation of WBAN is limited to Zigbee [47–49] and Bluetooth [53, 54] WPAN technologies. However, WPAN technologies do not comply with the medical standards in terms of QoS, reliability and increased data rate. Thus, a comprehensive and detailed implementation adhering to IEEE 802.15.6 standard

is yet to be performed. Moreover, a test-bed implementation would provide crucial insight into the mechanisms and available resources in a sensor node. Such knowledge can be exploited for efficient practical incorporation of CR features in the sensor nodes. ***Therefore, motivated by the lack of adequate implementation work regarding IEEE 802.15.6, the next aim is to develop a WBAN that is based on the IEEE 802.15.6 scheduled access MAC protocol, capable of tracking multiple attributes of a patient in real-time and integrate it within a remote heath monitoring e-healthcare system. Furthermore, leveraging on our developed detailed OPNET simulation model, we focus on making the developed WBAN energy-efficient for longer battery life of sensor nodes. Additionally, to facilitate an energy-efficient backhaul transmission that incurs low data transfer costs to the users, we also propose and implement a fast Discrete Wavelet Transform (DWT) based data compression algorithm at the BNC, termed herein as B-DWT. In this regard, the aim is to ensure faster execution of B-DWT at the BNC with low memory foot-print.***

Focusing on CR test-bed implementation for DSA, it is imperative that detailed test-bed modeling and performance evaluation with test-bed parameters allows users to study the device characteristics in real environment under operational conditions at any realistic scale at real speeds. It gives an insight into the working of the device and helps in understanding the trade-off between different test-bed parameters. This allows us to re-modify the existing analytical expressions with test-bed related parameters and study them from new viewpoints. Considering the design complexities in real-time CR modeling, it is obvious that most of the works [88–90] have been focused towards offline non-real time processing, and even fewer [91, 97] works have implemented in real-time CR model for the SUs. While RECOG [91] configures the Access Points with cognitive abilities to implement real-time applications, the soft real-time model in [97] utilizes the knowledge of the frequency hopping based PU traffic behavior to host video-streaming services. However, the model in [91] suffers from the issues of energy-efficiency and cost-effectiveness due to the use of two transceivers, whereas the model in [97] does not consider a generic CRN and is thus not widely acceptable. In short, none of these works deploy "truly cognitive SU terminals" that must be equipped with sensing, decision, management and mobility functionalities. To this end, spectrum sensing [76] is by far the most important component for the establishment of SU. Furthermore, energy-detection is the most common sensing technique used in validation of a wide range of CR algorithms that rely on spectrum sensing as one of its enabling methods. Apart from this, another challenge towards real-time processing in SUs is the efficient utilization of the limited on-board resources such as the Field Programmable Gate Array (FPGA) and Embedded Processor (EP) resources. ***Taking all these into account, the focus of this study is to model a prototype of real-time CR interface or SU through optimal characterization, design and***

implementation of resource and energy-efficient energy detector for DSA to ultimately enable opportunistic IP enabled communication over PU channels. The developed CR interface will serve as test-bed for future improvements and medium for proof-of-concept of proposed models.

Thereafter, the focus shifts from implementation of WBAN and CR to the detailed analytical study of IEEE 802.15.6 scheduled access MAC protocol leading to optimization of the network performance and sensor node energy-efficiency using CR based adaptive techniques. Detailed analytical modeling and performance evaluation allows users to study a communication network and analyze its performance even before the system is implemented. It gives an insight into the system performance and helps us understand the tradeoff between different system parameters. Moreover, it allows a system designer to incorporate methods to optimize network parameters at the design stage thereby maximizing the system performance [98]. Performance evaluation of IEEE 802.15.6 MAC protocols through analytical modeling has mainly been focused towards the CSMA/CA [64–66], and slotted Aloha [67] based contented medium access. As for the contention free scheduled access, Tachtatzis et al. [99] performed energy analysis of the scheduled access modes in the context of medical applications. However, this work does not put forward a complete performance evaluation of the standard. ***Taking all these into account, the focus of this work is on the detailed analytical study of the scheduled access mode leading to closed form expressions for the frame delay; reliability of data transfer; throughput; energy consumption and Energy-Efficiency (EE) of the sensor nodes. The next aim to exploit the observations of the study and leverage CR capabilities of our already developed sensor nodes to implement adaptation of the allocation intervals and payload sizes based on the channel SNR to achieve the maximum EE for a particular average frame delay and reliability constraints.***

Having developed, characterized and optimized the basic WBAN setup and a real-time CR terminal for DSA within a CRN, the focus shifts towards integrating these two technologies to address the need for low cost solutions that will encourage rapid adaptation of ICT in the field of healthcare particularly for remote healthcare monitoring and also address the impending spectrum efficiency issues faced by next generation wireless networks due to the advent of IoT solutions like the ubiquitous health monitoring. Backhaul CRN for DSA will enable NRT pervasive healthcare which will allow periodic monitoring of patients in both outdoor as well as indoor environments. However, this imposes strict reliability requirements for the CRN. One of the issues regarding reliability in CRN is the sudden arrival of a PU during SU communication. In this regard, handoff through cross-layer interaction between CR MAC and PHY layers has received considerable attention in [85, 86]. Handoff ensures continuous SU communication by switching to unoccupied PU channels. However, the reliability/robustness

requirement of healthcare services require addressing of other possible data loss scenarios like inability to initiate and/or continue communication due to unavailability of no or proper PU channels. Literature survey revealed that there has been no effort in this regard from practical design and implementation perspective. A possible solution to this problem is giving SUs the intelligence to switch to other licensed WAN technologies if it fails to sustain a communication over the CRN. Apart from reliability, another essential requirement of any proposed model targeted towards battery operated SUs like BNCs is the need to ensure maximum possible energy-efficiency. However, the major limitation of the existing research work related to energy studies [84] in the field of DSA using CR is that they do not consider the optimization of energy-efficiency as a ratio of throughput to the energy consumption. ***These serve as the motivations for the next work in the thesis that focuses on a complete design and implementation of cross-layer based intelligent WBAN gateway, which is the BNC, using CR technology that facilitates cost-efficient WBAN backhaul transmission by leveraging the novel idea of cross-layer message passing between CR MAC and upper management layer to facilitate session management and switching between CR backhaul and conventional licensed WAN. The next aim is to maximize the energy-efficiency of the backhaul transmission through optimization of inter-sensing duration by the BNC using computationally efficient convex optimization techniques.*** Note that, in the present scenario we consider the fundamental centralized CRN model as envisioned in IEEE 802.22 [46], where the role of the CBS is to assign PU channels to the SUs based on information derived from a whitespace database. The additional protection to PU communication through spectrum sensing is to be ensured by the SUs.

There is yet another popular CRN architecture where the CBS performs all necessary cognitive actions for PU channel access [100], thereby simplifying the SU design. It is intuitive that this method will be more energy-efficient for the SUs but at the cost of i) increased resource requirement at the CBS, for example- additional transceivers for CRN control channel, powerful processors to perform optimizations on behalf of all SUs, and ii) more message transfer between SU and CBS. Thus considering that resource in not a constraint for the CBS, the last phase of the work deals with a centralized CRN to facilitate energy-efficient NRT data transmission by SUs like the BNC of WBANs. As explained earlier, there has been limited efforts in the domain of energy-efficient transmission over CRN. Major cause of energy wastage in CRN is due to collisions between SU and PU systems. Minimization of such interference can thus guarantee enhanced energy-efficiency as well as reliability in transmission. One possible way to mitigate this interference is through exploitation of prediction techniques in CRN. In this regard, Hidden Markov Model (HMM) [101] based prediction has been used in [87, 102] to facilitate handoff in CRNs.

However, the possibility of using this prediction information towards energy-efficient NRT SU transmission is yet to be explored. Apart from identifying and optimizing the predictable PU channels for improved NRT SU communication, the Cognitive Base Station (CBS) also needs to fairly allocate the predictable channels among the SUs so as to minimize the total battery consumption. Centralized resource allocation in CRs is discussed in [103–105]. However, they are either maximizing throughput or are database driven which do not consider sensing uncertainties. ***Accordingly, with the focus on increasing both the energy-efficiency and interference rejection capabilities of SUs, the next step of this work is to develop a framework for centralized CRN at the CBS that incorporates a hardware based HMM predictor engine on reconfigurable hardware to minimize the prediction time, followed by detection of predictable PU channels under sensing uncertainties with optimization of the inter sensing-prediction duration and lastly fairly allocating the predictable channels among the NRT SUs to minimize the total battery consumption in the CRN.***

It is thus inferred from this section that there is a strong motivation for conducting the proposed research work in the domain of energy-efficient WBAN with CR enabled features followed by its integration over backhaul CRN for cost-efficient, spectral efficient and energy-efficient remote health monitoring. In this regard, the primary objectives of this thesis are outlined as follows.

Objectives of the Thesis

❶ **Development of a comprehensive simulation model for IEEE 802.15.6 scheduled access MAC and implementation of the same in real test-bed** for energy-efficient tracking of multiple attributes of a patient in real-time, followed by its integration within e-healthcare system with added features like on-board compression of data for backhaul transmission.

❷ **Prototype modeling of real-time CR interface (SU)** through characterization and implementation of resource/ energy-efficient energy detection based sensing for DSA over licensed PU channels.

❸ **Analytical modeling of IEEE 802.15.6 scheduled access MAC under non-ideal channel conditions** to study its performance against varied system parameters, **followed by CR based adaptive parameter configuration based on the WBAN channel condition**.

❹ **Design and implementation of a novel WBAN gateway, called BodyCog-BNC**, that employs CR backhaul communication for cost-efficient remote health monitoring

while ensuring reliability in data transfer and maximum energy-efficiency, and also analyzing it to derive closed form expressions for major performance indicators.

❺ **Designing a Centralized Scheduling, Sensing and Prediction (CSSP) framework** for a CRN for energy-efficient non-real time communication as encountered in remote health monitoring using WBAN.

1.4 Thesis Organization

The thesis is henceforth organized as follows.

❖ After the detailed discussions pertaining to the general introduction, contribution and outline of the thesis in Chapter 1, ***Chapter 2 provides the details related to the background study involving WBAN and CR technologies***. A technical overview of the WBAN technology is provided along with a discussion on the MAC and PHY layer specifications as laid out by IEEE 802.15.6 standard for its implementation. We also elaborate on the integration aspects of WBAN within an e-healthcare framework. Next, the evolution of the CR technology is traced from being adaptive systems to its application for DSA. Thereafter, we provide a brief overview of the adaptive aspects of CR systems, the CR cycle and the CRN architecture for DSA. This is followed by a discussion on the wide array of applications of both the technologies and their related design and implementation challenges. Finally, we highlight how CR platforms can be leveraged to alleviate the various challenges faced by WBAN both as a standalone network and when deployed over an e-healthcare architecture while also addressing the design challenges faced during such CR implementations.

❖ It is evident from the background study of Chapter 2 that there is an enormous scope of IEEE 802.15.6 based WBAN in facilitating proactive, affordable and ubiquitous PHS. Accordingly, the first step towards conducting state-of-art research with this standard is the design and development of a real life-like simulation model that will serve as a platform for validating analytical observations and also facilitate performance analysis and optimization of designed WBANs. ***Therefore, Chapter 3 deals with the design of simulation models for WBAN as per the IEEE 802.15.6 specifications***. Literature survey revealed several limitations in the existing simulation models of Wireless Sensor Networks (WSNs) in general and WBANs in particular. Furthermore, there has been very limited work on scheduled access MAC of IEEE 802.15.6. Due to this, we developed a detailed simulation model in OPNET Modeler 16.0 of WBAN following scheduled access

MAC of IEEE 802.15.6 protocol employing a hierarchical top-down approach, starting at the network level, followed by the node level, right up to the process level. In addition to design of simulation platform, another aspect that is of great significance is using the simulation model for actual energy-efficient design and implementation of WBAN on test-bed to facilitate real-time health monitoring and non-real time transfer of small amounts of WBAN captured data to remote server in an e-healthcare framework. A WBAN test-bed model will also provide important insight into the sensor node mechanism and resources, which can be exploited later for embedding CR enabled adaptability. Therefore, ***Chapter 3 also deals with the hardware and software designs to implement and optimize (with the help of the simulation model) a WBAN based on scheduled access MAC of IEEE 802.15.6 standard for e-healthcare***. Additionally, we also propose a DWT based data compression technique (B-DWT) to facilitate energy-efficient and low cost backhaul data transmission by BNC using licensed WAN technologies like GPRS and GSM. After suitable hardware design, we exploit our developed simulation model to perform performance analysis and characterization of our WBAN. Finally, the advantages of the proposed B-DWT technique are also established along with the basics of remote server and database storage.

Publications:

i) **Journal:** Lecture Notes in Computer Science (LNCS), Springer Scopus Indexed (One of the 12 papers selected among 134 submissions).

ii) **International Conference Proc. :** IEEE COMSNETS, Bangalore, India, Jan'18.

❖ Chapter 2 has already established the potential of CRN in alleviating some of the major concerns such as spectrum scarcity issues arising due to the deployment of prolific amount of IoT services like e-healthcare and the necessity for minimizing the data transfer costs involved in remote health monitoring. Also, Chapter 3 has laid the ground work for the implementation of remote health monitoring using WBAN. However, the work in Chapter 3 was focused primarily on WBAN which utilized licensed WAN for backhaul transmission. However, to introduce CRN at the backhaul of WBAN and truly take advantage of DSA, the first step should be the proper design of a real-time CR interface (i.e. SU) that can be used for opportunistic IP enabled communication over PU channels in a CRN. ***Chapter 4 addresses this issue of practical realization of real-time SUs through proposed test-bed design, characterization of energy detection based sensing and implementation of a generic CRN test-bed where SUs leverage our proposed Practical Energy-Efficient Energy Detection (PED) method to sense the PU channels with high accuracy and then successfully transfer IP packets while keeping the interference to***

PUs within pre-determined threshold. The PED method is further integrated within a proposed Energy Detection based CR MAC (ECR-MAC) framework developed at the Embedded Processor (EP) for real-time SU operation. Further, performance analysis is also performed to establish the superiority of PED method in terms of reduced energy consumption in spectrum sensing and also study the characteristics of SU operation viz. interference to PU, detection performance and ROC of spectrum sensing under varied operating conditions.

Publications:

i) **Journal:** Elsevier Computers and Electrical Engineering Journal, vol. 45, Jul'15.

ii) **International Conference Proc. :** IEEE OPTRONIX, Kolkata, India, Mar'19.

Having developed the simulation and test-bed setups of WBAN and CRN in Chapter 3 and Chapter 4 respectively, we now turn our focus towards a finer level of study and optimization followed by related design and implementation (using our already established setups) regarding-

i) WBAN communication as per IEEE 802.15.6 scheduled access mode augmented with CR enabled adaptive features.
ii) WBAN gateway design to interface WBAN with backhaul CRN for cost-efficient remote health monitoring over an e-healthcare platform.
iii) Optimization in CRN backhaul communication to facilitate energy-efficient NRT communication.

The aforementioned topics are elaborated in the following chapters.

❖ The focus shifts from implementation to detailed analytical study of WBAN based on IEEE 802.15.6 scheduled access MAC, followed by suitable optimization to achieve optimal system performance. ***Specifically, Chapter 5 deals with detailed mathematical derivations of closed form expressions of key performance indicators of WBAN leading to comprehensive performance analysis and subsequent optimization through suitable tuning of system parameters by exploiting CR capabilities of sensor nodes under non-ideal channel conditions***. In this regard, expressions of average frame waiting delay, throughput, energy consumption and energy-efficiency of the sensor nodes were derived using queuing techniques. We also elaborate on the non-ideal channel characteristics of WBAN and its effect on the performance indicators. Following this, to lend credibility to the derived expressions, we validate the analytical model through simulations performed using our OPNET model developed in Chapter 3. In addition, we

perform detailed analysis of system performance for variations in allocation intervals, traffic loads,payload sizes, beacon intervals, information data rate, error probability due to different modulation schemes and channel SNRs. Finally, by taking note of the trade-offs in system performance with respect to the selection of allocation intervals and payload sizes, we propose an implementable Look-up Table (LUT) based approach that allows our already developed sensor nodes in Chapter 3 to leverage their CR capabilities to sense the channel SNR and adapt their allocation intervals and payload sizes to achieve maximum energy-efficiency under frame delay and reliability constraints.

Publications:

i) **Journal:** IEEE Transactions on Mobile Computing, Feb'19.

ii) **International Conference Proc. :** IEEE RADIO, Reunion Island, France, Oct'16 (Awarded in YSA Competition).

❖ After suitably studying, optimizing and implementing the standalone WBAN operation in Chapter 5, and also characterizing and developing a real-time CR terminal in Chapter 4, the next important objective is to design and implement a BNC as a gateway between WBAN and backhaul CRN to facilitate spectrum efficient and cost-efficient remote health monitoring. ***In this aspect, Chapter 6 deals with design and implementation of an intelligent WBAN gateway, termed as BodyCog-BNC, that uses CR to opportunistically access licensed PU channels to facilitate spectral-efficient, cost-efficient and reliable NRT backhaul transmission of WBAN data***. For this, we develop a protocol stack for BodyCog-BNC that incorporates our proposed cross-layer based BodyCog-BNC Management Entity (BME) and BodyCog-BNC CR MAC (BCR-MAC) units. Thereafter, we perform complete design and implementation of the BME and BCR-MAC by developing the BME Development (BMED) framework and BCR-MAC Development (BCRD) framework respectively. The operation of these units are based on cross-layer message passing that enables intelligent session management and spectrum agility depending on the state of the CRN. Furthermore, with the additional requirement of maximizing the energy-efficiency of backhaul CR transmission, we formulate our proposed Inter-Sensing Time Optimization (ISTO) algorithm that uses Karush-Kuhn-Tucker (KKT) based convex optimization to optimally select the inter-sensing duration of the CR cycle under sensing uncertainties while keeping the PU interference under predetermined threshold. Closed form analytical expressions are also derived to perform analysis of the developed BodyCog-BNC in terms of average energy consumption, probability of switching from CR interface to licensed WAN, the speed of such switching and the cost-efficiency. Thereafter, we conduct a comprehensive performance evaluation of BodyCog-BNC for varied

healthcare applications under different PU activities, detected PU SNRs, control channel SNRs and CR cost regimes, which establishes its superiority in facilitating reliable cost-efficient backhaul communication by showing drastic improvement over the existing use of licensed WAN technologies. Finally, by leveraging i) the WBAN BNC developed in Chapter 3, ii) the real-time CR terminal created in Chapter 4 and iiii) our proposed BMED and BCRD architectures, we implement a prototype of BodyCog-BNC and provide a proof of concept of the feasibility of BodyCog-BNC in enabling NRT remote health monitoring.

Publications:

i) **Patent:** "Cross-Layer Apparatus and Method for Cognitive Radio System"- Filed

ii) **Journal:** Elsevier Physical Communication, May'19.

iii) **International Conference Proc. :** IEEE TENSYMP, Ahmedabad, India, May'15.

❖ Chapter 6 has already presented the novel idea of exploiting backhaul CRN to address all the concerns faced by WBAN with respect to low cost backhaul communication and also that faced by next generation networks in tackling the issue of spectrum crunch due to increasing number of IoT services. However, in Chapter 6 we have shown the integration of the BodyCog-BNC into a basic CRN as envisioned in IEEE 802.22 [46], where the protection to incumbent PU communication needs to ensured by SUs through spectrum sensing. However, we now consider the alternate popular CRN policy [100] where the CBS performs all necessary cognitive actions for PU channel access, thereby simplifying the SU (BNC) design. Considering that the CBS has ample resources to execute complex operations, ***Chapter 7 proposes a centralized scheduling, sensing and enhanced HMM based prediction framework, termed CSSP, at the CBS to facilitate highly energy-efficient NRT data transfer as encountered in WBAN based remote health monitoring***. To this end, we design and implement our proposed Hardware based HMM (H2M2) engine at the CR PHY of CBS that reduces the prediction time significantly thereby improving the system performance. Thereafter, through performance analysis we establish that H2M2 reduces interference between SU and PU but at the cost of reduced throughput. To address this, we introduce our devised Inter Sensing-Prediction Time Optimization (ISPTO) algorithm that maximizes SU throughput under sensing uncertainties and PU interference constraint. Following this, we formulate the problem of minimizing the total battery consumption of all the NRT SUs in the CRN by allocating the appropriate predictable channels to suitable users based on the operating conditions. For this purpose, we propose Battery Consumption Minimizing Scheduler (BCMS) that solves the channel assignment problem in polynomial time and also ensures fairness while channel

assignment. Detailed performance analysis is conducted to demonstrate the remarkable improvement in energy-efficiency due to use of CSSP over high PU activity channels as compared to traditional sensing frameworks. Finally, the practical utility of the system is established with respect to WBAN based remote health monitoring by developing a prototype model of H2M2 in FPGA board and using it in association with the CRN test-bed developed in Chapter 4 through a hardware co-simulation environment that shows a suitable direction of use for future IoT applications.

Publications:

i) **Patent:** "Method and Apparatus for Energy Efficient Data Transmission in Cognitive Radio System"- Filed

ii) **Journal:** Wiley International Journal of Communication Systems, vol. 31(13), Sep' 18

iii) **International Conference Proc. :** IEEE IACC, Andhra Pradesh, India, Feb'16.

1.5 Flow of Thesis with Summary of Contributions

The flow of research contributions in this thesis is illustrated by the schematic diagram in the next picture.

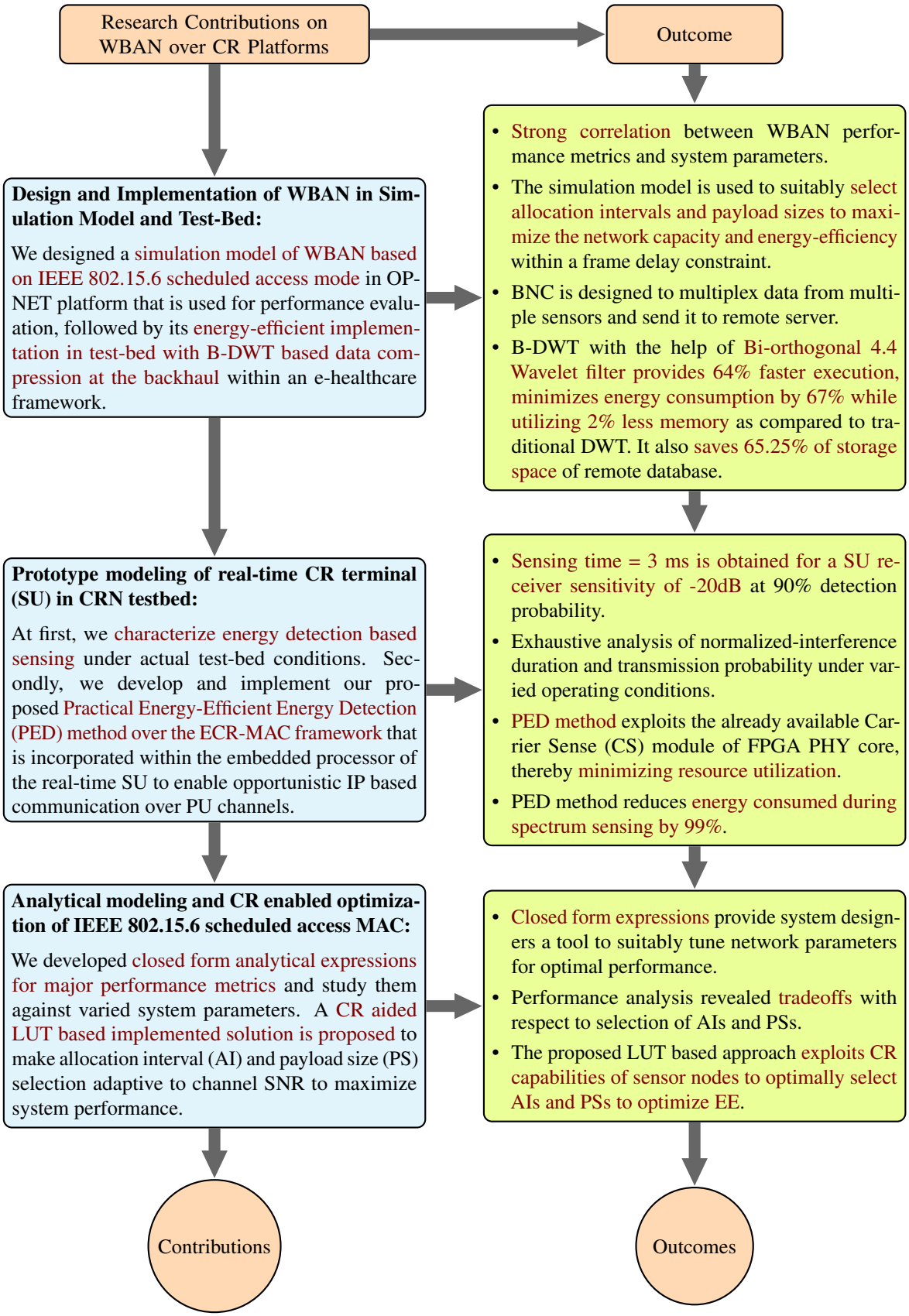
Research Contributions on WBAN over CR Platforms
Outcome
Design and Implementation of WBAN in Simulation Model and Test-Bed:
We designed a simulation model of WBAN based on IEEE 802.15.6 scheduled access mode in OPNET platform that is used for performance evaluation, followed by its energy-efficient implementation in test-bed with B-DWT based data compression at the backhaul within an e-healthcare framework.
Strong correlation between WBAN performance metrics and system parameters.
The simulation model is used to suitably select allocation intervals and payload sizes to maximize the network capacity and energy-efficiency within a frame delay constraint.
BNC is designed to multiplex data from multiple sensors and send it to remote server.
B-DWT with the help of Bi-orthogonal 4.4 Wavelet filter provides 64% faster execution, minimizes energy consumption by 67% while utilizing 2% less memory as compared to traditional DWT. It also saves 65.25% of storage space of remote database.
Prototype modeling of real-time CR terminal (SU) in CRN testbed:
At first, we characterize energy detection based sensing under actual test-bed conditions. Secondly, we develop and implement our proposed Practical Energy-Efficient Energy Detection (PED) method over the ECR-MAC framework that is incorporated within the embedded processor of the real-time SU to enable opportunistic IP based communication over PU channels.
Sensing time = 3 ms is obtained for a SU receiver sensitivity of -20dB at 90% detection probability.
Exhaustive analysis of normalized-interference duration and transmission probability under varied operating conditions.
PED method exploits the already available Carrier Sense (CS) module of FPGA PHY core, thereby minimizing resource utilization.
PED method reduces energy consumed during spectrum sensing by 99%.
Analytical modeling and CR enabled optimization of IEEE 802.15.6 scheduled access MAC:
We developed closed form analytical expressions for major performance metrics and study them against varied system parameters. A CR aided LUT based implemented solution is proposed to make allocation interval (AI) and payload size (PS) selection adaptive to channel SNR to maximize system performance.
Closed form expressions provide system designers a tool to suitably tune network parameters for optimal performance.
Performance analysis revealed tradeoffs with respect to selection of AIs and PSs.
The proposed LUT based approach exploits CR capabilities of sensor nodes to optimally select AIs and PSs to optimize EE.
Contributions
Outcomes

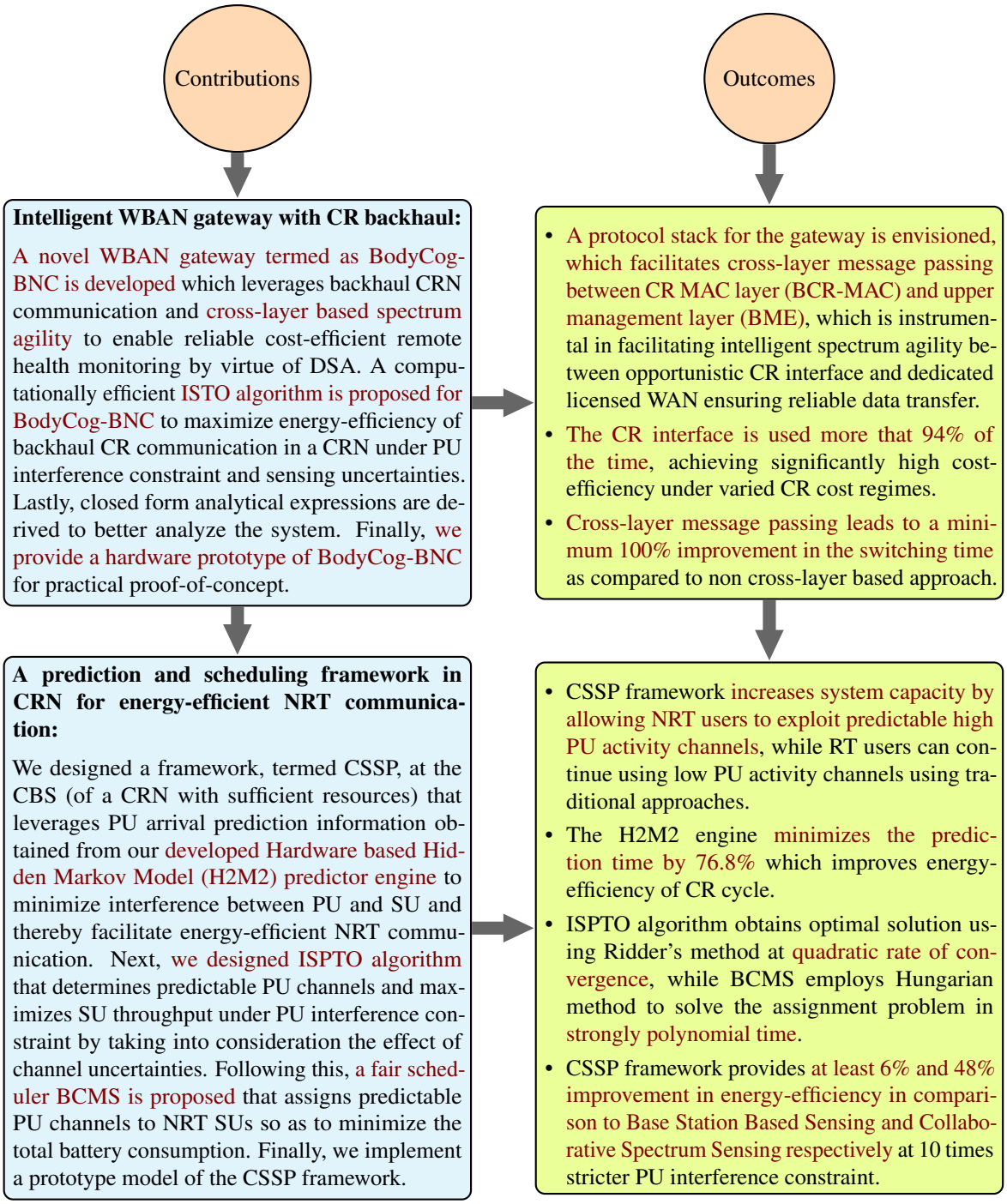
Contributions
Outcomes
Intelligent WBAN gateway with CR backhaul:
A novel WBAN gateway termed as BodyCog-BNC is developed which leverages backhaul CRN communication and cross-layer based spectrum agility to enable reliable cost-efficient remote health monitoring by virtue of DSA. A computationally efficient ISTO algorithm is proposed for BodyCog-BNC to maximize energy-efficiency of backhaul CR communication in a CRN under PU interference constraint and sensing uncertainties. Lastly, closed form analytical expressions are derived to better analyze the system. Finally, we provide a hardware prototype of BodyCog-BNC for practical proof-of-concept.
• A protocol stack for the gateway is envisioned, which facilitates cross-layer message passing between CR MAC layer (BCR-MAC) and upper management layer (BME), which is instrumental in facilitating intelligent spectrum agility between opportunistic CR interface and dedicated licensed WAN ensuring reliable data transfer.
• The CR interface is used more that 94% of the time, achieving significantly high cost-efficiency under varied CR cost regimes.
• Cross-layer message passing leads to a minimum 100% improvement in the switching time as compared to non cross-layer based approach.
A prediction and scheduling framework in CRN for energy-efficient NRT communication:
We designed a framework, termed CSSP, at the CBS (of a CRN with sufficient resources) that leverages PU arrival prediction information obtained from our developed Hardware based Hidden Markov Model (H2M2) predictor engine to minimize interference between PU and SU and thereby facilitate energy-efficient NRT communication. Next, we designed ISPTO algorithm that determines predictable PU channels and maximizes SU throughput under PU interference constraint by taking into consideration the effect of channel uncertainties. Following this, a fair scheduler BCMS is proposed that assigns predictable PU channels to NRT SUs so as to minimize the total battery consumption. Finally, we implement a prototype model of the CSSP framework.
• CSSP framework increases system capacity by allowing NRT users to exploit predictable high PU activity channels, while RT users can continue using low PU activity channels using traditional approaches.
• The H2M2 engine minimizes the prediction time by 76.8% which improves energy-efficiency of CR cycle.
• ISPTO algorithm obtains optimal solution using Ridder's method at quadratic rate of convergence, while BCMS employs Hungarian method to solve the assignment problem in strongly polynomial time.
• CSSP framework provides at least 6% and 48% improvement in energy-efficiency in comparison to Base Station Based Sensing and Collaborative Spectrum Sensing respectively at 10 times stricter PU interference constraint.

Chapter 2

Background Study: WBAN and CR Technologies

❝ *Study the past, it would define the future.* ❞

-Confucius, Philosopher

Comprehensive literature survey in the previous chapter has already laid the foundation for the proposed research work in the thesis. It is quite clear from the interest in this domain that WBAN is envisioned as a key solution towards providing a proactive, affordable and ubiquitous healthcare for the citizens. At the same time, it is evident that CR is an essential technique for achieving highly energy-efficient WBAN communication under non-ideal channel conditions and also creating low cost energy-efficient backhaul communication opportunities for remote health monitoring through DSA in the next generation networks such as 5G networks [8]. Thus, the focus of work in this thesis is to deploy healthcare monitoring applications by jointly using energy-efficient WBAN and CR platforms.

Accordingly, this chapter provides a technical overview of both these disciplines with special emphasis on their practical relevance and highlighting the challenges and complexities involved in such systems. In accordance with the challenges faced by WBAN (both access and backhaul communication), we illustrate how our proposed methods can address them through the application of CR technology. However, in doing so, we will encounter certain CR specific design and implementation challenges which are duly addressed in the ensuing chapters.

2.1 Introduction

Ubiquitous healthcare is an emerging technology that promises increase in efficiency, accuracy and availability of medical treatment. This is due to the rapid advancements of wireless communication and semiconductor technologies which led to the development of small and intelligent sensors that can be used on, around, or implanted in the human body. In this context, WBANs which are special purpose sensor networks constitute an active field of research and development as it offers the potential of great improvement in the delivery and monitoring of healthcare [35]. However, WBAN also introduces a number of challenges such as scarcity of hardware and radio communication resources, the special properties of the radio environment under which they operate and different QoS needs for different sensor nodes operating simultaneously in WBAN. These challenges need to be tackled without sacrificing the need for high energy-efficiency of the sensor nodes and QoS (like delay) requirements for healthcare applications. ***Therefore, the design, analysis and implementation of WBAN require thorough examination of the critical factors affecting performance such as the channel models and the MAC protocols employed to coordinate different sensor nodes***. Furthermore, by exploiting the Cognitive Radio (CR) ability of the sensor nodes we can make WBAN adapt to the channel conditions so as to maximize their energy-efficiency while satisfying their QoS needs. ***Therefore, the development of an energy-efficient WBAN also requires the study of the general mechanism of a CR system***.

Moreover, integration of WBAN with ICT technologies can enable administration of healthcare delivery in a non-invasive manner. It will offer cost savings, and improve the quality of life of the patients. Based on the application, the gateway of WBAN termed as Body Network Controller (BNC) can use long distance wireless backhaul communication technologies to connect to external database server or healthcare center. For this, one of the primary requirement is proper access to radio spectrum. However, two big waves in the wireless world are driving the need for more spectrum. First is the boom in bandwidth savvy applications like video and voice applications, which demand far more capacity than previous mobile applications. Second is the emerging Internet of Things (IoT) applications that could quickly overwhelm networks with the volume of connected devices. Remote health care monitoring is one such IoT application. A CRN [10, 74, 106] is one of the promising candidates that aims at solving this spectrum scarcity problem through DSA. It allows these applications to access the idle frequency slots in different spectrum bands [38], and in doing so, increase the overall spectrum utilization. In addition, as discussed in Chapter 1, backhaul CR communication can enable cost-efficient remote health monitoring which will allow healthcare providers to reach out to all sections of society. Thus, WBAN based remote health monitoring is a suitable candidate to exploit backhaul CRN technology, and is

therefore, another primary focus of research in this thesis. However, DSA over licensed PU channels presents some unique challenges related to reliability in communication. More in detail, the unreliability in spectrum sensing operation can often lead to collisions between PU and BNC transmission. This implies that the BNC must re-send the data leading to more energy consumption. Other sources of unreliability include error in CRN control channel and unavailability of suitable free PU channels. Since healthcare applications require high degree of reliability in transmission, all the aforementioned issues need to be taken into consideration prior to deploying WBAN over CRN backhaul, while also ensuring maximum energy-efficiency for the BNCs. ***Therefore, the use of CR enabled DSA for low cost energy-efficient WBAN backhaul communication require thorough study of the primary components of a CRN***.

2.1.1 Contributions of this Chapter

As both WBAN and CR technologies have established their strong presence in the respective domains, this chapter provides a background study of these two technologies. The significant contributions are summarized as follows.

❶ In this chapter, first we provide a technical overview of the WBAN technology and the MAC and PHY layer specifications laid out by IEEE 802.15.6 standard for its implementation. We also illustrate the three-tier e-healthcare architecture to utilize WBAN for remote health monitoring. Thereafter, the key applications areas of WBAN are discussed along with the challenges in its design and implementation.

❷ This is followed by the discussion on the CR technology, its evolution from adaptive systems to its application for DSA. Following this, we provide a brief overview of the adaptive aspects of CR systems, the CR cycle and the Cognitive Radio Network architecture for DSA. Thereafter, the applications of the CR technology and the services that stand to benefit from it are highlighted. Finally, the potential design challenges are suitably discussed.

❸ Lastly, in view of the applications and challenges of both WBAN and CR, we discuss our proposed methods of integration of these two technologies in the context of adaptive energy-efficient WBAN communication and cost-efficient/ energy-efficient data transfer from WBAN over backhaul to remote server.

2.1.2 Chapter Organization

This chapter is organized as follows. Section 2.2 provides an overview of WBAN, its applications and technological aspects. Next, in Section 2.3, we present a detailed discussion on the CR technology from the viewpoint of adaptive systems and dynamic spectrum access. Thereafter, Section 2.4 elaborates the potential prospects and applications of CR technology in WBAN.

2.2 WBANs: Applications and Technologies

WBAN is commonly regarded as a key enabling technology for personal healthcare [17]. The sensors of the WBAN continuously monitor the physiological signals of a patient and send them to the BNC. The primary implementation strategies of the WBAN include (i) as a standalone network, which allows citizens to have more responsibility in managing their own health, and (ii) as part of e-healthcare architecture, which enables remote health monitoring. Accordingly, in this section, first we provide a brief overview of the WBAN technology along with its benefits and applications. Then, we introduce the IEEE 802.15.6 standard for WBAN and the primary challenges in its implementation.

2.2.1 Overview of WBAN Technology

The basic topology of standalone WBAN was depicted earlier in Figure 1.1 and now by the red dotted-circle in Figure 2.1. Under both scenarios, the WBAN represents a standard one-hop star topology. The node in the center of the star is placed on a location like the waist [99, 107] or wrist. This node at the center of the network is termed as the Body Network Controller (BNC) as it coordinates the activities of the sensor nodes. The BNC can also be visualized as a smartphone with the special ability to communicate with sensors. The sensors sense their data and transmit it to the BNC with minimal or no collision. The BNC after collection of these data can display them graphically to give real-time feedback to the user.

Apart from helping users track their own vitals, WBAN when incorporated within an e-healthcare architecture can help realize a truly pervasive health monitoring system. The basic three tier e-healthcare architecture is shown in Figure 2.1. The three different tiers are as follows:

- Tier-1 (Access Layer): Intra-WBAN communication
- Tier-2 (Convergence Layer/ Backhaul): Inter-WBAN communication
- Tier-3 (Service Layer): Beyond-WBAN communication

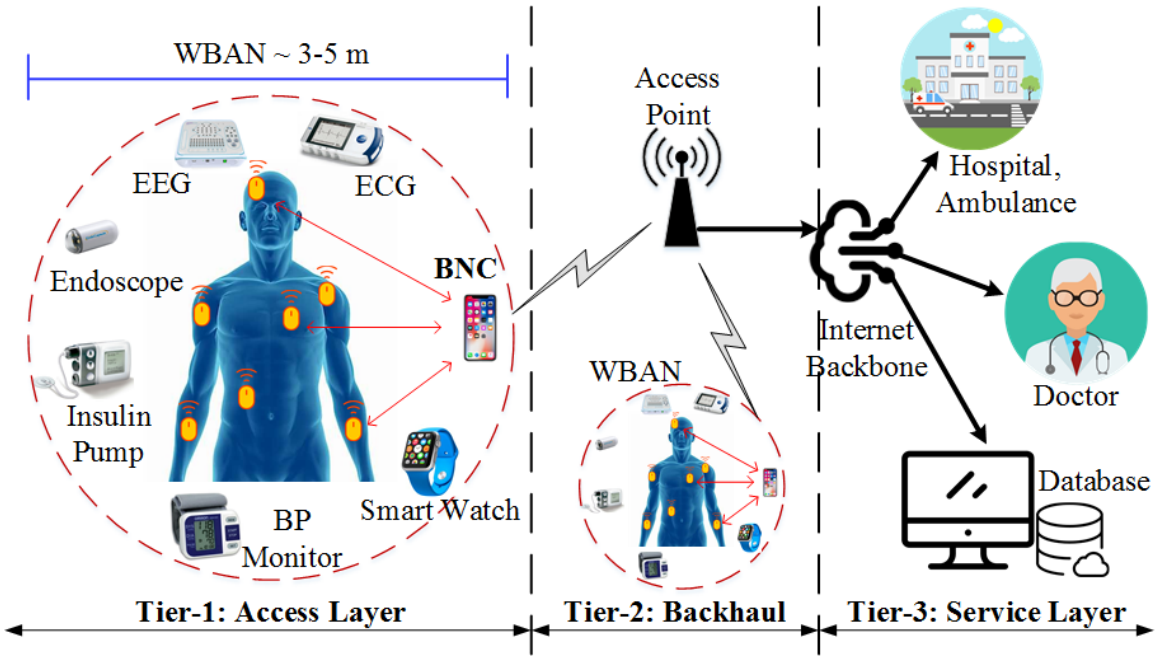

Fig. 2.1 3-tier e-healthcare architecture where the red dotted-circle represents a WBAN.

Tier-1: Access Layer- This basically denotes the network interaction of WBAN nodes and their respective transmission ranges ($\sim$ 3 meters) in and around the human body. The WBAN depicted earlier in Figure 1.1 is the Access Layer denoted as Tier-1 of Figure 1.3.

Tier-2: Convergence Layer/Backhaul- This tier represents the communication between BNC and one or more access points (APs) or Base Stations (BSs) as the case maybe. The APs can be considered as part of the infrastructure, or even be placed strategically in a dynamic environment to handle emergency situations. Tier-2 communication aims to interconnect WBANs with various networks such as WLANs, or long distance communication technologies like GPRS, 3G, LTE, upcoming 5G networks, which can easily be accessed in daily life as well as cellular networks and the Internet [35]. The more technologies supported by a WBAN, the easier for them to be integrated with applications. In this regard, the medium distance technologies like WLAN can enable real time tracking of patient data in home or hospital environment [108], whereas long distance communication technologies by using IP communication can facilitate truly ubiquitous Non-Real Time (NRT) transfer of recorded WBAN data over to Tier-3 as explained next.

Tier-3: Service Layer- The design of this communication tier is for use in metropolitan areas. An Internet gateway can be used to bridge the connection between Tier-2 and this tier [6]. However, the design of Tier-3 for communication is application-specific. For example, in a medical environment a database is one of the most important components of the service layer as it includes the medical history and profile of the user. Based on this, doctors or

patients can be notified of an emergency status through either the Internet or a Short Message Service (SMS). Additionally, Tier-3 allows storing all necessary information of a patient which can be used for their treatment [35].

2.2.2 WBAN Applications

WBAN has a wide array of applications including military, ubiquitous health care, sport, entertainment and many other areas. These applications can be classified as either *medical* or *non-medical* as can be seen as Table 2.1. The main characteristic in all WBAN applications is improving the user's quality of life [6].

Table 2.1 Applications of WBAN

Medical	Real-Time	Assessing soldier fatigue and battle readiness
		Aiding professional and amateur sport training
		Sleep staging
		Biofeedback
	Non-Real Time	Remote monitoring as an alternative to in-clinic follow-up
		Aid patients with hypertension
		Keep track of chemo patients
		Study epileptic seizures
		Ambient assisted living
Non-Medical		Real-time streaming
		Entertainment applications
		Secure authentication

2.2.2.1 Medical Applications

WBANs have a huge potential to revolutionize the future of health care monitoring by diagnosing many life threatening diseases and providing real-time patient monitoring [108]. Accordingly, the medical applications can be further classified based on the architecture of WBAN: i) Real-Time (RT) monitoring applications, ii) Non-Real Time (NRT) applications.

Real-Time Medical Applications

Most of the real-time applications employ a standalone WBAN providing real-time feedback to the user. Some of these applications are mentioned below:

1) *Assessing Soldier Fatigue and Battle Readiness*- By using WBANs, the activity of soldiers in the battlefield can be readily monitored even under harsh conditions, which can

be instrumental in reducing the probability of injury while providing improved monitoring and care in case of injury.

2) *Aiding Professional and Amateur Sport Training*- WBANs can be used to provide monitoring parameters and real time feedback to the users allowing performance improvement and preventing injuries related to incorrect training [109].

3) *Sleep Staging*- On an average about 27% of the world population suffers from sleep disorders. Such disorders can lead to cardiovascular diseases, sleepiness at work place and drowsy driving. Sleep disorders can be realized through a polysomnography test which requires analysis of a number of biopotentials recorded overnight in a sleep laboratory. However, this test involves a lot of wires that disturb the patient's motion and initiates artifacts and noise that reduce the signal quality. WBANs are capable of eliminating cable clutter, thereby effectively improving the quality of the signal recorded [110].

4) *Biofeedback*- Biofeedback refers to the measurement of physiological activity plus other potential useful parameters and feed them back to the user allowing him to learn how to control and modify his physiological activity with the aim of improving his health and performance [111, 112]. To this end, the WBAN sensors implanted or placed in the human body can monitor physiological parameters, and help patients to maintain their health through biofeedback phenomena such as temperature analysis, blood pressure detection, Electrocardiography (ECG), Electromyography (EMG), among others.

Non-Real Time Medical Applications

The NRT medical applications primarily rely on long distance backhaul communication to provide pervasive healthcare to citizens. Some of these applications are mentioned below:

1) *Remote Monitoring as an Alternative to In-Clinic Follow-up*-Telemedicine enables remote delivery of patient care using integrated health information systems and telecommunication technologies and allows scientists, physicians and other medical professionals around the world to serve more patients. In fact, thanks to body sensors for providing sensed signals, that can be gathered and effectively stored in remote database or processed to obtain reliable and accurate physiological estimations and allow distant doctor to have near-real time opinions for medical diagnosis and prescription. Such smart health care system can provide applications for diagnostic procedure, maintenance of chronic condition and supervised recovery from a surgical procedure. Thus, this comes as a safe, cost-effective and comfortable alternative to face-to-face follow-up visits. For example: Short interval ECGs can be periodically sent to physicians/ remote database over backhaul even while traveling, and different alerts can be configured online. An example of a similar system is CardioMessenger [113] developed by

Biotronik in Germany that uses cellular network as backhaul technology. Significant events can be reported by fax, e-mail or text message in order to ensure optimal follow-up.

2) *Aid Patients with Hypertension*- A 24x7 healthcare monitoring of patients with chronic condition like hypertension is not practical for healthcare providers. However, regular monitoring can be greatly beneficial for increasing patient outcomes.

3) *Keep Track of Chemo Patients*- The hospital can give out smart watches with inbuilt sensors to patients to help them stick to their medication regiment and additionally provide the ability to easily and regularly track and report their symptoms and temperature.

4) *Study Epileptic Seizures*-Some patients with epileptic seizures experience negative side effects when they are on their medication or are otherwise still at risk. Using sensors, the BNC can collect information about patients' seizures to help understand and diagnose these neurological conditions. This can be accomplished by collecting data before, during and after a seizure and sending it to remote healthcare facility or records for analysis.

5) *Ambient Assisted Living*- The ubiquitous Internet connectivity of WBANs allows for networking of the devices and services in home care known as Ambient Assisted Living (AAL), where each WBAN wirelessly communicates with a back-end medical network [114]. AAL aims to prolong the self-conducted care of patients that are assisted in their home, minimizing the dependency on intensive personal care, increasing quality of life and decreasing society costs. In fact, ambient assisted living will foster a new generation of IT systems with characteristics such as anticipatory behaviour, context awareness, user friendliness and flexibility [115].

2.2.2.2 Non-Medical Applications

Though the primary aim of WBANs is to serve the medical applications, for completeness of the topic we also list some of the non-medical applications where it can be useful.

1) *Real Time Streaming*- This class of applications involve video streaming such as video clip capturing by the camera in a cellular phone, and 3D video. Audio streaming is also possible through voice communication for headsets for instance listening to music, listening to the bus schedule information on the bus stop, or explanation of art at the museum, or multicasting for conference calls. This category also includes vital sign and body information-based entertainment service, stream transfer which is used for remote control of entertainment devices, body gesture recognition/motion capture, identification, emotion detection and to monitor forgotten things by sending an alert to the owner.

2) *Entertainment Applications*- This category consists of social networking and gaming applications. Appliances such as MP3-players, microphones, head-mounted displays, cameras, and advanced computer appliances can be used as devices integrated in WBANs. They can be used in virtual reality and gaming purposes (game control with hand gesture, mobile body motion game and virtual world game), exchanging digital profile/business card, personal item tracking and consumer electronics.

3) *Secure Authentication*- This application refers to utilizing both physiological and behavioral biometrics such as iris recognition, fingerprints and facial patterns. This is one of the key applications of WBANs due to duplicability and forgery, which has motivated the use of new behavioral/physical characteristics of the human body, in essence multi-modal biometric, gait and electroencephalography [35].

2.2.3 IEEE 802.15.6 Standard for WBAN

In its initial stages, WBAN communications primarily followed the Bluetooth [21], Bluetooth Low Energy (BLE) [116], Zigee/ IEEE 802.15.4 [22] standardization. However, these standards are not suited for WBAN-communications. The Bluetooth and Zigbee standards were designed to support WPANs operating on low data rates. The purpose of it was to provide an efficient low-power and low-complexity, short-range radio frequency based wireless communication standard with a support for node-mobility [58]. However, these protocols failed to meet the increased Quality of Service (QoS), reliability and data rate needs for WBAN. Coming to BLE, it was adopted towards the backend of 2010 for low data rate (small packets) and infrequent communication from nodes to a hub in a mobile phone or web service where the critical low power requirement is needed. It was not designed for applications requiring high reliability and has inefficient support for multiple nodes. In addition, all the aforementioned standards do not satisfy the medical communication requirements because of close proximity to the human body tissue. Thus, a standard model was required for the successful implementation of WBANs addressing both its consumer electronics and medical applications.

In view of the aforementioned shortcomings, IEEE 802.15.6 Task Group in 2012 provided a new set of PHY layer and MAC layer specifications [23], particularly for wireless communications involving WBANs. It describes its aim as follows: “To develop a communication standard for low power devices and operation on, in or around the human body (but not limited to humans) to serve a variety of applications including medical, consumer electronics, personal entertainment and other.”

2.2.3.1 Requirements of WBANs in IEEE 802.15.6

The main requirements of IEEE 802.15.6 standard are listed below [61, 109, 117–119]:

- WBAN links should support bit rates ranging from 10 Kbps to 10 Mbps (see Figure 1.2).
- Packet Error Rate (PER) should be less than 10% for a 256 octet payload for a majority (95%) of the best performing links based on PER.
- Nodes should be capable of being removed and added to the network in less than 3 seconds.
- Each WBAN has to be capable of supporting 256 nodes.
- Reliable communication should be ensured by the nodes in all conditions even when the person is on the move. Unstable channel may lead to reduced channel capacity but it should not cause data loss. Such non-ideal channel conditions can arise due to postural body movements of a person which may result in shadowing effect and channel fading. Moreover, WBAN nodes may move individually with respect to each other, or the WBAN itself may move location resulting in interference.
- Jitter, latency and reliability should be supported for WBAN applications that require them. Latency should be less than 125 ms in medical applications and less than 250 ms in non-medical applications whilst jitter should be less than 50 ms.
- Co-existence of on-body and in-body WBANs within range should be supported.
- Up to 10 randomly distributed, co-located WBANs should be supported by the physical layer in a $6m^3$ cube.
- The transmission power of WBAN nodes should range between 0.1mW (-10dBm) to 1mW (0dBm). This complies with the FCC's Specific Absorption Rate (SAR) of the of 1.6 W/Kg in 1g of body tissue [1].
- WBANs should be able to operate in heterogenous environment by cooperating with other co-located networks to receive information.
- A WBAN can employ different technologies such as UWB in addition to narrow-band transmission to cover different environments and support high data rates.
- WBANs must incorporate QoS management features to be self-healing and secure as well as allowing priority services.
- WBANs should be able to incorporate power saving mechanisms to operate under power constrained environment.

2.2.3.2 IEEE 802.15.6 MAC Layer Specifications

Within a WBAN, the BNC, also termed as the hub, coordinates the channel access for the sensors. For this, IEEE 802.15.6 working group defines a MAC layer on top of the PHY

[1] http://www.fcc.gov/oet/rfsafety/sar.html

layer. Broadly, there are three mechanisms by which the hub coordinates the channel access for the sensors. They are as follows:

1. Beacon mode with beacon period superframe boundaries
2. Non-beacon mode with superframe boundaries
3. Non-beacon mode without superframe boundaries

Out of these, the most commonly used and accepted access mode by researchers and developers is the beacon mode with superframe boundaries [64–66]. It specifies a time reference for the nodes and hub in WBAN which divides the time axis into beacon periods (superframes) bounded by periodic beacon transmissions as shown in Figure 2.2 [23], where B stands for beacon. Each super-frame is further composed of allocation slots of equal length T_S and numbered from 0, 1,...,j..., X, where $X \leq 255$. The allocation slots are further classified into different access phases that define precisely what kind of channel access can be employed within it. It consists of an Exclusive Access Phase 1 (EAP1), a Random Access Phase 1 (RAP1), a Type I/II phase, an Exclusive Access Phase 2 (EAP 2), a Random Access Phase 2 (RAP 2), a Managed Access Phase (MAP), and a Contention Access Phase (CAP). The hub transmits a B2 frame to mark the beginning of a non-zero CAP.

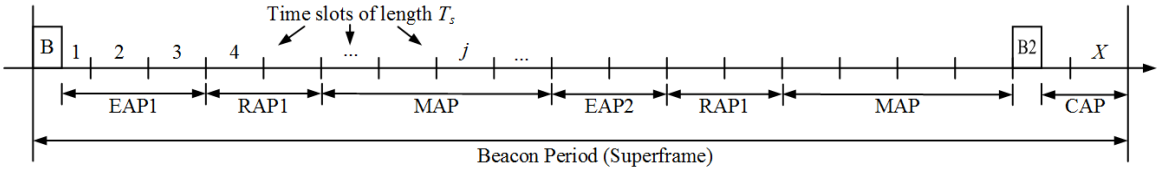

Fig. 2.2 Layout of access phases in a beacon period (superframe) for beacon mode.

The different access mechanisms within the access phases can be classified as-

1) *Scheduled access and variants (connection-oriented contention-free access)*- In this access mechanism, the hub uses MAP to arrange scheduled uplink, scheduled downlink, and scheduled bilink allocation intervals. Scheduled allocations may be 1-periodic or m-periodic allocations, except that a node shall not have both 1-periodic and m-periodic allocations in the same BAN.

2) *Unscheduled and improvised access (connectionless contention-free access)* – This access mechanism utilizes posting or polling for resource allocation.

3) *Random access mechanism*– In this access mechanism, the nodes strive for resource allocation via either the slotted Aloha procedure or CSMA/CA. EAP1 and EAP2 are utilized for high priority traffic such as reporting emergency events; while CAP, RAP1 and RAP2 are only used for regular traffic.

Based on the application requirements, except RAP1, the hub may disable any of these access periods by setting the duration length to zero.

2.2.3.3 IEEE 802.15.6 PHY Layer Specifications

The PHY layer of IEEE 802.15.6 [23] is responsible for the following tasks: activation and deactivation of the radio transceiver, Clear Channel Assessment (CCA) within the current channel and reliable data transmission and reception. The choice of the physical layer depends on the target application: medical/non-medical, in, on and off-body. The PHY layer provides a procedure for transforming a Physical layer Service Data Unit (PSDU) into a Physical layer Protocol Data Unit (PPDU). In this regard, IEEE 802.15.6 specifies three different PHY layers:

1. Narrow Band (NB),
2. Ultra-Wide Band (UWB), and
3. Human Body Communication (HBC).

We elaborate on these PHY layers by their frequency bands, modulation options, and some key features. The frequency bands and bandwidths of the different PHY layers are shown in Figure 2.3 [17] and summarized in Table 2.2 [23].

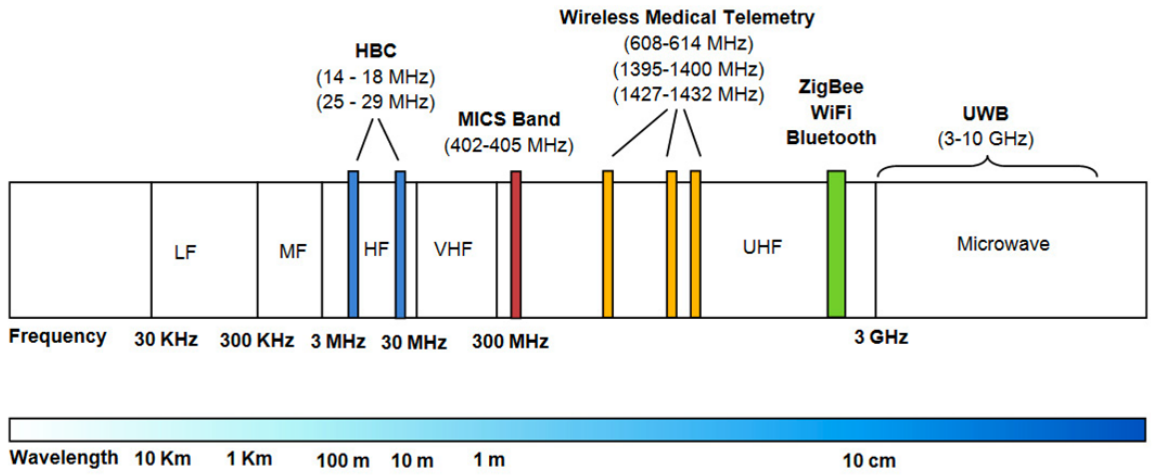

Fig. 2.3 IEEE 802.15.6 frequency bands [17].

Table 2.2 Frquency bands and bandwidths of different PHY layers of IEEE 802.15.6 [23]

PHY Layer	Frequency	Bandwidth
Human Body Communication	16 MHz	4 MHz
	27 MHz	4 MHz
Narrow Band Communication	402-405 MHz	300kHz
	420-450 MHz	300 kHz
	863-870 MHz	400 kHz
	902-928 MHz	500 kHz
	950-958 MHz	400kHz
	2360-2400 MHz	1 MHz
	2400-2438.5 MHz	1 MHz
UWB Communication	3.2-4.7 GHz	499 MHz
	6.2-10.3 GHz	499 MHz

Narrow Band (NB) PHY Layer

The narrowband proposals are used for both medical and non-medical systems. NB PHY is responsible for data transmission/reception, activation or deactivation of the radio transceiver and CCA in the current channel. Based on the NB specifications, in order to construct PPDU, the PSDU has to be pre-appended with a Physical Layer Convergence Protocol (PLCP) Preamble and a PLCP Header as shown in Figure 2.4. The PCLP preamble aids the receiver in carrier-offset recovery, packet detection and timing synchronization. The PCLP header is sent after the PCLP preamble via the data rates given in its operating frequency band. It transfers the necessary information required for successfully decoding a packet to its receiver. The PLCP Header can be further decomposed into PHY Header, Header Check Sequence (HCS) and BCH Parity bits. The PSDU, which is the last component of PPDU contains a MAC header, a MAC frame body and a Frame Check Sequence (FCS) [23].

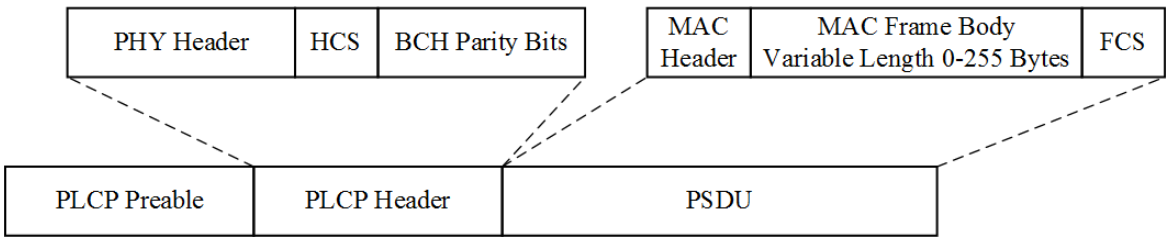

Fig. 2.4 Standard PPDU structure.

For NB PHY, seven frequency bands are proposed including Medical Implant Communication Service (MICS) within 402-405 MHz, Wireless Medical Telemetry Service (WMTS), and Industrial, Scientific, and Medical (ISM) band which comprises of 863-870 MHz, 902-928 MHz, 950-958 MHz, 2400-2483 MHz bands. The un-licensed ISM band in 2400-2483 MHz suffers strong interference [120] from other co-existing wireless devices which use technologies like IEEE 802.15.4 and IEEE 802.15.1. The sixth band (2360-2400 MHz) of NB PHY is assigned for medical device use. Importantly the 2360-2400 MHz band is not an ISM band; hence, interference is significantly reduced compared to the 2400+ ISM band. Considering the 420-450 MHz band, the sub-band 433.05-434.79 MHz is an ISM band which experiences both less interference and superior transmission properties such as less shadowing and attenuation from the body similar to MICS bands. NB PHY uses Differential 8-Phase Shift Keying (D8PSK), Differential Binary Phase Shift Keying (DBPSK) and Differential Quadrature Phase Shift Keying (DQPSK) modulation techniques except at 420- 450 MHz where it uses the Gaussian Minimum Shift Keying (GMSK) modulation technique.

Ultra-Wide Band (UWB) PHY Layer

UWB systems are mostly suitable for the WBAN non-medical system. The UWB PHY is used for communication between on-body devices and for communication between on-body and off-body devices. The UWB system has some advantages such as low radiated power, large bandwidth to mitigate multipath effects, and scalability of the data rates.

The design of UWB PHY is not only in order to improve the robustness of the WBAN, but also provides opportunities for implementation of high performance, low complexity and low power consumption operation. There are two different types of UWB technologies included in the UWB PHY. Namely, Impulse Radio UWB (IR-UWB) and Wideband Frequency Modulation (FM-UWB). In IR-UWB, the transmitter only needs to operate during the pulse transmission, producing a strong duty cycle on the radio and the expensive baseline power consumption is minimized. FM-UWB exploits high modulation index of Frequency Modulation (FM) to obtain an UWB signal. FM-UWB implements processing gain by increasing the transmission bandwidth of a message signal similarly to a spread-spectrum system. This constant-envelope approach, where peak power equals average power, yields a flat spectrum with steep spectral roll-off. Due to the high processing gain, FM-UWB technology combines low complexity with robustness against interference and multipath.

Two frequency bands exist in the UWB PHY: high band and low band; each of which are divided into channels with a bandwidth of 499.2 MHz. The low band only has 3 channels: (1-3). Channel 2 is considered as a mandatory channel with the central frequency of 3993.6

MHz. The high band has eight channels: (4-11). Channel seven is considered as a mandatory channel with the central frequency of 7987.2 MHz. All other channels are considered to be optional. At least one of the mandatory channels has to be supported by a UWB device. Data rates are typically in the range of 0.5 Mbps to 10 Mbps with 0.4882 Mbps for the mandatory channel [120].

Human Body Communication (HBC) PHY Layer

Human Body Communication (HBC) is also called Electric Field Communication (EFC) in some early literature, because EFC is the basis behind the physical realization of HBC that uses human body for medium access. In EFC, data is sent across devices placed on or near the body by a near electric field. Its transmitter is implemented with only digital circuits and needs one electrode, instead of antenna. The realization of the receiver needs no RF modules, which makes equipment easy to carry and power consumption is very low. The HBC PHY has a bandwidth of 4 MHz and operates in two frequency bands centered at 16 MHz and 27 MHz. The United States, Japan and Korea support both of these frequency bands whereas Europe only supports the 27 MHz operating band. The data rates are distributed in 164.1kbps, 328.1kbps, 656.3kbps, or 1312.5kbps.

2.2.4 Challenges in WBAN

The challenges in relation to design and deployment of WBAN are highlighted as follows:

1. **Non-Ideal Channel Model-** One of the primary aspects of efficient WBAN design is to ensure reliable operation considering that one of the target applications is healthcare. Meeting this requirement needs accurate propagation modeling of the channel. The modeling should consider the peculiarities of the WBAN channel i.e. on-body, off-body and in-body. In this regard, Smith et al. in [61] have considered the WBAN channels and the IEEE 802.15.6 standard to provide an insight into the propagation characterizations. It was shown that small-scale fading in narrowband communications is best modeled by either lognormal distribution or gamma distribution. While UWB communication is best modeled by lognormal distribution. Any proposed PHY or MAC layer method should therefore take into consideration the appropriate channel model and also evaluate the non-ideal effects such as degradation in channel SNR leading to bit-error rate, corresponding re-transmission and resulting delays in data communication. Channel SNR can also vary due to mobility of the WBANs. Though WBAN as a unit is relatively static, however the entire WBAN can be mobile due to movement of concerned patients. Therefore, a

WBAN should be adaptive enough to vary its operating parameters so as to maximize its performance under all conditions.

2. **Energy-Efficiency-** One of the main constraints in WBANs is the limited power supply of the sensor nodes. It is even more critical for implant nodes, where frequent battery replacement is not a viable option. A widely accepted metric to estimate the effect of an algorithm or protocol on battery consumption is its energy-efficiency. Mathematically, energy-efficiency is given as the ratio of throughput obtained to the energy consumed. It is inversely related to the total battery consumed to send a certain amount of data. Therefore, higher the energy-efficiency, lesser is the battery consumption. However, improving throughput and reducing energy consumption are two conflicting aspects of communication. Hence, careful modeling and study is required to ensure maximum energy-efficiency of a proposed method while still satisfying the QoS requirements like frame delay of the healthcare applications. In addition to this, intelligent duty-cycling [33] to prolong battery life is also an important consideration for sensor nodes which are involved in periodic monitoring of physiological signals.

   With regards to a BNC, since it is likely to be rechargeable, the energy-efficiency of a BNC is less critical as compared to sensor nodes. However, it still needs to be maximized so as to prolong the intervals between battery recharges, and thereby save the cost of electricity. Therefore, the NRT backhaul transmission by the BNC needs to made energy-efficient by means of techniques like data compression that can reduce the amount of data to be transmitted and adaptation to communication channel conditions for optimal performance.

3. **Resource Constraint-** All the sensors nodes and the BNCs are primarily resource constrained microcontroller based devices with limited storage and processor power. This means less buffer space for storage and limited processing speed. Hence, a computationally intensive algorithm might take up significant amount of communication time leading to buffer overflow and packet loss. Thus, any proposed solution needs to be lightweight and easily implementable which has less memory footprint and small processing time. In this regard, faster memory read and write operations can be leveraged as opposed to complex mathematical evaluations by low power microcontrollers.

4. **Interference-** It is highly likely that a WBAN may encounter other WBANs in its vicinity. Therefore, coexistence and/or interference mitigation between a WBAN and its neighbor WBANs is a crucial consideration. To this end, IEEE 802.15.6 [23] have proposed multiple techniques such a beacon shifting and frequency hopping and active superframe interleaving. Apart from the afore-mentioned techniques, other available methods involv-

ing application of game theory, iterative water-filling based power allocation can also be adapted for interference mitigation.

5. **Security-** Little study has been done in the area of security for WBANs. Additionally, due to stringent resource constraints in terms of power, memory, communication rate and computational capability as well as inherent security vulnerabilities, the security specifications proposed for other networks are not applicable to WBANs. The practical deployment of WBANs and the integration of convenient security mechanisms requires knowledge of the security requirements of WBANs [121].

6. **Cost-Efficiency of Backhaul Transmission-** One of the primary objectives of Remote Health Monitoring (RHM) is to provide affordable pervasive healthcare. Therefore, reducing the operational cost of a WBAN for RHM is of vital importance. Among the several factors affecting the cost of RHM, one of the recurring components is the cost involved in transferring data over backhaul. Though the cable Internet connectivity is widely spread and low cost, but mobile Internet connectivity is yet to go long way for low cost solution, especially in developing country. Apart from data compression which obviously reduces the data transfer cost, a possible solution to address this issue is by employing Dynamic Spectrum Access (DSA) over licensed bands to opportunistically send small amount of NRT healthcare data without interfering with the licensed users.

Thus, it is inferred from this section that several unique challenges and constraints are posed by WBAN. The primary requirements of WBAN is to ensure highly energy-efficient and reliable transfer of healthcare information from sensor to BNC while satisfying the strict QoS needs. While for backhaul transmission, the primary concerns are energy-efficiency and cost-efficiency. Taking cue from this, in the next section we study Cognitive Radio technology which can an enabler of the above-mentioned objectives.

2.3 Cognitive Radio: From Adaptive Wireless Systems to Dynamic Spectrum Access

In the late 1990s, nearly all telecommunications radios comprised of a Digital Signal Processor (DSP) to implement modulation and signal processing functions, and a General Purpose Processor (GPP) to realize operator interface, network signaling, and system overhead functions. This architecture is attractive to a manufacturer as the same basic electronics can be reused for each new radio design, thereby reducing engineering development, enabling volume purchasing, and optimizing production of a common platform, while retaining the

flexibility for sophisticated waveforms and protocols. To tap the power, attractiveness to the consumer market and the ability to add additional functionality that is highly tuned to market specific applications, some manufacturers called their radios *Software Defined Radios (SDRs)*. SDR has been defined as a radio platform whose functionality is at least partially controlled or implemented in software.

In the late 2000s, many radios made the software functionality available for various classes of adaptivity and significantly extend user support functionality. This initiated the generation of *Cognitive Radios (CRs)*. Thus, with minimal additional hardware, additional software features will enable users, network operators, spectrum owners, and regulators to accomplish much more than with the fixed application radios of an earlier generation.

As discussed, CRs are highly agile wireless platforms capable of autonomously choosing operating parameters based on both prevailing radio and network conditions [75, 122]. Consequently, CRs have the potential to revolutionize how devices perform wireless networking. For instance, CRs are capable of transmitting in unoccupied wireless spectrum while minimizing interference with other signals in the spectral vicinity; that is, *Dynamic Spectrum Access* [10, 11, 123]. Therefore, in this section, first we discuss the general relationship between CR and SDR to realize an adaptive wireless communication system. Thereafter, we study how DSA is made possible using CR technology. Following this, we list the varied application areas of CR that lays the foundation for its use towards WBAN and remote health monitoring. Lastly, we discuss the different challenges in realizing an individual CR node or a Cognitive Radio Network (CRN).

2.3.1 SDR and CR Relationship to Realize Adaptive Wireless Systems

It is useful to define what the authors refer to as a cognitive radio. Cognitive radio can be described as a node with an ability to form an awareness of its environment and context, make decisions and inferences from this information combined with knowledge of the user's objectives, act in a manner that attempts to accomplish the user's objectives, and optionally learn from these experiences for possible use in the future [75, 124]. The foundation of a cognitive radio is essentially a wireless communications stack capable of being dynamically reconfigured. *One of the ways of implementing CR is by using a SDR, which is a wireless device where some or all of the physical layer (PHY) and the rest of the communications stack is implemented in software, or can be configured using a software mechanism. Cognitive functionality may have an influence on all or many of the layers in a communications stack and is not just limited to the PHY only*.

Therefore, as highlighted above, SDR is one of the core enabling technology for cognitive radio. SDR can provide a very flexible radio functionality by avoiding the use of application

specific fixed analog circuits and components. One of the most popular definitions of cognitive radio, in fact, supports the above argument clearly: "A cognitive radio is an SDR that is aware of its environment, internal state, and location, and autonomously adjusts its operations to achieve designated objectives."

One of the simplest conceptual model that describes the relation between CR and SDR can be described as shown in Figure 2.5. In this simple model, CR is wrapped around SDR. This model fits well to the aforementioned definition of CR, where the combination of cognitive engine, SDR, and the other supporting functionalities (e.g. sensing) results in cognitive radio. Cognitive engine is responsible for optimizing or controlling the SDR (which comprises all the layers of a communication system) based on some input parameters such as that are sensed or learned from the radio environment, user's context, and network condition. Cognitive engine is aware of the radio's hardware resources and capabilities as well as the other input parameters that are mentioned above. Hence, it tries to satisfy the radio link requirements of a higher layer application or user with the available resources such as spectrum in terms of bandwidth (both in time allocated and frequency allocated) and power. Compared to hardware radio where the radio can perform only single or very limited amount of radio functionality, SDR is built around software based digital signal processing along with software tunable Radio Frequency (RF) components. Hence, SDR represents a very flexible and generic radio platform which is capable of operating with many different operating parameters at different layers of the protocol stack. For example, at the PHY it may be the selection of different bandwidths over a wide range of frequencies and using many different modulation and waveform formats; while at the MAC layer it may be selection of different access periods, packet sizes or relays based on channel conditions; similarly, at the Network layer it may be selection of optimal routing path in a network.

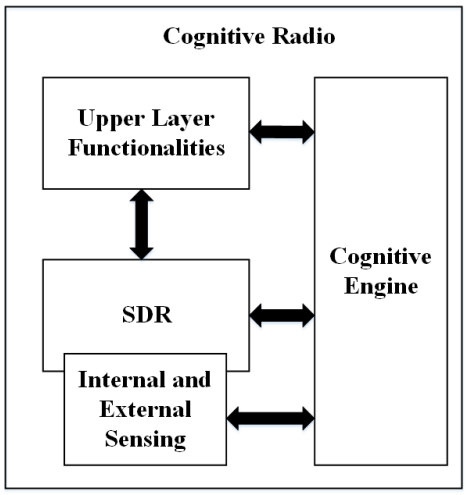

Fig. 2.5 The illustration of relationship between SDR and cognitive radio [34].

From this, it follows that CR functionality requires at least the following capabilities:

- **Flexibility and agility**, the ability to change the waveform and other radio operational parameters on the fly.
- **Sensing**, the ability to observe and measure the state of the environment, including spectral occupancy. Sensing is necessary if the device is to change its operation based on its current knowledge of RF environment.
- **Learning and adaptability**, the ability to analyze sensory input, to recognize patterns, and modify internal operational behavior based on the analysis of a new situation, not only based on pre-coded algorithms but also as a result of a learning mechanism.

Equipped with the above mentioned capabilities we now discuss one of the most significant applications of CR which is Dynamic Spectrum Access.

2.3.2 Dynamic Spectrum Access

With the increasing demand for additional bandwidth to support existing and new services, both spectrum policy makers and communication technologists are seeking solutions for this apparent spectrum scarcity. Additionally, in this era of IoT, there is an upscale surge in the use of device-to-device communications and vehicular communications that in turn aggravates the spectrum congestion problem. Meanwhile, measurement studies have shown that much of the licensed spectrum is relatively unused across time and frequency [38, 125–129]. Nevertheless, current regulatory requirements prohibit unlicensed transmissions in these bands, constraining them instead to several heavily populated, interference-prone frequency bands. To provide the necessary bandwidth required by current and future wireless services and applications, the FCC has commenced work on the concept of unlicensed users "borrowing" spectrum from spectrum licensees [130]. This approach to spectral usage is known as Dynamic Spectrum Access (DSA). With recent developments in CR technology, it is now possible for these systems to simultaneously respect the rights of incumbent license holders while providing additional flexibility and access to spectrum.

An example of how DSA would work can be illustrated in Figure 2.6 [131], where parts of the spectrum between 928 MHz and 948 MHz are occupied over both frequency and time. However, it can be observed that there also exists portions of the spectrum that are unoccupied for a significant period of time, making them suitable candidates for secondary access by unlicensed wireless devices in a DSA framework. Nevertheless, when accessing these unoccupied frequency ranges within licensed spectrum, the secondary wireless device must ensure that it does not interfere with the operations of the Primary User

(PU) transmissions. Interference may occur when the Out-Of-Band (OOB) radiation of the secondary transmission exceeds the tolerable levels, contaminating the PU transmission if located relatively close in the frequency domain. Simultaneously, given the time-varying nature of wireless transmissions, a spectrum that might be unoccupied at one time instant could potentially be occupied at a subsequent time instant. Consequently, the CR platform must be environmentally aware and rapidly reconfigurable to prevent Secondary User (SU) interference of PU transmissions.

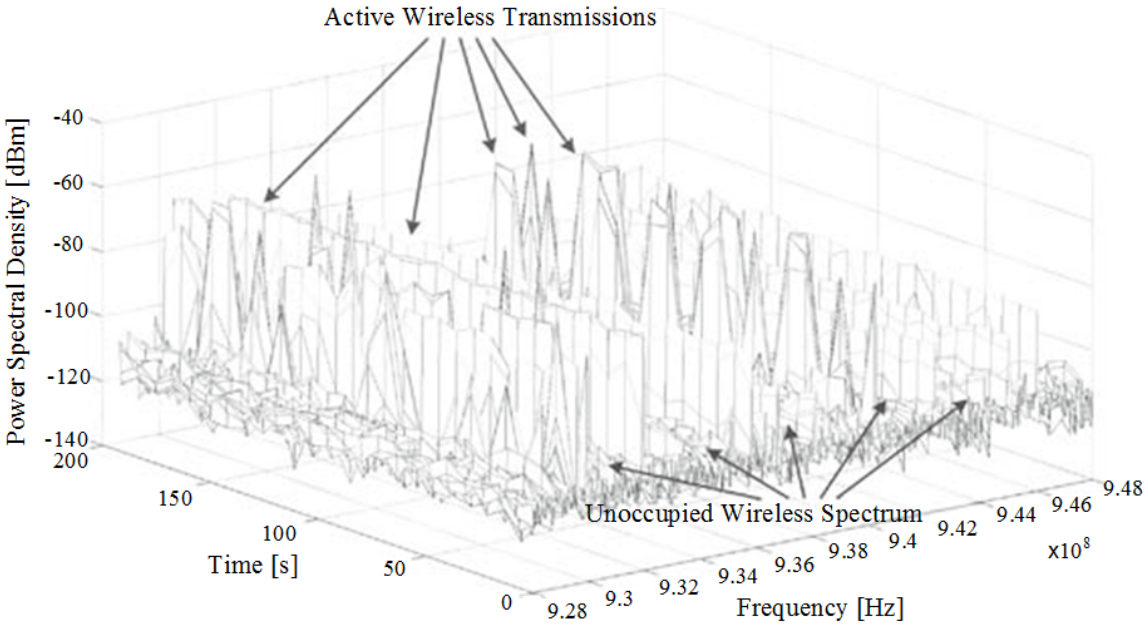

Fig. 2.6 Example of spectrum holes in the frequency band 928–948 MHz [131].

Two types of spectrum access are proposed for the SUs in CRN. The first policy is the Opportunistic Spectrum Access (OSA) [132] or overlay access scheme, where the SUs can access the spectrum on temporal basis provided that the PUs are absent. The second policy is the Concurrent Spectrum Access (CSA) [132] or underlay spectrum access, where the SU transmits with restrained transmission power so as to maintain the interference to PU below a certain threshold level. Both these policies are depicted in Figure 2.7.

The basic cognitive capability of a CR user as discussed in the previous sub-section allows the SUs to follow a basic CR cycle which is discussed next.

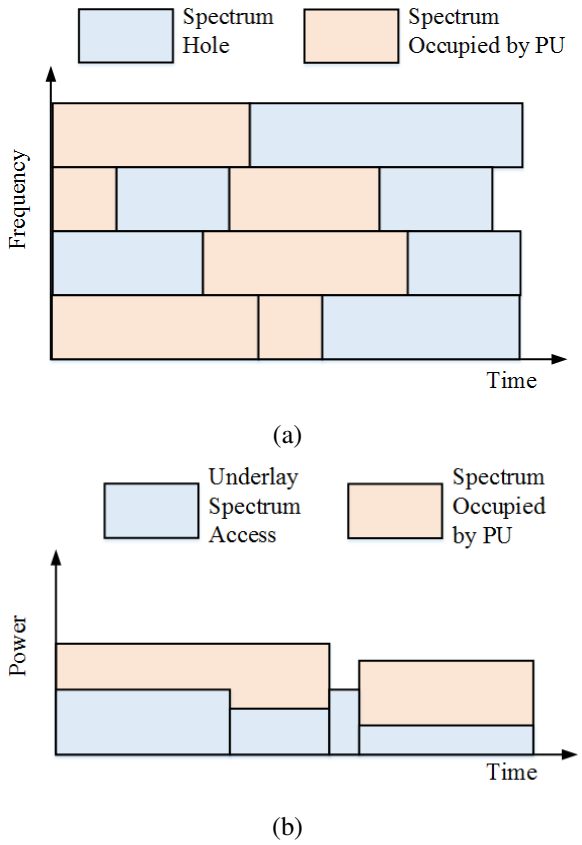

Fig. 2.7 Dynamic spectrum access in CRN with respect to (a) Overlay policy, and (b) Underlay policy.

2.3.2.1 CR Cycle

The basic CR cycle is depicted in Figure 2.8. Every SU follows this CR cycle with minor modifications and performs the following essential operations.

1. *Spectrum Sensing*- This is one of the most critical aspects of CRN, where the CR detects the spectrum holes through periodic sensing mechanisms (energy detection, matched filter, cyclostationary feature detection etc.) and determines the suitability of a particular wireless channel for hosting SU applications. It is imperative that higher the accuracy of sensing, more is the success rate in terms of increasing system capacity and subsequent spectrum utilization. On the other hand, imperfect spectrum sensing can lead to the undesirable conditions of false-alarm (where channel is detected busy even though it is idle) and miss-detection (where channel is detected idle when it is actually occupied by PU). Both of them can severely degrade the SU performance in terms of system under-utilization as well as increased levels of harmful interference with the PUs.

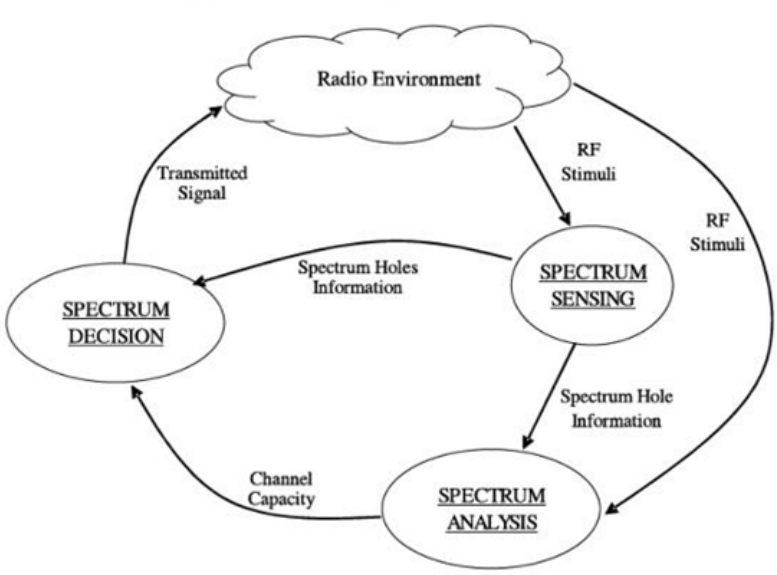

Fig. 2.8 Basic CR cycle [10].

2. *Spectrum Analysis*- This step follows the spectrum sensing part, where the SU uses the sensing outcome to analyze the channel conditions before considering the wireless channel as an "opportunity" for transmission. This is important because considering the unreliability of the wireless environment, the sensed channel must be analyzed and characterized in terms of different factors (including interference levels, path loss, wireless link errors, link layer delay, holding time of PUs, etc.). Based on this analysis, the SU enters the third phase.

3. *Spectrum Decision*- Here the SU takes any of the three decisions namely: i) the decision to transmit in the current channel considering favorable channel conditions for the underlying SU transmissions; ii) the decision to halt transmission when the current channel is analyzed to be unsuitable for sending SU packets. This is followed by the decision to perform spectrum handoff to another available idle channel; and finally, iii) the decision to drop from the channel when the operating channel is inapt for SU transmissions and no other idle channel is available at that time instant.

Collectively, spectrum sensing, spectrum analysis and spectrum decision constitute the CR cycle. Thereafter, when these SUs are deployed in the network along with the PUs, the network becomes a Cognitive Radio Network. The resultant network architecture is discussed as follows.

2.3.2.2 Cognitive Radio Network

The components of the CRN architecture, as shown in Figure 2.9, can be classified in two groups as the primary network and the CR network. The CRN may be further categorized as either infrastructure based network or an ad-hoc network.

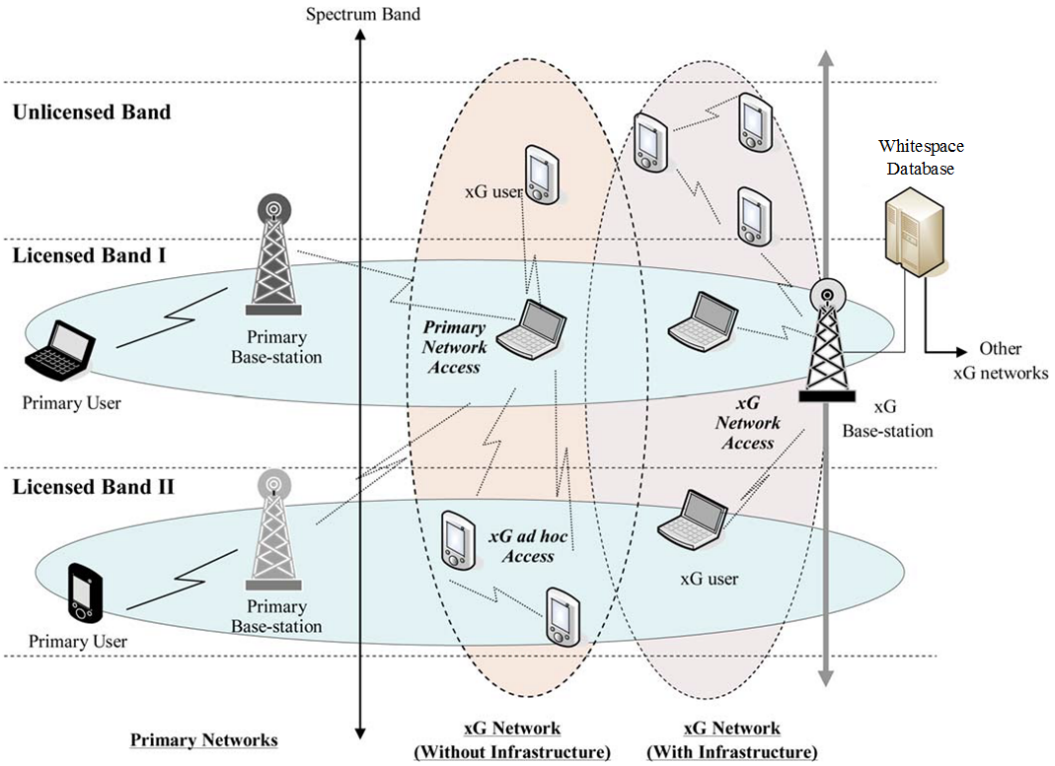

Fig. 2.9 CRN Architecture [10].

In the infrastructure-based network, the CRN comprises of the SUs, the Centralized Base Station (CBS) and White Space Database [10]. These base stations provide single hop connection to the SUs by means of which these SUs can access other networks like the Internet. The white space database helps in providing PU activity information of the PU channels in the CRN. The centralized CRN is most suitable for backhaul/long distance communication and communication requiring Internet access like in ubiquitous remote health monitoring.

In the ad-hoc network, the SUs operate independently, either non-cooperatively [133] or in collaboration with each other [134, 135]. There is no centralized entity to control their actions. As with any ad-hoc network, the efficiency of the ad-hoc CRN depends on the timely decision-making capabilities of the SUs, which, unless properly planned, can severely restrict the overall system capacity of the network.

In this thesis, we are primarily concerned with the use of backhaul CRN for deployment of efficient remote health monitoring as an IoT application over next generation cellular networks like 5G. Therefore, it is imperative that we study the possible scenarios of integration of CRN within 5G cellular networks. For this, Hong et al. in [8] have proposed to use Cognitive cellular networks which are defined as cellular networks that employ CR to lease addition spectrum outside the licensed cellular bands [136]. Among the different architectures proposed in [8], the architecture which is of great interest to our specific objective is illustrated in Figure 2.10. It shows a standalone CRN that overlays the existing licensed cellular network. A Base Station (BS) may have both or one of the radio interfaces. As illustrated in Figure 2.10, one usage scenario is to use the power-limited cognitive Radio Resource (RR)[2] for users near a macrocell BS, while the licensed RR is reserved to serve users further away. Another promising case is to deploy cognitive small cells (or femtocells) that use cognitive RR to cover traffic hotspots or coverage gaps. Compared to licensed-band-based small cells, cognitive small cells can offer potentially higher capacity and better interference protection to the macrocell. Another possible usage scenario highlights service differentiation. For example, services with strict QoS requirements can be scheduled to the (higher cost and more reliable) licensed radio interface, whereas services with relaxed QoS requirements can be delivered over the (lower cost and less reliable) cognitive radio interface. We are interested in exploiting the last concept of service differentiation where CR backhaul can be used for cost-efficient transfer of NRT healthcare information while incorporating innovative ways to ensure high reliability and energy-efficiency.

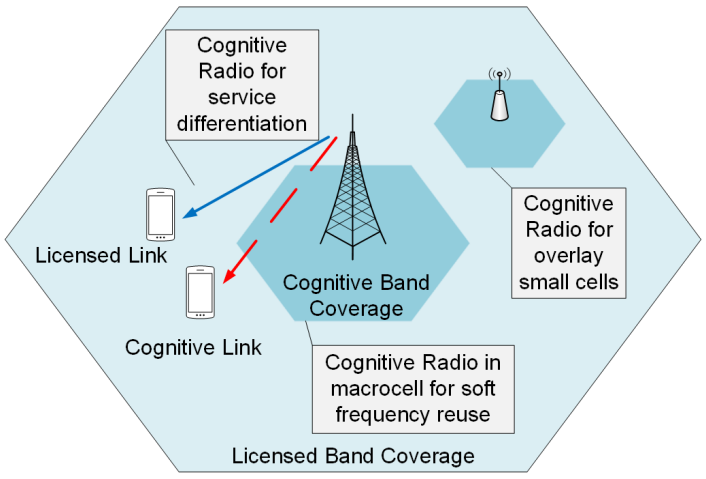

Fig. 2.10 Architecture and usage scenarios of cognitive cellular networks [8].

[2]The radio resource (RR) at a particular band can be characterized by the bandwidth, maximum transmit power, and reliability (or availability)

2.3.3 Cognitive Wireless Communication Applications

Cognitive radio comes with multitudes of features. The majority of these attributes are "Awareness", "Sensing", "Learning", and "Adaptation". For better understanding and organization of each application and their relationship with "cognitive concept" we classify the CR applications as:

i) Wireless resource optimizing applications
ii) Communication quality enhancing applications
iii) Service specific applications

In general, many of these applications across groups can benefit from each other, their territories may overlap, and they can (individually or combined) work together to improve wireless communication. As resource optimization and quality enhancement applications are closely related they are discussed under the same heading as follows.

2.3.3.1 Resource Optimization and Quality Enhancing Applications

Wireless resources are limited. This scarcity in resources demands careful consideration and planning in their usage. The conventional radio resources encompass spectrum, network infrastructure, power and battery. Table 2.3 summarizes the various resources and their respective applications. We briefly illustrate each resource related application separately.

Table 2.3 CR applications in wireless communication

Wireless resources	**Brief description of related CR applications**
Knowledge	Awareness of available knowledge and sensing their changes Utilization of knowledge
Power	Prioritizing tasks according to power level Power control according to channel and mobile position Power control according to audio and visual activity
Energy	Maximizing battery life by optimizing transmission power, transmission time, channel sensing time, duty cycle, packet size, modulation level
Spectrum	Detection, accessing and management of available spectrum
Network	Cross layer optimization Autonomous selection of optimum route and topology Network security against intruders/hackers Self diagnosis and repair of network components

1) *Knowledge*- Knowledge comprises of information on the individual entities within a communication link. Measured and predicted values of channel related information such as link quality, Signal-to-noise Ratio (SNR), and channel fading parameters might also be considered as knowledge. This knowledge can be used to appropriately select suitable parameters. For example- awareness of channel conditions such as fading characteristics, noise and/or interference levels will help select suitable Forward Error Correction (FEC) scheme, interleaving length, modulation order, and type, etc. Similarly, spectrum knowledge beyond traditional concept of fixed spectrum can lead to transmission over variable spectrums and variable dimensions of channel space.

2) *Power*- Optimizing power is vital for maintaining sustained wireless communication link. Major CR applications involving power optimization are adaptive power control according to link quality, optimizing power by shutting off in case of low priority applications to better utilize it in case of emergency such as "911", adaptive routing mechanism based on available power of other nodes.

3) *Energy*- Optimizing the energy consumption of a wireless node/system allows the communicating nodes to prolong their battery life and/or extend the life-cycle between successive recharges and also enable greener communications. For example, maximizing the energy-efficiency of implant sensor nodes within human body, like in pacemaker, will allow patients to use their devices for long periods of time without the need for a replacement, which might require the patient to undergo a inconvenient, cumbersome and costly medical procedure. CR due to its adaptive ability can optimize the transmission parameters like transmission power, transmission time, channel sensing time, duty-cycle, packet size etc. to allow systems/nodes pump out more data over a network for lesser energy consumption, thereby maximizing the energy-efficiency.

4) *Spectrum*- The overcrowded spectrum partitioning impose additional usage of available spectrum in alternate dimensions and instances (such as different times of day). Cognitive intelligence brought forth a breakthrough in this "additional usage" of spectrum such as cellular GSM bands, spectrum holes in unused public safety bands or TV bands, unlicensed bands in ISM and 60GHz bands. Utilizing these bands require the DSA capability that broadly follows the cognition cycle described in Figure 2.8.

5) *Network*- Optimizing network within a specific link can depend on individual and/or multiple participating nodes. Individual node task carried out by CR that affects overall network performance involves cross-layer optimization where functions of multiple protocol stacks are optimized or considered jointly, and network learning which includes utilizing network resources so as to improve network capacity, handle multiple applications, and

prioritize applications at times of network congestion. The collaborative network tasks performed over multiple nodes include i) optimum route identification and re-configuration to network resource utilization and minimization of network delay and cost, ii) autonomous change of network topology to establish and maintain communication between source and destination, iii) detecting or diagnosing faulty parts of a network and providing self-healing without human intervention, thereby minimizing network downtime.

6) *Interference-* Interference in wireless systems limits the expansion of communication domain in terms of user, network, spectrum, time, space and geographical coverage capacity. CR helps mitigate interference such as self-interference due to inter-symbol interference and/or inter-carrier interference by dynamically sensing frequency and time selectivity of channel and adjusting its own transmitter/receiver parameters or other user interference. In spectrum sharing environment, CR can intelligently determine the presence of PU using several parameters such as SNR values, channel fading parameters, spectrum usage statistics, and geographical location and avoid any possible interference on primary from secondary or vice versa.

7) *Link Adaptation-* A communication link can be affected by a number of factors such as radio environment, mobility, data rate, available spectrum, network, and individual application requirements. CR employs various techniques to handle these factors and maintain desired link quality. The techniques involve adaptive source coding based on the type of data such as voice, text, video etc., adaptive channel coding, adaptive modulation to balance power efficiency and spectrum efficiency, adaptive carrier frequency selection by sensing available spectrum and accordingly adapting its carrier frequency. Also there are some technology specific adaptations available such as selection of cyclic prefix size, Fast Fourier Transform (FFT) size, and number of carriers in Orthogonal Frequency Division Multiplexing (OFDM), and adaptive selection of duty cycle and number of pulses per bit in impulse radio based UWB technology [137].

2.3.3.2 Service Specific Applications

Service specific / end user products utilize the benefits of cognitive influence in wireless communication applications. It may be impossible to capture all present and future products within this section therefore, some of the major ones are described here.

1) *Office and Home Environment-* In an office environment, the CR can prioritize a radio network connection according to pre-set priority status. For example, a conference among the CEOs can receive the highest priority in network connection and available spectrum occupancy. Then the next level of priority is set forth and so on. The priorities can be set at

times of network initialization and can be updated on a regular basis within a central control. Each wireless work station can communicate with the central control and download the priority table. Similarly, in a home environment, data transfer application like gaming and video streaming over CR enabled WiFi may have higher priority as compared to Machine-to-Machine (M2M) communications like periodic temperature update.

2) *Low Cost Broadband Connectivity*- A significant advantage of opportunistic spectrum usage due to DSA is the ability to offer cost-effective broadband access in general and more particularly in remote and rural areas. This is particularly important from the perspective of developing nations such as India [138]. Here, unlike cable internet, the cost of mobile internet is still considerably higher. This acts as a fundamental deterrent towards adaptation of humanitarian technologies such as remote health monitoring at every strata of the society. To this end, IEEE 802.22 standard for Wireless Regional Area Networks (WRANs) [39] is the first CR standard that proposes to use several un-utilized Very High Frequency (VHF) and Ultra-High Frequency (UHF) TV broadcasting bands to provide cost-effective wireless broadband access to rural areas. This unused spectrum is also known as the Television Band White Space (TVWS). Thus CR through DSA can be leveraged to provide low cost broadband connectivity to people which in effect will drive other IoT services like remote monitoring/e-Healthcare.

3) *QoS and QoS Management*- CR can be used to prioritize certain applications to satisfy specific QoS needs. This may include prioritizing connection such as dropping streaming audio if there is an incoming call; selection of appropriate channel bandwidth that matches endpoint codecs and allowing adaptive compression to balance application and voice bandwidth usage. CR can also intelligently degrade the supplied services in accordance with link quality changes and battery power reduction.

4) *Emergency and Disaster Relief*- In a disaster situation, the private wireless networks such as a cellular networks can be inoperable and the public safety spectrum can be overcrowded due to numerous emergency connections. Under such situation, cognitive radio can utilize available licensed/unlicensed spectrum holes and heterogeneous network components to create and maintain temporary emergency connection. As an example, CR can establish a communication link over GSM band using WLAN access points.

5) *Underwater Acoustic Communications*- Typically, the Underwater Acoustic Communication (UWC) based systems are prone to high levels of path-loss and noise. Therefore, sharing this spectrum among different underwater systems (underwater vehicles, fleet, acoustic sensor networks for underwater exploration, etc.) is a challenging task, given the fact that this spectrum exhibits spatio-temporal variations in its characteristics. For example, the path-loss

of the medium changes with depth and seasons, the noise is amplified by waves and human activities, and the nearby active sonars can diversely affect the environment. Thus, CR can be used to mitigate these interferences by selecting suitable channels with less interference and adaptation of transmission power to minimize interference with other existing underwater devices and sonars.

6) *Smart Grid-* Increasing population coupled with higher demands for power have put severe constraints on the existing power grids, as a result of which system reliability, power quality and consumer satisfaction have witnessed a gradual decline over the years. In addition, the harsh environmental conditions surrounding these power grids including dynamic topology changes, interference and fading concerns, and connectivity issues have created challenging problems in relation to establishing wireless communication in these grids. Consequently, this has led to the development of CR enabled next-generation power grids, commonly referred to as "Smart-Grids" (SG). These SGs are modernized versions of the traditional power grids and comprise of the advanced ICT infrastructure. CR technology further aims to increase the system capacity by addressing the challenges of wireless link failures and extreme environmental conditions in these power grids, through DSA based spectral management policies [139]. In this regard, CRN can be put to good use for several SG services such as, i) advanced metering architecture, ii) distributed electric generation, iii) power outage detection, and iv) wide area monitoring.

7) *Health Monitoring-* The application of cognitive radio can also bring improvements in areas of proactive and affordable health-monitoring both at personal level through RT WBAN communication and at the remote level via efficient NRT backhaul communication. This is the topic of this thesis and we will elaborate on this in the next section.

2.3.4 Challenges in CR

In view of the complexities inherent in general CR systems and DSA via CRNs, the key challenges in relation to their successful design and deployment are highlighted in this section as follows.

1. **Sensing Issues-** The primary challenge lying in the design of the CR module for DSA is the ability to detect the PU presence with minimum complexity in a very short time [140] and ensure successful transmission by SU (if that channel is idle). Another challenge in spectrum sensing is keeping the interference to PUs within a pre-determined threshold. Interferences to PUs can arise due to uncertainties in sensing such as false-alarm and miss-detection. Possible solutions to minimizing these interferences to PUs involve collaborative sensing among SUs, optimization of sensing and inter-sensing durations or

use of prediction techniques as proposed later in this thesis. In addition, depending on the application level requirements there might be further need to achieve different objectives like maximization of throughput, energy-efficiency while satisfying different constraints such as delay limit, maximum energy consumption or minimum throughput etc.

2. **Spectrum Management Issues-** Different spectrum management issues are faced by individual CR nodes and centralized CBS of a CRN. The spectrum analysis by a CR node to determine the quality of a channel must not be based on SNR values alone. Rather, different parameters like PU traffic activity, path-loss, fading and shadowing models, etc. must be taken into account during analysis. Also, spectrum decision by a CBS is greatly affected in heterogeneous networks, where different types of SUs exist (for example, RT and NRT SUs). Care must be taken to ensure assignment of suitable channels, design of queuing models and call admission control policies to satisfy the overall objectives such as maximization of the number of users in the system without compromising the service quality, or minimization of the total energy consumption of all the SUs. Finally, spectrum management must also include the necessary framework that will support different SUs while allowing the reconfiguration of the underlying CR modules.

3. **Spectrum Mobility Issues-** When several channels are available to the SUs in a CRN, the decision framework must decide the target channels where SUs can perform handoff as and when required. This requires the design of suitable Target Channel Sequence (TCS) for each SU, which should be updated with time to capture the variation in network dynamics. Then, the next challenge lies in performing the spectrum handoff without causing serious degradation to the supported applications. This is a difficult task, given the fact that spectrum handoff requires SUs to change their operating frequency and involves significant overhead depending on the underlying hardware.

4. **Spectrum Sharing Issues-** Different spectrum sharing issues might arise depending on the type of the CR system. Some of the possible scenarios are discussed below. For non-coordinating CR users sharing the same channel (e.g.- unlicensed channel), there is a need to consider the effect of an individual action on other existing systems. One solution is to employ game theoretic approach to construct individual objective functions called utility functions that considers both the gain in individual performance and degradation of performance other systems. For example, increase in power to attain higher throughput might cause interference to other coexisting users, the same might be applicable to every user in the system. This can be viewed as a game and solved in a distributed manner to achieve Nash equilibrium. Considering SUs in a CRN, the spectrum sharing issue can be addressed through cooperation and coordination among the entities. One solution is

to use Common Control Channel (CCC) which allows the signaling message to be sent over a dedicated channel. Use of CCC can enhance the coordination among these SUs both in infrastructure based networks and ad-hoc networks. However, PUs have authority to access the licensed channel and CCC is not exempted from this. Thus CCC must be regularly updated and this updated information should be communicated to the SUs.

5. **Layered Model Issues-** Apart from the MAC layer issues (spectrum sharing, management) and PHY layer operations (spectrum sensing, reconfiguration, transmission), challenges exist in the upper layers of the SUs. For example, the opportunistic nature of PU channel access in a CRN means that the channels may be blocked due to random PU activities. Then, either the transmission needs to be re-routed or else the SUs must wait for the recovery of the original path, which is again a spectrum decision problem that needs to addressed by upper layers. Also, the typical congestion control mechanisms in the transport layer cannot directly be applied to the CRN. This is attributed to the unique problem in CRN where it is difficult to determine the exact cause of packet drop, that is, whether packet loss occurred due to congestion or due to emergence of the PUs. One solution is to develop explicit mechanisms where the source nodes can determine the PU activity through detection mechanisms and accordingly control their data traffic rate.

6. **Cross-layer Design Issues-** It is pretty evident from the background study in this section that cross-layer design is an integral aspect in a CR system. The most important is the cross-layer interaction between the MAC layer (for spectrum management and/or decision making) and the PHY layer (for spectrum sensing and/or transmission operations). The challenge lies in designing the related policies in each layer in such a way that they complement each other. For example, if the channel SNR of WBAN degrades, then the allocation interval of sensor nodes in scheduled access mode of MAC protocol needs to be increased to keep frame delay for different applications within permissible limit. Similarly, the payload sizes may be reduced to improve the reliability of data transfer. We will discuss more on this later in Chapter 5. Likewise, in DSA, during spectrum handoff, cross-layer interaction is required among the PHY, MAC, Transport and Application layers. To cite an instance, whenever an SU changes its operating frequency based on the handoff design, the same information has to be used by the Transport and Application layers so as to minimize the abrupt degradation in service quality.

7. **Resource Constraint Issues-** The available resources, in terms of computation power, memory, storage etc., in a SU or CBS is also an important consideration in designing efficient algorithms. For instance, the computation complexity of an algorithm needs to

be analyzed from the perspective of feasibility in real test-bed to realize its applicability in real world scenario.

8. **Cognitive Radio Policy Issues**- Policy related issues primarily deal with the way the PU channels are assessed and/or sensed. There are many factors that may affect the CRN policy makers and the network operators while selecting a specific model. Some of the important factors are- standardization requirement, resource and cost considerations etc. In this regard, the fundamental model for centralized CRN as envisioned in IEEE 802.22 [12] directs the CBS to assign PU channels to the SUs based on information derived from a white-space database. While additional protection to PU communication can be ensured by the SUs through spectrum sensing. As compared to this, another CRN architecture, as used by Tamal et al. in [100], allows a CBS to perform all necessary cognitive actions for PU channel access. An obvious advantage of this model is simpler SU design, however this is at the cost of complex framework for the CBS requiring more resources.

Thus, it is inferred from this section that unique challenges and constraints are posed by CR based communication in comparison to traditional wireless networks. On top of that, when application-oriented studies are carried out by leveraging CR technologies either as an adaptive system or through DSA, the additional requirements of these applications must also be taken care of. This demands joint formulation of application-oriented policies such that both the application objectives as well as the fundamental objective of CR systems are fulfilled. Taking cue from this, the next section presents the application oriented study of CR enabled RT WBAN applications and the NRT transfer of WBAN captured data over CRN.

2.4 WBAN over CR Platforms: Prospects and Applications

As already discussed in the previous section, the primary objective of CR technology is to make a transceiver adaptive to its environment so as to maximize its performance under all conditions. While that of CRN is to reduce spectrum congestion, utilize the bandwidth at the maximum and provide low cost broadband access. At the same time, considering the immense importance of WBAN in personal healthcare, supporting highly energy-efficient WBAN communication under non-ideal channel conditions and allowing WBAN to transfer near-real time IoT enabled data at low-cost to remote server is an imminent requirement. Therefore, the afore-mentioned requirements of WBAN make it a suitable candidate to be implemented over CR platform. Accordingly, Table 2.4 summarizes the challenges faced by WBAN (with respect to both access and backhaul communication) as highlighted in Section 2.2.4 and how they are addressed in this thesis through the application of CR technology.

However, as already discussed in Section 2.3.4, the CR implementation also presents specific challenges which need to be addressed. Accordingly, Table 2.4 also lists the techniques adapted by us to mitigate such CR specific issues.

Table 2.4 Summary of WBAN and CR challenges as addressed in this thesis

WBAN Challenges	**CR Solution to WBAN issues**	**Challenges in CR Implementation**	**Solutions to the CR Issues**
Non-Ideal WBAN channel conditions leading to reduced reliability, increased frame delay and lower energy-efficiency of sensor nodes.	An Adaptive MAC protocol following IEEE 802.15.6 standard that allows the sensor nodes to modify the MAC & PHY parameters (payload sizes and allocation intervals in scheduled access mode) based on the channel condition and optimize the energy-efficiency of the nodes under frame delay and reliability constraints.	Exploiting complex numerical techniques to implement adaptive allocation intervals and payload sizes will be resource intensive for low power microcontrollers of the sensor nodes and will thereby affect real-time delay constrained WBAN communication.	Instead of numerical approach, a LUT based technique to adapt the allocation intervals and payload sizes based on channel SNR will be more efficient.
The WBAN backhaul communication faces the following challenges- Spectrum congestion in conventional networks due to huge volume of IoT applications like remote health monitoring and high data transfer cost over licensed WAN technologies.	DSA over licensed bands using a centralized CRN overlaid on a licensed cellular WAN will provide enhancement in spectrum capacity and a low cost solution for data transfer.	Need to ensure reliable data transfer to the remote server taking into account the opportunistic nature of CRN. Need to ensure maximum energy-efficiency for BNC transmission over CRN while keeping the interference to PUs within predetermined limits. Based on the CRN policies and available resources the CBS in centralized CRN may perform selective operations.	A cross-layered BNC is proposed that allows switching from backhaul CRN to licensed WAN interface of the BNC in the event of failure in attaining a channel from CBS or sustaining communication over allocated PU channels. Regarding energy-efficiency maximization, first we consider the situation when the CBS only allocates channel and obtains PU activity information. Based on this CRN policy, we propose methods that allow channel sensing and energy-efficiency maximization to be performed by BNCs while taking into account PU interference constraint and sensing uncertainties. In case, the CBS has sufficient resources, then we propose a centralized framework that exploits efficient prediction technique at the CBS to significantly minimize the interference of backhaul communication with PU transmission and thereby improve the energy-efficiency. Moreover, the CBS can apply a proposed fair scheduling mechanism to allocate predictable PU channels to appropriate NRT users in the network to minimize the total battery consumption.

Chapter 3

Modeling of WBAN based on IEEE 802.15.6 Scheduled Access MAC using OPNET with Energy-Efficient Test-Bed Implementation for e-Healthcare

❝ *Design is not just what it looks like and feels like. Design is how it works.*❞

-Steve Jobs, Apple Inc.

As clearly evident from the previous chapters, there is an enormous scope of IEEE 802.15.6 based WBAN in facilitating proactive, affordable and ubiquitous PHS. However, use of WBAN also presents stringent challenges with respect to ensuring high energy-efficiency and satisfying strict QoS constraints coupled with different MAC layer requirements and non-ideal channel characteristics. This necessitates the need to conduct intensive research in this emerging discipline with respect to performance analysis and optimizations that are suitably validated or guided by simulation results. Accuracy and credibility of the simulation output in these studies are strongly dependent on the proper design of the simulation model. However, in the absence of any such simulation model of WBAN based on IEEE 802.15.6 standard, the first step towards conducting full-fledged research in this domain is to develop a comprehensive simulation model. This model will serve as a platform for validating analytical observations and also facilitate performance analysis and optimization of designed WBANs in the thesis. ***Accordingly, one of the objectives of this Chapter is to build a detailed simulation model in OPNET Modeler 16.0 of WBAN following Scheduled Access MAC (SAM) of IEEE 802.15.6 protocol employing a hierarchical top-down approach, starting at the network level, followed by the node level, right up to the process level.***

In the next phase of work, we use the simulation model for energy-efficient design and implementation of WBAN on real test-bed to facilitate real-time health monitoring and non-real time transfer of small amounts of WBAN captured data to remote server in an e-healthcare framework. The designed WBAN test-bed in general, and the WBAN BNC in particular, will serve as the precursor to designing the gateway between WBAN and backhaul CRN, which will be the topic of discussion later in Chapter 6. Through the developed test-bed model we also gain important insight into the sensor node mechanism and resources, which we later exploit for embedding CR enabled adaptability in Chapter 5. Therefore, ***this chapter also deals with the hardware and software designs to implement and optimize (with the help of the simulation model) a WBAN based on IEEE 802.15.6 SAM for e-healthcare***. Additionally, we also propose a DWT based data compression technique (B-DWT) to facilitate energy-efficient and low cost backhaul data transmission by BNC using licensed WAN technologies like GPRS and GSM. After suitable hardware design, we exploit our simulation model to perform performance analysis and characterization of our WBAN. Finally, the advantages of the proposed B-DWT technique are also established along with the basics of remote server and database storage.

3.1 Introduction

Personal Health Systems (PHS) through wearable devices is considered as a key solution towards enabling proactive, affordable and ubiquitous healthcare monitoring. It allows monitoring of one's vital physiological signals like electrocardiograms (ECG), electromyogram (EMG), pulse oximeters, dosimeters, movement alarms and many more, while allowing them to engage in their normal activities instead of staying at hospital or home or close to a specialized medical device. This can be achieved through a network consisting of intelligent, low-power, micro and nano-technology sensors and actuators, which can be placed on the body, or implanted in the human body (or even in the blood stream), providing timely data. Such networks are commonly referred to as Wireless Body Area Networks (WBANs) [17]. They allow citizens/patients to have more responsibility in managing their own health and interacting, whenever is necessary, with care providers. In addition to proactive healthcare, long-term use of WBANs also reduces healthcare costs by removing the need for costly in-clinic visits or in-hospital monitoring of patients.

Further, due to the remarkable progress in Internet and Communication Technologies (ICT), WBANs can be integrated with Internet by transmitting the data using long distance communication technologies comprising Wide-Area Access Networks (WANs) like cellular communications, e.g. GSM, GPRS, 3G, 4G. This is termed as the *convergence layer or back-*

haul of a WBAN. Whereas, the WBAN comprising of the sensors and hub communicating over short distance close to the body is also termed as the *access layer*. The convergence layer provides mobility to the patients allowing them to carry on their daily activities in both outdoor as well as indoor environments while still facilitating ubiquitous remote monitoring of the patient's health over the Internet. Importantly, as WBANs provide large time intervals of medical data, doctors will have a clearer view of the patient's status [6].

Existing Wireless Personal Area Network (WPAN) technologies like Zigbee (IEEE 802.15.4) [22] have previously been used for designing WBANs. However, these standards were meant to support low cost and low data rate communications and they do not satisfy the QoS, reliability, high data rate and medical requirements of WBAN [17]. To address this, IEEE has recently come up with IEEE 802.15.6 [23] standard. The standard provides a new set of PHY and MAC layer specifications. The MAC layer supports both contention based access using CSMA/CA, slotted Aloha and contention free scheduled access.

SAM allows the sensor nodes to transmit their data during specific Allocation Intervals (AIs). Literature survey revealed that the IEEE 802.15.6 based CSMA/CA and Slotted Aloha MAC received a lot of attention through simulation and analytical modeling studies. In this regard, the performance of CSMA/CA MAC is studied under saturation traffic in [64] and non-saturation traffic in [65]. While, the throughput analysis of slotted Aloha was performed in [67]. However, scheduled access mechanism of IEEE 802.15.6 is yet to be explored. Since it is based on the concept of TDMA, it provides advantages like energy-efficient transmission, bounded delay, reduced collision under high network load with correlated traffic [31], thereby prolonging sensor battery life time.

3.1.1 Importance of SAM in Healthcare Monitoring

Patient monitoring using biomedical sensors is a popular WBAN application that can continuously or periodically monitor chronic and non-chronic diseases. In most of these cases the traffic is often correlated [31]. For example, to get a clearer picture of a patient's overall health, a physician requires a complete view of the patient's vitals namely temperature, blood pressure, ECG which have to be recorded simultaneously at periodic intervals. Similarly, for tracking the performance of an athlete, a WBAN need to continuously track high data rate applications like EMG, ECG, along with low data rate signals like temperature. Contention based MAC is not suitable in such cases of high traffic correlation [31] as they encounter heavy collisions and extra energy consumption. Schedule-based protocols such as TDMA, provide good solutions to the traffic correlation. These protocols are energy conserving protocols because the duty cycle is reduced and there are no contention, idle listening, and overhearing problems [31]. Usually, CSMA/CA is considered to be appropriate for

low, urgent, adaptive, scalable traffic patterns and frequent network changes, whereas the TDMA is recommended for high periodic traffic and infrequent network changes [28–30]. A comparison between TDMA and CSMA protocols is reported in [32]. It is shown that TDMA method is more suitable for nondynamic types of networks. Fortunately, WBAN has a nondynamic network structure (fixed network topology), which forms the basis for further investigations on TDMA MAC by Marinkovic et al. in [33]. Further detailed account of other related works based on TDMA in WBAN is provided in Chapter 5.

Networks with high correlated traffic may have sensors transmitting at low and/or medium to high data rates. To this end, Tachtazis et al. in [99] addressed the low data rate case by considering m-periodic allocations of IEEE 802.15.6 SAM. In m-periodic SAM [23], devices and hubs exchange frames in every m superframes. However, the analysis for medium to high data rate applications which requires 1-periodic SAM is yet to be carried out. Therefore, to adress this scenario, in this work, we consider the *1-periodic allocation* of IEEE 802.15.6 SAM [23], where nodes exchange frames with the hub in their scheduled AIs in every superframe. Further, we will focus only on *uplink traffic*, as it is the most commonly encountered traffic which is extensively considered for analysis in the literature [65, 66].

3.2 Related Work and Motivation

In this section, we review some of the available simulation models that can be used for modeling WBAN, and establish the motivation behind selecting OPNET simulation platform [95] for our work. Following this, we discuss some of the implementation works related to WBAN, and bring out the novelty aspects of this chapter from the implementation perspective.

3.2.1 Available Simulation Models/Tools

NS2 [92] is one of the best known network simulators used for modeling WSNs. However, NS-2 is considered to be too general, less accurate and thus inappropriate for WSN simulation. OMNet ++ [93] is another well-known component-based simulator. But it is perhaps even more generic that NS-2. OMNET++ has a framework called Castalia [94] to extend its functionality. Castalia is developed for networks of low power wireless sensor nodes. Castalia provides an implementation of IEEE 802.15.6 MAC. However, the lack of a proper Graphical User Interface (GUI) makes coding, realizing network environment and performing simulation a rather complicated process.

In [141], the author developed an simulation model in OPNET platform [95] for the IEEE 802.15.4 standard, profiled for healthcare applications. That model implements the

slotted and the unslotted CSMA/CA MAC protocols. A very reliable model of the IEEE 802.15.4/ZigBee protocols for WSNs is provided in [96]. It does not use the OPNET Modeler standard library for Zigbee implementation. Hence, the results obtained were very reliable. This motivated us to use the design philosophy in [96] and extend it for IEEE 802.15.6 SAM. Due to the afore-mentioned reasons and because of the accuracy and elaborate GUI of OPNET, we use OPNET 16.0 Modeler [95] for developing the IEEE 802.15.6 simulation model based on SAM.

OPNET is one of the widely used simulation software for modeling and simulation of communication networks. It has the distinct advantage of model design, data collection and data analysis. OPNET implements a naturally pipelining structure of actual communication networks through a hierarchical design approach. Through discrete event simulation it allows users to analyze both the behavior and performance of modeled systems. Moreover, it allows flexible modeling of the behavior of various nodes in a network through Finite State Machine and high-level programming, thereby supporting realistic modeling of most of the different communications protocols, algorithms, and transmission technologies [96, 142].

3.2.2 Hardware Prototype for WBAN Implementation- Existing Works and Requirements

Earlier works related to design of WBANs considered low power Wireless Personal Area Network (WPAN) technologies such as Zigbee (IEEE 802.15.4) [22, 47–49] and Bluetooth (IEEE 802.15.1) [21, 53, 54]. However, as highlighted earlier, WPAN technologies do not comply with the medical standards in terms of QoS, reliability and increased data rate. In this aspect, IEEE 802.15.6 is a more suitable choice. However, literature survey revealed that implementation of a WBAN setup based on the MAC protocol as envisioned in IEEE 802.15.6 is scarce. Moreover, to the best of author's knowledge no work has implemented the scheduled access mechanism of IEEE 802.15.6 in a WBAN for real-time health monitoring. To this end, the aim of this work is to implement a WBAN that is based on the IEEE 802.15.6 SAM protocol, capable of tracking multiple attributes of a patient in real-time. WBAN when viewed as a standalone network allows patients to have a real-time view of their vitals, giving them more control over their own health. However, in this work, to stay true to the IoT vision, we devise a remote heath monitoring e-Healthcare system that supports database storage of samples of near real-time also termed as non-real time (NRT) data transmitted at regular intervals by WBANs of multiple patients located anywhere in the world. For this, we design our WBAN BNC to multiplex multiple sensor data and transfer them over the Internet using cellular backhaul technology to a Remote Server (RS). The RS de-multiplexes the data and

stores it in database to provide complete health history of a patient to healthcare personnel and patients via web and mobile apps. Hardware and software designs have been developed to reach our goals.

Moreover, with the need to reduce data transfer costs and energy-consumption over backhaul, we were motivated to look into compression algorithms that would allow non-stationary signals such as ECG which are collected by WBAN to be compressed without significant loss of data prior to backhaul transmission. Additionally, the transmitted compressed data can also be leveraged for efficient storage of the huge volume of healthcare information at the remote database of an e-healthcare system. A concise overview of the most relevant compression techniques can be found in [143, 144]. Our focus is on physiological signal compression solutions that are implementable in real time on WBAN BNC, which is a low power microcontroller with limited resources. Additionally, the algorithms should achieve competitive Compression Data Ratios (CDRs) while being amenable to efficient, fast, and low memory footprint implementation on our target platforms. These algorithms are all based on the Discrete Wavelet Transform (DWT) [145, 146]. So in order to make our system more robust and energy-efficient, we implement a very classical DWT in our BNC and perform extensive performance analysis to determine the best combination of wavelet filter and compression and provide benchmarks in performance for future works. Interestingly, our BNC DWT (B-DWT) implementation based on the concept of Finite Impulse Response (FIR) moving average filters [147] showed significant performance improvements in terms of execution speed and memory utilization over the traditional DWT.

Furthermore, motivated by the need to prolong battery life of the sensor nodes, we made our WBAN energy-efficient. For this we performed performance analysis of our setup in OPNET simulator [95] using our custom-made WBAN simulation model. Through performance analysis we derived the optimal AIs that maximize network capacity while satisfying the frame delay constraints and also obtained the payload sizes needed to maximize the energy-efficiency of sensor nodes.

Some of the applications of our system include- i) remote monitoring as a cost-effective and comfortable alternative to in-clinic cardiac treatment follow up, e.g. short interval ECGs can be periodically sent to database, ii) regular monitoring of patients with hypertension, iii) keeping track of conditions of chemo patients, and iv) collecting data before, during and after an epileptic seizure and sending it to remote healthcare facility.

3.2.3 Contributions of this Chapter

The main contributions of this chapter are as follows:

❶ A custom made simulation model is developed in OPNET for WBAN as per the IEEE 802.15.6 SAM. For this, we follow an in-depth top-down hierarchical approach comprising of three layers, namely network model, node model and process model.
❷ The simulation model is then used for performance evaluation of WBAN under ideal channel conditions through study of metrics such as average frame delay, throughput, energy consumption of sensor nodes for variations in parameters like Allocation Intervals (AIs) and Payload Sizes (PSs).
❸ With regards to implementation of WBAN setup for e-healthcare, we describe the detailed hardware interfacing among different components that are required for designing the sensor nodes and BNC.
❹ We also elaborate the process of multiplexing data at the BNC from multiple sensor nodes which are simultaneously monitoring different physiological signals (e.g. ECG, temperature). In addition, the BNC is also devised to collect and store different data fragments of a single data stream sent by a particular sensor node. All the collected data are stored using multiple queues that lead to efficient memory management at the sensor nodes.
❺ Next, we describe our proposed fast B-DWT algorithm to compress the collected data (eg. ECG) prior to transferring the data to remote server.
❻ We also design a basic remote server and database to store compressed/uncompressed data for pervasive access.
❼ Following the hardware design, we obtain the optimal allocation intervals for ECG and temperature monitoring using the developed OPNET simulation model maximizing the network capacity within a frame delay constraint. We also determine the optimal payload sizes that maximize the energy-efficiency of the sensor nodes.
❽ Finally, through a comprehensive performance analysis of the proposed B-DWT algorithm we establish its performance superiority in terms of efficient memory utilization and execution speed. Thereafter, we determine the best wavelet filter and compression level that allows a balanced trade-off between the amount of data compression and information loss.

3.2.4 Chapter Organization

This chapter is organized as follows. We start by highlighting the salient features of IEEE 802.15.6 scheduled access MAC in Section 3.3. Then in Section 3.4, we describe our OPNET model in detail following a hierarchical top-down approach, starting at the network level, followed by the node level, right up to the process level. In Section 3.5, we provide the simulation results and analyze the different WBAN performance metrics and also validate the

functionality of the model. Following this, the focus shifts towards test-bed implementation of WBAN. Section 3.6 gives an overview of the e-healthcare system model, and DWT based data compression. Section 3.7 and 3.8 presents the design of sensor nodes and BNC respectively. The implementation of scheduled access MAC is provided in Section 3.9 (See Appendix D.1 for Demo Video Link). Section 3.10 describes the implementation of the proposed B-DWT algorithm at BNC. In Section 3.11, we discuss the performance analysis and characterization of our WBAN setup and B-DWT algorithm. Section 3.12 deals with the RS and database design. Finally, we conclude this chapter in Section 3.13.

3.3 Overview of IEEE 802.15.6 SAM

The IEEE 802.15.6 [23] standard specifies the PHY layer and the MAC sub-layer for WBAN. Within a WBAN all the sensor nodes are coordinated by their respective hubs for medium access. Further, one WBAN can have only one hub and multiple nodes communicating in star topology. Each hub and node is internally partitioned into PHY and MAC sub-layer. For transmission, the MAC sublayer accepts packets (MAC service data units or MSDUs) from its higher Application Layer (APP layer), appends MAC header and Frame Check Sequence (FCS) to produce MAC Protocol Data Unit (MPDU) also known as Physical Service Data Unit (PSDU), which is then forwarded to the PHY layer. Lastly, PHY layer appends its header to form the Physical Protocol Data Unit (PPDU) that is transmitted over a channel to the receiver. On reception, the reverse operation happens. In this section, we give a brief overview of the MAC sublayer protocol, more specifically the scheduled access mode.

For medium access to be scheduled in time, the time axis is divided into beacon period or superframes. Referring to the IEEE 802.15.6 superframe structure given in Figure 2.2, we remark that all phases except RAP1 may have a zero length. In this chapter, since we focus on scheduled 1-periodic uplink allocation, we keep EAP1, RAP1 and MAP and set all other phases to zero. The superframe structure as followed in this work is shown in Figure 3.1.

To start a scheduled allocation, the node sends Connection Request frame to the hub, requesting the required AIs of MAP i.e. the number of allocation slots needed. In response,

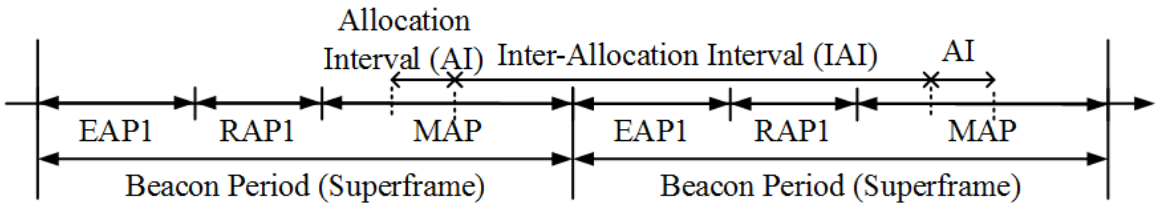

Fig. 3.1 Layout of access phases as followed in this work.

the hub sends a connection assignment frame containing information about the AIs which have been accepted by the hub. The frame transactions for connection establishment happens in the contention access phases. In 1-periodic SAM, every sensor node is allocated their requested AI within the MAP at fixed locations of every superframe (Figure 3.1), where only uplink transmission of that particular sensor node is allowed without interference or collision from other sensor node transmissions. This is similar to static TDMA as in [148]. Upon obtaining a scheduled uplink allocation, the node may initiate a frame transaction with the hub at the start each of the AIs, if the frame transaction and an appropriate guard time fit into the AI. A frame transaction comprises of the node transmitting a data frame and waiting for a corresponding Immediate Acknowledgment (I-Ack) frame from the hub, separated by a Short Inter-Frame Spacing (SIFS). If an I-Ack frame is not received within the expected time, the node resends the data frame. The maximum number of such resends is denoted by R. The basic principle behind the scheduled access mode is shown in Figure 3.2. The assignment for a particular sensor node remains valid until i) the node ends the scheduled allocation by sending a disconnection request at a pre-determined time, for instance in case of periodic monitoring at regular intervals, or ii) the session is aborted by the hub after failing to receive any frame in the last $mScheduledAllocationAborted$ AIs.

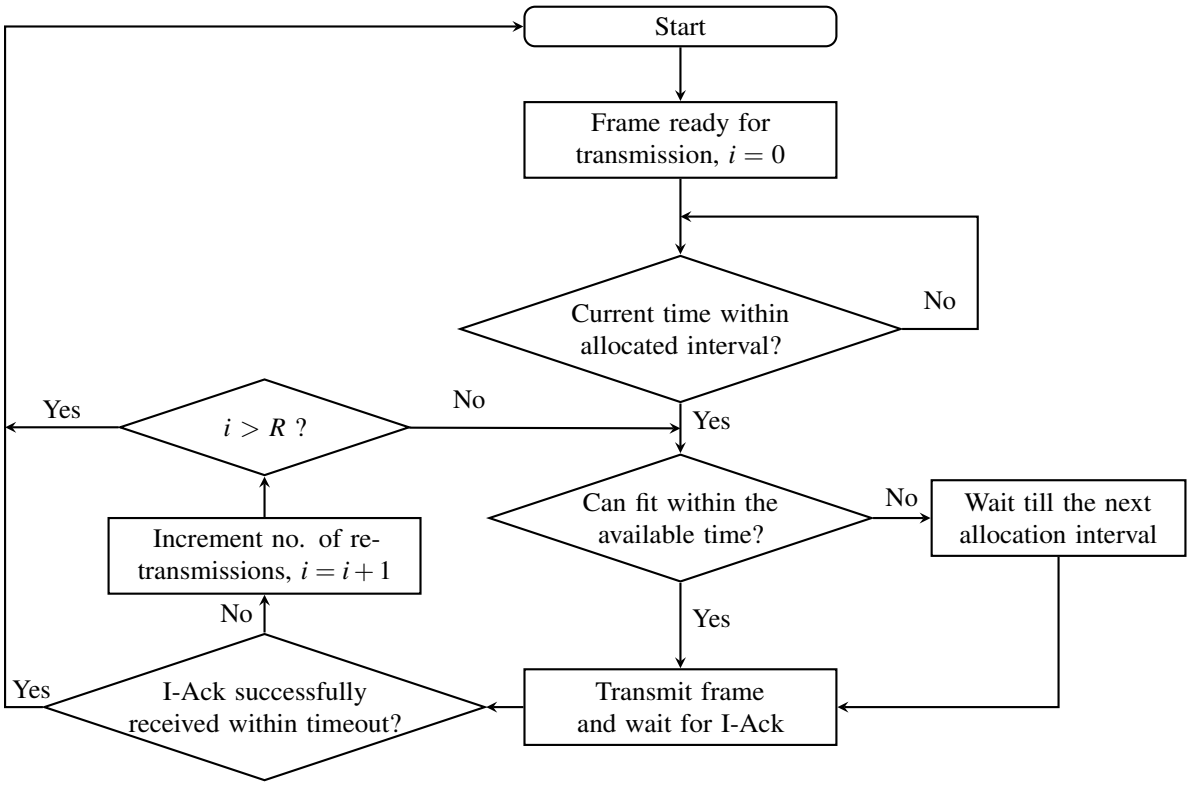

Fig. 3.2 IEEE 802.15.6 scheduled access mechanism.

3.4 OPNET Simulation Model

OPNET Modeler 16.0.A [95] is chosen as the simulation platform as it offers high level customization for its nodes. It allows accurate modeling, simulation, collection and analysis of wide range of statistical data for wireless networks. For designing a simulation model of IEEE 802.15.6 we draw on the concepts presented in [96] on designing IEEE 802.15.4 based ZigBee protocol in OPNET. During the establishment of a WBAN based on IEEE 802.15.6 SAM, OPNET divides the Design Model into three layers namely:

i) Network model,
ii) Node model, and
iii) Process model.

This is achieved through Object-oriented software technology and Layered Modeling Techniques. In this section, we describe the methods involved at each of these layers in designing the OPNET model.

3.4.1 The Network Layer Model

A network layer model defines the overall scope of a system to be simulated. It is a high-level description of the objects, also known as nodes, contained in the system. The network model specifies the nodes in the system, as well as their physical locations, interconnections and configurations.

Our simulation model supports WBAN star topology, with all sensor nodes communicating directly with the hub, thereby enabling single hop communications, as shown in Figure 3.3.

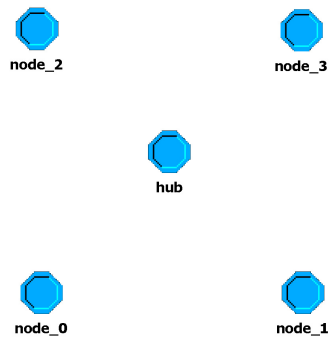

Fig. 3.3 The network layer model of WBAN.

3.4.2 The Node Layer Model

This section presents the methods used to specify the internal structure and therefore much of the capabilities of communication nodes. As introduced in Section 3.4.1, a WBAN is comprised of two types of nodes, namely hubs and sensor nodes. The hierarchical design of each module of WBAN sensor node/ hub is shown in Figure 3.4. Based on a layered protocol architecture, the node layer model is divided into the following three layers:

i) Application (APP) Layer,
ii) Medium Access Control (MAC) layer, and
iii) Physical (PHY) layer.

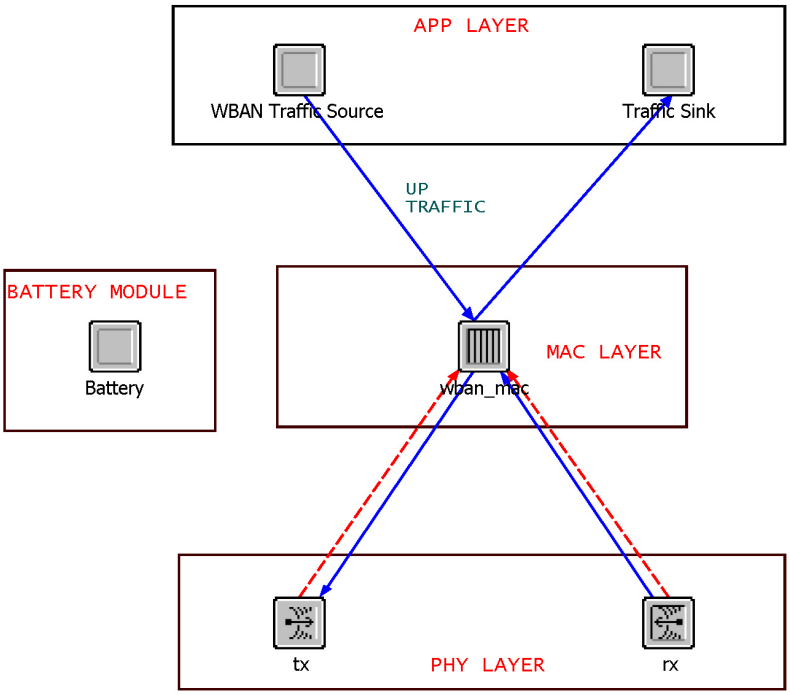

Fig. 3.4 The node layer model of hub/ sensor node.

In Figure 3.4, the Application Layer comprises of i) *WBAN Traffic Source* that is responsible for generating packets or MSDUs with traffic load as mentioned in node domain attributes shown in Figure 3.5, and ii) *Traffic Sink* that receives packets from the WBAN MAC layer and processes them appropriately. The *sch_mac* module is a queue module that implements the MAC layer functionality with the responsibility of i) receiving packets from APP layer followed by encapsulation into MPDUs that are sent to the PHY layer for transmission, or ii) decapsulation of MPDUs obtained from PHY layer before passing them

on to the APP layer. Furthermore, in the MAC layer we have incorporated the scheduled access mechanism of IEEE 802.15.6. Additionally, the MAC layer of a hub forms beacons frames. The MAC layer also has the capability to get channel access information from the physical layer for implementing the basic CSMA/CA algorithm as incorporated in [96] for transmitting management frames like Connection Request and Connection Assignment. The PHY layer performs Narrowband communications with the help of wireless transceiver (*tx* for transmitter and *rx* for receiver) over 2.4 GHz as per the standard, with data transmission and reception using QPSK/ BPSK modulation. The data frame transmission and reception relationship is shown through the blue line in Figure 3.4. Whereas, the red dotted line represents a statistic wire, which does not affect the normal data transmission. The statistic wire is used by the MAC to obtain PHY layer channel information.

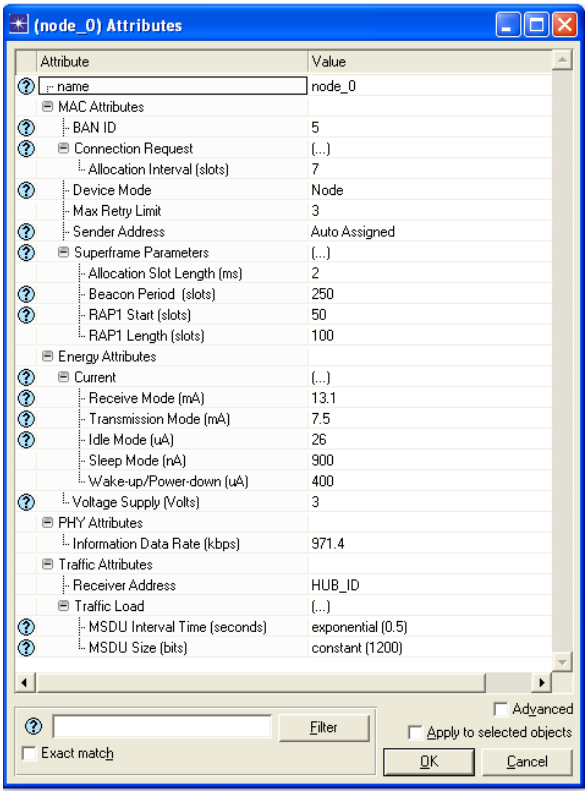

Fig. 3.5 Node Attributes.

In addition, the node model also has a *Battery Module* (Figure 3.4), that essentially computes the energy consumption of each node during transmission, reception and idle stages of the node. The Battery module performs this through interrupt driven Interface Control Information (ICI) interchange with the *sch_mac*. We now describe the process model of each of these modules.

3.4.3 The Process Layer Model

Process models specify the behavior of processor and queue modules which exist in the Node domain. Process models can be used to implement a wide variety of hardware and software subsystems, including communication protocols, algorithms, shared resources such as disks or memory, operating systems, queuing disciplines, specialized traffic generators, custom statistic collectors, and so on. Our process models are designed so as to work for both the hub and the sensor node on conditional basis. This reduces the complexity of the modeling, as many of the basic functionality for both the hub and sensor node are identical. We will highlight the major differentiating features between the two when applicable.

3.4.3.1 Model design for traffic generation

The *WBAN Traffic Source* module is responsible for generating packets having different traffic patterns or Traffic Loads (TLs). It draws on the functionality of a basic source module in OPNET and extends it to build an advanced generator capable of producing MSDUs of varied traffic patterns. The module supports the setting of different packet inter-arrival time intervals like constant, exponential and other distribution function, packet size, start time and end time. The process model of *WBAN Traffic Source* is shown in Figure 3.6.

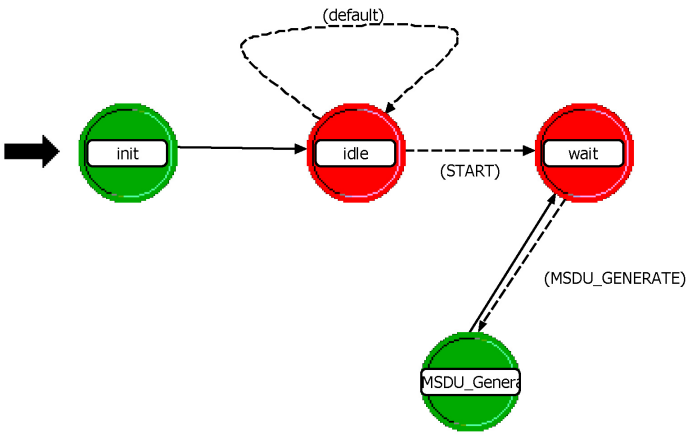

Fig. 3.6 The process model of *WBAN Traffic Source*.

In Figure 3.6, initially the process model is in *init* state in which statistics needed to be gathered in simulation are registered and initialized, following which the process model enters into *wait* state. The MSDU_GENERATE macro is defined to specify the transition from *wait* state to the forced *MSDU_Generate* state when an MSDU is scheduled to be generated next. At the *MSDU_Generate* state the required MSDU is generated as per the set packet size and then a self-interrupt is scheduled at the instant when the next MSDU will

be generated as per the set packet inter-arrival time. Thus, multiple packets are generated through scheduling of self-interrupts corresponding to their next-packet generation instants. The MSDUs thus generated are forwarded to the *sch_mac* module for further processing.

3.4.3.2 Principle of MAC protocol design of WBAN node

Based on the scheduled access mechanism of IEEE 802.15.6 MAC protocol and the modeling methods of OPNET, the process model of *sch_mac* built in this work is as shown below in Figure 3.7.

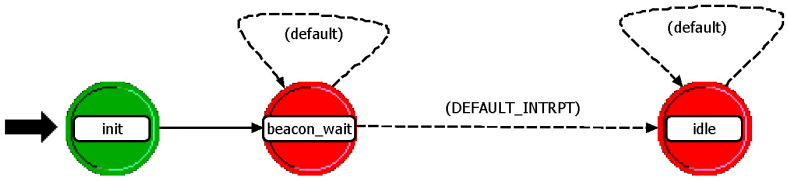

Fig. 3.7 The process model of *sch_mac*.

Similar to the previous process model, in Figure 3.7 the *init* state initializes the different statistics variables and interrupt handles. Moreover, at the *init* state, the hub extracts the superframe parameters from the node domain attributes shown in Figure 3.5 and sets the relevant fields in the Beacon MSDU frame. Since OPNET provides direct support for packet format - packet format editor, we create the Beacon MSDU frame format as per the IEEE 802.15.6 standard [23] with all the relevant fields as shown in Figure 3.8. Thereafter, the hub sends the first beacon frame and moves to the *beacon_wait* state, while the sensor node has already entered the *beacon_wait* state waiting for the beacon to arrive. On receiving the beacon, the sensor node extracts the beacon and updates the different superframe parameters based on the Beacon MSDU fields (Figure 3.8). Following this, the hub schedules the next beacon frame transmission and the sensor node prepares for the Connection Request frame transmission. In addition, both the hub and sensor node schedules various self-interrupts to indicate start/end of EAP/RAP, more on this later. It must be noted that the beacon transmitted by the hub is also received by it and then discarded. However, this is significant because the reception of the beacon triggers a packet interrupt on both the hub and sensor node and activates the DEFAULT_INTRPT transition, which transfers them to the *idle* state. At the *idle* state, the process model waits for next interrupt to occur. Once an interrupt happens, it executes the exit-executive [95] function *mac_interrupt_handling()*, which allows the process to take action based on the interrupt type. The realization of the interrupt handling mechanism in OPNET can be seen in Figure 3.9. We now discuss the different categories of interrupt and their significance in brief.

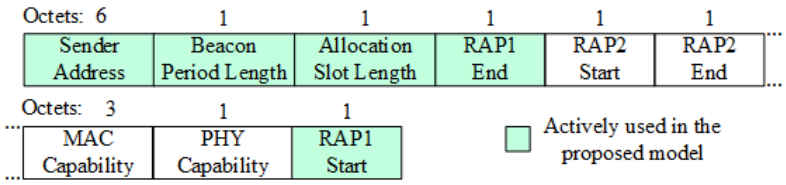

Fig. 3.8 Beacon MSDU Frame format.

```
switch (op_intrpt_type()) {
  case OPC_INTRPT_STRM: //Stream interrupt
    handle_incoming_frame(); //Handle the incoming frame
    break;
  case OPC_INTRPT_SELF: //Self-interrupts
    switch (op_intrpt_type ()) { // User self-interrupt codes
      case SELF_INTERRUPT_CODE#1:
        ...
        break;
      case SELF_INTERRUPT_CODE#2:
        ...
        break;
      default:
    }
  case OPC_INTRPT_STAT: //Statistic interrupts from PHY
    switch (op_intrpt_stat ()) { // User self-interrupt codes
      case BUSY_RX_STAT: // Stat from busy receiver
        ...
        break;
      case BUSY_TX_STAT: // Stat from busy transmitter
        ...
        break;
      default:
    }
  case OPC_INTRPT_ENDSIM: // Simulation end interrupt
    ...
    break;
  default:
}
```

Fig. 3.9 The interrupt handling mechanism of *mac_interrupt_handling()*

3.4.3.3 Interrupt handling by the MAC

As shown on Figure 3.9, the *mac_interrupt_handling()* function allows *sch_mac* to handle the following three kinds of interrupts:

1. Arriving frame interrupt,
2. A scheduled self-interrupt, and
3. Statistic interrupt arising from the PHY layer.

Arriving frame interrupt: A frame may arrive at the MAC as either:

i) an MSDU from the *WBAN Traffic Source* module, or
ii) a PPDU from the receiver *rx* radio.

An MSDU will be converted into MPDU and enqueued in a DATA sub-queue. The MPDU format [23] is shown below in Figure 3.10 along with its major fields. In this regard, it must be pointed out that the *sch_mac* module of a node maintains two sub-queues: one for data MPDUs (DATA sub-queue) and the other for management MPDUs (MGM sub-queue). The data frames are the MSDUs arriving from the traffic generator, whereas the Management frames are the Beacons, Connection Request and Connection Assignment frames.

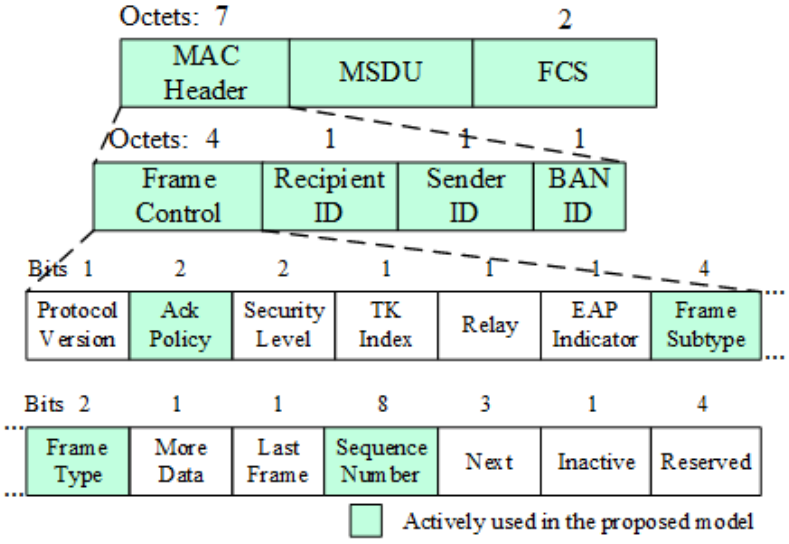

Fig. 3.10 MPDU Frame format.

A PPDU from the physical layer is forwarded over the packet stream from *rx* radio to *sch_mac*. The MPDU (or PSDU) is extracted from the PPDU and it is examined for bit errors due to non-ideal channel characteristics that might have corrupted it. In case of an error or reception of a duplicate frame, the received frame is discarded and the frame

re-transmission policy is followed. Data, Connection Request and Connection Assignment frames follow I-Ack policy, whereas Beacon frame follows a No Acknowledgment (N-Ack) policy. Alternatively, if the received packet is successfully received, we check if the MPDU is actually meant for the sensor node by comparing the BAN ID, Recipient ID and Sender ID present in the MPDU header (Figure 3.10) respectively with the BAN ID, node ID and expected Sender ID for the sensor node. Upon successfully filtering the incoming MPDU, the process handles the MPDU based on its frame type, i.e. whether it is a Data, Management or an I-Ack frame. This is identified from a Frame Type field in the frame MPDU as shown in Figure 3.10. Furthermore, a Frame Subtype field helps distinguish between the different Management type frames. A detailed discussion of the handling of Data, I-Ack, Connection Request and Connection Assignment frames will be taken up later in appropriate sections.

Scheduled self-interrupt: A OPNET process through its Kernel Procedure (KP) *op_intrpt_schedule_self()* has the ability to schedule self-interrupts. It allows the invoking process to schedule an interrupt at an appropriate simulation time. The self-interrupt is associated with an identification code, e.g. SELF_INTERRUPT_CODE#1 in Figure 3.9. The code can be obtained when the interrupt invokes the process, using the KP *op_intrpt_code()*. The self-interrupts used in our OPNET model can be categorized into the following classes-

i) Superframe self-interrupts,
ii) Frame transmission self-interrupts. and
iii) CSMA/CA self-interrupts

The superframe self-interrupts indicate the end of Beacon interval, and the start and end of different access-phases. Whereas, the frame transmission self-interrupts indicate actions associated with frame transmission. These are mainly- attempting a frame transmission, start of transmission, timeout for receiving I-Ack and sending I-Ack. The transmission mechanism is described later in detail.

The CSMA/CA mechanism used in our model is mainly for assisting the sensor nodes and hub transmit the Connection Request and Connection Assignment frames during the contention periods. For this purpose, the CSMA/CA mechanism in our model is very fundamental drawing on the methods used in [96]. The CSMA/CA self-interrupts mainly comprise of start and end of the Clear Channel Assessment (CCA) period. At the interrupt instants, the process checks whether the channel is busy by reading the statistic wire from the radio *rx*. If the medium is idle, transmission is allowed at the end of a back-off interval. We will not elaborate on the CSMA/CA mechanism further in this chapter.

Statistic interrupt arising from the PHY layer: The *sch_mac* module has two statistic wires coming from the radio *tx* and *rx* at the PHY layer. The statistic wires are configured to return a Boolean value (0.0 or 1.0) which represents whether any packets are currently being received (for *rx*) or transmitted (for *tx*) on a channel. The interrupt from these statistic wires are mainly utilized for updating the battery module using ICI for keeping track of the energy consumption. ICI allows information to be transferred from *sch_mac*, where the statistic event is generated, to the Battery module, where the energy consumption of the node is updated. The mechanism followed is as follows: When transmission or reception of a packet over the channel is complete, with the help of the statistic interrupts the total duration of the frame transaction is computed and that information is conveyed to the Battery module using ICI through scheduled remote interrupt.

3.4.3.4 Connection Establishment Mechanism of MAC

As pointed out earlier, after a sensor node receives the first Beacon from the hub, it creates the Connection Request MSDU containing the requested allocation length obtained from the node attributes (Figure 3.5). The MSDU is then encapsulated within an MPDU with the receiver address set to the address of the hub and the Ack policy set to I-Ack policy. The connection request MPDU thus prepared is enqueued in the MGT sub-queue and transmitted in the EAP1 or RAP1 following the transmission mechanism that is explained in the next sub-section.

After the Connection Request MSDU frame is received and extracted, the hub prepares the Connection Assignment MSDU. The hub maintains:

i) a variable *nat* that identifies the first non-allocated time slot, and
ii) an array *map_node* that maps each MAP time-slot to the assigned sensor node by storing their node ids.

For assigning an allocation interval to the sensor node, the hub checks whether the requested allocation interval can be fit with the first non-allocated time slot and the end of the MAP. If it can be fit, then the allocation interval is assigned to the sensor node. Thereafter, the hub mentions the start and end of the allocation intervals as '*nat*' and '*nat* + requested allocation interval+1' respectively in the Connection Assignment MSDU. The variable *nat* and the array *map_node* maintained by the hub are also updated accordingly. The MSDU is then encapsulated in an MPDU and enqueued in MGT sub-queue.

3.4.3.5 Transmission Mechanism of MAC

When the *sch_mac* process is waiting in its *inactive* state (Figure 3.7), the transmission mechanism described herein allows it to take action based on the occurring self-interrupt and the status of the sub-queues. Note that, an inactive state in Figure 3.11 refers to both idle and sleep states shown in Figure 3.12 which are discussed in the next sub-section. Figure 3.11 shows the flowchart of the transmission mechanism of the *sch_mac* . Here, we mainly focus on the mechanism at the sensor node. Upon being invoked by either the start of EAP1, RAP1, the assigned allocation interval in MAP, an I-Ack timeout or an arriving MSDU packet from *WBAN Traffic Source*, the process schedules a self-interrupt at the current simulation time with code ATTEMPT_FRAME_TRANSMISSION_CODE. If the interrupts invoke the process during the EAP1 or RAP1, the process checks whether the MGT sub-queue is non-empty or any Management frame like Connection Request, Connection Assignment or Beacon (for hub) is selected to be transmitted. If neither of these conditions are satisfied, the module returns to the *inactive* state. But when either of the condition is true, or if the current time is within the allocation interval, the process checks the following arguments in order-

i) confirming that no frame transaction is in progress,
ii) whether any frame is already selected for transmission (indicated by the Boolean variable *frame_selected*) which may have been deferred or failed in a previous transmission, if not then extract the topmost MPDU from the MGT sub-queue, or if it is empty draw an MPDU from the non-empty DATA sub-queue and set *frame_selected* = True, and
iii) whether the number of re-transmission attempts (*no_of_retries*) of a selected frame is within the maximum re-transmission limit (*max_retrans_limit*).

If either of the above arguments are un-successful/false, the process returns to its *inactive* state.

When a frame is selected for transmission, the process checks whether the frame along with its an I-Ack and a guard time can be fit within the end of the current access phase or the allocation interval. If it is a fit, only then the process increments *no_of_retries* and makes a transmission attempt. Additionally, to transmit a Management frame within an EAP1/RAP1 the process follows the CSMA/CA mechanism. If the MPDU follows an I-Ack policy, then, before transmission a copy of the MPDU is made and the I-Ack timer is started. Upon reception of an I-Ack frame within the timeout, the timer will be stopped or else the process makes a re-transmission attempt.

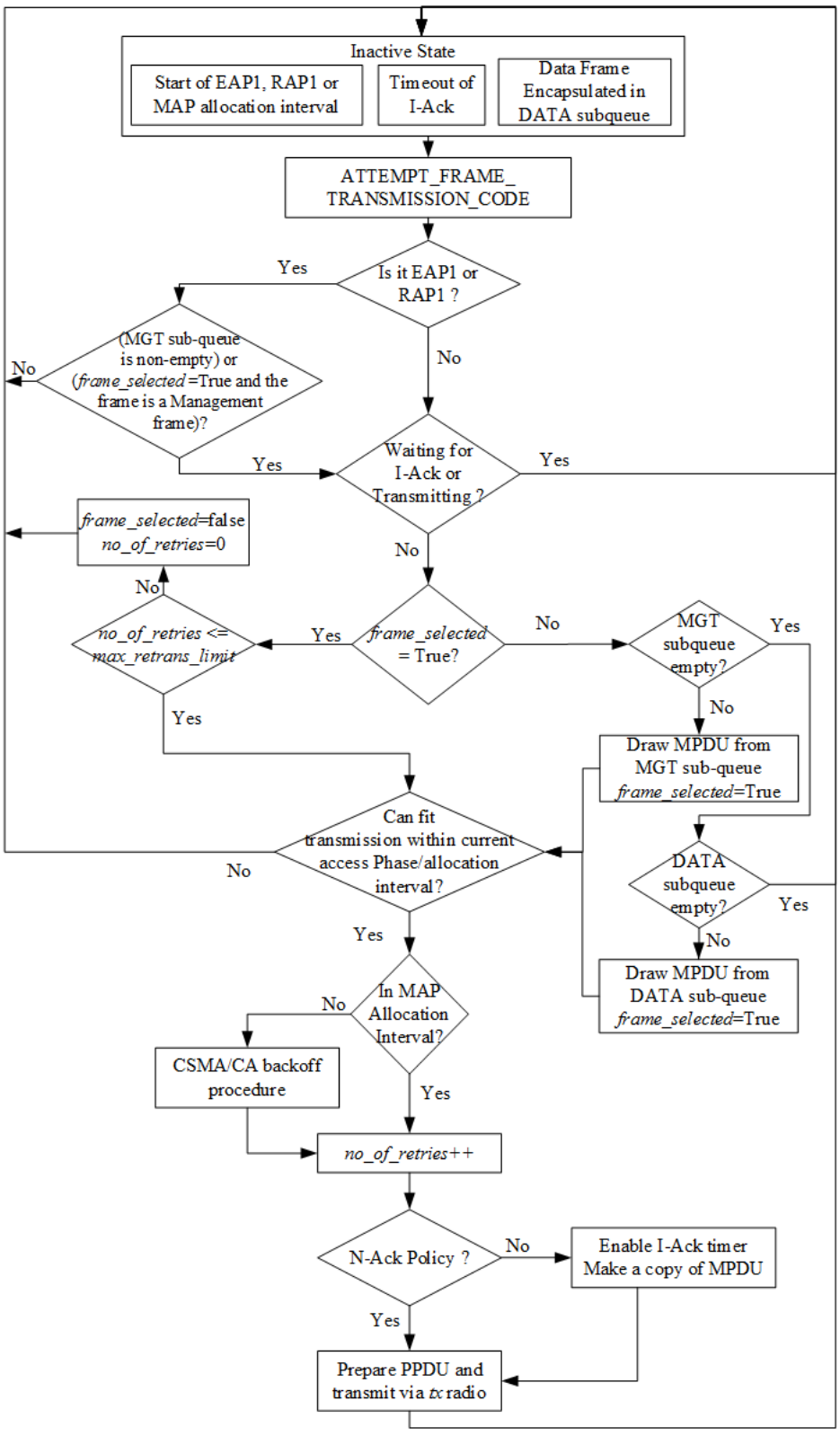

Fig. 3.11 Flowchart illustrating transmission mechanism of *sch_mac*.

3.4.3.6 Model Design of Battery Module

The Battery module is responsible for calculating the total energy consumed by the nodes. Transmission and reception of frames consumes the major energy of a node. In addition, small energy is also consumed when the node is idle while waiting for reception of I-ACK frame. Further, motivated by the need to minimize the energy consumed by the sensor node, we adapt the Low Duty Cycling (LDC) technique envisioned by Marinkovic et al. in [33] and consider the following approach during a SAM session:

i) A sensor node remains active when a frame is serviced. However, when the service of a frame is deferred, the sensors will go to sleep sate (i.e. transceivers are powered down), and wake up prior to the beginning of the upcoming AI. Note that in sleep mode, the Analog to Digital Converters (ADCs) and the internal timers of sensor nodes remain active, which provide the interrupts necessary for wake up.
ii) When the queue of a sensor node becomes empty, it goes to sleep. Following this, it will again wake up prior to the service of the next incoming packet.
iii) The sensor node also wakes up for periodic synchronization with the hub through reception of a beacon. Periodic synchronization is required by the sensor nodes to compensate for their relative clock drifts with respect to the hub [23]. As per IEEE 802.15.6, the sensor node needs to re-synchronize every SI_n superframes termed as the $mNominalSynchInterval$. After re-synchronization the node again goes to sleep.

Based on the above-mentioned LDC approach and the transmission mechanism highlighted earlier, we represent the state of a sensor node during normal data communication (excluding the re-synchronization) by a Finite State Machine (FSM) as shown in Figure 3.12.

The current consumptions of the node during these activities along with the supply voltage are mentioned in the PHY layer Node Attributes as shown in Figure 3.5. Let I_t mA, I_r mA, I_i µA, I_s nA and I_{wup} mA denote the current consumptions of the node when it is transmitting, receiving, idle, sleeping and waking-up/turning-off its transceivers respectively, and let V_s volt denote the voltage supply. The energy dissipation calculation is done by the *energy_comp* state shown in Figure 3.13.

We highlighted earlier that the *Battery* module updates the energy consumption with the help of the ICI packets that are associated with remote interrupts invoked by *sch_mac*. Some of these remote interrupts in turn are dependent on the statistic interrupts from the PHY layer. The ICI contains information about the time duration of transmission or reception. Moreover, these remote interrupts are associated with codes, namely TRANS_CODE to indicate a transmission event and REC_CODE to indicate reception event. The process obtains these codes associated with the remote interrupts, extracts the duration of transmission from the ICI

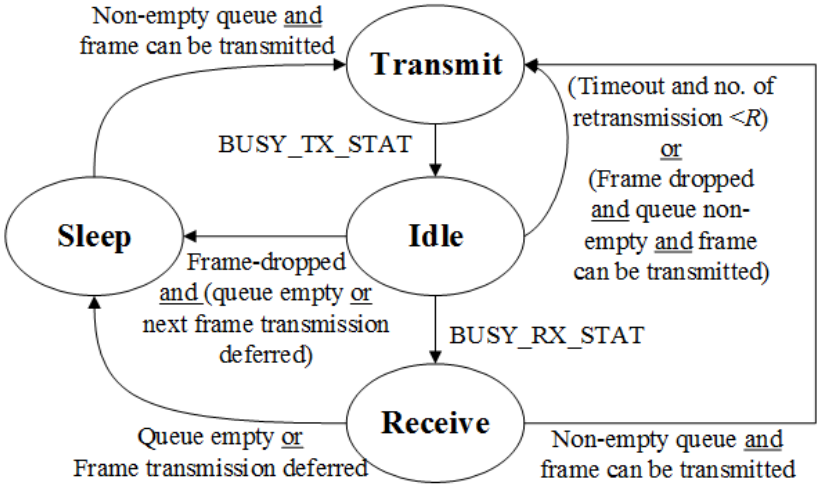

Fig. 3.12 FSM representation of sensor node states during data communication.

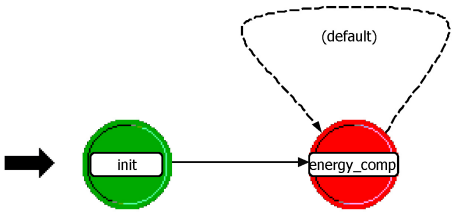

Fig. 3.13 The process model of *Battery* module.

packet, and updates the energy consumed by the sensor node. Let us denote the transmission and reception time by t_{trans} and t_{rec} respectively. So, the energy consumption is evaluated as:

$$E_{trans} = I_t \times 10^{-3} \times t_{trans} \times V_s \tag{3.1}$$

$$E_{rec} = I_r \times 10^{-3} \times t_{rec} \times V_s \tag{3.2}$$

where E_{trans}, E_{rec} denote the energies consumed during transmission, and reception respectively. Note that the E_{rec} calculated in (3.2) is also used for calculating the energy consumed in reception of beacon during re-synchronization.

As shown in Figure 3.12, if the DATA sub-queue of the node becomes empty or there is a frame deferral, the node powers down its transceivers (sleep). Accordingly, the *sc_mac* sends a remote interrupt to the *Battery* module to intimate the start of the sleep state. We use a variable *sleep_start_time* to keep track of the last time this remote interrupt was invoked. A sleep period ends when the sensor node makes the next transmission attempt, and the battery module is intimated using the corresponding remote interrupt. Thereafter, the battery module

computes the energy consumed in sleep mode as,

$$\begin{aligned} E_{sleep} =& I_s \times 10^{-9} \times (current\_time - sleep\_start\_time) \times V_s \\ &+ 2t_{wup}(I_{wup} \times 10^{-6} - I_s \times 10^{-9}) \times V_s \end{aligned} \tag{3.3}$$

Where *current_time* gives the present simulation time when the interrupt associated with the transmission event was invoked. t_{wup} denotes the wake-up time/ turn-off time of the transceivers, and I_{wup} represents the corresponding current consumed.

Following the above approach, we also derive the energy consumed during re-synchronization (except for beacon reception part), where the sensor node wakes-up guard time (GT_n) prior to the reception of the beacon as,

$$\begin{aligned} E_{sync} =& I_s \times 10^{-9} \times (current\_time - sleep\_start\_time) \times V_s \\ &+ I_i \times 10^{-6} \times GT_n \times V_s + 2t_{wup}(I_{wup} \times 10^{-6} - I_s \times 10^{-9}) \times V_s \end{aligned} \tag{3.4}$$

Similar to (3.3), following Figure 3.12, we also calculate the energy consumed (E_{idle}) when the sensor node is waiting idly for reception of I-Ack from the hub as

$$E_{idle} = I_i \times 10^{-6} \times (current\_time - last\_idle\_time) \times V_s \tag{3.5}$$

The variable *last_idle_time* keeps track of the last time the remote interrupt corresponding to the transmission event was invoked and *current_time* gives the present simulation time when the remote interrupt associated with either i) the reception event of an I-Ack, or ii) the next event (as per Figure 3.12) due to I-Ack timeout were invoked. The time interval between these two instants give the idle duration as shown in (3.5). The energies thus computed using (3.1)-(3.5) are updated into a global variable that gives the total energy consumed.

3.4.3.7 Model Design of Sink Module

The sink module is similar to the OPNET provided basic sink module that disposes off serviced packets. Destroying packets that are no longer needed frees up memory to be reused during simulation. Along with this we update a few statistics namely the end-to-end delay of the packets, the number of bits and packets received. In the next Section, we illustrate the variation in these performance metrics with respect to some system parameters and also validate the model functionality.

3.5 Performance Analysis using OPNET Model

The IEEE 802.15.6 SAM is analyzed in this Section by simulating our developed WBAN based on OPNET under ideal channel conditions. An Ideal channel refers to a channel having high SNR (above 25dB). We evaluate the performance in terms of average waiting delay of the frames, the average throughput and energy consumption of the sensor nodes. The performance analysis and analytical modeling of WBAN under low to medium channel SNR scenarios will be performed later in Chapter 5.

The simulations are performed for a WBAN with sensors and hubs communicating in a one-hop star topology as shown in Figure 3.3. At the PHY layer we use QPSK modulation and an information data rate of 971.4kbps for *tx* and *rx* modules. We have performed the simulations for a Electrocardiogram signal having 300 bytes/sec incoming data rate.The system parameters used for simulation [23, 25, 66, 99] are summarized in Table 3.1.

Table 3.1 Simulation parameters

Parameters	**Values**	**Parameters**	**Values**
Slot length, T_S	2ms	PPDU Header	214 bits
Max. retry limit, R	3	Voltage Supply, V_s	3V
sifs	75 μs	Transmit current, I_t	7.5 mA
Guard time, GT_n	120 μs	Receive current, I_r	13.1 mA
Beacon Period, X	250 slots	Idle current, I_i	26 μA
Sync Interval, SI_n	$8X$slots	Sleep current, I_s	900 nA
RAP1 Start	50^{th} slot	Wake-up current, I_{wup}	400 μA
RAP1 End	100^{th} slot	Wake-up time, t_{wup}	1.5ms
MAC Header	7 bytes	Simulation Time	30 min
MAC FCS	2 bytes		

The variations of average frame waiting delay, the energy consumed by the sensor node and the average throughput for the ECG sensor node having payload size (P_{size}) of 150 bytes with respect to different AIs under ideal channel conditions are shown in Figure 3.14. It is noted from Figure 3.14a that with increase in AI, the waiting delay decreases. This is because as the value of AI increases, the deferral probability of a frame and Inter-Allocation Interval (IAI) decreases and the frames are serviced more easily resulting in the lower average waiting delay. We also observe from Figure 3.14b that the energy consumption initially decreases and then gradually increases with increase in AI. For a small AI, the frame service time is more which leads to a lower probability of the queue being empty. This results in frequent frame deferral causing powering down of the transceivers at the beginning of an IAI followed by waking-up prior to the start of the next AI. Due to this reason, the energy

consumption has a higher value at smaller AIs. Also it is observed that at larger values of AI the energy consumption increases with increase in AI length. This is a straightforward impact of the increase in the probability of an empty queue which leads to a rise in the number of transceiver turn-offs after service of a frame. Lastly, in Figure 3.14c we see that the throughput remains unchanged for changes in AI, the value being equal to the incoming data rate. This is to be expected as the outgoing data rate of a stable queue is equal to the incoming data rate.

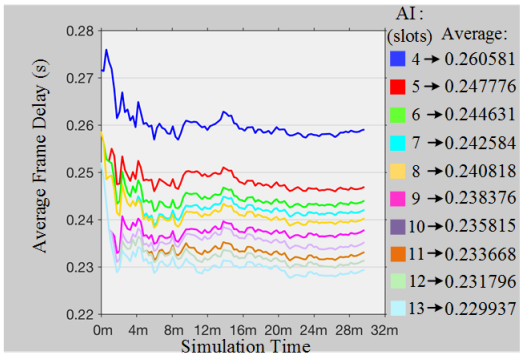

(a) Average frame delay

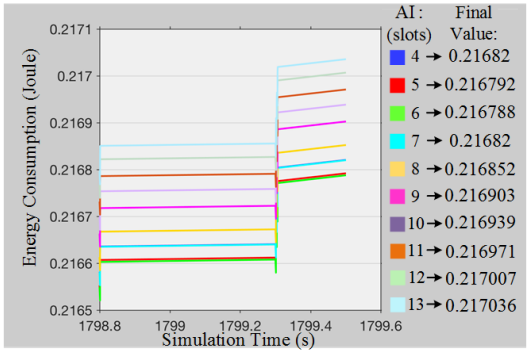

(b) Energy consumption

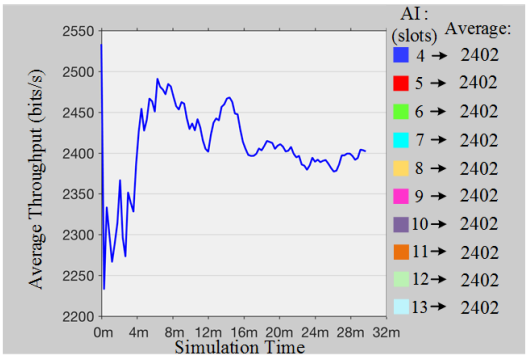

(c) Average throughput

Fig. 3.14 Variation of performance metrics with respect to allocation intervals under ideal channel condition for ECG sensor node @300bytes/s with payload size = 150 bytes.

Next, we present the analysis of average waiting delay, throughput and energy consumption of the sensor node with respect to variations in Payload Sizes (PSs) as shown in Figure 3.15 under ideal channel conditions, while keeping the AI fixed at 11 slots. In this regard, it can be observed from Figure 3.15a that with changes in PS the average value to the delay do not show remarkable variation. This observation can be explained from the inverse relation between PS (P_{size}) and arrival rate (λ), as $P_{size}\,\lambda$ = incoming rate. Elaborating on this, as P_{size} increases λ decreases or viceversa. Figure 3.15b shows the variation of the average

energy consumption of a sensor node with respect to the PSs. We note that for a given AI, the energy consumption of a sensor node is lower for larger PS. With increase in PS, the arrival rate of the packets to the queue (λ) decreases. Since the header size (MAC+PHY) for a transmitted frame is constant, the number of header bit transmission decreases with decrease in frame transmission rate, which is equal to packet arrival rate. This explains the concerned decrease in the energy consumption. Finally, from Figure 3.15c, we remark that under ideal channel conditions, similar to Figure 3.14c, the throughput essentially remains unchanged with variations in PSs.

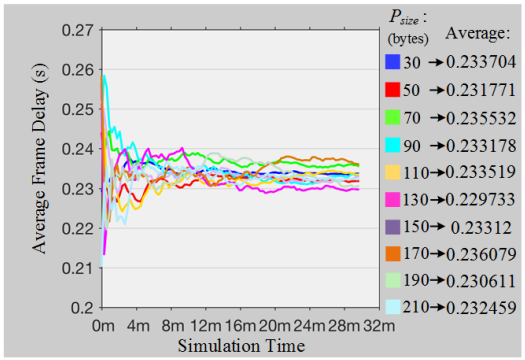

(a) Average frame delay

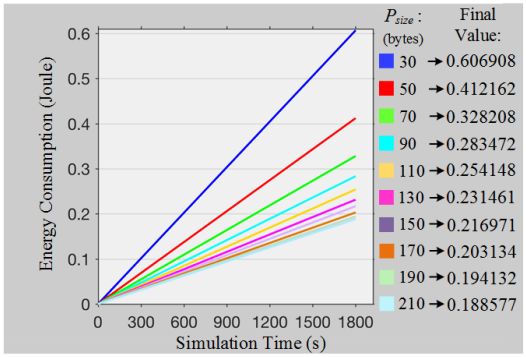

(b) Energy consumption

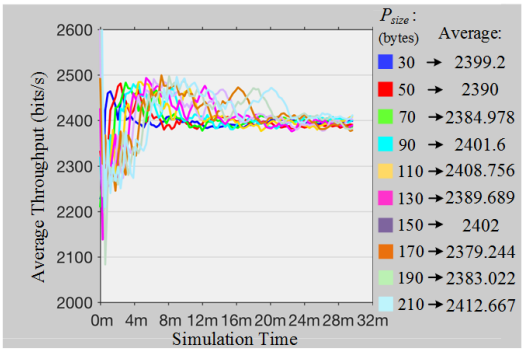

(c) Average throughput

Fig. 3.15 Variation of performance metrics with respect to payload sizes (P_{size}) under ideal channel condition for ECG sensor node @300bytes/s with AI of 11 slots.

Lastly, in Figure 3.16 we validate the implementation and functionality of our designed OPNET simulation model. Figure 3.16c highlights that the hub successfully captures the data transmitted simultaneously by two nodes using scheduled allocations. For illustration, we consider Node-0 transfers Electroencaphalogram (EEG) data @ 500 bytes/s with larger payload size (Figure 3.16a), and Node-1 transfers the ECG data @300 bytes/s data with a

smaller payload size (Figure 3.16b). In this regard, the nodes use allocation intervals of 10 and 7 slots respectively.

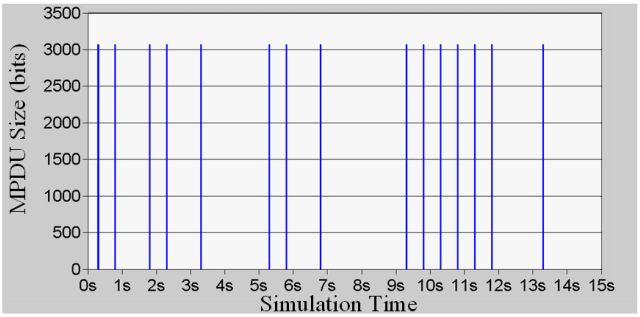

(a) Transmitted Data MPDUs by Node-0

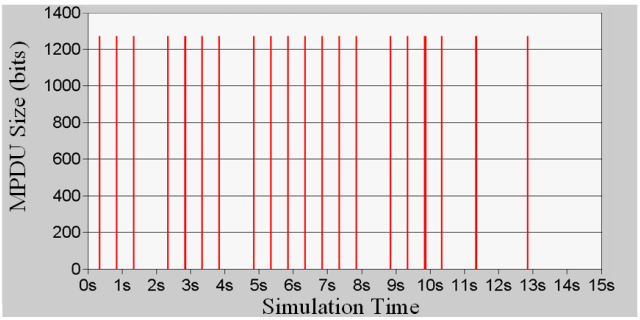

(b) Transmitted Data MPDUs by Node-1

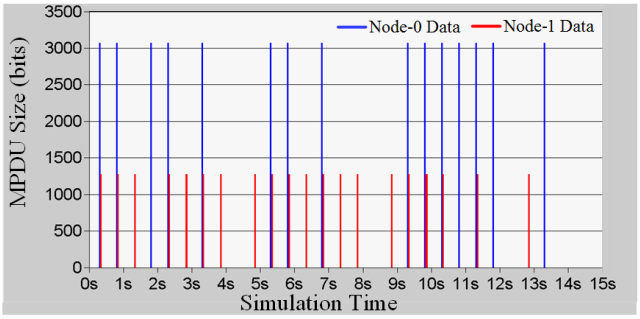

(c) Received Data MPDUs by Hub

Fig. 3.16 Multi-sensor communication in WBAN using scheduled access MAC.

Having designed the simulation model of WBAN based on IEEE 802.15.6 Scheduled Access MAC, the focus now shifts toward implementation of the same in test-bed for e-healthcare. Following which, we leverage our designed simulation model in OPNET to optimize the developed test-bed model performance.

3.6 System Model of WBAN based e-Healthcare System

The WBAN based e-Healthcare system developed here uses a three-tier architecture as shown in Figure 3.17. The first tier known as the *access layer* comprises of the WBAN operating over 433MHz ISM band. At the WBAN, multiple sensors connected to a patient/ human body sense and collect physiological data and transmits them over the 433 MHz band to a BNC. The communication is this layer is short-range communication. The sensor nodes communicate in a star topology, with the BNC acting as the hub that coordinates the sensors in transmitting their data. We use the terms BNC and hub interchangeably with respect to WBAN. In this chapter, we implement, characterize and optimize, first of its kind, the scheduled access MAC protocol as envisioned in IEEE 802.15.6 to control and coordinate the different sensors nodes in the WBAN. The 433 MHz band is selected as – i) it is un-licensed and thus no licensing issues, ii) less penetration loss, and iii) allows high-level integration with radio frequency IC technology leading to smaller size and lower power consumption.

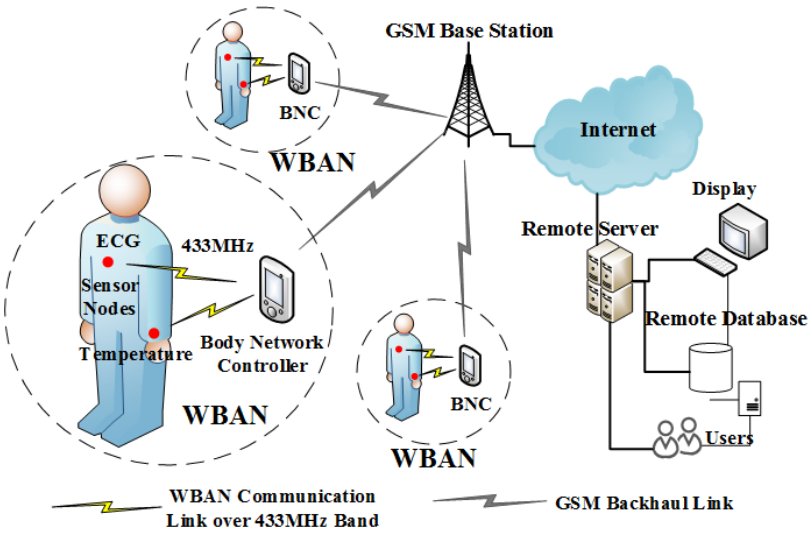

Fig. 3.17 WBAN based e-healthcare architecture.

In this work, we mainly focus on designing WBAN for an e-healthcare application that uses a database to store small portions of real-time WBAN data. To demonstrate the feasibility of just a couple of the several use-case scenarios, we consider monitoring ECG and temperature of a patient with individual sensors. For ECG tracking, we allow the ECG sensor to transmit a 2 second ECG data to the BNC at regular intervals of 2 hours. While for temperature monitoring, only one sample is transmitted every 2 hours. During normal transfer, the sensor nodes employ the LDC technique described in Section 3.4.3.6. After sending the data, the sensors go for hibernation. In hibernation mode, in addition to the

transceivers, the ADCs of the sensor nodes are also powered down. It is worth mentioning that the designed WBAN based on scheduled access MAC can be easily altered to monitor data continuously at the BNC (see Figure 3.29b). A possible scenario can be bed-side monitoring (connecting a PC to BNC) or tracking of ones' vitals in real-time on smartphone (considering BNC as part of a smartphone). This is achieved by disabling the hibernation periods and allowing the sensors to continuously monitor the physiological signals.

After multiplexing data from the sensor nodes, the BNC compresses the signals comprising of several samples of information. In our example scenario, we compress the 2 second ECG signal using our proposed computationally and memory efficient B-DWT algorithm into considerably smaller number of samples, which reduces the energy consumed and cost of data transfer in backhaul transmission. The compressed data stream is also appended with additional header information that facilitates in the reconstruction of the original signal. Hence, after multiplexing and compression, the BNC sends the data to a RS over a TCP/IP Internet connection via a Wide Area Network Base Station (BS). In this work, for transferring the data collected from WBAN to the BS, the BNC uses General Packet Radio Service (GPRS) over a Global System for Mobile Communications (GSM) network operating in 850/900MHz band. This comprises the second tier known as the *convergence layer or backhaul*. The backhaul supports wide area communication, thereby enabling patient mobility.

Lastly, after being forwarded by the BS, the data enters the *service layer*. The BS is connected to the service layer through an Internet gateway. The service layer is application specific. In our design, we intend to capture small amounts of medical data at the RS and store them in a database. The physiological signals which are compressed at the BNC are stored in the database in their compressed form along with their associated header information, thereby saving database storage resources. When the compressed signal needs to be read from the database for further diagnosis, the RS or a user application uses the additional header information to implement inverse DWT to reconstruct the original signal (see Figure 3.30).

3.6.1 Overview of DWT based Data Compression

DWT provides an effective data reduction scheme for non-stationary signals like ECG wave [143]. This is because DWT provides time localization of frequency content of the signal. Since the main information in most of the common non-stationary signals lies at low frequencies, the time localization of these lower frequencies will be more precise. Moreover, the high frequency DWT coefficients are less prominent and can be discarded without any major loss of information.

The major challenge in incorporating DWT at BNC is to make the microcontroller of the BNC perform real-time signal processing in addition to digitization, data storage and communication. It is not a trivial task considering the limited performances of the microcontroller in terms of memory resources and arithmetic power and the algorithmic complexities. We propose a B-DWT algorithm to optimize the DWT through advanced wavelet filters for its calculation by the low-power and low-memory microcontrollers in the BNC. Traditional DWT-based compression algorithm [149] performs several unnecessary arithmetic operations, which implies significant performance penalty. Through our proposed B-DWT algorithm we performed several implementation optimizations for improved execution time and optimal memory utilization, as subsequently explained.

The success of decomposition of a signal into DWT coefficients, followed by compression and then reconstruction to retrieve the original signal depends not only on the level of compression but also on the high-pass and low-pass filters used in sub-band coding [149]. In Section 3.11.3, a comprehensive performance testing of all the major wavelet filters is provided, and depending on the level of compression and the associated permissible information loss, a suitable wavelet filter is selected for the system.

In the following sections, we discuss the design and implementation details of the different components needed to realize the system model as envisioned in Figure 3.17.

3.7 Wireless Sensor Node Design and Data Generation

We design our own sensor nodes that have the capability of capturing the physiological signals with high fidelity and transmit the captured data wirelessly over 433MHz ISM band. The basic block diagram of this design is given in Figure 3.18.

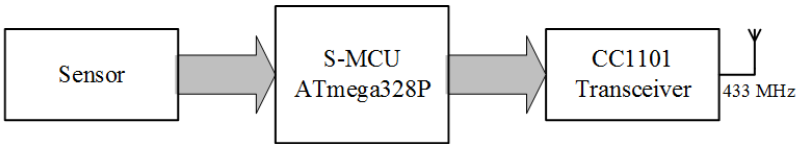

Fig. 3.18 Building blocks of sensor node.

As shown in Figure 3.18, the sensor node comprises of an 8-bit 16MHz ATmega328P Microcontroller Unit (S-MCU) that is interfaced with a sensor and a wireless CC1101 transceiver [150]. The S-MCU is part of an Arduino Uno microcontroller board and has 2KB of SRAM and 1KB of EEPROM [151]. The sensors are application specific. For ECG monitoring we use AD8232 sensor [152], which is an integrated signal conditioning block. It is designed to collect, amplify and filter small bio-potential signals from a human body in the

presence of noisy conditions, such as those created by motion or remote electrode placement. While for temperature monitoring we employ LM35 sensor. Figure 3.19 shows the hardware realizations of the ECG setup, and Figure 3.20 represents the major components of the sensor node through a functional layered diagram with inter-layer coupling. The S-MCU samples the analog data of the signals, digitizes them with the help of the ADC and stores them. The sampling frequencies of various physiological signals are given in Table 3.2 [108]. After obtaining the data, the S-MCU will pack the data into MAC frames called MAC Protocol Data Units (MPDUs) by appending headers. Based on the scheduled access mechanism, the S-MCU will transmit the data to the hub over the 433MHz ISM band using the CC1101 transceivers. The CC1101 wireless chip is selected because of low-power consumption, overall cost saving, small size, fast data transfer and less penetration loss at 433MHz bands. Furthermore, the CC1101 along with its open-source Panstamp library [153] for Arduino gives the flexibility of designing our own MAC protocols. In the following, we elaborate on the sensing and transmission mechanisms in more detail.

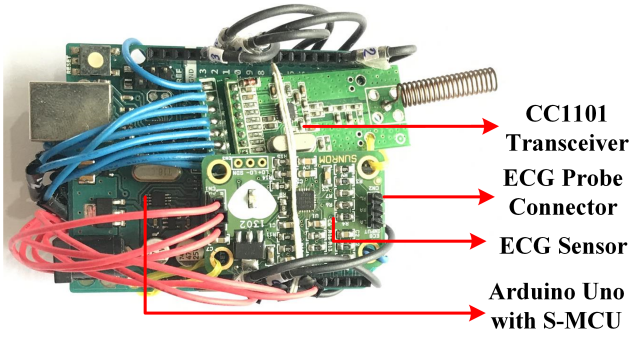

Fig. 3.19 Developed sensor node with ECG sensor.

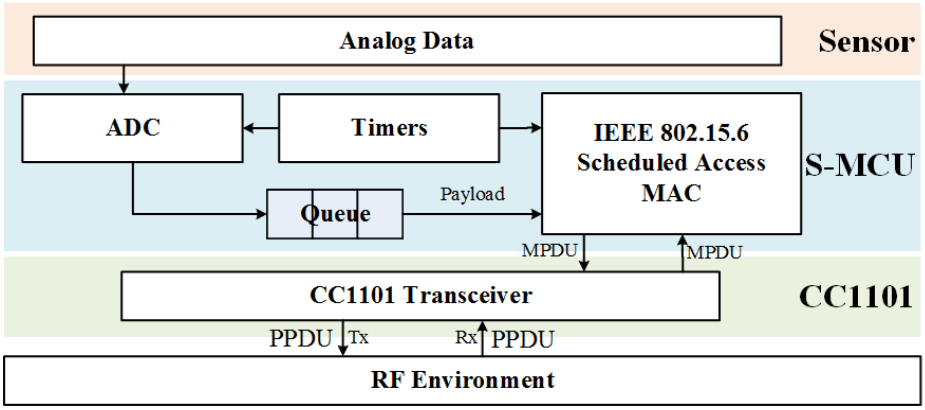

Fig. 3.20 Layered diagram of sensor node with inter-layer coupling.

Table 3.2 Physiological signal frequencies [108]

Data Stream	Signal Frequency (Hz)	Data Stream	Signal Frequency (Hz)
ECG	0.01 - 250	EEG	0.5 - 60
Respiratory Rate	0.1 - 10	Body Temperature	0 - 0.1
Blood Pressure	0 - 50	EMG	10 - 500

3.7.1 Sensing Mechanism

For sensing the physiological signals, the S-MCU takes help of timer interrupts. Atmega328P has 3 timers. Each of the timers has a counter that is incremented on each tick of the timer's clock. In Clear Timer on Compare match (CTC) mode, timer interrupts are triggered when the counter reaches a specified value stored in the compare match register. Once a timer counter reaches this value it will clear on the next tick of the timer's clock, and continue to count up to the compare match value again. We can also set the speed at which the timer increments the counter using a prescaler. Upon setting the compare match value and prescaler, we generate timer interrupts at the required sampling intervals for the signals. When interrupted, S-MCU executes its Interrupt Service Routine (ISR), which triggers the ADC to read the analog value of the signal and enqueues its corresponding digital value in a First-In-First-Out (FIFO) queue. This is shown in Figure 3.20.

3.7.2 Interfacing CC1101 with S-MCU

CC1101 provides extensive hardware support for data buffering, packet handling, burst transmissions, link quality indication and clear channel assessment. The main operating parameters and 64-byte transceiver FIFOs of CC1101 can be controlled via a Serial Peripheral Interface (SPI), where the S-MCU is the "master", while the CC1101 serves as its "slave". We use Panstamp library [153] for Arduino to communicate between S-MCU and the CC1101. More specifically, we implement the CC1101 class contained in the Panstamp library. It provides simple mechanisms to configure the CC1101 registers to operate in 433MHz band and use GFSK modulation scheme. The CC1101 class also allows us to send and receive wireless frames termed as Physical Layer Protocol Data Units (PPDUs). The most interesting methods are the `receiveData` and `sendData`. In order to detect an incoming packet, we configure CC1101 to interrupt the S-MCU Interrupt Pin (INT0). Whenever the INT0 pin of S-MCU goes low, the interrupt is triggered and the S-MCU reads the incoming PPDU stored in the RX FIFO register of CC1101 using the `receiveData` command. While, the `sendData` is a method which enables S-MCU to send a data packet via the CC1101 RF transmitter.

It takes the PPDU to be sent as an argument. Next, we discuss the CC1101 PPDU frame format.

3.7.3 CC1101 PPDU Frame Format

A CC1101 PPDU frame format is configurable and consists of a fixed length preamble, a synchronization (SYNC) word, optional length byte, optional address byte (not used as similar field is in the MPDU), variable length MPDU and an optional 2-byte Cyclic Redundancy Check (CRC) field as shown in Figure 3.21 [150]. The *preamble*, *SYNC word* and *CRC* fields are defined at the registers of CC1101 and are inserted automatically during transmission (Tx) and removed during reception (Rx).

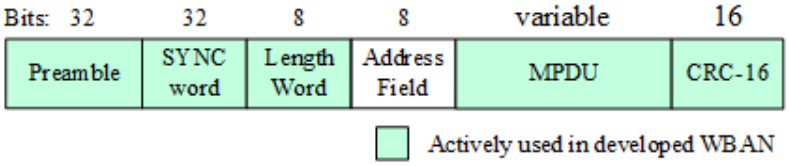

Fig. 3.21 CC1101 PPDU frame format.

We employ a variable packet length mode, where the MPDU length is configured by the first byte after the sync word. The maximum length of MPDU is 60 bytes. This is governed by the CRC capabilities of CC1101. We set the *Length* field to 'MPDU size' bytes. The actual length of CC1101 data buffer is 63 bytes. However, 3 status bytes are inserted within a received PPDU adjacent to its MPDU. These three status bytes contain Received Signal Strength Indicator (RSSI), Link Quality Indicator Values (LQI) and CRC_OK values. In Rx mode, when a sync word is detected, the RSSI value at the RSSI register is inserted in the RSSI byte. *In Chapter 5, we show that a sensor node can exploit this RSSI value to derive the corresponding channel SNR, and thereafter use the same for cognitive adaptation of the AI and PS to maximize its energy-efficiency*. The LQI is a metric of the current quality of the received signal. In CRC auto flush mode, CC1101 will flush the entire Rx FIFO if the CRC check fails and it will set CRC_OK field to '0'.

3.7.4 MPDU Frame Format

The MPDU frame prepared by S-MCU (Figure 3.20) consists of a fixed length MAC header and a variable-length MAC frame body/payload as shown in Figure 3.22 [23]. The payload contains the sensor data. The *Recipient ID* denotes the ID of the recipient of the current frame. The *Sender ID* is set to the ID of the sender of the current frame. The *BAN ID* field is

set to the ID of the BAN in which the current frame is transferred. The *Ack Policy field* is set to I-Ack to indicate the immediate acknowledgment requirement of data, connection request and connection assignment frames. The *Frame Type* and *Frame Subtype* fields indicate the type and sub-type of the current frame respectively according to Table 3.3. It must be pointed out that the *Frame Subtype* field for allocation mapped data is user configurable that we use for representing 15 different physiological signals. If more number of sensors are needed in a WBAN, then we can use the reserved fields in the MPDU. The *Last Frame* field is used to indicate the last frame transmitted in an AI.

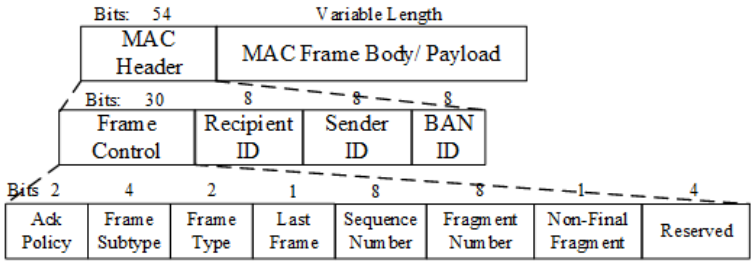

Fig. 3.22 CC1101 MPDU frame format.

Table 3.3 Frame Type and Frame Subtype field encoding [23]

Frame Type value	**Frame Type name**	**Frame Subtype value**	**Frame Subtype name**
00	Management	0000	Beacon
00	Management	1000	Connection Request
00	Management	1001	Connection Assignment
01	Control	0000	I-Ack
10	Data	1000-1111	Allocation Mapped Data

The *Sequence Number* field prevents reception of duplicate MAC Service Data Unit (MSDU) at the receiver. It is denoted with the same value for frames containing fragments of the same MSDU. The *Fragment Number* field in data frames is used to indicate frames containing the fragments of the same MSDU. The *Non-final Fragment* field in data frames is set to one if the frame contains a non-final fragment of a fragmented MSDU.

For example, in case of transfer of a 2s ECG data sampled at 200Hz, a total of 400 integer samples are generated. If we fragment the data stream into 20 data samples (each of 2 bytes), then there will be 20 such 40-byte data payloads. Each of these data payloads constitute an MSDU fragment. Then there will be 20 data fragments having same sequence number but incrementing fragment number. Whereas, the sequence number will be incremented for the next 2s ECG data. These fields play vital roles in multiplexing data from multiple sensor nodes at the BNC and will be discussed in the next section.

3.8 BNC Design with Multiplexing of Multiple Sensors and B-DWT based Compression of Data

We designed a BNC to realize the scenario shown in Figure 3.17. The BNC is developed based on the internal structure as shown in Figure 3.23. The ATmega328P MCU of the BNC (H-MCU) controls the WBAN communication as a hub using CC1101 transceiver. The WBAN communications needs to satisfy QoS constraints as mentioned in IEEE 802.15.6 standard [23]. Therefore, it comes as a straight forward deduction that it is not possible to engage H-MCU in backhaul communication Therefore, we add another MCU comprising of an 8-bit 16MHz ATmega2560 MCU termed as the Client MCU (C-MCU) as shown in Figure 3.23. We will justify the terminology shortly. The C-MCU is part of an Arduino Mega microcontroller board and has 8KB of SRAM and 4KB of EEPROM [154]. The higher specifications of ATmega2560 is needed for 1) queuing data from multiple sensors, 2) handle TCP-IP communications, 3)B-DWT based compression of data such as the ECG samples, and 4) to allow scope for future optimizations with respect to the backhaul communication. For supporting backhaul communication, we have a GSM shield connected to the C-MCU. With the GSM shield, it is possible to leverage the GPRS data communication to access the Internet. The GSM shield is fitted with a Subscriber Identity Module (SIM) card that is used to access a GSM network of a communications provider. Figure 3.24 shows the hardware realization of the BNC. The interfacing of CC1101 with H-MCU is similar to that of the sensor nodes, and thus needs no further mention. However, the interfacing between H-MCU and C-MCU needs an elaborate explanation. Next, we discuss this interfacing, and describe the process of transferring the data collected from multiple sensor nodes to the RS.

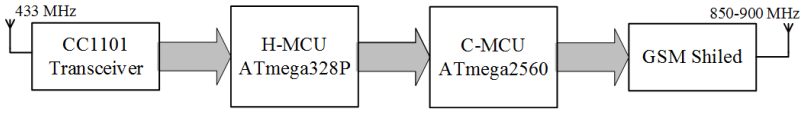

Fig. 3.23 Building blocks of body network controller.

3.8.1 Interfacing H-MCU with C-MCU for Data Multiplexing with B-DWT based compression

The H-MCU communicates with C-MCU via Universal Asynchronous Receiver/ Transmitter (UART) interface. Here, the H-MCU takes bytes of data and transmits the individual bits in a sequential fashion to the C-MCU. Figure 3.25 illustrates the process of transferring and multiplexing the data collected by H-MCU from multiple sensors to the C-MCU. When the

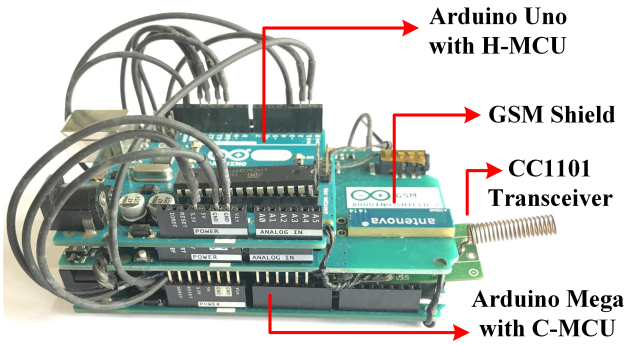

Fig. 3.24 Developed body network controller.

H-MCU receives a data MPDU from a sensor within an AI, it extracts the payload, the *Frame Subtype* (FS) field, the *Non-Final Fragment* (NFF) field and prepares H-MCU packet. It then transfers the H-MCU packet, as shown in Figure 3.25, to the C-MCU over the UART interface. The FS field helps C-MCU decode the signal, while the NFF helps C-MCU identify the final payload of a fragmented MSDU.

Upon detecting a packet over the UART interface, C-MCU parses the incoming integer numbers. The first number of an incoming H-MCU packet corresponds to its size, which helps C-MCU identify the boundaries of the packet. The next field is the *Frame Subtype* field. For our proposed BNC, we employ this field to multiplex data from multiple sensors within a particular WBAN of a patient. To enforce minimal memory utilization, we employ a multiple queue memory management system for the C-MCU. Where one queue corresponds to one particular physiological signal (having distinct Frame Subtype) as shown in Figure 3.25. The *cus_id* field inserted by C-MCU will help the RS identify the patient and efficiently store the data in the database, more on this later. The advantage of the queue management system is that the individual queues are flexible enough to adjust their lengths as per the number of samples within an MSDU (fragmented or non-fragmented) that it stores. This leads to less wastage of memory space, unlike fixed length array. The intelligent nature of the BNC allows the C-MCU to take action when a complete MSDU is received from H-MCU. This is identified from the Non-Final Fragment field (see Figure 3.25). It must be noted, that prior to queuing the data bytes from H-MCU into C-MCU packets, the integer data are re-converted to actual analog floating-point values that were digitized at the ADC of the sensor nodes. Upon reception of a complete MSDU, the BNC is pre-programmed to perform B-DWT data compression on certain signals with particular *Frame Subtype*. The compression status of a signal is indicated by the *dwt_flag* field of C-MCU packet which is set to '1' if a signal is to be compressed, else it is set to '0' . The *dwt_flag* will intimate the RS about the compression status of a received C-MCU packet, which needs to be stored accordingly.

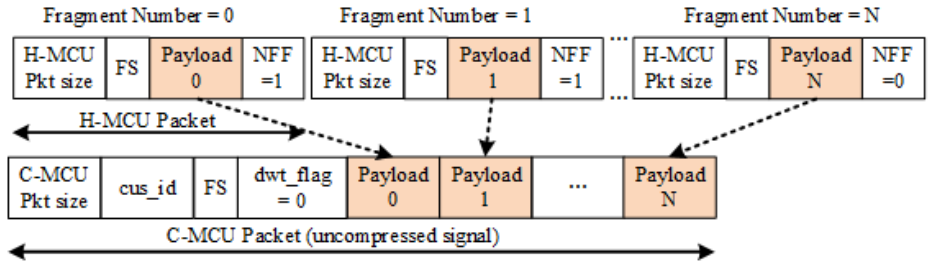

(a) Preperation of uncompressed C-MCU packet

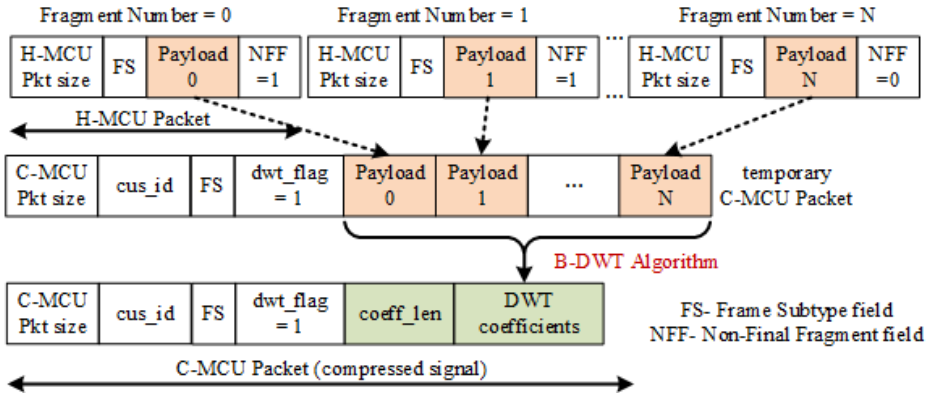

(b) Preperation of compressed C-MCU packet with DWT coefficients

Fig. 3.25 Multiplexing different fragments from sensors with data that requires (a) no compression, (b)B-DWT compression for preparation of C-MCU packets.

In case a signal is to be transmitted in uncompressed form (eg. Temperature values), the resulting C-MCU packet is prepared directly from the H-MCU packets as shown in Figure 3.25a. However, for signals that require compression (eg. ECG samples), prior to preparing the final C-MCU packet with DWT coefficients, the C-MCU prepares a 'temporary C-MCU packet' comprising of all the payloads of the concerned H-MCU packets as illustrated in Figure 3.25b. Thereafter, the C-MCU compresses the original signal using B-DWT to prepare the final C-MCU packet. In addition to the already existing fields, the C-MCU appends an extra field denoted by *coeff_len* ahead of the DWT coefficients. The *coeff_len* denotes the length of different levels of DWT coefficients which will be discussed later in Section 3.10.1. The *coeff_len* field is instrumental in facilitating future reconstruction of signal from the DWT coefficients. The C-MCU packet thus prepared is transferred to the RS using the GSM shield.

3.8.2 TCP/IP Client Server Interaction using GSM Shield

The GSM library for Arduino allows the C-MCU to act as a client and use TCP/IP communication to send data to the RS over the Internet. To connect to the Internet, we provide the GPRS Access Point Name (APN) of the cellular provider. The GPRS APN is the gateway between the cellular network and the Internet. The RS has a known dynamic DNS (DDNS) address, '`server.ddns.net`' and runs a Remote Server Application Program (RSAP), that opens a TCP/IP server socket at port 8080 and listens to incoming client connections.

In our designed WBAN, different sensors send their MSDU to the BNC at regular intervals (in the order of hour). After a complete MSDU is received, compressed (in needed) and packed into a C-MCU packet, it is ready to be transmitted over to the RS. The C-MCU creates a *GPRS_Client* connection to the RSAP socket `@server.ddns.net:8080`. When the connection is accepted by the RSAP, the C-MCU packet is written out and then *GPRS_Client* socket is closed. The C-MCU packet received at the RS is then inserted into a database. A detailed discussion on the database management is given later in Section 3.12.

3.9 Implementation of Scheduled Access MAC

In order to achieve a seamless and reliable communication between different sensor nodes and the BNC, we use the scheduled access mechanism of IEEE 802.15.6. For this, the S-MCU of sensor nodes and H-MCU of BNC needs to handle the following three kinds of operations: i) Superframe generation, ii) Connection Establishment, and iii) Data Transmission/ Reception We now discuss these operations in detail.

3.9.1 Superframe Generation

In our designed WBAN, the sensors and hub operate within the superframe structure as depicted in Figure 3.1. To achieve this, the H-MCU and S-MCU takes help of Timer interrupts, whose ISR pseudo-code is given in Algorithm 3.1.

We maintain a variable *mac_state* that defines the current access phase of the sensor node/hub. A timer interrupt executes the ISR, checks the current *mac_state*, and based on it changes *mac_state* to the value corresponding to next access phase. The ISR also updates the compare match register of the timer to trigger the next interrupt at the end of the current access phase. Additionally, at the beginning of EAP1, the hub broadcasts a Beacon MPDU allowing the sensor nodes to tune their individual timer clocks to the hub's clock and also update the access phase lengths in case of a change.

Algorithm 3.1 Timer interrupt subroutine for superframe generation

```
1:  ISR(TIMER1_COMPA_vect){
2:      switch (mac_state){ // MAC states
3:          case EAP1: //End of EAP1
4:              mac_state = RAP1; //Start of RAP1
5:              set compare match register for interrupt at end of RAP1
6:          break;
7:          case RAP1: //End of RAP1
8:              mac_state = MAP1; //Start of MAP1
9:              set compare match register for interrupt at end of MAP1
10:         break;
11:         case MAP1: //End of MAP1
12:             mac_state = EAP1; //Start of EAP1
13:             set compare match register for interrupt at end of EAP1
14:         break;
15:     {
16: {
```

3.9.2 Connection Establishment

Prior to beginning its transmission, a sensor node must obtain a scheduled allocation from the hub by sending a Connection Request frame within EAP1 or RAP1. The MSDU of Connection Request frame contains the requested AI. If the hub can fit the requested AI within the available MAP barring the already granted allocations, then the hub sends a Connection Assignment frame, informing the acceptance. Note that IEEE 802.15.6 [23] has the provision for both secured and un-secured WBAN session. An implementation of the secured communication is beyond the scope of this chapter, however it will be incorporated in our setup in the future.

For transferring the Connection Request or Connection Assignment frames, the S-MCU and H-MCU uses Tx-if-Clear Channel Assessment (CCA) mechanism of CC1101. The CCA functionality makes use of the Carrier Sense (CS) feature of CC1101. The CS is asserted when the RSSI is above a programmable absolute threshold, and de-asserted when RSSI is below the same threshold. The RSSI threshold value (in dBm) in our setup is set at -91.5dBm based on the CC1101 specification sheet [150]. In Tx-if-CCA mode, before transmission, the CC1101 strobes the Rx, waits 500µs for a valid RSSI, and compares it with the threshold for CS. If CS is asserted, then the channel is busy or else the PPDU loaded in Tx FIFO buffer of CC1101 is transmitted.

After connection establishment, the CCA function of CC1101 for sensor nodes is disabled as sensor nodes do not require CCA for scheduled access. We now discuss the data transmission and reception mechanism in the scheduled AIs.

3.9.3 Data Transmission and Reception

Upon obtaining a scheduled uplink allocation, if the queue of the sensor node is not-empty, then the sensor node can initiate a frame transaction with the hub within its AIs. However, the sensor node will only initiate transmission if the frame transaction and an appropriate guard time fit within the current timer instant and the end of the AI, as shown in Figure 3.26. If the frame cannot be transmitted, it will be deferred till the next AI. A frame transaction comprises of the sensor node transmitting a CC1101 PPDU and waiting for a corresponding Immediate Acknowledgment frame (I-Ack) from the hub, separated by a Short Inter-Frame Spacing (SIFS). If an I-Ack is not received within the expected time, the node resends the data frame. The maximum number of such resends is denoted by R. The I-Ack timeout is detected by enabling another timer, termed I-Ack timer, within the sensor node. The timeout is set to the time required to transmit an I-Ack frame plus the SIFS period. In this regard, the superframe parameters, frame lengths and other system parameters are given in Table 3.4.

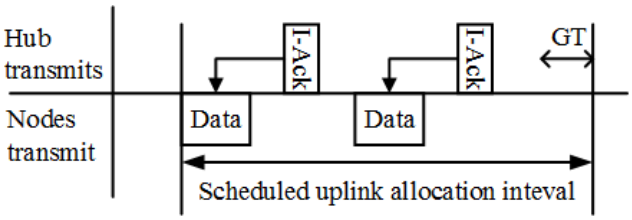

Fig. 3.26 Frame transactions in scheduled uplink allocations.

Upon reception of a PPDU at the hub, the H-MCU examines its CRC_OK status bit. If the CRC check fails, then the hub discards the received frame. Upon timeout, the sensor node will retransmit the frame. However, if the PPDU passes the CRC check, then the MPDU will be extracted. Next, we check if the MPDU is actually meant for the sensor node by comparing the *BAN ID*, *Sender ID* and *Recipient ID* present in the MPDU header (Figure 3.22) respectively with the *BAN ID*, *Recipient ID* of the expected sensor node and hub ID. H-MCU also checks for a duplicate frame using the *Sequence Number* and *Fragment Number* fields of the MPDU. Upon successfully filtering the incoming PPDU, the sensor data is handled by H-MCU and sent to C-MCU, as described in Section 3.8.1. In response to the successful filtering of the received MPDU, H-MCU prepares the corresponding I-Ack frame by setting its *Recipient ID* field to the sensor node ID, *Sender ID* field to the hub ID

and *Sequence Number* and *Fragment Number* to that of the received MPDU frame. Upon successfully receiving the I-Ack frame, the sensor node loads the TX FIFO of its CC1101 with the next data PPDU to be sent.

In order to prolong the battery life of sensor nodes, the following techniques are adapted-

i) During normal uplink data transfer, we follow the LDC technique of Section 3.4.3.6, and
ii) after completion of the transmission of an MSDU and all fragments thereof, S-MCU puts sensor node to hibernation state.

In either of the modes, when the CC1101 transceiver is powered down, the power and crystal oscillator of CC1101 are turned off. Again, when the sensor node wakes up, S-MCU selects the CC1101 chip to wake it from the inactive state.

3.10 Implementation of B-DWT for Data Compression

DWT, in practice, employs wavelet filters comprising of a pair of finite half-band low and high pass filters [149]. Let us assume that the impulse response of these FIR filters be represented by $H_d[n]$ and $L_d[n]$ respectively, and the length of these filters be denoted by K. The procedure starts with passing the input sequence $x[n]$ comprising of N samples through $H_d[n]$ and $L_d[n]$ simultaneously, which doubles the frequency resolution. As per Nyquist theorem, half the samples now become redundant and hence are removed through down sampling by 2. The down sampling process reduces the time-resolution by half. The output of $H_d[n]$ followed by the down sampling, known as *Detail Coefficients*, comprises the first level of DWT coefficients. Whereas, the output of $L_d[n]$ after down sampling, called *Approximation Coefficients*, is again subjected to filtering through $H_d[n]$ and $L_d[n]$ with subsequent sub-sampling, and the process continues until L levels of decomposition are performed. We now introduce our proposed B-DWT.

3.10.1 Proposed B-DWT Algorithm

For the proposed B-DWT algorithm, we employ the analysis of moving average filters [147], that allows us to mathematically express the DWT process as,

$$y_{high}[n] = \sum_{t=0}^{K-1} (H_d[t]x[2n-t]) \tag{3.6}$$

$$y_{low}[n] = \sum_{t=0}^{K-1} (L_d[t]x[2n-t]) \tag{3.7}$$

Where, $y_{high}[n]$ and $y_{low}[n]$ are the outputs of the high-pass and low-pass filters after sub-sampling by 2. By intelligently exploiting (3.6) and (3.7), our proposed B-DWT can provide improvement in execution speed by effectively reducing the number of arithmetic operations. Additionally, B-DWT intelligently utilizes the C-MCU memory allocated for storing input signal to hold the output data that will be utilized in the calculation of DWT coefficients of subsequent levels. This saves memory space in the resource constrained C-MCU which can now be more efficiently utilized. The psedo-code of B-DWT is provided in Algorithm 3.2.

At the beginning of the B-DWT algorithm, initialization of all the variables is performed. tot_dwt_len denotes the length of the L level DWT of the input signal $x[n]$ without any compression, and it can be obtained mathematically. $y[n]$ is the set of yet to be attained DWT coefficients. M keeps track of the length of the input signal at each filtering stage. $start\_ind$ and end_ind marks the beginning and end of the location in $y[n]$ where the DWT coefficients at each stage are to be inserted. As discussed previously, in DWT based compression, the first level of high frequency DWT coefficients of length $\lfloor (N+K-1)/2 \rfloor$ are generally discarded. Therefore, in order to save memory space of C-MCU and reduce execution time, the length of $y[n]$ is reduced as in (line: 4 of Algorithm 3.2). Thereafter, in the *for* loop of (line 8 of Algorithm 3.2) the detail and approximation coefficients are obtained from sub-loops in (lines: 10 and 21 of Algorithm 3.2) respectively. Note that, an advantage in terms of less number of computations can be gained from (lines: 12 and 22 of Algorithm 3.2) which essentially performs the down sampling but prior to the filtering process. More specifically, at each filtering stage the proposed B-DWT technique uses $(L-1)(L+M-2)/2$ number of additions and $L(L+M-1)/2$ multiplications. Whereas, normal DWT implementation takes $(L-1)(L+2M-1)/2$ number of additions and $L(L+2M-1)/2$ multiplications to get the same result. Hence, at each filtering stage B-DWT requires almost half the number of computations as compared to normal DWT, thereby drastically reducing the execution time. After evaluating the DWT coefficients at a particular level, the final stage of the B-DWT pertains to the utilization of the approximation coefficients for the next level. Since, we opt to enforce minimal memory utilization, the *for* loop of (line 30 of Algorithm 3.2) aptly overwrites the input signal at $x[n]$ with the approximation coefficients. Thereafter, M, $start\_ind$ and end_ind are updated before proceeding to the next level. Finally, after the computation of L levels of DWT, depending on the required degree of compression, the output signal of length C is generated from $y[n]$ in (line 36 of Algorithm 3.2). Lastly, the length of each of the L levels of DWT coefficients and the actual input signal length N are updated in $coeff\_len$ field of C-MCU packet (Figure 3.25).

Algorithm 3.2 Computation of DWT Coefficients by B-DWT Algorithm

Initialization

tot_dwt_len=length of dwt output;
N= length of input signal, K=length of filter, C=length of compressed signal;
$x[0:N-1]$=input signal, $x[N:N+K-2]=0$;
$y[0:tot\_dwt\_len-\lfloor(N+K-1)/2\rfloor-1]=\{0\}$;
$H_d[0:K-1]$=High pass filter coefficients;
$L_d[0:K-1]$=Low pass filter coefficients;
$M=N$, $end\_ind=tot\_dwt\_len$, $start\_ind=0$, $k=0$, $i=0$, $j=0$;
for $j=1:L$ **do**
    $start\_ind=end\_ind-\lfloor(M+K-1)/2\rfloor$;

Calculation of Detail Coefficients

    for $k=0:\lfloor(M+K-1)/2\rfloor-1$ **do**
        if $j>2$ **then**
            $i=2k+1$;
            if $i<(K-1)$ **then**
                $y[start\_ind+k]=\sum_{t=0}^{i}H_d[t]\times x[i-t]$;
            else
                $y[start\_ind+k]=\sum_{t=0}^{K-1}H_d[t]\times x[K-1-i]$;
            end if
        end if
    end for
    $end\_ind=start\_ind$;

Calculation of Approximation Coefficients

    for $k=0:\lfloor(M+K-1)/2\rfloor-1$ **do**
        $i=2k+1$;
        if $i<K-1$ **then**
            $y[k]=\sum_{t=0}^{i}L_d[t]\times x[i-t]$;
        else
            $y[k]=\sum_{t=0}^{K-1}L_d[t]\times x[K-1-t]$;
        end if
    end for
    if $j<L$ **then**
        for $k=0:\lfloor(M+K-1)/2\rfloor-1$ **do**
            $x[k]=y[k]$;
        end for
    end if
    $M=\lfloor(M+K-1)/2\rfloor$;
end for
output_signal = $y[0:C-1]$, where $C\leq\lfloor(N+K-1)/2\rfloor$;

3.11 Performance Evaluation and Optimization of Developed WBAN Setup

In this section, we analyze the performance of our designed WBAN access layer. For this, we exploit our simulation model for WBAN in OPNET simulator [95] based on the scheduled access mechanism of IEEE 802.15.6 MAC protocol. The requirements stated in [23] mention an operating range of 3m for WBANs. At this distance, we were not able to record any CRC error for the received frames. We, therefore, consider an ideal channel for our OPNET model, and analyze the system performance metrics namely, average frame delay and energy consumption of the sensor nodes. Recollect that, in Section 3.5, it was observed that the throughput remained essentially constant with respect to changes in allocation intervals and payload sizes, hence we skip throughput analysis in this section.

Through performance analysis, we also choose the appropriate system parameters. We determine the AIs to maximize network capacity while maintaining a frame delay constraint, and also select a payload size to achieve minimum energy consumption (i.e. maximum energy-efficiency) of sensor nodes. Network capacity is defined as the number of sensors that can be accommodated within the MAP for scheduled access. The AIs assigned to the sensors play a significant role in determining the network capacity. More AIs assigned to a particular sensor node means less number of AIs left for other nodes, and thus lowers network capacity. Since the variation of energy consumption of sensor nodes with AIs is not significant under ideal channel conditions, as observed in Figure 3.14b, we neglect this effect in our optimization. However, this effect will be studied later in great detail in Chapter 5 under non-ideal channel conditions .

This section also deals with the analysis of the proposed B-DWT based compression of ECG signal samples generated by AD8232 sensor. Then, it reports the most suitable wavelet filter to achieve optimal compression within acceptable information loss. Finally, we provide some real test-bed results pertaining to implementation of B-DWT in C-MCU to establish its superior real-time performance with respect to normal DWT process.

3.11.1 Performance Analysis of WBAN Communication

We evaluate the performance of our setup in terms of the afore-mentioned metrics through simulations in our OPNET model. For simulation, the parameters followed are same as the hardware setup. The complete list of system parameters is given in Table 3.4. The transceiver specific parameters of CC1101 are obtained from its data-sheet [150]. The OPNET model is designed based on a slotted time-reference, with each slot equivalent to 2ms. Accordingly,

we refer to superframe parameters in terms of time-slots. However, for building our hardware setup, we implement the equivalent times in floating point variables.

Table 3.4 System parameters

Parameters	**Values**	**Parameters**	**Values**
Data Rate	38.4kbps	Voltage Supply, V_s	3V
SIFS	75 μs	Transmit Current	16 mA
Guard Time, GT	120 μs	Receive Current	15 mA
Beacon Period	0.5s	Idle Current	1. 7mA
EAP1 Length	0.05s	Sleep Current	0.2 μA
RAP1 Length	0.05s	Wake-up Current	240 μA
MAP Length	0.4s	Wake-up Time	1.5 ms

As highlighted in Section 3.6, we tested our hardware model for ECG and temperature monitoring. The monitoring of ECG signal is more complicated as compared to temperature. Unlike temperature (0.1 sample/s), sending an ECG signal requires continual and undisturbed sampling period of 200 samples/s or 400 bytes/s. Therefore, performance analysis for ECG sensor node needs special attention. We run the simulations in OPNET for 5mins in case of ECG and 2 hours in case of temperature, where the nodes generate data continuously without any sleep interval during the simulation run. This helps us get accurate average values for the performance metrics.

The nodes generate traffic with constant traffic distribution. In case of ECG sensing, for a selected payload size (of a single fragment) of P_{size} bytes/packet, the arrival rate (λ) is obtained as

$$\lambda = \frac{400}{P_{size}} \text{packets/s} \tag{3.8}$$

Figure 3.27 shows the variation of average frame delay for ECG monitoring with respect to the size of the payloads for different AIs. It must be noted, that the CC1101 PPDU frame format limits the maximum payload size to 52 bytes. In this figure, it can be observed that as the AI increases, delay decreases. For larger AIs, the event of deferral of frame transmissions decreases. Less deferral corresponds to less waiting delay for the frames in the queue. This leads to the perception that higher AIs are better for the system. However, as we increase the AI, the network capacity also decreases. Hence, we select an AI that just satisfies the maximum frame delay constraint. For our setup, we consider a delay constraint of 150ms [23]. From Figure 3.27, we can observe that an AI of 90 slots (0.18s) satisfies this delay constraint. It is also observed that for a fixed AI, variation in moderate payload sizes does not affect frame delay significantly. Larger payloads lead to more deferrals, but reduced packet arrival rates tend to balance that effect. Thus, the queue length and waiting delay does not

vary much with changes in payload size. However, very small payload sizes (< 20 slots) lead to high frame delay due to high packet arrival rate as per (3.8). A high packet arrival rate will cause buffer overflow and thus packet loss and high delay.

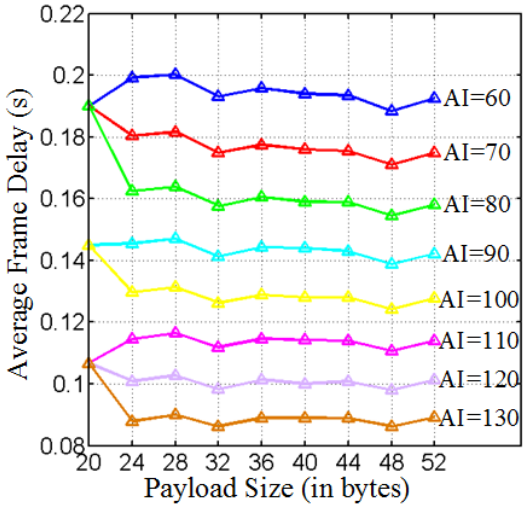

Fig. 3.27 Variation of average frame delay with respect to payload size of ECG transmission within WBAN for different Allocation Intervals (AI) in 2ms slots.

We illustrate the variation of total energy consumption of the ECG node transceiver with respect to the payload sizes in Figure 3.28. It is observed that as payload size increases, the energy consumption decreases. This is similar to the observations of Figure 3.15b. Therefore, we remark that higher payload size leads to more energy-efficient transmissions. Hence, we consider a payload size of 52 bytes for ECG node.

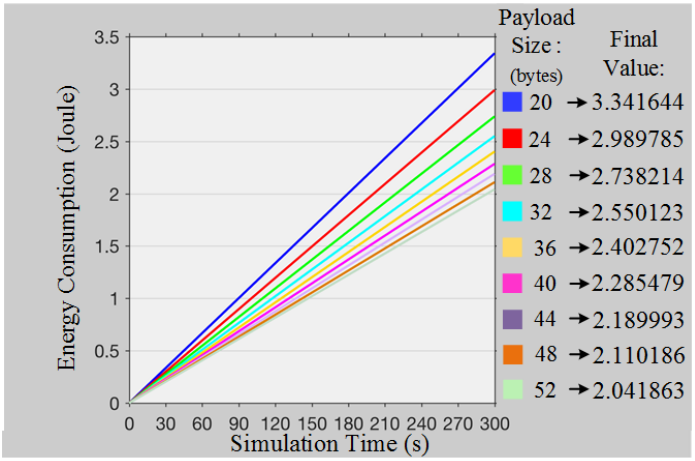

Fig. 3.28 Variation of energy consumption for continuous transmission by ECG node for varied payload sizes.

Compared to ECG, modeling temperature monitoring is much simpler. Only one 2-byte sample needs to be transmitted every sleep interval. So, determining a payload size is not required. As for AI, we performed a delay analysis in OPNET and determined 5 slots (0.01s) as the AI length for temperature monitoring.

Likewise, the WBAN sensor nodes in our setup have been tuned to the optimal AIs and payload sizes. To validate the functionality and capability of the scheduled access mode in providing real-time tracking of physiological parameters, the H-MCU was directly monitored via a serial monitoring tool. As shown in some exemplifying screenshots in Figure 3.29, the hub arranges the superframe structure as highlighted in Figure 3.1, the sensor nodes efficiently transmit the frames in their AIs and we obtain both ECG and temperature data simultaneously at the monitoring tool. Note that, in order to get a continuous monitoring graph, the ECG is sampled continuous and the temperature is sent in every superframe without sleep intervals. The continuous simultaneous monitoring of ECG and temperature is further elaborated through a video demonstration [1].

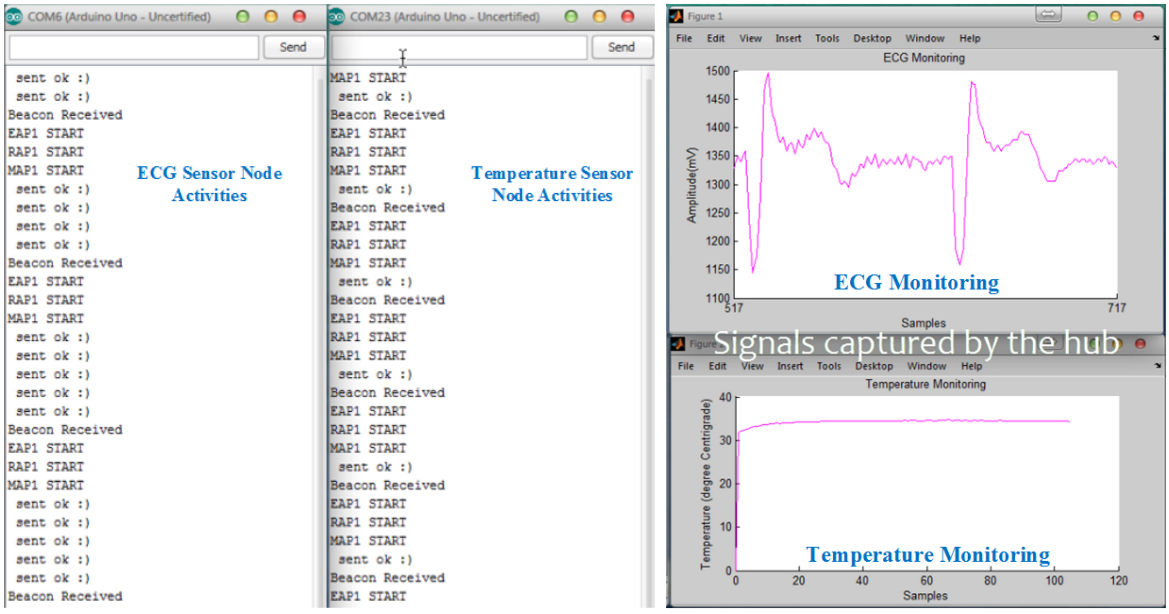

(a) (b)

Fig. 3.29 Snapshot: (a) Simultaneous activities of ECG and temperature nodes, (b) Simultaneous monitoring of continuous ECG and temperature at hub.

[1] Video@ https://www.dropbox.com/s/tb6guwr0ha0bsc2/SAM_Demo.mp4?dl=0.

3.11.2 Performance Metrics for DWT Analysis

The two metrics that are commonly used to measure the performance of DWT analysis are [146],

i) *Percentage Root Mean Difference (PRD)* to measure distortion between the original signal and the reconstructed signal. Mathematically,

$$PRD = \sqrt{\frac{\sum_{n=1}^{N} (x[n] - \hat{x}[n])^2}{\sum_{n=1}^{N} (x[n])^2}} \times 100\% \tag{3.9}$$

ii) *Compression Ratio or Compressed Data Ratio (CDR)*, defined as the ratio of the number of bits representing the original signal to the number of bits required to store the compressed signal. Mathematically,

$$CDR = \frac{B_{original}}{B_{compressed}} \tag{3.10}$$

Where, $B_{original}$ and $B_{compressed}$ are the bit rates of the original and compressed signals respectively.

3.11.3 Peformance Analysis of proposed B-DWT

Table 3.5 compares the output PRD and CDR averaged over the 400 sample ECG signal for B-DWT performed using different DWT filters over 5 levels (i.e. $L = 5$). With increasing compression, the CDR improves, however the PRD also increases. This is expected because more compression means discarding more number of DWT coefficients, which results in eliminating increased number of coefficients at lower frequency levels containing significant meaningful information. Therefore, a tradeoff is required between the desired level of compression (CDR) and the acceptable PRD.

The relationship between the measured PRD and the diagnostic distortion is established based on the work of Zigel et al. on the weighted diagnostic measure for ECG signal compression [155], which classifies the different values of PRD based on the signal quality perceived by a specialist. Table 3.6 reports the resulting different quality classes and corresponding PRD. A filter is selected which provides an acceptable PRD with the maximum amount of compression. *Biorthogonal 4.4 filter* produces the best results for B-DWT. A "very good" signal reconstruction quality (corresponding to PRD below 2%, see Table 3.6) can be reached for CDRs up to 3.03. Finally, it is worthwhile mentioning that the used metric, PRD may

Table 3.5 CDR and PRD at different levels of DWT for varied wavelet filters

Wavelet Family	**Wavelets**	**Level-1**		**Level-2**		**Level-3**		**Level-4**		**Level-5**	
		CDR	PRD	CDR	PRD	CDR	PRD	CDR	PRD	CDR	PRD
Biorthogonal	bior1.1	15.38	4.56	7.84	3.79	3.96	3.07	1.99	1.97	1	0
	bior1.3	11.76	4.66	6.35	3.97	3.42	2.40	1.82	2.00	0.95	0
	bior2.2	11.76	5.06	6.35	2.92	3.42	2.03	1.82	1.12	0.95	0
	bior2.4	9.52	4.24	5.33	3.41	3.03	1.76	1.68	1.11	0.90	0
	bior3.1	13.33	6.20	7.02	3.97	3.67	2.27	1.90	0.69	0.97	0
	bior4.4	9.52	4.25	5.33	3.40	**3.03**	**1.68**	1.68	0.94	0.90	0
Reverse Biorthogonal	rbio1.1	15.38	4.56	7.84	3.79	3.96	3.07	1.99	1.96	1.0	0
	rbio1.3	11.76	4.36	6.35	3.49	3.42	1.79	1.82	1.51	0.95	0
	rbio1.5	9.52	4.41	5.33	3.46	3.03	2.58	1.68	1.39	0.90	0
	rbio2.2	11.76	4.59	6.35	3.31	3.42	2.68	1.82	1.47	0.95	0
	rbio2.6	8.00	4.35	4.60	3.60	2.70	2.52	1.56	0.94	0.86	0
	rbio3.1	13.33	14.75	7.02	9.79	3.67	6.95	1.90	2.27	0.97	0
	rbio3.5	8.70	4.55	4.94	3.60	2.86	2.61	1.61	0.54	0.88	0
Daubechies	db1	15.38	4.56	7.84	3.79	3.96	3.07	1.99	1.96	1.0	0
	db4	10.53	4.20	5.80	3.53	3.20	2.36	1.74	0.61	0.92	0
Coiflets	coif1	11.76	4.47	6.35	2.89	3.42	2.26	1.82	1.31	0.95	0
	coif2	8.70	4.29	4.94	3.51	2.86	2.64	1.61	1.04	0.88	0
	coif3	7.14	4.37	4.17	3.51	2.50	2.41	1.47	0.95	0.83	0
	coif4	5.88	4.39	3.51	3.71	2.17	2.45	1.33	0.90	0.78	0
Symlets	sym2	13.33	5.14	7.02	3.78	3.67	1.86	1.90	1.31	0.97	0
	sym4	10.53	4.24	5.80	3.18	3.20	2.46	1.74	1.22	0.92	0

not always reflect the reconstruction quality. Hence, Figure 3.30 is plotted to illustrate that the proposed B-DWT algorithm produces acceptable signal after signal reconstruction. As evident from Figure 3.30b the last 310 DWT coefficients are insignificant and hence omitted. From Figure 3.30c it can be easily seen that transmitting only the first 132 DWT coefficients (3.03 CDR or 67% compression) followed by signal reconstruction preserves the original signal information. Interestingly, the reconstructed signal does not contain the high frequency noise and is smoother than the original signal in Figure 3.30a. Consequently, while incurring no significant information loss, B-DWT could efficiently provide three-fold energy and cost saving in transmission over long distance backhaul link and thus making our e-healthcare architecture more energy-efficient and cost effective.

Table 3.6 PRD and corresponding quality class [155]

PRD	**Reconstructed Signal Quality**
0∼2%	"Very good" quality
2∼9 %	"Very good" or "good" quality
$\geq$ 9 %	Not possible to determine the quality group

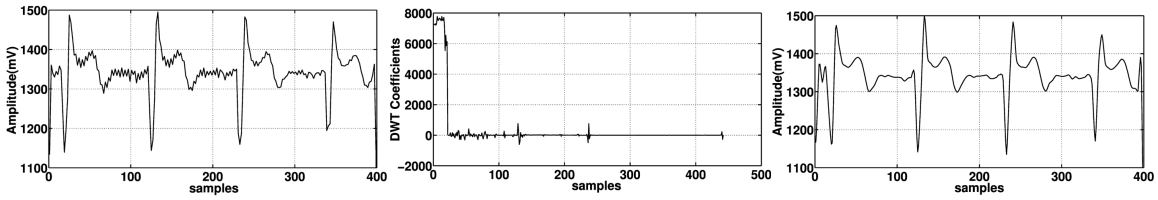

(a) Original ECG (b) DWT coefficients (c) Reconstructed ECG

Fig. 3.30 (a) 2s ECG signal captured by AD8232 sensor, (b) DWT signal compressed using Bior.4.4 filter, (c) Reconstructed signal from 1st 132 DWT coeff.

3.12 Remote Server and Database

In this section, the implementation of the Remote Server (RS) and the development of a database to store the captured data is described. For the RS, we have used MATLAB TCP server framework. As highlighted previously, the RS receives the C-MCU packets from the BNC. The RS is further configured to insert the data into a database called Remote DB in a formatted manner as illustrated in Figure 3.31. As seen in Figure 3.31, the database maintains separate Microsoft Excel files (*.xlsx*) for each patient and names them according to their Customer IDs. Each *.xlsx* file has separate worksheets for storing records of different physiological signals in chronological order of the time the data were collected. The time of the data collection is registered by the RS. To achieve this structured and sorted Remote DB, the RS exploits the header information contained with C-MCU packets. More specifically, the *cus_id* helps in selecting the *.xlsx* file, the *Frame Subtype* field allows to identify the worksheet, and the *dwt_flag* field facilitates in identifying whether the data contained in the C-MCU packet is compressed. If *dwt_flaq*=1 (as in in case of ECG), the corresponding DWT coefficients are stored along with the contents of the *coeff_len* field of C-MCU packet. As shown in Figure 3.31, for a single record of ECG monitoring we store the all the 132 DWT coefficients preceded by the *coeff_len*, values, while for temperature only a single value (uncompressed) is stored. In must be highlighted that, instead of storing all the 400 samples

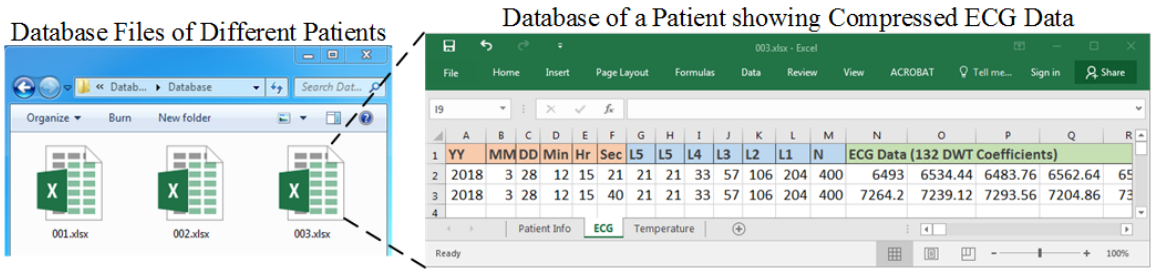

Fig. 3.31 Snapshot of remote database.

of a 2s ECG signal, B-DWT allows Remote DB to store the same signal in terms of 132 DWT coefficients and seven *coeff_len* values leading to a significant 65.25% reduction in database storage utilization.

The presence of this database decouples the process of data collection and analysis/visualization. The latter can be achieved with the help of different automated data analytics tools such as Microsoft Power BI. Therefore, doctors and other operators do not need to directly query the database for information. A detailed discussion of the data analytics tool is beyond the scope of this work. However, it is worth to mention that the different analytics tools will not only help in visualizing the received data and deliver deeper insights into a patient's conditions, but also enable integration of the system to cloud and web services. This will further enable other services like bringing the data into mobile handsets, and therefore, provide ubiquitous access to the patient's information stored in the database. Moreover, the healthcare service providers can also leverage on Cloud messaging services like Google Cloud Messages (GCM) to send Push Notifications to the mobile devices of medical staff in case of an emergency.

3.13 Conclusion

In this chapter, we have designed a simulation model in OPNET Modeler for a WBAN as per the IEEE 802.15.6 standard focused towards its scheduled access mechanism. For this, the network model, the node model and the process model are designed and realized. We provide the detailed interrupt-based design of the process model of the MAC of sensor nodes and hub. More specifically, we implemented the superframe generation, frame transmission, connection establishment and energy computation mechanisms of the scheduled access mode. Further, we study the performance in terms of variation of average frame delay, throughput and energy consumption of the sensor nodes with respect to system parameters like traffic loads and allocation intervals. The results obtained reflect efficient simulation design with sufficient credibility. Thus, the model established in this chapter can be used in future research work like validation of derived analytical models, performance analysis of WBAN setups, followed by suitable optimizations.

In this chapter, we also present a WBAN that can be used to remotely monitor and store multiple physiological signals of patients. For this, we implement, first of its kind, schedule access mechanism of IEEE 802.15.6 to monitor ECG and temperature simultaneously. In this regard, detailed hardware implementation involving interfacing of MCU of sensor nodes with CC1101 low power transceiver is discussed. We also remark that, in Chpater 5 we enable the sensor node the exploit the RSSI value inserted by CC1101 after packet reception to derive

the corresponding channel SNR, and thereafter use the same for cognitive adaptation of the AI and PS to maximize its energy-efficiency. Focusing on the present chapter, we elaborate the process of multiplexing of data from multiple sensor nodes at the BNC. In addition, we also propose a fast B-DWT algorithm at the BNC to compress long data streams into DWT coefficients in real-time that would allow the BNC to transfer the data over a backhaul network in an energy-efficient and cost effective manner. In this regard, the BNC is used to connect to a GSM cellular network to send the collected data over the Internet to a Remote Server (RS). Moreover, the RS is configured to accept data from multiple patients and store in a database. This would allow users to access patient data anywhere, anytime through web service and mobile applications.

To characterize and optimize the designed WBAN, we perform its performance analysis in OPNET. To this aim, we obtain the optimal Allocation Intervals (AIs) for ECG and temperature monitoring, that maximizes the network capacity within a frame delay constraint. Furthermore, the optimal payload sizes are obtained to maximize the energy-efficiency of the sensor nodes. Additionally, through a comprehensive performance analysis of the proposed B-DWT algorithm we found Bi-orthogonal 4.4 Wavelet filter as the most suitable filter providing 67% signal compression with less than 2% information loss. Moreover, B-DWT is found to be 64% faster in terms of execution speed and 2% more memory efficient as compared to traditional DWT. To add to this, the storage of the physiological signals in their compressed form at the remote database also allows a significant 65.25% reduction in database storage utilization. Currently we are working to make the WBAN communication secured, and interface the database with analytics tool and cloud services to provide a user interface for secured pervasive access of the data.

Chapter 4

Characterization and Resource/Energy-Efficient Implementation of Energy Detector for Real-Time CR using WARP

❝ *I think that in the discussion of natural problems we ought to begin not with the Scriptures, but with experiments, and demonstrations*❞

-Galileo Galilei

It is evident from Chapter 2 that CRN has the potential of alleviating some of the major concerns such as spectrum scarcity issues arising due to the deployment of prolific amount of IoT services like e-healthcare and the necessity for minimizing the data transfer costs involved in remote health monitoring. Also, Chapter 3 has laid the ground work for the implementation of remote health monitoring using WBAN. However, the work in Chapter 3 was focused primarily on WBAN which utilized licensed WAN for backhaul transmission. To introduce CRN at the backhaul of WBAN and truly take advantage of DSA, the first step should be the proper design of a real-time CR interface (i.e. SU) that can be used by the BNC for opportunistically sending its NRT data over PU channels in a CRN. Other motivations for developing a CR platform in hardware test-bed is firstly to use it for obtaining key operational parameters from test-bed, and secondly for validating the research findings through future proof of concepts and render them suitable for widespread deployment.

One of the fundamental functions of any SU is efficient sensing of the spectrum to detect spectrum holes in the PU channel. Therefore, it is imperative that particular attention is given towards characterization and implementation of spectrum sensing in real test-bed. The critical aspects of such implementation include i) efficient utilization of the on-board resources of

the SU, and ii) ensuring maximum energy-efficiency. ***Taking all of these into account, this chapter provides a practical realization of real-time SUs through proposed test-bed design, characterization of energy detection based sensing and implementation of a generic CRN test-bed where SUs leverage our proposed Practical Energy-Efficient Energy Detection (PED) method to sense the PU channels with high accuracy and then successfully transfer IP packets while keeping the interference to PUs within pre-determined threshold***.

4.1 Introduction

In recent years there has been an increasing demand of wireless services. However, traditionally spectrum is licensed to operators and each system has to operate within a limited frequency band. As the unlicensed spectrum is already congested, there is a need to find new ways to exploit licensed radio spectrum. Recent studies have shown that the actual licensed spectrum remains unoccupied for large periods of time [156] termed as 'white spaces'. Cognitive Radio (CR) [157, 10] technology can be used to sense these 'white spaces'. Opportunistic users also called Secondary Users (SUs) can leverage the CR technology to exploit the 'white spaces' without causing harmful interference to the incumbent Primary Users (PUs). The aim of this chapter is to build a practical real-time SU in a CR test-bed that is capable of taking intelligent standalone decisions enabling opportunistic transmission over PU channels. This would facilitate testing and validation of new proposed CR related concepts and algorithms in real test-bed setup. For this, SUs need to have CR capabilities, such as sensing the spectrum reliably to determine whether it is being used by a PU and change the radio parameters to exploit the unused part of the spectrum.

Spectrum sensing is by far the most important component for the establishment of SU. Spectrum sensing is the task of obtaining awareness about the spectrum usage and existence of PUs in a geographical area. This awareness can be obtained by using geolocation and database, by using beacons, or by local spectrum sensing at cognitive radios [158, 159, 76] or a combination of any of these within a network. In this chapter, we focus on spectrum sensing performed by SUs because of its broader application areas and lower infrastructure requirement. When used with geolocation database, local spectrum sensing can provide even superior spectrum efficiency for a Cognitive Radio Network (CRN).

Three schemes are generally used for local detection of PU presence through spectrum sensing. These are: matched filter based detection, energy detection and cyclostationary feature detection. Among these, both matched filter and cyclostationary feature detection require some priori information about the PU signal to be known to the SU. However, if the receiver cannot gather sufficient information about the PU signal, for example, if only the

power of the random Gaussian noise is known to the SU receiver, the optimal detector is an energy detector [160]. Despite of the poor performance of energy detector under low SNR conditions and noise uncertainty [161], it is still widely used as a signal detection method in real time systems because of its lower complexity. Furthermore, energy detection is the most common sensing technique used in validation of a wide range of CR algorithms that rely on spectrum sensing as one of its enabling methods.

Some of the common techniques to improve the performance of energy detection involves use of longer sensing duration and higher receiver sensitivity [77]. Fortunately, in current practical test-beds for CRs, the Analog to Digital Converter (ADC) frequency of a receiver is quite high. This greatly reduces the sensing time with high receiver sensitivities. For example, Ghasemi et al. in [77] reports a sensing time of 100ms for a single SU for a very low receiver sensitivity of -20dB. However, recent CR test-beds which have high ADC frequencies of 40MHz reduces the individual sensing time to 3ms, as will be discussed later in this chapter. Due to the aforementioned reasons, individual energy detection based sensing is highly favorable for low complexity implementation of highly efficient CRs.

Literature survey revealed that most of CR related work has been focused towards theoretical research and software simulation, which need further validation on practical hardware platform to observe their performance in real situation and feasibility of implementation. To this end, we aim to build a standalone SU in test-bed. For this, it is essential to perform a detailed test-bed modeling of the energy detection based spectrum sensing, evaluate its performance and possibly optimize it.

4.1.1 Importance of Test-Bed Modeling and Performance Evaluation

Detailed test-bed modeling and performance evaluation with test-bed parameters allows users to study the device characteristics in real environment under operational conditions at any realistic scale at real speeds. It gives an insight into the working of the device and helps in understanding the tradeoff between different test-bed parameters. This allows us to re-modify the existing analytical expressions with test-bed related parameters and study them from new viewpoints.

One such aspect of test-bed deployment of CR is the intelligent exploitation of the limited on-board resources of the SU. The resources are utilized based on specific applications. There are two types of resources available for efficient SU deployment -

i) **Field Programmable Gate Array (FPGA) hardware resources**- Low-level Physical (PHY) layer entities like transceivers, packet buffers, registers, packet detectors, energy

detectors are implemented in the FPGA. In addition, any operation that requires parallel processing for faster execution can be implemented at the PHY core.

ii) **Soft-core Embedded Processor (EP) resources**- This is based on sequential execution of instructions and mainly used for higher Medium Access Control (MAC) layer operations that act on the information collected at the PHY layer and then imbibe intelligence to the SU.

Efficient implementation of CR through intelligent utilization of the afore-mentioned limited resources opens up new possibilities of achieving more efficient SU performance. Lastly, a test-bed setup for CRN also allows system designers to validate new ideas in practical scenarios as a proof of concept. This may lead to discovery of possible deployment issues and incorporation of appropriate modifications in the proposed algorithms to address such issues.

4.1.2 Available CR Test-Bed Platforms

Although many works have been proposed to improve the performance of spectrum sensing and dynamic spectrum access and sharing, most of them only focus on the theoretical modeling and analysis and few of them have been verified in a practical system. Therefore, CR platforms need to be developed as a real world test-bed that can verify the theoretical analysis. Generally, CR is characterized by self-adaptive mechanisms which rely on *software radio technologies*. In this regard, generally Software Defined Radio (SDR) platforms like GNU-radio based Universal Software Radio Peripheral (USRP) [162], Wireless Open Access Research Platform (WARP) [163] and Berkeley Emulation Engine 2 (BEE2) [164] have been used for developing CR test-beds. A comprehensive survey on the SDR architectures available for CR test-beds is conducted in [165].

GNU Radio is a free software toolkit for building software radios [162]. The USRP is the device that interfaces GNU Radio and the real environment. GNU Radio is the software for exploring SDR and USRP is the hardware which implements it. GNU radio operates in computers and simulate the construction of simple software radios with USRP. It is an open-source framework and supports C++ and Python languages. C++ is used for the computational processing blocks, while Python is the glue that controls and coordinate these blocks. One of the main advantages of GNU radio is its low cost hardware, but that is because it does not have an on board processor. The performance of GNU radio is entirely dependent on a host computer that is connected to USRP via Universal Serial Bus (USB) interface. Since the low bandwidth of the USB connection limits the bandwidth between the software radio design with USRP, GNU Radio only supports narrow band communication

and low throughput. Due to the absence of an on-board processor, USRP cannot execute algorithms independently. This also limits the applicability of USRP to off-line physical layer prototyping, making it unsuitable for real-time Internet Protocol (IP) enabled communication.

WARP is an extensible, scalable and programmable wireless platform developed at Rice University [166] . It provides a freely available Open-Access Repository that supplies the archive for all parts of the platform, including documentation, libraries, designs, and application examples [166]. The Xilinx Virtex FPGA is used in the WARP board as the main computational processor and supplies embedded programming situation for PHY, MAC and network layer design with MATLAB simulink [163]. In addition, it also provides an on-board PowerPC (WARP v2) or Microblaze (WARP v3) processors for efficient MAC implementation. These on-board processors can be leveraged to realize an intelligent standalone communication node, where data is received as IP packets from an application through 1000/100 Mbps Ethernet interface, to achieve wide band communication and high throughput. The embedded processors are programmed in Xylinx SDK platform using C programming language. Moreover, like USRP, WARP also supports traditional off-line physical layer prototyping with a host Personal Computer (PC) controlling the board using WARP libraries for MATLAB called WARPLab framework. Lastly, the ability to connect multiple FPGAs together through high speed MGTs also makes the WARP scalable and extensible.

The BEE2 system is more advanced as compared to WARP and provides a scalable, modular solution for a range of advanced applications such as Digital Signal Processing (DSP) [164]. The BEE2 board includes 5 Vertex-2 Pro FPGAs. Each FPGA has a PowerPC 405 core, which minimizes the latency between the microprocessor and the reconfigurable fabric. Like in WARP, the PowerPC processor enables standalone node deployment in BEE2. The BEE2 uses Matlab/Simulink coupled with the Xilinx system generator as programmable tools to design a set of parameterized library blocks. One drawback of BEE2 is that it requires license to access certain sections of its repository. In summary, BEE2 is faster, with more communication ability, wider band communication, and is more scalable and extensible, but it is also more complex and expensive.

Due to the presence of on-board embedded processor, open-source framework and cost-effectiveness, we select WARP as the idle test-bed platform to conduct our CR based experimentation, validation and provide proof-of-concept for our proposed algorithms as introduced in later chapters.

4.1.3 Literature Survey and Motivation

Implementation of CR spectrum sensing using SDR boards has mainly been focused towards offline non-real time processing. In offline mode, the test-bed in general, and signal transmis-

sion, reception, signal processing and MAC layer processing in particular, are controlled by external computer software that interact with the boards. In this regard, Rashid et al. in [88] developed a CR system with spectrum sensing, spectrum management, spectrum decision and data transmission implemented in GNU radio and interacts with USRP as the hardware RF terminals. Similarly, in [89] Mandke et al. developed a flexible wireless test-bed called Hydra that uses the GNU radio platform and Click modular router to implement higher MAC and PHY layer algorithms in a Host PC while interacting with USRP radio terminals. The chief disadvantage is that end-to-end link performance is limited, not only by the computation needed by PHY algorithms, but also by the limited bandwidth of the USB 2.0 interface which connects the general purpose computer to the USRP front-end. Similar off-line spectrum sensing models for CRs were also developed using WARP by Lee et al. in [90]. As evident from the literature survey, implementation of MAC and PHY layer algorithms in on-board processor that would help realize a standalone SU is not possible in USRP and is yet to the realized in test-bed using WARP. The work in this chapter attempts to fill this gap.

In [90], Lee et al. did not implement the traditional energy detection based sensing probably due to noise uncertainty. However, energy detectors have very low complexity and are ideal for developing new PHY layer algorithms which leverage on sensing to provide the channel observations. This would provide a baseline which can then be tested for other sensing techniques as future projects. This motivated us to characterize the energy detection performance in a CR test-bed using WARP and then develop a sensing framework for its offline mode of operation. The off-line analysis and implementation provides the background needed to achieve the main goal of this chapter which is to build a real-time standalone SU with CR capabilities.

Offline processing and energy detection is ideal for testing new physical layer ideas. However, implementing those ideas in real-time in a standalone SU controlled by its on-board EP with no external control presents new challenges and opportunities for further optimizations. Considering the design complexities in real-time CR modeling, only few works [91, 97] have implemented it using the WARP boards. While RECOG [91] configures the Access Points with cognitive abilities to implement real-time applications, the soft real-time model in [97] utilizes the knowledge of the frequency hopping based PU traffic behavior to host video-streaming services. However, the model in [91] suffers from the issues of energy-efficiency and cost-effectiveness due to the use of two transceivers, whereas the model in [97] does not consider a generic CRN and is thus not widely acceptable. In short, none of these works deploy “truly cognitive SU terminals” that must be equipped with sensing, decision, management and mobility functionalities.

One of the primary challenges of implementing real-time CR interface is efficient utilization of the limited on-board resources as highlighted earlier. Moreover, a CR interface with its MAC and PHY tuned for real-time standalone SU operation can be leveraged for facilitating IP enabled communication. This in effect opens up immense opportunities for testing new applications and validation of new MAC layer ideas. Therefore, after drawing observations from the off-line mode, we model a Energy Detection based CR MAC (ECR-MAC) at the EP of WARP for implementing energy detection sensing. For the ECR-MAC, we propose a Practical Energy-Efficient Energy Detection (PED) method, which intelligently exploits the already available FPGA resources for practical realization of energy detection. Moreover, PED method not only enables efficient resource utilization but also minimizes the sensing time for PU detection based on the PU channel conditions. It is shown through performance analysis that PED method minimizes the energy consumed towards spectrum sensing. Therefore, our proposed PED method is more resource-efficient as well as energy-efficient as compared to the traditional energy detection based sensing.

4.1.4 Contributions of this Chapter

The main contributions of this chapter are as follows:

❶ For studying the energy detection sensing operation, we evaluate the sensing time and detection threshold by considering the probabilities of detection and false alarms in sensing. Based on this, we model the energy detection mechanism for efficient implementation in WARP. We extend the analysis to obtain the normalized interference duration between SU and PU transmissions, that is partly dependent on the uncertainties in sensing result.

❷ For characterization and performance analysis of energy detection in WARP, we take into account different operating conditions like the PU activity of a channel, detected PU SNR at the SU and SU receiver sensitivity.

❸ From the analysis we determine the Receiver Operating Characteristics (ROC) for WARP and its detection threshold that would provide satisfactory performance.

❹ Next, using the obtained parameters we implement and validate the operation of energy detection sensing over WARP test-bed in its off-line non-real time framework.

❺ As the most significant contribution of the chapter, after off-line validation, we utilize the real-time framework of WARP to design an independent and standalone SU to facilitate opportunistic IP enabled communication over PU channels. We introduce our proposed PED method and ECR-MAC framework for the on-board EP that exploits

the already existing Carrier Sense (CS) module in a transceiver system for resource efficient and energy-efficient implementation of energy detection framework.

❻ Thereafter, through performance analysis we validate the effectiveness of PED method in facilitating energy-efficient detection of PU presence as compared to traditional energy detector.

❼ Lastly, we validate the functionality of ECR-MAC framework by deploying opportunistic IP enabled SU communication over PU activity channels in our test-bed setup

4.1.5 Chapter Organization

This chapter is organized as follows. Section 4.2 outlines the system model that also includes the fundamentals of energy detection based sensing and PU activity modeling. In Section 4.3, we conduct performance analysis and characterization of energy detection in WARP. Next, Section 4.4 validates the characterization of energy detection through implementation using off-line WARPLab framework. Thereafter, Section 4.5 introduces our proposed PED method and ECR-MAC framework followed by the implementation of real-time CR interface using WARP boards. Finally, we conclude the chapter in Section 4.6.

4.2 System Model

We consider an overlay CR system comprising of a SU which needs to transmit data to a receiver by opportunistically accessing the PU channels of a PU system. For this, the SU senses a PU channel using energy detection based sensing for T_S duration for presence or absence of a PU. If the channel is sensed/observed to be ideal, then the transmission takes place for T_D duration. Else if the channel is busy, then the SU defers transmission for inter-sensing duration T_D. The sensing-transmission cycle of SU, also termed as CR cycle, is shown in Figure 4.1. The total frame duration of the CR frame is denoted by $T_F = T_S + T_D$. Figure 4.1 also highlights that a SU transmission can cause undue interference to PU transmission when,

- the SU miss-detects the presence of PU and starts transmission,
- the SU correctly detects the absence of PU and begins transmission, but PU returns in the channel within the inter-sensing duration

To address the above issues, the SU must make sure that the interference to PU is kept within a pre-determined threshold.

It is worth mentioning that, in the event of successive user-defined B number of busy sensing observations, the SU may perform handoff, i.e. it may jump to another PU channel

for transmission. A discussion on handoff or its target channel sequence is beyond the scope of this chapter and an elaborate study in this regard can be found in [167]. Therefore, in this chapter, we do not consider the handoff event, and the SU remains in the same channel even after successive busy sensing observations.

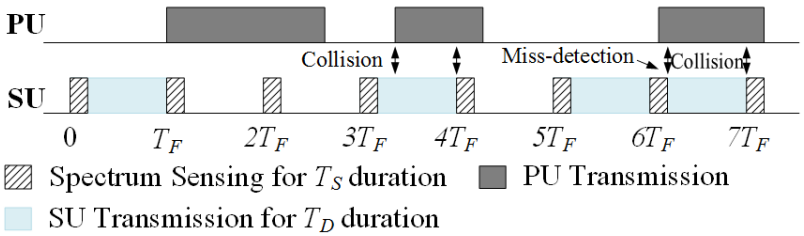

Fig. 4.1 Timing behavior of PU and SU with possible collision instances.

Figure 4.2 shows the several functional entities of a standalone SU developed on WARP board along with the inter-layer coupling. The MAC layer at the Embedded Processor (EP) of a SU incorporates the sensing scheduling and spectrum access units. *Sensing Scheduling* unit controls certain timers that set the start and end of sensing and inter-sensing durations, thereby maintaining the CR cycle. The *Spectrum Access* unit is responsible for accessing and obtaining the current channel observation from the Spectrum Sensing unit. Based on the sensing observation, it decides whether to remain idle or transmit in the following inter-sensing duration. For transmission, the MAC accepts packets from the higher layer, encompasses them into CR frames by appending CR MAC headers and forwards them to the CR PHY layer for transmission. Lastly, the CR PHY layer at the FGPA core of SU comprises of the *Spectrum Sensing* unit and the transceiver radio modules for transmission over the radio frequency environment.

It is worth mentioning that the SU depicted in Figure 4.2 is a standalone entity that we aim to develop in this chapter. However, in off-line mode, the WARP EP is deactivated and the WARP PHY layer resources are controlled by a host PC. The software framework at the PC, called WARPLab, takes all the spectrum related decisions. This shown in Figure 4.3a. Whereas, in real-time mode, a host which may be a PC provides only the higher application layer data packets to the CR MAC layer at the EP of SU for transmission. This is highlighted in Figure 4.3b. Real-time mode of operation facilitates IP based communication between two hosts as illustrated in 4.3b. Whereas, in off-line mode the communication is restricted within different radio boards that are controlled by a single host PC.

In the following sub-sections, we first model the PU activity, and then introduce the performance parameters for energy detection based sensing and subsequent transmission.

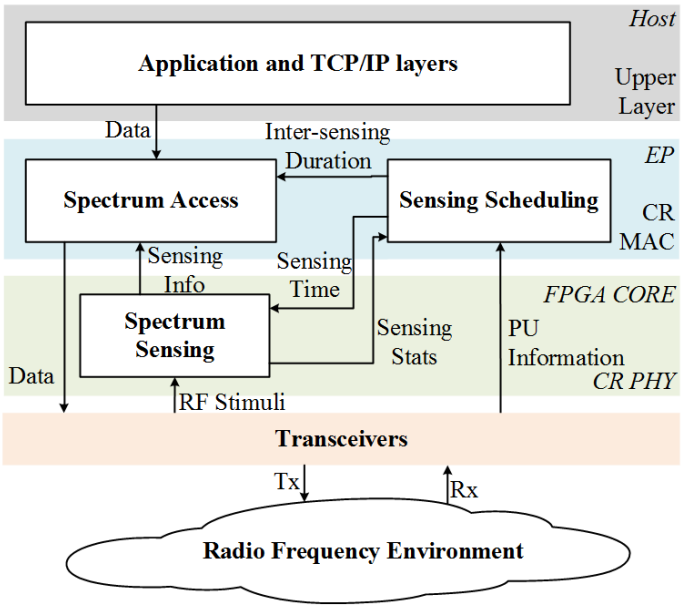

Fig. 4.2 Functional block diagram of a standalone SU with data from host PC.

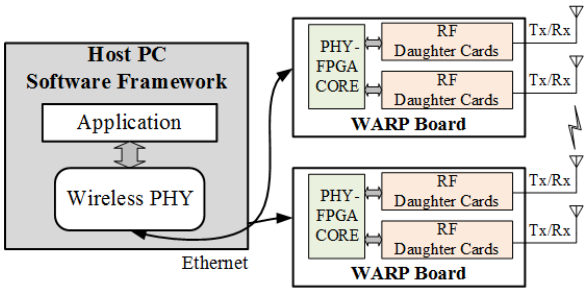

(a) Off-line mode of operation

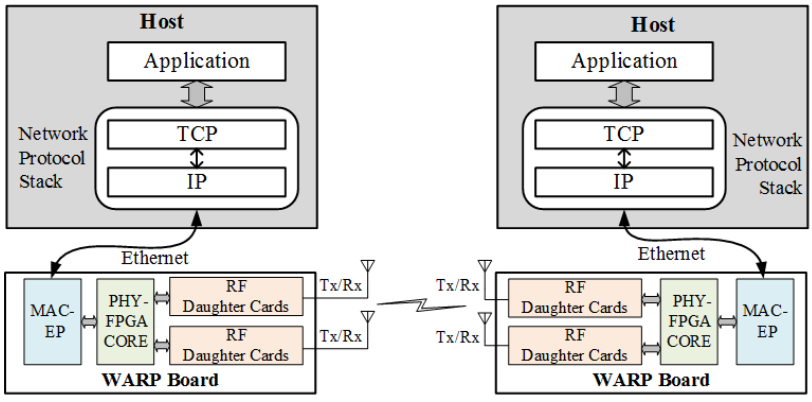

(b) Real-time mode of operation

Fig. 4.3 Block diagram of SUs composed of WARP nodes for off-line and real-time operations

4.2.1 PU Activity Modeling

The PU system has multiple non-overlapping orthogonal PU channels of bandwidth WHz. The occupancy state of a channel due to PU is modeled as a non-time slotted two-state ON/OFF Continuous Time Markov Chain (CTMC), which is the most popular model in literature. For PU activity modeling, 27% of the total schemes have used this model [168]. This model is also used in public-safety bands for approximating spectrum usage, in IEEE 802.11b for modeling the presence of PUs, and it is the most famous model for voice [168–170]. The durations of PU's ON state (hypothesis H_1 or busy period) and OFF state (hypothesis H_0 or idle period) are represented by exponentially distributed i.i.d. random variables X and Y, with probability density functions (p.d.f.) $f_X(t) = \lambda e^{-\lambda t}$ and $f_Y(t) = \mu e^{-\mu t}$ having parameters λ and μ respectively. Thus, the average busy period (t_{on}) is $1/\lambda$, and the average idle period (t_{off}) is $1/\mu$. Therefore, the probability of a channel being busy, simply termed as PU activity, is denoted by $P(H_1) = \dfrac{t_{on}}{t_{on}+t_{off}}$. While the idle channel probability is $P(H_0) = \dfrac{t_{off}}{t_{on}+t_{off}}$.

4.2.2 Energy Detection

It is reasonable to assume that the SU does not have a priori knowledge of the PU signal characteristics such as the modulation type, packet format or pulse shape. In this scenario, the optimal detector is an energy detector [160], which is also one of the most commonly used detection technique in CRs [10]. The goal of spectrum sensing is to decide between the following two hypotheses,

$$x(t) = \begin{cases} n(t), H_0 \\ \\ h\,s(t) + n(t), H_1 \end{cases} \tag{4.1}$$

where, $x(t)$ is the SU received signal, $s(t)$ is the primary signal, $n(t)$ is the Gaussian white noise at the receiver of the SU with no noise un-certainty and h denotes the gain of wireless channel between the SU and the PU.

The energy-detector performs non-coherent signal detection by integrating squared versions of N_S number of received signal samples that are received during sensing time T_S. We can relate N_S and T_S as,

$$T_S = \frac{N_S}{f_{ADC}} \tag{4.2}$$

where f_{ADC} is the sampling frequency of the Analog-to-Digital Converter (ADC) of the SU radio transceivers. The energy of the signal thus obtained is then compared to a set threshold

as shown in Figure 4.4. Let λ_{th} be the detection threshold of the SU. The Neyman-Pearson method of obtaining λ_{th} is discussed next.

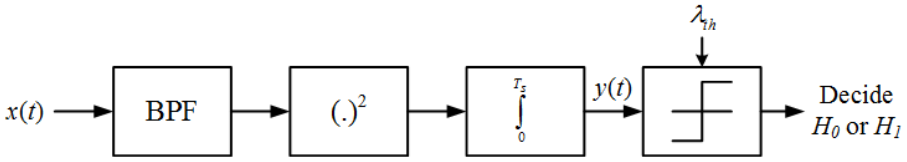

Fig. 4.4 Block diagram of energy detector.

The energy collected (Y) by the SU during the sensing time T_S can be obtained as,

$$Y = \sum_{n=1}^{N_S} |x[n]|^2 \tag{4.3}$$

Following the work of Urkowitz [171], Y may be shown to have the following distribution,

$$Y = \begin{cases} \chi^2_{N_S}, H_0 \\ \chi^2_{N_S}(2\gamma_{PU}), H_1 \end{cases} \tag{4.4}$$

where, $\chi^2_{N_S}$ and $\chi^2_{N_S}(2\gamma_{PU})$ denote central and non-central chi-square distributions respectively with a non-centrality parameter of $2\gamma_{PU}$ for the latter. γ_{PU} represents the received PU Signal-to-Noise Ratio (SNR) at the SU. According to the central limits theorem, if $N_S > 125$, Y can be approximated as a Gaussian random variable with distribution,

$$Y \sim \begin{cases} N(N_S\sigma_0^2, 2N_S\sigma_0^4), H_0 \\ N(N_S\sigma_1^2, 2N_S\sigma_1^4), H_1 \end{cases} \tag{4.5}$$

where, σ_0^2 denotes the variance of white noise at the SU and σ_1^2 denotes the variance of Y under H_1.

For a zero mean white noise, the noise power (N_0) at the SU can be obtained as,

$$N_0 = \frac{1}{N_S}\sum_{k=1}^{N_S} n^2[k] = E\left\{n^2[k]\right\} = Var\left\{n[k]\right\} = \sigma_0^2 \tag{4.6}$$

Further, it can be shown that,

$$\sigma_1^2 = \sigma_0^2(1+\gamma_{PU}) \tag{4.7}$$

The received PU signal power at the SU can be calculated as,

$$S_0 = \frac{Y}{N_S} - N_0 \tag{4.8}$$

The detection performance of spectrum sensing is crucial to the performance of both primary and CR systems. This is primarily determined on the basis of two metrics:

i) probability of false-alarm, and
ii) probability of detection.

Probability of false-alarm denotes the probability of the SU declaring that a PU is present when the spectrum is actually free. Whereas, *probability of detection* denotes the probability of the SU declaring that a PU is present when the spectrum is indeed occupied by the PU. Mathematically, the probability of false-alarm (P_f) of the SU can be obtained as,

$$P_f = P(Y > \lambda / H_0) = Q\left(\frac{\lambda_{th} - N_S\sigma_0^2}{\sqrt{2N_S\sigma_0^4}}\right) \tag{4.9}$$

Similarly, the detection probability (Pd) of the SU can be obtained as,

$$P_d = P(Y > \lambda / H_1) = Q\left(\frac{\lambda_{th} - N_S\sigma_1^2}{\sqrt{2N_S\sigma_1^4}}\right) \tag{4.10}$$

where σ_0^2 and σ_1^2 are obtained using (4.6) and (4.7) respectively, and $Q(\cdot)$ is the Q-function. Let the SU false-alarm constraint be set to κ. Then, solving (4.9) we can obtain the detection threshold (λ_{th}) of SU as,

$$\lambda_{th} = \sqrt{2N_S\sigma_0^4}\,Q^{-1}(\kappa) + N_S\sigma_0^2 \tag{4.11}$$

Further, we can obtain the number of samples required for the SU to sense a PU at a minimum PU SNR, $\gamma_{PU,min}$ (also known as receiver sensitivity) with detection probability $P_d = \chi$ under the false-alarm constraint $P_f = \kappa$ can be obtained upon simplification using (4.10) and (4.11) as,

$$N_S = 2 \times \left[\left\{ Q^{-1}(\kappa) - (1 + \gamma_{PU,\min})Q^{-1}(\chi) \right\} / \gamma_{PU,\min} \right]^2 \tag{4.12}$$

Using (4.12) and (4.2) we obtain a fixed sensing time for our designed CR system using WARP and perform further performance analysis of energy detection based sensing under varied PU activity and SNR conditions.

4.2.3 Transmission

Two metrics that are commonly used to characterize the SU performance during transmission:

i) transmission probability, and
ii) normalized interference duration

It is worth mentioning that there are other metrics namely throughput, energy consumption and energy-efficiency of a SU and they will be taken up later in appropriate chapters.

A SU may initiate transmission under two conditions: i) the channel is actually busy but the sensing decision indicates an idle channel (miss-detection) with probability $(1-P_d)$, and ii) the channel is idle and the sensing decision correctly identifies this (not false alarm) with probability $(1-P_f)$. Then, the *transmission probability* (P_{trans}) can be expressed as,

$$P_{trans} = P(H_1)\,(1-P_d) + P(H_0)(1-P_f) \tag{4.13}$$

We define the *normalized interference duration* (ε) as the ratio of the expected non-effective CR communication or the collision duration to the inter-sensing duration, which is defined as,

$$\varepsilon = \frac{T_C}{T_D} \tag{4.14}$$

where T_C is the expected collision duration of the SU due to interference with the PU within the inter-sensing duration T_D. We now analyze the different possibilities of collisions between SU and PU transmissions.

(A) In the event of a miss-detection, the SU will initiate data transmission and generate interference to the PU in its inter-sensing block T_D. Under this scenario, two different cases of interference might arise:

i) The channel does not change its state in the inter-sensing interval (T_D), and so the interference lasts for the entire T_D duration.
ii) The channel changes its state after t_1 during the inter-sensing duration. Then, the interference will last for t_1.

Therefore, in case of a miss-detection we can express the average non-effective communication duration (T_{bc}) as,

$$T_{bc} = \int_{T_D}^{\infty} f_X(t_1) T_D \,\mathrm{d}t_1 + \int_0^{T_D} f_X(t_1) t_1 \,\mathrm{d}t_1 \tag{4.15}$$

Solving (4.15) using the p.d.f. of exponential ON time ($f_X(t)$) we obtain T_{bc} as,

$$T_{bc} = \frac{1}{\lambda} \times \left(1 - e^{-\lambda T_D}\right) \tag{4.16}$$

(B) We now consider the scenario where the SU correctly identifies an idle channel during its sensing time and starts communication. Despite the correct detection, the SU may still generate interference with PU within its inter-sensing duration. This happens if the channel state changes after t_1 in the inter-sensing interval. Then, the interference will appear for $(T_D - t_1)$. So in case of a not false-alarm we can express the non-effective communication duration (T_{ic}) as,

$$T_{ic} = \int_0^{T_D} f_Y(t_1)\,(T_D - t_1)\,\mathrm{d}t_1 \tag{4.17}$$

Solving (4.17) using the p.d.f. of exponential OFF time ($f_Y(t)$) we have T_{ic} as,

$$T_{ic} = T_D - \frac{1}{\mu} \times (1 - e^{-\mu T_D}) \tag{4.18}$$

Therefore, the expected collision duration (T_C) can be obtained using (4.16) and (4.18) as,

$$T_C = P(H_1)\,(1 - P_d) T_{bc} + P(H_0)(1 - P_f) T_{ic} \tag{4.19}$$

A CR system should be designed so that the normalized interference duration (ε) in (4.14) is kept within a pre-determined threshold. This ensures that the interference to PU communication due to opportunistic SU transmission does not exceed the prescribed limit. Mathematically, this can be represented as,

$$\varepsilon \leq \Gamma \tag{4.20}$$

4.3 Performance Analysis and Characterization of Energy Detection in WARP

In this section, we perform a simulation study in MATLAB and analyze the performance of energy detection based sensing and transmission under different receiver sensitivities, channel SNRs and PU traffic usages. Based on the design philosophy highlighted in the

previous section, we evaluate the performance in terms of detection probability, transmission probability and normalized interference duration.

4.3.1 Simulation Settings

In our simulations, we utilize the WARP radio boards to model the transceivers of SU CR modules. More specifically, we consider the sampling frequency of the ADC (f_{ADC}) of the SU receiver to be equal to that of the WARP board, i.e. $f_{ADC} = 40$MHz. The PU activity of the channels follow an exponential ON-OFF distribution with mean duty-cycle $t_{on} + t_{off} = 3$s. To obtain the sensing time, we draw on the assumptions presented in [172], where the optimal sensing time has been evaluated for detection probability $\chi = 0.9$, and false alarm constraint $\kappa = 0.1$.

Further, to keep parity between the simulation results and designed hardware prototype, we take into account the following considerations. The ADC of WARP has a sampling frequency of 40 MHz with a buffer size of 2^{14}. Generally, WARP avoids first 1000 received signal samples out of 2^{14} samples. Excluding this 1000 samples, WARP takes 0.384 ms to sense the samples contained in an entire buffer. Hence, the time taken for sensing N_S samples for PU detection using WARP can be obtained as,

$$T_S = 0.384 \times \frac{N_S}{2^{14} - 1000} \tag{4.21}$$

4.3.2 Analysis of Receiver Operating Characteristics (ROC)

We illustrate the variation of the detection probability (P_d) with respect to the PU SNR at SU for different SU receiver sensitivities $(\gamma_{PU,min})$ in Figure 4.5a, which is also known as the Receiver Operating Characteristics (ROC). It is observed that as PU SNR at the SU increases, the detection probability increases. Higher SNR corresponds to higher accumulated energy within the sensing time, which leads to better PU detection. Also, we notice that for any given PU SNR, the detection probability increases with decrease in the value of $\gamma_{PU,min}$. From the expression of N_S in (4.12) and P_d in (4.10), we discern the inverse proportionality of $\gamma_{PU,min}$ and P_d. Hence, we remark that the more a receiver is sensitive, the better is its detection performance. However, this comes at the cost of increased sensing time. This is illustrated in Figure 4.5b. It is noted that with the decrease in $\gamma_{PU,min}$, the sensing time increases drastically. This variation can be explained from (4.12). As $\gamma_{PU,min}$ gradually decreases, the value of the number of samples required to detect the PU presence with probability $\chi = 0.9$ increases. This increases the sensing time obtained using (4.21), thereby leading to more energy consumption. Therefore, it is very essential to set a receiver sensitivity

that balances the detection performance and sensing time. For our designed system we set $\gamma_{PU,min} = -20$dB, which is also duly supported by related works in the literature [172]. For $\gamma_{PU,min} = -20$dB, the receiver sensitivity is set sufficiently low to allow good detection of PU for a wide range of detected PU SNRs at the SU. As shown in Figure 4.5b, for $\gamma_{PU,min} = -20$dB, we obtain the sensing time $T_S = 3$ms which corresponds to the required number of samples obtained using (4.12) as $N_S = 131072$.

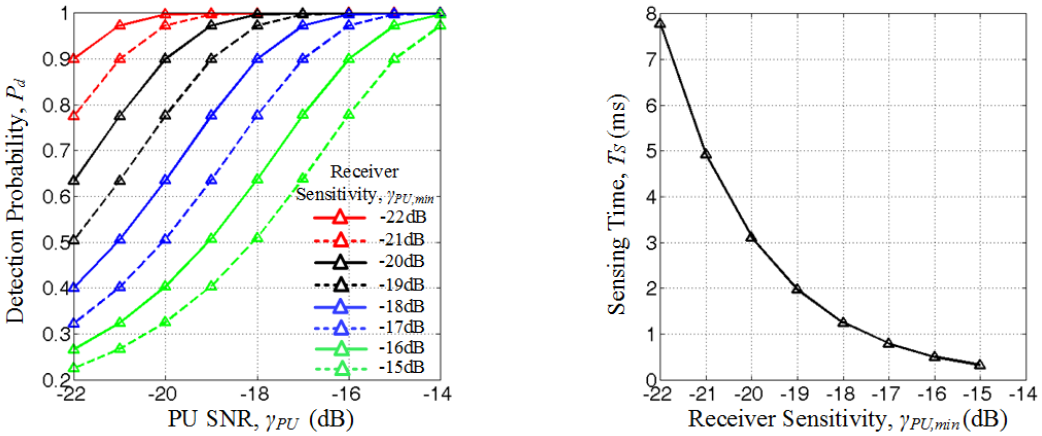

(a) Receiver operating characteristics

(b) Sensing time vs receiver sensitivity

Fig. 4.5 Variation of (a) detection probability under different PU SNRs and receiver sensitivities, (b) sensing time with respect to different receiver sensitivities.

4.3.3 Analysis of Normalized Interference Duration

In interference-tolerant CR networks, a practical and reliable way to manage the mutual interference of SU and PU transmissions is by keeping the normalized interference duration within the pre-specified threshold Γ. The variations of normalized interference duration with the inter-sensing time (T_D) for different PU activities at -20dB and -19dB detected PU SNR are shown in Figures 4.6a and 4.6b respectively. From both the figures it is observed that as T_D increases the normalized interference increases. Higher T_D corresponds to higher probability of return of PU during transmission by SU within a detected white-space, which adds to the concerned increased interference. Further, keeping T_D and detected PU SNR fixed, it can be seen that the interference decreases with decrease in PU activity. Lower PU activity means less PU ON time and more empty spaces, which contributes toward lower mean collision duration.

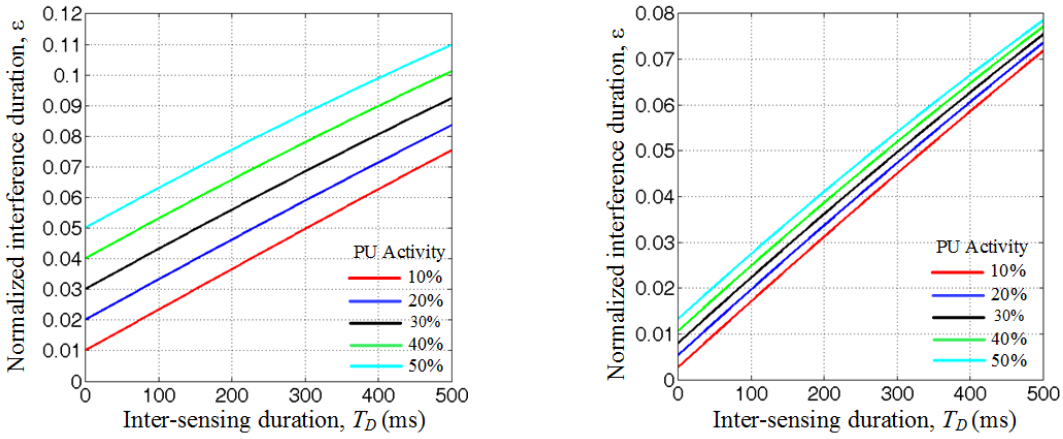

(a) PU SNR, $\gamma_{PU} = -20$dB

(b) PU SNR, $\gamma_{PU} = -19$dB

Fig. 4.6 Variation of normalized interference duration with respect to inter-sensing duration for different PU activities and detected PU SNRs.

4.3.4 Analysis of Transmission Probability

Figure 4.7 shows the variation of transmission probability (P_{trans}) with respect to the PU SNRs and PU activities. In this figure, it can be observed that as the PU SNR decreases, the transmission probability increases, resulting in more throughput for the SUs. Lower PU SNR leads to more miss-detections which leads to more SU transmission opportunities. However, the increased SU transmission is at the cost of more interference to the PU as evident from Figures 4.6a and 4.6b.

Furthermore, it is also noted from Figure 4.7 that as the value of PU activity increases, P_{trans} decreases. This is to be expected as higher PU activity corresponds to less number of white spaces available for transmission. Therefore, it comes as straightforward deduction that as lower PU activity channels are characterized by high transmission probability, they are idle for deployment of SUs with high throughput and low delay requirement, e.g. Real Time applications. Whereas, for Non-Real Time applications both high and low PU activity channels may be suitable. However, energy-efficiency of SU is a consideration. More in detail, a lower PU activity (less than 50%) will allow the SU to attain higher throughput for the energy consumed by it towards spectrum sensing. We study this scenario in great detail in Chapter 6. However, if the channel sensing is performed by some other entity like a Cognitive Base Station (CBS) in a CR network, even higher PU activity channels may be suitable for NRT transmission. However, this comes at the obvious cost of more network resources. We consider such a network in Chapter 7.

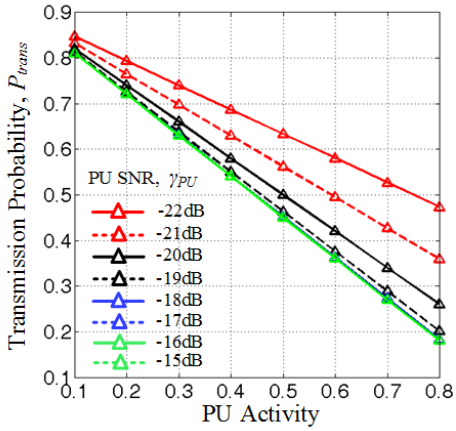

Fig. 4.7 Variation of transmission probability with respect to different PU activities and detected PU SNRs.

4.4 Implementation of Energy Detection based Sensing using WARPLab

In order to develop a real-time standalone SU using WARP, at first we start with the off-line non-real time WARPLab framework to develop an energy detection model for WARP. In addition, this developed WARPLab model will also enable verification of new physical layer ideas based on spectrum sensing. In this thesis, we use this developed model later for the proof of concept of our proposed Centralized Scheduling, Sensing and Prediction (CSSP) framework as discussed in Chapter 7.

In this subsection, we first describe the test-bed setup for effective execution of WARPLab framework. Thereafter, we highlight the implementation of energy detection sensing using WARPLab.

4.4.1 Test-bed Setup for WARPLab framework

We develop the energy detection based sensing model using WARPLab in the absence of noise uncertainty. A detailed distributed overlay spectrum sharing CR system in the 2.4 GHz unlicensed spectrum has been considered consisting of one PU and one SU as shown in Figure 4.8. The location of the SU radio is varied with respect to the PU transmitter as explained later in Section 4.4.3. The WARP v2 board is configured with WARPLab v6 [166] bit stream from a PC via a JTAG cable. Further, we communicate with WARP board through MATLAB running on the PC via Ethernet cable.

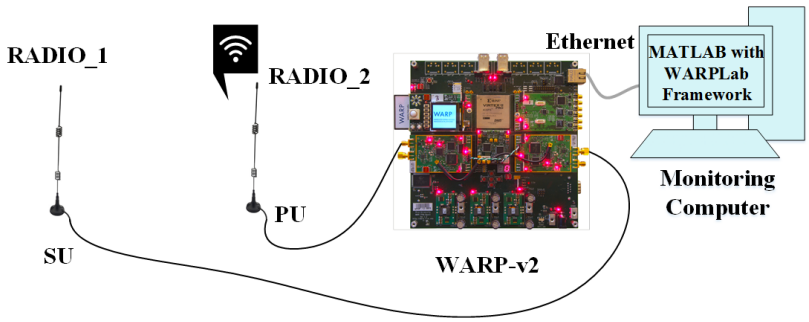

Fig. 4.8 Test-bed setup for energy detection using WARPLab.

Lee et al. in [90] implemented the PU and SU sub-systems on two different WARP boards controlled by the same PC. In this regard, to better utilize the resources we use a single WARP board to implement the PU and the SU. For this experiment, the WAPRLab MATLAB script is configured to implement one radio daughter card of the board as the PU and another as the SU. The received signal at the SU is stored in the buffers of the radio daughter cards. The stored data in the buffers are then read by the MATLAB script, which uses energy based detection, as illustrated in Section 4.2.2, to sense the presence or absence of the PU. The PU channel is centered at 9.5 MHz having a bandwidth of 18MHz. The baseband signal is then translated to channel 9 of 2.4GHz RF spectrum by up-conversion.

4.4.2 Energy Detection Algorithm for WARPLab

We use a single WARP v2 kit to implement energy detection based sensing. A single kit consists of four trans-receiver radios, out of which two has been used. RADIO_2 serves as the primary transmitter (Tx mode) and RADIO_1 as the SU transceiver. RADIO_2 primary signal is generated using exponential ON-OFF distribution as explained in Section 4.2.1. At first, we configure RADIO_1 (SU) to operate as a receiver (Rx mode) and then calculate the noise powers N_0 using (4.6). Thereafter, the MATLAB script calculates the detection threshold λ_{th} using (4.11), performs energy detection sensing in Rx mode and obtain the respective detection bits. Figure 4.9 gives a flow chart of the sequence of events.

4.4.3 WARPLab based Results

In this sub-section, we present the results of the implementation of energy detection based sensing using WARPLab. In this regard, following the flowchart in Figure 4.9, we calculate the noise power (in dB) at the WARP receiver as,

$$N_0 = \sigma_0^2 = -123.3\text{dB} \tag{4.22}$$

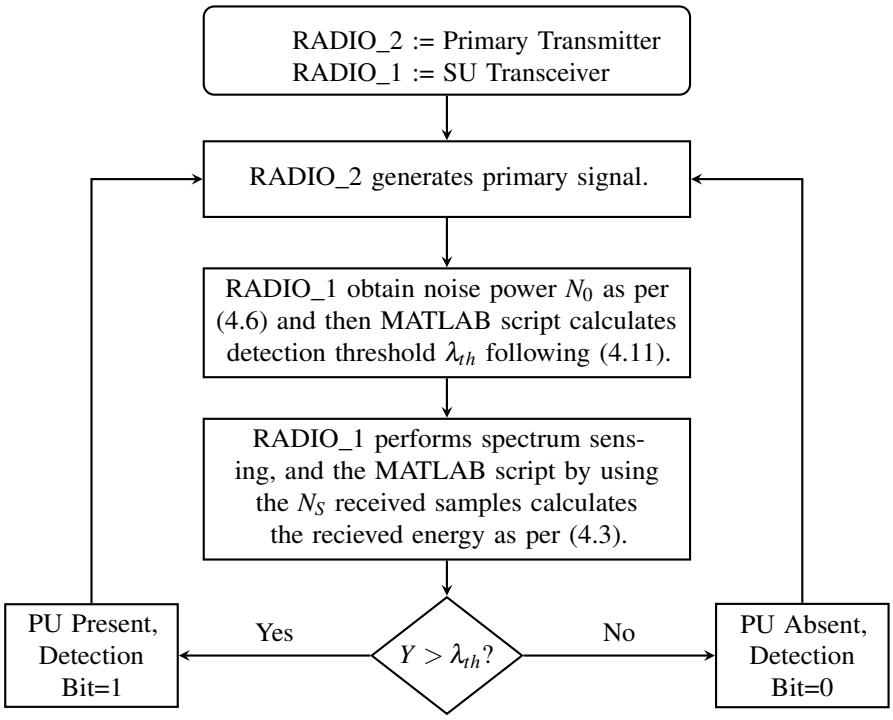

Fig. 4.9 Flowchart of implementation of energy detection in WARP using WARPLab.

Thereafter, using $N_S = 131072$ (obtained in Section 4.3.2) we calculate the detection threshold (λ_{th}) (in dB) using (4.11) as,

$$\lambda_{th} = -72.05\text{dB} \tag{4.23}$$

Figure 4.10a shows the transmitted PU signal over CR environment, while Figure 4.10b shows the raw received signal at the SU during PU transmission where the PU SNR at the SU is -10.63 dB. The un-deterministic PU signals are detected with the help of energy detection threshold obtained from (4.23), and the detection bits are shown in Figure 4.10c, which depicts the correct detection of PU presence.

4.5 Design and Implementation of Resource-Efficient and Energy-Efficient Energy Detection in Real-Time CR Test-bed using WARP

After initial testing and validation of the energy detection based sensing for CR in offline mode using WARPLab framework, we now utilize the WARP Real-Time (WARP-RT) framework to design an independent and standalone SU with efficient implementation of energy detection

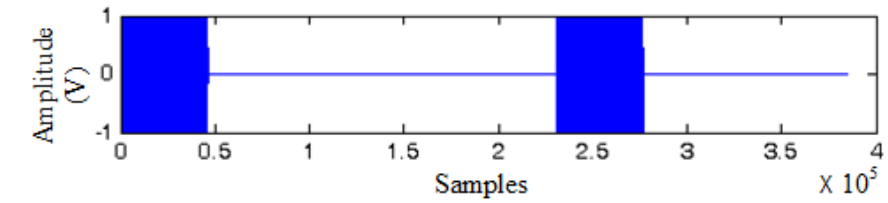

(a) PU transmitted signal

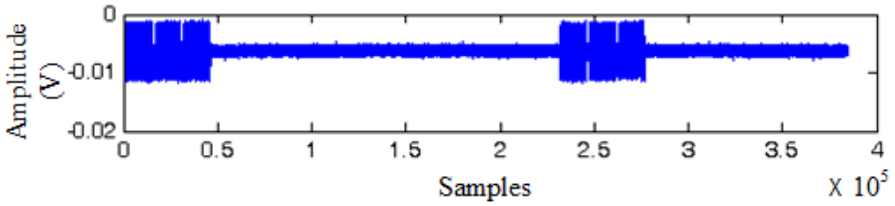

(b) SU received signal

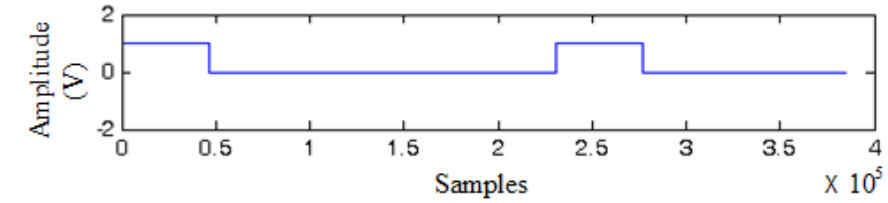

(c) Detection bits

Fig. 4.10 Primary user transmission and SU received signal with detection bit.

based sensing to facilitate opportunistic IP enabled communication over PU channels. To this end, as highlighted previously, for implementing energy detection based sensing we are motivated to exploit the already existing Carrier Sense (CS) module in a transceiver system that are used in protocols like Carrier Sense Multiple Access (CSMA). This prevents us from designing a separate energy detection module at the FPGA core specifically for CR use, thereby leading to efficient utilization of FPGA resources. Furthermore, we propose a Practical Energy-Efficient Energy Detection (PED) method for the CR MAC layer running in the CR Embedded Processor (EP) that intelligently exploits the CS module at the PHY core of the SU. Moreover, a real-time test-bed setup with SU having intelligent EP capable of taking standalone decisions can be leveraged for performance analysis, validation and proof-of-concept for new application and MAC layer ideas. In our work, we have duly used this design for validation of our proposed concepts later in Chapter 6.

In this Section, we first design the Energy Detection based CR MAC (ECR-MAC) for the SU EP which incorporates the proposed PED method for spectrum sensing. Following this, we validate the working of the ECR-MAC in a test-bed setup. Lastly, we quantify the improvement in energy-efficiency due to PED method.

4.5.1 ECR-MAC with Proposed PED Method

Prior to introducing our proposed PED method, we give a brief overview of the working of a CS module. Thereafter, we explain the PED method.

4.5.1.1 Carrier Sense (CS) Module

The CS module senses the channel for a maximum duration of t_s ($t_s << T_S$) and returns a binary result denoted by variable b. It collects the samples and computes the total energy accumulated at the current instant. However, at any instant during its operation if it detects that the total energy computed within its accumulator is higher than a threshold λ_{CS}, then it returns a binary value $b = 1$ (busy) to the ECR-MAC. The threshold energy for CS module (λ_{CS}) is set to the total energy accumulated within t_s duration if the individual signal samples received has constant power $THRES_{RSSI}$ ($THRES_{dB}$ in dB). For a given ADC frequency (f_{ADC}), the threshold energy of CS module (λ_{CS}) can expressed mathematically as,

$$\lambda_{CS} = f_{ADC}\, t_s\, 10^{THRES_{dB}/10} \tag{4.24}$$

If the total energy accumulated within t_s duration is less than λ_{CS}, then CS module returns $b = 0$ (idle). In addition, under normal CS operation as implemented in CSMA, the CS module accumulator is reset before the next operation.

4.5.1.2 Proposed PED Method and ECR-MAC Framework

The elementary CS module can be effectively utilized within our designed ECR-MAC framework to energy-efficiently sense the PU channel. This constitutes the proposed PED method. The primary activities of ECR-MAC are shown in Figure 4.11.

To keep track of the sensing and transmission time durations, we exploit the WARP 80MHz Timer (TMR), which is set in the count-up mode. For maintaining the boundaries of the sense interval (T_S) and optimal inter-sense duration (T_D^*) we declare two variables T_{cur_sense} and $T_{cur\_intersense}$ that are used to read the TMR and store the current time instant within sensing and inter-sensing durations respectively. Lastly, ECR-MAC maintains a variable $transmit\_flag$ which indicates the sensing observation, i.e. it is set to '1' if the PU channel is sensed to be idle, or else if a channel is busy it is set to '0'. Depending on the variable, ECR-MAC begins or defers transmission respectively.

The PED method operates within the devised ECR-MAC framework as follows:

1. For sensing a PU channel, the ECR-MAC iteratively accesses the CS module for a maximum of T_S duration. (Figure 4.11 (1)). If the CS module returns $b = 1$ (Figure

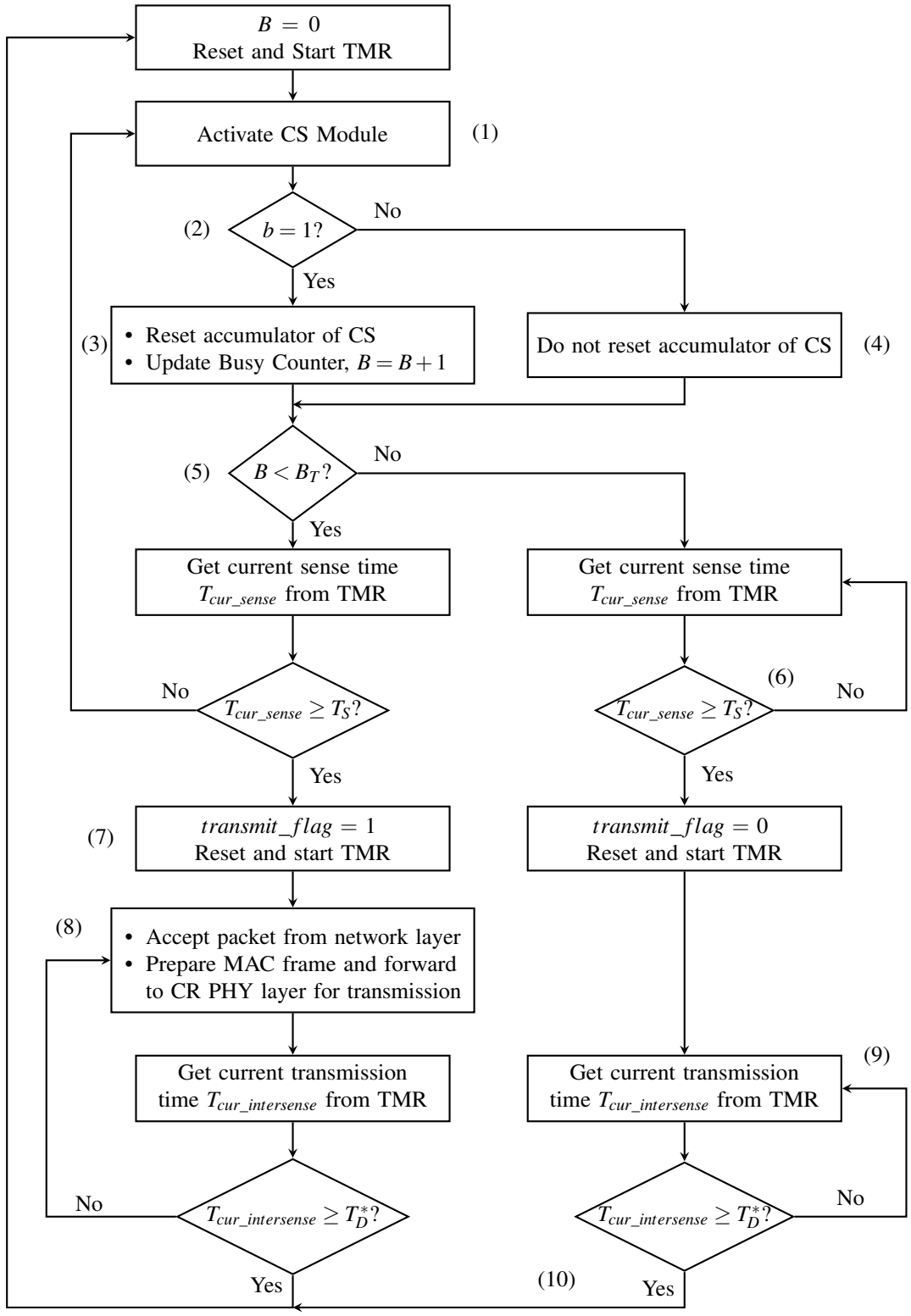

Fig. 4.11 Flowchart of implementation of ECR-MAC in WARP using WARP-RT framework.

4.11 (2)), then ECR-MAC increments a busy counter B and resets the accumulator of CS module (Figure 4.11 (3)).

2. In the event that the CS module returns $b = 0$, ECR-MAC does not reset the accumulator of CS module (Figure 4.11 (4)). We achieve this through a small change in ECR-MAC conditional programming. This essentially allows the ECR-MAC to utilize the already accumulated energy in a CS module which was not utilized towards incrementing the busy counter.

3. To determine whether the total cumulative signal energy accumulated till the current instant within the sensing time T_S exceeds energy detection threshold λ_{th}, the busy counter B is compared against a maximum threshold B_T, where,

$$B_T = \frac{\lambda_{th}}{\lambda_{CS}} \tag{4.25}$$

4. If at the end of a CS module operation, we attain $B \geq B_T$ (Figure 4.11 (5)), then the ECR-MAC infers the channel as busy, stops sensing, remains idle for the rest of the sensing duration (Figure 4.11 (6)) and sets the $transmit\_flag = 0$. This practical technique makes sensing even more energy-efficient and resource-efficient. It is resource-efficient because it enables intelligent exploitation of available resources, i.e. the CS module, without the need for the design of a separate energy detector at the PHY core. While it is energy-efficient because during a busy channel with moderately good PU SNR, the accumulated energy will be above the threshold even before the sensing time is complete, thereby allowing the SU to switch off the radio-modules and reduce energy consumption.

5. When the channel is completely idle, the maximum number of times CS module can be accessed is $N_C = \frac{T_S}{t_s}$). Consequently, if at the end of sense interval we have $B < B_T$, then ECR-MAC sets $transmit\_flag = 1$. (Figure 4.11 (7)).

6. If $transmit\_flag = 1$, ECR-MAC accepts packets from network layer, encapsulates it in a MAC frame and forwards it to CR PHY layer for transmission (Figure 4.11 (8)). However, if $transmit\_flag = 0$, ECR-MAC remains inactive (also termed as sleep) for the inter-sense duration (Figure 4.11 (9)).

7. Upon expiry of the inter-sense duration, ECR-MAC again begins channel sensing (Figure 4.11 (10)).

4.5.2 Energy Consumption Analysis of PED Method

In this sub-section, we conduct a performance analysis of the PED method in MATLAB. For this, we use the sensing duration of $T_S = 3$ms that was calculated earlier in Section 4.3.2 for $\gamma_{PU,min} = -20$dB and detection threshold of $\lambda_{th} = -72.04$dB. Figure 4.12 shows the probability of detecting a PU using the PED method for different PU SNRs at a particular instant within the sensing time T_S . It is noted that the time required to detect a PU with certain probability decreases with increase in PU SNR. Higher PU SNR leads to accumulation of samples with larger power in the CS module which leads to reduction in the time needed to exceed the energy detection threshold λ_{th}. Figure 4.13a shows the effective sensing time for PED method to attain a 90% detection probability under different PU SNRs. A smaller effective sensing time leads to reduction in the energy consumed towards sensing a channel as busy. This improvement in energy consumption is highlighted in Figure 4.13b. As observed, higher PU SNR leads to more reduction in energy consumption.

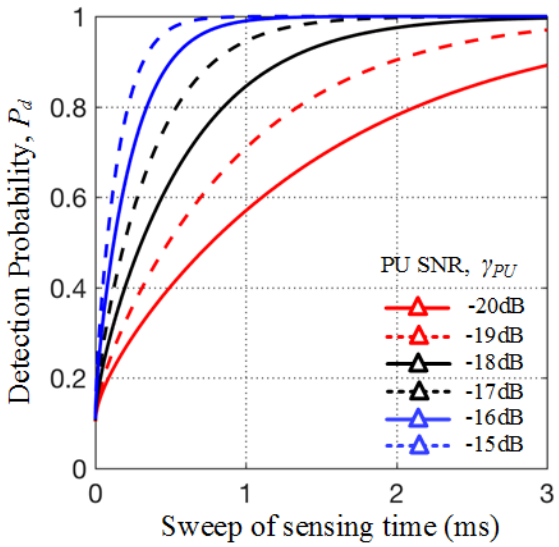

Fig. 4.12 Variation of detection probability for different detected PU SNRs at different instants of sweeping through the sensing time of duration $T_S = 3ms$.

4.5.3 Test-bed Setup and Validation of ECR-MAC framework

Based on the system-model highlighted in Section 4.2, we consider the test-bed shown in Figure 4.14 for testing and validating the functionality of ECR-MAC as highlighted in Section 4.5.1. The test-bed includes-

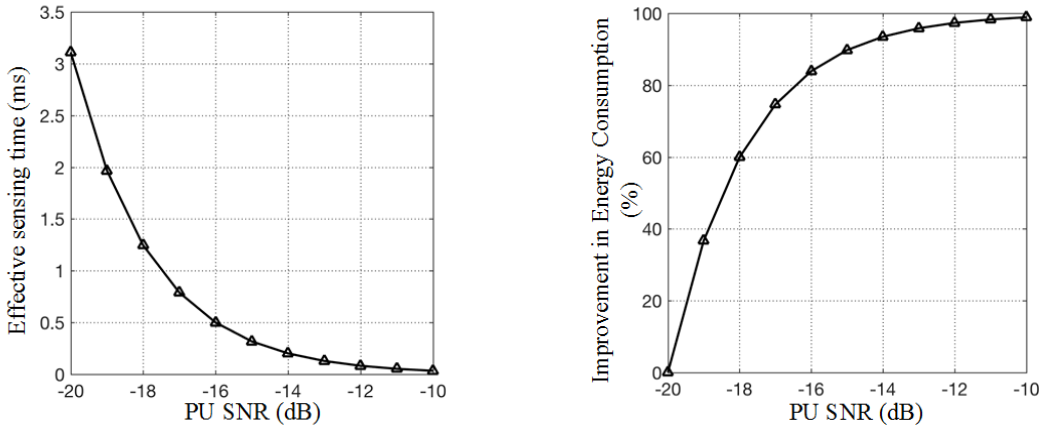

(a) (b)

Fig. 4.13 Variation of (a) Effective sensing time for $P_d = 0.9$, and (b) Percentage improvement in energy consumption due to PED method, with respect to different detected PU SNRs.

1. A PU system developed using 2 laptops with built in 100MBps IEEE 802.11a cards. The PU system emulates the incumbent PU transmitter (PU-Tx) and receiver pair (PU-Rx) with exponential ON-OFF traffic. The PU system uses channel 9 of 2.4GHz frequency band for video communication. The exponential traffic is generated by turning the video transmission ON and OFF using an automated tool for intervals governed by the exponential ON-OFF distribution. The time-period of the distribution is set to 3s and the PU activity is set to 20%.
2. A SU is composed of a Personal Computer (PC) connected to WARP v3 board whose Microblaze embedded processor is modified with our proposed ECR-MAC as per the algorithm shown in Figure 4.11. Leveraging on the PED method of ECR-MAC framework, the SU PC detects whitespaces in the PU channel and transmits UDP video to a receiver.
3. A PC connected to a WARP v2 board configured as a Normal receiver (N-Rx) receives the data transmitted by the SU.

In the designed ECR-MAC framework, the threshold and sensing time for the CS module are set to $THRES_{dB} = -113.31dB$, and $t_s = 30\mu s$ respectively. Moreover, as obtained previously, we set the SU sensing time $T_S = 3$ms. The inter-sensing duration T_D is set such that the normalized interference duration $\varepsilon = \Gamma = 0.06$ (for a certain detected PU SNR and set PU activity). Lastly, we calculate the maximum number of times the CS module can be accessed within the sensing duration of 3ms as $N_C = 100$ and obtain $B_T = 11$ using (4.25).

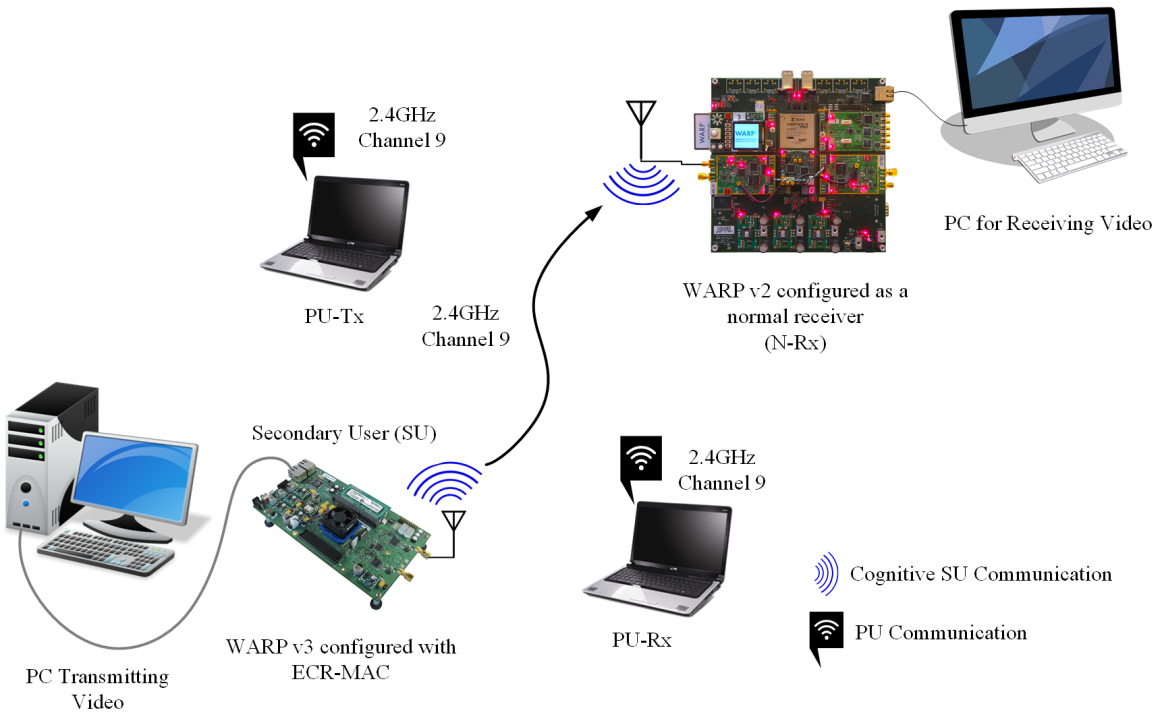

Fig. 4.14 Test-bed setup for demonstration of functionality of ECR-MAC framework.

For studying the activities of the SU and PU, we respectively monitor the incoming traffic at the Ethernet terminals of PU-Rx and N-Rx PCs with Network Emulator for Windows Toolkit Software. A snapshot of the real-time operation as recorded in the software is shown in Figure 4.15. It depicts that the ECR-MAC successfully detects the gaps in PU transmission and transmits its video successfully to the N-Rx.

Furthermore, we use a software called Putty [173] to monitor the internal activities of the ECR-MAC via USB-UART interface of WARP. It helps in debugging the sensing-transmission cycle executed by ECR-MAC. Figure 4.16 highlights two screenshots of the ECR-MAC activities when the channel is completely empty (Figure 4.16a) and when it is busy (Figure 4.16b). To illustrate the sensing operation, we continue channel sensing for the entire T_S duration and display the maximum value attained by busy counter. For easier representation, we denote the complete sensing time as $N_C = 100$. As shown in Figure 4.15, the ECR-MAC successfully performs energy detection based sensing and accurately detects the PU presence/absence.

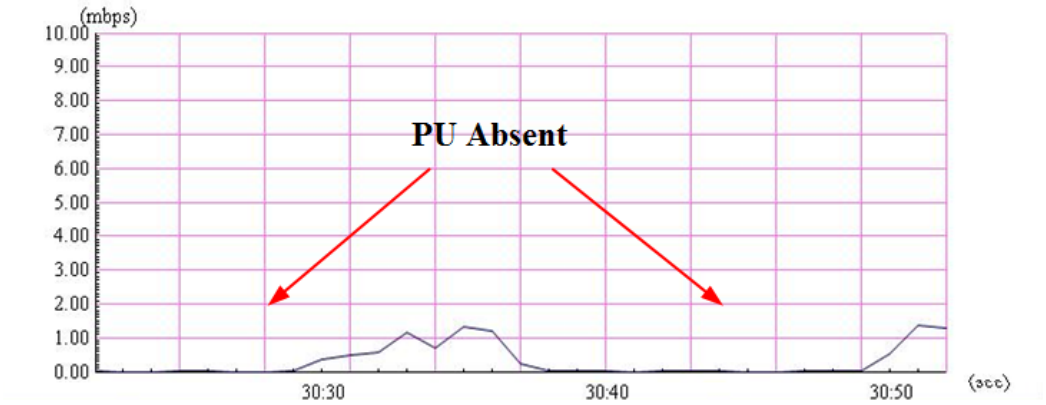

(a) PU transmitted signal

(b) Received SU video signal at N-Rx

Fig. 4.15 Network Emulator screenshots displaying the ability of ECR-MAC in facilitating SU transmission during spectrum holes in PU channel.

4.6 Conclusion

In this chapter, we have provided a holistic test-bed development, analysis and characterization of a CR based SU, which uses energy detection based spectrum sensing as one of its enabling methods. To this end, first we study the analytical modeling of various performance metrics of energy detecton sensing, namely receiver operating characteristics, normalized interference duration, and transmission probability. Following this, we conduct a comprehensive performance analysis of energy detection sensing in terms of the aforementioned performance metrics against system parameters like PU channel activity, SU receiver sensitivity, PU SNR, sensing time. The performance study revealed the trade-offs in achieving high detection probability with low receiver-sensitivity but at the cost of longer sensing time. Therefore, to address this inherent trade-off in WARP, we obtain a sensing time of 3ms for a receiver sensitivity of -20dB at 90% detection probability. We validate the effectiveness

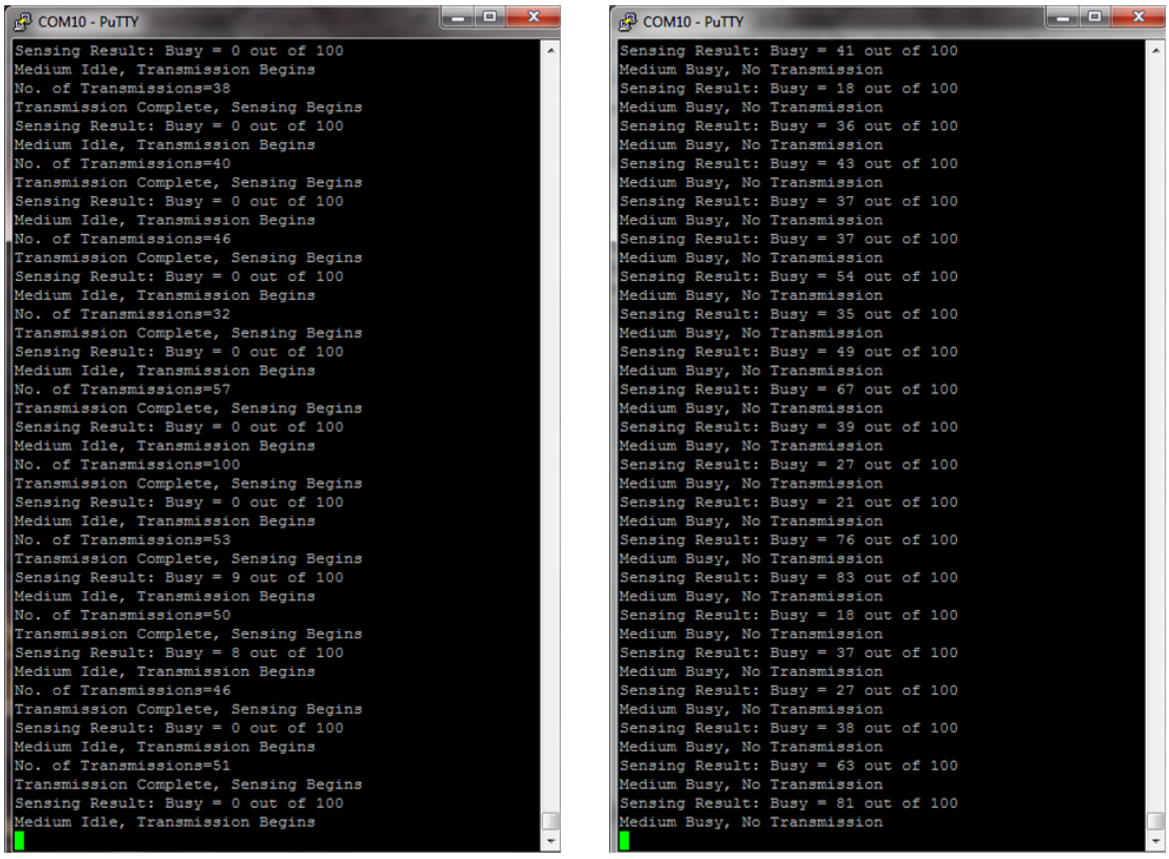

(a) Idle PU channel (b) Busy PU Channel

Fig. 4.16 Putty Screenshots showing internal operation of ECR-MAC when (a) PU channel is idle, (b) PU channel is busy.

of this characterization by successfully implementing energy detection in off-line mode using the WARPLab framework. Finally, motivated by the need to develop a real-time CR enabled SU, we introduce our proposed Practical Energy-Efficient Energy Detection (PED) method that efficiently uses the existing Carrier Sense (CS) module of a transceiver system to implement the energy detection based sensing as characterized earlier. In addition to being resource efficient, the PED method is also made energy-efficient in its sensing operation by incorporating within our proposed Energy Detection based CR MAC (ECR-MAC) framework developed at the embedded processor of WARP. Lastly, through a test-bed validation we demonstrate how ECR-MAC can be used to realize the real-time CR interface of a SU to facilitate IP enabled communication like video streaming over opportunistic PU channels.

Chapter 5

Performance Analysis of Scheduled Access Mode of the IEEE 802.15.6 MAC Protocol under Non-Ideal Channel Conditions

❝ *The advantage of the analytical approach is that it is widely applicable, and it can provide a considerable amount of qualitative information even with a relatively poor resolving power.*❞

- Christian de Duve, Nobel Laureat, Cytologist and Biochemist

After suitably designing the simulation model and test-bed model for WBAN, the next focus is the detailed analytical study of WBAN based on IEEE 802.15.6 scheduled access MAC, followed by suitable optimization to achieve optimal system performance. Detailed analytical modeling and performance evaluation allows users to study a communication network and analyze its performance even before the system is implemented. It gives an insight into the system performance and helps us understand the tradeoff between different system parameters. Moreover, it allows a system designer to choose optimal network parameters at the design stage thereby maximizing the system performance.

Delay, throughput and energy consumption are some of the most vital performance metrics for the sensor nodes of WBAN. Average delay of data frames is an important QoS metric for real-time health monitoring. Average throughput of sensor node helps in estimating the network capacity. While, average energy consumption analysis gives an estimate of the sensor life time. From this, we can also obtain energy-efficiency, which is defined as the ratio of the average throughput to energy consumption. It indicates how

efficiently energy is being utilized towards data transmission. ***For these reasons, in this chapter, we provide detailed mathematical derivations of closed form expressions of key performance indicators of WBAN leading to comprehensive performance analysis and subsequent optimization through suitable tuning of system parameters by exploiting CR capabilities of sensor nodes under non-ideal channel conditions***.

Initially, the expressions of average frame waiting delay, throughput, energy consumption and energy-efficiency of the sensor nodes are derived using queuing techniques. We also elaborate on the non-ideal channel characteristics of WBAN and its effect on the performance indicators. Following this, to lend credibility to the derived expressions, we validate the analytical model through simulations performed using our OPNET model developed in Chapter 3. In addition, we perform detailed analysis of system performance for variations in allocation intervals, traffic loads,payload sizes, beacon intervals, information data rate, error probability due to different modulation schemes and channel SNRs. Finally, by taking note of the trade-offs in system performance with respect to the selection of allocation intervals and payload sizes in IEEE 802.15.6 scheduled access mode, we propose an implementable LUT based approach that allows our already developed sensor nodes in Chapter 3 to leverage their CR capabilities to adapt their allocation intervals and payload sizes based on the channel SNR to achieve maximum energy-efficiency under frame delay and reliability constraints.

5.1 Introduction

Pervasive monitoring of human physiological parameters through wearable wireless medical sensors forming a network known as Wireless Body Area Network (WBAN), which is a key solution towards achieving an affordable and proactive healthcare [17]. It allows ubiquitous healthcare monitoring providing early diagnosis of diseases for patients and enhances patient mobility leading to speedy recovery. With the rise of embedded systems and advances in sensors such networks are becoming a reality [25].

A WBAN comprises of wireless sensors measuring physiological parameters of human body, and sending the data to a hub that is placed close to the body (within 3m) [17], [23]. The applications include: electromyogram, electrocardiogram, pulse oximeter, dosimeter and many more. The hub then forwards the data to an access point which may be connected to Internet, allowing ubiquitous health monitoring.

Current communication technology such as ZigBee [22] is not meant for WBAN-communications. ZigBee was primarily designed for wireless personal area networks operating at low data rates. It does not support increase in data rate, Quality of Service (QoS) and reliability needed for WBANs. To address this, IEEE 802.15.6 [23] Task Group developed

a short-range wireless communication standard for low power devices functional on, in, or around the human body meant to serve medical as well as entertainment applications. IEEE 802.15.6 supports QoS, data rates up to 10Mbps, extremely low power and high reliability.

Medium access control (MAC) protocols are one of the key enabling techniques of WBANs [25]. They play a vital role in determining the performance of WBAN in terms of the battery life of the energy constrained sensor nodes and the delay in sending a data packet to the hub. Contention free Time Division Multiple Access (TDMA) and contention based CSMA/CA or Slotted Aloha are the two basic MAC mechanisms used in WBANs to support variety of periodic and urgent traffic [26]. Both of these access mechanisms have their own advantages and shortcomings which depend on factors like data rate and network conditions [27]. Therefore, to integrate their advantages, IEEE 802.15.6 provides a hybrid MAC protocol that supports both CSMA-CA, Slotted Aloha and TDMA based Scheduled Access MAC (SAM). Since in depth study of SAM is still limited, in this chapter we perform its detailed analytical modeling, evaluate its performance and then optimize for maximum energy-efficiency.

5.1.1 Importance of SAM in Healthcare Monitoring

Patient monitoring using biomedical sensors is a popular WBAN application that can continuously or periodically monitor chronic and non-chronic diseases. In most of these cases the traffic is often correlated [31]. For example, to get a clearer picture of a patient's overall health, a physician requires a complete view of the patient's vitals namely temperature, blood pressure, ECG which have to be recorded simultaneously at periodic intervals. Similarly, for tracking the performance of an athlete, a WBAN need to continuously track high data rate applications like EMG, ECG, along with low data rate signals like temperature. Contention based MAC is not suitable in such cases of high traffic correlation [31] as they encounter heavy collisions and extra energy consumption. Schedule-based protocols such as TDMA, provide good solutions to the traffic correlation. These protocols are energy conserving protocols because the duty cycle is reduced and there are no contention, idle listening, and overhearing problems [31]. Usually, CSMA/CA is considered to be appropriate for low, urgent, adaptive, scalable traffic patterns and frequent network changes, whereas the TDMA is recommended for high periodic traffic and infrequent network changes [28–30]. A comparison between TDMA and CSMA protocols is reported in [32]. It is shown that TDMA method is more suitable for nondynamic types of networks. Fortunately, WBAN has a nondynamic network structure (fixed network topology), which forms the basis for further investigations on TDMA MAC by Marinkovic et al. in [33]. Further detailed account

of other related works based on TDMA in WBAN is provided in Section 5.2, which shows its active interest among researchers.

5.1.2 Different Modes of IEEE 802.15.6 SAM

The above sub-section establishes the significance of TDMA based SAM protocols in WBANs with high correlated traffic scenarios. Moreover, such networks may have sensors transmitting at low and/or medium to high data rates. To this end, Tachtazis et al. in [99] addressed the low data rate case by considering m-periodic allocations of IEEE 802.15.6 SAM. In m-periodic SAM [23], devices and hubs exchange frames in every m superframes. However, the analysis for medium to high data rate applications which requires 1-periodic SAM is yet to be carried out. Therefore, to adress this scenario, in this chapter, we consider the *1-periodic allocation* of IEEE 802.15.6 SAM [23], where nodes exchange frames with the hub in their scheduled Allocation Intervals (AIs) in every superframe. Further, we will focus only on *uplink traffic*, as it is the most commonly encountered traffic and also has been extensively considered for analysis in the literature [65, 66].

IEEE 802.15.6 [23] also suggests two different access continuation and termination mechanisms for 1-periodic uplink SAM in Sections 6.7.4/6.7.5 and Section 6.8 of [23]. We designate these two modes respectively as *Primary* and *Supplementary* (one which is not meant as a substitute of the primary mode). In the *Primary* mode, a connection can be terminated any time by the sensor node by transmission of a Modified Connection Request frame to the hub. This connection termination mechanism can be readily exploited in WBANs with high correlated and periodic traffic having either i) sensor nodes that are pre-defined to start and stop their sessions, as reported in [31], e.g. transmission of a five minute ECG signal at regular intervals of several hours, or ii) user initiated start and stop of a highly correlated monitoring session, as in case of the athlete monitoring. However, to avert situations where a sensor node might misuse such allocations, the standard recommends aborting connections which have not generated traffic for a considerable amount of time (equal to *mScheduledAllocationAborted* AIs). This also has the following interpretation: the presence of the abort mechanism ensures that even in the event of a momentary empty queue, neither the sensors nor the hub relinquish or reclaim the AIs until it exceeds the prescribed *mScheduledAllocationAborted* AIs. Even for high data rate applications (like EEG, EMG), such instances of empty queue are likely to arise as the service rate of a data frame is supposed to be greater than the packet arrival rate as illustrated by Rashwand et al. in [65]. However, such moments are quickly followed by more data packets.

Contrary to the primary mode, the *supplementary* mode exploits the *More Data* or *Last Frame* fields of transmitted frames to respectively convey whether there are any Data (or

Management) type frames pending for transmission or if this is the last frame to be transmitted in the present AI. Based on the appropriate combination, the AI will be reclaimed by the hub. This supplementary mode of operation can be beneficial for emergency applications with finite backlogged data [174], or sensor nodes with finite buffered traffic [175, 176] under high network load. On completion of the data transmission, such nodes which may not be pre-programmed can utilize the supplementary mode of SAM as an effective means of terminating a session. However, for high data rate applications it will often lead to frequent disconnections. This will result in unnecessary energy consumption and network delays which arises as a result of the subsequent connection establishment that is based on contention based CSMA/CA or Slotted Aloha, that in effect nullifies the advantages of using TDMA based SAM. The aforementioned reasons motivate us to base the analysis in this chapter following the primary mode of SAM. In addition, in Section 5.3.2, we propose a possible method that would allow both primary and supplementary modes to co-exist and be used according to the application needs.

5.2 Related Work and Motivation

In this section, we review the seminal works in the field of i) performance analysis in IEEE 802.15.6, ii) TDMA based WBAN MAC protocols, iii) queuing analysis of TDMA systems, and iv) generic vacation based queuing analysis, to bring out the motivation and novelty aspects of this work.

Performance analysis of IEEE 802.15.6 MAC protocols: The evaluation of the MAC protocols through analytical modeling has mainly been focused towards the CSMA/CA and slotted Aloha based contented medium access. Rashwand et al. in [65] provided frame delay analysis for CSMA/CA based MAC using queuing theory under realistic non-saturated traffic considering the empty state of a sensor node queue for error-prone channel conditions. In this regard, Sarkar et al. [66] provide further in depth analysis of reliability, throughput, delay and power consumption in CSMA/CA mode under saturated traffic and non-ideal fading channel conditions. In [177, 178], a non-Markovian analysis of the CSMA/CA access mode is provided in terms of throughput and delay limits. Chowdury et al. [67] analyzed the throughput performance of the slotted Aloha under varied traffic loads.

As for the contention free SAM, Tachtatzis et al. [99] performed energy analysis of the m-periodic uplink SAM in the context of medical applications. It considers only low traffic scenarios where a data frame is completely transmitted within a single AI without considerations for retransmission and frame deferrals. As evident from the literature survey, the work on IEEE 802.15.6 based SAM is very limited. This necessitate the need to perform

a detailed theoretical analysis of the IEEE 802.15.6 SAM, particularly for serving medium to high data rate applications leveraging the 1-periodic uplink SAM. Some of the relevant related work on general TDMA based MAC in WBAN are reviewed next.

TDMA based WBAN MAC: Focusing on TDMA based protocols, the authors in [175, 176] modify the existing IEEE 802.15.4 superframe to allocate more than one slots to the users based on their traffic. Similarly, Mohhamad et al. in [174] modify the IEEE 802.15.6 superframe to serve emergency data. However, in these works the nodes have buffered packets and the allocated slots are released to other nodes when the transmission is completed, which bear resemblance with the supplementary mode of IEEE 802.15.6 SAM. However, buffering of packets from high data rate applications, which is a point of interest in this chapter, in memory limited sensor nodes is not a feasible approach. In this regard, Marinkovi'c et al. in [33] proposes an Energy-Efficient Low Duty Cycle (EELDC) MAC protocol which supports streaming of large amount of data in WBAN. However, one major area where this user-defined MAC protocol differs from IEEE 802.15.6 is the allocation of only a single slot to a sensor within a superframe and the presence of separate reserved slots for packet re-transmission. Liu et al. [179] proposed a MAC for WBAN based on TDMA with QoS provisioning and energy-efficient design for different types of traffic. It is based on scheduling of sensor node transmissions by the hub at every superframe. The delay experienced by data frames in [179] is calculated using a traditional vacation based queuing system, which considers that after a sensor node finishes its scheduled transmission slots it goes to sleep which is viewed as the server's vacation. The work in [179] differs from IEEE 802.15.6 standard in the following aspects: i) Primary mode of SAM is based on fixed transmission order in every superframe, ii) when the queue of a node becomes empty within an AI, it does not immediately go for a vacation, however it may employ a Low Duty Cycling (LDC) technique as envisioned in [33] to reduce energy consumption, and iii) it does not consider the provision of deferring a frame transaction if it cannot be fitted into the present AI. A frame transaction includes transmission of a data frame and reception of an acknowledgement. The last two of the above-mentioned points prevent application of standard results of traditional vacation based queuing systems for SAM. We now review some seminal works on queuing analysis of TDMA based systems and general vacation based queuing systems.

Queuing Analysis of TDMA Systems: Performance analysis of traditional TDMA MAC is well investigated in [180, 181, 148]. Lam [148] discussed the analysis for TDMA with fixed slot assignment. In this chapter, the average delay was derived by obtaining the steady state Probability Generating Function (PGF) of queue length. The equilibrium point analysis for the fixed point TDMA and its derivation of average message delay is performed

by Tasaka in [181]. However, these works [181, 148] are not meant specifically for the IEEE 802.15.6. More in detail, in these works, the authors need not take into account the deferral of a frame transaction within an AI, and the presence of acknowledgment frames corresponding to every data message, or retransmission of data messages in case of an error in the transmission. All these factors make IEEE 802.15.6 SAM different from the traditional TDMA schemes and thereby calls for separate analysis. For the analysis, we adapt an approach that is inspired from M/G/1 systems with vacations. However, unlike [179], the modeling of the queue for SAM differs from traditional vacation or periodic vacation based systems. Before highlighting the significant differences, we briefly review some of the works on vacation based queuing systems.

Vacation based Queuing Systems: Traditionally, a server goes into vacation once the queue becomes empty [182]. Upon returning from vacation, if the server finds jobs waiting it starts serving them, or else it goes for another vacation. This vacation model as used in [179, 183] is not suitable for SAM. In [184, 185], for analyzing LTE/UMTS dowlink traffic, the authors considered that a node instead of immediately going to sleep (vacation) dwells in an inactivity region where a packet upon arrival at the base station will be served immediately. This has similarity with uplink SAM, where a queue of a sensor node after becoming empty within an AI will remain idle till the start of the IAI. However, unlike [184, 185], an IAI starts after the completion of an AI in a strictly periodic manner, irrespective of the state of the queue. For instance, consider that the time available within an AI is not adequate for completing the next frame transaction. Then, the service of the frame will be deferred to the next AI. As for the server (hub), it is in IAI (like being in vacation), but the node is still holding the frame which is waiting for service to resume in the next AI. Addressing this, in this chapter we model the service time to encompass the IAI in case of deferral. Furthermore, at the end of an IAI even if a queue is empty, instead of going for another vacation, as in [184, 185], the hub will serve a packet arriving within the AI immediately. Moreover, as compared to these works, we obtain different service times based on the state of the node in SAM. Doshi in [186] surveys the available vacation models for cyclic server queues. However, none of these provide a suitable match for SAM, where the server is modeled to go to vacation either when the queue is empty or when a specific number of jobs have been served.

In this chapter, we provide a detailed mathematical treatment of SAM and formulate the expressions for all the essential performance metrics like frame delay, throughput, energy consumption, reliability, and energy-efficiency. In addition, motivated by the LDC approach undertaken by Marinkovic et al. in [33], we incorporate the same in our analysis for ensuring minimal energy consumption. Further, inspired by Sarkar's work [66] for CSMA/CA, in

this chapter we consider non-ideal fading channel properties to model and analyze the aforementioned parameters for TDMA based SAM in WBAN. It is to be mentioned that none of the existing works have considered BCH coding, as mentioned in IEEE 802.15.6 [23], and its effect on the performance of MAC protocols. BCH coding provides a significant Signal-to-Noise Ratio (SNR) gain for systems [187]. Therefore, in our work, along with other parameters we also consider the effect of BCH coding to analyze the derived metrics for varied channel SNRs.

5.2.1 Contributions of this Chapter

We consider the primary mode of IEEE 802.15.6 1-periodic uplink SAM and perform the following:

❶ For delay analysis we evaluate the service time of the data frames and the PGF of queue length by considering the acknowledgment, deferral and retransmission policies of the standard. We extend the analysis to obtain throughput as a departure process from the queue. Lastly, we calculate the energy consumption of a sensor node by considering LDC.
❷ We also evaluate other necessary parameters like reliability in data transfer, and energy-efficiency of the nodes.
❸ Further, we take into consideration log-normal fading channel [61] characteristics and incorporate BCH coding, first of its kind, into the performance analysis.
❹ Our analytical model is validated with simulation results obtained from our customized IEEE 802.15.6 SAM built for WBAN in OPNET (Chapter 3).
❺ For performance analysis we take into account different system parameters like the length of AIs, Payload Sizes (PSs), varied traffic loads, beacon intervals, data transmission rate, non-ideal channel errors and SNRs, and then determine the optimal (and minimum) AIs and PSs for a certain traffic load that maximize the energy-efficiency of sensor nodes under frame delay and reliability constraints.
❻ Finally, we show how a system designer can prepare Look-Up Table (LUT) that allows nodes to adapt their optimum AIs and PSs based on the channel SNR.

5.2.2 Chapter Organization

This chapter is organized as follows. In Section 5.3 the system model is outlined. Section 5.4 presents the delay analysis. The throughput analysis and energy consumption analysis are provided in Section 5.5 and Section 5.6 receptively. Section 5.7 elaborates the non-ideal

channel modeling. In Section 5.8, first we validate our analytical model, and then conduct an extensive performance analysis of the aforementioned attributes and subsequently the optimal AI and PS are obtained in Section 5.9. Finally, we conclude the chapter in Section 5.10.

5.3 System Model

5.3.1 Basic Framework of IEEE 802.15.6

We consider a single hop star-topology where multiple sensor nodes and a hub are organized to form a WBAN, which is coordinated by the hub for medium access. The frames are exchanged between nodes and the hub.

All nodes and hubs comprise of a PHY layer and a MAC sublayer. For a node that has data to transmit, the MAC accepts *packets* (also termed as MAC service data units or MSDUs) from its higher application layer. The MAC sublayer then passes MAC *frames* (also known as MAC protocol data units or MPDUs) to the PHY layer. An MPDU comprises of MAC header and Frame Check Sequence (FCS) appended to the MSDU. Further, the PHY layer prior of transmission over the channel appends its header to the MPDU to produce PHY frame (also known as Physical protocol data unit or PPDU). In this chapter, unless specifically mentioned otherwise, the term frame refers to a PPDU, as MPDU and PPDU have a one-to-one mapping with the inclusion of PHY header in the PPDU.

All nodes and the hub need to establish a time reference base, if their medium access is to be scheduled in time. Therefore, as shown in Figure 5.1a [23], the time axis is divided into beacon periods (superframes) and each superframe is composed of allocation slots of equal length T_S and numbered from $0, 1, \cdots, j, \cdots, X$, where $X \leq 255$.

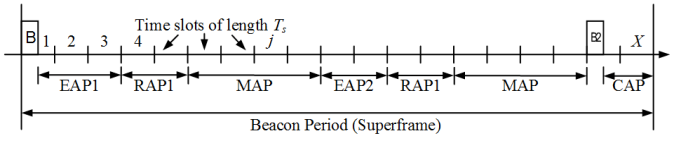

(a)

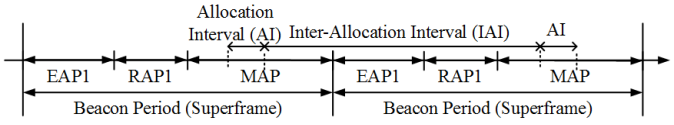

(b)

Fig. 5.1 (a) Layout of superframe and access phases in IEEE 802.15.6, (b) Layout of access phases as followed in this chapter.

In beacon mode operation, the hub communicates the boundaries of the superframe and synchronizes the sensor nodes through periodic transmission of beacons as shown in Figure 5.1a. The hub organizes applicable access phases in each superframe as illustrated in Figure 5.1a, where B stands for Beacon. The hub may place the access phases— Exclusive Access Phases (EAP1 and EAP2), Random Access Phase (RAP1 and RAP2), Managed Access Phase (MAP), and Contention Access Phase (CAP)— in the order shown in Figure 5.1a. Except RAP1, the hub may set the length of all other access phases to zero. The access during EAPs, RAPs and CAP is based on contention mechanism and access during MAP is scheduled. In this work, we focus on scheduled access in MAP. Therefore, we keep EAP1, RAP1 and MAP and set the lengths of all other access phases to zero as shown in Figure 5.1b. EAP1 is kept for emergency applications that may occur in a WBAN, while RAP1 is required for exchange of management frames such as in case of connection establishment of SAM session. It must be noted that for SAM, both CAP and RAP1 serves the same purpose. Thus, provided both CAP and RAP1 are of same length, the cyclic nature of SAM ensures that the steady state analysis and results presented in this chapter remain valid irrespective of whether RAP1 or CAP is set to zero.

5.3.2 SAM: Connection Establishment, Access Continuation and Termination

Connection Establishment: To obtain one or more new scheduled allocations, a sensor node shall send a Connection Request frame to the hub. For this the node may use CSMA/CA or slotted Aloha in contention periods (RAP1 in this case). The Connection Request contains- i) the wakeup period request which is set to one for 1-periodic allocations, and ii) Uplink Request Information Element (IE). Through these IEs, the sensor nodes request the hub for creation or modification of one or more scheduled allocations. Specifically, the nodes mention the *User Priority (UP)*, the *Minimum Length* N_M^{min} of AI required to barely satisfy the QoS metrics like delay and reliability, and the desired/optimum *Allocation Length* N_M^* for each superframe that maximizes the node energy-efficiency. Note that, the symbol N_M is used to represent any AI length. Our analysis presented in this Chapter will ultimately lead to the determination of the range $[N_M^{min}, N_M^*]$ and the corresponding PSs (P_{size} in bytes) based on the traffic load of the sensor nodes, channel SNR, superframe parameters and applicable data rates. To grant scheduled allocations requested by the sensor nodes, the hub may employ scheduling to assign AIs to the appropriate nodes based their request. Since, IEEE 802.15.6 SAM governs communication after an AI has been assigned to a node, a detailed discussion on the assignment problem is beyond the scope of this Chapter. However,

it is worth mentioning that the solution will depend on - i) number of nodes, ii) the node priorities, and iii) the number of available free MAP slots. After obtaining a solution, the hub sends Connection Assignment frames to the nodes, containing Assignment IEs that inform nodes about the accepted AIs.

Session Continuation and Termination: In primary mode of 1-periodic SAM, every sensor node is allocated their requested AIs within the MAP at fixed non-overlapping locations of every superframe (Figure 5.1b), where only uplink transmission of that particular sensor node is allowed without interference or collision from other sensor node transmissions. This is similar to static TDMA as in [148], which has the following features- i) due to the cyclic nature of allocation, the steady state analysis is dependent only on the length of the AI and not on the relative location of AI, and ii) the analysis for a sensor node performance does not depend on other sensor node transmissions which occur outside its AI [148]. The assignment for a particular sensor node remains valid until- i) the node ends the scheduled allocation by sending a disconnection request at a pre-determined time, for instance in case of periodic monitoring at regular intervals, ii) a connection change request is generated from the node to modify the session parameters, e.g. request to change the length of the AI due to change in channel SNR, or iii) the session is aborted by the hub after failing to receive any frame in the last $mScheduledAllocationAborted$ AIs.

In this chapter, we strictly follow the primary mode. But to facilitate coexistence with the supplementary mode, we propose the following possible implementation. The supplementary mode sets the *More Data* field of MPDU to 0 if there are no more data or management frames pending for transmission, thereby relinquishing the AI [23]. Based on this, the supplementary mode can be transformed into primary mode by allowing a sensor node to set $MoreData = 1$ to intimate the hub about the pending Modified Connection Request management frame, which is to be finally transmitted to terminate the SAM session. This will prevent the hub from relinquishing the AI. When $MoreData = 1$, the $LastFrame$ field is set to 1 to intimate the hub about deferral of frame transaction, which is explained next.

5.3.3 SAM: Uplink Data Communication

Upon receiving the Connection Assignment frame from the hub, a sensor node may initiate a data frame transaction with the hub anywhere within its AIs, if the data frame, acknowledgment and an appropriate guard time (GT) [23] can fit into the current AI of N_M slots. This is illustrated in Figure 5.2. The data frames are of fixed length l (slots) and l_b (bits) and arrives at the sensor node (denoted U) according to a Poisson process with mean arrival rate λ. It is reasonable to expect that multiple data frame transmissions can occur within a single AI. If the time duration between the current time and the end of the current AI is not long

enough to fit a frame transaction, the node shall defer the transmission till its next AI. The node sleeps in the time duration between two successive AIs defined as the Inter-Allocation Interval (IAI) as shown in Figure 5.1b. During IAI, the node can generate new packets which will be stored in a queue maintained by it and transmitted later during an AI.

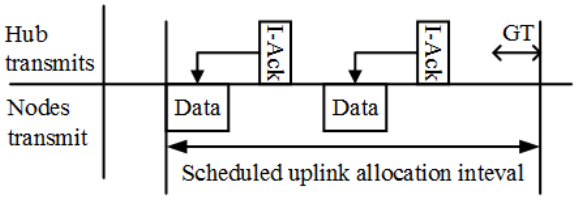

Fig. 5.2 Frame transactions in scheduled uplink allocation interval.

The system is modeled with non-ideal channel conditions, and for Immediate Acknowledgment (I-Ack) Policy [23]. An I-Ack frame is transmitted by the hub to acknowledge successful receipt of the previous frame. The size of I-Ack frame is denoted by *ack* (slots) and ack_b (bits). Let *ber* denotes the Bit Error Rate (BER) of the channel due to the error-prone non-ideal nature of the channel. Therefore, the probability that the data frame and its corresponding I-Ack frame are transmitted without getting corrupted by any error can be denoted as, $\eta = (1 - ber)^{l_b + ack_b}$. Detailed modeling of the non-ideal channel in WBAN will be discussed later in Section 5.7. In the event of an un-successful reception of either the data frame or its I-Ack, the node retransmits the data frame. The data frame is dropped after it exceeds the maximum limit *R* for such retransmissions.

5.3.4 Low Duty Cycling

For minimizing the energy consumed by a sensor node we adapt the duty cycling approach envisioned by Marinkovic et al. in [33]. In [33], a duty cycle is defined as the fraction of time that a sensor is in an "active" state. For the sensor, this is the time the transceiver is ON (RF activity time), regardless if it is transmitting data, receiving data, or idly waiting for an I-Ack. The TDMA based protocol envisioned in [33], allows sensor nodes to go to power down state after a frame has been transmitted. During power down (or sleep) mode, only the internal time counter and ADC sampling are active, which provide the appropriate *interrupts* necessary to wake up the sensor node. Based on this, we consider the following duty cycling approach during a SAM session:

1. A sensor node remains active when a frame is serviced. However, when the service of a frame is deferred, the sensors will go to sleep state, and wake up prior to the beginning of the upcoming AI.

2. When the queue of a sensor node becomes empty, it goes to sleep. Following this, it will again wake up prior to the service of the next incoming packet.
3. The sensor node also wakes up for periodic synchronization with the hub through reception of a beacon. Periodic synchronization is required by the sensor nodes to compensate for their relative clock drifts with respect to the hub [23]. As per IEEE 802.15.6, the sensor node needs to re-synchronize every SI_n superframes termed as the $mNominalSynchInterval$. After re-synchronization sensor node again goes to sleep.

Note that, similar to [33, 99], in this chapter we focus only on the energy consumed by the transceiver of a node.

5.3.5 Assumptions

We make following assumptions to simplify the analysis presented in this chapter:

- The connection assignment process is a one-time operation that does not affect steady state analysis related to data frame transmission in SAM.
- The time before a SAM session is aborted i.e. $mScheduledAllocationAborted$ AIs is sufficiently long to not affect the steady state analysis. The default value of $mScheduledAllocationAborted$ is 32 [23]. For example- in case of beacon periods of 0.3s or 0.5s, the equivalent time before a session can be aborted will be 9.6 mins and 16 mins respectively. The probability of a frame not arriving for 9.6 mins or 16 mins within an active session is almost zero for a Poisson arrival process for the concerned medium to high data rate applications.
- To simplify the analysis, initially we do not consider the guard time (GT_n) within an AI as GT_n is in the order of micro-seconds whereas the AIs are in the order of several milli-seconds. However, the final results are derived by incorporating GT_n through a simple transformation,

$$N_M \rightarrow N_M - \frac{GT_n}{T_S} \tag{5.1}$$

Equation 5.1 considers the guard time as part of the IAI. However, this incorporation of GT_n do not make any noticeable changes to delay or throughput calculations. While for energy calculations, its effect is noteworthy only during periodic re-synchronization that is taken up separately in Section 5.6.

In the following sections, we calculate the average frame delay, throughput and energy consumption of the sensor node. Table 5.1 summarizes the symbols used in the chapter.

Table 5.1 Summary of symbols used

Symbol	Meaning
X	Beacon interval
T_S	Allocation slot length
N_M	Allocation interval length
P_{size}	Payload size
l, l_b	Data frame length (in slots and bits)
ack, ack_b	I-Ack frame length (in slots and bits)
ber_u, ber, ser_u, ser	Uncoded/Coded BER and SER
γ	Channel SNR
η, η_d, η_a	Successful transfer prob of a data and I-Ack pair, a single data frame and a single I-Ack
R	Re-transmission limit
λ	Packet arrival rate
$sifs$	Short inter-frame space
GT_n, SI_n	Guard time and Synchronization Interval
L_s, L_c	Successful & unsuccessful transaction time
L_d	IAI length or Deferral time
$\mathscr{L}_A(s)$ $\mathscr{L}_B(s)$ $\mathscr{L}_C(s)$	$\mathscr{L}T$[a] of service times of different scenarios
$\overline{X}_a$ $\overline{X}_b$ $\overline{X}_c$	Mean service time of different scenarios
n	No. of Frames Slots with an AI
r	Remainder of AI not covered by frame slots
$\Pi(z)$	PGF[b] of number of frames in queue
a_i, b_i, c_i	No. of packet arrivals in i^{th} frame departure
$A(z)$, $B(z)$, $C(z)$	PGF of a_i, b_i, c_i
$\mathscr{L}_M(s)$, $\mathscr{L}_I(s)$	$\mathscr{L}T$ of MAP duration and IAI
$\bar{I}$	Mean IAI
$\overline{W}$	Mean waiting delay
T	Average throughput
D	Average inter-departure time
p_s	Reliability of data transfer
$I_t, I_r, I_i, I_{wup}, I_s$	Current consumptions while Tx, Rx, in idle state, powering on/down and in sleep state
V_s	Supply voltage
E_{avg}	Average energy consumed by sensor node
EE	Energy-efficiency
μ, σ	Log-normal channel coefficients

[a] $\mathscr{L}T$=Laplace Transform, [b]PGF=Probability Generating Function.

5.4 Waiting Delay Analysis

We analyze the delay of a packet arriving at sensor node U by employing embedded Markov chain analysis [182]. In this analysis, the Markov chain of the number of frames in the queue of U is embedded just after the frame departure instants and we consider how the system evolves from one departure instant to the next. A frame departure instant is defined as the time instant when the service of a particular frame is complete. While the service time is defined as the time a node takes to start its transmission attempt till the time it has been successfully transmitted or dropped when it exceeds the maximum retry limit. Due to the inherent nature of the cyclic ordering of AI and IAI, a frame to be serviced will experience different service times based on the arrival of the frame and/or the arrival/departure of previous frames. Therefore, we also evaluate the average service time of a frame under the various scenarios considered for embedded Markov Chain analysis. To this aim, we perform computations in Laplace domain which makes the analysis simpler. Note that, due to presence of an erroneous channel, the service time of a frame may comprise of multiple data frame transactions. A data frame transaction between node U and the hub comprises of the actual data frame transmission, the reception of corresponding acknowledgment from the hub and a short inter-frame space ($sifs$) between the transmission and reception. Therefore, the time spent towards a data frame transaction is denoted as $L_x = l + ack + sifs$. Subscript 'x' is replaced by 's' or 'c' for successful or unsuccessful transmission respectively.

5.4.1 Embedded Markov Chain Analysis

The embedded Markov chain analysis obtains a relation for the number of frames (PPDU) left in the queue by a frame departure. The Markov chain analysis can be treated under the following three scenarios:

(S1) i^{th} frame departure leaves the queue empty and

- (S1a) the $(i+1)^{\text{th}}$ packet (MSDU) arrives during an AI.
- (S1b) the $(i+1)^{\text{th}}$ packet arrives during a IAI.

(S2) i^{th} frame departure leaves the queue non-empty.

We perform embedded Markov chain analysis for each scenario to derive the expression for the number of frames left in the queue just after a frame departure. Let n_i be the number of frames left behind in the queue after i^{th} frame departure. We relate the states of the queue at the i^{th} and $(i+1)^{\text{th}}$ instants and derive the relations for n_{i+1}. Thereafter, we derive the service time of the frame for each scenario.

5.4.1.1 Scenario S1a: Empty queue after i^{th} frame departure and the next $(i+1)^{\text{th}}$ packet arrives during an AI

This scenario is illustrated in Figure 5.3, which depicts that the number of frames left behind in the queue after the $(i+1)^{\text{th}}$ frame departure will be equal to the a_{i+1} packets that have arrived during the service time of that frame. This can be expressed as

$$n_{i+1} = a_{i+1}, \qquad j = 0, n_i = 0 \tag{5.2}$$

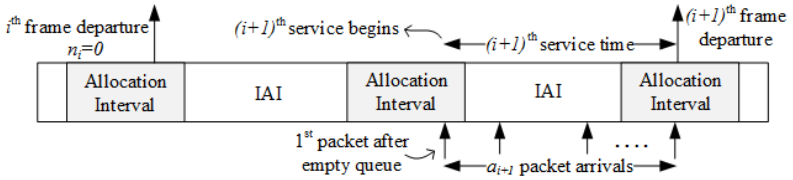

Fig. 5.3 Frame departure and packet arrivals for Scenario S1a.

As evident from (5.2), the condition of the $(i+1)^{\text{th}}$ packet arriving during an AI means that no packet arrival occurred after the queue became empty in any of the earlier AIs and IAIs (i.e. $j = 0$). Thus, the probability ($\widehat{F_0}$) that the $(i+1)^{\text{th}}$ packet arrives in an AI after the i^{th} frame departure leaves the queue empty can be obtained upon simplification as

$$\begin{aligned} \widehat{F_0} &= (1 - f_{M,0}^{(1)}) + f_{M,0}^{(1)} f_0^* (1 - f_{M,0}) \left[1 + f_0^* f_{M,0} + \cdots\right] \\ &= \frac{(1 - f_{M,0}^{(1)}) + f_0^* \left(f_{M,0}^{(1)} - f_{M,0}\right)}{1 - f_0^* f_{M,0}} \end{aligned} \tag{5.3}$$

where $f_{M,0}$ is the probability of no packet arrival during an AI (except for the 1st AI of frame departure), and is given as

$$f_{M,0} = \mathscr{L}_M(\lambda) \tag{5.4}$$

where, $\mathscr{L}_M(s) = \mathscr{L}(\delta(t - N_M T_S)) = e^{-sN_M T_S}$ is the Laplace transform ($\mathscr{L}T$) of the pdf of the AI of N_M slots and '$\mathscr{L}$' denotes the Laplace transform operator. Furthermore, f_j^* denotes the probability of j packet arrivals during an IAI. Let $\mathscr{L}_I(s) = e^{-sL_d T_S}$ denote the $\mathscr{L}T$ of the pdf of IAI of length $L_d = (X - N_M)$ slots (see Figure 5.1b). Then the PGF of the number of packet arrivals during an IAI can be related to f_j^* as $\mathscr{L}_I(\lambda - \lambda z) = \sum_{j=0}^{\infty} f_j^* z^j$ [182]. Thus, f_0^* is given as

$$f_0^* = \mathscr{L}_I(\lambda) \tag{5.5}$$

Lastly, we denote $f_{M,0}^{(1)}$ as the probability of no packet arrivals in the first AI between the instant when the i^{th} frame departure leaves the queue empty and the end of that AI. Let t

denote the time of departure of the i^{th} frame with respect to the start of the AI. Since t can lie anywhere between L_sT_S and N_MT_S with equal probability, $f_{M,0}^{(1)}$ can be obtained as

$$f_{M,0}^{(1)} = \int_{L_sT_S}^{N_MT_S} \frac{e^{-\lambda(N_MT_S-t)}}{(N_M-L_s)T_S}\,\mathrm{d}t = \frac{1}{\lambda}\frac{1-e^{-\lambda(N_M-L_s)T_S}}{(N_M-L_s)T_S} \tag{5.6}$$

We also calculate the PGF ($A(z)$) of the number of packet arrivals during a frame service time in scenario S1a as

$$A(z) = \mathscr{L}_A(\lambda - \lambda z) \tag{5.7}$$

where $\mathscr{L}_A(s)$ is the $\mathscr{L}T$ of the pdf of the service time of a frame under scenario S1a, which is derived next. Equation (5.2) and the PGF obtained in (5.7) will be used for further delay analysis in Section 5.4.2.

Evaluation of pdf of service time of frame under S1a: $\mathscr{L}_A(s)$

In Figure 5.4, we draw a Continuous Time Markov Chain (CTMC) that considers all possibilities of arrival of a new frame within an AI and its subsequent service as per IEEE 802.15.6 SAM. For developing the CTMC, in Figure 5.5a we visualize the AI to be composed of $n = \lfloor N_M/L_s \rfloor$ Frame Slots (FS) each with L_s slot duration in addition to the last r slot duration, where $r = N_M \% L_s$. The symbol '%' denotes the modulus operator. Further, for this scenario S1a, we consider each FS of the AI where a packet first arrives to be composed of sections as shown in Figure 5.5b. For example, in the u^{th} FS, the section AS(u,1) denotes the first r slot duration and section AS(u,2) represents the next $(L_s - r)$ slot duration. The last section of L_s slots is denoted as AS(d) because a frame arriving in this interval will be deferred. This division of a FS into sections will not be required for evaluation of Scenarios S1b and S2. In the CTMC of Figure 5.4, the blocks S(u,1), $u = 1,2,\cdots,n$; S(u,2), $u = 1,2,\cdots,(n-1)$; and S(d) corresponds to the arrival of a packet in sections AS(u,1), AS(u,2) and AS(d) of an AI respectively (refer Figure 5.5b). Using the uniformity property of Poisson arrivals [188] it can be shown that, given a packet arrives within an AI, the arrival instant relative to the start of the AI is uniformly distributed over AI length. This explains the probabilities associated with the blocks in Figure 5.4. The analysis based on this CTMC is divided into two parts. First, we obtain the $\mathscr{L}T$ of pdf of the time taken for service of a frame in each of these blocks and also their corresponding mean service times. Then, following Figure 5.4, we combine the service times of individual blocks to obtain the mean service time of a frame for Scenario S1a.

The internal structure of one block of each category (S(u,1), S(u,2) and S(d)) is shown in detail in Figure 5.6. The CTMC is modeled after the states of the node when a new frame starts its first transmission attempt till the moment it is serviced. For the CTMC, we consider

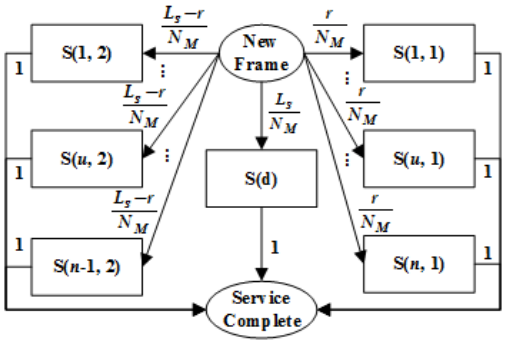

Fig. 5.4 CTMC for service of a data frame under Scenario S1a.

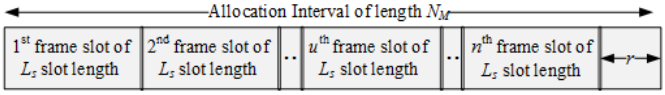

(a) Viewing AI as composed of Frame Slots (FS)

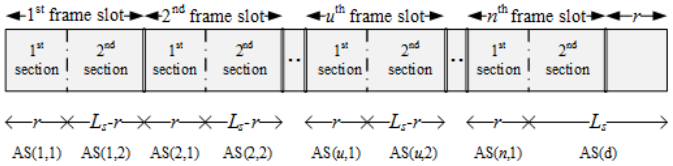

(b) Each FS is considered to have sections particularly for Scenario S1a

Fig. 5.5 Composition of an Allocation Interval (AI).

the general case of $n < R$. However, following Figure 5.6, the final expressions are obtained for any value of n and R. The CTMC is constructed as a 3-tuple with the following states:

1. (k, u, T) representing the k^{th} transmission attempt of the frame at u^{th} FS (symbol 'T' denotes Transmission),
2. (k, u, N) representing deferral of the k^{th} transmission attempt of the frame at u^{th} FS (symbol 'N' denotes No-transmission).

For block S(u,1), $u = 1, 2, \cdots, n$, as shown in Figure 5.6a, a packet first arriving within section AS(u,1), will make its next transmission attempt (in case of an error with probability $(1-\eta)$) in AS($u+1$, 1). Similar argument also holds for block S(u,2), $u = 1, 2, \cdots, (n-1)$, as shown in Figure 5.6b. The subsequent transmission attempts within the AI follow similar pattern until a frame deferral occurs, which is discussed next. After an unsuccessful transmission attempt at state $(k, n$,T) in Figure 5.6a and state $(k, n-1$, T) in Figure 5.6b, it is observed that the $(k+1)^{\text{th}}$ transmission in both the cases is deferred and the node moves to state ($k+1$, 1, N). Time spent in state ($k+1$, 1, N) for blocks S(u,1), $u = 1, 2, \cdots, n$, and S(u,2), $u = 1, 2, \cdots, (n-1)$, can be obtained as $\left(L_d + \frac{r}{2}\right)$ and $\left(L_d + \frac{L_s+r}{2}\right)$ slots respectively.

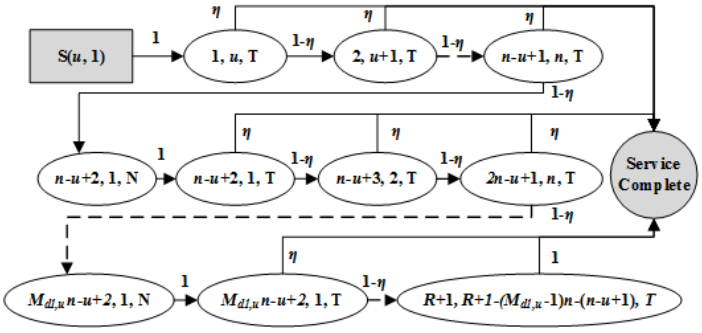

(a) CTMC for block S(u,1)

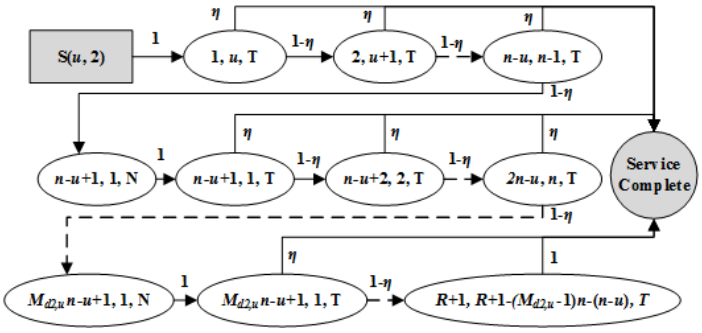

(b) CTMC for block S(u,2)

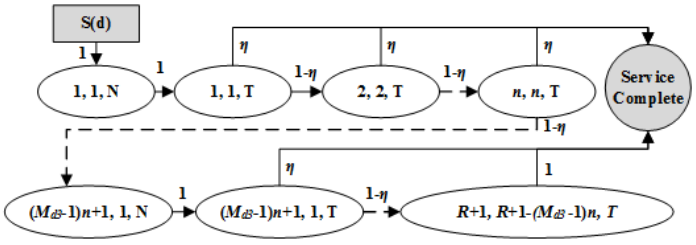

(c) CTMC for block S(d)

Fig. 5.6 CTMC for different blocks of Figure 5.4 for $n < R$.

It is to be noted that after the 1st deferral, every transmission attempt until the frame is serviced will always be at the beginning of a FS.

At a finer level of detail, it can be observed that the states occurring after the first deferral of a frame in blocks S($u-1$,2) and S(u,1) for $u = 2,3,\cdots,n-1$ are same. This repetition of states in the CTMC of Figure 5.4 is done for simplifying the derivation of the service time of a frame for each block. Finally, considering block S(d) in Figure 5.6c, we observe that the first transmission attempt is deferred for $\left(L_d + \frac{L_s}{2}\right)$ slots till the beginning of the next AI.

Following Figure 5.6, we derive the $\mathscr{L}T$ of the pdf of the service time of a frame arriving in blocks S(u,1), $u = 1,2,\cdots,n$; S(u,2), $u = 1,2,\cdots,(n-1)$; and S(d) ($\mathscr{L}_{A1,u}(s), \mathscr{L}_{A2,u}(s)$ and $\mathscr{L}_{A3}(s)$) respectively in (5.8), (5.9) and (5.10).

$$\mathscr{L}_{A1,u}(s) = e^{-sL_sT_S}\eta\left[\sum_{\substack{j=0\\ j\le R}}^{n-u}(1-\eta)^j e^{-sjL_cT_S} \quad + \right.$$
$$\left.(1-\eta)^{n-u+1}e^{-s(n-u+1)L_cT_S}e^{-s\left(L_d+\frac{r}{2}\right)T_S}\sum_{\substack{m_d=1\\ R>n-u}}^{M_{d1,u}}\left\{(1-\eta)^{(m_d-1)n}e^{-s(m_d-1)XT_S}\sum_{\substack{q=0\\ q+(m_d-1)n\\ +(n-u+1)\le R}}^{n-1}(1-\eta)^q e^{-sqL_cT_S}\right\}\right]$$
$$+(1-\eta)^{R+1}\left[e^{-s(R+1)L_cT_S}\Big|_{(n-u)\ge R} + e^{-s\left(L_d+\frac{r}{2}\right)T_S}e^{-s(M_{d1,u}-1)XT_S}e^{-s\left(R+1-(M_{d1,u}-1)n\right)L_cT_S}\Big|_{(n-u)<R}\right] \tag{5.8}$$

$$\mathscr{L}_{A2,u}(s) = e^{-sL_sT_S}\eta\left[\sum_{\substack{j=0\\ j\le R}}^{n-u-1}(1-\eta)^j e^{-sjL_cT_S} \quad + \right.$$
$$\left.(1-\eta)^{n-u}e^{-s(n-u)L_cT_S}e^{-s\left(L_d+\frac{L_s+r}{2}\right)T_S}\sum_{\substack{m_d=1\\ R+1>n-u}}^{M_{d2,u}}\left\{(1-\eta)^{(m_d-1)n}e^{-s(m_d-1)XT_S}\sum_{\substack{q=0\\ q+(m_d-1)n\\ +(n-u)\le R}}^{n-1}(1-\eta)^q e^{-sqL_cT_S}\right\}\right]$$
$$+(1-\eta)^{R+1}\left[e^{-s(R+1)L_cT_S}\Big|_{(n-u-1)\ge R} + e^{-s\left(L_d+\frac{L_s+r}{2}\right)T_S}e^{-s(M_{d2,u}-1)XT_S}e^{-s\left(R+1-(M_{d2,u}-1)n\right)L_cT_S}\Big|_{(n-u-1)<R}\right] \tag{5.9}$$

$$\mathscr{L}_{A3}(s) = \eta e^{-sL_sT_S}e^{-s\left(L_d+\frac{L_s}{2}\right)T_S}\sum_{m_d=1}^{M_{d3}}\left\{(1-\eta)^{(m_d-1)n}e^{-s(m_d-1)XT_S}\sum_{\substack{q=0\\ q+(m_d-1)n\le R}}^{n-1}(1-\eta)^q e^{-sqL_cT_S}\right\}$$
$$+(1-\eta)^{R+1}e^{-s\left(L_d+\frac{L_s}{2}\right)T_S}e^{-s(M_{d3}-1)XT_S}e^{-s(R+1-(M_{d3}-1)n)L_cT_S} \tag{5.10}$$

Where, $M_{d1,u}$, $M_{d2,u}$, and M_{d3} denote the maximum number of AIs (barring the 1st AI) that the service of a frame may extend for blocks S(u,1), S(u,2) and S(d) respectively, and are obtained as

$$M_{d1,u} = \left\lceil \frac{(R+1)-(n-u+1)}{n} \right\rceil \tag{5.11}$$

$$M_{d2,u} = \left\lceil \frac{(R+1)-(n-u)}{n} \right\rceil \tag{5.12}$$

$$M_{d3} = \left\lceil \frac{(R+1)}{n} \right\rceil \tag{5.13}$$

Equation (5.8) comprises of two parts: the first part deals with a successful frame transaction, which may occur after a number of unsuccessful transmission attempts, while the second part is related to a frame being dropped, which occurs after the number of transmission attempts have exceeded $(R+1)$. Considering the successful frame transaction, the conditions placed beneath each summation symbol signifies the possible scenarios where the final successful transmission might occur for a packet arriving in u^{th} FS of the first AI. The expressions associated with $(j \leq R)$ refers to the possibility of successful transaction occurring in the $(j+1)^{\text{th}}$ FS of the first AI, whereas the condition $q+(m_d-1)n+(n-u+1) \leq R$ refers to the possibility of the successful transmission occurring in the q^{th} FS of $(m_d+1)^{\text{th}}$ AI. Similarly, the dropped frame scenario will occur in the first AI if $(n-u) \geq R$ or else it will occur in the successive AIs following the deferral procedure. Likewise, (5.9) and (5.10) can also explained following a similar argument.

From Figure 5.4, and combining (5.8), (5.9) and (5.10), we obtain

$$\mathscr{L}_A(s) = \frac{r}{N_M} \sum_{u=1}^{n} \mathscr{L}_{A1,u}(s) + \frac{L_s - r}{N_M} \sum_{u=1}^{n-1} \mathscr{L}_{A2,u}(s) + \frac{L_s}{N_M} \mathscr{L}_{A3}(s) \tag{5.14}$$

The mean service time $(\overline{X}_a)$ for a data frame under scenario S1a can be obtained by taking the first derivative of $\mathscr{L}_A(s)$ as $\overline{X}_a = -\mathscr{L}_A{}'(0)$, and the second order moment can be given as $\overline{X_a^2} = \mathscr{L}_A{}''(0)$.

5.4.1.2 Scenario S1b: Empty queue after i^{th} frame departure and the next $(i+1)^{\text{th}}$ packet arrives during an IAI

In this scenario, the service of the $(i+1)^{\text{th}}$ frame will begin after the end of the IAI in which it had arrived. There can be multiple packet arrivals during the IAI where the $(i+1)^{\text{th}}$ packet arrives. This event is illustrated in Figure 5.7. Hence, the probability (f_j) of j packet arrivals during an IAI for the first time since the queue became empty can be obtained upon

simplification using (5.5) as

$$f_j = f_{M,0}^{(1)} f_j^* \left[1 + f_{M,0} f_0^* + \cdots\right] = \frac{f_{M,0}^{(1)} f_j^*}{1 - f_0^* f_{M,0}}, j \geq 1 \tag{5.15}$$

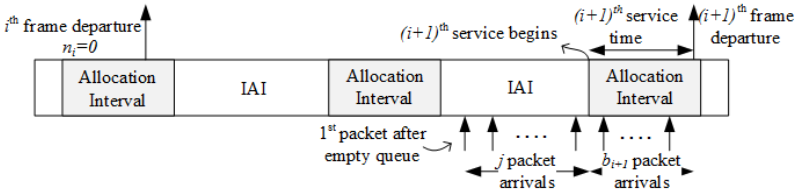

Fig. 5.7 Frame departure and packet arrivals for Scenario S1b.

From (5.15), we evaluate the PGF ($F(z)$) of the number of packet arrivals during an IAI for the first time since the queue became empty as

$$F(z) = \sum_{j=1}^{\infty} f_j z^j = \frac{\mathscr{L}_I(\lambda - \lambda z) - f_0^*}{1 - f_0^* f_{M,0}} \tag{5.16}$$

Thus, for this scenario, as depicted in Figure 5.7, we get the number of frames left after the $(i+1)^{\text{th}}$ frame departure as

$$n_{i+1} = j + b_{i+1} - 1, \qquad j \geq 1, n_i = 0 \tag{5.17}$$

where b_{i+1} is the number of packet arrivals during the service of the $(i+1)^{\text{th}}$ frame under Scenario S1b. Similar to (5.7), the PGF ($B(z)$) of the number of arrivals during the service time of a frame in this scenario can be obtained as

$$B(z) = \mathscr{L}_B(\lambda - \lambda z) \tag{5.18}$$

where $\mathscr{L}_B(s)$ is the $\mathscr{L}T$ of the pdf of the service time of a frame under Scenario S1b, which is derived next.

Evaluation of pdf of service time of frame under S1b: $\mathscr{L}_B(s)$

Under Scenario S1b, a packet arriving in an IAI will start its service at the beginning of the 1st FS of the AI following the IAI. Therefore, the service time of the frame will be similar to the packet arriving in block S(d) of Scenario S1a, except that there is no deferral and the

service begins at the start of the AI. Therefore, using (5.10) $\mathscr{L}_B(s)$ is related to $\mathscr{L}_{A3}(s)$ as

$$\mathscr{L}_B(s) = \mathscr{L}_{A3}(s)\, e^{s\left(L_d + \frac{L_s}{2}\right)T_S} \tag{5.19}$$

Finally, using (5.19), the mean service time for a data frame under Scenario S1b can be obtained as $\overline{X}_b = -\mathscr{L}_B{}'(0)$, and the second order moment can be given as $\overline{X_b^2} = \mathscr{L}_B{}''(0)$.

5.4.1.3 Scenario 2 (S2): Non-empty queue after i^{th} frame departure

Consider the case of non-empty queue when the i^{th} frame departs and immediately the node begins the service of the $(i+1)^{\text{th}}$ frame. While the frame is being serviced, new packets can arrive at the node, as shown in Figure 5.8, where there are c_{i+1} packet arrivals during the service of the $(i+1)^{\text{th}}$ frame. Thus, the number of frames left after the $(i+1)^{\text{th}}$ frame departure can be given by

$$n_{i+1} = n_i + c_{i+1} - 1 \qquad , n_i > 0 \tag{5.20}$$

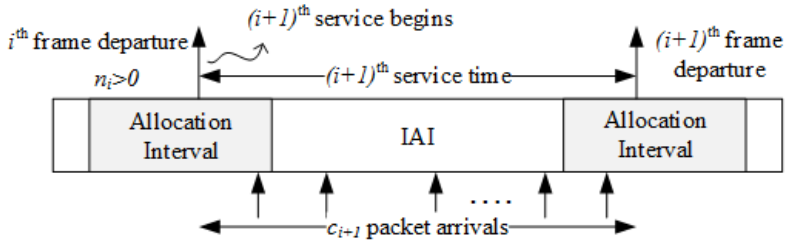

Fig. 5.8 Frame departure and packet arrivals for Scenario S2.

The PGF ($C(z)$) of the number of arrivals during the service time of a frame in this scenario is represented as

$$C(z) = \mathscr{L}_C(\lambda - \lambda z) \tag{5.21}$$

where $\mathscr{L}_C(s)$ is the $\mathscr{L}T$ of the pdf of the service time of a frame under Scenario S2.

Evaluation of moments of service time of frame under S2

Due to the inherent nature of Scenario 2, instead of obtaining the actual pdf $\mathscr{L}_C(s)$, we derive only its first two moments, i.e. the mean $\overline{X}_c = -\mathscr{L}_C{}'(0)$, and mean square value $\overline{X_c^2} = \mathscr{L}_C{}''(0)$, that will be used for further analysis in Section 5.4.2.

It is well established that for a stable queue the service rate must be greater than the packet arrival rate. Then the scenario of a non-empty queue will at some point arise after an

empty queue. Therefore, derivation of the moments of service time of the packets following the first packet arriving to an empty queue is the topic of interest. The evaluations can be split into two cases: Case1) the first packet to an empty queue arrives in an AI after which the queue remains non-empty, and Case2) the first packet to an empty queue arrives in an IAI after which the queue remains non-empty.

Case1) When the first packet to an empty queue arrives in an AI after which the queue remains non-empty: The probability that a packet arriving to an empty queue arrives in the AI is N_M/X. In Case1, similar to Scenario S1a, the arrival instant of the first packet is uniformly distributed within an AI. Therefore, the start of service of each frame following the first frame (till the queue remains non-empty) will also be uniformly distributed. Thus, the 1st and 2nd order moments of the service time of a frame in Case1 are given as, $\overline{X}_{c1} = \overline{X}_a$ and $\overline{X_{c1}^2} = \overline{X_a^2}$ respectively.

Case2) When the first packet to an empty queue arrives in an IAI after which the queue remains non-empty: Consider the case that the first packet arriving to an empty queue arrives in the IAI. The service of this 1st frame is already covered in Scenario S1b. However, the service of the following N_I (say) frames arriving within the IAI needs to be accounted for under Scenario 2. The service time of such frames depends on the position where their service starts with respect to the start of the AI, which in turn depend on the number of Poisson arrivals within an IAI of length L_d slots. The pdf of the service time of a frame which starts its service at the beginning of the u^{th} FS ($\mathscr{L}_{C2,u}(s)$) and one which starts just after the end of the n^{th} FS boundary (see Figure 5.5a), which we denote as the beginning of $(n+1)^{\text{th}}$ FS ($\mathscr{L}_{C2,n+1}(s)$) are respectively obtained using (5.8) and (5.10)) as

$$\mathscr{L}_{C2,u}(s) = \mathscr{L}_{A1,u}(s)\Big|_{rT_S/2 \to rT_S}, \quad u = 1,2,....,n \tag{5.22}$$

$$\mathscr{L}_{C2,n+1}(s) = \mathscr{L}_{A3}(s)\, e^{s\frac{L_s}{2}T_S} e^{-srT_S} \tag{5.23}$$

Where $rT_S/2 \to rT_S$ denotes replacing $rT_S/2$ in (5.8) with rT_S. The 1st and 2nd order moments of $\mathscr{L}_{C2,j}(s)$ are given as $\overline{X}_{c2,j} = -\mathscr{L}'_{C2,j}(0)$ and $\overline{X_{c2,j}^2} = \mathscr{L}''_{C2,j}(0)$, $j = 1,..,(n+1)$.

For deriving the moments of frame service time under Case2, we also obtain the average number of transmissions ($\overline{m}$) involved in the service of a frame as

$$\overline{m} = \left\lfloor \frac{1-(1-\eta)^{R+1}}{\eta} \right\rceil \tag{5.24}$$

Where '$\lfloor\cdot\rceil$' symbolizes rounding off to the nearest integer.

Using (5.22)-(5.24) and based on the cyclic nature of the AI and IAIs, the 1st and 2nd order moments of the service time under Case2 are obtained respectively as

$$\overline{X}_{c2} = \frac{\sum_{N_I=1}^{\infty} \left\{ \frac{(\lambda L_d T_S)^{N_I+1} e^{-\lambda L_d T_S}}{(N_I+1)!} \frac{1}{N_I} \sum_{k=1}^{N_I} \overline{X}_{c2,u_k} \right\}}{P_d(N_I \geq 1)} \tag{5.25}$$

$$\overline{X^2_{c2}} = \frac{\sum_{N_I=1}^{\infty} \left\{ \frac{(\lambda L_d T_S)^{N_I+1} e^{-\lambda L_d T_S}}{(N_I+1)!} \frac{1}{N_I} \sum_{k=1}^{N_I} \overline{X^2_{c2,u_k}} \right\}}{P_d(N_I \geq 1)} \tag{5.26}$$

In (5.25) and (5.26), we derive the moments for the N_I frames ($N_I > 1$) that may arrive after the first packet to an empty queue within an IAI . These moments are weighed against the probability of Poisson arrival of $(N_I + 1)$ packets within the IAI. Further, we leverage the cyclic nature of the AIs and IAIs and use (5.22) and (5.23) to provide the following iterative procedure where u_k and h_k are updated with each value of 'k' within the internal summations of (5.25) and (5.26),

$$u_k = \begin{cases} (h_k + \overline{m})\%(n+1), & h_k + \overline{m} < n+1 \\ (h_k + \overline{m})\%(n+1) + 1, & h_k + \overline{m} > n+1 \\ (h_k + \overline{m}), & h_k + \overline{m} = n+1 \end{cases} \tag{5.27}$$

$$h_k = \begin{cases} u_{k-1}, & u_{k-1} < n+1 \\ 1, & u_{k-1} = n+1 \end{cases} \tag{5.28}$$

Lastly, we normalize the summation in (5.25) and (5.26) with $P_d(N_I \geq 1)$, which is the probability of arrival of more than one packet within an IAI, and is given as

$$P_d(N_I \geq 1) = 1 - e^{-\lambda L_d T_S}(1 + \lambda L_d T_S) \tag{5.29}$$

Finally, the 1st and 2nd order moments of the service time of a frame in Scenario S2 are obtained respectively by combining the moments of Case1 and Case2 as

$$\overline{X}_c = \frac{N_M}{X}\overline{X}_{c1} + \frac{X - N_M}{X}\overline{X}_{c2} \tag{5.30}$$

$$\overline{X^2_c} = \frac{N_M}{X}\overline{X^2_{c1}} + \frac{X - N_M}{X}\overline{X^2_{c2}} \tag{5.31}$$

We now calculate the overall frame waiting delay using embedded Markov Chain Analysis in the next subsection.

5.4.2 Evaluation of Overall Frame Waiting Delay

The expression for the number of frames (n_{i+1}) left behind in the queue by the $(i+1)^{\text{th}}$ frame departure can be obtained by combining the equations (5.2), (5.17) and (5.20) for Scenario S1a, S1b and S2 respectively as

$$\begin{aligned} n_{i+1} &= a_{i+1}, && j=0, n_i=0 \\ &= j+b_{i+1}-1, && j\geq 1, n_i=0 \\ &= n_i+c_{i+1}-1, && n_i>0 \end{aligned} \tag{5.32}$$

Using the unit-step function $U(x)$, (5.32) can be expressed in more compact form as

$$\begin{aligned} n_{i+1} = a_{i+1} &+ (n_i+c_{i+1}-a_{i+1}-1)U(n_i-1) \\ &+ U(j-1)\left[1-U(n_i-1)\right]\left[j+b_{i+1}-a_{i+1}-1\right] \end{aligned} \tag{5.33}$$

Hence, the PGF of the equilibrium state distribution of the number of frames in the queue of U at frame departure instants can be evaluated as [182]

$$\begin{aligned} \Pi(z) = E(z^{n_{i+1}}) &= A(z)\left[\pi_0\widehat{F}_0 + \pi_0\sum_{j=1}^{\infty} f_j z^{b_{i+1}-a_{i+1}+j-1} + \sum_{n_i=1}^{\infty}\pi_{n_i} z^{c_{i+1}-a_{i+1}+n_i-1}\right] \\ &= A(z)\pi_0\widehat{F}_0 + \pi_0 B(z)\frac{F(z)}{z} + \frac{C(z)}{z}\left(\Pi(z)-\pi_0\right) \end{aligned} \tag{5.34}$$

The first, second and third terms of (5.34) correspond to Scenarios S1a, S1b and S2 respectively. Here, π_{n_i} denotes the steady-state probability of n_i frames in the queue. Using (5.16), and upon simplifying (5.34) we get

$$\Pi(z) = \pi_0\frac{C(z)-B(z)F(z)-z\widehat{F}_0A(z)}{C(z)-z} \tag{5.35}$$

Using the normalization relation $\Pi(1)=1$ we get

$$\pi_0 = \frac{(1-\lambda\overline{X}_c)}{\widehat{F}_0(1+\lambda\overline{X}_a)+F(1)\lambda\overline{X}_b+F'(1)-\lambda\overline{X}_c} \tag{5.36}$$

As per Kleinrock's Result [188] and PASTA Property [189], (5.33) will also give the steady state distribution observed at any arbitrary chosen time instant. Hence, the average number of frames in the queue of node (U) under equilibrium can be given from Little's law.

Therefore, using equation (5.35) and applying Little's law we obtain,

$$\Pi'(1) = \lambda W = \frac{\pi_0}{2(1-\lambda\overline{X}_c)}\Big[2F'(1)\lambda\overline{X}_b + 2\widehat{F}_0\lambda\overline{X}_a + F''(1) + \widehat{F}_0\lambda^2\overline{X_a^2} + F(1)\lambda^2\overline{X_b^2} - \lambda^2\overline{X_c^2}\Big] + \frac{\lambda^2\overline{X_c^2}}{2(1-\lambda\overline{X}_c)} \tag{5.37}$$

where W is the mean waiting time (in s) of data frames, and $F'(1)$ and $F''(1)$ are obtained from (5.16) as

$$F'(1) = \frac{f_{M,0}^{(1)}\lambda\,\bar{I}}{1 - f_0^* f_{M,0}} \tag{5.38}$$

$$F''(1) = \frac{f_{M,0}^{(1)}\lambda^2\,\overline{I^2}}{1 - f_0^* f_{M,0}} \tag{5.39}$$

where $\bar{I} = -\mathscr{L}_I'(0) = L_d T_S$ denotes the average duration of IAI. $\overline{I^2} = \mathscr{L}_I''(0)$ is the 2^{nd} order moment.

It is worth emphasizing that (5.37) gives the closed form expression for derivation of the W as a function of superframe parameters like beacon period (X), allocation interval (N_M); traffic loads (λ and P_{size}); transmission data rate which determines frame transaction time; and channel bit-error-rate (*ber*) which in turn depends on channel SNR.

5.5 Throughput Analysis

The throughput T of node U is defined as the number of data bits departing from the queue maintained by the node and successfully transmitted over to the hub per unit time. Let D denote the mean inter-departure time of frames from the queue, and p_s represents the probability of successful transmission of the data frames with payload size of P_{size} bytes. Then, mathematically T (bits/sec) is defined as

$$T = (8 \times P_{size}) \times \frac{1}{D} \times p_s \tag{5.40}$$

5.5.1 Evaluation of p_s: Reliability or Probability of Successful Transfer of Data Frames

A successful data transfer occurs if a data frame of l_b bits is successfully transmitted over the error-prone non-ideal channel to the hub. Note that, l_b denotes the average length of the PHY frames (PLCP Preamble+ PLCP Header+ MAC header + MSDU length or payload or packet

size + MAC FCS length) in bits. The probability that the data frame is transmitted without getting corrupted by any bit error can be denoted as, $\eta_d = (1 - ber)^{l_b}$. In case of an error in transmission, the node re-transmits the data frame where the maximum re-transmission limit is denoted by R. Thus, the probability of successful data transfer (p_s) also known as reliability can be given by

$$p_s = 1 - (1 - \eta_d)^{R+1} \tag{5.41}$$

5.5.2 Evaluation of D: Inter-Departure Time of Frames

Based on the concept of flow balance, for a queue to be stable the incoming rate must be equal to the outgoing rate. Therefore, we state Lemma 1 as available in literature [182].

Lemma 1 *For a Poisson arrival process to a queue with rate λ , the departure process is also Poisson with same rate.*

In this sub-section, we derive the closed form expressions for the inter-departure time as it will provide the foundation for energy consumption analysis in the next section. Additionally, solving the derived final expression of D in any simulator will provide a proof for Lemma 1.

The inter-departure time analysis can be considered under two separate scenarios:

1. a frame departure leaves the queue non-empty, and
2. a frame departure leaves the queue empty

Let D_1 and D_2 denote the average inter-departure times for the above two scenarios, respectively. The overall average inter-departure time D can be expressed as

$$D = (1 - \pi_0)D_1 + \pi_0 D_2 \tag{5.42}$$

5.5.2.1 D_1 evaluation: Frame departure leaves queue non-empty

Since in this scenario the service of the next frame will start immediately, the average inter-departure time (D_1) in this case will be equal to $\overline{X}_c$, i.e.

$$D_1 = \overline{X}_c \tag{5.43}$$

5.5.2.2 D_2 evaluation: Frame departure leaves queue empty

Since there are no frames present, the next frame departure will happen after the next incoming packet is serviced. This event is illustrated in Figure 5.9. Similar to Section 5.4.1.1,

t denotes the time of departure of the frame with respect to the start of the AI. Hence, t can lie anywhere between L_sT_S and N_MT_S with equal probability. To evaluate D_2, we consider a shift in the time axis starting from t. Regarding the arrival instant of the next packet, we can identify two events. Event 1) next packet arrives in an AI, and 2) next packet arrives in an IAI. As per Section 5.4.1, the service time of the frame under these two events will be $\overline{X}_a$ and $\overline{X}_b$ respectively. Additionally, the service of a frame arriving at an empty queue within an IAI will start after the end of the IAI, whereas for a frame arriving within AI it will start immediately. Therefore, following Figure 5.9 with shifted time-reference, the average time taken ($Z(t)$) for the next frame to depart after the previous frame leaves the queue empty at time t can be calculated as

$$\begin{aligned} Z(t) = &\int_0^{N_MT_S-t} f_\lambda(\tau)(\tau+\overline{X}_a)d\tau + \int_{N_MT_S-t}^{XT_S-t} f_\lambda(\tau)(XT_S-t+\overline{X}_b)d\tau + \\ &\int_{XT_S-t}^{(X+N_M)T_S-t} f_\lambda(\tau)(\tau+\overline{X}_a)d\tau + \int_{(X+N_M)T_S-t}^{2XT_S-t} f_\lambda(\tau)(2XT_S-t+\overline{X}_b)d\tau + \cdots \qquad (5.44) \\ = &\overline{X}_a + \frac{1}{\lambda} + \frac{e^{\lambda t}}{1-e^{\lambda XT_S}}\left[e^{-\lambda N_MT_S}(X-N_M)T_S - \left(e^{-\lambda N_MT_S}-e^{-\lambda XT_S}\right)\left(\frac{1}{\lambda}+\overline{X}_a-\overline{X}_b\right)\right] \end{aligned}$$

Where τ is a dummy variable that represents the arrival instant of the next packet with respect to the origin of the shifted time reference and it follows an exponential distribution $f_\lambda(\tau) = \lambda e^{-\lambda\tau}$. Using the uniform distribution of t between L_sT_S and N_MT_S, the average inter-departure time of the frame under this scenario (D_2) can be obtained by taking the mean of (5.44) with respect to t as,

$$D_2 = E\{Z(t)\} \qquad (5.45)$$

Equation (5.45) involves calculation of the mean of $e^{\lambda t}$ of (5.44), which is obtained as $E\{e^{\lambda t}\} = \frac{e^{\lambda N_MT_S}-e^{\lambda L_sT_S}}{\lambda(N_M-L_s)T_S}$.

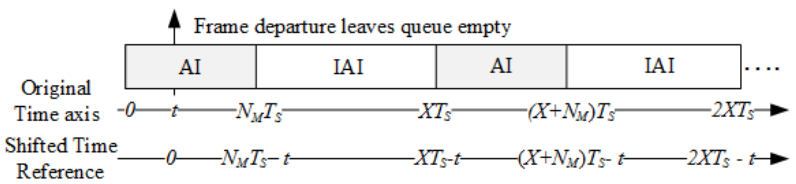

Fig. 5.9 Shifting of time reference for inter-departure time analysis.

5.6 Energy Consumption Analysis

Energy consumption is one of the most important performance parameters for WBAN. It helps in estimating the average life-span of the nodes. In SAM, considering LDC, energy is consumed by sensor node U towards transmission, reception, when a node is idle while waiting for an I-Ack, when waking up or powering down the transceivers and when the node is sleeping with transceivers powered down. These energy consumptions can be related to the current consumptions of the node as given in Table 5.2. I_t, I_r , I_i, I_{wup} and I_s are the current consumptions of the node while transmitting, receiving, in idle state, when waking up/powering down and when it is in sleep state respectively. Whereas, V_s denotes the node power supply.

Table 5.2 Energies consumed during different sensor node activities

Activity	**Energy Consumption**	**Remarks**
Transmission of data frame	$\xi_{d,t} = V_s I_t t_d$	t_d= Duration of data frame transmission
Reception of I-Ack Frame	$\xi_{a,r} = V_s I_r t_{ack}$	t_{ack}= Duration of I-Ack frame reception
Waiting for an I-Ack Frame	$\xi_{a,i} = V_s I_i t_{ack}$	
Waiting in sifs	$\xi_{sifs} = V_s I_i sifs$	
Waking-up or powering-down	$\xi_{wup} = V_s I_{wup} t_{wup}$	t_{wup} = Waking-up/ powering-down time
Sleep current not consumed during waking-up or powering-down	$\xi_{s,wup} = V_s I_s t_{wup}$	For adjusting the extra energy consumed in waking-up/powering-down
Reception of beacon	$\xi_b = V_s I_r t_b$	t_b= Duration of beacon reception
Sleep current not consumed during beacon reception	$\xi_{s,b} = V_s I_s t_b$	For adjusting the extra energy consumed in beacon reception

Let E_D denotes the average energy consumed between the departure of two frames. Furthermore, additional energy is consumed by sensor nodes during re-synchronization. During re-synchronization, the sensor node wakes up GT_n time prior to the reception of beacon. Based on this, the average energy consumed (E_{avg}) by the sensor node in operating

time T_{op} can be expressed as,

$$E_{avg} = \frac{T_{op}}{D} E_D + \frac{T_{op}}{SI_n T_S} \left[2\left(\xi_{wup} - \xi_{s,wup}\right) + \left(\xi_b - \xi_{s,b}\right) + GT_n V_s (I_i - I_s) \right] \tag{5.46}$$

At a finer level of detail, observe the subtraction of $2\xi_{s,wup}$ which is an adjustment to accommodate the energy consumed during sensor node wake-up and power-down within an otherwise sleep duration. Similarly, the adjustment terms $\xi_{s,wup}, \xi_{s,b}$, and $GT_n V_s I_s$ accommodate the additional energies consumed during re-synchronization.

The derivation of E_D is identical to the derivation of D. Therefore, following Section 5.5.2, E_D can be obtained as,

$$E_D = (1 - \pi_0)\overline{E}_c + \pi_0 E_Z \tag{5.47}$$

Where E_Z refers to the energy consumed under Scenario 2 of Section 5.5.2, which is obtained following (5.44),(5.45) as

$$\begin{aligned} E_Z = 2\left(\xi_{wup} - \xi_{s,wup}\right) + \overline{E}_a + \frac{V_s I_s}{\lambda} + \frac{V_s I_s E\{e^{\lambda t}\}}{1 - e^{\lambda X T_S}} \Big[& e^{-\lambda N_M T_S} (X - N_M) T_S - \\ & \left(e^{-\lambda N_M T_S} - e^{-\lambda X T_S}\right) \left(\frac{1}{\lambda} + \frac{\overline{E}_a - \overline{E}_b}{V_s I_s}\right) \Big] \end{aligned} \tag{5.48}$$

Note that, when the queue becomes empty, the sensor node goes to sleep, and subsequently wakes up when the next incoming packet is to be serviced. The terms $\overline{E}_a$, $\overline{E}_b$, $\overline{E}_c$ refer to the average energies consumed during service of a frame under scenarios S1a, S1b and S2 respectively of Section 5.4.1 and are obtained as $\overline{E}_a = -\mathscr{L}'_{E,A}(0)$, $\overline{E}_b = -\mathscr{L}'_{E,B}(0)$ and $\overline{E}_c = -\mathscr{L}'_{E,C}(0)$ respectively. Where, $\mathscr{L}_{E,A}(s), \mathscr{L}_{E,B}(s), \mathscr{L}_{E,C}(s)$ are the $\mathscr{L}T$ of the pdfs of the respective energies consumed. The derivation $\mathscr{L}_{E,A}(s), \mathscr{L}_{E,B}(s)$ and the 1st order moment of $\mathscr{L}_{E,C}(s)$ (i.e. $\overline{E}_c$) are identical to their service time counterparts except certain terms replaced as summarized in Table 5.3. Accordingly, based on Table 5.3, the $\mathscr{L}T$s of service times like $\mathscr{L}_{A1,u}(s)$, $\mathscr{L}_{A2,u}(s)$, $\mathscr{L}_{A3}(s)$, $\mathscr{L}_{C2,u}(s)$ and $\mathscr{L}_{C2,n+1}(s)$ get transformed into the $\mathscr{L}T$s of the pdf of the respective energy consumptions as, $\mathscr{L}_{E,A1,u}(s)$, $\mathscr{L}_{E,A2,u}(s)$, $\mathscr{L}_{E,A3}(s)$, $\mathscr{L}_{E,C2,u}(s)$ and $\mathscr{L}_{E,C2,n+1}(s)$. Similarly, service time moments $\overline{X}_a$, $\overline{X}_{c1}$ and $\overline{X}_{c2,j}$ get transformed to their respective energy consumption moments as, $\overline{E}_a$, $\overline{E}_{c1}$ and $\overline{E}_{c2,j}$.

Table 5.3 Energies consumed during service of a frame

Service Time Terms	Corresponding Energies Consumed
L_sT_S in (5.8)-(5.10)	$E_{Ls} = \xi_{d,t} + \xi_{a,r} + \xi_{sifs}$ Applicable to all instances except those mentioned later in this table
L_cT_S in (5.8)-(5.10)	$E_{Lc} = \eta_d \left(\xi_{d,t} + \xi_{a,r} + \xi_{sifs}\right) + (1 - \eta_d)\left(\xi_{d,t} + \xi_{a,i} + \xi_{sifs}\right)$
L_dT_S in (5.8)-(5.10)	$E_{Ld} = L_dT_SI_sV_s + 2(\xi_{wup} - \xi_{s,wup})$
rT_S in in (5.8)-(5.10), (5.22), (5.23)	$E_r = rT_SI_sV_s$
XT_S in (5.8)-(5.10)	$E_X = nE_{Lc} + E_r + E_{Ld}$
$\left(L_d + \frac{L_s+r}{2}\right)T_S$ in (5.9)	$E_{Ld} + \frac{1}{2}(L_sT_SI_sV_s + E_r)$
$\left(L_d + \frac{L_s}{2}\right)T_S$ in (5.10), (5.19)	$E_{Ld} + \frac{1}{2}L_sT_SI_sV_s$
$\left(\frac{L_s}{2} - r\right)T_S$ in (5.23)	$\frac{1}{2}L_sT_SI_sV_s - E_r$

Energy-Efficiency

Energy-efficiency of a sensor node is defined as the throughput achieved by the node for the energy consumed by it. Energy-efficiency (EE) in bits/s/watt of a sensor node can be given as the ratio of the average throughput (T) to the average power consumed (P_{avg}) i.e. energy consumed per unit time. Therefore, using (5.40) and (5.46) we get

$$EE = \frac{T}{P_{avg}} \tag{5.49}$$

where $P_{avg} = \frac{E_{avg}}{T_{op}}$ with E_{avg} obtained using (5.46).

5.7 Analysis of Non-Ideal Channel Characteristics

In order to design a highly reliable WBAN it is essential to characterize the wireless channel between the sensor nodes and the hub that are fixed on the body surface. A number of studies have addressed the WBAN channel modeling problems. Smith et al. [61] show lognormal distribution to be the best fit for small-scale fading in narrowband communications. In similar research work based on on-body channels [63], where communication is across the surface of the human body and off-body [62], have both reported small-scale fading following log-normal distribution. Motivated by this we consider a log-normal channel for modeling the wireless channel and then derive its Bit Error Rate (BER).

Prior to transmission of the MPDU (also known as Physical Service Data Unit or PSDU), IEEE 802.15.6 allows encoding using a systematic BCH encoder [23] with a code rate of (51,63) that has a 2-bit error-correcting capability. Since error can be corrected, the (51,63) BCH encoder produces a coding gain. Taking this into consideration, we obtain the coded BER of the log-normal channel for different channel SNRs through simulations. The coded BER thus obtained will then be utilized in our developed analytical model for further performance analysis of IEEE 802.15.6 SAM. To this end, in this section we also show the resulting probability of successful transfer of data frames or reliability in WBAN for different payload sizes under varied channel SNRs.

5.7.1 Log-Normal Channel Modeling

Consider the channel gain of the wireless fading channel be denoted by h. Then the effective channel SNR γ at the receiver is given by

$$\gamma = |h|^2 \frac{E_b}{N_o} = |h|^2 \gamma_0 \tag{5.50}$$

where $\gamma_0 = E_b/N_o$ is the given value of bit energy to noise ratio also known as the reference SNR. To find the average uncoded error probability, more specifically the uncoded symbol error probability or Symbol Error Rate (SER), over all random values of γ, the pdf of γ i.e. $p_\Upsilon(\gamma)$ needs to be evaluated from the pdf of a log-normal channel.

The log-normal pdf ($p_H(h)$) for an envelope H with log mean μ and log standard deviation σ, may be given as [61],

$$p_H(h) = \frac{1}{h\sigma\sqrt{2\pi}} \exp\left(\frac{-[\log(h)-\mu]^2}{2\sigma^2}\right), h > 0 \tag{5.51}$$

The pdf ($p_\Upsilon(\gamma)$) of SNR γ is obtained by differentiating its Cumulative Distribution Function (CDF) ($F_\Upsilon(\gamma)$), which is related to the CDF of h ($F_H(h)$) using (5.50). Therefore,

$$p_\Upsilon(\gamma) = F_\Upsilon{}'(\gamma) = F_H{}'\left(\sqrt{\frac{\gamma}{\gamma_0}}\right) = \frac{1}{2\sqrt{\gamma_0\gamma}} p_H\left(\sqrt{\frac{\gamma}{\gamma_0}}\right) \tag{5.52}$$

Equation (5.52) can be simplified by using $p_H(h)$ from (5.51).

5.7.2 Bit Error Rate

First we calculate the uncoded BER (ber_u) and then utilize it for coded BER calculation. To obtain ber_u we start by obtaining the uncoded SER (ser_u). For an m-bit binary symbol, SER is related to BER as $ser_u = 1-(1-ber_u)^m$.

The SER depends on the particular modulation process utilized at the physical layer. As per IEEE 802.15.6, for 2360-2483.5 MHz bands, the DBPSK and DQPSK modulation schemes are supported. We calculate average SER (ser_u) as

$$ser_u = \int_0^\infty P_e(\gamma) p_\Upsilon(\gamma) d\gamma \tag{5.53}$$

where $P_e(\gamma)$ is the conditional error probability. For completeness, we give $P_e(\gamma)$ for DBPSK and DQPSK from [66] as

$$P_e(\gamma)_{DBPSK} = \frac{1}{2} e^{-\gamma} \tag{5.54}$$

$$P_e(\gamma)_{DQPSK} = Q(a\sqrt{\gamma}, b\sqrt{\gamma}) - \frac{1}{2} I_0(ab\gamma) e^{-\frac{a^2+b^2}{2}\gamma} \tag{5.55}$$

where $a = \sqrt{2-\sqrt{2}}, b = \sqrt{2+\sqrt{2}}$ and $Q(\cdot)$ is the Marcum Q-function and $I_0(\cdot)$ is the modified Bessel Function of the first kind and zero-order. Using ser_u from (5.53), we get the uncoded BER for DBPSK ($m = 1$) and DQPSK ($m = 2$).

After obtaining the uncoded BER, the focus shifts to determining the coded BER through simulations conducted in MATLAB. We consider BCH (51,63) encoder to encode the data and produce the transmitted message, then use the obtained uncoded BER to introduce error in the encoded message, thereby obtaining the received message. The received message is then decoded and compared with the transmitted data to obtain the coded BER (ber).

For this purpose, readings were taken with the narrowband communication parameters as given in Table 5.4 [23], and for modeling the log-normal channel we consider log mean $\mu = -7.25$ and log standard deviation $\sigma = 0.73$[61].

Table 5.4 Modulation parameters for 2360-2483.5 MHz

Information Data Rate (kbps)	Modulation	Code Rate	Spreading Factor (S)	Symbol Rate (ksps)
485.7	$\pi/2$-BPSK	51/63	1	600
971.4	$\pi/4$-QPSK	51/63	1	600

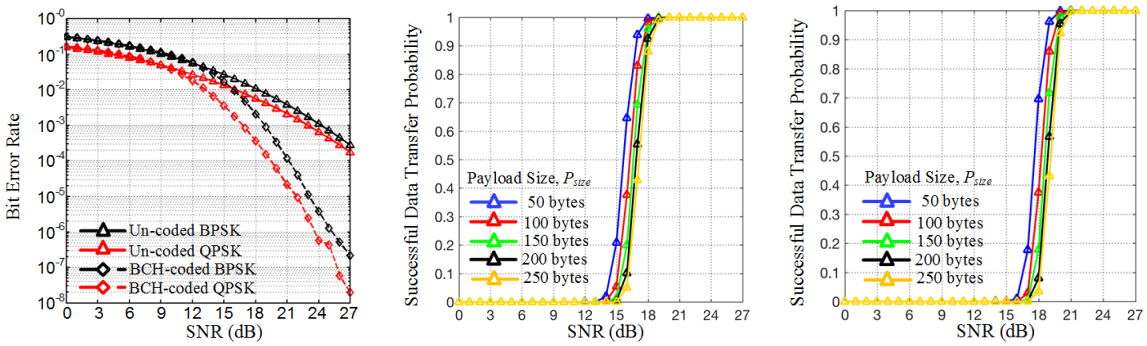

(a) (b) 971.4kbps-DQPSK (c) 485.7kbps-DBPSK

Fig. 5.10 Variation with respect to SNR of (a) BER and (b), (c) Probability of successful data transfer against different payload sizes.

Figure 5.10a shows the significant coding gain due to BCH code for WBAN. It must be noted that the uncoded SER (not shown in Figure 5.10a) of DQPSK is higher than that of DBPSK. However, in Figure 5.10a we see a slightly lower coded/uncoded BER for DQPSK as compared to DBPSK. This is because for higher SNR the ber_u of DQPSK is half of its ser_u.

The effect of BER or the channel SNR is best observed through its effect on the reliability (p_s) in data transfer. To this aim, in Figures 5.10b and 5.10c, we vary the payload size (P_{size}) of the transmitted data and study the variation in p_s considering different channel SNRs for both DQPSK and DBPSK respectively. In this regard, the MAC header, FCS and PPDU header sizes are mentioned in Table 5.6. With an increase in channel SNR, the successful packet transmission probability increases drastically due to the improved BER performance. Further, for larger P_{size}, the probability that the data frames will be affected by channel error will be high resulting in lower probabilities of successful data transfer. Most importantly, Figures 5.10b and 5.10c help in determining the SNR for a particular TL beyond which the reliability in data transfer is guaranteed to satisfy a minimum reliability constraint $p_{s,min}$, which as per the standard is 0.9 [17].

5.8 Performance Analysis

We solve our analytical model using MATLAB platform to obtain the average waiting delay of frames (W), the throughput (T) and energy consumption (E_{avg}) of the sensor nodes. In this section, first we validate our analytical model by comparing with simulation results of the IEEE 802.15.6 SAM obatined using OPNET simulator [95]. The detailed modeling of

IEEE 802.15.6 SAM in OPNET was discussed earlier in Chapter 3. After validating the accurateness of the analytical model, we conduct a comprehensive performance analysis of primary mode of IEEE 802.15.6 1-periodic uplink SAM.

For experiments in OPNET simulator and in analytical model, we consider that the nodes generate Poisson traffic as per the Traffic Load (TL) parameters given in Table 5.5 [190]. The WBAN operates in 2.4 GHz band having a log-normal fading channel as modeled in Section 5.7 following the coded BER curve as shown in Figure 5.10a. We set the data transmission rate at 971.4kbps and set the modulation parameters and transmission rates according to the IEEE 802.15.6 standard (Table 5.6). The beacon period X is set to 250 time slots, while the EAP and RAP lengths are fixed at 50 and 100 slots respectively and the length of MAP is set to 100 slots. The rest of the system parameters used for simulation are as shown in Table 5.6 [25, 23, 66, 99]. The transceiver current consumptions are based on Nordic nRF24L01+ [191] transceivers that operate in the 2.4GHz band. We run the simulations in OPNET for 30mins, i.e. the operating time $T_{op} = 1800$s, and then compare and contrast the variation of the performance metrics under different channel conditions.

Table 5.5 Different Traffic Load (TL) parameters [190]

TL	**Data Stream**	**Data Rate (bytes/s)** (λP_{size})
1	Respiration	93.75
2	Blood Pressure	150
3	Electrocardiogram (ECG)	300
4	Electroencephalogram (EEG)	500
5	Pulse Oxymeter	1000
6	Electromyogram (EMG)	3000

Table 5.6 Simulation parameters

Parameters	**Values**	**Parameters**	**Values**
Slot length, T_S	2ms	Voltage Supply, V_s	3V
Max. retry limit, R	3	Transmit current, I_t	7.5 mA
sifs	75 μs	Receive current, I_r	13.1 mA
Guard time, GT_n	120 μs	Idle current, I_i	26 μA
MAC Header	7 bytes	Wake-up current, I_{wup}	400 μA
MAC FCS	2 bytes	Sleep current, I_s	900 nA
PPDU Header	214 bits	Wake-up time, t_{wup}	1.5ms
Sync Interval, SI_n	$8X$slots	Operational Time, T_{op}	30 min

Table 5.7 Validation of Analytical (Ana) results with Simulation (Sim) data for TL-3, data rate = 971.4 kbps, beacon period X = 250 slots

Ideal Channel with P_{size}=150 bytes							**Non-Ideal Channel (SNR = 18dB) with N_M=11 slots**						
[a] N_M	[b] W (s)		[c] T (bits/s)		[d] E_{avg} (Joule)		[e] P_{size}	[b] W (s)		[c] T (bits/s)		[d] E_{avg} (Joule)	
(slots)	Sim	Ana	Sim	Ana	Sim	Ana	(bytes)	Sim	Ana	Sim	Ana	Sim	Ana
4	0.2606	0.2537	2402	2400	0.21682	0.21665	30	0.2384	0.2405	2401.87	2394.91	0.78282	0.8466
5	0.2478	0.2473	2402	2400	0.21679	0.21664	50	0.2359	0.2401	2370.22	2389.13	0.54832	0.59881
6	0.2446	0.2449	2402	2400	0.21679	0.21667	70	0.2355	0.2397	2363.82	2380.14	0.45426	0.49592
7	0.2426	0.2432	2402	2400	0.21682	0.21669	90	0.2370	0.2397	2406.80	2367.40	0.41087	0.44139
8	0.2408	0.2415	2402	2400	0.21685	0.21672	110	0.2394	0.2403	2401.91	2350.52	0.38288	0.40891
9	0.2384	0.2398	2402	2400	0.21690	0.21675	130	0.2392	0.2408	2338.84	2329.29	0.35977	0.38832
10	0.2358	0.2382	2402	2400	0.21694	0.21677	150	0.2452	0.2412	2274.67	2303.60	0.34266	0.37488
11	0.2337	0.2365	2402	2400	0.21697	0.21680	170	0.2430	0.2424	2274.22	2273.50	0.34163	0.36603
12	0.2318	0.2348	2402	2400	0.21700	0.21683	190	0.2456	0.2435	2263.11	2239.13	0.34164	0.36031
13	0.2299	0.2332	2402	2400	0.21703	0.21686	210	0.2498	0.2441	2111.2	2200.71	0.32720	0.35676

[a]N_M = AI length, [b]W = Avg. waiting delay, [c]T = Avg. throughput, [d]E_{avg}= Avg. energy consumed in T_{op} = 30min, [e]P_{size} = Payload size.

The simulation results are summarized in Table 5.7 along with the analytical results for comparison. Related detailed plots from OPNET are provided further in Appendix A. All the results in Table 5.7 indicate reasonably close match between the simulation and analytical results, thereby strongly validating our derived analytical model.

We now conduct extensive performance analysis of the IEEE 802.15.6 SAM. In addition to earlier simulation settings, we perform various tests for the 485.7 kbps data rate (Table 5.4). Also, to see the effect of varied beacon intervals, along with the 250 slot beacon interval we also take a 150 slot beacon interval where the EAP1, RAP1 and MAP durations are set to 25, 25 and 100 slots respectively.

5.8.1 Effect of Variation of Allocation Intervals

In this sub-section, we present the analysis of average waiting delay and energy consumption with respect to variations in AIs. We do not consider throughput since it remains constant for changes in AI as evident from Table 5.7.

In Figure 5.11, keeping PS fixed, we illustrate the variation of average frame delay versus the AIs against different channel SNRs, data transmission rates and Beacon Period (BP). From the figures it is observed that as the AI increases, delay of the frames decreases. This is because as the value of AI increases, the deferral probability of a frame and IAI decreases and the frames are serviced more easily resulting in the lower average waiting delay. We also observe that under lower channel SNR the delay is higher. This is expected as lower SNR leads to more bit errors and hence more re-transmissions, which increases the service time.

Moreover, comparing Figures 5.11a and 5.11b reveals that for lower data rate the waiting delay increases. Lower data rate leads to longer frame transmission time, and hence larger service duration which leads to more deferrals and thus longer delays. As an effect, we find that for maintaining the same delay, one needs to select more AIs for lower data rate as compared to higher data rates.

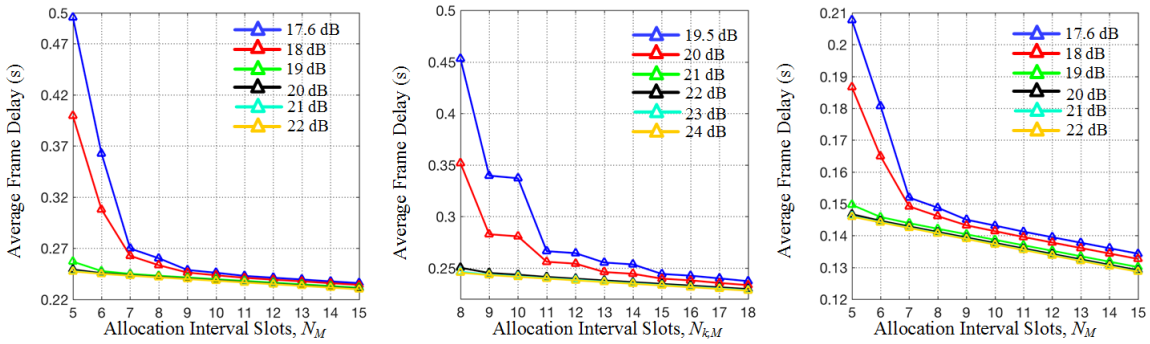

(a) 971.4kbps, 250 slot BP (b) 485.7kbps, 250 slot BP (c) 971.4kbps, 150 slot BP

Fig. 5.11 Variation of average frame delay with respect to allocation intervals under different channel SNRs for TL-3 with P_{size}= 150 bytes.

Further, from Figures 5.11a and 5.11c it is observed that as the BP decreases, waiting delay decreases. Smaller BP corresponds to lower IAI, which reduces the service duration and the probability that a new packet to an empty queue will arrive during an IAI. As a consequence, the waiting delay is reduced drastically.

Next, in Figure 5.12, keeping the PS fixed, we vary the AI for different channel SNRs, data rates and BPs to observe their impact on the average energy consumption of the sensor nodes within an operating time of 30 minutes. It is observed that increase in AI leads to initial decrease in energy consumption followed by a gradual rise. For a small AI, the frame service time is more which leads to a lower probability of the queue being empty. This results in frequent frame deferral causing powering down of the transceivers at the beginning of an IAI followed by waking-up prior to the start of the next AI. Due to this reason, the energy consumption has a higher value at smaller AIs. Also it is observed that at larger values of AI the energy consumption increases with increase in AI length. This is a straightforward impact of the increase in the probability of an empty queue which leads to a rise in the number of transceiver turn-offs after service of a frame. Furthermore, as shown in Figure 5.12, increasing channel SNR reduces energy consumption. This is expected as higher channel SNR is associated with lower BER that results in increased reliability of data transfer with reduced number of re-transmissions.

From Figures 5.12a and 5.12b, it is observed that the energy consumption decreases with increase in data rate. Higher data rate corresponds to lower transmission and reception time for the frames leading to lower amount of energy exhausted for those operations. Lastly, comparing Figures 5.12a and 5.12c we note that the energy consumption is higher for lower BPs. From the expression of energy consumption (5.46), we remark that the increase in energy consumption at smaller BPs is due to the decrease in the synch interval SI_n.

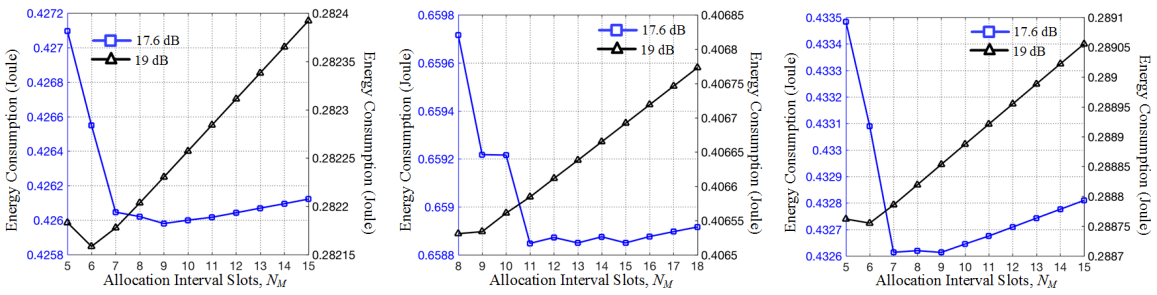

(a) 971.4kbps, 250 slot BP (b) 485.7kbps, 250 slot BP (c) 971.4kbps, 150 slot BP

Fig. 5.12 Variation of average energy consumption with respect to allocation intervals under different channel SNRs for TL-3 with P_{size}= 150 bytes.

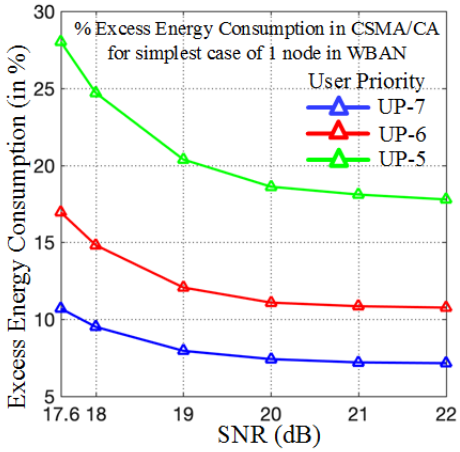

Fig. 5.13 Comparison of SAM with CSMA/CA for different channel SNRs and TL-3 with P_{size}= 150 bytes.

Finally, Figure 5.13 provides a basic comparison of SAM with CSMA/CA of IEEE 802.15.6 for medium/high rate applications. As evident, even in a collision free scenario CSMA/CA consumes more energy. This is due to listen-before-talk and use of backoff counter in CSMA/CA [23].

5.8.2 Effect of Variation of Payload Sizes

In this sub-section, we present the analysis of average waiting delay, throughput, energy consumption and energy-efficiency with respect to variations in PSs (with fixed AI) as shown in Figure 5.14. In this regard, it can be observed from Figure 5.14a that as P_{size} increases, the frame delay initially decreases and then increases. Smaller PS leads to higher packet arrival rate (λ) resulting in increased delay. Whereas, for a too long PS, the reliability decreases which causes more re-transmissions and deferrals, thereby increasing its delay.

Figure 5.14b shows the variation of the average throughput with respect to the PSs that satisfy a minimum 90% reliability [17] in data transfer. From the expression for throughput (5.40), we discern the direct proportionality of reliability with the average throughput. Therefore, as a straightforward deduction from Figure 5.10, we remark that with decrease in PS and/or increase in channel SNR the throughput increases due to the increase in reliability of data transfer.

Figure 5.14c shows the variation of the average energy consumption of a sensor node with respect to the PSs for different channel SNRs. We note that for a given AI and channel SNR, the energy consumption of a sensor node is lower for larger PS. As PS increases: i) the average number of transmissions involved in the service of a frame ($\overline{m}$) increases due to

reduced reliability, and ii) the arrival rate of the packets to the queue (λ) decreases. Since the header size (MAC+PHY) for a transmitted frame is constant, the number of header bit transmission decreases with decrease in frame transmission rate, which is equal to packet arrival rate (as per Lemma 1). As deduced from Figure 5.14c, with increase in PS, the latter effect of decrease in the number of transmitted header bits overpowers the increase in number of re-transmissions due to the reduced reliability, which explains the concerned decrease in the energy consumption. Also similar to Figure 5.12, in Figure 5.14c we observe that the energy consumption increases with decrease in channel SNR.

After obtaining the average throughput and energy consumption of individual sensor nodes, we plot the variation of their energy-efficiency with respect to channel SNRs for different PSs in Figure 5.14d. We observe that the energy-efficiency increases with channel SNR since both throughput and energy consumption improves. But more importantly, it can be observed that at high channel SNR, as PS increases the energy-efficiency increases.

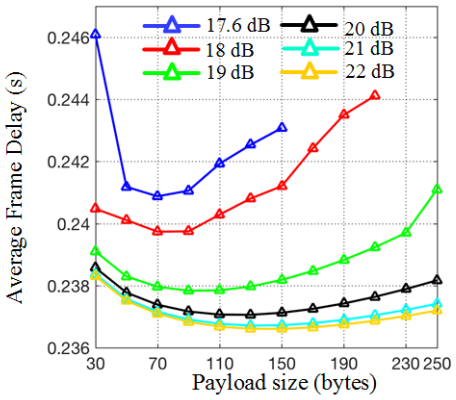

(a) Average Frame Delay

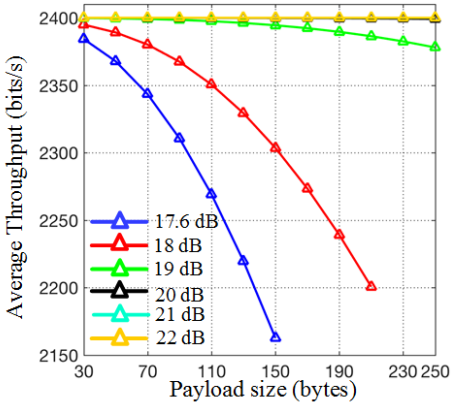

(b) Average Throughput

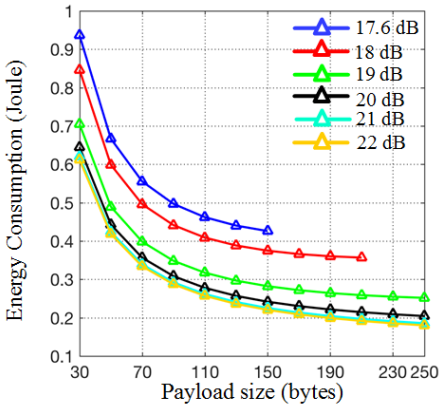

(c) Average Energy Consumption

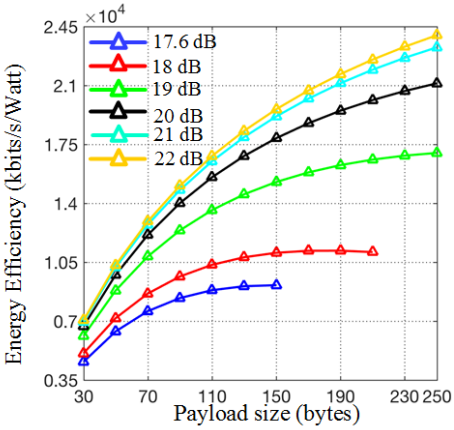

(d) Energy-Efficiency

Fig. 5.14 Performance under different PSs and channel SNRs for TL-3 with P_{size}= 150 bytes, data transmission rate=971.4 kbps, BP $X = 250$ slots.

Hence, we remark that for higher channel SNR, the decrease in energy consumption due to increase in PS as observed in Figure 5.14c outweighs the reduction in throughput as seen in Figure 5.14b. However, for lower channel SNRs, we observe that energy-efficiency follows a concave curve. At low channel SNR, the reliability is noted to be the lowest resulting is reduced throughput, which explains the concerned decrease in energy-efficiency for higher PS.

Thus, in this section we observe tradeoffs with respect to the selection of AIs and PSs. Using the information obtained, in the next Section we propose a method to assign optimal AIs and PSs for sensor nodes based on the traffic load, channel SNR, beacon period and data transmission rate.

5.9 Optimal Allocation Interval and Payload Size

Suppose we have the constraint that the average waiting delay (W) that a frame experiences should be less than W_{max}, and the reliability in data transfer (p_s) should be greater than $p_{s,min}$. As per IEEE 802.15.6, the maximum tolerable delay limit should be less than 250ms [25], and the minimum reliability requirement $p_{s,min} = 0.9$ [17]. Based on this information and the previous observations, the following optimization problem has been formulated.

5.9.1 Energy-Efficiency Maximization Problem

The selection of the optimal AI and PS for a node can be cast as its energy-efficiency (EE) maximization problem under its maximum delay and minimum reliability constraints. This optimization problem is expressed as,

$$\mathbf{P1}: \quad \max_{N_M, P_{size}} EE\left(N_M, P_{size}\right) \tag{5.56}$$

$$s.t. \quad W\left(N_M, P_{size}\right) \leq W_{max} \tag{5.57}$$

$$p_s\left(P_{size}\right) \geq p_{s,min} \tag{5.58}$$

$$0 \leq N_M \leq l_{map}, 0 \leq P_{size} \leq 255 \tag{5.59}$$

where we get EE, W, p_s from (5.49), (5.37), (5.41) respectively. l_{map} in constraint (5.59) is the MAP length in slots and 255 bytes denotes the max payload permitted by IEEE 802.15.6.

We solve problem **P1** offline using exhaustive search to obtain the optimal AI (N_M^*) and PS (P_{size}^*). Figs. 5.15a, 5.15b give the N_M^* (in slots) and P_{size}^* (in bytes) for all TLs and channel SNRs for 971.4kbps data transmission rate, 250 slot BP, and $l_{map} = 100$. The delay constraint W_{max} for 250 slot BP is set to 250ms. From the plot in Figure 5.15a, it is observed

that keeping the SNR fixed, TLs with higher data rate need more AIs. Inspecting Figure 5.15b, reveals that the optimal PS for a particular SNR is in general equal to the PS that achieves the maximum energy-efficiency while satisfying constraint (5.58). However, this is a general trend and exceptions are possible particularly at low SNRs and the exact solution is dependent on the operating conditions. Moreover, for higher TLs (TL-4,5,6), increasing channel SNR decreases the optimal AIs. Whereas, for lower TLs, with increase in SNR, N_M^* initially increases and then decreases. Finally, from Figure 5.15c it is evident that a stricter delay constraint can be satisfied by requesting higher number of AIs from the hub. This observation is a straightforward deduction from Figure 5.11a. Thus, the QoS needs for various applications manifests itself through different AI length requirements. Note that in designing WBAN it is also required to set the beacon period so as to satisfy the strictest delay constraint among the TLs.

5.9.2 Minimum Allocation Interval

The optimal N_M^* is the desired AI of a sensor node for a particular channel SNR which can be specified in the *Allocation Length* field of its Uplink Request IE. However, due to several reasons such as large number of nodes, and/or priority of other nodes, this desired AI might not always be granted by the hub. Hence, it is also essential for the node to specify the minimum AI length N_M^{min} in the *Minimum Length* field which satisfies constraints (5.57) and (5.58). To obtain N_M^{min}, we employ the following 2-step offline exhaustive search technique: i) obtain the minimum AI, $N_M = N_M^{min}$ that satisfies (5.57), (5.58), (5.59), ii) keeping AI fixed at N_M^{min}, obtain PS P_{size}^{min} that provides the maximum energy-efficiency.

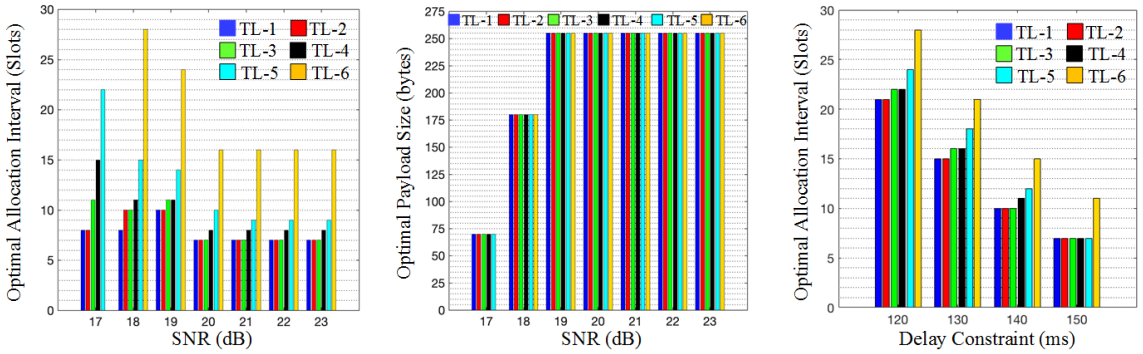

(a) Optimum allocation intervals (b) Optimum payload sizes (c) 971.4kbps,150 slot BP,20dB SNR

Fig. 5.15 Variation of optimum AIs and PSs with respect to (a), (b) channel SNRs and (c) delay constraints for different TLs.

5.9.3 Proposed LUT based Solution

After obtaining the optimum and minimum values offline, we prepare a static Look-Up Table (LUT) for the sensor node (with fixed TL) that specifies the range $[N_M^{min}, N_M^*]$ and the associated PSs corresponding to the channel SNR of a log-normal fading channel (Note- except P_{size}^*, other PSs are obtained following Section 5.9.2 for the respective AI values). We propose to store the static LUT locally at the sensor node, and hence can be leveraged easily for adapting its AI and PS based on the channel SNR. Recollect that in Section 3.7.3, we illustrated how the CC1101 transceiver inserts the RSSI value as a status byte within the received PPDU adjacent to its MPDU. This RSSI value can be used to derive the corresponding channel SNR. Thereafter, the sensor node can leverage its LUT for adapting the AI and PS based on the present channel SNR. This can be viewed as ***cognitive adaptation*** of parameters by the sensor nodes based on the prevailing channel condition. The adaptation can be implemented by sending a Connection Request frame to the hub during SAM session initiation or through Modified Connection Request frame during an ongoing session, where the minimum and optimum AI are mentioned in the Uplink IEs. Thereafter, based on the assigned AI by the hub (see Section 5.3.2), the sensor node selects the corresponding PS from its LUT. The cost of maintaining such LUTs is minimal as only a small amount of memory will be utilized to store the LUT as arrays. It is also worth mentioning that the LUTs do not require dynamic updating since- i) the traffic generated in sensor nodes employing the primary mode of 1-periodic SAM falls under normal traffic category [31] having pre-determined fixed data rate, and ii) the channel state (σ and μ) of the log-normal channel is based on the placement of the sensor node and hub on the body, which is pre-specified as per the interested application. Accordingly, based on the application requirement, a system designer can obtain the appropriate channel coefficients from [61], and thereafter can prepare the LUT using our proposed analytical model. Table 5.8 presents an example of such an LUT for TL-3, with 971.4kbps data rate and 250 slot BP for $\mu = -7.25, \sigma = 0.73$.

Table 5.8 LUT for TL-3 with AIs and PSs (971.4 kbps, 250 slot BP, 100 slot MAP)

SNR (dB)	N_M (slots)	P_{size} (bytes)	SNR (dB)	N_M (slots)	P_{size} (bytes)	SNR (dB)	N_M (slots)	P_{size} (bytes)
	[a] 9	65		[a] 6	175		[a] 5	185
17	10	65		7	225	20	6	250
	[b] 11	70		8	235		[b] 7	255
	[a] 8	125	19	9	250		[a] 5	185
18	9	155		10	255	21	6	250
	[b] 10	180		[b] 11	255		[b] 7	255

[a] Minimum AI Length (N_M^{min}), [b] Optimum AI Length (N_M^*)

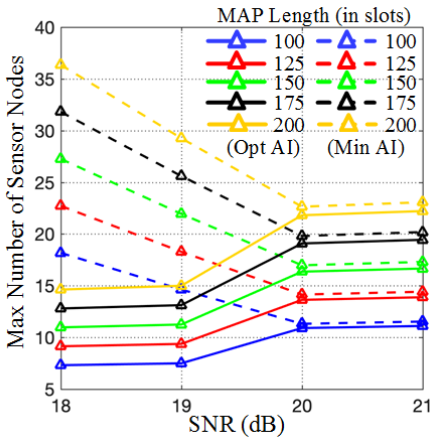

Fig. 5.16 Variation of network capacity with respect to channel SNR and MAP length when nodes are assigned only optimal or minimum AIs (971.4kbps data rate, 250 slot BP

The average total number of nodes in a WBAN obtained by considering the special cases of assigning all uniformly distributed nodes (Table 5.5) either optimum or minimum AIs would be the minimum and maximum network capacity respectively for a certain MAP length and channel SNR. This claim is noticeable from Figure 5.16. As evident, a system designer must set the MAP length to support the required number of nodes under medium to high channel SNR.

5.10 Conclusion

In this work, a detailed analysis of IEEE 802.15.6 SAM for WBAN is presented. We take into account the I-Ack policy, a log-normal fading channel, BCH encoding and low-duty cycling. The delay experienced by the frames is evaluated by deriving their service times and PGF of the queue size. Furthermore, we derive the throughput and energy consumption of the nodes considering the departure process of frames from the queue. We also analyze the Energy-Efficiency (EE) of sensor nodes and reliability of data transfer. The closed form expressions of these metrics allow their derivation as a function of various system parameters including traffic loads, Payload Sizes (PSs), beacon periods, transmission rate, Allocation Intervals (AIs) and channel SNRs. The validity of the derived model is confirmed by the closeness of the analytical and simulation results. Further, we study the variations of the performance metrics against the above mentioned system parameters. Thereby, it is concluded, through analysis, that by choosing optimal AI and PS we can maximize the EE of sensor nodes while satisfying frame delay and reliability constraints. Lastly, we highlight the significance of the analytical model in providing the system designers a tool to obtain LUTs

for sensor nodes for adaptively optimizing the AIs and PSs based on the channel SNRs to transfer physiological signals of varied data rate through WBAN.

Chapter 6

Design, Implementation and Analysis of Cognitive Radio Enabled Intelligent WBAN Gateway for Cost-Efficient Remote Health Monitoring

❝ *The goal of real healthcare reform must be high-quality universal coverage in a cost-effective way* ❞

-Bernie Sanders, United States Senator

After suitably studying, optimizing and implementing the standalone WBAN operation in Chapter 5, and also characterizing and developing a real-time CR terminal in Chapter 4, the next important objective is to design and implement a BNC as a gateway between WBAN and backhaul CRN to facilitate spectrum efficient and cost-efficient remote health monitoring. This is envisioned to address the basic challenges to deployment of NRT IoT services like healthcare monitoring over future 5G networks, which include tackling the increasing demand for wireless spectrum and the rise in data transfer costs, particularly in developing countries. ***Therefore, this chapter deals with design and implementation of an intelligent WBAN gateway, termed as BodyCog-BNC, that uses CR to opportunistically access licensed PU channels to facilitate spectral-efficient, cost-efficient and reliable NRT backhaul transmission of WBAN data***.

To this end, we develop and implement a cross-layer based modified protocol stack at the BodyCog-BNC comprising of BodyCog-BNC Management Entity (BME) and BodyCog-BNC CR Medium Access Control (BCR-MAC) units. The operation of these units are based

on cross-layer message passing that enables intelligent session management and spectrum agility depending on the state of the CRN. Furthermore, we consider a basic CRN/CBS as envisioned in IEEE 802.22, where the function of CBS is limited to assigning channels to SUs. Additional protection against PU interference has be ensured through spectrum sensing by the opportunistic users. Therefore, with the additional requirement of maximizing the energy-efficiency of backhaul CR transmission, we incorporate optimization algorithms within CR terminals of individual BNCs to achieve maximum possible energy-efficiency. To this aim, we formulate our proposed Inter-Sensing Time Optimization (ISTO) algorithm that uses KKT based convex optimization to optimally select the inter-sensing duration of the CR cycle under sensing uncertainties while keeping the PU interference under predetermined threshold. Closed form analytical expression are also derived to perform analysis of the developed BodyCog-BNC in terms of average energy consumption, probability of switching from CR interface to licensed WAN, the speed of such switching and the cost-efficiency. Thereafter, we conduct a comprehensive performance evaluation of BodyCog-BNC for varied healthcare applications under different PU activities, detected PU SNRs, control channel SNRs and CR cost regimes, which establishes its superiority in facilitating reliable cost-efficient backhaul communication by showing drastic improvement over the existing use of licensed WAN technologies. Finally, by leveraging i) the WBAN BNC developed in Chapter 3, ii) the real-time CR terminal created in Chapter 4, and iiii) our proposed cross-layer based design of BME and BCR-MAC, we implement a prototype of BodyCog-BNC and provide a proof of concept of the feasibility of BodyCog-BNC in enabling NRT remote health monitoring.

6.1 Introduction

The rise in healthcare expenditures [192–194] and the need for detection and prevention of fatal diseases at an early stage requires the healthcare system to be more affordable and proactive. One key solution to this is the use of wearable wireless medical sensors forming Wireless Body Area Networks (WBANs) [17]. WBANs typically consist of low power micro and nano-technology sensors placed on or in the body that sense physiological signals and wirelessly transmit the information using technologies like IEEE 802.15.6 [23] or Zigbee [22] to a gateway termed as Body Network Controller (BNC) [17]. The medical applications of WBAN include monitoring of electrocardiograms (ECG), electromyogram (EMG), pulse oximeters, dosimeters, movement alarms and many more. Recent advances in the design of Internet of Things (IoT) technologies allow the BNC to connect to Internet. The use of WBAN over IoT platform thus can guarantee continuous ubiquitous monitoring of one's

physiological parameters thereby providing greater mobility and flexibility to patients. As WBANs provide large time intervals of medical data which are stored in the cloud or remote server, the doctors can now access the patient records remotely giving them a clearer view of the patient's status [6]. Additionally, the integration of wireless wide area networks, for example, 2G, 2.5G, 3G as backhaul and the Internet provides greater patient mobility and global health-care connectivity [195] of WBAN. This enhanced patient mobility in turn facilitates speedy recovery. Clinical studies show that remote monitoring reduces time to detect clinical events [196], and hospitalizations [197]. Thus, remote monitoring not only increases the quality of patient care, but improves clinical efficiency and substantially reduces healthcare costs.

The licensed bands of 2G (GSM), 2.5G or 3G forming Wide-Area Access Networks (WANs) for backhaul communication can provide guaranteed quality of service [37]. Although these licensed spectra generally served well in the past, there is a dramatic increase in their access for mobile services in the recent years. Industry analysts predict that by 2020 about 50 billion devices are supposed to be connected to mobile networks worldwide, which include devices/sensors sending information between Machine-to-Machine(M2M), to servers, or to the cloud [198]. This increasing demand for wireless spectrum has led to spectral congestion. Therefore, there is a need to address this spectrum scarcity problem.

Additionally, use of licensed WAN technologies involve high data transfer costs. Though the cable Internet connectivity is widely spread and low-cost, but mobile Internet connectivity is yet to go long way for low-cost solution, especially in developing countries. Hence, a technology that enables low-cost long distance data transfer while still giving the same level of mobility and connectivity as licensed WAN will act a driving factor not only from the end user's perspective but also for the IoT and healthcare industry.

6.1.1 Cognitive Radio Backhaul: A Suitable Choice for NRT WBAN Applications

The spectrum scarcity problem can be addressed by the Cognitive Radio (CR) technology, while at the same time reducing the cost of connectivity through opportunistic sharing of idle spectrum, known as Dynamic Spectrum Access (DSA) [75]. CR technology allows unlicensed Secondary Users (SUs) to opportunistically use under utilized licensed bands without causing harmful interference to the incumbent Primary Users (PUs). Thus, CR is beneficial for both the network operators as well as the users:

User Perspective- As DSA is fundamentally opportunistic, the cost of sharing the spectrum is expected to be much lower than the cost of purchasing a licensed band [8].

This would make IoT services like healthcare monitoring more affordable to public particularly in developing nations, where the cost of data transfer is still high.

Network Operator Perspective- As the CR technology allows the SUs to utilize the unoccupied white spaces of the PU spectrum, it greatly enhances the spectral efficiency of the system. In effect, it enhances the user base of a network catering to specific applications. Additionally, the payoffs from SUs adds to the profit of the operators.

Thus CR is being considered as a promising technology to tackle, or at least partly address, the above challenges in the upcoming 5G cellular networks [8].

WBAN applications require high level of reliability, and the way to ensuring the reliability depends on the type of application. WBAN applications can be classified into- i) Real Time (RT) application, like continuous streaming of physiological signals, and ii) Non-Real Time (NRT) application, which is the offline (stored) transfer of data at regular intervals. Since CR technology is opportunistic in nature, it is affected by the sudden arrival of PU in a channel. CR handles such scenarios through handoff [167], wherein it switches to some other vacant PU channel to continue its communication. However, such handoff procedure is often associated with data loss at the Medium AccessControl (MAC) layer [100]. This data loss can be mitigated through re-transmission by Transmission Control Protocol (TCP) [199] at the upper transport layer. However, TCP does not satisfy the delay requirements of RT applications. Hence, RT WBAN applications will have to rely on licensed WAN technology with dedicated channels. Whereas, for NRT applications there are no strict delay requirements. Therefore, CR may be an ideal candidate for cost-efficient and spectral efficient reliable NRT WBAN backhaul communication. It is also worth emphasizing that RT continuous monitoring is mainly required in hospital environment, where short distance backhaul communication technology like IEEE 802.11 [200] based Wireless Local Area Network (WLAN) is more suitable. Whereas, NRT applications require the mobility provided by long distance backhaul technology to enable periodic monitoring of patients in both outdoor as well as indoor environments.

To the best of authors' knowledge, only few attempts have been made to leverage the use of CR technology specifically for reliable and cost-efficient NRT communication. To this end, in this chapter we propose an intelligent WBAN controller termed as *BodyCog-BNC* that exploits the flexibility of CR technology to realize a seamless integration of WBAN with both backhaul CR Network (CRN) and licensed WAN to enable NRT WBAN communication. The term *BodyCog* refers to the integrated architecture of WBAN and CRN. The proposed BodyCog-BNC can be visualized as a mobile phone with additional capability to communicate with the sensors in the access layer and forward the data using the already

present licensed WAN modules (GSM/GPRS/3G/4G) or the next generation CR modules. The sensors may be standalone or located in a smart watch [201] which communicates with the phone (BodyCog-BNC) over the access layer.

Some of the application areas of BodyCog-BNC for NRT health monitoring include:

i) *Remote Monitoring as a complement to in-clinic cardiac treatment follow-up*: Short interval ECGs (compressed significantly as shown in Section 3.10) can be periodically sent to physicians/remote database over CR backhaul even while traveling, and different alerts can be configured online. An example of a similar system is CardioMessenger [113] developed by Biotronik in Germany that uses cellular network as backhaul technology. Significant events can be reported by fax, e-mail or text message in order to ensure optimal follow-up. Thus, this comes as a safe, cost-effective and comfortable alternative to face-to-face follow-up visits. Additionally, any emergency time-critical event detected by BodyCog-BNC can be communicated immediately using existing licensed WAN technology.

ii) *Aid Patients with Hypertension*: A 24x7 healthcare monitoring of patients with chronic condition like hypertension is not practical for healthcare providers. However, regular monitoring can be greatly beneficial for increasing patient outcomes.

iii) *Keep track of chemo patients*: The hospital can give out smart watches with inbuilt sensors to patients to help them stick to their medication regiment and additionally provide the ability to easily and regularly track and report their symptoms and temperature.

iv) *Study epileptic seizures*: Some patients with epileptic seizures experience negative side effects when they are on their medication or are otherwise still at risk. Using sensors, BodyCog-BNC can collect information about patients'seizures to help understand and diagnose these neurological conditions. This can be accomplished by collecting data before, during and after a seizure and sending it to remote healthcare facility or records for analysis.

6.1.2 Motivation

In the present literature, there are very few works that have considered a comprehensive design, analysis and implementation of the CR technology to enable reliable, cost-efficient NRT communication. Most of the works has been focused towards RT applications like VoIP [100], video etc. More in detail, for RT applications, the authors did not have to take into consideration the high reliability requirement imposed by NRT applications. High reliability

requires handling the data loss due to- i) channel errors during normal communications, ii) handoff, and iii) inability to initiate and/or continue communication due to unavailability of no or proper PU channels. The former two scenarios are addressed in the literature through re-transmission at MAC layer [199] and quick handoff with presence of TCP [199] at upper layer respectively. However, the last scenario is yet to be explored. A possible solution to this problem is to provide CR the intelligence to switch to other licensed WAN technologies within TCP timeout if it fails to sustain a communication over the CRN. This requires the CR MAC layer to communicate with upper layers which can enable switching between two different technologies, termed as *spectrum agility*.

Cross-layer message passing in CR has been well investigated in [86, 85], however, mostly from the perspective of CR MAC and physical layer (PHY). IEEE 802.22 [86] and C-MAC [85] deals with spectrum handoff through Incumbent Detection Recovery protocol in centralized CRN. In C-MAC [85] , during beacon periods, SUs switch among the network channels by listening to beacon frames and acquiring information about the state of PU channels from PHY layer. As evident, the use of cross-layer interaction is limited to CR MAC and PHY layer, giving CR the ability to switch only between PU channels. This motivated us to design and implement cross-layer interaction between CR MAC and upper layers to facilitate spectrum agility for BodyCog-BNC.

It can be anticipated that compared to licensed WAN technologies, employing CR will come with the extra overhead of channel sensing and control messaging with the Cognitive Base Station (CBS) of CRN. This will impact the energy consumption of the BNC. However, the proposed BodyCog-BNC is shown to outperform the costlier conventional licensed WAN technologies in terms of cost-efficiency. *Cost-Efficiency* takes into account both the data transfer cost and the cost of electricity needed for recharging the batteries of BNC to replenish the energy consumption. However, driven by the motivation to make the CR backhaul communication of BodyCog-BNC as energy-efficient as possible, we propose an energy-efficiency maximization algorithm. Ma et. al. in [81] discusses a periodic spectrum sensing framework, in which each frame consists of a sensing block and an inter-sensing block. Sensing duration optimization is proposed in [202] and [203] to improve the channel efficiency. In [82], a periodic sensing timing is proposed to improve the channel utilization of CR users while limiting their interference with PUs, taking into consideration the impact of false-alarm and miss-detection (Section 4.2). Unfortunately, very few of the former works take into account the energy consumption. In [84], to maximize the channel utilization, an opportunistic spectrum access strategy is introduced for a slotted SU overlaying an un-slotted primary network under interference constraint and energy consumption constraint. However, none of the works consider optimization of energy-efficiency, which is the ratio of throughput

to energy consumption. To this end, the present work proposes an algorithm to determine the optimal inter-sensing duration that maximizes the energy-efficiency of CR transmission in the presence of sensing uncertainties over a PU channel under a pre-determined PU interference constraint . In addition, the algorithm also identifies the usable PU channels and also facilitates efficient cross-layer based decisions.

6.1.3 Contributions of this Chapter

The main contributions of this article are summarized below.

❶ The proposed WBAN gateway, i.e. BodyCog-BNC is designed to facilitate cost-efficient and reliable NRT backhaul transmission of WBAN data using CR technology to opportunistically access the white spaces in licensed PU channels. It will be shown through analysis that BodyCog-BNC provides a cost-efficient healthcare IoT solution for the users and a profitable avenue for network operators.

❷ A cross-layer based *BodyCog-BNC Management Entity (BME)* is thus developed and implemented at the management layer of the BNC that exploits the cross-layer message passing with CR MAC layer to facilitate spectrum agility and session management. Session management comprises of connection, disconnection and other session related decisions by the BME based on information from the CR MAC layer. Whereas, spectrum agility is the ability to intelligently switch from CR backhaul to licensed WAN when required.

❸ We also design and implement a cross-layer based CR MAC for BodyCog-BNC, termed as *BCR-MAC*, which facilitates spectrum agility at the BME. To this aim, BCR-MAC manages the connection to the CBS through control message exchange. However, in the event of failure in this control message exchange, or unavailability of proper CR channels, or successive handoff events due to presence of multiple PUs in different channels, the BCR-MAC through cross-layer message passing intimates the BME to initiate spectrum agility so as gracefully switch to the licensed WAN. The simulation studies show that the cross-layer based design provides a significant enhancement of switching speed in case of spectrum agility as compared to a non cross-layer based approach.

❹ In this work, we have also optimized the CR backhaul communication through a proposed *Inter-Sensing Time Optimization (ISTO) algorithm*. ISTO is implemented at the BCR-MAC and maximizes the energy-efficiency of transmission over a PU channel allocated by CBS while still satisfying the strict PU interference constraint

under sensing uncertainties. Furthermore, the ISTO algorithm also identifies whether an allocated channel is suitable for CR communication.

❺ For performance analysis of BodyCog-BNC, we derived the closed form mathematical expressions for different metrics like the average energy consumption, probability of switching from CR interface to licensed WAN, the speed of such switching and the cost-efficiency.

❻ Lastly, through a proof of concept we show a hardware prototype implementation of the BodyCog-BNC and then validate its ability in enabling NRT data transmission over a CRN.

6.1.4 Chapter Organization

The chapter is organized as follows. In Section 6.2, the BodyCog architecture is outlined, whilst the protocol stack of the proposed BodyCog-BNC along with its design overview is outlined in Section 6.3. Section 6.4 discusses the design and implementation of the BME. While Section 6.5 describes the design and implementation of the BCR-MAC. Section 6.6 introduces the ISTO algorithm. The performance metrics are introduced and derived in Section 6.7. Thereafter, Section 6.8 discusses the performance analysis of the BodyCog-BNC. Section 6.9 demonstrates the prototype implementation and test-bed validation of BodyCog-BNC (See Appendix D.2 for Demo Video Link). Finally, we conclude the chapter in Section 6.10.

6.2 BodyCog Architecture

The integrated architecture of WBAN over CR backhaul to support ubiquitous NRT remote healthcare monitoring is named as BodyCog architecture and is shown in Figure 6.1. It aims to send small amounts of WBAN captured data at regular intervals to a Remote Server (RS) via the nearest Cognitive Base Station (CBS) of a centralized CRN. The BodyCog consists of three logical layers: 1) the access layer comprising of WBAN, 2) the backhaul convergence layer that includes the centralized CRN and licensed WAN, and 3) the service layer comprising of a RS.

6.3 Protocol Stack and Design of BodyCog-BNC

According to [204, 205], for any M2M communication in IoT, the protocol stack should be i) Energy-Efficient, ii) Internet-Enabled, and iii) Highly Reliable. To this end, Aijaz et. al. in

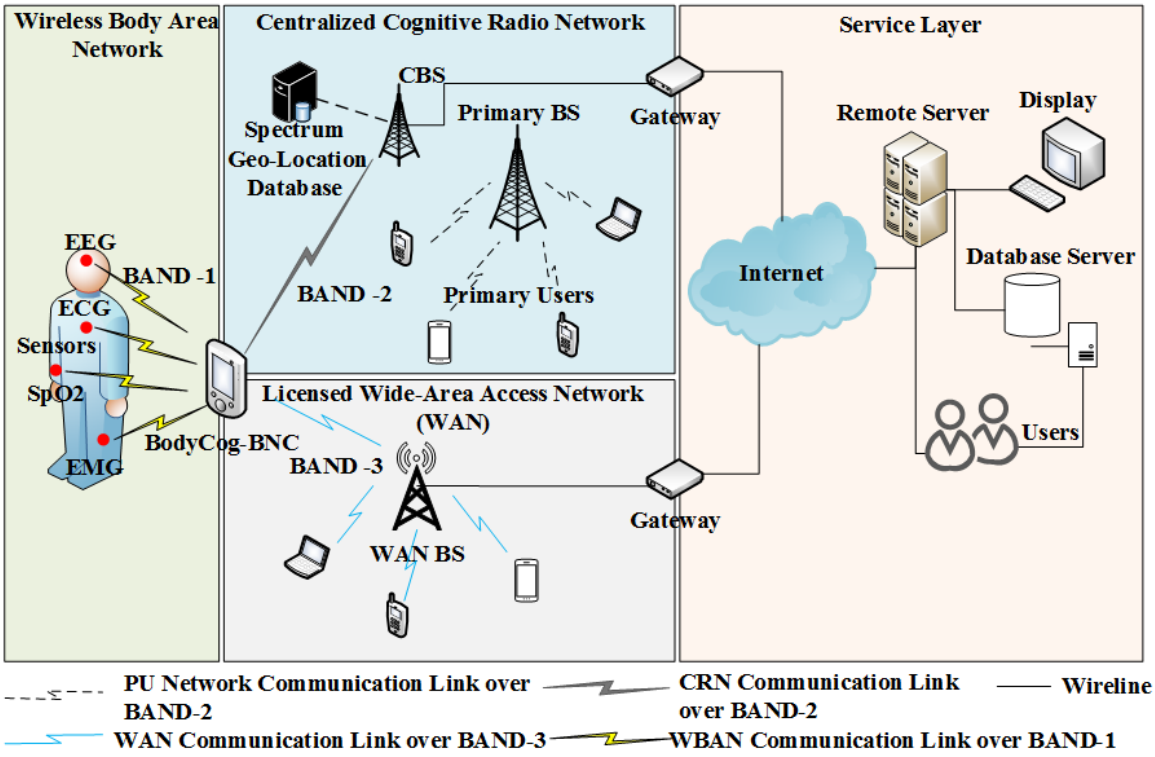

Fig. 6.1 BodyCog architecture along with a licensed WAN for spectrum agility.

[204] proposed a protocol stack to enable cognitive M2M communication, which is focused towards access layer communication. However, to facilitate NRT cognitive communication at the convergence layer and enable BodyCog-BNC to take intelligent decisions based on the states of the PU channels, the existing cognitive M2M protocol stack needs to be revised with additional capabilities. For example, it should be "flexible" enough to switch to other licensed WAN technologies like cellular network in case of non-availability of PU channel. Hence, a modified cross-layer based protocol stack for the BodyCog-BNC is devised as shown in Figure 6.2. The dotted lines in Figure 6.2 highlight the layer wise communication in the BodyCog architecture. The BNC design to implement the protocol stack is illustrated in Figure 6.3, where SAP denotes a service access point between two layers.

At the PHY and MAC layer of the WBAN, standards like IEEE 802.15.6 [23] or Zigbee [22] may be adapted to satisfy specific QoS needs of WBAN applications. As shown in Figure. 6.3, a WBAN Microcontroller Unit (MCU) with the help of the wireless transceivers operating in BAND-1 coordinates all the activities of the sensors and BNC in the WBAN access layer. The WBAN MCU collects physiological signals in Real Time (RT). However, based on the application, the communication over convergence layer may be RT or NRT. We focus on NRT communication. For example, suppose the BodyCog-BNC captures a 2 second

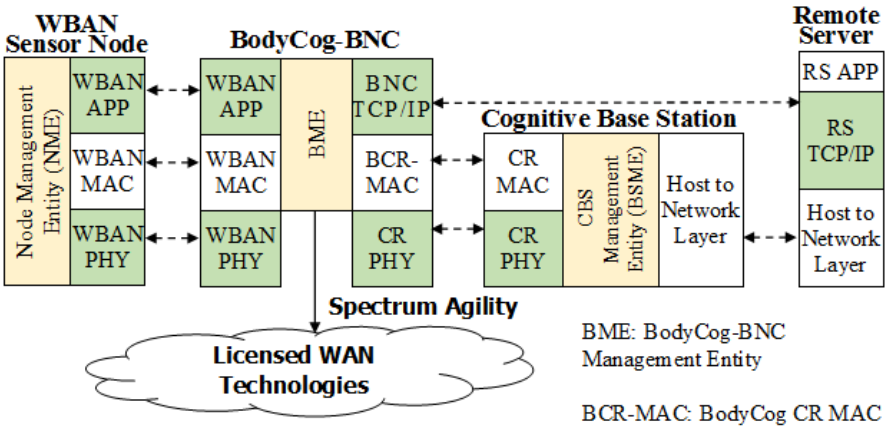

Fig. 6.2 Complete BodyCog protocol stack with layer wise communication of BodyCog-BNC.

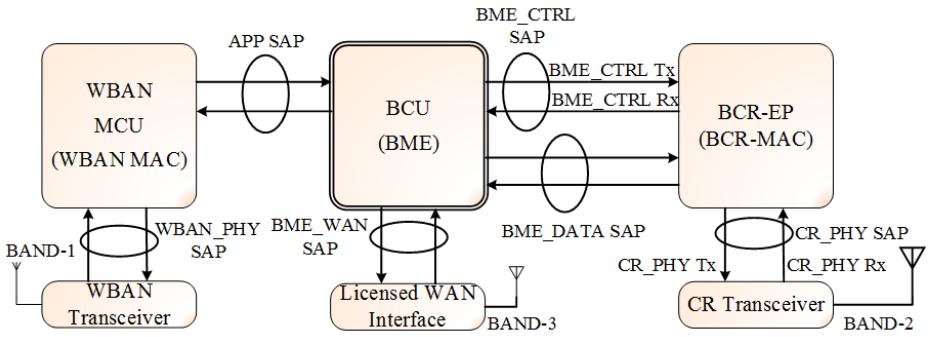

Fig. 6.3 BodyCog-BNC Design.

electrocardiogram (ECG) signal from WBAN sensors at 200Hz. The BNC then compresses the 6.4kb data. Thereafter, it acts as a mobile gateway and initiates the data transfer over the low-cost backhaul CRN. Furthermore, the WBAN access layer and BodyCog-BNC may be scheduled to capture and transfer the 2s ECG signal every few hours to generate a comprehensive record for a patient at the remote server database.

The proposed protocol stack and design of BodyCog-BNC comprises of a cross-layer based BodyCog-BNC Management Entity (BME) which forms a management layer. The BME is implemented at the BodyCog-BNC microcontroller unit (BCU) (see Figure 6.3). The BME communicates with an Embedded Processor (EP) housing the BodyCog-BNC CR MAC (BCR-MAC) by exploiting cross-layer message passing via the BME_CTRL SAP. BME_CTRL SAP comprises of BME_CTRL Tx and BME_CTRL Rx for message passing in the direction as highlighted in Figure 6.3. Leveraging on the cross-layer message passing, the BME facilitates-

i) session management
ii) spectrum agility

Once a session is established with the remote server over the backhaul CRN, the BCU transfers the data to CR embedded processor via the BME_DATA SAP. However, if the BCR-MAC intimates BME about the inability of the CRN to support the data transmission, then BME performs spectrum agility and intelligently switches to licensed WAN and sends data via BME_WAN SAP.

Along with the BME, the BCU also implements the transport layer functionality. At the transport layer, a reliable data stream is required to transfer sensitive medical data to the remote server. Thus, conventional connection oriented Transmission Control Protocol (TCP) is adapted. The physical partitioning between BME and TCP/IP layer is hard to mandate, and thus BME is inter-changeably termed as the TCP client.

The intelligence at the CR end of BodyCog-BNC is imposed by the proposed cross-layer based CR MAC, termed as BCR-MAC, which is implemented at the BodyCog-BNC CR Embedded Processor (BCR-EP), as shown in Figure 6.3. Figure 6.4 shows the functional diagram of the proposed BCR-MAC and the inter-layer coupling. The major functions of the BCR-MAC are as follows:

i) provides access (*spectrum access*) to the backhaul CRN through connection and disconnection procedures with the CBS and cross-layer message passing with BME,
ii) performs *spectrum sensing* of an allocated PU channel with the help of signal energy obtained from the CR PHY layer via CR_PHY SAP (see Figure 6.3),
iii) implements a proposed Inter-Sensing Time Optimization (ISTO) algorithm to maximize the energy-efficiency of transmission over a PU channel by selecting the optimal inter-sensing duration (*sensing scheduling*),
iv) enables handoff (*spectrum mobility*) to a new channel in case PU is detected in the current allocated PU channel, and
v) facilitates *spectrum agility* at the BME through cross-layer message passing due to un-availability of vacant PU channels in the CRN, or unsuccessful control message exchange with CBS, or successive handoffs.

BCR-MAC relies on the detection of unoccupied PU spectrum through spectrum sensing. Therefore, in the next sub-section we present the BCR-MAC channel access and highlight the sensing-transmission cycle.

The WBAN layer includes all the sensors for sensing vital medical health information like heart-beat, blood oxygen and glucose level, temperature etc. This data is communicated to our proposed portable gateway controller called BodyCog-BNC over frequency BAND-1, as shown in Figure 6.1. The communication in this layer can be compliant to either IEEE 802.15.6 [23] or Zigbee [22] standard.

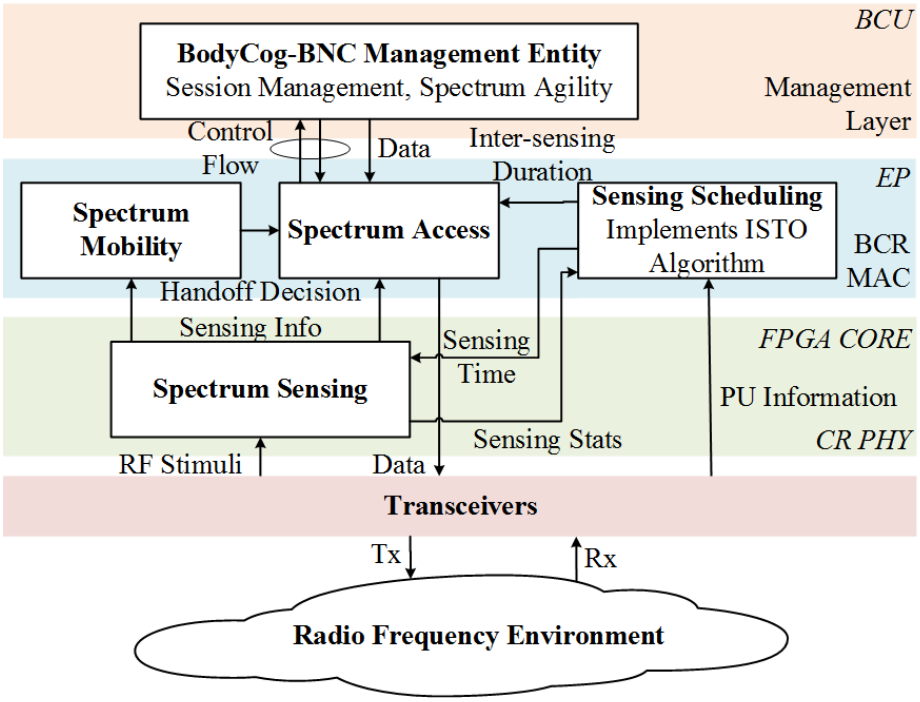

Fig. 6.4 Spectrum functions at the BCR-MAC.

The BodyCog-BNC is responsible for managing the transfer of WBAN data collected from the sensors to the remote server in an energy-efficient and cost-efficient way. The design of BodyCog-BNC is the main contribution of this work which acts as the gateway interface between WBAN and CRN/ licensed WAN. BodyCog-BNC is designed such as to enable communication with different WBAN standards. It supports the CR protocols and is also capable of session management and spectrum agility. BodyCog-BNC is thus an intelligent device and the core of BodyCog architecture. A detailed overview of the BNC design is presented in the next section.

The backhaul CRN allows the PUs and the BodyCog Platform to coexist and operate in the same frequency range, BAND-2 (Figure 6.1). We consider a centralized overlay CRN with a CBS serving multiple SUs. The BodyCog-BNC serves as one of the SUs from the viewpoint of the CRN. The Primary Network (PN) has multiple non-overlapping orthogonal PU channels of bandwidth W Hz. The occupancy state of a channel due to PU is modeled as a non-time slotted two-state ON/OFF Continuous Time Markov Chain (CTMC) [169, 168, 170]. The durations of PU's ON state (hypothesis H_1 or busy period) and OFF state (hypothesis H_0 or idle period) are represented by exponentially distributed i.i.d. random variables X and Y, with probability density functions $f_X(t) = \lambda e^{-\lambda t}$ and $f_Y(t) = \mu e^{-\mu t}$ having parameters λ and μ respectively. Thus, the average busy period (t_{on}) is $1/\lambda$, and the average idle period (t_{off}) is $1/\mu$. Therefore, the probability of a channel being busy, simply

termed as PU activity, is denoted by $P(H_1) = \frac{t_{on}}{t_{on}+t_{off}}$. While the idle channel probability is $P(H_0) = \frac{t_{off}}{t_{on}+t_{off}}$. It is assumed that the CBS retrieves the PU channel occupancy data, t_{on} and t_{off} from an external entity such as a white space database [206, 207].

We consider that a common control channel is available to the SUs [208, 44]. Each SU is equipped with a single half-duplex radio [85], which can either transmit or receive/sense, but not both at the same time. To obtain a data channel for transmission, a SU upon reception of a beacon sends a channel request to the CBS over the control channel and waits for a successful channel assignment message. The CBS after gathering all the information from the SUs, determines a transmission schedule applying a fair scheduling policy [209, 105] and broadcasts it to the users via channel assignment messages. The fair scheduling policy allows the CBS to maintain a table of weights. Let w_i be the weight for the i^{th} SU (SU_i) that is obtained as the ratio of the number of channel requests granted to SU_i to total number of requests from SU_i up to the current instant. The fair scheduling assigns the best quality channels (e.g. lowest PU activity channel having the highest detected PU Signal-to-Noise Ratio) to the SUs in ascending order of their weights. If the channel assigned is not found suitable for transmission by the SU, it may request another channel from the CBS during a negotiation period. However, it is most likely that the channel assigned by CBS will be suitable and accepted by the SUs. A detailed discussion on the various fair scheduling policies in literature is provided in [209, 105]. Thus, the CBS coordinates 'in which channel' the BNCs should tune in order to transmit their packets.

Lastly, at the RS, a Remote Server Application Program (RSAP) is designed so as to communicate with BodyCog-BNC over TCP/IP link. This allows the RS to monitor the patient's health ubiquitously and periodically over the Internet irrespective of its location.

6.3.1 BCR-MAC Sensing-Transmission Cycle

BCR-MAC employs a time slotted protocol as shown in Figure 6.5 with period $T_F > 0$. At the beginning of each slot, the allocated PU channel is sensed for sensing duration T_S by the BCR-MAC through CR PHY layer. Then depending on whether the channel is idle or busy, it will remain silent or access the channel for transmission/reception with inter-sensing duration T_D. It is reasonable to assume that the CRN does not have a priori knowledge of the PU signal characteristics such as the modulation type, packet format or pulse shape. In this scenario, the optimal detector is an energy detector [160], which is also one of the most commonly used detection technique in CRNs [83]. Therefore, in this sub-section, we derive the essential energy detection sensing performance metrics and the sensing time (T_S).

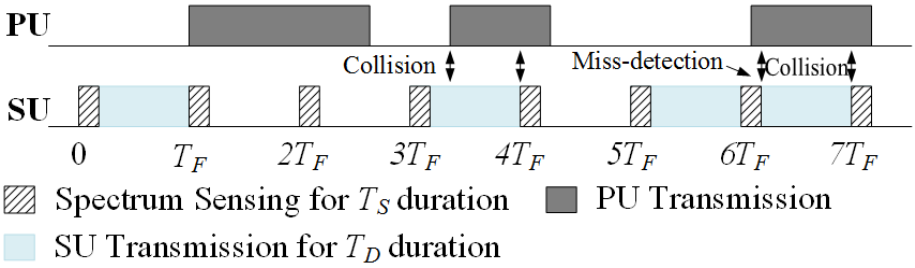

Fig. 6.5 Timing behavior of PU and SU with possible collision instances.

The energy detector performs non-coherent signal detection by integrating squared versions of received signal samples. The PU signal is detected by comparing the received signal energy with a threshold computed using an estimated noise power as described in Section 4.2. The detection threshold λ_{th} of the CR PHY of BodyCog-BNC, in the presence of white Gaussian noise at the receiver, can be given by,

$$\lambda_{th} = \sqrt{2N_S N_0^2} Q^{-1}(P_f) + N_S N_0 \tag{6.1}$$

where N_S denotes the number of received samples used for detection, N_0 represents the noise power calculated at the receiver and P_f is the false-alarm probability constraint [160] for the system which is set a priori as $P_f = \kappa$.

Using the threshold obtained in (6.1), the BNC can detect the presence of PU with detection probability P_d [160], given as (Section 4.2),

$$P_d = Q\left(\frac{\lambda_{th} - N_S N_0(1+\gamma_{PU})}{\sqrt{2N_S}N_0(1+\gamma_{PU})}\right) \tag{6.2}$$

where γ_{PU} is the PU SNR detected at the CBS, $Q(\cdot)$ is the Q-function.

Thus, the number of samples required to sense a PU signal at minimum PU SNR, $\gamma_{PU,min}$ (also known as receiver sensitivity) with a detection probability $P_d = \chi$ under the false-alarm constraint $P_f = \kappa$ can be obtained using (6.1) and (6.2) as,

$$N_S = 2 \times \left[\left\{ Q^{-1}(\kappa) - (1+\gamma_{PU,min}) Q^{-1}(\chi) \right\} / \gamma_{PU,min} \right]^2 \tag{6.3}$$

Using N_S obtained in (6.3) we can calculate the sensing time T_S based on the Analog to Digital Converter (ADC) frequency (f_{ADC}) of the CR radio module as,

$$T_S = \frac{N_S}{f_{ADC}} \tag{6.4}$$

6.4 Design and Implementation of BME

This section describes the BME session management and spectrum agility functions. For this, the BME exploits the cross-layer message passing with BCR-MAC via the BME_CTRL SAP. Using the cross-layer message passing, we model the *BME TCP/IP Client-Server (BTCS)* framework as a Finite State Machine (FSM) for interaction with Remote Server (RS). Following this, we show how to follow the development steps at the BCU, more specifically BME, to implement the BTCS framework from its FSM.

6.4.1 Cross-Layer Messages between BME and BCR-MAC

The cross-layer interaction between BME and BCR-MAC follows the control message flow as shown in Figure 6.6. The messages are described as follows:

- CONN_REQ: When the WBAN APP layer has NRT data to send via CR interface, the BME initiates the CR session by sending CONN_REQ message to the BCR-MAC.
- CONN_ACCPT/CONN_FAIL: The CONN_ACCPT message is issued by the BCR-MAC to BME to inform when backhaul communication can take place through the CR interface of BodyCog-BNC. However, if the CRN is not suitable for communication, then BCR-MAC responds with CONN_FAIL message.
- DISCON_REQ: With this message BME intimates BCR-MAC to release its PU channel to CBS.
- DISCON_ACK: BCR-MAC confirms disconnection from CBS with the DISCON_ACK message.

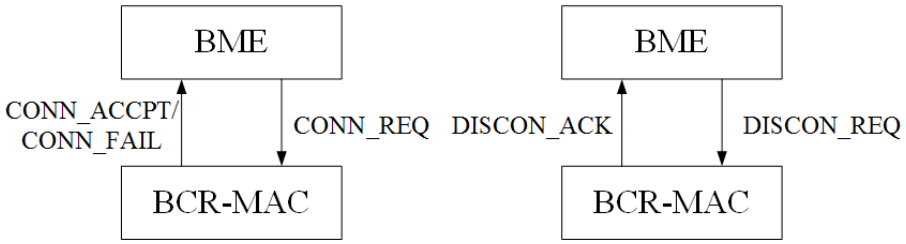

Fig. 6.6 Cross-layer messages between BME and BCR-MAC.

The detailed explanation on the BCR-MAC functionality is provided in Section 6.5. Next, we highlight the BME development architecture designed to handle the cross-layer message passing and exploit them to enable NRT communication over the BTCS framework.

6.4.2 The BME Development Architecture

To handle cross-layer message passing and design the BME we developed a *BME Development (BMED)* architecture, which is implemented at the BNC micro-controller Unit (BCU) (Figure 6.3). Within the architecture we define several macros and functions in C programming language [210] to enable development of the BTCS framework from the FSM of BME. The developed codes are compiled along with the macros and functions. Figure 6.7 shows the BMED architecture. The BMED framework (Figure 6.7 (1)) consists of- i) BCU interrupts at the APP SAP (Figure 6.7 (2)) and BME_CTRL Rx (Figure 6.7 (3)), ii) a data queue (Figure 6.7 (4)) to store compressed WBAN data, and iii) the main control loop (Figure 6.7 (5)) of BME. An incoming WBAN data stream from WBAN APP layer (Figure 6.7 (6)) via APP_SAP can generate two types of events:

i) APP_DATA_START: Generated when BME starts receiving data from APP layer.
ii) APP_DATA_END: Generated when the entire APP layer data is received at the BME.

Whereas in case of BME_CTRL Rx, the cross-layer messages described in Section 6.4.1 are implemented as events. An event at either APP SAP or BME_CTRL Rx interrupts the main control loop and transfers the control to their respective Interrupt Service Routines (ISRs), i.e. APP_SAP_ISR (Figure 6.7 (7)) or BME_CTRL_Rx_ISR (Figure 6.7 (8)). Based on the FSM state, the event and the state-event transition table, the ISR determines the action

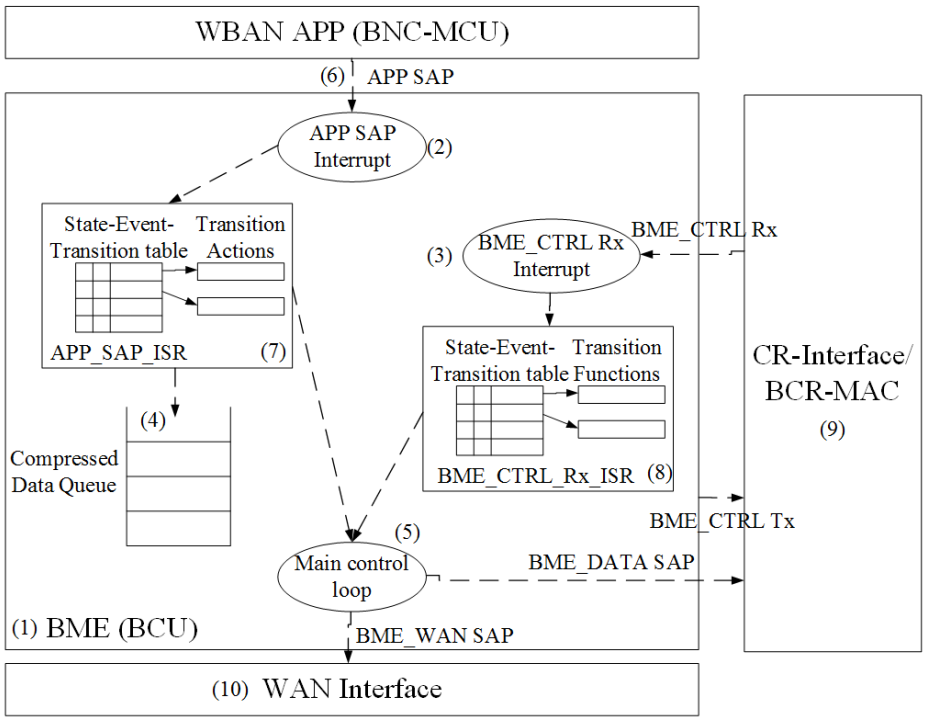

Fig. 6.7 The BMED framework architecture at the BME.

to be executed and possibly generate new events. Therefore, to implement BME, we define the state-event-transition table and the actions for the ISRs that are derived from the FSM developed to realize the BTCS framework, which is discussed next.

6.4.3 Developing BTCS Framework from FSM

In order to achieve a seamless and reliable interoperability with the Internet, the interlinking of BCR-MAC control messages with TCP/IP layer has been exploited in the BodyCog-BNC design. The integration of TCP/IP functionalities into BodyCog-BNC makes BodyCog architecture IoT aware. As stated previously, we treat the BME as a TCP client. The different components of BTCS framework are highlighted in Figure 6.8. In Figure 6.8, *CR_Client* and *WAN_Client* denotes the BME client connections over CR interface (Figure 6.7 (9)) and WAN interface (Figure 6.7 (10)) respectively. The Remote Server Application Program (RSAP) starts a server session by opening a TCP/IP server socket at the dynamic DNS address `server.ddns.net` and port 8080 (Figure 6.8 (1)) and waits for the BME client to connect with. When the connection is established, RSAP reads the data sent out by BME client. The overall TCP/IP behavior is controlled by the cross-layer interaction between BME and BCR-MAC, which is represented through a FSM in Figure 6.9. The FSM focuses on the states, events and the actions of the BME that allows us to construct the state-event-transition table and the actions of BMED (Figure 6.7), thereby facilitating BME implementation. In the following, we provide an elaborate explanation of BME operation using the FSM.

Figure 6.9 illustrates the state transition diagram of the BME FSM. Initially, the FSM is in INACTIVE state.

1. When the WBAN APP layer starts sending data to the BME, APP_DATA_START event is invoked. This allows the BME to receive the WBAN data samples in the APP_DATA_RECEIVING state (Transition 1 in Figure 6.9). On reception of the complete WBAN data, APP_DATA_STOP event is generated and BME implements Discrete Wavelet Transform (DWT) based data compression to reduce the number of samples to be transmitted over the backhaul link (Figure 6.8 (2)). The data compression is initiated through the DATA_COMPRESS action of BME, and the compressed data is stored in 'Compressed Data Queue' (Figure 6.7 (4)). When the compression is complete, BME sends CONN_REQ message to the BCR-MAC over BME_CTRL Tx requesting access to the CRN. The FSM now enters the CONN_RESP_PENDING state (see Transition 2 in Figure 6.9).
2. Upon reception of CONN_REQ, the BCR-MAC exchanges control message with CBS and builds the response message. If a suitable channel is obtained from the CBS, BCR-MAC

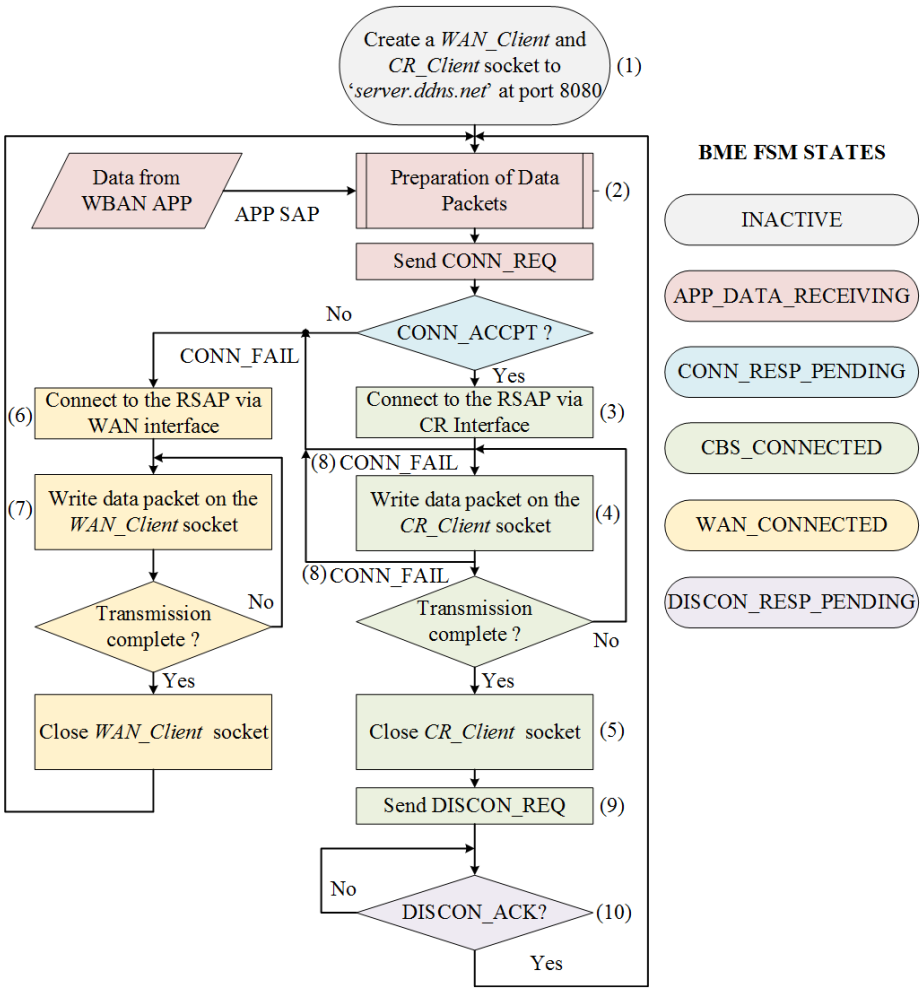

Fig. 6.8 Flowchart of the BTCS framework at BME.

replies with the CONN_ACCPT message to the BME and a CR session is established. The FSM moves to the CBS_CONNECTED state (see Transition 3 in Figure 6.9), and the transition is indicated by the internally generated CONNECT_CBS action. The CONNECT_CBS action allows the BME to create a *CR_Client* connection to RSAP server socket (Figure 6.8 (3)), and then prepare a copy of the 'Compressed Data Queue'. After the copied data is written out (Figure 6.8 (4)) in the CBS_CONNECTED state, the *CR_Client* socket is closed (Figure 6.8 (5)).

3. Suppose that the CBS fails to assign a free or suitable PU channel. Then the BCR-MAC sends a CONN_FAIL message to the BME. Upon receipt of CONN_FAIL, the FSM performs spectrum agility and enters the WAN_CONNECTED state (see Transition 4 in Figure 6.9). For spectrum agility, BME internally generates the CONNECT_WAN action which activates the WAN interface, connects the SAP server using *WAN_Client*

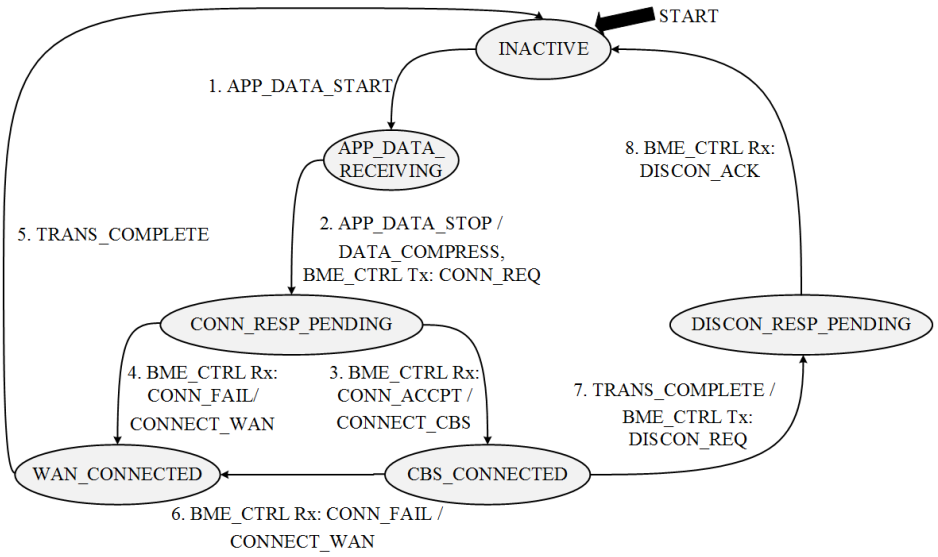

Fig. 6.9 BME FSM state transition diagram.

(Figure 6.8 (6,7)), make a copy of the compressed data and complete transmission of that copied data in WAN_CONNECTED state. After completion of transmission (indicated by generation of TRANS_COMPLETE event), the FSM moves to the INACTIVE state (see Transition 5 in Figure 6.9).

4. Suppose that during an ongoing CR session, a PU suddenly arrives in the allocated PU channel. The BCR-MAC is robust enough to perform handoff to another free PU channel assigned by the CBS. However, in case of presence of PUs in multiple PU channels or the assigned channels being not suitable for communication, the BCR-MAC interrupts the CR session at the BME by sending CONN_FAIL message (Figure 6.8 (8)). The FSM moves to the WAN_CONNECTED state (see Transition 6 in Figure 6.9), performs spectrum agility, prepares a fresh copy of the 'Compressed Data Queue' and continues the communication over the WAN interface.
5. On the successful completion of the transfer of compressed data over the CR interface, the BME sends the DISCON_REQ message to the BCR-MAC (Figure 6.8 (9)) via BME_CTRL Tx. The FSM moves from CR_CONNECTED state to DISCON_RESP_PENDING state (see Transition 7 in Figure 6.9). BCR-MAC after successfully releasing the PU channel to CBS, sends DISCON_ACK message to BME confirming the disconnection of the CR session (Figure 6.8 (10)) . Thereafter, the FSM enters the INACTIVE state (see Transition 8 in Figure 6.9), waiting for the next data stream from the WBAN APP layer.

Note that, the 'Compressed Data Queue' is emptied only after the successful data transfer to the RS, i.e. when a TRANS_COMPLETE event is generated at the BME.

6.4.4 BMED Implementation of BTCS framework

Using the FSM diagram illustrated in Figure 6.9, we describe the setup of the BMED architecture at the BCU. First we define the different states, events, actions and ISRs. Then the implementation of the actions within ISR is described. To this end, we use macros and functions to execute different BME functionalities. This makes the coding independent of the BCU hardware platform. A separate platform specific header file maps the macros and functions to the hardware specific execution steps.

6.4.4.1 States, Events, Actions and ISRs of BMED

The BMED definitions for the BME states, events, actions and ISRs are shown in Figure 6.10 and described as follows:

```
START_DEFINE_BME_STATE
    BME_STATE (INACTIVE)
    BME_STATE (APP_DATA_RECEIVING)
    BME_STATE (CONN_RESP_PENDING)
    ...
END_DEFINE_BME_STATE

START_DEFINE_BME_EVENT
    BME_EVENT (APP_DATA_START)
    BME_EVENT (APP_DATA_STOP)
    BME_EVENT (receive_BME_CTRL_Rx)
    BME_EVENT (TRANS_COMPLETE)
END_DEFINE_BME_EVENT

START_DEFINE_BME_ACTION
    BME_ACTION (send_BME_CTRL_Tx)
    BME_ACTION (DATA_COMPRESS)
    BME_ACTION (CONNECT_CBS)
    BME_ACTION (CONNECT_WAN)
END_DEFINE_BME_ACTION

DECLARE_BME_ISR (APP_SAP_ISR)
DECLARE_BME_ISR (BME_CTRL_Rx_ISR)
```

Fig. 6.10 The definition of states, events, actions and ISRs for BME.

- Lines 1-6 define the BME FSM states using the macros START_DEFINE_BME_STATE and END_DEFINE_BME_STATE. The BME_STATE macro defines individual states (e.g. CONN_RESP_PENDING, etc in Figure 6.9).
- Lines 7-12 define the BME FSM events using the macros START_DEFINE_BME_EVENT and END_DEFINE_BME_EVENT. The BME_EVENT macro defines individual events (e.g. APP_DATA_START, etc in Figure 6.9).
- Lines 13-18 define the BME FSM actions using the macros START_DEFINE_BME_ACTION and END_DEFINE_BME_ACTION. The BME_ACTION macro defines individual actions. For example, send_BME_CTRL_Tx denotes the action of sending a cross-layer message to BCR-MAC via the BME_CTRL Tx. These actions are implemented as per the state-event-transition table maintained by the ISRs.
- Lines 19-20 declare the BME ISRs using the macros DECLARE_BME_ISR.

6.4.4.2 ISR and State-Event-Transition Table Implementation within BMED

In this section, we describe the BMED steps to implement BME_CTRL_Rx_ISR as an example to illustrate how to develop the BME from its FSM. Figure 6.11 shows the C-code for the BME_CTRL_Rx_ISR. This ISR is executed when there is an incoming cross-layer message over the BME_CTRL Rx from the BCR-MAC. The BME main control loop is interrupted and the program control is shifted to the ISR.

- Line 1 invokes the START_BME_ISR macro to start the ISR BME_CTRL_Rx_ISR declared at Line 20 of Figure 6.10.
- Lines 2-3 declare two enumerated data type variables: vREC_BME_CTRL_MSG and vBME_STATE. These variables are used to store the incoming cross layer message from BCR-MAC and the current BME FSM state respectively.
- Line 4 uses the function CHECK_BME_STATE to obtain the current BME FSM state and store it in vBME_STATE.
- Line 5 uses the BME_parseInMsg function to parse the incoming message associated with the receive_BME_CTRL_Rx event and store it in the variable vREC_BME_CTRL_MSG.
- Line 6 initiates the switch-case statements that compare the vREC_BME_CTRL_MSG to the possible incoming cross-layer messages (Lines 7 and 12). The switch-case model provides the actual implementation of the state-event-transition table shown in Figure 6.7, and is explained next.
- Lines 8 and 13 compare vBME_STATE with the possible BME FSM states. Thereafter, depending on the current BME FSM state the appropriate transition actions are executed.
- Lines 9 and 14 use the BME_EXECUTE function to execute the CONNECT_CBS or CONNECT_WAN actions respectively.

```
 1: START_BME_ISR (BME_CTRL_Rx_ISR)
 2: tBME_CTRL_MSG vREC_BME_CTRL_MSG;
 3: tBME_STATE vBME_STATE;
 4: vBME_STATE = CHECK_BME_STATE ();
 5: vREC_BME_CTRL_MSG = BME_parseInMsg (receive_BME_CTRL_Rx);
 6: switch (vREC_BME_CTRL_MSG){
 7:       case CONN_ACCPT:
 8:             if (vBME_STATE = = CONN_RESP_PENDING){
 9:                   BME_EXECUTE (CONNECT_CBS);
10:                   BME_CHANGE_STATE_TO (CBS_CONNECTED);}
11:             break;
12:       case CONN_FAIL:
13:             if(vBME_STATE==(CONN_RESP_PENDING || CBS_CONNECTED)){
14:                   BME_EXECUTE (CONNECT_WAN);
15:                   BME_CHANGE_STATE_TO (WAN_CONNECTED);}
16:             break;
17:       default:
18:             break;}
19: END_BME_ISR (BME_CTRL_Rx_ISR)
```

Fig. 6.11 The C-code of the ISR BME_CTRL_Rx_ISR.

- Line 10 and 15 uses the BME_CHANGE_TO_STATE macro to move the BME FSM to CBS_CONNECTED or WAN_CONNECTED states respectively.
- Line 19 exits the ISR.

After the end of the BME_CTRL_Rx_ISR, the program returns to the main control loop. Depending on the current FSM state, which in this case will be either CBS_CONNECTED or WAN_CONNECTED, the program executes the functions necessary to transfer data over either the CR or WAN interface respectively.

6.5 Design and Implementation of BCR-MAC

The BCR-MAC serves as the heart of the cognitive radio functions at the backhaul link of BodyCog-BNC. In this section, we describe the spectrum access, sensing scheduling, spectrum mobility and facilitation of spectrum agility functions of BCR-MAC. Similar to the previous section, first we highlight the control messages exchanged between BCR-MAC and CBS. Next, we describe the *BCR-MAC Development (BCRD) architecture*, which models the BCR-MAC functionality as a FSM. Then we explain how BCRD framework leverages on the FSM to implement the BCR-MAC.

6.5.1 Control Messages between BCR-MAC and CBS

The control messages exchanged between BCR-MAC and CBS are as follows:

- CHAN_REQ: Upon receiving a CONN_REQ from BME, the CHAN_REQ message is initiated by the BCR-MAC to request a PU channel from CBS for transmission.
- CHAN_SUCS: If a PU channel is available for transmission then the CBS responds with CHAN_SUCS message.
- CHAN_FAIL: The CHAN_FAIL message is issued by the CBS if no PU channel is available for transmission.
- CHAN_RLS: With this message the BCR-MAC releases its channel to the CBS.
- CHAN_RLSD: CBS acknowledges the disconnection with CHAN_RLSD message.

It is worth mentioning that all the control messages except CHAN_RLS and CHAN_RLSD are sent over the control channel.

6.5.2 The BCR-MAC Development Architecture

The BCRD framework architecture as shown in Figure 6.12 is developed to assist development of BCR-MAC from its FSM. It is implemented at the BCR-EP (Figure 6.3). As illustrated in Figure 6.12, the BCRD framework handles the cross-layer message passing with BME and the data received from both CR-PHY and BME. The framework (Figure 6.12(1)) consists of three primary BCR-EP external interrupts: i) BME_CTRL Tx (Figure 6.12 (2)), ii) BME_DATA SAP (Figure 6.12 (3)), and iii) CR_PHY Rx (Figure 6.12 (4)). In addition, it includes two Timer (TMR) (Figure 6.12 (5)) interrupts which are controlled and generated internally by BCR-MAC.

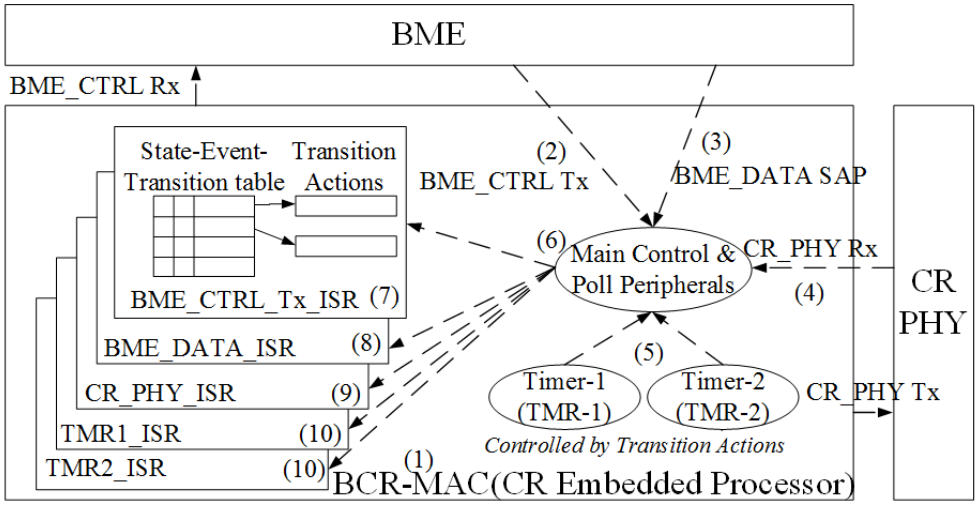

Fig. 6.12 The BCRD framework architecture at the BCR-MAC.

The main control loop (Figure 6.12 (6)) of BCRD architecture continuously polls the interrupts, and the actual processing happens via the respective ISRs, as follows:

i) The BME_CTRL_Tx_ISR (Figure 6.12 (7)) is executed when an incoming cross-layer message is received from BME.
ii) The BME_DATA_ISR (Figure 6.12 (8)) is called when a new data/ payload is received from the BME for transmission.
iii) The CR_PHY_ISR (Figure 6.12 (9)) is a callback for the reception of wireless frames from the CR_PHY Rx. The received frames include control messages and immediate acknowledgments (I-Ack) from the CBS.
iv) The TMR1_ISR and TMR2_ISR (Figure 6.12 (10)) are responsible for handling internally generated timeout events, which are explained next.

Sticking to the FSM design philosophy, the ISRs execute their actions based on state-event-transition tables that are generated from the FSM. Therefore, in the following sub-section we describe the FSM of BCR-MAC.

6.5.3 Developing BCR-MAC from FSM

Figure 6.13 shows the execution flow of BCR-MAC for normal communication over CRN with connection and disconnection procedures. In this figure, a dashed arrow represents a cross-layer message between BME and BCR-MAC. A solid arrow represents a control message between BCR-MAC and CBS. The BCR-MAC maintains a FSM to handle the cross-layer and control messages. In Figure 6.13, an oval represents a BCR-MAC FSM state. The complete FSM state transition diagram is illustrated in Figure 6.14. Initially the BCR-MAC is in INACTIVE state indicating that no CR activation request is initiated by the BME and the BME_DATA SAP interrupt is disabled.

1. When the BME wants to start a server session it sends CONN_REQ over BME_CTRL Tx (Figure 6.13 (1)) that requests the BCR-MAC to forward the request for a free PU channel to the CBS. The BCR-MAC FSM enters the BEACON_WAIT state (see Transition 1 in Figure 6.14).
2. On reception of a BEACON from CBS, the BCR-MAC sends CHAN_REQ (Figure 6.13 (2.2)) to the CBS, starts TMR-1 (Figure 6.13 (2.3)) and waits for CHAN_SUCS. The FSM moves from BEACON_WAIT to CHAN_SUCS_PENDING (see Transition 2 in Figure 6.14). The TMR-1 period is set to the time needed to send a CHAN_REQ control frame and receive its corresponding CHAN_SUCS confirmation. We assume that this CHAN_REQ message is corrupted by noise, and will be re-transmitted next.

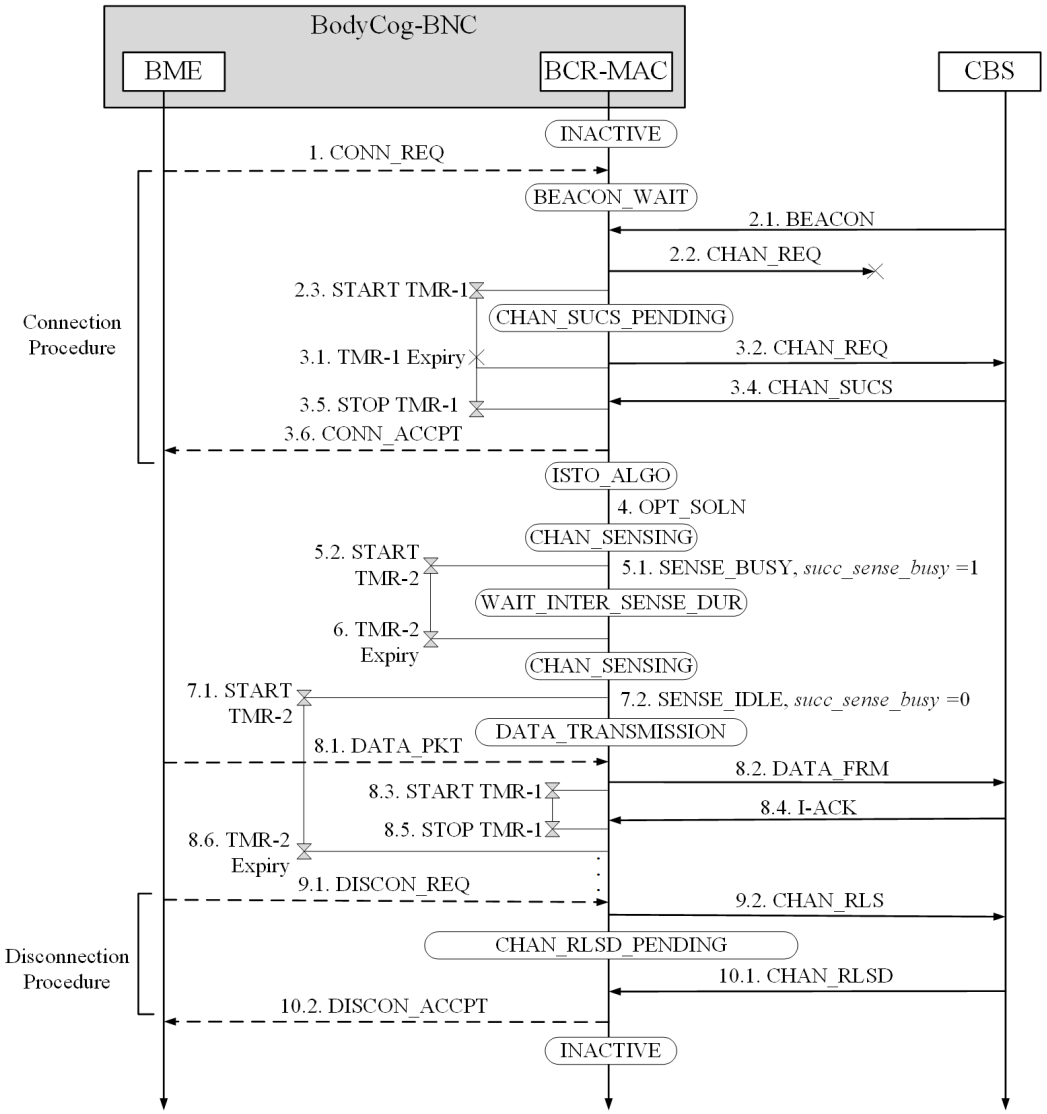

Fig. 6.13 BCR-MAC flowchart with general connection and disconnection procedures.

3. If the control messages are corrupted by bit level errors, then the received message at either CBS or BCR-MAC will be discarded, leading to expiry of the timer. On expiry of TMR-1 (Figure 6.13 (3.1)), the CHAN_REQ message is re-transmitted by BCR-MAC (Figure 6.13 (3.2)). The FSM remains at CHAN_SUCS_PENDING state (see Transition 3.1 in Figure 6.14). We assume that this CHAN_REQ message is received by CBS followed by successful transmission of CHAN_SUCS message as illustrated in point 5.
4. Suppose, that all the channels in CRN are pre-occupied and not available for allocation to SUs. In such scenario, the CBS fails to assign a free channel to BNC and sends CHAN_FAIL message. Upon receiving CHAN-FAIL, BCR-MAC will inform BME about the connection failure via CONN_FAIL message. Furthermore, if the number of

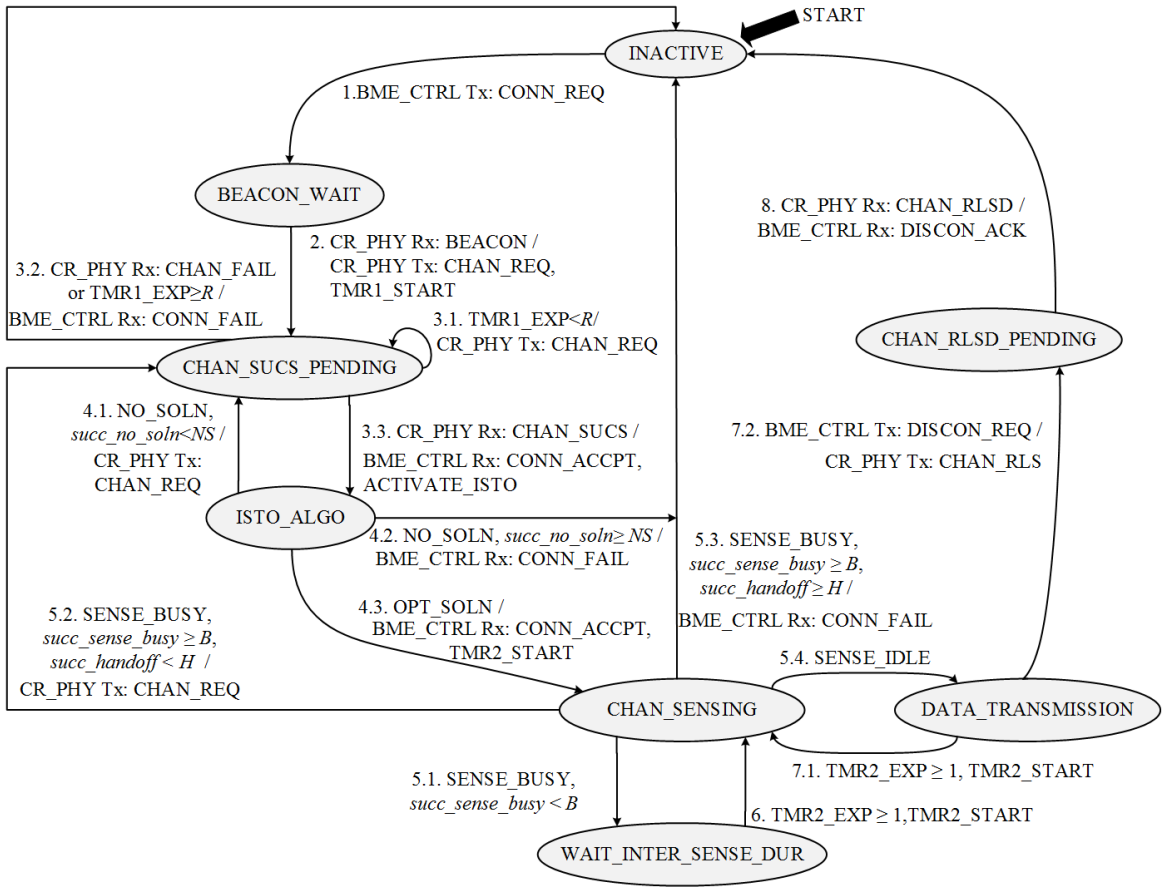

Fig. 6.14 BCR-MAC FSM state transition diagram.

CHAN_REQ re-transmissions exceed the maximum limit, set to R, then BCR-MAC will send CONN_FAIL message to BME. For either of the above mentioned events, the FSM will move from CHAN_SUCS_PENDING to INACTIVE state (see Transition 3.2 in Figure 6.14). Upon receiving CONN_FAIL, the BME performs spectrum agility and intelligently switches to licensed WAN.

5. Suppose that the CHAN_SUCS is received by BCR-MAC before the TMR-1 expires (Figure 6.13 (3.4)). Then the BCR-MAC stops the TMR-1 (Figure 6.13 (3.5)) and invokes ACTIVATE_ISTO action to implement ISTO algorithm. The FSM now enters the ISTO_ALGO state (see Transition 3.3 in Figure 6.14). The ISTO algorithm determines the optimal inter-sensing duration that provides the maximum energy-efficiency towards CR communication over the channel assigned by CBS under sensing uncertainties while keeping the interference to PU within permitted threshold. In addition, BCR-MAC also leverages the ISTO algorithm to determine whether an assigned PU channel is suitable for communication.

6. If ISTO algorithm determines that there is no optimal solution for the received channel, then a NO_SOLN event is invoked that causes the BCR-MAC to send another CHAN_REQ to the CBS. The FSM moves from ISTO_ALGO back to the CHAN_SUCS_PENDING state (see Transition 4.1 in Figure 6.14). The BCR-MAC maintains a variable *succ_no_soln* that keeps track of the number of successive NO_SOLN events. If $succ\_no\_soln \geq NS$, then BCR-MAC issues a CONN_FAIL message to the BME and moves to INACTIVE state (see Transition 4.2 in Figure 6.14).
7. When ISTO algorithm obtains the optimal inter-sensing duration, the BCR-MAC invokes the OPT_SOLN event (Figure 6.13 (4)), resets *succ_no_soln* to 0 and BCR-MAC sends CONN_ACCPT message to BME. The FSM enters the CHAN_SENSING state (see Transition 4.3 in Figure 6.14).
8. At the CHAN_SENSING state the BCR-MAC invokes energy detection based spectrum sensing, and senses the channel for T_s duration. If the channel is sensed to be busy, then the SENSE_BUSY event (Figure 6.13 (5.1)) is invoked that starts the TMR-2 timer (Figure 6.13 (5.2)). The FSM moves from CHAN_SENSING to WAIT_INTER_SENSE_DUR state (see Transition 5.1 in Figure 6.14) where the BCR-MAC remains inactive/ sleeps. The TMR-2 period is set to the optimal inter-sensing duration, T_D^*.
9. On expiry of the TMR-2 timer (Figure 6.13 (6)), the BCR-MAC wakes up and moves to the CHAN_SENSING state (see Transition 6 in Figure 6.14). The BCR-MAC maintains a variable *succ_sense_busy* that keeps track of the number of successive SENSE_BUSY events. If $succ\_sense\_busy \geq B$, then BCR-MAC triggers a handoff assuming that a PU has arrived in the channel. The BCR-MAC requests a new channel from CBS using the CHAN_REQ message and moves to CHAN_SUCS_PENDING state (see Transition 5.2 in Figure 6.14). To keep track of the number of the successive handoff events, BCR-MAC uses the $succ\_handoff$ variable. If $succ\_handoff \geq H$, then BCR-MAC issues a CONN_FAIL message to the BME and moves to INACTIVE state (see Transition 5.3 in Figure 6.14). On reception of CONN_FAIL, BME initiates spectrum agility. This ensures intelligent switching of BNC from CRN to licensed WAN in case of presence of PUs in multiple PU channels.
10. If the channel is sensed to be idle, then the SENSE_IDLE event is invoked that starts the TMR-2 timer (Figure 6.13 (7.1)), resets *succ_sense_busy* and $succ\_handoff$ to 0 and enables the BME_DATA SAP interrupt allowing the BME to transfer its data packet (DATA_PKT) to the BCR-MAC (Figure 6.13 (8.1)). The BCR-MAC then forwards it as data frame (DATA_FRM) to the CBS (Figure 6.13 (8.2). The FSM moves from CHAN_SENSING to DATA_TRANSMISSION state (see Transition 5.4 in Figure 6.14). During transmission, a media access similar to the Stop-and-Wait Automatic Repeat-

Request (ARQ) protocol [211] is used (Figure 6.13 (8.2-8.5)), but with the additional feature of sequence number to address the issue of reception of duplicate packets. The ARQ protocol exploits TMR-1 interrupt for re-transmission of DATA_FRM in the event of timeout due to loss of a DATA_FRM and/or its corresponding I-ACK frame while transmission due to non-ideal channel conditions. On expiry of TMR-2, the FSM moves back to the CHAN_SENSING state (see Transition 7.1 in Figure 6.14).

11. When data transmission is complete, BME sends DISCON_REQ to BCR-MAC (Figure 6.13 (9.1)), which forwards the request of releasing the PU channel to the CBS by transmitting CHAN_RLS (Figure 6.13 (9.2)) message over the allocated channel. The FSM moves from its present state to CHAN_RLSD_PENDING (see Transition 7.2 in Figure 6.14).
12. On reception of CHAN_RLSD confirmation from CBS (Figure 6.13 (10.1)), the BCR-MAC sends DISCON_ACCPT message to BME (Figure 6.13 (10.2)) and then the FSM returns to the INACTIVE state, waiting for the next CONN_REQ message from BME to arrive (see Transition 8 in Figure 6.14).

6.5.4 Implementation of BCR-MAC

Leveraging on the BCR-MAC FSM diagram in Figure 6.14, we illustrate the setup steps for BCRD architecture to implement BCR-MAC at the BCR-EP. Much like the BME implementation steps, first we define the states, events and transition actions and then show the implementation of ISRs following the FSM of BCR-MAC.

6.5.4.1 States, Events, Actions and ISRs of BCRD

The definition of the various states, events, actions and ISRs are given in Figure 6.15, which are described as follows:

- Lines 1-6 define the BCR-MAC FSM states using the macros START_DEFINE_BCR_STATE and END_DEFINE_BCR_STATE. The BCR_STATE macro defines individual states (e.g. BEACON_WAIT, etc in Figure 6.14).
- Lines 7-16 define the BCR FSM events using the macros START_DEFINE_BCR_EVENT and END_DEFINE_BCR_EVENT. The BCR_EVENT macro defines individual events (e.g. TMR1_EXP, etc in Figure 6.14)
- Lines 17-26 define the BCR FSM actions using the macros START_DEFINE_BCR_ACTION and END_DEFINE_BCR_ACTION. The BCR_ACTION macro defines individual actions. For example, send_BME_CTRL_Rx denotes the action of sending a cross-layer

message to BME via the BME_CTRL Rx. These actions are implemented as per the state-event-transition table maintained by the ISRs.

- Lines 27-31 declare the BCR-MAC ISRs using the macros DECLARE_BCR_ISR.

```
 1: START_DEFINE_BCR_STATE
 2:         BCR_STATE (INACTIVE)
 3:         BCR_STATE (BEACON_WAIT)
 4:         BCR_STATE (CHAN_SUCS_PENDING)
 5:         ...
 6: END_DEFINE_BCR_STATE

 7: START_DEFINE_BCR_EVENT
 8:         BCR_EVENT (TMR1_EXP)
 9:         BCR_EVENT (TMR2_EXP)
10:         BCR_EVENT (receive_BME_CTRL_Tx)
11:         BCR_EVENT (receive_CR_PHY_Rx)
12:         BCR_EVENT (OPT_SOLN)
13:         BCR_EVENT (NO_SOLN)
14:         BCR_EVENT (SENSE_IDLE)
15:         BCR_EVENT (SENSE_BUSY)
16: END_DEFINE_BCR_EVENT

17: START_DEFINE_BCR_ACTION
18:         BCR_ACTION (send_BME_CTRL_Rx)
19:         BCR_ACTION (send_CR_PHY_Tx)
20:         BCR_ACTION (receive_BME_DATA_SAP)
21:         BCR_ACTION (ACTIVATE_ISTO)
22:         BCR_ACTION (TMR1_START)
23:         BCR_ACTION (TMR1_STOP)
24:         BCR_ACTION (TMR2_START)
25:         BCR_ACTION (TMR2_STOP)
26: END_DEFINE_BCR_ACTION

27: DECLARE_BCR_ISR (BME_CTRL_Tx_ISR)
28: DECLARE_BCR_ISR (BME_DATA_ISR)
29: DECLARE_BCR_ISR (CR_PHY_ISR)
30: DECLARE_BCR_ISR (TMR1_ISR)
31: DECLARE_BCR_ISR (TMR2_ISR)
```

Fig. 6.15 The definition of states, events, actions and ISRs for BCR-MAC.

6.5.4.2 ISR and State-Event-Transition Table Implementation within BCRD

In this section, we describe the BCRD steps to implement CR_PHY_ISR as an example to illustrate how to develop the BCR-MAC from its FSM. Figure 6.16 shows the C-code for the CR_PHY_ISR. This ISR is executed when there is an incoming CR frame from CR_PHY Rx. The BCR-MAC main control loop is interrupted and the program control is shifted to the ISR.

- Line 1 invokes the START_BCR_ISR macro to start the ISR CR_PHY_ISR declared at Line 29 of Figure 6.15.
- Lines 2-4 declare three enumerated data type variables: pREC_BCR_CR_frame, vREC_BCR_-CBS_CTRL_MSG and vBCR_STATE. These variables are used to store the incoming CR frame from CR_PHY Rx, any control message extracted from the received CR frame and the current BCR-MAC FSM state respectively.
- Line 5 uses the function CHECK_BCR_STATE to obtain the current BCR-MAC FSM state are store it in vBCR_STATE.
- Line 6 uses the BCR_parseInMsg function to parse the incoming message associated with the receive_CR_PHY_Rx event and store its address in the pointer variable pREC_BCR_CR_-frame.
- Line 7 invokes the BCR_goodHeader function to examine the reception of a good CR frame. This essentially examines the received CR frame for errors due to non-ideal wireless channel characteristics that might have corrupted it. In case of an error, the received frame is discarded and the ISR exits as in Line 8.
- Line 9-10 uses the functions BCR_check_destAddr and BCR_check_seqNum to check whether the received frame is actually meant for the recipient and/or to ascertain non-reception of a duplicate frame.
- Line 11 uses the function BCR_extractCtrlMsg to extract the control message from pREC_BCR_CR_frame and store it in vREC_BCR_CBS_CTRL_MSG.
- Line 12 initiates the switch-case statements that compare the vREC_BCR_CBS_CTRL_MSG to the possible incoming control messages from CBS (Lines 13, 19, 25, 30, and 35). The switch-case model provides the actual implementation of the state-event-transition table shown in Figure 6.12, and follows the same principles as followed in Section 6.4.4 for BMED architecture.
- Line 43 exits the ISR and the program returns to the main control.

```
START_BCR_ISR (CR_PHY_ISR)
tBCR_CBS_MSG* pREC_BCR_CR_frame;
tBCR_CBS_CTRL_MSG vREC_BCR_CBS_CTRL_MSG;
tBCR_STATE vBCR_STATE;
vBCR_STATE = CHECK_BCR_STATE ();
pREC_BCR_CR_frame = BCR_parseInMsg (receive_CR_PHY_Rx);
if (BCR_goodHeader (pREC_BCR_CR_frame) = = badHeader){
    return;}
if (∼ (BCR_check_destAddr (pREC_BCR_CR_frame) &&
        BCR_check_seqNum (pREC_BCR_CR_frame))){
    return;}
vREC_BCR_CBS_CTRL_MSG = BCR_extractCtrlMsg (pREC_BCR_CR_frame);
switch (vREC_BCR_CBS_CTRL_MSG){
    case BEACON:
        if (vBCR_STATE = = BEACON_WAIT){
            send_CR_PHY_Tx (CHAN_REQ);
            BCR_EXECUTE (TMR1_START);
            BCR_CHANGE_STATE_TO (CHAN_SUCS_PENDING);}
        break;
    case CHAN_SUCS:
        if (vBCR_STATE = = CHAN_SUCS_PENDING){
            send_BME_CTRL_Rx (CONN_ACCPT);
            BCR_EXECUTE (ACTIVATE_ISTO);
            BCR_CHANGE_STATE_TO (ISTO_ALGO);}
        break;
    case CHAN_FAIL:
        if (vBCR_STATE = = CHAN_SUCS_PENDING){
            send_BME_CTRL_Rx (CONN_FAIL);
            BCR_CHANGE_STATE_TO (INACTIVE);}
        break;
    case CHAN_RLSD:
        if (vBCR_STATE = = CHAN_RLSD_PENDING){
            send_BME_CTRL_Rx (DISCON_ACK);
            BCR_CHANGE_STATE_TO (INACTIVE);}
        break;
    case I-ACK:
        if ((vBCR_STATE = = DATA_TRANSMISSION)&&(TMR1_active ()){
            BCR_EXECUTE (TMR1_STOP);
            BCR_discardDataFrameCopy ();
            BCR_enableBMEDataSAP ();}
        break;
    default:
        break;}
END_BCR_ISR (CR_PHY_ISR)
```

Fig. 6.16 The C-code of the ISR CR_PHY_ISR.

6.6 Optimization of CR Inter-Sensing Duration

In this Section, first we perform an energy-efficiency study of sensing-transmission cycle highlighted in Section 6.3.1. Thereafter, we present the ISTO algorithm executed during the BCR-MAC ISTO_ALGO state (Figure 6.14) to maximize the energy-efficiency for transmission over a single PU channel by varying the inter-sensing duration (T_D) under certain constraints. A very short T_D leads to less communication opportunities for the BCR-MAC in ideal periods resulting in reduced throughput. Additionally, there would also be more energy consumption due to frequent sensing resulting from smaller T_D. On the other hand, a long transmission duration increases interference probability of PU reoccupying the channel during transmission by BCR-MAC. Therefore, we need to determine the optimal inter-sensing duration that maximizes both the throughput and energy-consumption i.e. the energy-efficiency.

Two metrics are used to characterize the performance of CR backhaul transmission over a single channel by BCR-MAC: i) energy-efficiency, and ii) normalized interference duration. *Energy-efficiency* (η) is defined as the ratio of the normalized throughput-time (T) to the normalized energy consumed (E), which can be expressed as,

$$\eta = \frac{\mathrm{T}}{\mathrm{E}} \tag{6.5}$$

Normalized throughput-time is defined as the ratio of the net time available for successful transmission without collision within a single CR frame to the total frame duration. Similarly, we define *normalized energy consumption* as the ratio of the total energy consumed during sensing and transmission in a CR frame to the frame duration. The normalized throughput-time and normalized energy consumption can respectively be given as,

$$\mathrm{T} = P_{trans}\,\frac{T_D - T_C}{T_S + T_D} \tag{6.6}$$

$$\mathrm{E} = \frac{I_r T_S + P_{trans} I_t T_D}{T_S + T_D} \tag{6.7}$$

Where, T_S and T_D are the sensing duration and inter-sensing duration respectively. As introduced in previous sub-section, T_C is the expected collision duration of the BCR-MAC due to interference with the PU within the inter-sensing duration T_D, P_{trans} is the transmission probability within a single channel, and I_r and I_t are the current consumptions of CR radio-modules in receiving and transmitting modes respectively. Lastly, we define *normalized interference duration* (ε) as the ratio of the collision duration to the inter-sensing duration,

which is defined as,

$$\varepsilon = \frac{T_C}{T_D} \tag{6.8}$$

A BCR-MAC may initiate transmission under two conditions: i) the channel is actually busy but the sensing decision indicates an idle channel (miss-detection) with probability $(1-P_d)$, and ii) the channel is idle and the sensing decision correctly identifies this (not false-alarm) with probability $(1-P_f)$. The probabilities $(1-P_d)$ and P_f denote the sensing uncertainties. Then, the transmission probability (P_{trans}) can be expressed as,

$$P_{trans} = P(H_1)(1-P_d) + P(H_0)(1-P_f) \tag{6.9}$$

Let T_{bc} and T_{ic} denote the average collision durations within the inter-sensing duration T_D, for the above mentioned two cases respectively. The expected collision T_C can be expressed as,

$$T_C = P(H_1)(1-P_d)T_{bc} + P(H_0)(1-P_f)T_{ic} \tag{6.10}$$

The average non-effective communication durations T_{bc} and T_{ic} were presented in Section 4.2.3 as,

$$T_{bc} = 1/\lambda \left(1 - e^{-\lambda T_D}\right) \tag{6.11}$$

$$T_{ic} = T_D - 1/\mu \left(1 - e^{-\mu T_D}\right) \tag{6.12}$$

Equations (6.11) and (6.12) are derived considering different underlying interfering cases between BCR-MAC and PU for the given inter-sensing duration T_D.

6.6.1 CR Energy-Efficiency Maximization Problem

We formulate the energy-efficiency maximization problem for transmission over a single CR channel as follows:

$$\mathbf{P1}: \quad \max_{T_D} \eta(T_D) \tag{6.13}$$

$$s.t. \quad \varepsilon(T_D) \leq \Gamma \tag{6.14}$$

$$T_D \geq 0 \tag{6.15}$$

Where, Γ in constraint (6.14) is a predefined normalized interference duration threshold to protect the PU communication. The false-alarm probability P_f in **P1** is equal to the constraint

κ used for deriving sensing samples in (6.3). While, the detection probability P_d depends on the detected PU SNR at the BodyCog-BNC γ_{PU}.

The objective function in (6.13) is concave in nature. The proof of concavity is provided in B.1. Therefore, problem **P1** can be solved to obtain the global optimum solution (T_D^*) using classical optimization techniques satisfying the Karush Kuhn Tucker (KKT) conditions.

Lemma 1: (KKT Conditions): For optimum solution T_D^* of Problem **P1** there exists a unique Lagrangian multiplier λ_1^* such that,

$$\frac{\partial \eta\left(T_D^*\right)}{\partial T_D} + \lambda_1^* \frac{\partial \varepsilon\left(T_D^*\right)}{\partial T_D} = 0 \tag{6.16}$$

$$\lambda_1^* \left[\varepsilon\left(T_D^*\right) - \Gamma\right] = 0 \tag{6.17}$$

$$\varepsilon\left(T_D^*\right) - \Gamma \leq 0 \tag{6.18}$$

$$\lambda_1^* \leq 0 \tag{6.19}$$

Equations (6.16)-(6.19) respectively are the optimality, complementary slackness, feasibility and non-negativity KKT conditions [212] obtained from **P1**. For the proposed computationally efficient solution, the optimization problem is solved by iterating through the various possible combinations of λ_1^* in (6.19) and then finding T_D^* that satisfies conditions (6.16)-(6.18). The aforementioned KKT conditions motivate the following Inter-Sensing Time Optimization (ISTO) algorithm.

6.6.2 Inter-Sensing Time Optimization (ISTO) Algorithm

The ISTO algorithm implemented by BCR-MAC operates following the pseudocode given in Algorithm 6.1. After initialization of PU timing parameters t_{on} and t_{off}, and obtaining the average PU SNR, ISTO algorithm tries to find the optimal solution by setting constraint (6.14) inactive ('Case 1' of Algorithm 6.1) and then solving (6.16) through Newton-Raphson (NR) technique [213] (lines: 2 and 3 of Algorithm 6.1). NR method is a numerical technique to iteratively solve equations until a convergence is reached. If the resulting solution $T_{D,1}$ satisfies the feasibility conditions and constraint (6.15) then we get the optimal solution. Note that an inherent advantage of Problem **P1** is that (6.14) and (6.15) form two boundaries of the solution. This is certainly a desirable characteristic and means that if $T_{D,1}$ is not the optimum solution, then the same, if exits, will lie on the boundary of (6.14) (line: 7 of Algorithm 6.1) and must lie within the boundary (6.15). So, if $T_{D,1}$ is not the optimum solution, the algorithm tries the final step of activating constraint (6.14) ('Case 2' of Algorithm 6.1) to obtain solution $T_{D,2}$. If $T_{D,2}$ does not satisfy the feasibility conditions and constraint (6.15) then there is no solution and the BCR-MAC needs a new channel. Consequently, the

BCR-MAC invokes the NO_SOLN event (see Transition 4.1 in Figure 6.14). A no solution essentially means the allocated PU channel is not "good" for CR backhaul communication.

Algorithm 6.1 Inter-Sensing Time Optimization (ISTO) Algorithm

Initialization: Initialize t_{on} and t_{off}, obtain γ_{PU}
Case 1: Let $\lambda_1^* = 0$
Solve (6.16) by Newton-Raphson (NR) method to obtain $T_{D,1}$
if $\varepsilon(T_{D,1}) < \Gamma$ and $T_{D,1} > 0$ **then**
    Optimal solution $T_D^* = T_{D,1}$
else if $\varepsilon(T_{D,1}) \geq \Gamma$ **then**
    Case 2: Let $\lambda_1^* < 0$
    From (6.17), solving $\varepsilon(T_{D,2}) = \Gamma$ by NR method we get $T_{D,2}$
    Solve (6.16) to obtain λ_1^*
    if $\lambda_1^* < 0$ and $T_{D,2} > 0$ **then**
        Optimal solution $T_D^* = T_{D,2}$
    else
        No Solution
    end if
end if

6.7 Analytical Derivation of Performance Metrics

In this section, we obtain the closed form expressions of the primary performance metrics for backhaul transmission of BodyCog-BNC, viz. average energy consumption, cost-efficiency, CR utilization probability and speed of spectrum agility. The symbols appearing in the analysis are summarized in Table 6.1.

6.7.1 Average Energy Consumption (E_{avg})

Energy consumption is one of the most important parameters that helps in estimating the period for which the rechargeable batteries of Body-BNC will last. For NRT backhaul communication, we consider that the BodCog-BNC has D_{bits} of data (in bits) to transmit. The data is generated from the WBAN and thereafter compressed by the BME. We now compute the average energy consumed towards transmission of the D_{bits} data.

Table 6.1 Symbols used

Symbol	Description	Symbol	Description
t_{on}, t_{off}	Average PU activity ON and OFF period	ξ_S	Energy used in single channel sensing
λ_{th}	Energy detection threshold	$\xi_{t,ctrl}$	Energy used in control channel transmission
N_S	No. of samples received for PU detection	$\xi_{r,ctrl}$	Energy used in control channel reception
N_0	Noise power	$\xi_{i,ctrl}$	Energy used in waiting over control channel
P_d, P_f	PU detection and false-alarm probability	ξ_{WAN}	Energy used in licensed WAN transmission
γ_{PU}	Detected PU SNR at SU/BNC	t_{ctrl}	Time taken in control channel transmission
$\gamma_{PU,min}$	Receiver sensitivity	$t_{ISTO,j}$	Time taken in ISTO over j^{th} PU channel
T_S, T_D	Sensing and Inter-sensing duration	t_{WAN}	Time taken in licensed WAN transmission
R	Control message re-transmission limit	ber	Bit error rate of control channel
B	Successive channel busy before handoff	η_{ctrl}	Successful control message transmission probability
H	Successive handoffs before spectrum agility	$\eta_{ctrl,p}$	Successful control message exchange probability
η	Energy-efficiency of CR transmission	$P_{s,ctrl}$	Successful control message exchange probability
T	Normalized throughput-time in a CR frame	$P_{us,ctrl}$	Unsuccessful control message exchange probability
I_t, I_r, I_i	Current consumed during transmission, reception and ISTO or waiting for a frame	$E_{s,ctrl}$, $E_{us,ctrl}$	Average energy consumed in successful and unsuccessful control message exchange
V_S	Supply voltage of radio modules	$T_{s,ctrl}$	Successful control message exchange time
E	Normalized energy consumed in a CR frame	$T_{us,ctrl}$	Unsuccessful control message exchange time
P_{trans}	Transmission probability over a PU channel	E_{avg}	Avg. energy consumed by BodyCog-BNC
ε	Normalized PU interference duration	P_{switch}	CR to WAN switching probability
Γ	Normalized PU interference threshold	T_{switch}	CR to WAN switching time
T_C	Avg. collision duration within T_D	CE	Cost-efficiency of BodyCog-BNC
D_{bits}	Size of transmitted data	C_{conv}	Cost of using only conventional licensed WAN
H_{bits}	Size of header of CR frames	$C_{BodyCog}$	Cost of using BodyCog-BNC (i.e. CR+WAN)
$\xi_{t,j}$	Energy used in j^{th} PU channel transmission	c_{energy}	Cost of electricity
$\xi_{dis,j}$	Energy used in j^{th} PU channel disconnection	c_{dat}	Cost of data transfer over licensed WAN
$\xi_{ISTO,j}$	Energy used in ISTO over j^{th} PU channel	ζ	Coefficient indicating the CR cost regime

Let ξ_s, $\xi_{t,j}$, $\xi_{dis,j}$ and $\xi_{ISTO,j}$ respectively denote the energy consumption of BodyCog-BNC for a single sensing, transmission, disconnection procedure and execution of ISTO algorithm over the j^{th} assigned PU channel. Further, let $\xi_{t,ctrl}$, $\xi_{r,ctrl}$ and $\xi_{i,ctrl}$ respectively denote the energy consumed while transmitting, receiving and waiting for a control message of size H_{bits} over the control channel. H_{bits} is also the size of the header of CR frames appended by BCR-MAC. Lastly, let ξ_{WAN} denotes the energy consumption for transmission over the licensed WAN. These energy consumptions can be obtained as,

$$\xi_s = I_r V_s T_S \tag{6.20}$$

$$\xi_{t,j} = \frac{E_{CR,j}}{T_{CR,j}} (D_{bits} + H_{bits}) \tag{6.21}$$

$$\xi_{dis,j} = \frac{E_{CR,j}}{T_{CR,j}} \left(1 + \frac{I_r}{I_t}\right) H_{bits} \tag{6.22}$$

$$\xi_{ISTO,j} = I_i V_s t_{ISTO,j} \tag{6.23}$$

$$\xi_{t,ctrl} = I_t V_s t_{ctrl} \tag{6.24}$$

$$\xi_{r,ctrl} = I_r V_s t_{ctrl} \tag{6.25}$$

$$\xi_{i,ctrl} = I_i V_s t_{ctrl} \tag{6.26}$$

$$\xi_{WAN} = I_t V_s t_{WAN} \tag{6.27}$$

where I_r, I_t and I_i are respectively the currents consumed by radio modules towards reception, transmission and when either executing ISTO algorithm or waiting for reception of a message. V_s represents the supply voltage of radio modules. In this regard, we assume that both the CR and WAN interfaces are developed using identical radio boards with similar current consumptions. Further, T_S denotes the spectrum sensing time. $t_{ISTO,j}$ is the time taken to perform ISTO for j^{th} assigned PU channel. t_{ctrl} and t_{WAN} respectively denote the times taken for transmission of control message over the control channel and data over the licensed WAN respectively, and are given as,

$$t_{ctrl} = \frac{H_{bits}}{C_{ctrl}} \tag{6.28}$$

$$t_{WAN} = \frac{D_{bits}}{C_{WAN}} \tag{6.29}$$

C_{ctrl} and C_{WAN} are the capacity of the CRN control channel and licensed WAN channel respectively and can be obtained using (6.32).

$E_{CR,j}$ and $T_{CR,j}$ in (6.21) respectively represent the energy consumed per CR frame for transmission and the number of bits successfully transmitted per CR frame over PU channel j, and can be obtained as,

$$E_{CR,j} = T_{D,j} I_t V_s \tag{6.30}$$

$$T_{CR,j} = \left(T_{D,j} - T_{C,j}\right) C_{CR,j} \tag{6.31}$$

where $T_{C,j}$ is the average collision duration obtained using (6.10) and $T_{D,j}$ is the optimal inter-sensing duration obtained from ISTO algorithm for j^{th} assigned PU channel. $C_{CR,j}$ is the capacity of j^{th} PU channel between BodyCog-BNC and CBS and is obtained using (6.32).

The capacity (C_x) of a channel 'x' depends on its bandwidth (W_x) and signal-to-noise ratio (SNR_x) and can be calculated by Shannon's formula as follows,

$$C_x = W_x \log_2 (1 + SNR_x) \tag{6.32}$$

Equation (6.32) provides the capacity of the channels, with 'x' replaced by '$ctrl$' for CRN control channel as in (6.28), 'WAN' for licensed WAN as in (6.29), and 'CR, j' for the j^{th} assigned PU channel between BodyCog-BNC and CBS as in (6.30)-(6.31).

6.7.1.1 Energy consumption in control channel

We consider that the control channel of CRN is non-ideal in nature with Gaussian white noise. Then the Bit Error Rate (BER) (ber) can be given as [71],

$$ber = Q\left(\sqrt{SNR_{ctrl}}\right) \tag{6.33}$$

where $Q(\cdot)$ denotes the Q-function.

Therefore, the probability that a control message of size H_{bits} is transmitted without getting corrupted by any errors can be denoted as, $\eta_{ctrl} = (1 - ber)^{H_{bits}}$. We now evaluate the average energy consumed for a successful and un-successful control message exchange.

A successful control message exchange comprises of a successful transmission of 'request' control message by BodyCog-BNC (e.g. CHAN_REQ) with probability η_{ctrl} followed by successful reception of the corresponding 'response' message from CBS (e.g. CHAN_SUCS) with probability η_{ctrl}. At a finer level of detail, the following scenarios may arise:

i) a 'request' message can be corrupted by noise; in that case there will be no 're-sponse' from the CBS. Subsequently, on non-reception of the 'response', BCR-MAC will re-transmit the 'request' message;
ii) a successful 'request' message transmission may not be followed by the CBS successfully transmitting the corresponding 'response' message. This will again lead to the BCR-MAC re-transmitting the 'request' message.

The above scenarios can reoccur until the maximum transmission limit R is exhausted by BCR-MAC. Let i denotes the total number of 'request' message transmissions and j denotes the total number of 'response' message transmissions for one particular scenario. Therefore, there are $(i-j)$ and $(j-1)$ unsuccessful 'request' and 'response' message transmissions respectively before one successful control message exchange. Based on the above scenarios, and using (6.24)-(6.26) the average energy consumption of BodyCog-BNC towards successful control message exchange $(E_{s,ctrl})$ can be given as,

$$E_{s,ctrl} = \sum_{i=1}^{R} \sum_{j=1}^{i} \left\{ i\,\xi_{t,ctrl} + j\,\xi_{r,ctrl} + (i-j)\,\xi_{i,ctrl} \right\} (1-\eta_{ctrl})^{(i-j)+(j-1)} \eta_{ctrl}^{j+1} \tag{6.34}$$

A control message exchange is un-successful if despite the BCR-MAC transmitting the 'request' control message R number of times, it did not successfully receive a 'response' from CBS. Extending the above analysis, the average energy consumption of BodyCog-BNC $(E_{us,ctrl})$ towards an un-successful control message exchange can be given as,

$$E_{us,ctrl} = \sum_{j=0}^{R} \left\{ R\,\xi_{t,ctrl} + j\,\xi_{r,ctrl} + (R-j)\,\xi_{i,ctrl} \right\} (1-\eta_{ctrl})^{(R-j)+(j)} \eta_{ctrl}^{j} \tag{6.35}$$

6.7.1.2 Scenario specific average energy consumptions (E_1, E_2, E_3)

We assume that the NRT data of size D_{bits} can transmitted within a single CR frame. The BCR-MAC FSM (in Figure 6.14) shows that a handoff is performed when a channel is sensed busy for B successive times. Further, in the event of H consecutive handoffs, the BCR-MAC performs spectrum agility, thereby allowing BME to switch to licensed WAN. For simplification of analysis, we consider that the ISTO algorithm provides an optimum solution for the channels provided by CBS. This is reasonable as the CBS has an approximate knowledge of PU activity from white-space database and PU SNR in the channel with the receiver sensitivity set sufficiently low. Based on this and the energy consumptions derived earlier, we present the average energy consumption analysis. To this end, we first consider

the simple case with $B = 2$ and $H = 2$ and then generalize the expression of the average energy consumption.

For $B = 2$ and $H = 2$ the average energy consumption analysis can be treated under three scenarios:

1. Successful transmission over the first assigned channel denoted as Ch-1 $(j = 1)$.
2. Successful transmission over the second channel denoted as Ch-2 $(j = 2)$ assigned after handoff from the first channel Ch-1.
3. Successful transmission using licensed WAN after switching (spectrum agility) from the CR interface.

Scenario 1 (S1): Successful transmission over the first-assigned channel (Ch-1) Consider the case when the frame transmission is successful using the first successfully assigned channel. The probability that a channel is successfully assigned is equal to the probability $(P_{s,ctrl})$ that the CHAN_REQ and CHAN_SUCS control message pair is successfully transmitted over the control channel. Therefore, $P_{s,ctrl}$ can be obtained as,

$$P_{s,ctrl} = \eta_{ctrl,p} \sum_{i=1}^{R} \left(1 - \eta_{ctrl,p}\right)^{i-1} \tag{6.36}$$

where, $\eta_{ctrl,p} = (1 - ber)^{2H_{bits}}$ is the successful transmission probability of one 'request-response ' pair between BCR-MAC and CBS. In this regard, the average time $(T_{s,ctrl})$ taken for successfully transmitting the control message pair can be calculated using (6.28) as,

$$T_{s,ctrl} = \eta_{ctrl,p} \sum_{i=1}^{R} 2i \times t_{ctrl} \left(1 - \eta_{ctrl,p}\right)^{i-1} \tag{6.37}$$

After the BCR-MAC successfully obtains a channel from CBS, the following scenarios may arise,

1. Ch-1 is sensed to be idle in the first sensing instant with probability $P_{S1,1} = P_{trans,1}$ obtained using (6.9).
2. Ch-1 is sensed to be busy in the first sensing instant but idle in the second sensing instant with probability $P_{S1,2} = P_{trans,1}\,(1 - P_{trans,1})$.

Therefore, the average energy consumption (E_1) under this scenario $S1$ can be obtained for $j = 1$ as,

$$\begin{aligned} E_1 =& P_{S1,1}[P_{s,ctrl}(\xi_s + \xi_{t,1} + \xi_{dis,1} + \xi_{ISTO,1}) + E_{s,ctrl}] \\ &+ P_{S1,2}[P_{s,ctrl}(2\xi_s + \xi_{t,1} + \xi_{dis,1} + \xi_{ISTO,1}) + E_{s,ctrl}] \end{aligned} \tag{6.38}$$

The $E_{s,ctrl}$ term in (6.38) is the average energy consumption of BodyCog-BNC towards successful CHAN_REQ and CHAN_SUCS control message exchange.

Scenario 2 (S2): Successful transmission over the second channel (Ch-2) assigned after handoff from Ch-1 Consider the case when the successfully allocated channel Ch-1 is sensed busy two consecutive times, then the BCR-MAC performs handoff with probability P_h given as,

$$P_h = P_{s,ctrl}(1 - P_{trans,1})^2 \tag{6.39}$$

Thereafter, the BCR-MAC successfully acquires a second channel Ch-2 with probability $P_{s,ctrl}$ from CBS and completes a successful transmission. Similar to scenario S1, two events may arise,

1. Ch-2 is sensed to be idle in the first sensing instant with probability $P_{S2,1} = P_{trans,2}$.
2. Ch-2 is sensed to be busy in the first sensing instant but idle in the second sensing instant with probability $P_{S2,2} = P_{trans,2}\,(1 - P_{trans,2})$.

Therefore, the average energy consumption (E_2) under scenario S2 can be obtained for $j = 2$ as,

$$\begin{aligned} E_2 =& P_h \left[P_{S2,1} \left\{ P_{s,ctrl} \left(3\xi_s + \xi_{t,2} + \xi_{ISTO,1} + \xi_{ISTO,2} + E_{s,ctrl} + \xi_{dis,2} \right) + E_{s,ctrl} \right\} \right. \\ &\left. + P_{S2,2} \left\{ P_{s,ctrl} \left(4\xi_s + \xi_{t,2} + \xi_{ISTO,1} + \xi_{ISTO,2} + E_{s,ctrl} + \xi_{dis,2} \right) + E_{s,ctrl} \right\} \right] \end{aligned} \tag{6.40}$$

Scenario 3 (S3): Successful transmission using licensed WAN after switching (spectrum agility) from the CR interface Consider the case when the BCR-MAC performs spectrum agility and allows BME to switch to WAN interface. This can occur under the following scenarios:

1. Un-successful control message exchange for the first channel request with probability $P_{us,ctrl}$ given as,

   $$P_{us,ctrl} = \left(1 - \eta_{ctrl,p}\right)^R \tag{6.41}$$

   The average time $(T_{us,ctrl})$ taken in an un-successful control message exchange can be calculated as,

   $$T_{us,ctrl} = 2R \times P_{us,ctrl} \times t_{ctrl} \tag{6.42}$$

2. Un-successful control message exchange for the second channel request during handoff with probability $P_h P_{us,ctrl}$.

3. Consecutive occurrence of two $(H = 2)$ handoff events, leading to spectrum agility with probability P_a given as,

$$P_a = P_{s,ctrl} P_h (1 - P_{trans,2})^2 \tag{6.43}$$

Therefore, the average energy consumption (E_3) under scenario S3 can be obtained as,

$$\begin{aligned} E_3 =& (E_{us,ctrl} + P_{us,ctrl}\xi_{WAN}) \\ &+ P_h \left(E_{us,ctrl} + P_{us,ctrl}(2\xi_s + \xi_{ISTO,1} + E_{s,ctrl} + \xi_{WAN})\right) \\ &+ P_a(4\xi_s + \xi_{ISTO,1} + \xi_{ISTO,2} + 2E_{s,ctrl} + \xi_{WAN}) \end{aligned} \tag{6.44}$$

It must be noted that there is no formal disconnection done by BCR-MAC in case of spectrum agility.

Finally, the average energy consumed (E_a) by BodyCog-BNC for $B = 2$ and $H = 2$ for the successful transfer of data can be obtained by combining (6.38), (6.40) and (6.44) as,

$$E_a = E_1 + E_2 + E_3 \tag{6.45}$$

Leveraging on the analysis presented for the above case of $B = 2$ and $H = 2$, we can obtain the generalized expression of average energy consumed (E_{avg}) by BodyCog-BNC for backhaul communication as given by (6.46) which enables a system designer to obtain the value of E_{avg} for any values of R, B and H during design process.

$$\begin{aligned} E_{avg} =& \sum_{i=1}^{H} \left[\left\{ \prod_{\substack{l=1 \\ i \neq 1}}^{i-1} (1 - P_{trans,l})^B \right\} (P_{s,ctrl})^{i-1} \sum_{j=1}^{B} \left[P_{trans,i} (1 - P_{trans,i})^{j-1} \right. \right. \\ & \left. \left. \left\{ P_{s,ctrl} \left(((i-1)B + j)\,\xi_s + \xi_{t,i} + \sum_{k=1}^{i} E_{ISTO,k} + (i-1)E_{s,ctrl} + \xi_{dis,i} \right) + E_{s,ctrl} \right\} \right] \right] \\ & + \sum_{i=1}^{H} \left[\left\{ \prod_{\substack{l=1 \\ i \neq 1}}^{i-1} (1 - P_{trans,l})^B \right\} (P_{s,ctrl})^{i-1} \left\{ P_{us,ctrl} \left((i-1)B \times \xi_s + \sum_{\substack{k=1 \\ i \neq 1}}^{i-1} E_{ISTO,k} + (i-1)E_{s,ctrl} + \xi_{WAN} \right) \right\} \right. \\ & \left. + E_{us,ctrl} \right] + \left[(P_{s,ctrl})^H \prod_{i=1}^{H} (1 - P_{trans,i})^B \left(H \times B \times \xi_s + \sum_{k=1}^{H} E_{ISTO,k} + H \times E_{s,ctrl} + \xi_{WAN} \right) \right] \end{aligned} \tag{6.46}$$

Equation (6.46) comprises of three addends where: the first term represents the average energy consumed towards successful transmission over CR backhaul, the second term calculates the average energy consumption for transmission using licensed WAN after

unsuccessful control message exchange, and the last term represents the average energy consumed for transmission using licensed WAN after H successive handoffs.

6.7.2 CR to WAN Switching Probability (P_{switch})

Switching probability P_{switch} is defined as the average probability of switching from CR interface to WAN, i.e. probability of performing spectrum agility. A lower value of switching probability indicates more utilization of the backhaul CRN and lesser switching to the WAN interface. Extending our discussion of sub-section 6.5.3, we can obtain switching probability from the second and third terms of (6.46) as,

$$P_{switch} = \sum_{i=1}^{H} \left[\left\{ \prod_{\substack{l=1 \\ i \neq 1}}^{i-1} \left(1 - P_{trans,l}\right)^{B} \right\} \left(P_{s,ctrl}\right)^{i-1} P_{us,ctrl} \right] + \left[\left(P_{s,ctrl}\right)^{H} \prod_{i=1}^{H} \left(1 - P_{trans,i}\right)^{B} \right] \tag{6.47}$$

6.7.3 CR to WAN Switching Time (T_{switch})

Switching time T_{switch} is defined as the average time taken for switching from CR interface to WAN to complete transmission. The expression for T_{switch} can be obtained from the second and third terms of (6.46) and is given in (6.48). The last term in (6.48) denotes the time taken in exchange of cross-layer messages of size $D_{crosslayer}$ between BME and BCR-MAC over the BME_CTRL SAP. The speed of message transfer across BME_CTRL SAP is denoted by R_{BME_CTRL}. The time taken for cross-layer message transfer is much smaller in comparison to the other terms and thus was omitted in energy calculations in (6.46).

$$\begin{aligned} T_{switch} = & \sum_{i=1}^{H} \left[\left\{ \prod_{\substack{l=1 \\ i \neq 1}}^{i-1} \left(1 - P_{trans,l}\right)^{B} \right\} \left(P_{s,ctrl}\right)^{i-1} \right. \\ & \left. \left\{ P_{us,ctrl} \left((i-1)B \times T_S + \sum_{\substack{k=1 \\ i \neq 1}}^{i-1} \left((B-1) \times T_{D,k} + t_{ISTO,k} \right) + (i-1) T_{s,ctrl} \right) \right\} + T_{us,ctrl} \right] \\ & + \left[\left(P_{s,ctrl}\right)^{H} \prod_{i=1}^{H} \left(1 - P_{trans,i}\right)^{B} \left(H \times B \times T_S + \sum_{k=1}^{H} \left((B-1) \times T_{D,k} + t_{ISTO,k} \right) + H \times T_{s,ctrl} \right) \right] \\ & + 3 \times \frac{D_{crosslayer}}{R_{BME\_CTRL}} \end{aligned} \tag{6.48}$$

6.7.4 Cost-Efficiency

Cost-efficiency (CE) of BodyCog-BNC is defined as the percentage improvement in cost $(C_{BodyCog})$ incurred to the user towards NRT backhaul data transmission by using BodyCog-BNC as compared to the cost of using only the conventional licensed WAN technology (C_{conv}). Mathematically, CE can be represented as,

$$CE = \frac{C_{conv} - C_{BodyCog}}{C_{conv}} \times 100\,\% \tag{6.49}$$

where, C_{conv} can be obtained as,

$$C_{conv} = c_{energy}\,\xi_{WAN} + c_{dat}\,D_{bits} \tag{6.50}$$

The first term in (6.50) represents the average cost of electricity consumed for recharging the battery of a BNC to replenish its energy consumed (in J) for transferring D_{bits} of data employing only conventional WAN technology. c_{energy} is the cost of electricity per unit Joule of energy consumed and ξ_{WAN} is obtained using (6.27). The second term of (6.50) denotes the cost of transferring data over a spectrum as charged by licensed WAN operators. c_{dat} represents the cost of using licensed WAN spectrum per bit of data transmitted and is set by operators after negotiating with the spectrum owner [214].

Similarly, $C_{BodyCog}$ in (6.49) can be obtained as,

$$C_{BodyCog} = c_{energy}\,E_{avg} + [P_{switch} + (1 - P_{switch})\zeta]\,c_{dat}\,D_{bits} \tag{6.51}$$

Where, E_{avg} is obtained using (6.46). $0 < \zeta < 1$ is the ratio of the cost of accessing the spectrum in an opportunistic manner using cognitive radio technology to the cost of leasing/purchasing the spectrum [214]. It is widely accepted that the cost of opportunistically accessing the spectrum is lower than the cost of leasing/purchasing a spectrum [214]. Values of ζ close to 0 indicate that the cost of CR access is small compared to spectrum leasing/purchasing. We call it *low CR cost regime*. Whereas, for values of ζ close to 1 we term it as *high CR cost regime*. Therefore, the cost-efficiency metric provides a unique metric that takes into account the extra energy utilized by BodyCog-BNC towards CR communication as compared to licensed WAN and presents the net gain in payoff for the users.

6.8 Performance Analysis

At first, we analyze the BodyCog-BNC to study the performance of ISTO algorithm in determining the optimal inter-sensing duration for a PU channel so as to maximize its energy-efficiency. Next, we evaluate the performance of the BodyCog-BNC backhaul communication in terms of average energy consumption, switching probability, switching time and cost-efficiency. We also compare and contrast the variations in these metrics against different possible operating conditions namely PU activity, detected PU SNR, control channel conditions, NRT data transferred and the CR cost regimes. Finally, we also show the superiority in performance of BodyCog-BNC in terms of cost-efficiency as compared to conventional licensed WAN technology. In this regard, the simulations are performed in MATLAB [215] for solving the optimization problem **P1** and to obtain the performance metrics.

6.8.1 Simulation Settings

In our simulations, the PU spectrum is divided into PU channels each of bandwidth $W = 5\,\text{MHz}$. The control channel also has a bandwidth of $W = 5\,\text{MHz}$. The PU activity of the channels follow an exponential ON-OFF distribution with mean duty-cycle $t_{on} + t_{off} = 3\,\text{s}$ [100]. The SNR of a data link between BodyCog-BNC and CBS follow an exponential process with mean SNR $= 10\,\text{dB}$ [105]. The SNR of the control channel also follows similar process with mean SNRs 10.5dB and 13.6dB for analysis under different BER conditions of 10^{-4} and 10^{-6} respectively (as per (6.33)). Further, for modeling the data transmission by BodyCog-BNC, we consider healthcare data generated from a WBAN. The sampling frequencies of various physiological signals, are given in Table 6.2 [108]. Table 6.2 also provides the corresponding data bits (D_{bits}) generated after three times compression of a 2s captured signal. Out of this, in this chapter, we show the results of performance analysis for the first three data streams (DS).

We utilize the Wireless Open-Access Research Platform (WARP) [166] radio boards to model the transceivers of CR and WAN interfaces. For obtaining their power consumption profile, readings were taken using an external ammeter connected in series with the WARP node's 12V power supply. The results revealed that, the node draws $I_t = 1.4\text{A}$, $I_r = 1.35\text{A}$ and $I_i = 1.3\text{A}$ current respectively in transmit, receive modes and when the WARP board processes ISTO algorithm or waits for reception of an acknowledgment.

To obtain the sensing time, we draw on the assumptions presented in [172], where the optimal sensing time has been evaluated for $P_d = \chi = 0.9$, receiver sensitivity $\gamma_{PU,min} = -20\,\text{dB}$, and $P_f = \kappa = 0.1$. Therefore, using (6.3) we obtain $N_S = 131072$. The WARP board

Table 6.2 Healthcare signal frequencies and data size

Data Stream (DS)	Signal Frequency (Hz)	Data Size for 2s signal (bits)	Compressed Data Size (D_i bits)
1. Body Temperature	0.1	32	32
2. ECG	200	12800	4224
3. EMG	500	32000	10560
4. Respiratory Rate	10	640	212
5. Blood Pressure	50	3200	1056
6. EEG	60	3840	1268
7. Galvanic Skin Resistance	20	1280	422

is equipped with a 40MHz ADC with a buffer size of 2^{14}. Generally, WARP avoids the first 1000 received samples. Using this and after some calculations, we obtain the sensing time $T_S = 3$ ms. Further, in our analysis, we consider the normalized interference threshold $\Gamma = 0.06$ for ISTO algorithm.

For designing the BCR-MAC, we consider the maximum number of re-transmissions for control message exchange i.e. $R = 3$, the maximum number of successive busy observations before a spectral handoff is executed i.e. $B = 2$ and the maximum number of successive handoffs before invoking spectrum agility to licensed WAN i.e. $H = 2$.

Lastly, in our simulations, for performing the cost-efficiency analysis we consider the current electricity and 3G data transfer costs prevailing in India, which is a developing nation. We set the cost of electricity as ₹4.89/kWh, i.e. $c_{energy} = ₹1.358 \times 10^{-6}$/J [216] and the basic cost of data transfer as ₹0.04 per 10kB data [217], i.e. $c_{dat} = ₹4 \times 10^{-6}$/bit.

6.8.2 Analysis of ISTO Performance

The objective of ISTO algorithm is to obtain the maximum energy-efficiency for backhaul CR transmission by selecting the optimum inter-sensing time (T_D^*). In this regard, the performance of ISTO algorithm depends on the PU activity and the sensing uncertainty denoted by the miss-detection probability $(1 - P_d)$ which in turn depends on the detected PU SNRs (γ_{PU}) . Accordingly, in Figure 6.17 we observe the variation of energy-efficiency (η) and normalized interference duration (ε) with T_D for different PU activities at detected PU SNRs -20dB and -19dB. Figures 6.17a and 6.17b show that the energy-efficiency is initially increasing and later decreasing with increased inter-sensing duration. Shorter T_D leads to less throughput and more energy consumed towards sensing, whereas a higher T_D corresponds to higher probability of return of PU during transmission by BodyCog-BNC within a detected

white-space, which leads to increase in interference to PU. The later effect is further evident from Figures 6.17c and 6.17d.

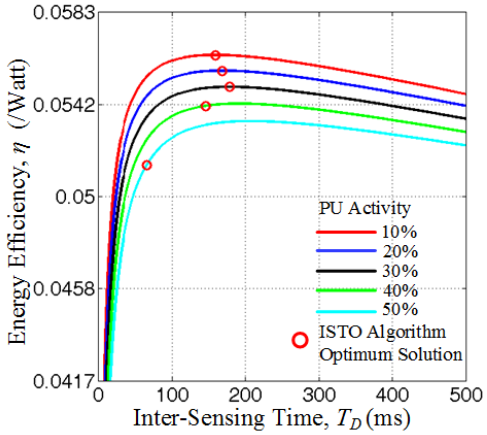

(a) Energy-efficiency for $\gamma_{PU} = -20\,\text{dB}$

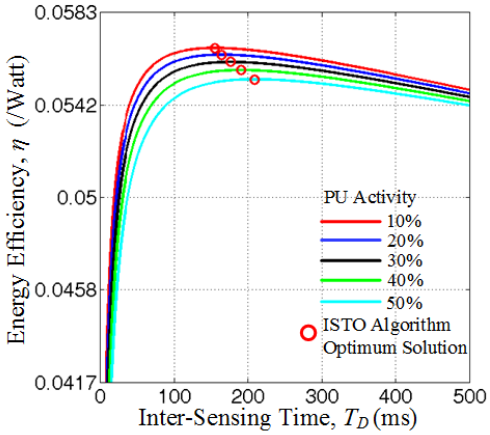

(b) Energy-efficiency for $\gamma_{PU} = -19\,\text{dB}$

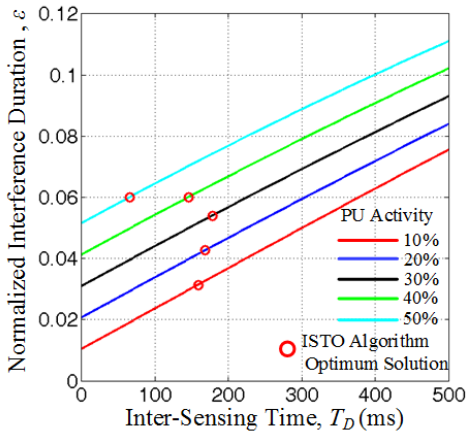

(c) Normalized interference duration for $\gamma_{PU} = -20\,\text{dB}$

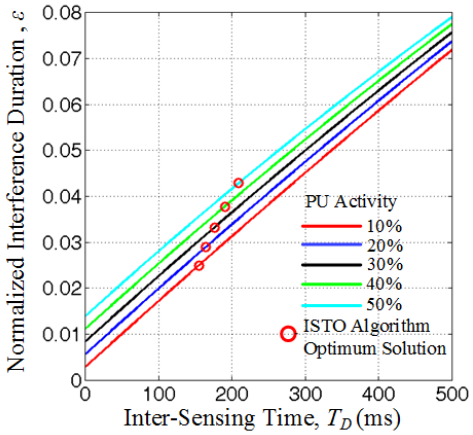

(d) Normalized interference duration for $\gamma_{PU} = -19\,\text{dB}$

Fig. 6.17 Variation of energy-efficiency and normalized interference duration with T_D for different PU activities.

Not withstanding the varied PU activity and detected PU SNR conditions, the ISTO algorithm accurately computes the optimal inter-sensing duration (T_D^*) for which the energy-efficiency is maximum which is evident from the 'red circles' in Figures 6.17a and 6.17b. In general, for a given detected PU SNR, the optimum inter-sensing duration increases with increase in PU activity. As a consequence, the inference at optimal points also increases with PU activity (Figures 6.17c and 6.17d). However, in order to comply with the pre-specified interference threshold Γ of the PUs, whenever 'Case 1' of ISTO algorithm gives an

inter-sensing duration for which constraint C1 (6.14) is not satisfied, the algorithm tries to find the solution on the boundary of C1. For example, in Figures 6.17a and 6.17c i.e. for $\gamma_{PU} = -20$dB, when the PU activity is as high as 40% and 50%, the optimal solution is on the boundary of constraint (6.14), for which the normalized interference is equal to Γ. Finally, a closer look at Figure 6.17 shows that for the same T_D and PU activity, higher PU SNRs (i.e. better detection probability) lead to better energy-efficiency and lesser interference.

The ISTO algorithm also helps BCR-MAC to identify any un-usuable channel that is allocated to it by the CBS. To study this, we vary the PU activities and detected PU SNRs of a PU channel to observe its impact on the outcome of the ISTO algorithm in terms of energy-efficiency and normalized interference duration. Similar to Figure 6.17, in Figures 6.18a and 6.18b we observe that at T_D^* the energy-efficiency decreases and collision increases with decrease in PU SNR and increase in PU activity. However, more importantly, ISTO algorithm declares the channels which fail to provide a solution as un-usable. In Figure 6.18, all such points which do not have a graph signifies that ISTO algorithm provided a no-solution under those conditions. In such scenarios, BCR-MAC after control message exchange with CBS switches to another channel or may perform spectral agility (see Section 6.5).

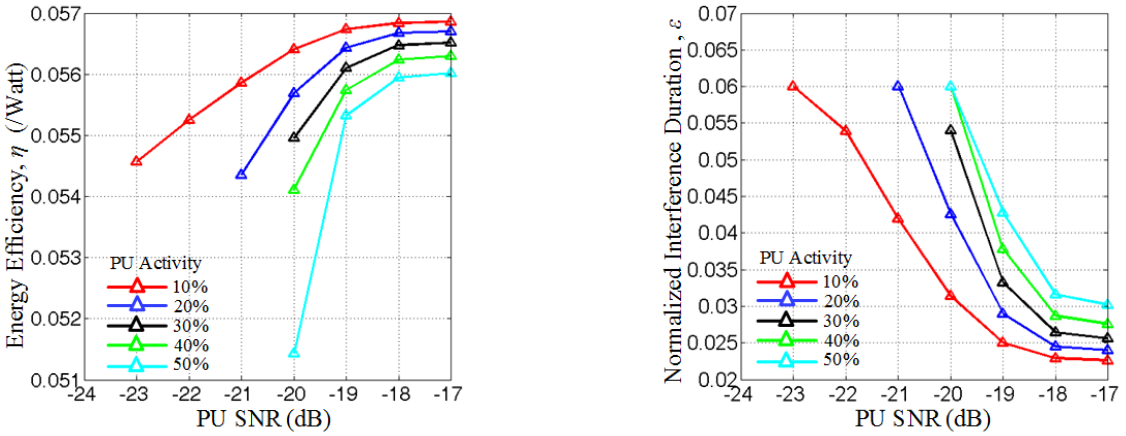

(a) (b)

Fig. 6.18 Variation of (a) energy-efficiency, and (b)normalized interference duration at T_D^* with detected PU SNR for different PU activities.

Finally, to observe the practicality of ISTO algorithm in real CR environment we implement it on 20MHz Microblaze processor of WARP v3 board. The efficiency of ISTO algorithm is determined through the time taken by the Newton Raphson (NR) techniques used for execution of its various steps, namely solving either 'Case 1' or 'Case 2' (see Algorithm

6.1). Keeping the detected PU SNR fixed at $\gamma_{PU} = -20\,\text{dB}$, it is seen that for PU activity less than 40%, ISTO algorithm takes 2.95ms for its entire operation. Whereas for higher PU activity the total time increases to 4.95ms. This is because for a PU activity greater than 40%, 'Case 1' of ISTO fails to reach a solution that satisfies the feasibility conditions and thereafter it moves to 'Case 2' leading to an increase in the time taken to provide the optimum solution.

6.8.3 Analysis of Average Energy Consumption

It is envisioned that by exploiting the opportunistic backhaul CR transmission, the BodyCog-BNC besides providing a solution to the spectrum scarcity problem will also facilitate cost-efficient backhaul transmission. To validate this, we take a closer look at the total cost incurred to a user (Section 6.7.4), which essentially comprises of two components: i) the energy cost, and ii) data transfer cost. Table 6.3 summarizes these two components when data streams DS-1, DS-2 and DS-3 are transferred employing the conventional licensed WAN technology and BodyCog-BNC. For BodyCog-BNC, we consider the worst case conditions, i.e. the first assigned PU channel has high PU activity of 50% and a low detected PU SNR of -20dB, a control channel SNR of -10.5dB which provides a bit-error rate of 10^{-4}, and a high CR cost regime. The PU activity and PU SNR of the second channel assigned after a handoff is uniformly distributed between 10% to 50% and -20dB to -17dB respectively. From Table 6.3, it is observed that the energy cost for BodyCog-BNC is more as compared to licensed WAN. This is to be expected as BodyCog-BNC performs additional cognitive actions leading to more energy consumption. However, the gain in cost saving for BodyCog-BNC in terms of data transfer cost is significantly higher as compared to its increased energy cost . This ultimately leads to 18-19% cost-efficiency (CE). The primary reason behind this is the lower cost of electricity as compared to the data transfer cost and the use of low cost CR backhaul. Therefore, it can be stated that, from the point of view of user payoffs data transfer cost is of greater concern than the energy cost, and BodyCog-BNC precisely addresses this concern as clearly evident from Table 6.3. Lastly, it is to be noted that with increase in data size, the energy consumed by BodyCog-BNC increases. However, the *CE* also increases because more data can be transmitted for the energy consumed.

Table 6.3 Cost incurred by licensed WAN and BodyCog-BNC

DS	**Licensed WAN**			**BodyCog-BNC (High CR Cost Regime $\zeta = 0.8$)**			
	Energy Cost	Data Cost	C_{conv}	Energy Cost	Data Cost	$C_{BodyCog}$	$CE\,\%$
DS-1	4.22×10^{-11}	1.28×10^{-4}	1.28×10^{-4}	2.44×10^{-7}	1.04×10^{-4}	1.04×10^{-4}	18.8
DS-2	5.57×10^{-9}	1.69×10^{-2}	1.69×10^{-2}	2.49×10^{-7}	1.37×10^{-2}	1.37×10^{-2}	18.98
DS-3	1.39×10^{-8}	4.22×10^{-2}	4.22×10^{-2}	2.58×10^{-7}	3.42×10^{-2}	3.42×10^{-2}	18.99

We now study the variation of the average energies consumed by BodyCog-BNC in Figure 6.19 under varied operating conditions. We consider DS-2 and vary the PU activity and detected PU SNR of the first channel to observe its impact on the performance. Additionally, we also observe the effect of variation in SNR of the non-ideal control channel at 10.5dB and 13.6dB. From Figure 6.19, it is observed that as the PU activity increases, average energy consumption becomes higher. This is caused by the fact that for high PU activity the probability of encountering a busy channel increases, which means wastage of time and energy in sensing a channel as busy and thereafter going through handoff and ultimately switching to licensed WAN. We also observe that, in general, the average energy consumption increases with increase in PU SNR. This variation can be explained from the perspective of miss-detection probability. As the detected PU SNR increases, the miss-detection probability decreases. This reduces the interference to PUs, however it also decreases the BNC transmission opportunities, leading to more energy consumed in sensing and handoffs. An exception to this trend can be observed at -20dB PU SNR for 40% and 50% PU activities, which have more energy consumptions than higher PU SNRs. This is because under these conditions ISTO algorithm obtains an optimal solution by solving 'Case 2' which involves more time as discussed in Section 6.8.2.

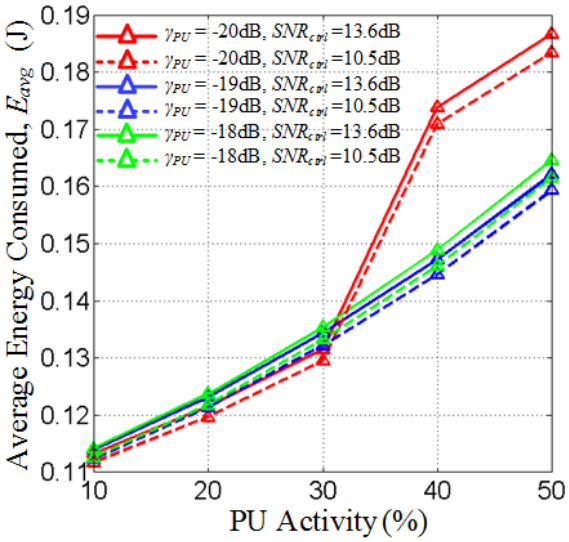

Fig. 6.19 Variation of average energy consumed by BodyCog-BNC for transferring DS-2 under different PU activities, PU SNRs (γ_{PU}) and control channel SNRs (SNR_{ctrl}).

The analysis presented above establishes the superior cost-efficiency of BodyCog-BNC under worst case conditions. Moreover, for completeness, we also need to perform a detailed evaluation of the *CE* under other operating conditions. However, prior to that, in the next

sub-section we analyze the factors influencing CE, namely the switching probability and switching time.

6.8.4 Analysis of Switching Probability and Switching Time

Figures 6.20a and 6.20b respectively show the variation of switching probability and switching time with respect to PU activity and detected PU SNR under varied control channel SNRs. In Figure 6.20a, we can observe that for a given detected PU SNR the switching probability increases with increase in PU activity of the first channel. Furthermore, for a fixed PU activity, as PU SNR increases switching probability increases. Similarly, as control channel SNR decreases the switching probability increases. The increase in switching probability also explains similar increase in the average switching time as shown in Figure 6.20b. The variations seen in Figure 6.20 can be explained following the arguments presented in the analysis of average energy consumption. Notwithstanding the aforementioned variations, it can be observed that the probability of switching to the licensed WAN even at high PU activity, high PU SNR and low control channel SNR is less than 6%. In other words, more that 94% of the time, the BodyCog-BNC uses the CRN for completing a successful backhaul transmission.

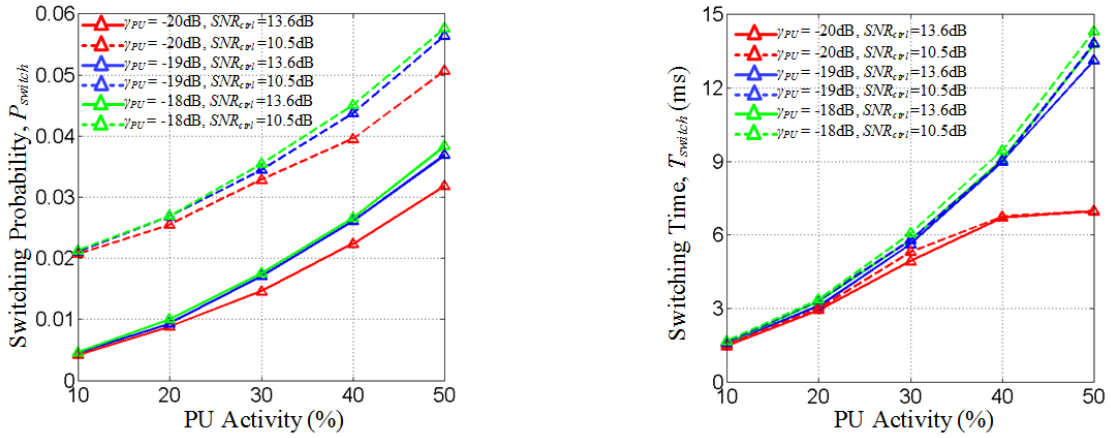

(a) (b)

Fig. 6.20 Variation of (a) switching probability, and (b)switching time under different PU activities, PU SNRs (γ_{PU}) and control channel SNRs (SNR_{ctrl}).

Lastly, a closer look at Figure 6.20b reveals that, even under worst case conditions the average switching speed is less than 14ms. This is achieved by exploiting the cross-layer message passing between BME and BCR-MAC. The BME session is established over a

TCP-IP client-server framework, with the BME acting as a TCP client. Generally, a Wiznet 5100 TCP-IP stack [218] has a default time-out period of 200ms and a maximum re-try count of 8, i.e. a TCP packet re-transmission will occur if there is no response from the remote peer within 200ms, and the maximum number of such re-transmissions is 8. Thus, in the absence of any cross-layer message passing between BME and BCR-MAC, it is only after 1.6s that the BME can ascertain the non-usability of CRN for backhaul communication, and thereafter switch to licensed WAN. Therefore, as observed, the proposed cross-layer message passing between BME and BCR-MAC helps the BodyCog-BNC achieve minimum 100% improvement in the switching time.

6.8.5 Analysis of Cost-Efficiency

Drawing from the results of the preceding sub-section, we now perform a detailed evaluation of the cost-efficiency (CE) of BodyCog-BNC in Figure 6.21. For this, we consider transmission of data stream DS-2 under different PU activities, PU SNRs and control channel SNRs. We consider two separate CR cost regimes: a) low cost regime with $\zeta = 0.2$, and b) high cost regime with $\zeta = 0.8$. From all the figures, it is observed that the BodyCog-BNC significantly improves the *CE* of backhaul transmission. This variation in *CE* can be explained by studying the changes in switching probability under different conditions as shown in Figure 6.20a. Lower switching probability corresponds to lesser utilization of the licensed WAN, which adds to the concerned cost-efficiency factor. The cost-efficiency results in Figure 6.21 prove that the low cost alternative provided by the use of CR technology in the backhaul will be lucrative to the users, more specifically in developing countries. CR technology aims to opportunistically access licensed spectrum thereby significantly reducing the data transfer costs. Furthermore, as observed previously in Table 6.3, with increase in data size the *CE* increases slightly, because more data can be transmitted for the energy consumed in channel sensing .

Lastly, by observing Figure 6.21a (low CR cost regime) and Figure 6.21b (high CR cost regime), we remark that irrespective of the cost regime imposed by the backhaul CRN, the BodyCog-BNC ensures significant cost-efficiency for the users. It should also be emphasized that the payoff from the users adds to profit of the network operators which is a direct consequence of the improved spectral efficiency achieved by the system leveraging on the DSA provided by CR technology.

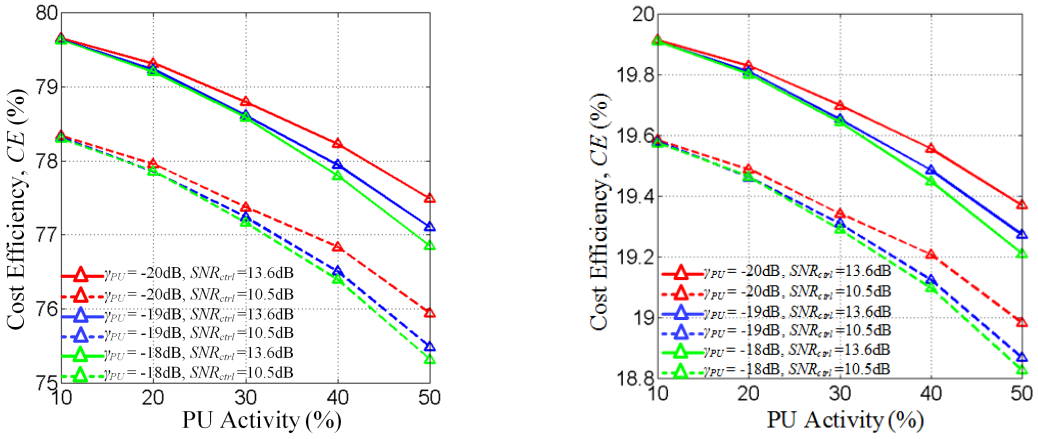

(a) Low CR cost regime

(b) High CR cost regime

Fig. 6.21 Variation of cost-efficiency of BodyCog-BNC for transferring DS-2 under different PU activities, PU SNRs (γ_{PU}) and control channel SNRs (SNR_{ctrl}).

6.9 Proof of Concept with Prototype Design

In this section, a prototype implementation of the proposed BodyCog-BNC and BodyCog architecture is described by means of a simple proof of concept of the design. It also validates the working functionality of different units and the novelty aspects of our system. For this design we leverage i) the WBAN BNC developed in Chapter 3, ii) the real-time CR terminal created in Chapter 4 and iiii) our proposed cross-layer based design of BME and BCR-MAC.

Figure 6.22 shows the comprehensive BodyCog prototype implementation in hardware which includes:

1. a sensor unit for ECG signal capture by AD8232 [152], which is an integrated signal conditioning block, as shown in Figure 6.23a;
2. a classic WBAN unit to facilitate transfer of ECG samples over 433MHz band using CC1101 transceivers [150], as shown in Figure 6.23a;
3. a BodyCog-BNC prototype as shown in Figure 6.23b, which is developed following the design principle highlighted in Figure 6.3;
4. a CBS designed using a WARP v2 board that uses two radio daughter cards- one for the control channel and the other for data transmission and reception;
5. For the CR system, we have selected the 2.4 GHz frequency band which has 12 channels of 20MHz bandwidth and have utilized 2 laptops with built in 100Mbps IEEE 802.11a cards to emulate the incumbent PU transmitter and receiver pair with exponential ON-OFF traffic.

In the following, we briefly highlight the salient features of our developed BodyCog-BNC prototype.

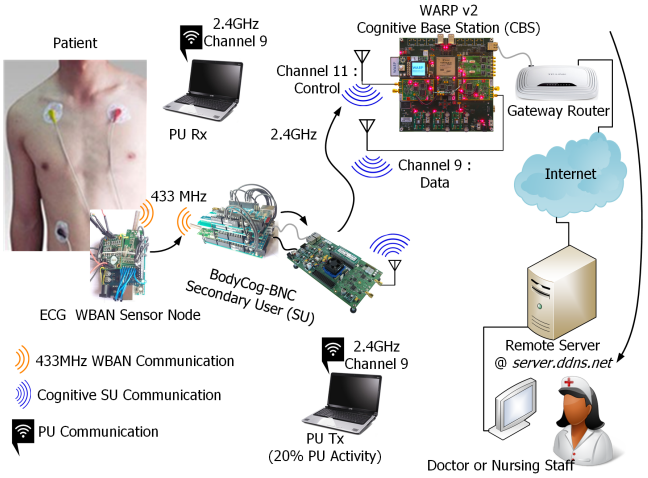

Fig. 6.22 Remote health monitoring system using BodyCog architecture and BodyCog-BNC.

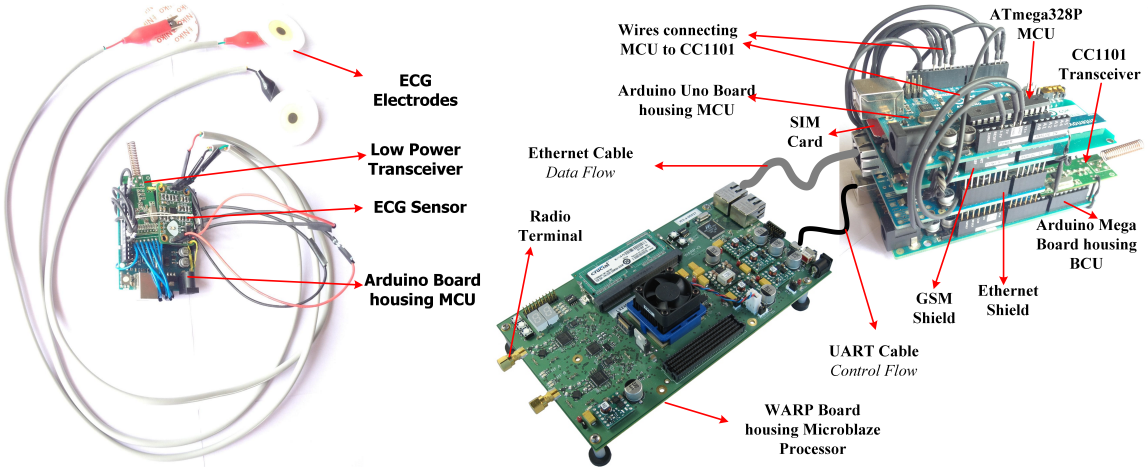

(a) Sensor node prototype (b) BodyCog-BNC prototype

Fig. 6.23 Interconnected boards and devices realizing a) Sensor node, and b) BodyCog-BNC prototype as envisioned in Figure 6.3.

6.9.1 BodyCog-BNC Prototype Design

With reference to the BNC design shown in Figure 6.3, the corresponding hardware components for the developed prototype are as follows:

i) **WBAN Microcontroller Unit (MCU)**- An 8bit 16MHz ATmega328P microcontroller of an Arduino Uno board [151].

ii) **WBAN Transceiver**- A TI CC1101 wireless transceiver to generate 433MHz ISM bands (BAND-1 of Figure 6.1) for sensor-BNC wireless connection. The wireless chips CC1101 are selected in this work because of the following reasons: overall cost saving, low-power consumption, small size, fast data transfer and less penetration loss at 433MHz ISM bands. This frequency range also allows high-level integration with radio frequency IC (RFIC) technology leading to smaller size and lower power consumption. In summary, higher frequencies cause severe penetration loss [219], whereas high level integration is difficult at lower frequencies. Moreover, using CC1101 together with the MCU gives the flexibility of designing user specific MAC protocols thereby making implementation of IEEE 802.15.6 based WBAN MAC protocols feasible in the future. CC1101 is interfaced with the MCU via Serial Peripheral Interface (SPI) communication bus that comprises the WBAN_PHY SAP (Figure 6.3).

iii) **BodyCog-BNC Microcontroller Unit (BCU)**- An 8-bit 16MHz ATmega2560 microcontroller unit, with upgraded 4-kB EEPROM and 8-kB RAM based on Arduino Mega board [154]. The BCU is programmed to receive data from MCU of BodyCog-BNC via the universal asynchronous transmitter/receiver (UART) communication bus (denoted UART-1) that comprises the APP SAP (Figure 6.3). Thereafter, BCU performs Discrete Wavelet Transform (Section 3.10) based data compression.

iv) **CR Embedded Processor and Transceiver**- A WARP v3 board with 40MHz Microblaze [166] Embedded Processor (EP), that houses the BCR-MAC protocol, and coordinates the CR communications over 2.4 GHz band (BAND-2 of Figure 6.1). BCU performs cross-layer message passing with EP via UART bus (denoted UART-0) which forms the BME_CTRL SAP (Figure 6.3). In addition, it transfers data to WARP via Ethernet connected through an Ethernet Shield [220] that constitute the DATA SAP (Figure 6.3).

v) **Licensed WAN Interface**- A GSM shield to connect to cellular network for switching to GSM bands (GSM 850MHz/900MHz) (BAND-3 of Figure 6.1).

A BodyCog-BNC needs to be extremely portable like a mobile phone thereby enabling patient mobility. All the components described above form a prototype for designing and testing the proposed BodyCog-BNC. Similar to the GSM module that is already present in mobile handsets, the WARP board can be envisioned as a CR module that may be featured in the next generation mobile phones for accessing the PU channels. The MCU and BCU units of BodyCog-BNC may be the additional features embedded for healthcare monitoring like

the Apple Health Kit [221]. Fabricating the BodyCog-BNC into a small form-factor based on this prototype design is an open research problem.

6.9.2 Operation of the Prototype

We demonstrate the feasibility of just one of the several possible use-case scenarios where the proposed BodyCog-BNC could find adoption. As an example, in the prototype BodyCog implementation, the AD8232 chip connected to the WBAN sensor board is exploited to periodically monitor the ECG signals for 2s. These periodic data could give physicians an extensive record to better diagnose the patient condition. With suitable programming and use of other sensors, this design can be extended for monitoring of other physiological signals with addition of emergency alert from user end or at the remote server.

When an incoming ECG signal event is detected by the MCU of BodyCog-BNC, it forwards the samples to the BCU. Once 400 ECG samples are ready, they are compressed by DWT technique using *Bi-orthogonal 4.4 wavelet filter* and the first 132 DWT coefficients are packetized providing 67% data compression. The ATmega2560 BCU takes 97.06 ms to executing the DWT based compression. We found Biorthogonal 4.4 filter (Section 3.11.3) to provide the best results for DWT: "very good" signal reconstruction quality [155] with the maximum amount of compression. Figure 6.24 is plotted to illustrate that the DWT data compression produces acceptable signal after signal reconstruction at the remote server end. Next, the BCU after cross-layer message passing with BCR-MAC communicates the data to the CBS over a PU channel in the absence of the incumbent PUs.

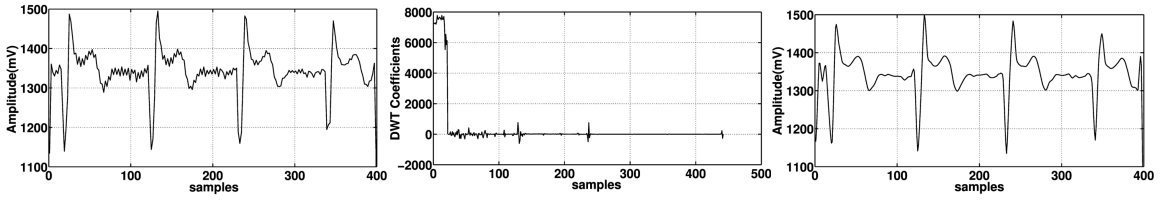

(a) Original captured ECG signal (b) DWT coefficients (c) Reconstructed ECG signal

Fig. 6.24 (a) 2s ECG signal captured by AD8232 sensor, (b) DWT signal compressed using Bior.4.4 filter, (c) Reconstructed signal from 1st 132 DWT coefficients.

For studying the BodyCog-BNC activities we use the following software:

i) *CommTunnel* [222]- It scans UART-0 to monitor the cross-layer message passing between BCU (i.e. BME) and CR embedded processor (i.e. BCR-MAC).

ii) *Putty* [173] – It monitors the internal activities of the BCR-MAC via USB-UART interface of WARP. It helps in debugging the control message exchange with CBS, ISTO algorithm, sensing-transmission cycle and the handoff mechanism.

The screenshots of Putty and CommTunnel in Figure 6.26 highlight the major functions of the proposed BME and BCR-MAC during normal data transfer over the CR interface. For this purpose, firstly through cross-layer message passing (indicated by green lines in Figure 6.26) BME intimates BCR-MAC to initiate connection with the CBS. Thereafter, through control message exchange over the control channel (channel 11 of the 2.4GHz band), a CR channel 9 of 2.4 GHz band having 20% PU activity with a total $t_{on}+t_{off}$ duration of 3s is successfully obtained from CBS. Then an optimal inter-sensing duration of 168ms is obtained by applying the ISTO algorithm for -20dB PU SNR and lastly the channel is sensed to be idle. For implementing the energy detection mechanism in WARP, we employ our designed ECR-MAC framework developed in Section 4.5.1, that incorporates our proposed energy-efficient and resource-efficient PED method. In this regard, for energy detection, the noise power is calculated as $N_o = -123.3\,\text{dB}$ and the energy detection threshold as $\lambda_{th} = -71.8\,\text{dB}$. In Figure 6.26b, we represent the total sensing time (T_S) as $N_C = 100$ units. We determine the PU channel as busy if total energy accumulated within T_S exceeds λ_{th}, which is denoted in terms of $B_T = 11$ units, where each unit represents -113.31 dB.

After a successful data transfer, the disconnection procedure is followed as per BCR-MAC protocol. Furthermore, the data received at CBS is sent to the remote server though a gateway router connected to the Internet. At the remote server, the RSAP performs inverse DWT of the received samples to give the ECG signal shown in Figure 6.24c. The other operating scenarios for the BodyCog-BNC are elaborated through a video demonstration [1].

Lastly, we demonstrate the efficiency of handoff procedure of the proposed BCR-MAC. A handoff event can be identified in packet sniffers like Wireshark [223] when there is a discontinuity in the packet arrivals at the receiver end. However, TCP communication used in BodyCog is discontinuous in nature, and a handoff event could not be differentiated from inter-packet arrivals. Therefore, a continuous User Datagram Protocol (UDP) communication like video streaming is considered. For this purpose, we connect one computer (PC-A) to WARP v3 running on BCR-MAC and another (PC-B) to WARP v2 board serving as CBS. In the absence of PU system, a UDP based video transmission is started from PC-A to PC-B and the packets are tracked at the receiving end with Wireshark. When a PU appears in the channel, BCR-MAC detects the PU's presence and a handoff event occurs as shown in Figure 6.25. More in detail, BCR-MAC requests the CBS for a new channel and upon getting a free channel, the video transmission resumes.

[1] Video @ https://www.dropbox.com/s/eqa0rimo03uja4c/BodyCog_Demo.mp4?dl=0

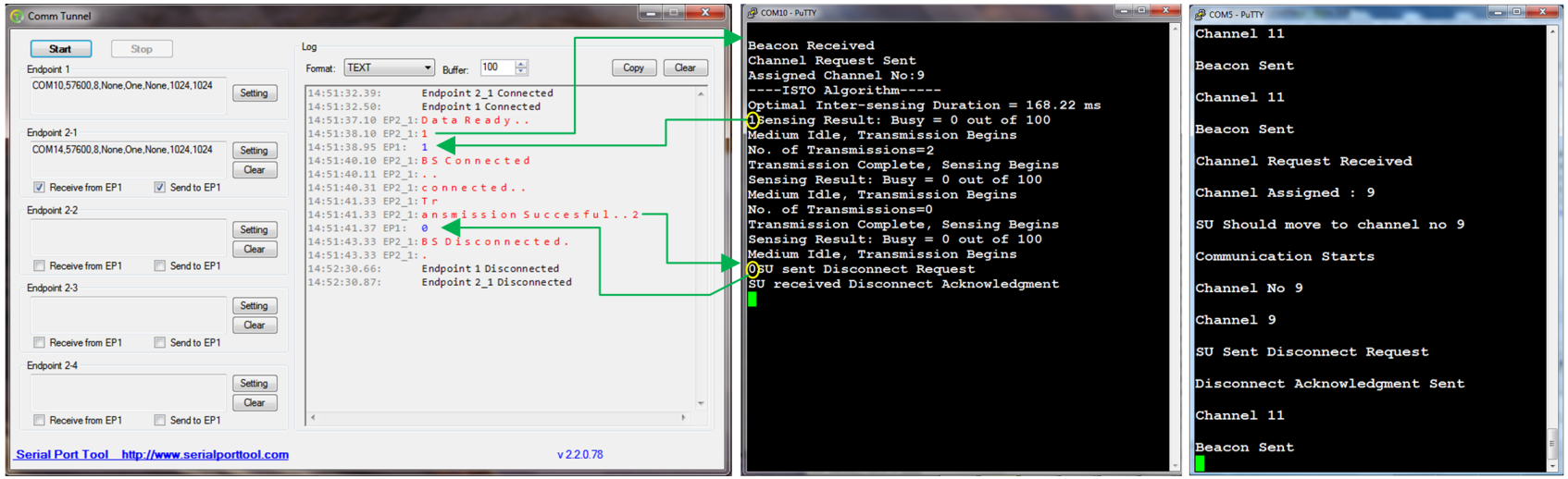

Fig. 6.26 Screenshots of (a) CommTunnel showing UART communication between BME (COM14) and WARP v3 (COM10), (b) Putty scanning BCR-MAC via USB-UART (COM 10) of WARP v3, (c) Putty scanning BS via USB-UART (COM 5) of WARP v2. Green lines indicate cross-layer interaction in BNC.

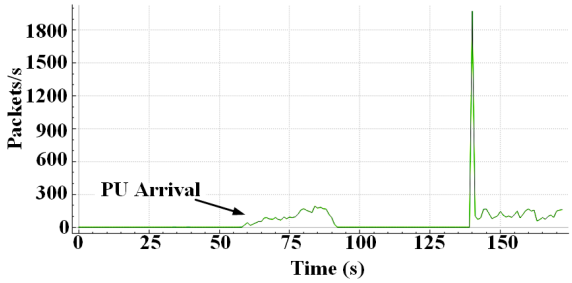

(a) PU signal

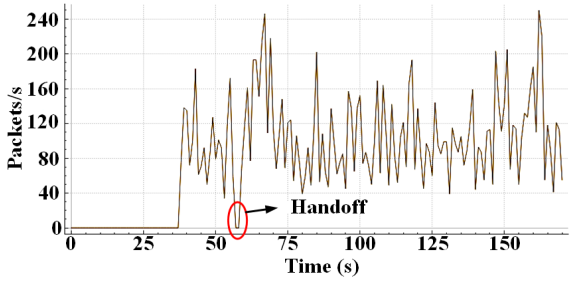

(b) Received continuous signal at CBS

Fig. 6.25 Screenshots of Wireshark showing handoff performed by BCR-MAC illustrated through continuous CR transmission.

6.10 Conclusion

In this chapter, we design and implement an intelligent WBAN gateway (controller) termed as BoyCog-BNC that uses CR technology to guarantee spectral efficient, cost-efficient and reliable NRT backhaul transmission of WBAN data. However, the inherent opportunistic mode of communication using the CR interface implies that to ensure reliability there is a need for devising ways to facilitate spectrum agility, i.e. switching to other backhaul technologies in the event that the CRN lacks vacant or suitable PU channels. To facilitate this, we introduce a modified protocol stack for the BNC comprising of our proposed cross-layer based BodyCog-BNC Management Entity (BME) and BodyCog CR MAC (BCR-MAC) units. We provide the complete design and implementation framework for the BME and BCR-MAC. These units exploit interrupt based intelligent cross-layer message passing to realize spectrum agility under varied scenarios, namely loss of control message between CBS and BNC or lack of proper PU channels or occurrence of successive handoffs in multiple PU channels. Further, to ensure maximum energy-efficiency for data transmission over backhaul CRN, we also propose an ISTO algorithm for BCR-MAC that uses KKT conditions to optimize the inter-sensing duration for a PU channel under sensing uncertainties while

keeping the interference to PU with a pre-determined limit. In addition, the ISTO algorithm also determines the suitability of a PU channel for communication.

To analyze the performance of BodyCog-BNC, we derive closed form mathematical expressions for obtaining its average energy consumption, switching probability, switching time and cost-efficiency in transmission. The closed form expressions of these metrics allow their derivations as a function of different parameters namely PU activity, detected PU SNR, control channel conditions, NRT data transferred and the CR cost regimes. This will enable a system designer to suitably select these parameters for optimal performance. Finally, it is concluded through analysis that the BodyCog-BNC efficiently uses the CR interface more than 94% of the time for backhaul communication, achieving a significantly high cost-efficiency as compared to conventional licensed WAN technologies. It is shown that the high cost-efficiency is ensured for a wide range of healthcare data and under varied CR cost regimes. Performance evaluations also highlight the superior enhancement in switching speed in case of spectrum agility. The use of cross-layer message passing leads to a minimum 100% improvement in the switching time as compared to non cross-layer based approach. Finally, we elaborate a developed hardware prototype of BodyCog-BNC and use it in a test-bed setup to validate the ability of BodyCog-BNC in enabling NRT remote healthcare monitoring.

Chapter 7

A Prediction and Scheduling Framework in Centralized Cognitive Radio Network for Energy-Efficient Non-Real Time Communication

❝ *Predicting the future isn't magic, it's artificial intelligence.* ❞

-Dave Waters

Chapter 6 has already presented the novel idea of exploiting backhaul CRN to address all the concerns faced by WBAN with respect to low cost backhaul communication and also that faced by next generation networks in tackling the issue of spectrum crunch due to increasing number of IoT services. However, in Chapter 6 we have shown the integration of the BodyCog-BNC into a basic CRN as envisioned in IEEE 802.22 [46], where additional protection to incumbent PU communication needs to ensured by SUs through spectrum sensing. However, we now consider the alternate popular CRN policy where the Cognitive Base Station (CBS) performs all necessary cognitive actions for PU channel access, thereby simplifying the SU (BNC) design. Considering that the CBS has sufficient resources to execute complex operations, ***this chapter proposes a centralized scheduling, sensing and enhanced Hidden Markov Model (HMM) based prediction framework, termed CSSP, at the CBS to facilitate highly energy-efficient Non-Real Time (NRT) data transfer as encountered in WBAN based remote health monitoring***.

To this end, we design and implement our proposed Hardware based HMM engine (H2M2) at the CR PHY of CBS that reduces the prediction time significantly thereby

improving the system performance. Thereafter, through performance analysis we establish that H2M2 reduces interference between SU and PU but at the cost of reduced throughput. To address this, we introduce our devised Inter Sensing-Prediction Time Optimization (ISPTO) algorithm that maximizes SU throughput under sensing uncertainties and PU interference constraint. Following this, we formulate the problem of minimizing the total battery consumption of all the NRT SUs in the CRN by allocating the appropriate predictable channels to suitable users based on the operating conditions. For this purpose, we propose Battery Consumption Minimizing Scheduler (BCMS) that solves the channel assignment problem in polynomial time and also ensures fairness. Detailed performance analysis is conducted to demonstrate the remarkable improvement in energy-efficiency due to use of CSSP over high PU activity channels as compared to traditional sensing frameworks. Finally, the practical utility of the system is established with respect to WBAN based remote health monitoring by developing a prototype model of H2M2 in Field Programmable Gate Array (FPGA) and using it in association with the CRN test-bed developed in Chapter 4 through a hardware co-simulation environment that shows a suitable direction of use for future IoT applications.

7.1 Introduction

Over the past few decades there has been a rapid increase in use of wireless communication services. Industry analysts predict that by 2020 about 50 billion devices are supposed to be connected to mobile networks worldwide which include devices/sensors sending information between Machine-to-Machine(M2M), to servers, or to the cloud. This explosion of devices connected to the Internet has been termed as the Internet of Things (IoT) [224]. This increasing demand for wireless spectrum has led to spectral congestion. On the contrary, studies by FCC have showed that the actual licensed spectrum remains unoccupied for large periods of time termed as 'white spaces'(for e.g., television broadcasting bands) [225, 75, 46]. The need for addressing this spectrum scarcity issue while utilizing the underutilized frequency slots led to the emergence of Cognitive Radio (CR) technology [75, 10]. CR can be used by unlicensed users known as Secondary Users (SUs) to sense these 'white spaces'and then share the spectrum with the licensed users termed as Primary Users (PUs) without causing harmful interference to the PUs. Hence, CR improves the spectral efficiency of the system. Thus, CR [75] is seen as a promising technology to tackle or at least partly address, the above challenges in the upcoming 5G cellular networks [8].

Some of the most prominent M2M application areas include healthcare (wireless body area network or WBAN, telemedicine, remote diagnosis, etc.), sensor networks (agriculture,

industrial monitoring) and smart grids (grid control, industrial metering, demand response) [226, 6]. These applications generate small amounts of data at regular intervals and send them over a long distance backhaul link in a reliable manner. Communication in such applications are in general delay tolerant or Non-Real Time (NRT), but demand high energy-efficiency that can minimize battery consumption and thereby prolong the battery life of the sensors.

7.1.1 Cognitive Radio Backhaul: A Suitable Choice

Using CR technology for the last mile backhaul communication in NRT applications not only addresses the spectrum scarcity problem but also enables low-cost data transfer [8, 227]. As the leased spectrum is fundamentally opportunistic, the cost of leasing the spectrum is expected to be much lower than the cost of purchasing a licensed band [8]. This would make IoT services like healthcare monitoring more affordable to public particularly in developing nations, where the cost of data transfer is still high. Besides, CR technology is inherently equipped to address the interference mitigation/reliability and energy-efficiency issues [75]. Therefore, a centralized Cognitive Radio Network (CRN) serving as a backhaul is an ideal candidate for low cost reliable energy-efficient NRT communications. To the best of authors' knowledge, only few attempts have been done to leverage the use of CRN specifically for NRT applications. Therefore, in this chapter, we propose a centralized CRN framework in order to ensure reliable energy-efficient communication for NRT SUs while coexisting with other SUs, more specifically Real Time (RT) users. The proposed framework is shown to outperform traditional CRN techniques like Base Station based Sensing (BSS) [228, 229, 91] and Collaborative Spectrum Sensing (CSS) [230] in terms of better energy-efficiency and interference mitigation capability.

7.1.2 Literature Survey and Motivation

In general, SUs rely on spectrum sensing [76] to opportunistically access PU channels. However, presence of noise and sudden arrival of PU during an ongoing SU transmission are common sources of collisions between SU and PU systems. Such collisions lead to wastage of energy/battery for SUs. Minimization of such interference can thus guarantee enhanced energy-efficiency as well as reliability in transmission. One possible way to mitigate this interference is through exploitation of prediction techniques in CRN. Several works such as [231–233] have employed Hidden Markov Model (HMM) [101] in CRN to predict the immediate future. To this end, Park et. al. in [231] proposes to use HMM based prediction in CRs to predict PU arrival based on the past channel sensing observations. The proposed method calculates the probabilistic correlation between the current channel status

and previous channel statuses using a Baum-Welch algorithm [234] in CR technology and predicting the future channel status based on the calculated probabilistic correlation using a forward algorithm [101]. This prediction information empowers the CR to take intelligent decisions. In [232], a HMM scheme predicts the next symbol in a TDMA PU traffic scenario. The presence of a Markov Chain for channel occupancy by PUs is further validated using real-time measurements in [233], which then uses the results to validate the HMM based modeling of CR based opportunistic PU channel access. However, the aforementioned works are primarily focused towards the analysis of HMM in CRN and do not put forward a framework for its implementation focused towards specific applications. In this regard, Akbar et. al. in [87] presented a Markov-based Channel Prediction Algorithm (MCPA), which allows the SUs to predict the arrival of PU using HMM based prediction and intelligently leave the channel that it currently occupies (also known as handoff) before the start of PU transmission. In [102], a method is proposed which uses HMM based prediction to reduce the number handoffs for a SU, thereby improving their throughput. A closer look reveals that when a PU returns to a channel the traffic intensity or PU channel activity increases [235]. Tumuluru et. al. in [235] and the performance analysis presented later in this chapter reports that with increase in PU activity, the number of slots occurring with busy channel status also increases resulting in more correlation in the PUs' channel occupancy data, which leads to the significantly better HMM prediction performance. The works in [87, 102] exploits this feature to initiate SU handoff, where upon arrival of PU in the channel there is an increase in the traffic intensity or PU channel activity. However, none of these works discuss the scope of applying the prediction information towards energy-efficient SU data communication.

Having established the superior performance of HMM based prediction in CRN under high PU activity, we look into the possibility of its exploitation towards energy-efficient SU data transmission with regards to both RT and NRT applications. To the best of our knowledge, none of the existing works in the literature report the use of HMM based prediction for minimizing collisions between PU and SU, and thereby facilitate energy-efficient SU data transmission in CRN. To this aim, we first consider a SU with RT application as a possible candidate. As reported extensively in [236], a high PU activity channel is not suited for sustaining RT communication over CRN. More in detail, a high PU activity channel due to its longer PU transmission durations increases the SU frame delay and reduces throughput. Such increased delay will not only fail to satisfy the strict delay requirements imposed by RT applications like VoIP and video streaming, but will also imply high buffer requirement for such SUs which may not be practical. Further, high PU activity channels also result in increased call drops during VoIP communication over CRN [100]. Therefore, a SU with RT application is not an ideal candidate for exploiting HMM based prediction for energy-efficient

data transmission over high PU activity channels. However, unlike RT SUs, NRT applications do not have strict delay and throughput requirements. Thus, the short white spaces in high PU activity channels could be efficiently utilized to send small amounts of NRT data. This motivated us to explore the possibility of an innovative framework which can leverage HMM based prediction over high PU activity channels to facilitate highly energy-efficient NRT communication and realize the IoT vision. The RT users in the CRN can continue to use low PU activity channels using traditional techniques such as BSS or CSS. It comes as a straight forward deduction that such a framework will also improve spectrum efficiency/capacity by allowing the utilization of both high and low PU activity channels in a CRN. Therefore, in this chapter we propose a framework that utilizes enhanced HMM based prediction for supporting energy-efficient and reliable NRT communication in a centralized CRN. To achieve this, we incorporate prediction within the traditional CR sensing-transmission cycle. Unlike most of existing works [87, 102] which advocate the use of HMM prediction for handoff, we use it to augment spectrum sensing by predicting the absence of PU during SU transmission, and thereby allowing communication with extremely low interference. Furthermore, HMM based prediction is a highly time intensive task. To address this issue, we designed a Hardware based HMM engine (H2M2) with enhanced prediction capability in terms of reduced prediction time. This can be achieved by reducing the total no of cycles by virtue of parallel processing and efficient pipelining, and operating the model at free running speed of re-configurable hardware like FPGA without setup and hold time violations. In our proposed framework, we exploit the superior prediction performance of H2M2 engine at the Cognitive Base Station (CBS) of the CRN. Additionally, the use of H2M2 for NRT data transmission presents other challenges that need to be addressed within the proposed framework and these are discussed next.

Initial performance analysis of our devised framework revealed that H2M2 guarantees less energy consumption due to its ability to limit interferences to PUs by avoiding miss-detections. However, it achieves this at the cost of reduced transmission opportunities, resulting in decreased throughput. This motivated us to improve the throughput of SUs while keeping the interference on PUs within a predetermined threshold. In this regard, several works [237–239] have focused on improving the throughput of CRN through a balance between sensing and transmission, while maintaining the PU interference as a constraint. A periodic sensing framework is discussed in [81], in which each frame consists of a sensing block and an inter-sensing block. Optimization of the sensing duration is proposed in [202], whereas [203] aims to improve the channel efficiency. In [82], a periodic sensing timing is proposed to improve the channel utilization of CR users while limiting their interference with PUs and also taking into account the impact of false alarm and miss-detection into consideration.

However, these works are not meant specifically taking prediction into consideration. More in detail, prediction leads to modified relations for transmission probabilities and interference to PUs. Therefore, incorporation of prediction within the traditional sensing-transmission cycle makes our proposed framework different from traditional CR cycle and thereby calls for separate analysis for maximization of throughput. To this end, the present work proposes an algorithm for the CBS to determine the optimal inter sensing-prediction duration that maximizes the SU throughput. In addition, the algorithm also identifies the high PU activity channels where prediction is most efficient.

As highlighted above, our proposed framework empowers the CBS to identify and optimize the predictable PU channels for improved NRT SU communication. Therefore, with the need to reduce the energy/battery consumption of NRT SUs, the next logical motivation is to devise a method that would allow the CBS to allocate the predictable PU channels to the NRT SUs in the most efficient manner. Centralized resource allocation in CRNs has been well-investigated in [103, 104], however, mostly from the perspective of throughput maximization. The fairness issues of a scheduler are considered in [209]. An energy-efficient scheduling mechanism for CRN has been presented in [105]. However, the channel access in [105] is mainly database driven without consideration of the PU channel activities, detected PU Signal to Noise Ratio (SNR) and the sensing uncertainty. Moreover, the scheduling in [105] is oriented towards RT applications with prolonged data transmission and continuous data arrival and hence the need to maintain certain throughput requirements. However, this does not apply for NRT users. Our scheduling requirement is assignment of the available predictable PU channels to NRT SUs so as to minimize the total battery consumption of the SUs. Furthermore, the scheduler must also take into account the sensing-prediction performance, the PU activity, detected PU SNR of the predictable channels and the data transfer requirements of the NRT SUs. To the best of our knowledge, such a scenario has not been studied and analyzed in the literature. Therefore, we complete our framework by incorporating a proposed scheduler that is fair in its resource allocation and also minimizes the total battery consumption of all the NRT SUs. Thus, owing to its scheduling and prediction features we term our proposed method as *Centralized Scheduling, Sensing and Prediction (CSSP)* framework.

7.1.3 Contributions of this Chapter

The main contributions of this article are summarized below.

❶ The proposed *CSSP framework* is developed by incorporating HMM based prediction within traditional sensing-transmission cycles of a centralized CRN. It is established

through performance analysis that CSSP outperforms established frameworks like BSS or CSS in terms of energy-efficiency and reliability. The reason for this improvement is the superior interference rejection capability of HMM based prediction under high PU activities channels. Consequently, CSSP framework also improves the spectral efficiency of CRN by assigning the un-exploited high PU activity channels exclusively to NRT SUs, while the RT users continue to use low activity channels through traditional approaches.

❷ We also minimize the prediction time by developing the *H2M2 engine* on re-configurable hardware at the CBS. H2M2 engine by virtue of its high-speed operation and efficient parallel processing and pipelining minimizes the prediction time significantly ensuring better energy-efficiency for the CRN.

❸ In this work, we have also optimized the framework through a proposed *Inter Sensing-Prediction Time Optimization (ISPTO)* algorithm. ISPTO runs at the CBS and maximizes the SU throughput for high PU activity channels while still satisfying the strict PU interference constraint. Furthermore, the ISPTO algorithm also identifies the predictable PU activity channels for efficient CRN performance.

❹ A novel *Battery Consumption Minimizing Scheduler (BCMS)* is also developed at the CBS and incorporated within the CSSP framework. BCMS assigns the predictable PU channels to the NRT SUs to minimize the total battery consumption of all the SUs. For this, it takes into account the PU activity and detected PU SNR of the channel, SU channel SNR and data lengths of SU transmission.

❺ Further, we integrate fairness into BCMS, which ensures that no NRT SU gets starved of transmission opportunities due to undue favor towards certain SUs. The designed BCMS is shown to outperform a heuristic scheduler both in terms of battery consumption minimization and fairness.

❻ Lastly, through a proof of concept we validate the ability of CSSP framework in enabling a WBAN to send its NRT data to the CBS by using H2M2 under high PU activity channels.

7.1.4 Chapter Organization

Our chapter is organized as follows. Section 7.2 outlines the system model and the CSSP framework. In Section 7.3, we present the design principles of H2M2 based prediction, following which Section 7.4 presents the elaborate hardware design of H2M2 on FPGA. Thereafter, in Section 7.5, we evaluate the performance of H2M2. Next, Section 7.6 introduces the throughput maximization problem and the proposed solution in the form of the ISPTO algorithm. Section 7.7 elaborates the problem formulation for BCMS and the

proposed solution. Section 7.8 discusses the performance analysis of the CSSP framework. Section 7.9 demonstrates the implementation of CSSP framework in test-bed. Finally, we conclude the chapter in Section 7.10.

7.2 System Model

We consider a centralized overlay CRN with a Cognitive Base Station (CBS) serving multiple SUs as shown in Figure 7.1. Based on the applications, the SUs can be either high-priority (real time or RT) or low-priority (non-RT or NRT) users. We focus on NRT users. Let K denotes the number of NRT users in the CRN. The Primary Network (PN) has multiple non-overlapping orthogonal PU channels of bandwidth W Hz. The occupancy state of a channel due to PU is modeled as a non-time slotted two-state ON/OFF Continuous Time Markov Chain (CTMC) [169, 168, 170]. The durations of PU's ON state (hypothesis H_1 or busy period) and OFF state (hypothesis H_0 or idle period) are represented by exponentially distributed i.i.d. random variables X and Y, with probability density functions $f_X(t) = \lambda e^{-\lambda t}$ and $f_Y(t) = \mu e^{-\mu t}$ having parameters λ and μ respectively. Thus, the average busy period (t_{on}) is $1/\lambda$, and the average idle period (t_{off}) is $1/\mu$. Therefore, the probability of a channel being busy, simply termed as PU activity, is denoted by $P(H_1) = \dfrac{t_{on}}{t_{on}+t_{off}}$. While the idle channel probability is $P(H_0) = \dfrac{t_{off}}{t_{on}+t_{off}}$. It is assumed that the CBS retrieves the PU channel occupancy data, t_{on} and t_{off} from an external entity such as a white space database [206, 207]. Further, to provide channel access to NRT SUs, along with the retrieved PU activity information the CBS performs spectrum sensing and prediction using a proposed H2M2 engine over select *predictable* channels.

As discussed above, the CBS performs prediction only over selected channels, also known as *predictable* channels. A predictable channel is defined as a channel where H2M2 can efficiently predict the PU presence while minimizing the interference between SU and PU within a predetermined threshold. Let F denotes the number of such predictable channels. The CBS utilizes the PU activity information (from database) and the detected PU SNR and then classifies the channel as predictable based on our proposed *Inter Sensing-Prediction Time Optimization (ISPTO) algorithm*. ISPTO algorithm also determines the optimal inter sensing-prediction time for the predictable channels, that maximizes the SU throughput within the PU interference threshold. It will be shown later through performance analysis that the predictable channels are characterized by high PU activities within a certain range, that depends on the PU SNR. It is worth mentioning that, high PU activity channels cannot satisfy strict RT requirements like high throughput and low delay. However, by exploiting

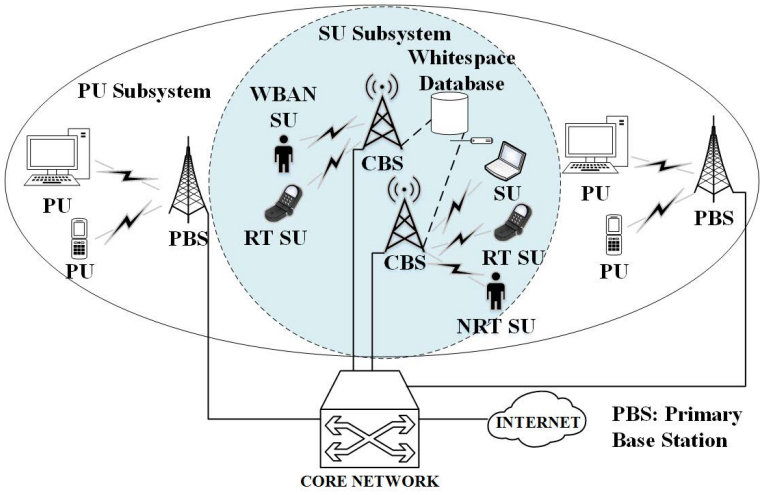

Fig. 7.1 Centralized cognitive radio network architecture.

the developed framework, the predictable channels are able to provide highly reliable and energy-efficient communication for NRT SUs.

7.2.1 Centralized Scheduling, Sensing and Prediction (CSSP) Framework

The time-line of the proposed *CSSP framework* is shown in Figure 7.2. It is assumed that a common control channel is available to the SUs at any time [208, 44]. Each SU is equipped with a single half-duplex radio [85], which can either transmit or receive/sense, but not both at the same time. To obtain a data channel for transmission, a SU upon reception of a beacon sends a channel request to the CBS over the control channel and waits for a successful channel assignment message. An NRT user SU_i in its channel request includes its state $[D_i]$. $[D_i]$ is the number of data bits that SU_i needs to send. For example, a WBAN Controller needs 6.4kb data to transmit a recorded 2 second electrocardiogram (ECG) signal captured at 200Hz. The CBS after gathering all the information from the NRT SUs, determines a transmission schedule applying a proposed scheduling policy and broadcasts it to the NRT users via channel assignment messages. In this regard, we propose the *Battery Consumption Minimizing Scheduler (BCMS)* that utilizes the information generated from ISPTO algorithm to assign suitable predictable channels to the NRT SUs so as to minimize the total battery consumption. The channel assignment message contains information about the granted channel, if any, and the derived optimal inter sensing-prediction duration T_D^*. It comes as a straight forward deduction that the CSSP framework also improves the spectral efficiency of CRN. The improvement is an effect of assigning the NRT users to un-utilized predictable high PU activity channels while the RT users use the traditional low PU activity channels. More

in detail, if the channel request comes from a RT SU, CBS assigns them non-predictable low PU activity channels. Following which, the RT SUs follow traditional sensing-transmission policies like BSS or CSS. Figure 7.3 shows the several functional entities of CBS where the CSSP framework is incorporated at the MAC layer and the H2M2 engine is developed at the PHY core of CBS.

When a predictable channel is assigned, the NRT SU waits (in sleep state) for the CBS to i) complete spectrum sensing, and ii) predict the PU channel occupancy state in the next sensing instant using the H2M2 engine. Based on the current sensing and prediction result, CBS informs the decision '*transmit*' over the control channel to the SU, which wakes up to receive and act on the decision. If $transmit = 1$, the NRT SU transmits its data to the CBS over the assigned channel. In the event when $transmit = 0$, the SU defers transmission (sleeps) until the *transmit* bit is HIGH. The developed sensing-transmission-prediction cycle is shown in Figure 7.2 and highlighted next.

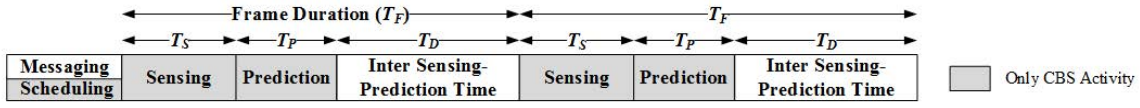

Fig. 7.2 Timeline of the proposed CSSP framework.

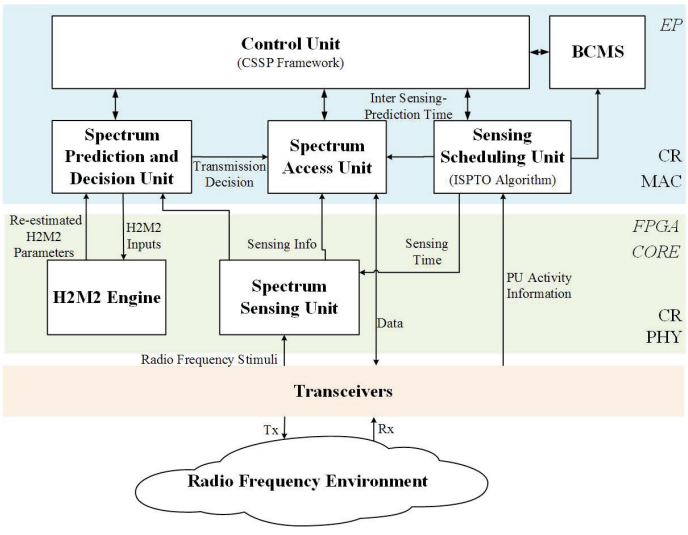

Fig. 7.3 Functional block diagram for the CBS.

7.2.2 Sensing-Prediction-Transmission Cycle: Modified CR Frame

Spectrum sensing is performed to provide protection against arrival of incumbent PUs in a channel. Traditionally, spectrum sensing is followed by transmission. However, due to

the presence of noise, spectrum sensing cannot guarantee a certain detection of the ON and OFF states. This uncertainty in sensing observations often leads to collision between SU and PU transmissions causing bit-level errors and energy loss for the SUs. In order to minimize these uncertainties in sensing decisions we introduce prediction between sensing and transmission as shown in Figure 7.2. The CBS and SU employ a time slotted protocol over the predictable PU channels with frame duration $T_F > 0$. The sensing duration is denoted by T_S, the prediction time by H2M2 is represented by T_P, and T_D denotes the inter sensing-prediction time. The SUs transmit during T_D depending on the CBS decision. We assume that the control messaging period is significantly shorter as compared to other periods.

7.2.2.1 Sensing

It is reasonable to assume that the CRN does not have a priori knowledge of the PU signal characteristics such as the modulation type, packet format or pulse shape. In this scenario, the optimal detector is an energy detector [160], which is also one of the most commonly used detection technique in CRNs [83]. The energy detector performs non-coherent signal detection by integrating squared versions of received signal samples. The PU signal is detected by comparing the received signal energy with a threshold computed using an estimated noise power as described in Section 4.2. The detection threshold (λ_{th}) of the CBS, in the presence of white Gaussian noise at the receiver, can be represented as,

$$\lambda_{th} = \sqrt{2N_S N_0^2} Q^{-1}(P_f) + N_S N_0 \tag{7.1}$$

where N_S denotes the number of received samples used for detection, N_0 represents the noise power calculated at the receiver and P_f is the false-alarm probability constraint [160] for the system.

Using the threshold obtained in (7.1), the CBS can detect the presence of PU with detection probability P_d [160], given as (Section 4.2.2),

$$P_d = Q\left(\frac{\lambda_{th} - N_S N_0(1+\gamma_{PU})}{\sqrt{2N_S}N_0(1+\gamma_{PU})}\right) \tag{7.2}$$

where γ_{PU} is the PU SNR detected at the CBS, $Q(\cdot)$ is the Q-function.

Thus, the number of samples required for the CBS to sense a PU signal at minimum PU SNR, $\gamma_{PU,min}$ (also known as receiver sensitivity) with a detection probability $P_d = \chi$ under the false-alarm constraint $P_f = \kappa$ can be obtained using (7.1) and (7.2) as,

$$N_S = 2 \times \left[\left\{ Q^{-1}(\kappa) - (1+\gamma_{PU,min})\, Q^{-1}(\chi) \right\} / \gamma_{PU,min} \right]^2 \tag{7.3}$$

Using N_S obtained in (7.3) we can calculate the sensing time T_S based on the ADC frequency of the CR radio module. This is described later in Section 7.8.

7.2.2.2 Prediction

A closer look at (7.2) reveals that, due to the presence of noise there is a possibility of miss-detection of PU. This causes transmission on the channel even when the PU is present, leading to collision and wastage of energy. To this end, we propose to reduce the miss-detection probability (P_m) through the incorporation of prediction. The fundamental principle behind prediction using H2M2 is through observation (sensing) over the most recent N sensing slots and predicting the presence of PU in the next i.e. $(N+1)^{\text{th}}$ sensing instant.

It is worth emphasizing that, if the prediction was performed by the NRT SUs, it would require them to sense a channel in every CR frame to generate the most recent N sensing observations. However, NRT users like those in WBAN transmit small amounts of data at regular intervals in the range of hours. Thus, observing the channel continuously even when there is no data to send will not meet the energy-efficiency requirements of such battery operated NRT users. This justifies our proposition of centralized sensing and H2M2 based prediction at the CBS. In the following section, we describe the design of the H2M2 engine and the detailed operating principle behind prediction.

7.3 Design Principle of H2M2 Predictor

The H2M2 engine is based on the principle of HMM to predict PU arrivals using the past observations with intelligent decisions for PU's presence and absence in the next sensing instant. HMM prediction is a highly intensive process that can consume significant amount of time. This has an impact on the energy-efficiency of the CR frame when we integrate prediction within the sensing transmission cycle of our CSSP framework. To address this concern, we developed an H2M2 engine at the PHY layer FPGA core. The proposed H2M2 engine minimizes the prediction significantly. This is achieved by 1) reducing the total number of cycles through parallel processing and efficient pipelining, and 2) operating the model at free running speed of FPGA processor without setup and hold time violations while still interacting with a slow MAC processor of CBS. In this section, we briefly describe the principle of prediction process in H2M2, and in the next section we provide an detailed description of the design.

7.3.1 Working Principle of H2M2

The conceived H2M2 engine has been put into effect according to its integration within the CSSP framework as illustrated in Figure 7.4a. The input and output ports of H2M2 engine are shown in Figure 7.4b. As shown, the sensing observation O is sent from the sensing unit through MAC layer to the H2M2 engine (Figure 7.3). In addition, the channel transition probabilities $A = (a_{ij}, i, j = \{1,2\})$, observation probabilities $B = (b_{ij}, i, j = \{1,2\})$ and initial steady-state distribution $\pi = (\pi_i, i = \{1,2\})$ [101] are also communicated to H2M2. These HMM parameters are further illustrated in Figure 7.5. a_{ij} denotes the probability of transition from channel State-i in the present sensing instant to channel State-j in the next sensing instant. Where, State-1 ($S^{(1)}$) corresponds to OFF state and State-2 ($S^{(2)}$) corresponds to ON state. The state transition probabilities can be expressed in matrix form [84] as,

$$A = \begin{bmatrix} a_{11} & a_{12} \\ a_{21} & a_{22} \end{bmatrix} = \frac{1}{\lambda+\mu} \begin{bmatrix} \lambda+\mu e^{-(\lambda+\mu)T_F} & \mu-\mu e^{-(\lambda+\mu)T_F} \\ \lambda-\lambda e^{-(\lambda+\mu)T_F} & \mu+\lambda e^{-(\lambda+\mu)T_F} \end{bmatrix} \tag{7.4}$$

When the channel is in OFF state at time t_0, then the probability of PU being OFF at time $t_0 + T_F$, i.e. a_{11} is given by the upper left entry in the transition matrix, i.e. $\frac{1}{\lambda+\mu}\left(\lambda+\mu e^{-(\lambda+\mu)T_F}\right)$.

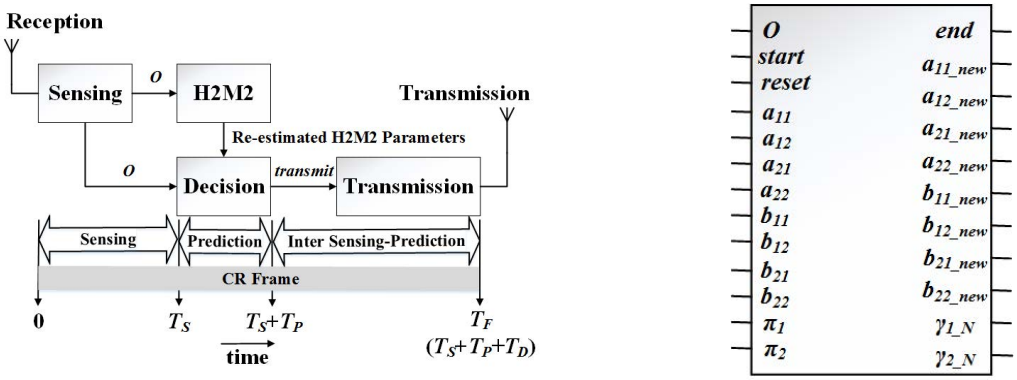

(a) (b)

Fig. 7.4 (a) CR frame in CSSP framework with H2M2, (b) H2M2 engine

Further, b_{12} represents the false-alarm probability (P_f) of observing State-2 when the channel is in State-1. Therefore, b_{11} is equal to $\left(1-P_f\right)$. Similarly, b_{22} and b_{21} are the detection probability P_d and miss-detection probability $P_m = (1-P_d)$ respectively. Lastly, π_i denotes the probability of being in State-i at the beginning of a prediction cycle.

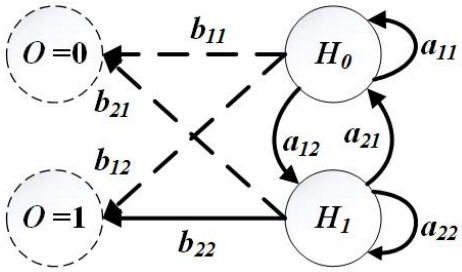

Fig. 7.5 Hidden Markov model for cognitive radio.

Since the FPGA is operated in free running mode, the front end of H2M2 is designed to collect observations from the slow MAC processor and store them in a FIFO register. Upon applying a pulse to the positive edge triggered *start* port, every new observation O from the sensing unit is stored in this FIFO register. Prediction starts after the FIFO register is full. Thereafter, every new observation replaces the oldest value in the FIFO, and H2M2 provides prediction results for the next sensing slot.

The output ports represent re-estimated values of a_{ij}, b_{ij} indicated by a_{ij_new}, b_{ij_new} respectively, where $i, j = \{1,2\}$. γ_{1_N} and γ_{2_N} are the respective estimated probabilities of being in State-1 and State-2 at N^{th} sensing instant. The optimal re-estimated parameters are obtained after I iterations and then sent to the decision unit (Figure 7.3) to predict the most probable observation in the next sensing slot.

7.3.2 Decision Process

H2M2 aims at predicting the observation at the next sensing instant. Consider the following observation sequence $\mathbf{O} = \{O_1, O_2, \cdots, O_N\}$ representing the most recent N sensing results. The idle and busy sensing decisions are represented by 0 and 1 respectively. Let $P(O_{N+1} = 0|\mathbf{O}, \Lambda)$ and $P(O_{N+1} = 1|\mathbf{O}, \Lambda)$ denote the probabilities of observing an idle and busy state respectively at the $(N+1)^{\text{th}}$ instant given the observation sequence $\mathbf{O}$ and HMM model $\Lambda = \langle A, B, \pi \rangle$. Then the prediction rule can be given by,

$$prediction = \begin{cases} 0, \text{if} P(O_{N+1} = 0|\mathbf{O}, \Lambda) > P(O_{N+1} = 1|\mathbf{O}, \Lambda) \\ 1, \text{if} P(O_{N+1} = 1|\mathbf{O}, \Lambda) \geq P(O_{N+1} = 0|\mathbf{O}, \Lambda) \end{cases} \tag{7.5}$$

More specifically, for the next sensing slot, if the probability of observing an idle state is more than the probability of observing a busy state, then the decision block makes the logical

decision for free channel void of PU. The probabilities in (7.5) can be expressed as,

$$P(O_{N+1}=0|\mathbf{O},\Lambda) = P(H_{0,N+1})b_{11\_new} + P(H_{1,N+1})b_{21\_new} \tag{7.6}$$

$$P(O_{N+1}=1|\mathbf{O},\Lambda) = P(H_{0,N+1})b_{12\_new} + P(H_{1,N+1})b_{22\_new} \tag{7.7}$$

Where, $P(H_{0,N+1})$ and $P(H_{1,N+1})$ are the probabilities that the channel states at $(N+1)^{\text{th}}$ sensing slot are H_0 and H_1 respectively. If S_i denotes the channel state during i^{th} sensing instant then,

$$P(H_{0,N+1}) = P(S_{N+1}=0|\mathbf{O},\Lambda) = \gamma_{1\_N}a_{11\_new} + \gamma_{2\_N}a_{21\_new} \tag{7.8}$$

$$P(H_{1,N+1}) = P(S_{N+1}=1|\mathbf{O},\Lambda) = \gamma_{1\_N}a_{12\_new} + \gamma_{2\_N}a_{22\_new} \tag{7.9}$$

Based on the values of O and $prediction$, the decision block prepares its decision variable $transmit$ to be communicated to the NRT SU. Then $transmit = 1$ is only possible iff the present observation is 0 and it is predicted that there will be no PU arrival during SU transmission. For all other cases $transmit = 0$. This can be represented as,

$$transmit = 1 \text{ iff } O = 0 \text{ and } prediction = 0 \tag{7.10}$$

At a finer level of detail, (7.10) implies that even in the event of a miss-detection, the probable collision between SU and PU transmissions can be averted if H2M2 correctly predicts the presence of PU in the channel. Thus, the effective miss-detection probability is reduced. In Section 7.5, we evaluate the performance of H2M2 in avoiding the miss-detections and creating transmission opportunities.

7.4 H2M2 Design

The designed H2M2 engine operates on fixed point data because fixed-point calculations require less memory and less processor time to perform. Also, the logic circuits of fixed-point hardware are much less complicated than those of floating-point hardware. In H2M2, for high accuracy we use a 16-bit fixed point precision with 14-bit binary point. The block diagram of this design is shown in Figure 7.6. The design comprises of a data flow path and a control flow path. Both the paths are closely interlinked with message interchange. Each submodule remains in standby mode and will start its activities when triggered by an event that may come from some other submodule. Once activated, it will run independent of other blocks. Hence, careful study of the clock cycles is required to align the activities of different blocks of H2M2. The details of these sub-blocks are discussed below.

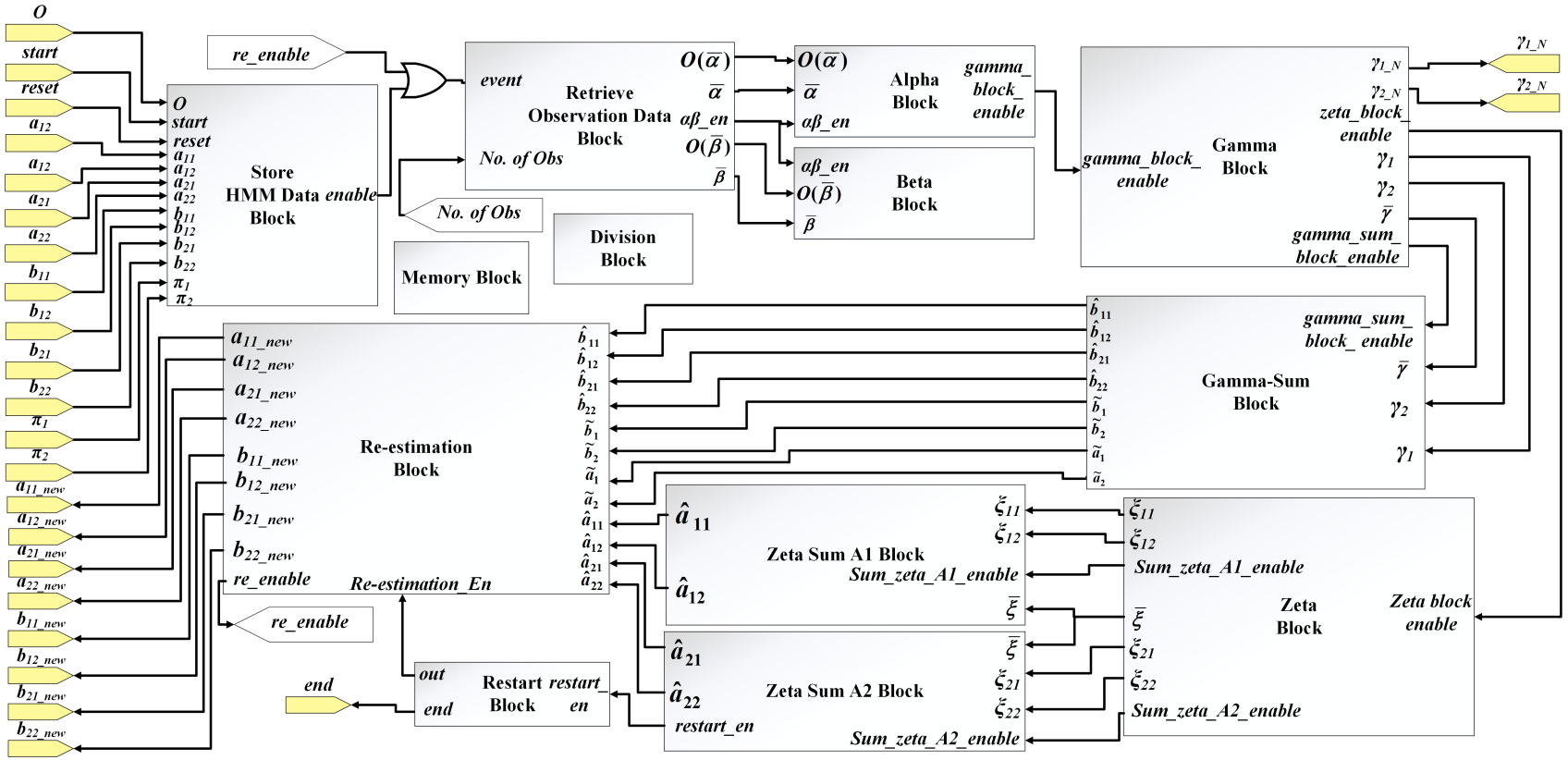

Fig. 7.6 Block Diagram of H2M2 Circuit.

7.4.1 Memory Block

The memory block in H2M2 consists of the read and write circuitry associated with the following shared memories:

- O-Block- N registers for storing N observations
- $\langle a_{11}\rangle, \langle a_{12}\rangle, \langle a_{21}\rangle, \langle a_{22}\rangle$- stores state transition probabilities a_{11}, a_{12}, a_{21} and a_{22} respectively.
- $\langle b_{11}\rangle, \langle b_{12}\rangle, \langle b_{21}\rangle, \langle b_{22}\rangle$- stores observation probabilities b_{11}, b_{12}, b_{21} and b_{22} respectively.
- $\langle \pi_1\rangle, \langle \pi_2\rangle$ - stores steady state probabilities π_1 and π_2 respectively.
- $\langle \alpha_1\rangle, \langle \alpha_2\rangle$ - stores forward probabilities $\alpha_1(i)$ and $\alpha_2(i)$ respectively, $i = 0, 1, \cdot\cdot, T-1$;
- $\langle \beta_1\rangle, \langle \beta_2\rangle$ - stores backward probabilities $\beta_1(i)$ and $\beta_2(i)$ respectively, $i = 0, 1, \cdot\cdot, T-1$;

Figure 7.7 shows the general circuitry for data read and writes operations for a memory in H2M2. The circuit of Figure 7.7 allows different submodules to access the same shared memory at different times. In Figure 7.7, the memory is accessed by P number of submodules at disjoint time instants. Most of the submodules perform only read operation except submodule-1 that needs to write data onto the memory. When submodule-j wants to read a data, it makes its *enable line* (enj) high which enables the memory. At the same time a encoder gives an output 'j' that selects the corresponding address line $addj$ and the data is read out of the location mentioned in $addj$. Thereafter, the read data is passed on to the output line rj, which is then utilized by submodule-j. Similarly, for write operation first $dataj$ is written when *write enable* (wr_enj) signal is set to HIGH and then read out.

In Figure 7.7, it is shown how the multiple address lines from different submodules are multiplexed with the help of encoder and a multiplexer. However, $\langle b_{i1}\rangle$ and $\langle b_{i2}\rangle$, $i = 1, 2$ are both enabled at the same time but depending on the selected address i.e. 0 or 1 (which is the value of an observation) the output of one is passed. For instance, $\langle b_{i1}\rangle$ is chosen if the selected address is 0 or else $\langle b_{i2}\rangle$ is selected. Therefore, b_{ij} is also represented as $b_i(O_k)$, which means the outputs of $\langle b_{i1}\rangle$ or $\langle b_{i2}\rangle$ will be selected depending on whether the observation at k^{th} instant is 0 or 1 respectively.

7.4.1.1 O-Memory Block

The O-memory block is a specially designed set of N registers (FIFO) that holds the most recent N observations. The loading of observations into these registers was explained in Section 7.3.1 and the circuit diagram is shown in Figure 7.8a. In this regard, for illustration we consider $N = 100$. The loading of the registers is coupled with O_{en} signal, which is explained in the next sub-section.

The read circuitry of O-block is similar to that shown in Figure 7.7. However, since O-block is not a single memory but a collection of *N* registers, the 'Memory' in Figure 7.7 will be replaced by Figure 7.8b. For representing 100 registers minimum address width of seven (D0-D6) will be required. To read one particular register, these address lines need to be de-multiplexed. For this purpose, design of Figure 7.8b has been based on the basic concepts of address de-multiplexing.

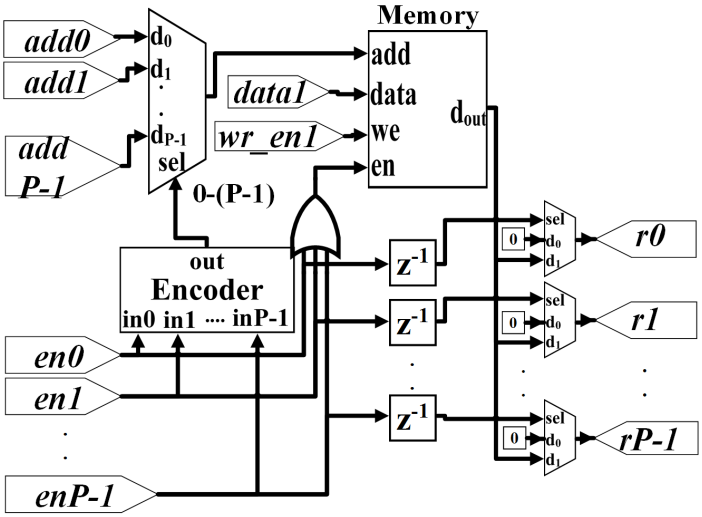

Fig. 7.7 Generalised read and write circuitry for memory blocks in H2M2.

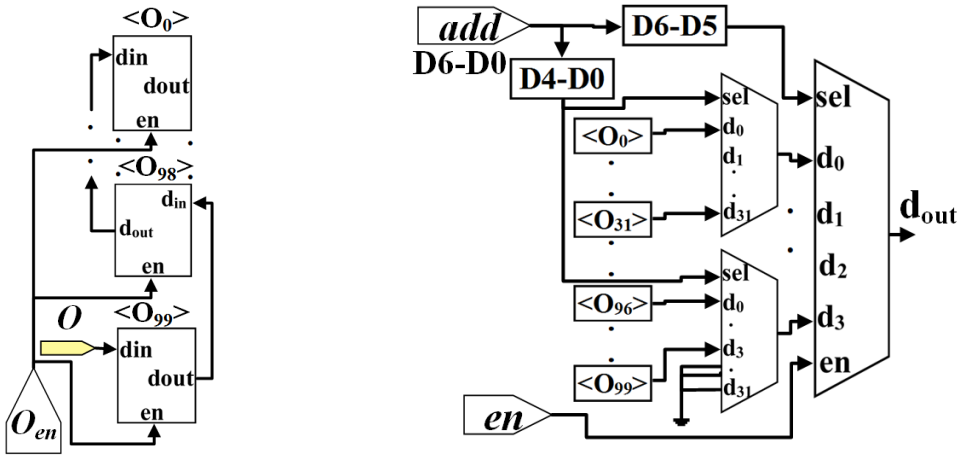

(a) (b)

Fig. 7.8 Design of O-Block for (a)Write, (b)Read.

7.4.2 Store HMM Data Block

This block primarily deals with storing of the observations coming from the sensing module in to observation memory block (O Block). However, since the FPGA is operated in free running mode, the front end of this block has been designed such that data can be collected from the slow processor (sensing module) which sends observation data to it.

7.4.2.1 Front End

This front end is instrumental in operating FPGA in free running mode while still interacting with a slow speed processor, like a computer over Ethernet connection or an embedded soft-core processor, which traditionally is a major bottleneck in such communications. This is possible by making the front end positive edge-triggered. The circuit and its corresponding timing diagram are shown in Figure 7.9.

In Figure 7.9a, each new observation O is coupled with a *start* signal. A textitstart signal comprises of 1,0 series. When *start* goes to '1' from '0' a pulse is generated that increments the accumulator (Acc.). Acc. keeps track of the total number of observation samples. It is primarily required after a *reset* pulse is applied when entire O-block is empty. If the Acc.

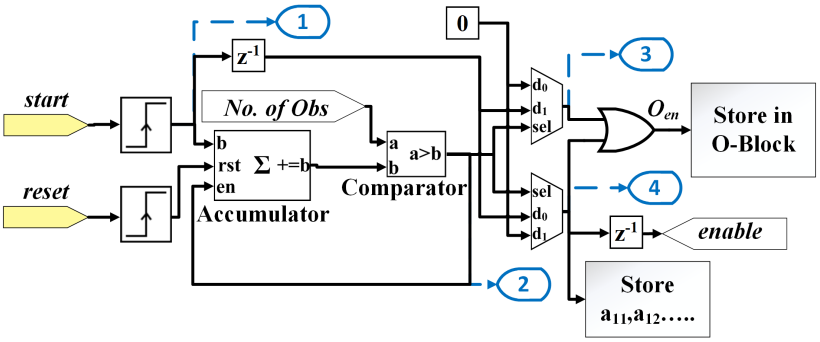

(a)

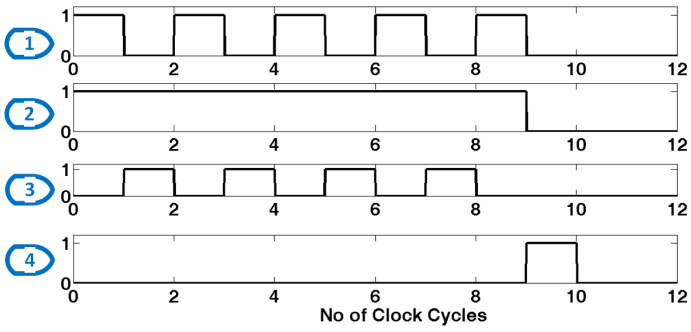

(b)

Fig. 7.9 Edge-triggered front-end- (a) Circuit diagram, (b) Timing Diagram.

count is less than the number of observations (N) then the 'd1' of upper MUX is active and the new observations are loaded into the observation matrix. In this case there is no prediction as the *enable* line is not activated. However, for the N^{th} and subsequent observations the positive edge of the start pulse is directed through 'd0' of lower MUX to store the present observation in the O-block along with storing of initial values of A, B, π in their respective shared memories and initialization of other shared memories like $\langle \alpha_i \rangle, \langle \beta_i \rangle$ memories. This pulse is then propagated through the *enable* line and passed on to next block i.e. Retrieve Observation data and the prediction process begins. Figure 7.9b shows the timing diagram of this operation. For illustration, N is assumed to be equal to 5. The *reset* input is required to set the accumulator back to zero, when the entire process needs to be initialized again.

7.4.3 Retreive Observation Data Block

This block deals with generating the time-indices $\overline{\alpha}$ and $\overline{\beta}$ needed for the operation of Alpha Block and Beta Block respectively. It also responsible for retrieving the observation values corresponding to $\overline{\alpha}$ and $\overline{\beta}$ and passing them on respectively to Alpha and Beta blocks. These observation values can be denoted as $O(\overline{\alpha})$ and $O(\overline{\beta})$ respectively. The most important circuit of this block is the Driving Circuit, which drives the operation of both Alpha and Beta blocks.

7.4.3.1 Driving Circuit

The driving circuit is a pulse generator that generates consecutive pulses of one timer clock cycle (1T) every 8T, and it allows for pipelining of different operations of Alpha and Beta blocks. The operation of the driving circuit can be explained from the AND gate in Figure 7.10. An *event* is said to occur (HIGH) when either *enable* from 'Store HMM Block' OR *re-enable* from 'Re-estimation Block' is HIGH. The HIGH *enable* signal is latched on by LATCH 1, fed onto the AND gate and also activates a free-running 7-bit counter.

The 3$^{\text{rd}}$ bit from the LSB is fed onto an inverter followed by a negative edge triggered circuit. This output has a period of 8T and is connected to the input of the AND gate. The output of the AND gate, denoted by $\alpha\beta\_en$ activates the 'Alpha and Beta Blocks'. So in this manner a train of N pulses are generated at an interval of 8T. The second counter in the circuit is part of a negative feedback and gives the count of the generated pulse. This later serves as an address, A, where $0 \leq A \leq N-1$ for retrieval of values from various memory blocks. After the N^{th} pulse- i) the output of the comparator becomes LOW, ii) the AND gate is disabled, and iii) the free running counter is disabled and reset, ready for the next *event* to occur.

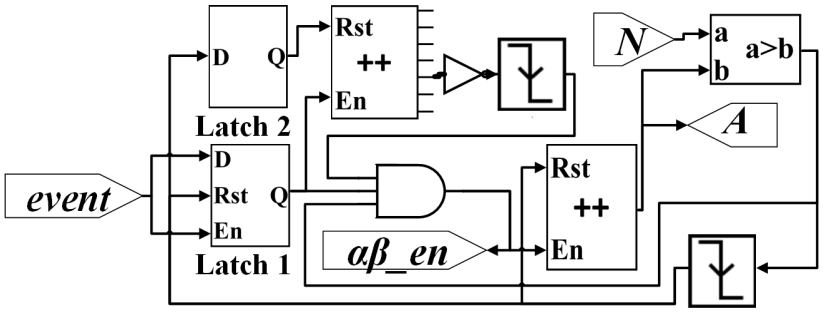

Fig. 7.10 Driving Circuit.

7.4.3.2 Generation of Alpha and Beta Block Time Indices

The address A has been generated to help in obtaining $\overline{\alpha}$ and $\overline{\beta}$, as shown below,

$$\overline{\alpha} = A, \qquad 0 \leq A \leq N-1 \tag{7.11}$$

$$\overline{\beta} = N-(A+1), \qquad 0 \leq A \leq N-1 \tag{7.12}$$

Since $\overline{\alpha}$ is the time-index for alpha block, it goes from 0 to $N-1$ in the forward direction. Similarly for the beta bock, $\overline{\beta}$ moves in the backward direction i.e. from $N-1$ to 0.

7.4.4 Alpha and Beta Block

7.4.4.1 Alpha Block

The alpha block calculates the forward variables [101],

$$\alpha_i(\overline{\alpha}) = P(O_1, O_2, ..., O_{\overline{\alpha}+1}, S_{\overline{\alpha}+1} = S^{(i)}|\Lambda), \quad i = 1,2 \tag{7.13}$$

where, $0 \leq \overline{\alpha} \leq N-1$. $\alpha_i(\overline{\alpha})$ is the probability of the partial observation sequence being $O_1, O_2, \cdots O_{\overline{\alpha}+1}$ from time 1 to $\overline{\alpha}+1$ and state $S_{\overline{\alpha}+1} = S^{(i)}$ at time $\overline{\alpha}+1$ given the HMM model Λ. $\alpha_1(\overline{\alpha})$ and $\alpha_2(\overline{\alpha})$ can be solved inductively as :

$$Initialization : \alpha_i(0) = \pi_i \times b_i(O_1), \quad i = 1,2 \tag{7.14}$$

$$Induction : (\text{for} \, 1 \leq \overline{\alpha} \leq N-1)$$

$$\alpha_1(\overline{\alpha}) = [\alpha_1(\overline{\alpha}-1) \times a_{11} + \alpha_2(\overline{\alpha}-1) \times a_{21}] \times b_1(O_{\overline{\alpha}+1}) \tag{7.15}$$

$$\alpha_2(\overline{\alpha}) = [\alpha_1(\overline{\alpha}-1) \times a_{12} + \alpha_2(\overline{\alpha}-1) \times a_{22}] \times b_2(O_{\overline{\alpha}+1}) \tag{7.16}$$

$$\alpha_i(\overline{\alpha}) = \alpha_i(\overline{\alpha}) / [\alpha_1(\overline{\alpha}) + \alpha_2(\overline{\alpha})] \quad i = 1, 2 \tag{7.17}$$

where $\alpha_i(\overline{\alpha}-1)$ and a_{ij} in the right hand side of (7.15) and (7.16) are obtained by reading $\langle\alpha_i\rangle$ and $\langle a_{ij}\rangle$ and the outcome of these operations are stored in their respective memory blocks through write operations. For example, $\alpha_i(\overline{\alpha}), i = 1,2$ that are obtained in (7.15)-(7.16) are written and updated in their respective memories $\langle\alpha_i\rangle$ at address $\overline{\alpha}$. Similar logic holds for all the equations in the sub-sections that follow. The address corresponding to a time will be one less as addresses start from '0' whereas time begins from '1'.

7.4.4.2 Beta Block

The beta block calculates the forward variables [101],

$$\beta_i(\overline{\beta}) = P(O_{\overline{\beta}+2}, O_{\overline{\beta}+3}, ..., O_N | S_{\overline{\beta}+1} = S^{(i)}, \Lambda), \quad i = 1,2 \tag{7.18}$$

where, $N-1 \geq \overline{\beta} \geq 0$. $\beta_i(\overline{\beta})$ is the probability of partial observation sequence being $O_{\overline{\beta}+2}, O_{\overline{\beta}+3}, ..., O_N$ from time $\overline{\beta}+2$ to N, given state $S_{\overline{\beta}+1} = S^{(i)}$ with the HMM model being Λ. $\beta_1(\overline{\beta})$ and $\beta_2(\overline{\beta})$ can be solved inductively, as follows:

$$Initialization : \beta_i(N-1) = 1, \quad i = 1,2 \tag{7.19}$$

$$Induction : (\text{for } N-2 \geq \overline{\beta} \geq 0)$$

$$\beta_1(\overline{\beta}) = a_{11}b_1(O_{\overline{\beta}+2})\beta_1(\overline{\beta}+1) + a_{12}b_2(O_{\overline{\beta}+2})\beta_2(\overline{\beta}+1) \tag{7.20}$$

$$\beta_2(\overline{\beta}) = a_{21}b_1(O_{\overline{\beta}+2})\beta_1(\overline{\beta}+1) + a_{22}b_2(O_{\overline{\beta}+2})\beta_2(\overline{\beta}+1) \tag{7.21}$$

$$\beta_i(\overline{\beta}) = \beta_1(\overline{\beta})/[\beta_1(\overline{\beta}) + \beta_2(\overline{\beta})] \tag{7.22}$$

Equations (7.17) and (7.22) are essentially scaling operations needed to keep the values of α_i and β_i within the precision range, otherwise these values tend to zero as N tends to a large number (>10) [101]. Moreover, (7.17) and (7.22) are also division operations, and any divider circuit is very resource intensive. A single divider needs 9 DSP blocks, so H2M2 can have at most two such dividers, and this comprises the *division block*. Thus, at a single instant the division block can perform two simultaneous division operations which take 4T. Therefore, the two alpha block operations of (7.17) that uses the division block would take 4T, followed by the beta block operations of (7.22). Further, when the beta block is using the division block, alpha block is performing its operations characterized by (7.15) and (7.16) thereby enabling pipelining. This is the reason behind setting the period of the driving circuit at 8T in Section 7.4.3.1. Figure 7.11 illustrates this pipelining between alpha and beta blocks. Once $\overline{\alpha}$ reaches $N-1$, *gamma_block_enable* is set to one and operation is transferred to gamma block.

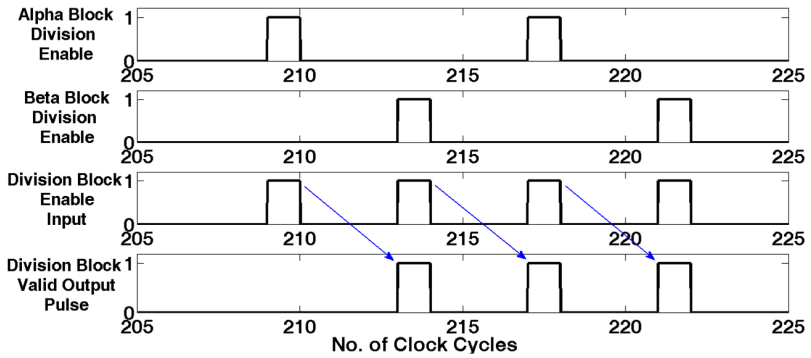

Fig. 7.11 Timing diagram of pipelining between alpha and beta blocks.

7.4.5 Gamma and Gamma-Sum Block

7.4.5.1 Gamma Block

The gamma variable $\gamma_i(\overline{\gamma})$, where $0 \leq \overline{\gamma} \leq N-1$ is given as,

$$\gamma_i(\overline{\gamma}) = P(S_{\overline{\gamma}+1} = S^{(i)}|O,\Lambda), \quad i = 1,2 \tag{7.23}$$

$\gamma_i(\overline{\gamma})$ is the probability of being in state $S^{(i)}$ at time $\overline{\gamma}+1$ given the observation sequence O, and the model Λ. Mathematically, this can be expressed as,

$$\gamma_i(\overline{\gamma}) = \frac{\alpha_i(\overline{\gamma}) \times \beta_i(\overline{\gamma})}{\sum_{i=1}^{2} \alpha_i(\overline{\gamma}) \times \beta_i(\overline{\gamma})}, \quad i = 1,2 \tag{7.24}$$

Similar to Alpha and Beta sub-modules, Gamma block also has a driving circuit like in Section 7.4.3 which generates the time index $\overline{\gamma}$ that drives the operations expressed in (7.24) along with gamma-sum block operations. Equation (7.24) represents two operations that are performed by the division block simultaneously. Since there is no need for pipelining, the time-period of driving circuit in gamma block is set as 4T. After (7.24), each $\gamma_i(\overline{\gamma})$ is transferred to gamma-sum block. The output ports γ_{1_N} and γ_{2_N} represent $\gamma_1(N-1)$ and $\gamma_2(N-1)$ respectively. After $\overline{\gamma}$ reaches $N-1$, the functions of gamma and gamma-sum blocks are over and gamma block sets *zeta_block_enable* to 1 and H2M2 moves on to Zeta Block.

7.4.5.2 Gamma-Sum Block

The function of gamma-sum block is to receive the values of gamma variables from gamma-block and perform summation operations using accumulators over $0 \leq \overline{\gamma} \leq N-1$ and store

the results in registers to be utilized later by Re-estimation block. These are represented in (7.25)-(7.27) from the concept of counting event occurrences.
Expected number of transitions from state $S^{(i)}$,

$$\tilde{a}_i = \sum_{\overline{\gamma}=0}^{N-2} \gamma_i(\overline{\gamma}), \quad i = 1,2 \tag{7.25}$$

Expected number of times in state $S^{(i)}$ and observing state j,

$$\hat{b}_{ij} = \sum_{\substack{\overline{\gamma}=0 \\ O_{\overline{\gamma}+1} = j \oplus 1}}^{N-1} \gamma_i(\overline{\gamma}), \quad i,j = 1,2 \tag{7.26}$$

Expected number of times in state $S^{(i)}$,

$$\tilde{b}_i = \sum_{\overline{\gamma}=0}^{N-1} \gamma_i(\overline{\gamma}), \quad i = 1,2 \tag{7.27}$$

The nomenclature of the variables in (7.25)-(7.27) will be clear after Section 7.4.8, which deals with the re-estimation block.

7.4.6 Zeta, Zeta-Sum A1 and Zeta-Sum A2 Block

7.4.6.1 Zeta Block

The HMM model parameters need to be re-estimated so as to maximize the probability of observation sequence given the model, $P(O|\Lambda)$ [101]. $P(O|\Lambda)$ can be locally maximized using an iterative procedure like Baum-Welch method. Zeta variables are defined as,

$$\xi_{ij}(\overline{\xi}) = P(S_{\overline{\xi}+1} = S^{(i)}, S_{\overline{\xi}+2} = S^{(j)}|O,\Lambda), \quad i,j = 1,2 \tag{7.28}$$

$\xi_{ij}(\overline{\xi})$ is the probability of being in state $S^{(i)}$ at time $\overline{\xi}+1$, and state $S^{(j)}$ at time $\overline{\xi}+2$, given the model Λ and observation sequence O. It is given as,

$$\xi_{ij}(\overline{\xi}) = \frac{\hat{\xi}_{ij}(\overline{\xi})}{\tilde{\xi}_{sum}(\overline{\xi})}, \quad i,j = 1,2 \tag{7.29}$$

where the numerator is,

$$\hat{\xi}_{ij}(\overline{\xi}) = \alpha_i(\overline{\xi}) \times a_{ij} \times b_j(O_{\overline{\xi}+2}) \times \beta_j(\overline{\xi}+1) \tag{7.30}$$

and the denominator is given as,

$$\tilde{\xi}_{sum}(\overline{\xi}) = \sum_{i=1}^{2}\sum_{i=1}^{2}\left[\hat{\xi}_{ij}(\overline{\xi})\right] \tag{7.31}$$

The driving circuit of Zeta block is activated when *zeta_block_enable* is set to HIGH. It generates the time index $\overline{\xi}$ that drives the operations of zeta block, zeta-sum A1 and zeta-sum A2 blocks. Equation (7.29) represents four division operations. Since only two division operations can be performed simultaneously in 4T, the time-period of driving circuit is set to 8T to complete all four divisions for a particular $\overline{\xi}$. After $\xi_{1j}(\overline{\xi})$, $j = 1,2$ are obtained simultaneously from (7.29) in the first 4T time duration, they are transferred to Zeta-Sum A1 block. Similarly, after $\xi_{2j}(\overline{\xi})$, $j = 1,2$ are obtained from (7.29) they are transferred to Zeta-Sum A2 block.

7.4.6.2 Zeta-Sum A1 and Zeta Sum A2 Block

Similar to gamma-sum block these sub-modules receive zeta block variables and accumulate them in registers over $0 \leq \overline{\xi} \leq N-2$ for use in the re-estimation process. The zeta-sum A1 operation can be given as,

$$\hat{a}_{1j} = \sum_{\overline{\xi}=0}^{N-2} \xi_{1j}(\overline{\xi}), \quad j = 1,2 \tag{7.32}$$

Similarly, the zeta-sum A2 operations can be given as,

$$\hat{a}_{2j} = \sum_{\overline{\xi}=0}^{N-2} \xi_{2j}(\overline{\xi}), \quad j = 1,2 \tag{7.33}$$

Where $\hat{a}_{ij}$ represents the expected number of transitions from state $S^{(i)}$ to state $S^{(j)}$. Once $\overline{\xi}$ reaches $N-2$ and $\hat{a}_{2j}$ is obtained, *restart_en* is set to 1.

7.4.7 Restart Block

This block checks whether H2M2 has undergone I number of iterations of re-estimations when *restart_en* becomes 1. If I iterations are yet to be completed, *reestimation_enable* is

set to 1 and H2M2 moves to re-estimation block. However, if H2M2 reaches I iterations, *end* is set to 1 and the entire operation of H2M2 ends.

7.4.8 Re-estimation Block

Re-estimation block receives all the variables stored in the registers of gamma-sum block and zeta-sum A1 block and zeta-sum A2 block and performs re-estimation to provide new values of a_{ij}, b_{ij} and $\pi_i, i, j = 1,2$. The new values are represented as a_{ij_new}, b_{ij_new} and π_{i_new} and are written into $\langle a_{ij}\rangle, \langle b_{ij}\rangle$ and $\langle \pi_i\rangle, i, j = 1,2$ respectively overwriting the previous values.

$$a_{ij\_new} = \frac{\hat{a}_{ij}}{\tilde{a}_i}, \quad i, j = 1, 2 \tag{7.34}$$

$$b_{ij\_new} = \frac{\hat{b}_{ij}}{\tilde{b}_i}, \quad i, j = 1, 2 \tag{7.35}$$

$$\begin{aligned} \pi_{i\_new} &= \text{expected number of times in state} S^{(i)} \text{at time} t = 1 \\ &= \gamma_i(0), \quad i = 1, 2 \end{aligned} \tag{7.36}$$

As π_{i_new} in (7.36) is obtained in gamma-block it is written into $\langle \pi_i\rangle$ there. After all the new H2M2 variables have been obtained, *re-enable* is set to 1 for 1T and a new iteration of operations begins from Retrieve Observation Data block.

7.5 Evaluation of H2M2 Performance

In this section, we analyze the ability of H2M2 in i) avoiding miss-detections, and ii) creating transmission opportunities. First, we present two probabilities that quantify these properties. Next, we analyze these metrics for variations in HMM parameters, more specifically the state transition probabilities. The conclusions drawn from the analysis will be utilized in the next section to formulate the ISPTO algorithm for optimizing the inter sensing-prediction duration.

7.5.1 Prediction Performance Metrics

To evaluate the capability of H2M2 in avoiding miss-detections we introduce the metric miss-avoidance probability (P_{ma}), which is defined as,

$$\begin{aligned} P_{ma} &= P(O_{1p}/O^{(0)}, H_1) \\ &= \frac{\text{Events when PU is predicted after miss-detection}}{\text{Events of miss-detetcion}} \end{aligned} \tag{7.37}$$

where O_{xp}, denotes the prediction result, with subscript 'x' replaced by '0' or '1' for predicting PU absence or presence respectively. Similarly, $O^{(x)}$ represents the present sensing result, with subscript 'x' replaced by '0' or '1' for observing PU absence or presence respectively.

Likewise, in order to evaluate the ability of H2M2 in creating transmission opportunities, we introduce the metric probability of transmission opportunity (P_o) and define it as

$$\begin{aligned} P_o &= P(O_{0p}/O^{(0)}) \\ &= \frac{\text{Events when H2M2 decision is to transmit}}{\text{Events when PU is not observed}} \end{aligned} \tag{7.38}$$

Both (7.37) and (7.38) are evaluated through the process of counting event occurrences as explained next.

7.5.2 Analysis of H2M2 Performance

We now present the simulations results for evaluating the probabilities given in (7.37) and (7.38). The simulations are conducted in MATLAB. First, we generate the PU states using the state transition probabilities given in (7.4). Then, we observe the states with detection probability $P_d = 0.9$ and false-alarm probability $P_f = 0.1$ to produce an observation sequence of $N = 100$. The observation sequence is then fed into the H2M2 engine that provides the prediction result after $I = 5$ iterations. We perform 10000 such Monte Carlo simulations to obtain the average probabilities P_{ma} and P_o for a particular set of state transition probabilities defined by the a_{11} and a_{21} values. Figures 7.12a and 7.12b show the variations in P_{ma} and P_o respectively for different values of a_{11} and a_{21}. It is observed that H2M2 offers significant gains in miss-avoidance probability at lower values of a_{11} and a_{21} but at the cost of reduced transmission opportunities.

A closer look at (7.4) reveals that the state transition probabilities depend on both the PU activity and the CR frame duration. More in detail, from Figure 7.12a we note that H2M2 offers better protection (P_{ma}) against miss-detection at higher PU activities. This particular observation is also supported by the findings of Tumuluru et al. in [235] regarding HMM prediction performance. Moreover, this makes H2M2 particularly favorable for NRT SUs. Such SUs can utilize the short spectral gaps of high PU activity channels to transmit their small NRT data with high reliability.

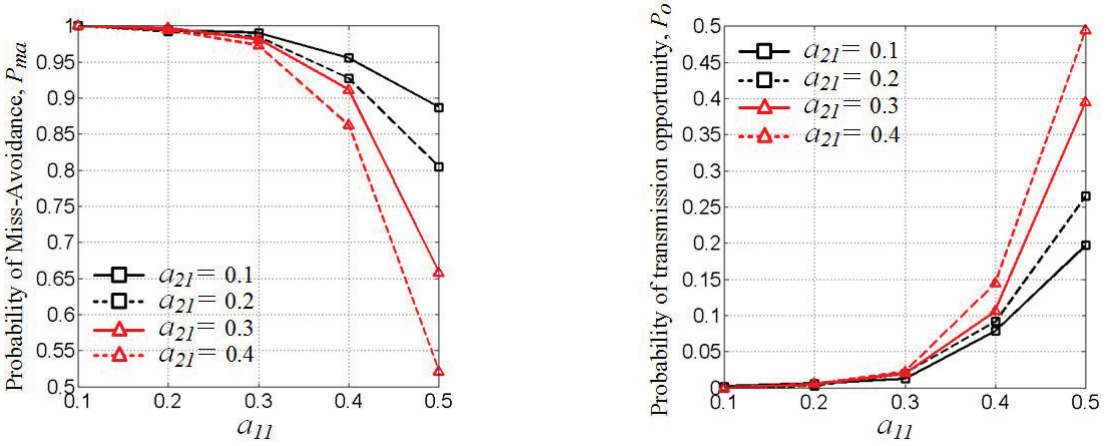

(a) (b)

Fig. 7.12 Variation of (a) P_{ma}, and (b) P_o with respect to transition probabilities a_{11} and a_{21}.

In addition, keeping the PU activity fixed, increasing the frame duration (T_F), more specifically the inter sensing-prediction duration (T_D), causes decrease in a_{11} and increase in a_{21}. Using the state transition probabilities, for a particular PU activity, a_{21} can be related to a_{11} as,

$$a_{21} = \frac{P(H_0)}{P(H_1)}(1 - a_{11}) \tag{7.39}$$

Note that for high PU activities $P(H_0) < P(H_1)$, therefore (7.39) reveals that the effect of T_D is more pronounced in a_{11} than in a_{21}. Therefore, increasing T_D improves P_{ma} but simultaneously decreases the transmission opportunities (P_o). Thus, we observe a trade-off with respect to the selection of inter sensing-prediction duration (T_D). Less T_D leads to better transmission opportunities hence higher throughput, however it also decreases the miss-avoidance probability, thereby increasing the collisions. More collisions lead to more energy consumption. Using the above information, in the next Section, we propose the Inter Sensing-Prediction Time Optimization (ISPTO) algorithm to assign the optimal T_D^* based on the channel PU activity and PU SNR.

Before describing the ISPTO algorithm, it is worth mentioning that the CBS maintains Look-Up Tables (LUTs), that provide the P_{ma} and P_o values of H2M2 for different values of a_{11} and a_{21} corrsponding to specfic detection probabilities $P_d = b_{22}$. The CBS can also employ estimated polynomial expressions of P_{ma} and P_o, but LUT is more accurate and provides better performance. It must be noted that, variations in P_d are an effect of change in detected PU SNR (γ_{PU}) at CBS as per (7.2). We maintain LUTs for $P_d = 0.90, 0.91, \cdots, 1$. Threferefore, the CSSP framework is designed to perform satisfactorily for a PU channel with detected PU SNR $\gamma_{PU} \geq \gamma_{PU,min}$. In our work, we devised such LUTs for $N = 100$, $I = 5$, $\gamma_{PU,min} = -20dB$ and $P_f = \kappa = 0.1$. Further, to avoid very large LUTs we maintain a resolution of 0.01 for a_{11} and a_{21} values. The receiver sensitivity $\gamma_{PU,min}$ and false-alarm constraint are general practices in CR literature [172], while the optimal number of observations (N) and iterations (I) will be validated later through analysis in Section 7.8.

7.6 Optimization of Inter Sensing-Prediction Duration

H2M2 engine aims at reducing the collisions between SU and PU transmissions by minimizing the events of miss-detections in high PU activity channels. An obvious benefit to this is the reduction in wastage of energy for the battery operated NRT SUs. However, H2M2 achieves this at the cost of reduced transmission opportunities. To address this, in this section we propose the ISPTO algorithm that leverages the trade-off between P_{ma} and P_o highlighted in the previous section to determine the optimal inter sensing-prediction duration (T_D^*), which maximizes the throughput while keeping the interference to the PUs within a threshold for a particular high PU activity channel having PU SNR $\gamma_{PU} \geq \gamma_{PU,min}$.

The throughput is represented through a *normalized throughput-time* metric. It is defined as the ratio of the net time available to NRT SUs within a single CR frame for successful transmission without collision to the total frame duration. It can be given as,

$$\mathrm{T} = P_{trans} \frac{T_D - T_C}{T_S + T_P + T_D} \tag{7.40}$$

where, T_S, T_P and T_D are the sensing, prediction and inter sensing-prediction durations respectively. T_C is the expected collision duration within T_D due to interference with the PU and P_{trans} is the probability of transmission over the PU channel. Lastly, we represent the interference to PU due to SU transmission using the *normalized interference duration* metric, which is defined as,

$$\varepsilon = \frac{T_C}{T_D} \tag{7.41}$$

An NRT SU initiates data transmission when the CBS predicts the absence of PU in the next sensing instant and the present observation indicates an ideal state. In this regard, a CBS observes an ideal state under two conditions: i) miss-detection with probability $(1-P_d)$, and ii) not false-alarm with probability $\left(1-P_f\right)$. Then, the transmission probability P_{trans} can be given as,

$$P_{trans} = P_o \left[P(H_0)\left(1-P_f\right) + P(H_1)\left(1-P_d\right)\right] \tag{7.42}$$

Let T_{bc} and T_{ic} denote the average collision durations within the inter-sensing duration T_D, for the above mentioned two cases respectively. The average collision duration (T_C) is derived as in Appendix C.1 and expressed as,

$$T_C = \left(T_{bc} - T_{ic}\right)\left(1-P_{ma}\right)\left(1-P_d\right)P(H_1) + T_{ic}\,P_{trans} \tag{7.43}$$

Zhou et. al in [82] presented the average collision durations T_{bc} and T_{ic} as,

$$T_{bc} = 1/\lambda \left(1 - e^{-\lambda T_D}\right) \tag{7.44}$$

$$T_{ic} = T_D - 1/\mu \left(1 - e^{-\mu T_D}\right) \tag{7.45}$$

Equations (7.44) and (7.45) are derived considering different underlying interfering cases between the SU and PU for the given inter-sensing duration T_D. We draw on the expressions presented in [82], however their occurrence probabilities are modified due to prediction. This is highlighted further in Appendix C.1.

7.6.1 Normalized Throughput-Time Maximization Problem

We formulate the normalized throughput-time maximization problem as follows:

$$\mathbf{P1}: \quad \max_{T_D} \mathrm{T} \tag{7.46}$$

$$s.t. \quad \varepsilon \leq \Gamma \tag{7.47}$$

$$T_D \geq 0 \tag{7.48}$$

where Γ in constraint (7.47) is a predefined normalized interference duration threshold to protect the PU communication. The value of P_f in **P1** is kept equal to the constraint (κ) used for the obtaining the LUTs and deriving the sensing time.

The objective function (7.46) and the constraint (7.47) are non-convex in nature. This is due to the presence of P_{ma} and P_o that are obtained from the LUT of H2M2 for values of a_{11} and a_{21}, that in turn depends on T_D. Therefore, **P1** cannot be solved through classical optimization techniques based on Karush-Kuhn-Tucker (KKT) conditions. Inspecting the nature of T in (7.40) and ε in (7.41), reveals that both are strictly decreasing functions of T_D (see Figure 7.16), such that for $T_{D,1} < T_{D,2}$ we have

$$\mathrm{T}(T_{D,1}) > \mathrm{T}(T_{D,2}) \tag{7.49}$$

$$\varepsilon(T_{D,1}) > \varepsilon(T_{D,2}) \tag{7.50}$$

This observation is in lines with the performance analysis of H2M2 that was as conducted in Section 7.5. Increasing T_D leads to decrease in probability of transmission opportunity (P_o) and thus reduces the throughput-time. On the contrary, the miss-avoidance probability (P_{ma}) increases with increase in T_D, thereby reducing the normalized interference duration. Thus, the optimal solution of **P1** (T_D^*) must lie at the boundary of constraint (7.47), such that,

$$f(T_D^*) = 0 \tag{7.51}$$

where $f(T_D) = \varepsilon(T_D) - \Gamma$. Equation (7.51) can be solved using various root finding numerical techniques available in the literature such as Ridder's method [240], Regula Falsi, Secant Method or Bisection Techniques [241]. Ridder's method has quadratic rate of convergence unlike linear convergence of Regula Falsi. Secant method has the disadvantage that the root does not necessarily remain bracketed, also its convergence rate is 1.618 which is less than that of Ridder's method. Bisection method provides the surest solution, but is extremely slow. Therefore, in this chapter, we use Ridder's method to solve (7.51). The proof of convergence is provided next for the solution to (7.51).

7.6.1.1 Proof of Convergence

The Ridder's method is a powerful and clever modification of the false-position method [241]. The false position method is a bracketing technique, whose convergence is ensured if the length of successive search spaces/brackets for finding the solution of (7.51) decreases with each iteration.

Assuming that the root is bracketed between $(T_{D,1}, T_{D,2})$, i.e. $f(T_{D,1})f(T_{D,2}) < 0$, where $T_{D,1} < T_{D,2}$, the new solution $T_{D,3}$ is

$$T_{D,3} = T_{D,1} + [-f(T_{D,1})] \frac{T_{D,1} - T_{D,2}}{f(T_{D,1}) - f(T_{D,2})} \tag{7.52}$$

Using (7.50) and (7.52), the relation between $T_{D,1}$, $T_{D,2}$ and $T_{D,3}$ can be obtained as,

$$T_{D,2} > T_{D,3} > T_{D,1} \tag{7.53}$$

Depending on whether $f(T_{D,1})f(T_{D,3}) < 0$ or $f(T_{D,2})f(T_{D,3}) < 0$, the root now lies within either $(T_{D,1}, T_{D,3})$ or $(T_{D,3}, T_{D,2})$ respectively. The process now finds the solution within the new brackets having smaller search spaces than the initial one. Therefore, it can be concluded that the strictly decreasing nature of ε in (7.50) ensures convergence of the solution in $O(M)$ time, where M is the number of iterations involved in the root finding technique. We now give our proposed ISPTO algorithm that is based on Ridder's method to obtain the optimal solution to (7.51).

7.6.2 ISPTO Algorithm

The ISPTO algorithm implemented by the CBS operates following the flowchart shown in Figure 7.13 for a PU channel with $\gamma_{PU} \geq \gamma_{PU,min}$. Briefly, at the beginning the initial bracket of the root is found using Binary search [241]. Thereafter, the improved root is obtained using Rider's formula [240]. In this regard, the value of the function $f(T_D)$ is obtained by exploiting the LUT for the current detection probability P_d. Lastly, the root is re-bracketed to find a closer solution. The iterations run till an optimum solution is reached within an error tolerance $\xi_{max} = 10^{-2}$ or the maximum iterations I_R are exhausted. I_R is significant in determining the range of predictable PU channels. For lower PU activity channels, increasing T_D does not lead to significant reduction in a_{11} (7.4). Hence, such channels will not satisfy the normalized interference constraint. In such cases, the ISTO algorithm will return a no-solution at the initial bracket finding stage. Thus, these PU channels are not considered as predictable channels. In the next section, we discuss about BCMS that assigns the available predictable channels to the NRT SUs.

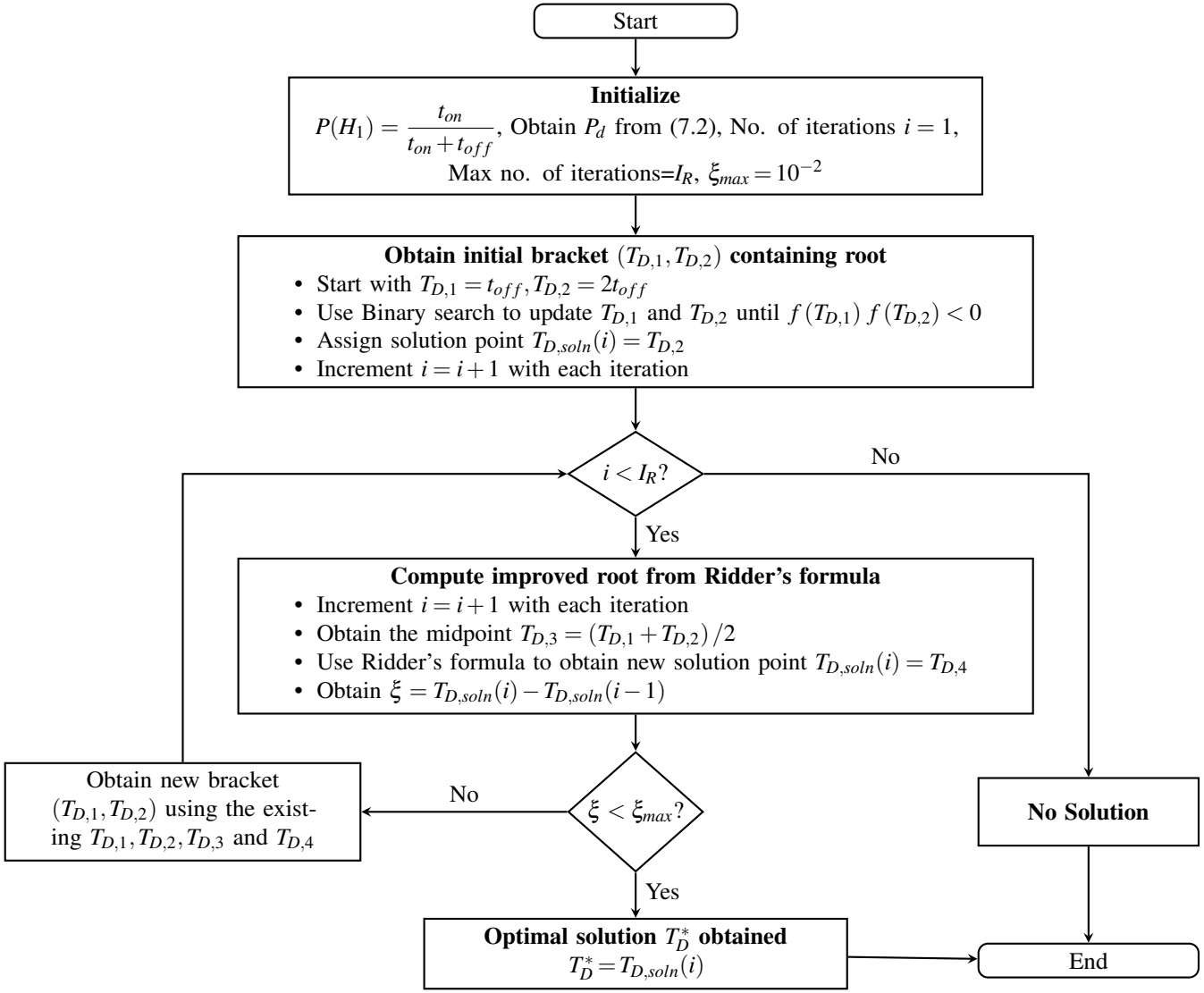

Fig. 7.13 Flowchart of ISPTO algorithm.

7.7 BCMS Design

The motivation behind designing a scheduler is to allow the SUs to transmit their data in the most efficient manner in a multi-channel scenario, that consumes the least amount of their battery. This is particularly significant because the NRT users are generally battery operated users such as sensor nodes and controllers like coordinator of WBAN. To this end, the proposed Battery Consumption Minimizing Scheduler (BCMS) aims at minimizing the total battery consumption of all the K number of NRT SUs by assigning them to F available predictable PU channels. Furthermore, we impose fairness into the scheduler to ensure no NRT SU gets starved from transmission opportunities. In this section, we first model the battery consumption of the sensor nodes and then formulate the assignment problem.

7.7.1 Battery Consumption Modeling

As illustrated in Figure 7.14, let $h_{i,j}$ denotes the channel between SU_i and CBS at predictable PU channel j, where $i \in 1,\cdots,K$ and $j \in 1,\cdots,F$. Further, let $P(H_{1,j})$ be the PU activity of predictable channel j with optimal inter-sensing duration $T_{D,j}$ that is determined by ISPTO algorithm. Capacity $(C_{i,j})$ of $h_{i,j}$ depends on the SNR $(SNR_{i,j})$ of link and the bandwidth of the channel (W). $C_{i,j}$ (bits/s) can be calculated by Shannon's formula as follows,

$$C_{i,j} = W\log_2\left(1+SNR_{i,j}\right) \tag{7.54}$$

The average number of bits $(T_{i,j})$ transmitted per CR frame by SU_i over assigned channel j can be obtained using (7.54) as,

$$T_{i,j} = P_{trans,j}\left(T_{D,j}-T_{C,j}\right)C_{i,j} \tag{7.55}$$

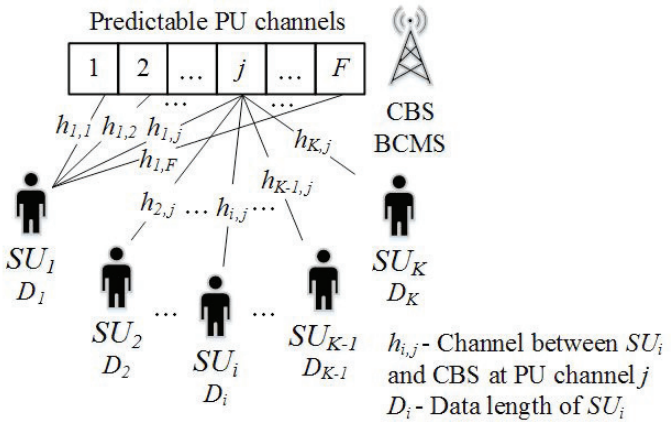

Fig. 7.14 Illustration of the heterogeneity in scheduling.

where $P_{trans,j}$ is the transmission probability for the j^{th} PU channel obtained using (7.42), and $T_{C,j}$ is the average collision duration within $T_{D,j}$ and is obtained using (7.43). The average energy (E_j) consumed in a single CR frame (Joules/CR frame) by an NRT SU for transmission over the j^{th} predictable PU channel can be calculated as,

$$E_j = P_{trans,j} T_{D,j} I_t V_s \tag{7.56}$$

where I_t denotes the current consumption of SU during transmission and V_s represents the power supply of the SU radio module.

Therefore, the average battery consumption $(B_{i,j})$ of SU_i for transmitting its D_i data bits over the j^{th} PU channel can be obtained using (7.55), (7.56) as,

$$B_{i,j} = \frac{E_j}{T_{i,j}} D_i \tag{7.57}$$

Consequently, the total battery consumption (B) of all the NRT SUs in the CRN can be represented as,

$$B = \sum_{i=1}^{K} \sum_{j=1}^{F} B_{i,j} A_{i,j} \tag{7.58}$$

where $A_{i,j}$ denotes the binary decision variable that designates the assignment status of SU_i at channel j. Specifically, if SU_i is allocated the j^{th} PU channel then $A_{i,j} = 1$, or else $A_{i,j} = 0$.

7.7.2 Total Battery Consumption Minimization Problem

We formulate the total battery consumption minimization problem as,

$$\mathbf{P2}: \quad \min_{\vec{A}} \sum_{i=1}^{K} \sum_{j=1}^{F} g_i^k B_{i,j} A_{i,j} \tag{7.59}$$

$$s.t. \quad \sum_{j=1}^{F} A_{i,j} = 1,\ i \in \{1, \cdots, K\} \tag{7.60}$$

$$\sum_{i=1}^{K} A_{i,j} = 1,\ j \in \{1, \cdots, F\} \tag{7.61}$$

$$A_{i,j} \in \{0,1\}, \forall i, j \tag{7.62}$$

where $\vec{A} = \left[A_{i,j},\, i \in 1,\cdots,K, j = 1,\cdots,F\right]$ is the assignment vector with elements $A_{i,j}$. Constraint (7.60) ensures that each SU is assigned to only one channel. Whereas, constraint (7.61) guarantees that a particular predictable channel is assigned to only one SU. In order to make BCMS fair in its channel assignment, we incorporate the index g_i, termed as *grant fair index*. g_i is defined as the ratio of the number of channel assignments granted to SU_i to the total number of channel requests from SU_i till the current moment. The grant fair index allows BCMS to favour the NRT SUs that are granted less number of channel assignments. Further, we introduce a degree of fairness, denoted by k. Higher degrees of k leads to better fairness.

Problem **P2** (7.59) is solved by BCMS after all the channels requests from the SUs are received at the CBS. BCMS obtains the optimal assignment vector $\vec{A}$ and informs the SUs via the control channel. Subsequently, SUs transmit their data bits over the assigned predictable channels. After completion, the SUs release their channels to the CBS. Problem **P2** is an assignment problem [242], which is a special case of transportation problem. It can be solved by finding the minimum weight perfect matching in a *weighted bipartite graph*. The graph is divided into two disjoint sets of SUs (U) and predictable channels (V), such that every edge connects a vertex in U to one in V. The weight of the edge between the i^{th} element in U and j^{th} element in V is $g_i^k B_{i,j}$. Such minimum weighted bipartite graphs can be solved by *Hungarian method* in strongly polynomial time [243]. The time complexity is given by $O(L^3)$ [244], where $L = \max(K,F)$.

7.7.3 Hungarian Algorithm for BCMS

The Hungarian algorithm implemented by BCMS follows the steps given in Algorithm 7.1. It uses an adjacency matrix also known as the cost matrix [243], where the entries in the matrix are the weights of edges in the bipartite graph. Let the set of SUs U represent the rows and the set of predictable channels V represent the columns. Thereafter, Algorithm 7.1 exploits Lemma 2 [243] for polynomial runtime complexity and guaranteed optimality.

Lemma 2 *If a number is added to or subtracted from all of the entries of any one row or column of a cost matrix, then an optimal assignment for the resulting cost matrix is also an optimal assignment for the original cost matrix.*

Based on this, in the first phase, row reductions and column reductions are carried out (Lines: 5 and 6 of Algorithm 7.1). In the second phase, the solution is optimized on iterative basis (Lines: 7-16 of Algorithm 7.1).

Algorithm 7.1 Hungarian Algorithm for BCMS

1: **Initialization:** Prepare the cost matrix **C** with elements $g_i^k B_{i,j}$, where $i \in 1, \cdots, K$ and $j \in 1, \cdots, F$
2: **if** $K \neq F$ **then**
3: Append zeros to convert **C** into $L \times L$ matrix, where $L = \max(K, F)$
4: **end if**
5: For each row of **C**, find the smallest element and subtract it from every element in its row
6: For each column of **C**, find the smallest element and subtract it from every element in its column
7: **loop**
8: Cover all zeros in **C** using minimum number (l) of horizontal and vertical lines
9: **if** $l = L$ **then** *(Test for Optimality)*
10: **return** : Optimal assignment corresponding to non-repeating zero entries covering all rows and columns
11: **else if** $l < L$ **then**
12: Determine the smallest entry (δ) not covered by any line
13: Subtract δ from each uncovered row
14: Add δ to covered column
15: **end if**
16: **end loop**

7.7.3.1 Time Complexity Analysis

The first two steps (Lines: 5 and 6 of Algorithm 7.1) in an effort to make the smallest element in each row and column equal to zero cover all the elements of the cost matrix **C**. This makes a total of $O(L^2)$ time.

In case the optimality test at Line: 9 of Algorithm 7.1 fails, then Lines: 13 and 14 of Algorithm 7.1 are repeated. Since these steps are similar to the first two steps, they have the same time complexity of $O(L^2)$ time.

In the worst case, there can be $O(L)$ number of such iterations (Lines: 13 and 14 of Algorithm 7.1), each taking $O(L^2)$ time, leading to a total running time of $O(L^3)$. Therefore, Hungarian algorithm provides optimal solution in strongly polynomial time.

To illustrate the significance of this, let us consider a Brute force solution which considers every possible assignment by checking every combination and seeing what yields the lowest battery consumption. However, there are $L!$ combinations to check, and for large L, this method becomes inefficient very quickly. Therefore, brute force method implies a complexity of $O(L!)$. Compared to this, the Hungarian algorithm is clearly much more efficient, thereby justifying its selection.

7.8 Performance Analysis of CSSP Framework

We analyze the CSSP framework to study the performance of ISPTO algorithm, H2M2 engine and BCMS. First, we present the performance of ISPTO algorithm in determining the optimal inter sensing-prediction time for a PU channel. Next, we illustrate the comparative performance analysis of CSSP with respect to BSS and CSS under different conditions. Then, we show the performance improvement in energy-efficiency of a CR frame due to H2M2 as compared to Software based HMM Prediction (SHMMP). Lastly, we evaluate BCMS performance in a multi-user, multi-channel scenario. BCMS performance is studied in terms of the total battery consumption minimization of the CRN and fairness. In this regard, the simulations are performed in MATLAB [215]. The H2M2 engine is developed in an ATLYS FPGA [245], that communicates with the MATLAB simulation environment using a developed MATLAB Hardware Co-simulation (M-Hwcosim) interface.

In the simulations, the spectrum is divided into PU channels of bandwidth W=5MHz. For example, if 20MHz WLAN bands comprise the PU spectrum, then each PU channel is a sub-band of bandwidth W within a WLAN band. The PU activity of the channels follow an exponential ON-OFF distribution with mean duty-cycle $t_{on} + t_{off}$=100ms [246]. The F predictable channels in the CRN have PU activities and detected PU SNR with uniform probability. The SNR of a link between SU and CBS follow an exponential process with mean SNR=2.5dB [105]. Further, for modeling the data transmitted by NRT SUs we consider healthcare data generated from a WBAN. The sampling frequencies of various physiological signals, are given in Table 7.1[108]. Table 7.1 also provides the corresponding data bits (D_i) generated in a 2s signal capture. The data streams are assigned to the SUs with uniform probability.

Table 7.1 Healthcare signal frequencies and data Size

Data Stream	**Signal Frequency (Hz)**	**Data Size (D_i) for 2s signal (bits)**
ECG	200	6400
Respiratory Rate	10	320
Blood Pressure	50	1600
EEG	60	1920
Body Temperature	0.1	16
EMG	500	16000
Galvanic Skin Resistance	20	640

We utilize the Wireless Open Access Research Platform (WARP) [166] radio boards to model the transceivers of CR modules. For obtaining their power consumption profile, readings were taken using an external ammeter connected in series with the WARP node's

12V power supply. The results revealed that, the node draws I_t =1.4A and I_r =1.35A current in transmit and receive modes respectively.

To obtain the sensing time, we draw on the assumptions presented in [172], where the optimal sensing time has been evaluated for $\chi = 0.9$, receiver sensitivity $\gamma_{PU,min}$ = -20 dB, and $\kappa = 0.1$. Therefore, using (7.3) we obtain N_S=131072. The WARP board is equipped with a 40MHz ADC with a buffer size of 2^{14}. Generally, WARP avoids the first 1000 received samples. Using this and after some calculations, we obtain the sensing time T_S = 3ms. Further, in our analysis, we consider the normalized interference threshold Γ=0.006 for ISPTO algorithm. It is worth mentioning that, owing to the improved interference rejection capabilities of H2M2 the threshold for ISPTO is set ten times less than the limits for BSS or CSS [82].

We illustrate the variation of normalized interference duration with the observation sequence length N of H2M2 in Figure 7.15a. Additionally, the log likelihood of generating an observation sequence $\mathbf{O}$, i.e. $\log(P(\mathbf{O}|\Lambda))$, by the H2M2 at every iteration is shown in Figure 7.15b. It is observed in Figure 7.15a that as N increases the interference decreases, however there is less variation beyond N=100. Similarly, $\log(P(\mathbf{O}|\Lambda))$ in Figure 7.15b shows convergence after 5 iterations. Therefore, for H2M2 the observation sequence length N is set to 100, and the maximum number of iterations I is set to 5.

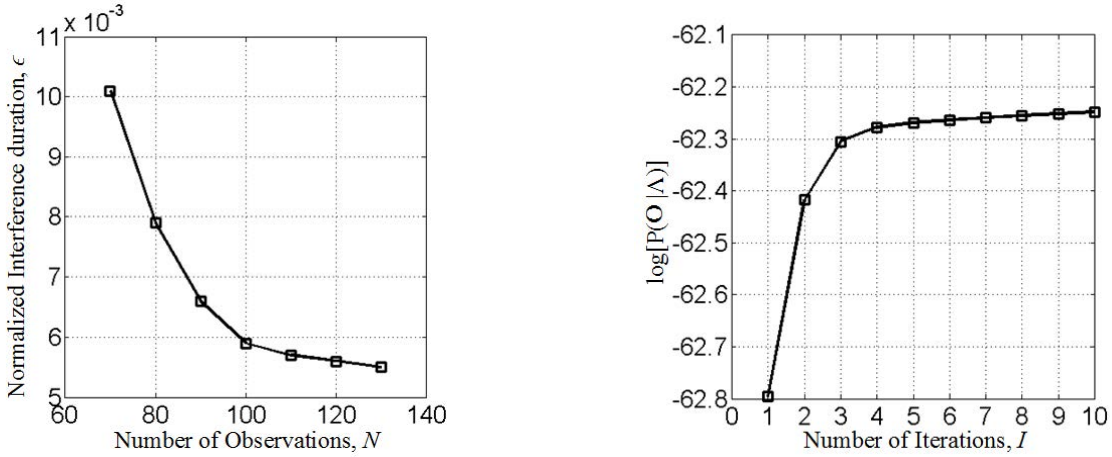

(a) (b)

Fig. 7.15 Variation of (a) ε with respect to N, and (b) $\log(P(\mathbf{O}|\lambda))$ with respect to I.

7.8.1 Analysis of ISPTO Performance

In this sub-section, the simulation results for ISPTO algorithm are presented. The variations of normalized throughput-time (T) (7.40) and the normalized collision duration (ε) (7.41) for different inter sensing-prediction durations T_D at $\gamma_{PU} = -20$dB are shown in Figures 7.16a and 7.16b respectively. It is noted that with the increase in T_D, both T and ε decreases. Furthermore, both the curves are observed to follow the strictly decreasing nature with respect to T_D satisfying (7.49) and (7.50). This variation can be explained from the relation between T_D, state transition probabilities and H2M2 performance as highlighted previously in Section 7.5. Briefly, as the value of T_D increases, the probability a_{11} decreases, which in turn, results in improvement in the miss-avoidance probability (P_{ma}) and thus decrease in interference. However, simultaneously the probability of transmission opportunity (P_o) also decreases, leading to lower throughput. Thus, we observe a trade-off with respect to the selection of T_D. ISPTO algorithm obtains the optimal inter sensing-prediction duration T_D^* at the boundary of the maximum permissible normalized interference threshold Γ=0.006. This is represented by the dotted line in Figure 7.16b . It is observed that, as the PU activity decreases T_D^* increases. Keeping T_D fixed in Figure 7.16b, it is noted that the normalized interference duration increases with decrease in PU activity. Lower PU activity leads to degraded prediction performance causing more collisions. Furthermore, it is seen that for PU activities less than 68%, ε never satisfies the interference threshold. Thus, for detected PU SNR of -20dB ($\gamma_{PU,min}$) the ISPTO algorithm selects the channels with PU activity greater that 68% as predictable channels.

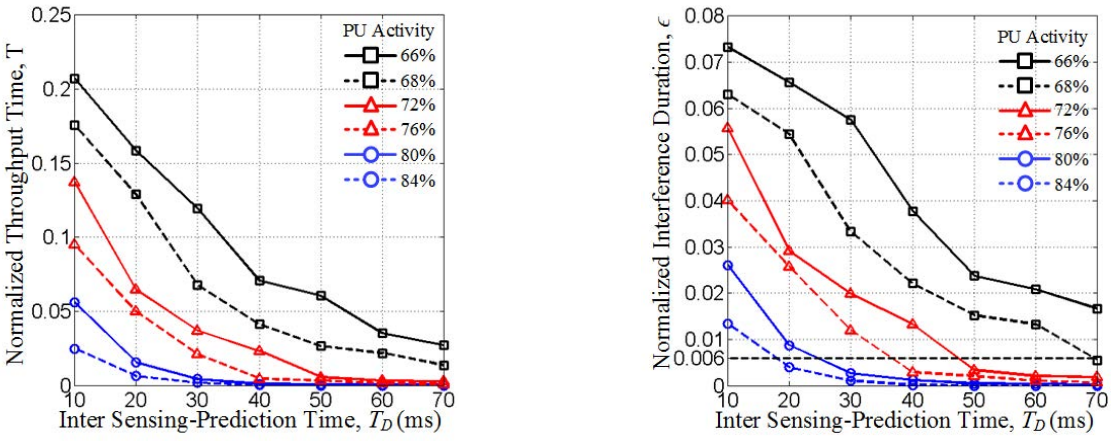

(a) (b)

Fig. 7.16 Variation of (a) T, and (b) ε with respect to T_D for different PU activities at $\gamma_{PU} = -20$dB.

In Figure 7.17, we vary the PU activity and detected PU SNR (γ_{PU}) at the CBS to observe its impact on the optimal inter sensing-prediction duration (T_D^*). Decrease in PU activity leads to increase in T_D^*, which is in lines with the observations reported in Figure 7.16b. Further, as shown in Figure 7.17, for a fixed PU activity T_D^* decreases with increase in γ_{PU}. Higher γ_{PU} corresponds to better detection probability. This leads to reduced collisions, which in turn reduces the value of T_D^*. A closer look at Figure 7.17, reveals that the lower bound of predictable PU activity range extends to 62% for $\gamma_{PU} = -18$dB, as compared to 68% for $\gamma_{PU} = -20$dB. This improvement at higher detected PU SNR is due to the reduced interference, which indicates that the lowest PU activity which satisfies the interference threshold will be less as compared to the lower PU SNRs. It is also worth mentioning that for $\gamma_{PU} = -18$dB, $P_d \approx 1$. Therefore, for $\gamma_{PU} > -18$dB there is no further improvement in predictable PU activity range.

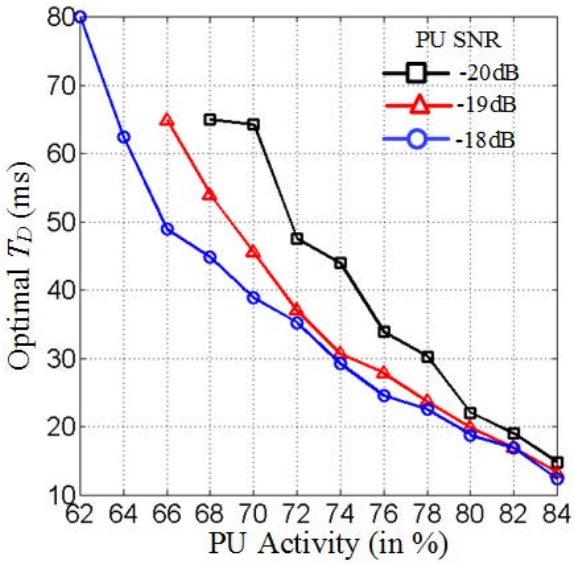

Fig. 7.17 Optimal inter sensing-prediction duration versus PU activity for different detected PU SNRs.

The performance of the different root-finding techniques in terms of the convergence time of the ISPTO algorithm for 78% PU activity and -20dB PU SNR is shown in Figure 7.18. From Figure 7.18, it is observed that Ridder's method offers the fastest convergence followed by Regula Falsi and Secant techniques. In this regard, the bisection method is found to be the slowest. This justifies our selection of Ridder's method for ISPTO algorithm.

Finally, we comment on the variation in energy-efficiency of the SUs at the optimal inter sensing-prediction duration. We define SU energy-efficiency (EE_{SU}) as the ratio of

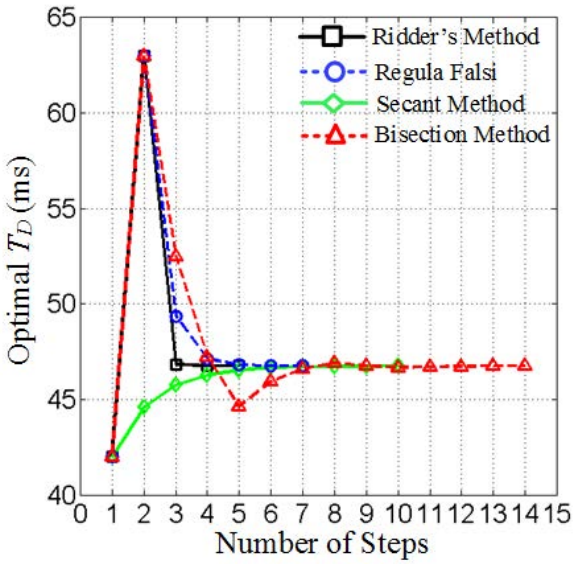

Fig. 7.18 Convergence of different root finding techniques in ISPTO algorithm.

normalized throughput time to the normalized SU energy consumption within a single CR frame. It is calculated as,

$$EE_{SU} = \frac{T_D - T_C}{T_D I_t V_s} \tag{7.63}$$

Examining (7.63) and (7.41) reveals that ideally EE_{SU} for all predictable PU channels should be same at $T_D = T_D^*$. However, slight variations are noted during simulations between different operating conditions. This is to be expected as the root finding method in ISPTO algorithm determines T_D^* within a certain degree of error tolerance. This error tolerance is limited by the resolution of the LUTs. Higher resolution will reduce these variations, however at the cost of very large LUTs. Thus, in this we limit the resolution of LUTs and error tolerance (ξ_{max}) to 10^{-2}, which provides an acceptable trade-off.

7.8.2 Comparative Analysis of Proposed CSSP Framework with Non-Predictive BSS and CSS

Figure 7.19a shows the variation of SU energy-efficiency (EE_{SU}) as defined in (7.63) with respect to the different PU activities for our proposed CSSP, traditional Base Station based Sensing (BSS) and Collaborative Spectrum Sensing (CSS) at $\gamma_{PU} = \gamma_{PU,min}$=-20dB. For CSS, we perform simulations against different number (n) of collaborating users. Additionally, for both BSS and CSS, we determine the optimal inter-sensing durations that maximize the

throughput time within a normalized interference duration constraint. In this regard, to avoid infeasible solutions, both CSS and BSS are evaluated for normalized interference constraints of 0.06, which is 10 times less than that of CSSP. In Figure 7.19a, we can observe that CSSP under predictable PU channels attains better EE_{SU} as compared to CSS and BSS. Due to the improved H2M2 performance in avoiding miss-detections, less energy is consumed towards successful transmission, thereby increasing the energy-efficiency. CSSP provides 48.43% improvement in EE_{SU} with respect to (w.r.t) CSS $(n = 1)$ and 6% improvement w.r.t BSS. This is more significant as the EE_{SU} improvement for CSSP is under stricter normalized interference constraint. The significantly lower value of EE_{SU} for CSS is because the SUs perform spectrum sensing for channel access.

Figures 7.19b and 7.19c respectively shows the variations of EE_{SU} and normalized interference duration (ε) with respect to the detected PU SNR (γ_{PU}) for CSSP at 78% PU activity, and BSS and CSS at 20% PU activity. Here, we can observe that CSSP outperforms both BSS and CSS.

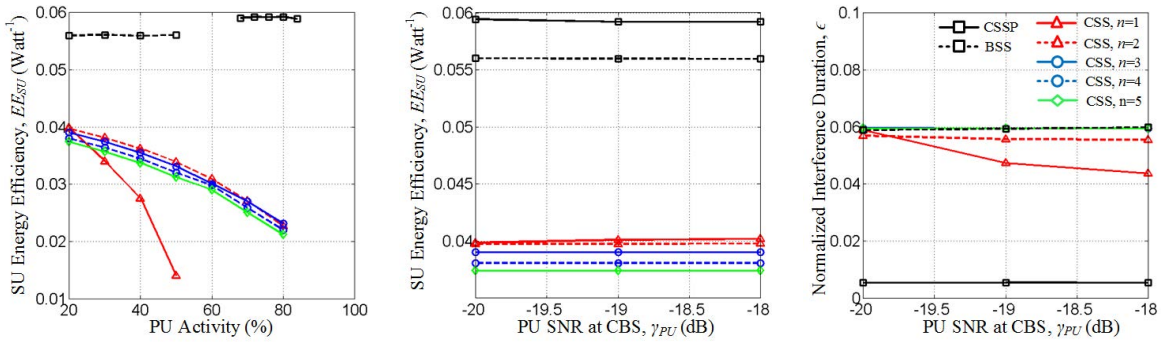

(a) Fixed PU SNR at CBS, γ_{PU}= -20dB

(b) Fixed PU activity (CSSP-78%),(BSS,CSS-20%)

(c) Fixed PU activity (CSSP-78%),(BSS,CSS-20%)

Fig. 7.19 (a) EE_{SU} versus PU activity, (b) EE_{SU} versus PU SNR at CBS, and (c) ε versus PU SNR at CBS for CSSP, BSS and CSS with different cooperating SUs.

7.8.3 Comparative Analysis of H2M2 with SHMMP

The performance of hardware implementation for HMMP can be analyzed from the time taken for re-estimating the HMM variables by H2M2 over 5 iterations utilizing 100 previous observations. The results of the study are summarized in Table 7.2. As evident, H2M2 reduces the number of clock cycles by 54% and that leads to 76.8% reduction in the time taken for prediction as compared to soft-core implementation of HMM prediction (SHMMP). This performance improvement is due to the efficient implementation of H2M2 on FPGA

at 40MHz without setup and hold-time violations and the use of parallel processing with pipelining that saves clock-cycles. This is contrary to sequential execution of instructions at lower 20MHz speed of soft-core processors like Microblaze. The setup time for H2M2 recorded after synthesis, mapping, placement and timing analysis of the design on FPGA is 17.7ns. Now the system clock period is 25ns. Therefore as the setup time is less than the clock period, H2M2 satisfies the setup time constraints.

Table 7.2 Performance improvement in H2M2 engine

Prediction Unit	Processor Speed	Clock Cycles	Time Taken
SHMMP	20MHz	26856	1.34ms
H2M2	40MHz	12381	0.31ms

The performance improvement achieved by H2M2 over SHMMP can be shown using CR frame energy-efficiency (EE_{CR}) metric. It can be calculated as,

$$EE_{CR} = \frac{P_{trans}(T_D - T_C)}{(T_S I_r + T_P I_P + P_{trans} T_D I_t) V_s} \tag{7.64}$$

where I_p=1.3A denotes the current consumed (in WARP board) by CBS during prediction and the other symbols have their usual meaning. The significance of EE_{CR} is that along with the SU energy consumption, it also considers the energy consumption of CBS. Figure 7.20 is plotted to illustrate the improvement in EE_{CR} due to H2M2 as compared to SHMMP under the same normalized interference constraint for $\gamma_{PU} = -20$dB. It is observed that for an

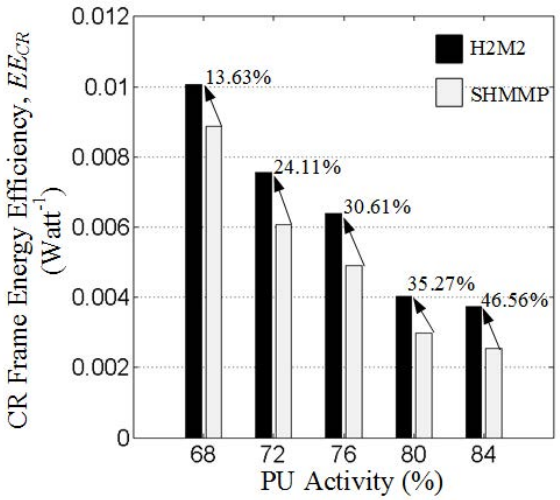

Fig. 7.20 Variation of EE_{CR} with respect to PU activity for H2M2 and SHMMP, with percentage improvement for H2M2.

84% PU activity there is a significant 46.55% improvement in EE_{CR}. Lower prediction time of H2M2 correspond to less energy consumption towards prediction, but more importantly higher inter sensing-prediction time, which adds to concerned EE_{CR} improvement. Moreover, we observe that for higher PU activities the percentage improvement increases. From the expression in (7.64) we discern the inverse proportionality of the improvement in EE_{CR} with T_D. Higher PU activities have smaller optimal T_D^*, and hence better improvements in EE_{CR}. Lastly, the increase in EE_{CR} with decrease in PU activity is attributed to the improvement in probability of transmission opportunity (P_o), which means that for the energy consumed by CBS more throughput is obtained from the CRN.

7.8.4 Analysis of BCMS Performance without Fairness

Having obtained the predictable channels and optimal T_D^* in ISPTO algorithm, we now analyze the performance of BCMS in minimizing the battery consumption of the NRT SUs. For this, first we deactivate fairness by setting $g_i = 1, i = 1, \cdots, K$. Then, in the next subsection we study the fairness of BCMS. To provide comparative analysis, we consider a Heuristic Battery Consumption Minimizing Scheduler (HBCMS). HBCMS greedily assigns each predictable PU channel to the NRT SU which consumes the minimum battery at that particular channel, i.e. lowest $B_{i,j}$. HBCMS operates in polynomial time in the order of $O(FK)$, where F is the number of available predictable PU channels and K is the number of NRT SUs requesting channel.

In Figure 7.21, we vary F to observe its impact on the BCMS performance. For this, we set $K = 20$. For each simulation setting, we obtain the results after 1000 Monte Carlo simulations. As shown in Figures 7.21a, 7.21b and 7.21c, initially the average battery consumption per NRT SU (β) increases with increase in F. This is due to increased number of channel assignments among the SUs. Alternatively, we can state that β decreases with decrease in F for $F < N$. This is to be expected, as among the many SUs requesting channel assignment, only those having lower data lengths or higher mean channel SNRs will be favored in general. Furthermore, for increase in F beyond $F = 20$, we observe that the battery consumption decreases. When $F > K$, BCMS chooses the most appropriate PU channels for assignment, while leaving the less energy-efficient channels un-assigned. Figure 7.21d depicts that BCMS performs better than HBCMS under all conditions with lower battery consumption.

Figure 7.21a also demonstrates the effect of SU channel SNRs on the battery consumption. In this scenario, we vary the ratio of SUs $(f_{snr}^{high} : f_{snr}^{low})$ having high mean SNR of 5dB and low mean SNR of 0dB. It is observed that as channel SNRs increase, the battery consumption

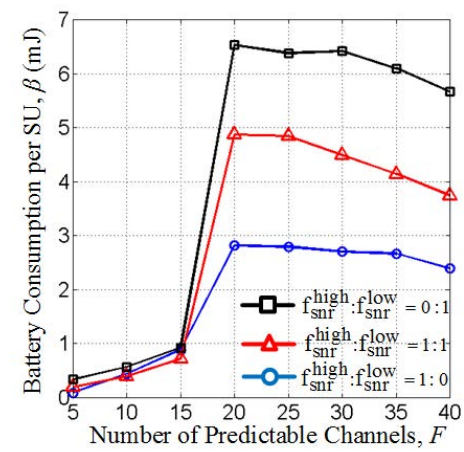

(a) Different ratio of NRT SU channel SNRs

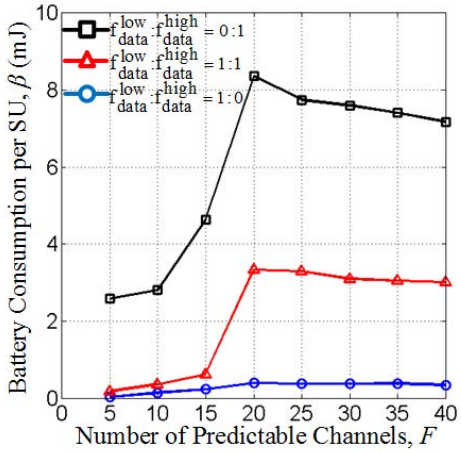

(b) Different ratio of NRT SU data lengths

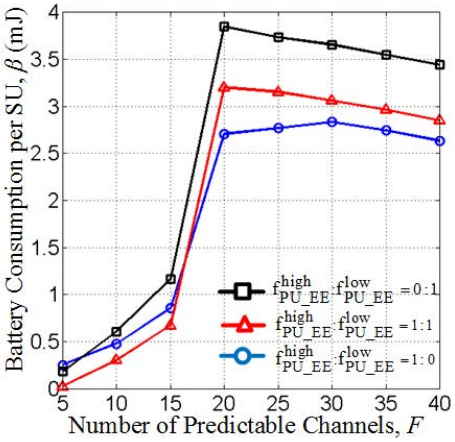

(c) Different ratio of PU activities with varied SU_{EE}

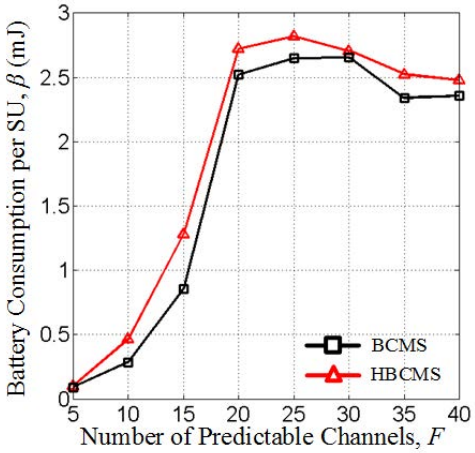

(d) BCMS vs HBCMS

Fig. 7.21 Variation of battery consumption per SU with respect to number of available predictable channels.

decreases. This is caused by the fact that higher SNR leads to more channel capacity, which reduces the transmission time and hence the battery consumption decreases.

Similarly, in Figure 7.21b we see the variation of β for different ratios of data sizes $(f_{data}^{low} : f_{data}^{high})$ among the NRT SUs. Referring to Table 7.1, we classify the 16, 320 and 640-bit data as low data sizes. It is noted that smaller data lengths lead to lesser battery consumption.

As discussed in Section 7.8.1, the SU energy-efficiency per CR frame (EE_{SU}) for T_D^* vary slightly for different PU activities and PU SNRs due to the unavoidable error tolerance of root

finding technique in ISPTO algorithm. Drawing from this observation, in Figure 7.21c we note the variation in β for different ratio of PU channels $(f_{PU\_EE}^{high} : f_{PU\_EE}^{low})$ classified based on their (EE_{SU}). As expected, the battery consumption decreases as the number of channels offering higher (EE_{SU}) increases. This highlights the capability of BCMS in assigning the most suitable PU activity channels while leaving the relatively less energy-efficient channels unassigned. Thereby, efficiently mitigating the small variations in EE_{SU} among the different PU activities at optimal T_D^*.

7.8.5 Analysis of BCMS Performance with Fairness

In this section, we illustrate the ability of BCMS to ensure fairness in channel assignment among different SUs. This prevents certain SUs from getting starved of channel assignments. Such a situation might arise if such SUs have low mean channel SNR or large data length. Therefore, ensuring fairness is necessary, even if it conflicts with the objective of minimizing the total battery consumption. We evaluate the fairness performance in terms of a metric known as *Gini Index*. Gini Index computes the deviation in resource allocation from the ideal fair allocation [247]. Gini index 0 denotes a perfectly fair allocation scheme, whereas an unfair allocation has high Gini Index. The Gini Index (F_{Gini}) can be calculated as,

$$F_{Gini} = \frac{1}{2K^2\bar{g}} \sum_{i=1}^{K} \sum_{j=1}^{K} \left| g_i - g_j \right| \tag{7.65}$$

$$\bar{g} = \frac{\sum_{i=1}^{K} g_i}{K} \tag{7.66}$$

Where g_i is the grant fair index of SU_i.

To illustrate the efficiency of BCMS in imposing fairness, we isolate two specific NRT SUs having contrasting characteristics for the scenario $K = 40$ and $F = 20$. More specifically, we consider a SU(SU_1) having 5dB mean channel SNR with a data length of 16bits, whereas another SU (SU_2) having 0dB mean channel SNR with 6400 data bits to send. Figure 7.22 shows the variation of the grant fair index for SU_1 and SU_2 over 200 successive simulation runs. We observe in Figure 7.22a that without fairness SU_2 does not receive any channel assignments, while SU_1 is favored. However, when fairness with degree $k = 1$ is imposed as in Figure 7.22b, there is improvement in the grant fair index of SU_1, and the difference in g_i between SU_1 and SU_2 is less. Furthermore, the fairness improves in Figure 7.22c as the degree of fairness is increased . The ability of BCMS in maintaining fairness among SUs can also be seen in Figure 7.23.

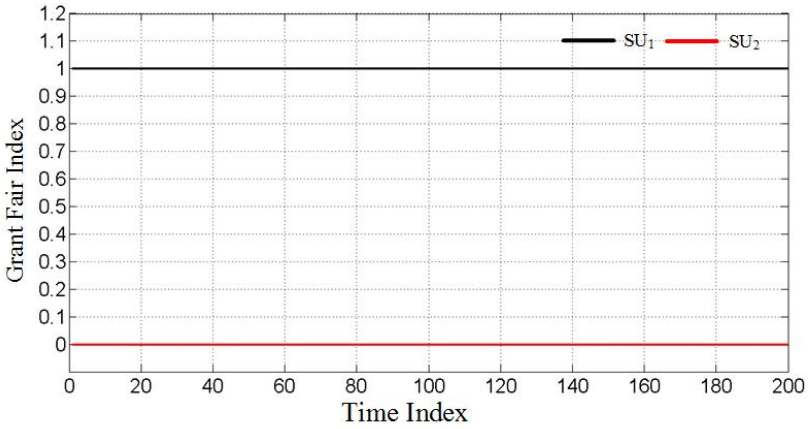

(a) No fairness

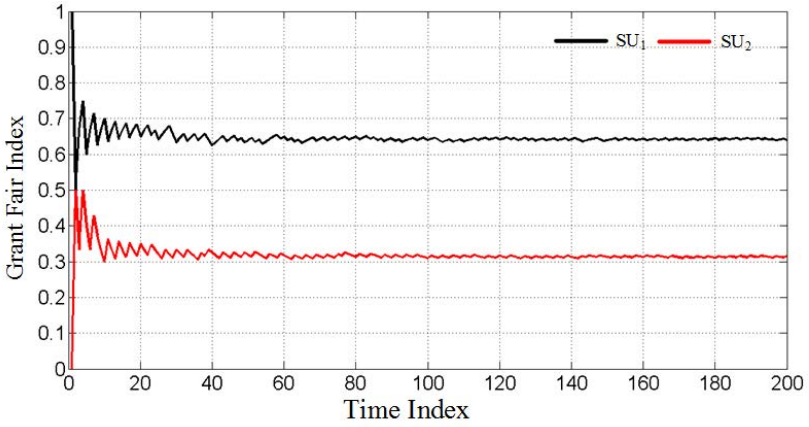

(b) Fairness with degree $k = 1$

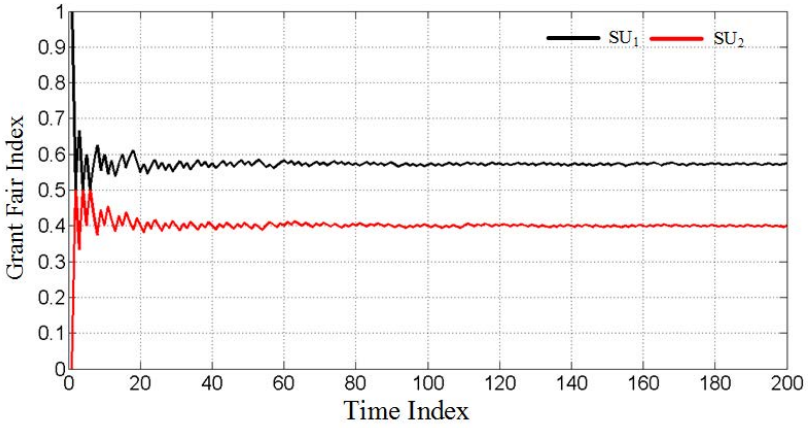

(c) Fairness with degree $k = 2$

Fig. 7.22 Variation of grant fair index for SU_1 and SU_2 with time. SU_1 has high mean channel SNR of 5dB and low data length of 16bits, SU_2 has low mean channel SNR of 0dB and high data length of 6400 bits.

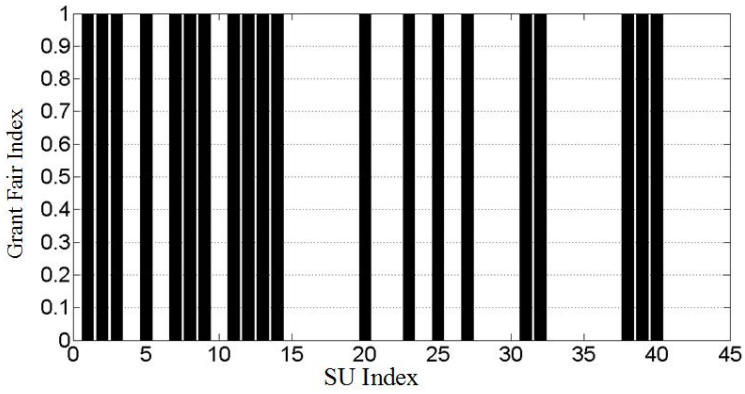

(a) No fairness

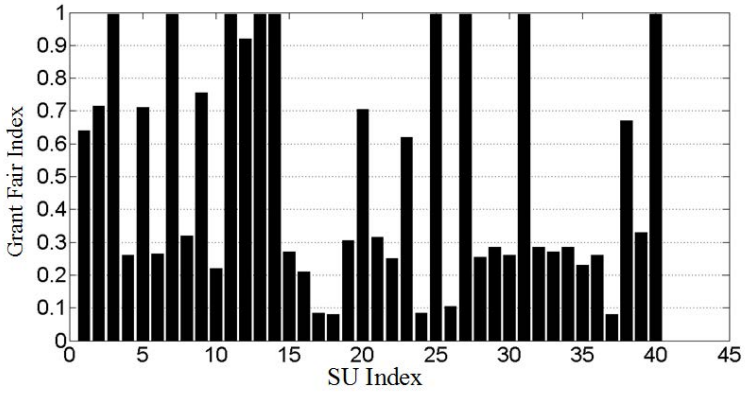

(b) Fairness with degree $k = 1$

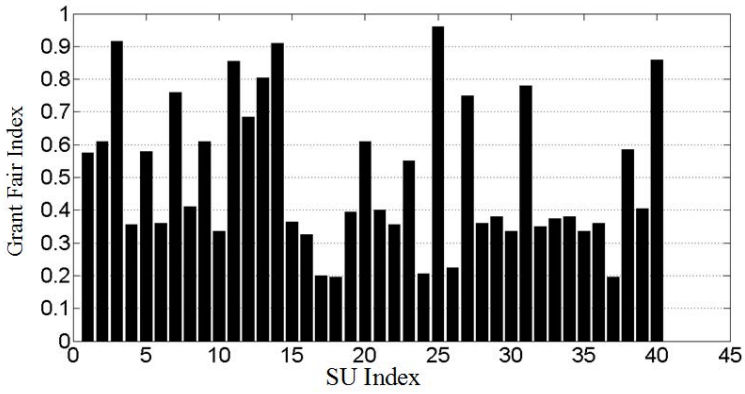

(c) Fairness with degree $k = 2$

Fig. 7.23 Grant fair index of different NRT SUs under various fairness settings.

Table 7.3 reports the performance of BCMS and HBCMS in terms of F_{Gini} and the average battery consumption per SU (β) under different fairness settings and number of SUs $K = 10$, $K = 30$ and $K = 40$. While the total number of predictable channels is kept fixed at $F = 20$. It can be concluded that BCMS outperforms HBCMS both in terms of F_{Gini} and β under all conditions. For a particular degree of fairness (k), the F_{Gini} value increases with increase in K. This is because, for larger values of K there are more unassigned SUs. In this regard, the decrease in β with increase in K is similar to the observation reported in Figure 7.21. Keeping K fixed, F_{Gini} improves with higher degrees of fairness (k). However, this improvement is at the cost of increased battery consumption. Therefore, a network designer while selecting the appropriate value of k needs to take into account the inherent trade-off between F_{Gini} and β.

Table 7.3 Performance of BCMS and HBCMS

k	Scheduler	K=10		K=30		K=40	
		F_{Gini}	β (mJ)	F_{Gini}	β (mJ)	F_{Gini}	β (mJ)
1	BCMS	0	0.62	0.2571	0.43	0.3505	0.38
	HBCMS	0	0.63	0.2627	0.535	0.3609	0.41
1.2	BCMS	0	0.62	0.2497	0.445	0.3255	0.405
	HBCMS	0	0.63	0.2566	0.55	0.3353	0.43
1.4	BCMS	0	0.62	0.2428	0.46	0.3036	0.43
	HBCMS	0	0.63	0.2473	0.54	0.3101	0.45
1.6	BCMS	0	0.62	0.2337	0.475	0.2843	0.445
	HBCMS	0	0.63	0.2374	0.53	0.2861	0.465
1.8	BCMS	0	0.62	0.2204	0.49	0.2631	0.465
	HBCMS	0	0.63	0.2244	0.535	0.2655	0.48
2	BCMS	0	0.62	0.2058	0.505	0.2443	0.48
	HBCMS	0	0.63	0.2065	0.56	0.245	0.495
0 (No Fairness)	BCMS	0	0.61	0.3333	0.315	0.5	0.25
	HBCMS	0	1.39	0.3333	0.385	0.5	0.32

7.9 Proof of Concept: NRT WBAN Transmission

In this section, a prototype implementation of the proposed CSSP framework and H2M2 engine is described and validated by means of a simple proof of concept representative of the main functionalities and aspects of novelty of our system.

We have developed a complete prototype implementation and validation scenario, as shown in Figure 7.24, which includes: 1) generation of a 10s ECG signal as output of a

WBAN using a MATLAB script [248] for the SU, 2) Discrete Wavelet Transform (DWT) based compression of the ECG signal into the first 512 DWT coefficients using bior4.4 filter as described in Section 3.11.3, 3) development of a CRN using WARP v2 board with one radio daughter card for the CBS and another radio daughter card for the SU, and 4) H2M2 implementation for prediction using ATLYS FPGA [245] board. For the PU system, we have selected the channel number 9 of 2.4 GHz frequency band and have utilized one radio daughter card of a WARP v3 board to emulate the incumbent PU transmitter with exponential ON-OFF traffic.

The CRN comprising of the CBS and SU radio daughter cards is controlled by a MATLAB script named as `CRN WARPLab` running on a PC. The CBS through `CRN WARPLab` script interacts with the H2M2 engine using our M-Hwcosim interface. The H2M2 engine that is developed on the standalone ATLYS FPGA emulates the actual hardware behavior of the proposed predictor engine, while reducing the turnaround time involved in developing the same at the PHY of WARP board. Further, to support spectrum sensing, we developed an energy detection model in the `CRN WARPLab` script which enables PU detection using the received samples captured by CBS radio daughter card of WARP v2 board. Furthermore, the PU system is also controlled by a MATLAB script termed `PU System WARPLab`, which generates the exponential ON-OFF distributed signal at 78% PU activity with $t_{on} + t_{off}$ = 100ms. The PU transmit power is set such that the detected PU SNR at the CBS is -20dB, i.e. $\gamma_{PU} = -20$dB.

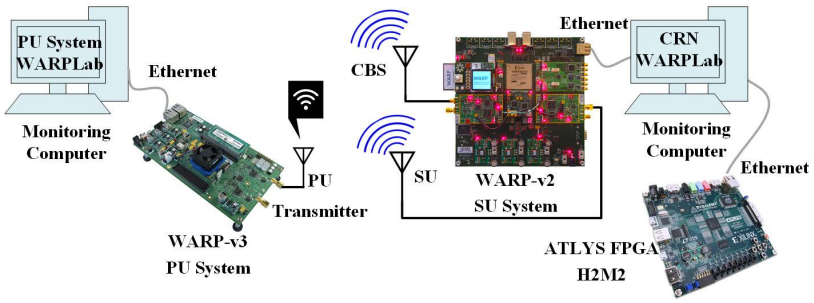

Fig. 7.24 Validation scenario for NRT communication over CSSP framework.

For enabling sharing of control information between CBS and SU, we design a control channel. The baseband frequency spectrum for the coexistence of primary signal and control channel is shown in our work [83]. It is worth noting that all communications have been setup in a slotted manner, with each slot duration being equal to the 0.384ms which is the time taken by WARP board to transmit or read the complete buffer of 2^{14} samples excluding 1000 delay samples. Following which all the timing parameters, viz. sensing time, transmission time, ON and OFF times of PU signals, have been mapped into equivalent number of slots.

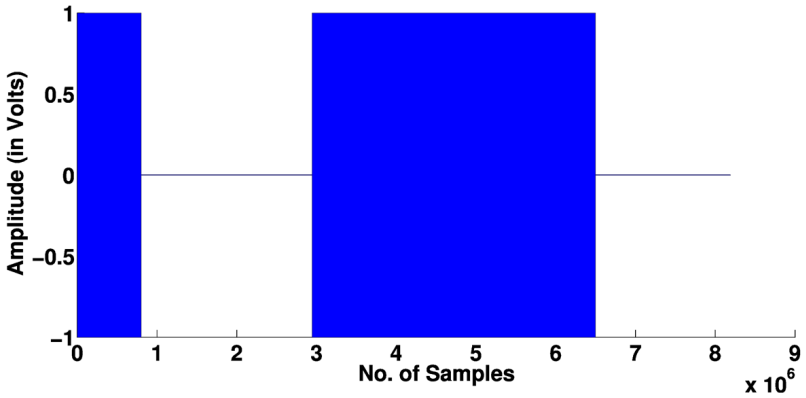

(a) PU transmistted signal

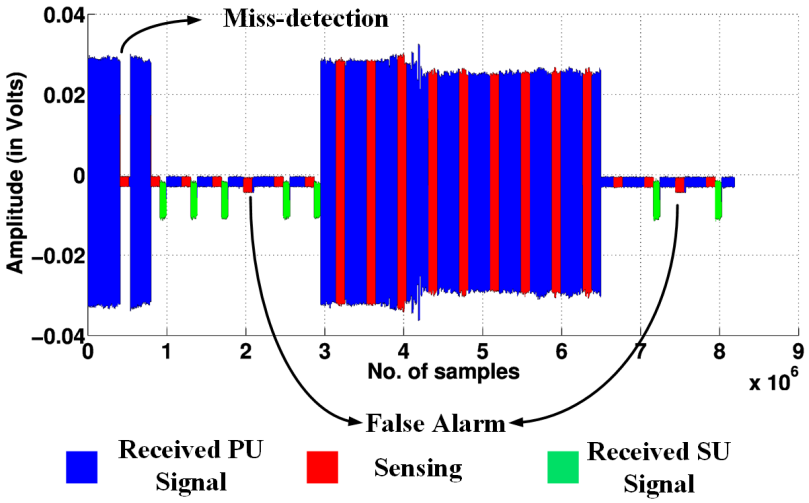

(b) CBS received signal

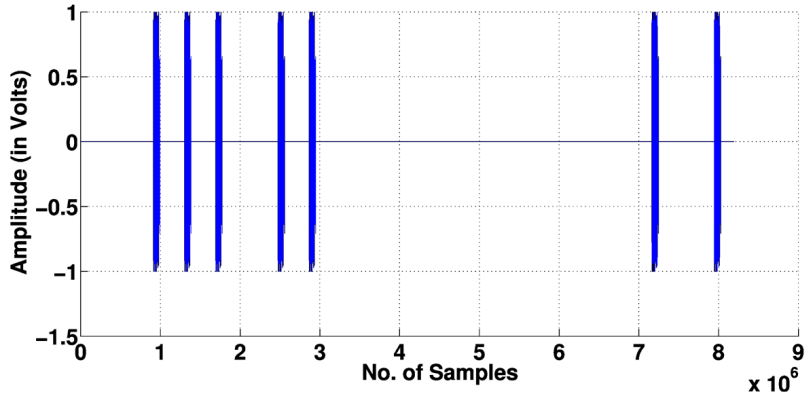

(c) Transmitted signal by NRT SU

Fig. 7.25 Activities of PU, CBS and NRT SU.

The MATLAB plots in Figure 7.25 highlight the major functions of the PU, CBS and SU. When the SU has a compressed ECG signal ready for transmission, it sends a request to the CBS over the control channel. Upon receiving the request, the CBS radio senses the PU signal through energy detection using `CRN WARPLab` script for 3ms at intervals of T_D^*=30.3ms. The received PU signal at the CBS during this periodic sensing is shown in Figure 7.25b. Additionally, for illustration purpose the received PU signal during the inter-sensing durations has also been shown. After sensing, the observation is then sent to the free running ATLYS board with the help of M-Hwcosim interface. Upon obtaining the re-estimated H2M2 parameters, the CBS radio communicates the transmission decision, *transmit* over the control channel to SU radio. When $transmit = 1$, the SU radio transmits its data. Such SU data transmission instances are shown in Figure 7.25c. The transmission time is 1.18ms.

Finally, through Figure 7.25b we demonstrate the efficiency of H2M2 in the CSSP framework. It is observed that the SU could successfully transmit in the white spaces avoiding the miss-detections. As shown in Figure 7.25b, in the event of a miss-detection, H2M2 accurately predicts the presence of PU and doesn't allow SU transmission, thereby reducing the miss-detection probability. Some instances of false-alarm which prevents SU transmission are also observed in Figure 7.25b. False alarm occurs when the received PU signal at the CBS is slightly higher than the noise-floor. It can be expected that this accidental false-alarm might disturb the H2M2 training observation sequence. However, interestingly when a white-space is detected in the next sensing instance following the false-alarm, the SU could successfully transmit. Thus, this illustrates that a false-alarm does not disturb the H2M2 performance.

7.10 Conclusion

In this work, we have proposed the *Centralized Scheduling, Sensing and Prediction (CSSP) framework* for a CRN to enable energy-efficient Non-Real Time (NRT) communication for SUs . To this end, an enhanced HMM based prediction is incorporated within the traditional CR sensing-transmission cycle. Further, by designing *H2M2 engine* the prediction time is minimized in the order of 76.8% and thus improving the energy-efficiency of the CR cycle. The CBS leverages on the ability of H2M2 to minimize the miss-detection probability of spectrum sensing at high PU activities, thereby limiting interference to PUs. The reduced collisions between PU and SU transmissions guarantee less energy consumption for the NRT SUs at the cost of reduced transmission opportunities decreasing the throughput. For this, a non-convex optimization problem is formulated and solved by our proposed *ISPTO*

algorithm to maximize the throughput of SUs in PU channels by obtaining the optimal inter sensing-prediction duration. ISPTO employs Ridder's method for faster quadratic rate of convergence than other root finding techniques and provides a solution for predictable PU channels. Based on the outcome of the ISPTO algorithm, our proposed *BCMS* assigns the predictable PU channels to the NRT SUs to minimize the total battery consumption of the SUs. For channel assignment, BCMS considers the diversity in data transmission lengths of the NRT SUs, SU channel SNRs, PU channel activities, detected PU channel SNR at the CBS and solves the resource allocation problem in polynomial time using Hungarian technique. BCMS also provides *fairness* among NRT SUs through the grant fair index and degree of fairness variables as provided in the chapter.

Performance analysis shows that the proposed CSSP framework provides atleast 6% and 48% improvement in energy-efficiency in comparison to BSS and CSS respectively at 10 times stricter PU interference constraint. Moreover, ISPTO algorithm determines that the channels having the minimum PU SNR of -20dB are predictable when their PU activities are greater than 68%. This predictable PU activity range improves to 62% for PU SNR greater than equal to -18dB. Therefore, the CSSP framework improves the spectral efficiency of CRN by assigning the un-utilized high PU activity channels exclusively to NRT SUs, while the RT users continue to use low activity channels through traditional approaches. We have also showed that BCMS can obtain better (lower) battery consumption and fairness performance as compared to a heuristic scheduler. Furthermore, it is shown that by choosing the appropriate degree of fairness a network designer can obtain the required level of balance between fairness and battery consumption. Finally, an NRT WBAN communication use case is implemented in testbed to validate the functionality of CSSP framework that shows a suitable direction of use for future IoT applications. As a future work, we are extending adaptive transmission power mechanism in this work.

Chapter 8

Concluding Remarks

❝ *Quality is not an act, it is a habit.*❞

-Aristotle

Wireless Body Area Network (WBAN) is indeed a technology that allows citizens/patients to have more responsibility in managing their own health. Moreover, allowing interaction with care providers, whenever necessary. This is considered as a key solution towards providing an affordable and proactive healthcare system. In February 2012, IEEE provided IEEE 802.15.6 standard for the successful implementation of WBANs addressing both its consumer electronics and medical applications. Further, due to the remarkable progress in Internet and Communication Technologies (ICT), WBANs can be integrated with Internet by transmitting the data using long distance backhaul/convergence layer technologies comprising Wide-Area Access Networks (WANs) like cellular communications, e.g. GSM, GPRS, 3G, 4G. The convergence layer provides mobility to the patients allowing them to carry on their daily activities in both outdoor as well as indoor environments while still facilitating ubiquitous remote monitoring of the patient's health over the Internet. However, the aforementioned advantages of WBANs do not come without its own challenges both at the access and convergence layer. At the access layer, the primary challenges include enhancing the battery life of the sensor nodes while maintaining the strict QoS and reliability requirements of the medical applications under non-ideal channel conditions. While at the convergence layer, the primary challenges are i) efficient handling of the increasing demand for spectrum due to prolific increase in the number of IoT devices/applications such as remote health monitoring, and ii) minimization of the cost of data transfer over the backhaul. In this work, we address the aforementioned challenges through the application of Cognitive Radio (CR) technology. At the WBAN access layer, we employ CR technology to enable a sensor node to adapt its parameters according to the environment so as to maximize its performance under all

conditions. Whereas at the backhaul, we exploit CR in the form of Dynamic Spectrum Access (DSA) or backhaul Cognitive Radio Network (CRN) to reduce spectrum congestion, utilize the bandwidth at the maximum and provide low cost broadband access for remote health monitoring.

Prior to making the access layer sensor nodes cognitive in nature, we conduct intensive performance analysis and design of WBAN based on IEEE 802.15.6. Additionally, in this work we consider the Scheduled Access MAC (SAM) protocol as it provides good solutions to the traffic correlation. These protocols are energy conserving protocols because the duty cycle is reduced and there are no contention, idle listening, and overhearing problems. As for the backhaul CRN, in this thesis we deal with the design and implementation aspects to enable Non-Real Time (NRT) energy-efficient and cost-efficient transfer of small amounts of WBAN collected medical data to the remote end over CRN. However, the research methodologies in this thesis can be made equally applicable to other NRT data transfer cases as encountered in several IoT and Machine-to-Machine (M2M) applications.

This chapter provides a brief summary of the research accomplishments carried out in this thesis, in accordance with the overall objectives of research (as stated in Chapter 1), and also discusses the future aspects of system and application development that can be pursued based on the obtained outcome in the thesis.

8.1 Summary of Research Accomplishments

Due to the absence of any simulation model of WBAN based on IEEE 802.15.6 standard, the first step in this thesis is to develop a comprehensive simulation model. This model serves as a platform for validating analytical observations and also facilitate performance analysis and optimization of designed WBANs in the thesis. ***Accordingly, this thesis builds a detailed simulation model in OPNET Modeler 16.0 of WBAN following IEEE 802.15.6 SAM.*** For this, we perform detailed network, node and process level modeling as per the rules outlined in the standard. Extensive analysis is performed to study correlation between performance metrics like average frame delay, throughput and energy consumption of the sensor nodes and system parameters like traffic loads, Payload Sizes (PSs) and Allocation Intervals (AIs). The developed simulation model can be used in future research work like validation of derived analytical models, performance analysis of WBAN setups, followed by suitable optimization. The designed simulation model can also be implemented as training tools to acquaint researchers with the fundamental ideas of MAC protocols of IEEE 802.15.6 in general and SAM in particular. ***In the next phase of work, we use the simulation model for energy-efficient design and implementation of WBAN on real test-***

bed to facilitate real-time health monitoring and non-real time transfer of small amounts of WBAN captured data to remote server in an e-healthcare framework. In this regard, the complete implementation specific details are provided pertaining to the selection of components and their extensive implementation involving interfacing of MCU of sensor nodes with CC1101 low power transceiver. A proposed technique to multiplex data from multiple sensors is highlighted. Lastly, we leverage the OPNET model to characterize and optimize the designed WBAN. We obtain the optimal AIs for ECG and temperature monitoring using the developed OPNET simulation model maximizing the network capacity within a frame delay constraint. Furthermore, we show the development of a state-of-the art BNC which has the ability to collect data from multiple sensors of a patient, compress them using a proposed Discrete Wavelet Transform (DWT) based technique for the BNC called B-DWT, and thereafter, send the data to Remote Server (RS) over cellular network. We also determined *Bi-orthogonal 4.4 Wavelet filter* as the most suitable filter for B-DWT algorithm providing 67% signal compression with less than 2% information loss. Our proposed B-DWT outperforms traditional DWT in terms of 64% faster execution time and takes 2% less memory of resource constraint BNC. The overall WBAN setup is successfully integrated within an e-healthcare framework which collects and stores data from multiple patients for pervasive access. The developed test-bed model of WBAN serves as a precursor to efficient integration of CR features for real-time adaptation of system parameters based on channel conditions.

Prior to deploying WBAN over CR backhaul, it is imperative that we develop a real-time CR interface that enables opportunistic IP based communication for the SUs over licensed PU channels in a practical hardware test-bed. This requires an efficient spectrum sensing mechanism for the SU. ***To this end, we perform analytical and simulation study of the performance of energy detection based sensing under sensing uncertainties and varied PU activities.*** We obtain the Receiver Operating Characteristics (ROC) for energy detection based sensing with respect to different receiver sensitivities, which is the minimum PU SNR that can be detected with 90% probability. In addition, we keep the interference to PU channels within predetermined limit and study the normalized interference metric. ***Thereafter, we characterize energy detection based sensing in an actual test-bed comprising of WARP boards.*** In case of WARP, we obtain a sensing time of 3ms for a SU receiver sensitivity of -20dB. The variation of sensing time is also shown for varied receiver sensitivity. Following this, we model an Energy Detection based CR MAC (ECR-MAC) at the Embedded Processor (EP) of WARP. ***The ECR-MAC employs a proposed Practical Energy-Efficient Energy Detection (PED) method which exploits the already available FPGA resources for practical realization of energy detection.*** PED method shows a significant reduction in energy

consumed for spectrum sensing at higher detected PU SNRs. For example, the effective sensing time to detect a PU signal with detected SNR=-10dB for a detection probability of 0.9 is obtained as 0.3ms, therefore there is almost 99% reduction in energy consumption upon employing PED method as against traditional energy detection method. Lastly, we validate the functionality of ECR-MAC framework by deploying opportunistic IP enabled SU communication over PU activity channels in our developed test-bed setup.

After suitably designing the simulation model and test-bed model for WBAN, ***the focus shifts to the detailed analytical study of WBAN based on IEEE 802.15.6 SAM under non-ideal channel conditions, followed by CR enabled optimization to achieve optimal system performance.*** The need for a detailed study of IEEE 802.15.6 SAM is addressed by conducting a comprehensive mathematical analysis. Applying queuing theory, we derive the average waiting delay of the frames, the throughput and energy consumption of the sensor nodes. For this, we take into account the presence of immediate acknowledgment, non-ideal channel fading and BCH encoding. We also analyze the Energy Efficiency (EE) of sensor nodes and reliability of data transfer. Detailed analysis is performed over both analytical and developed OPNET simulation model to study WBAN performance against different system parameters like the length of allocation intervals, varied traffic loads, payload sizes, beacon intervals, information data rate, error probability due to different modulation schemes and channel SNRs. Through the analysis, we determine optimal allocation intervals for the sensor nodes that maximize the energy-efficiency of sensor nodes under frame delay and reliability constraints. We also show how the proposed analytical model provides the system designers a tool to obtain LUTs stored locally at the sensor nodes for adaptively optimizing the AIs and PSs based on the channel SNRs. In this approach the sensor nodes use their CR ability to sense the channel SNR and adapt the AIs and PSs to the optimal values obtained from their LUTs.

A significant research contribution also been made in this thesis to address the problem of spectrum scarcity and the need for reliable cost-efficient remote health monitoring through design and implementation of a novel cross-layer based intelligent WBAN gateway called BodyCog-BNC, that exploits CR interface to perform DSA for NRT backhaul communication over PU channels in an opportunistic manner and also intelligently switch to conventional licensed WAN technologies when the CR backhaul is not suitable for communication. We term this intelligent switching ability of BodyCog-BNC as "spectrum agility". For this, two cross-layer based units are proposed for the BodyCog-BNC, namely BodyCog-BNC Management Entity (BME) and BodyCog CR MAC (BCR-MAC) which are part of our modified protocol stack for the BNC. For implementing the BME and BCR-MAC units we leverage on the Finite State Machine (FSM) based development

frameworks BME Development (BMED) architecture and BCR-MAC Development (BCRD) architecture respectively. Subsequently, we exploit these frameworks to implement interrupt based intelligent cross-layer message passing between BME and BCR-MAC and control message interchange between BCR-MAC and CBS. Leveraging this cross-layer message passing, we enable spectrum agility between CR interface and licensed WAN when i) the control channel of backhaul CRN is un-suitable for communication, or ii) the BNC encounters successive handoffs due to presence of PU in successive channels, or iii) the channel provided by CBS is not suitable for reliable communication. We have also optimized the CR backhaul communication through a proposed Inter-Sensing Time Optimization (ISTO) algorithm. It uses very efficient convex optimization techniques to maximize the energy-efficiency of transmission over PU channel allocated by CBS while still satisfying the strict PU interference constraint under sensing uncertainties. Further, we present closed form analytical expressions for different performance metrics like the average energy consumption, probability of switching from CR interface to licensed WAN, the time taken for such switching and the cost-efficiency in terms of PU activity, detected PU SNR, control channel conditions, NRT data transferred and the CR cost regimes. These expressions would help system designers suitably select system parameters like the number of handoffs allowed or properly selecting the CR cost regime so as to maximize the cost-efficiency for users and profits for the network operators. We show that the proposed BodyCog-BNC uses the CR interface more that 94% of the time for backhaul communication, achieving a significantly high cost-efficiency as compared to conventional licensed WAN technologies. Moreover, the high cost efficiency is ensured for a wide range of healthcare data and under varied CR cost regimes. Furthermore, the use of cross-layer message passing leads to a minimum 100% improvement in the switching time as compared to non cross-layer based approach. Lastly, a real hardware prototype of BodyCog-BNC is also designed to illustrate the feasibility of the proposed approach in enabling NRT remote healthcare monitoring. For this, we leverage both of our previously designed WBAN test-bed and CR test-bed.

Lastly, we consider backhaul CRNs with adequate resources at the CBS. In this case, significant gains in energy-efficiency of the NRT SUs (like WBAN BNCs) can be attained through sensing, prediction and scheduling at the CBS. ***To this end, we develop a Centralized Scheduling, Sensing and Prediction (CSSP) framework at the CBS.*** In the proposed framework, we incorporate Hidden Markov Model (HMM) based prediction within the traditional CR sensing transmission cycle. To minimize the prediction time, we design a Hardware based HMM engine (H2M2) to be used by the CBS. The H2M2 engine minimizes the prediction time by 76.8% and thus improves the energy efficiency of the CR cycle. H2M2 also minimizes energy consumption by reducing the collisions between SU and PU. However,

in doing so it also decreases the throughput of transmission. Therefore, to address this we develop an Inter Sensing-Prediction Time Optimization (ISPTO) algorithm, that identifies the predictable PU activity channels and maximizes the throughput within a PU interference threshold. The ISPTO alorithm that employs Ridder's method to obtain the optimal inter-sensing duration with quadratic rate of convergence. ISPTO algorithm also identifies the predictable PU channels by taking into consideration the effect of sensing uncertainties. ISPTO algorithm determines that the channels having the minimum PU SNR of -20dB are predictable when their PU activities are greater than 68%. This predictable PU activity range improves to 62% for PU SNR greater than equal to -18dB. Furthermore, to minimize the total battery consumption of all the SUs within CRN, a Battery Consumption Minimizing Scheduler (BCMS) is designed at the CBS that efficiently allocates the predictable PU channels to the NRT SUs. The BCMS employs Hungarian algorithm to solve the assignment problem in polynomial time and allocating the predictable channels to NRT SUs in the CRN. The proposed CSSP framework provides atleast 6% and 48% improvement in energy efficiency in comparison to Base Station Based Sensing and Collaborative Spectrum Sensing respectively at 10 times stricter PU interference constraint. We remark that, the CSSP framework allows NRT SUs to energy-efficiently send their data over high PU activity channels, whereas the RT users can continue using low PU activity channels through traditional sensing techniques. Therefore, by effectively allowing the utilization of both low and high PU activity channels, the CSSP framework also improves the CRN spectrum capacity. Finally, through a proof of concept we validate the ability of CSSP framework in enabling NRT communication.

In a nutshell the work in this thesis satisfactorily fulfills all the stated objectives through innovative research domains: i) facilitating energy-efficient WBAN communication through detailed analysis of MAC protocols, ii) enabling cost-efficient NRT backhaul data transmission with high energy efficiency , and iii) design and test-bed implementation. This is suitably demonstrated in Figure 8.1.

8.2 Future Scope

This thesis presented the research work to implement energy-efficient standalone WBAN with CR enabled features followed by its integration over backhaul CRN for cost-efficient, spectral efficient and energy-efficient remote health monitoring. In addition, formulating *WBAN transmission power adaptation*, and *appropriate WBAN MAC protocols* is essential to ensure optimal energy efficiency of sensor nodes when operating in unlicensed environment in the presence of other co-located systems. Similarly, considering our proposed CSSP framework, there is scope of further enhancement by *multiplexing multiple users in a white*

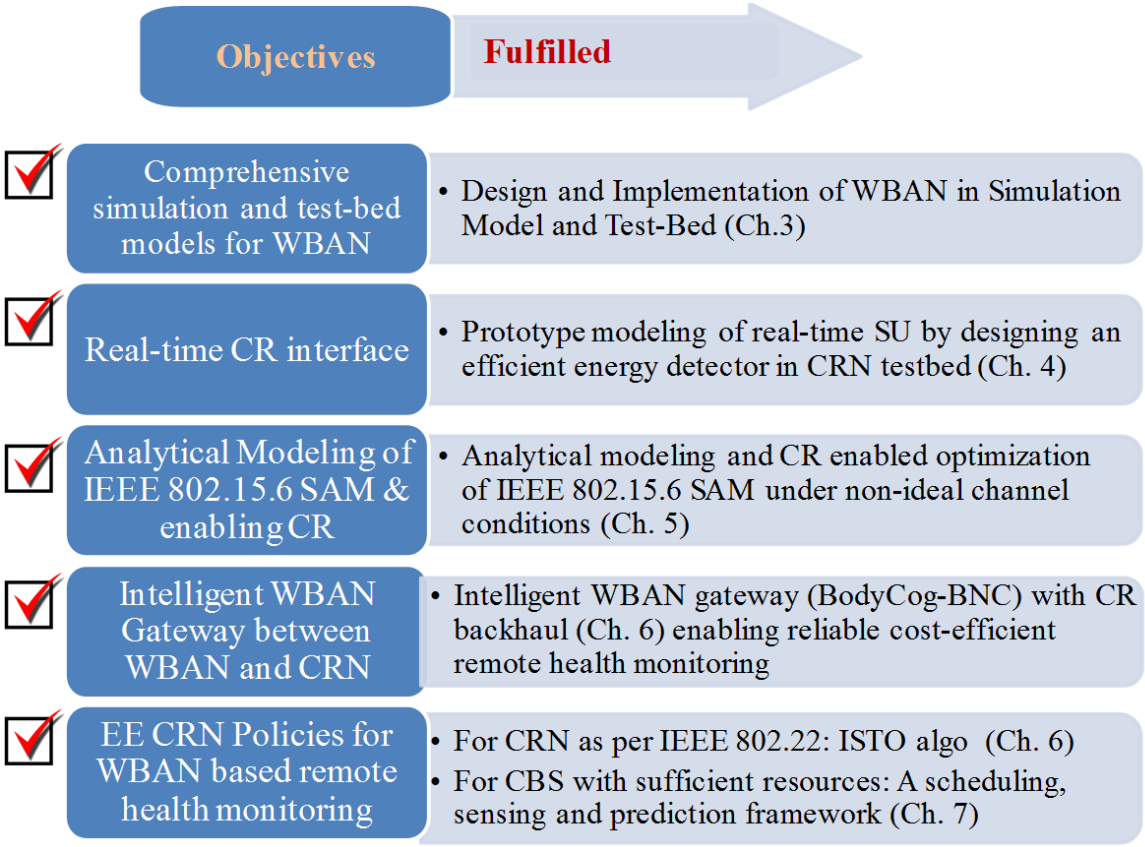

Fig. 8.1 Fulfillment of all the research objectives in the thesis

space detected by the CBS. In this regard, the research accomplishments in this thesis require further investigation in the following areas as listed below.

1. ***Design of efficient power adaptation strategies for WBAN sensor nodes for maximizing their energy-efficiency by taking into account several factors like frame delay, non-ideal channel conditions, reliability of data transfer, power budget etc.***

2. ***Design and analysis of WBAN MAC protocols that will enable a WBAN to adapt transmission power and also co-exist with other co-located heterogeneous wireless systems in the same channel.***

3. ***Suitable modification of the CSSP framework to enable transmission of multiple NRT users within a detected white-space.***

These issues are briefly discussed as follows.

1. ***Design of efficient power adaptation strategies for WBAN sensor nodes for maximizing their energy-efficiency by taking into account several factors like frame delay, non-ideal channel conditions, reliability of data transfer, power budget etc.***

Because of their structure and applications, coverage area of WBANs are quite likely to overlap each other, and due to limited available frequency bands, they will interfere with each other. This inter-network interference will cause serious problems in WBANs. It will decline the Signal-to-Interference Noise Ratio (SINR) and thereby cause throughput degradation and packet loss. Packet loss also leads to energy waste, which is the scarcest resource in WBANs. Furthermore, from the reliability point of view, interference may cause life critical packet loss and hence it is a serious threat to patients' lives. Although IEEE 802.15.6 supports channel hopping, superframe interleaving etc, transmission power control still plays an important role in the interference mitigation and resource management problem in wireless networks. Since multiple WBANs operate in a distributed manner, game theoretic approaches are being considered to address this issue. Therefore an efficiently designed power control game can help maximize the total system energy-efficiency by reducing cross-interference between links in different WBANs while consuming as little power as possible to achieve it.

2. ***Analysis of WBAN MAC protocols by incorporating co-existence and/or interference mitigation techniques***

A BNC/hub of a WBAN may need to employ mechanisms for enabling coexistence and/or interference mitigation between its WBAN and neighbor WBANs. To this end, IEEE 802.15.6 specifies Beacon Shifting, Channel Hopping, and Active Superframe Interleaving techniques. Furthermore, power adaptation is also another popular way of minimizing the effect of interference between different co-existing systems. This thesis has considered IEEE 802.15.6 SAM protocol for a single WBAN while assuming that coexistence issues do not affect steady state behavior. In this regard, it is necessary to conduct further analysis to investigate any effect of interference mitigation techniques on the performance analysis presented in this thesis.

3. ***Suitable modification of the CSSP framework to enable transmission of multiple NRT users within a detected white-space.***

Since an NRT SU transmission takes a very small duration, it is possible to mutiplex a number of NRT SUs within the inter-sensing duration. The assigned SUs can follow a TDMA based approach for uplink data transfer to CBS. However, this also increases the complexity of the scheduling mechanism of CBS. The assignment problem proposed for BCMS in this thesis considers assignment of single SU to the white-space of a PU channel. This needs to be modified to allow the CBS to optimally assign multiple SUs to a single PU channel.

References

[1] Global atlas on cardiovascular disease prevention and control-Geneva. *World Health Organization*, 2011.

[2] World Health Organization. Life expectancy at birth (years), 2017. Available: http://gamapserver.who.int/gho/interactive_charts/mbd/life_expectancy/atlas.html.

[3] The World Bank. World health organization global health expenditure database, 2018. Available: https://data.worldbank.org/indicator/SH.XPD.TOTL.ZS?end=2014&start=1995.

[4] S J Schieber, D K Bilyeu, D R Hardy, M R Katz, B B Kennelly, and M J Warshawsky. The unsustainable cost of health care. 2016.

[5] U Varshney. Pervasive healthcare: Applications, challenges and wireless solutions. *Communications of the Association for Information Systems*, 16(1):3, 2005.

[6] B Latré, B Braem, I Moerman, C Blondia, and P Demeester. A survey on wireless body area networks. *Wireless Networks*, 17(1):1–18, 2011.

[7] FCC. Notice of proposed rule making and order. *ET Docket no. 03-222*, 2003.

[8] X Hong, J Wang, C X Wang, and J Shi. Cognitive radio in 5G: A perspective on energy-spectral efficiency trade-off. *IEEE Communications Magazine*, 52(7):46–53, 2014.

[9] Q Zhao and B M Sadler. A survey of dynamic spectrum access. *IEEE Signal Processing Magazine*, 24(3):79–89, 2007.

[10] I F Akyildiz, W Y Lee, M C Vuran, and S Mohanty. NeXt generation/dynamic spectrum access/cognitive radio wireless networks: A survey. *Computer Networks*, 50(13):2127–2159, 2006.

[11] T A Weiss and F K Jondral. Spectrum pooling: An innovative strategy for the enhancement of spectrum efficiency. *IEEE Communications Magazine*, 42(3):8–14, 2004.

[12] IEEE Standards News. ISO approves the award-winning IEEE 802.22-2011 standard to provide broadband connectivity to rural and underserved global communities, 2017. Available: standards.ieee.org/news/2015/ieee_802.22.html.

[13] K Doughty, K Cameron, and P Garner. Three generations of telecare of the elderly. *Journal of Telemedicine and Telecare*, 2(2):71–80, 1996.

[14] P F Binkley. Predicting the potential of wearable technology. *IEEE Engineering in Medicine and Biology Magazine*, 22(3):23–27, 2003.

[15] Holter Systems Med-Electronics Inc. Holter monitor, 2005. Available: http://med-electronics.com.

[16] T Martin, E Jovanov, and D Raskovic. Issues in wearable computing for medical monitoring applications: A case study of a wearable ECG monitoring device. 4th International Symposium on Wearable Computers, pages 43–49, Atlanta, GA, 2000.

[17] S Movassaghi, M Abolhasan, J Lipman, D Smith, and A Jamalipour. Wireless body area networks: A survey. *IEEE Communications Surveys & Tutorials*, 16(3):1658–1686, 2014.

[18] Jawbone. Jawbone up, 2018. Available: https://jawbone.com/up.

[19] Fitbit. Fitbit app, 2018. Available: https://www.fitbit.com.

[20] Apple. Apple health kit, 2018. Available:developer.apple.com/reference/healthkit.

[21] IEEE standard for local and metropolitan area networks—Part 15.1: Wireless personal area networks (WPANs),. *IEEE Std*, 2005.

[22] IEEE standard for local and metropolitan area networks—Part 15.4: Low-rate wireless personal area networks (LR-WPANs). *IEEE Std*, 2011.

[23] IEEE standard for local and metropolitan area networks—part 15.6: Wireless body area networks. *IEEE Std.*, 2012.

[24] L Hanlen, D Smith, A Boulis, B Gilbert, V Chaganti, L Craven, D Fang, T Lamahewa, D Lewis, D Miniutti, et al. Wireless body area-networks: Toward a wearable intranet. *National ICT Australia*, 2011.

[25] G Z Yang and G Yang. *Body sensor networks*, volume 1. Springer, 2006.

[26] R Cavallari, F Martelli, R Rosini, C Buratti, and R Verdone. A survey on wireless body area networks: Technologies and design challenges. *IEEE Communications Surveys & Tutorials*, 16(3):1635–1657, 2014.

[27] C Zhang, Y Wang, Y Liang, M Shu, J Zhang, and L Ni. Low duty-cycling MAC protocol for low data-rate medical wireless body area networks. *Sensors*, 17(5):1134, 2017.

[28] J Yu, B Huang, X Cheng, and M Atiquzzaman. Shortest link scheduling algorithms in wireless networks under the sinr model. *IEEE Transactions on Vehicular Technology*, 66(3):2643–2657, 2017.

[29] M S Akbar, H Yu, and S Cang. Delay, reliability, and throughput based QoS profile: A MAC layer performance optimization mechanism for biomedical applications in wireless body area sensor networks. *Journal of Sensors*, 2016, 2016.

[30] J S Yoon, G S Ahn, S S Joo, and M J Lee. PNP-MAC: Preemptive slot allocation and non-preemptive transmission for providing QoS in body area networks. IEEE Consumer Communications and Networking Conference, pages 1–5, 2010.

[31] S Ullah and K S Kwak. An ultra low-power and traffic-adaptive medium access control protocol for wireless body area network. *Journal of Medical Systems*, 36(3):1021–1030, 2012.

[32] Victor Cionca, Thomas Newe, and Vasile Dadârlat. TDMA protocol requirements for wireless sensor networks. 2nd International Conference on Sensor Technologies and Applications, pages 30–35, 2008.

[33] S J Marinkovic, E M Popovici, C Spagnol, S Faul, and W P Marnane. Energy-efficient low duty cycle MAC protocol for wireless body area networks. *IEEE Transactions on Information Technology in Biomedicine*, 13(6):915–925, 2009.

[34] H Arslan. *Cognitive radio, software defined radio, and adaptive wireless systems*. Springer, 2007.

[35] M Chen, S Gonzalez, A Vasilakos, H Cao, and V C M Leung. Body area networks: A survey. *Mobile Networks and Applications*, 16(2):171–193, 2011.

[36] Wireless LAN medium access control (MAC) and physical layer (PHY) specifications. *IEEE Std. 802.11*, 1997.

[37] R L Evans. *QoS in integrated 3G networks*. Artech House, 2002.

[38] FCC. Spectrum policy task force report. *ET Docket no. 02-135*, 2002.

[39] A N Mody and G Chouinard. IEEE 802.22 wireless regional area networks enabling rural broadband wireless access using cognitive radio technology. *doc. : IEEE 802.22-10/0073r03*, 2010.

[40] C R Stevenson, G Chouinard, Z Lei, W Hu, SJ Shellhammer, and W Caldwell. IEEE 802.22: The first cognitive radio wireless regional area network standard. *IEEE Communications Magazine*, 47(1):130–138, 2009.

[41] J Huang, R A Berry, and M L Honig. Spectrum sharing with distributed interference compensation. 1st IEEE International Symposium on New Frontiers in Dynamic Spectrum Access Networks, DySPAN, pages 88–93, Baltimore, 2005.

[42] V Brik, E Rozner, S Banerjee, and P Bahl. DSAP: a protocol for coordinated spectrum access. 1st IEEE International Symposium on New Frontiers in Dynamic Spectrum Access Networks, DySPAN, pages 611–614, Baltimore, 2005.

[43] L Cao and H Zheng. Distributed spectrum allocation via local bargaining. IEEE Sensor and Ad Hoc Communications and Networks, SECON, pages 475–486, California, USA, 2005.

[44] L Ma, X Han, and C C Shen. Dynamic open spectrum sharing MAC protocol for wireless ad hoc networks. 1st IEEE International Symposium on New Frontiers in Dynamic Spectrum Access Networks, DySPAN, pages 203–213, Baltimore, 2005.

[45] S Sankaranarayanan, P Papadimitratos, A M Bradley, and S Hershey. A bandwidth sharing approach to improve licensed spectrum utilization. 1st IEEE International Symposium on New Frontiers in Dynamic Spectrum Access Networks, DySPAN, pages 279–288, Baltimore, 2005.

[46] IEEE standard for local and metropolitan area networks—Part 22: Wireless Regional Area Networks. *IEEE Std.*, 2012.

[47] T Gao, D Greenspan, M Welsh, R R Juang, and A Alm. Vital signs monitoring and patient tracking over a wireless network. 27th Annual International Conference of the IEEE Engineering in Medicine and Biology Society, EMBS, pages 102–105, China, 2006.

[48] C A Otto, E Jovanov, and A Milenkovic. A WBAN-based system for health monitoring at home. 3rd IEEE/EMBS International Summer School on Medical Devices and Biosensors, ISSS-MDBS, pages 20–23, NY, USA, 2006.

[49] C H Chan, C C Y Poon, R C S Wong, and Y T Zhang. A hybrid body sensor network for continuous and long-term measurement of arterial blood pressure. 4th IEEE/EMBS International Summer School and Symposium on Medical Devices and Biosensors, ISSS-MDBS, pages 121–123, United Kingdom, 2007.

[50] A Soomro and D Cavalcanti. Opportunities and challenges in using WPAN and WLAN technologies in medical environments. *IEEE Communications Magazine*, 45(2):114–122, 2007.

[51] M R Yuce and C K Ho. Implementation of body area networks based on MICS/WMTS medical bands for healthcare systems. 30th Annual International Conference of the IEEE Engineering in Medicine and Biology Society, EMBS, pages 3417–3421, Canada, 2008.

[52] U Anliker, J A Ward, P Lukowicz, G Troster, F Dolveck, M Baer, et al. AMON: A wearable multiparameter medical monitoring and alert system. *IEEE Transactions on Information Technology in Biomedicine*, 8(4):415–427, 2004.

[53] J M Choi, R S H Istepanian, A Alesanco, and H Wang. Hardware design & compression issues in compact bluetooth enabled wireless telecardiology system. 2nd International Conference on Broadband Networks, BroadNets, pages 1014–1015, MA, USA, 2005.

[54] M F A Rasid and B Woodward. Bluetooth telemedicine processor for multichannel biomedical signal transmission via mobile cellular networks. *IEEE Transactions on Information Technology in Biomedicine*, 9(1):35–43, 2005.

[55] FCC. MICS band plan, 2003.

[56] FCC. Wireless medical telemetry, 2000.

[57] S Hanna. Regulations and standards for wireless medical applications. 3rd International Symposium on Medical Information and Communication Technology, pages 23–26, MA, USA, 2009.

[58] Q Pang, S C Liew, J Y B Lee, and V Leung. Performance evaluation of an adaptive backoff scheme for WLAN. *Wireless Communications and Mobile Computing*, 4(8):867–879, 2004.

[59] R Gharpurey and P Kinget. *Ultra wideband: circuits, transceivers and systems*. Springer, 2008.

[60] M R Yuce, H C Keong, and M S Chae. Wideband communication for implantable and wearable systems. *IEEE Transactions on Microwave Theory and Techniques*, 57(10):2597–2604, 2009.

[61] D B Smith, D Miniutti, T A Lamahewa, and L W Hanlen. Propagation models for body-area networks: A survey and new outlook. *IEEE Antennas and Propagation Magazine*, 55(5):97–117, 2013.

[62] S L Cotton and W G Scanlon. Indoor channel characterisation for a wearable antenna array at 868 MHz. IEEE Wireless Communications and Networking Conference, WCNC, pages 1783–1788, NV, USA, 2006.

[63] A Fort, C Desset, P D Doncker, P Wambacq, and L V Biesen. An ultra-wideband body area propagation channel model-from statistics to implementation. *IEEE Transactions on Microwave Theory and Techniques*, 54(4):1820–1826, 2006.

[64] S Rashwand, J Mišić, and H Khazaei. Performance analysis of IEEE 802.15.6 under saturation condition and error-prone channel. IEEE Wireless Communications and Networking Conference, WCNC, pages 1167–1172, Mexico, 2011.

[65] S Rashwand, J Mišić, and V B Mišić. Analysis of CSMA/CA mechanism of IEEE 802.15.6 under non-saturation regime. *IEEE Transactions on Parallel and Distributed Systems*, 27(5):1279–1288, 2016.

[66] S Sarkar, S Misra, B Bandyopadhyay, C Chakraborty, and M S Obaidat. Performance analysis of IEEE 802.15.6 MAC protocol under non-ideal channel conditions and saturated traffic regime. *IEEE Transactions on Computers*, 64(10):2912–2925, 2015.

[67] M S Chowdhury, K Ashrafuzzaman, and K S Kwak. Saturation throughput analysis of IEEE 802.15.6 slotted aloha in heterogeneous conditions. *IEEE Wireless Communications Letters*, 3(3):257–260, 2014.

[68] M Sherman, A N Mody, R Martinez, C Rodriguez, and R Reddy. IEEE standards supporting cognitive radio and networks, dynamic spectrum access, and coexistence. *IEEE Communications Magazine*, 46(7), 2008.

[69] R C Santiago, K E Nolan, O Holland, L D Nardis, J M Ferro, N Barroca, L M Borges, F J Velez, V Goncalves, and I Balasingham. Cognitive radio for medical body area networks using ultra wideband. *IEEE Wireless Communications*, 19(4), 2012.

[70] P Phunchongharn, E Hossain, D Niyato, and S Camorlinga. A cognitive radio system for e-health applications in a hospital environment. *IEEE Wireless Communications*, 17(1), 2010.

[71] T S Rappaport. *Wireless communications: principles and practice*, volume 2. Prentice Hall, 1996.

[72] L Dai, B Wang, Y Yuan, S Han, I Chih-Lin, and Z Wang. Non-orthogonal multiple access for 5G: Solutions, challenges, opportunities, and future research trends. *IEEE Communications Magazine*, 53(9):74–81, 2015.

[73] F Boccardi, R W Heath, A Lozano, T L Marzetta, and P Popovski. Five disruptive technology directions for 5G. *IEEE Communications Magazine*, 52(2):74–80, 2014.

[74] J Mitola III. Cognitive radio for flexible mobile multimedia communications. *Mobile Networks and Applications*, 6(5):435–441, 2001.

[75] S Haykin. Cognitive radio: Brain-empowered wireless communications. *IEEE Journal on Selected Areas in Communications*, 23(2):201–220, 2005.

[76] T Yucek and H Arslan. A survey of spectrum sensing algorithms for cognitive radio applications. *IEEE Communications Surveys & Tutorials*, 11(1):116–130, 2009.

[77] A Ghasemi and E S Sousa. Spectrum sensing in cognitive radio networks: Requirements, challenges and design trade-offs. *IEEE Communications Magazine*, 46(4), 2008.

[78] D Cabric, S M Mishra, and R W Brodersen. Implementation issues in spectrum sensing for cognitive radios. 38th Asilomar conference on signals, systems and computers, pages 772–776, California, 2004.

[79] I F Akyildiz, W Y Lee, M C Vuran, and S Mohanty. A survey on spectrum management in cognitive radio networks. *IEEE Communications magazine*, 46(4), 2008.

[80] I Christian, S Moh, I Chung, and J Lee. Spectrum mobility in cognitive radio networks. *IEEE Communications Magazine*, 50(6), 2012.

[81] J Ma and Y G Li. A probability-based spectrum sensing scheme for cognitive radio. IEEE International Conference on Communications, ICC, pages 3416–3420, China, 2008.

[82] X W Zhou, Y Li, and Y H Kwon. Detection timing and channel selection for periodic spectrum sensing in cognitive radio. IEEE Global Telecommunications Conference, GLOBECOM, pages 1–5, LA, USA, 2008.

[83] T Manna and I S Misra. Implementation of relay based collaborative spectrum sensing using coalitional games in wireless cognitive radio networks. *Computers and Electrical Engineering*, 45:77–99, 2015.

[84] Y Xu, Y Sun, Y Li, Y Zhao, and H Zou. Joint sensing period and transmission time optimization for energy-constrained cognitive radios. *EURASIP Journal on Wireless Communications and Networking*, 2010(1):818–964, 2010.

[85] C Cordeiro and K Challapali. C-MAC: A cognitive MAC protocol for multi-channel wireless networks. In *2nd IEEE International Symposium on New Frontiers in Dynamic Spectrum Access Networks, DySPAN*, pages 147–157, Ireland, 2007.

[86] C Cordeiro, K Challapali, D Birru, and S Shankar. IEEE 802.22: The first worldwide wireless standard based on cognitive radios. 1st IEEE International Symposium on New Frontiers in Dynamic Spectrum Access Networks, DySPAN, pages 328–337, Baltimore, 2005.

[87] I A Akbar and W H Tranter. Dynamic spectrum allocation in cognitive radio using hidden markov models: Poisson distributed case. IEEE SoutheastCon, pages 196–201, Richmond, VA, 2007.

[88] R A Rashid, M A Sarijari, N Fisal, S K S Yusof, and S H S Ariffin. Enabling dynamic spectrum access for cognitive radio using software defined radio platform. IEEE Symposium on Wireless Technology and Applications, pages 180–185, Malaysia, 2011.

[89] K Mandke, S H Choi, G Kim, R Grant, R C Daniels, W Kim, R W Heath Jr, and S M Nettles. Early results on Hydra: A flexible MAC/PHY multihop testbed. 65th IEEE Vehicular Technology Conference, pages 1896–1900, Ireland, 2007.

[90] K H Lee, A Mate, and I T Lu. Practical implementation of time covariance based spectrum sensing methods using WARP. IEEE Long Island Systems, Applications and Technology Conference, pages 1–5, NY, USA, 2011.

[91] K Tan, K Kim, Y Xin, S Rangarajan, and P Mohapatra. RECOG: A sensing-based cognitive radio system with real-time application support. *IEEE Journal on Selected Areas in Communications*, 31(11):2504–2516, 2013.

[92] Information Sciences Institute. Network simulator NS-2, 2017. Available: www.isi.edu/nsnam/ns/.

[93] OpenSim Ltd. OMNeT++, 2017. Available: http://www.omnetpp.org/.

[94] National ICT(Australia). Castalia user manual, 2010. Available: http://castalia.npc.nicta.com.au/pdfs/Castalia-UserManual.pdf.

[95] Riverbed Technolgies. OPNET, 2012. Available: www.opnet.com.

[96] P JurcÃk, M Alves, E Tovar, Z Hanzálek, et al. A simulation model for the IEEE 802.15.4 protocol: Delay/throughput evaluation of the GTS mechanism. 15th International Symposium on Modeling, Analysis, and Simulation of Computer and Telecommunication Systems, MASCOTS, pages 109–116, Turkey, 2007.

[97] A Jain, V Sharma, and B Amrutur. Soft real time implementation of a cognitive radio testbed for frequency hopping primary satisfying QoS requirements. 20th National Conference on Communications, NCC, pages 1–6, India, 2014.

[98] J L Hammond and P P O'Reilly. *Performance analysis of local computer networks*. Addison-Wesley Longman Publishing Co., 1986.

[99] C Tachtatzis, F D Franco, D C Tracey, N F Timmons, and J Morrison. An energy analysis of IEEE 802.15.6 scheduled access modes. IEEE GLOBECOM Workshops (GC Wkshps), pages 1270–1275, 2010.

[100] T Chakraborty, IS Misra, and T Manna. Design and implementation of VoIP based two-tier cognitive radio network for improved spectrum utilization. *IEEE Systems Journal*, 10(1):370–381, 2016.

[101] L R Rabiner. A tutorial on hidden markov models and selected applications in speech recognition. *Proceedings of the IEEE*, 77(2):257–286, 1989.

[102] M T Soleimani, M Kahvand, and R Sarikhani. Handoff reduction based on prediction approach in cognitive radio networks. 15th IEEE International Conference on Communication Technology, pages 319–323, China, 2013.

[103] V K Tumuluru, P Wang, and D Niyato. A novel spectrum-scheduling scheme for multichannel cognitive radio network and performance analysis. *IEEE Transactions on Vehicular Technology*, 60(4):1849–1858, 2011.

[104] D Gözüpek and F Alagöz. Throughput and delay optimal scheduling in cognitive radio networks under interference temperature constraints. *Journal of Communications and Networks*, 11(2):148–156, 2009.

[105] S Bayhan and F Alagoz. Scheduling in centralized cognitive radio networks for energy efficiency. *IEEE Transactions on Vehicular Technology*, 62(2):582–595, 2013.

[106] Federal Communications Commission(FCC). Notice of proposed rule making and order: Facilitating opportunities for flexible, efficient, and reliable spectrum use employing cognitive radio technologies. *ET docket*, (03-108), 2005.

[107] R C Shah and M Yarvis. Characteristics of on-body 802.15.4 networks. 2nd IEEE workshop on Wireless mesh networks, WiMesh, pages 138–139, Virginia, USA, 2006.

[108] M R Yuce. Implementation of wireless body area networks for healthcare systems. *Sensors and Actuators A: Physical*, 162(1):116–129, 2010.

[109] S Ullah, P Khan, N Ullah, S Saleem, H Higgins, and K S Kwak. A review of wireless body area networks for medical applications. *arXiv:1001.0831*, 2010.

[110] N de Vicq, F Robert, J Penders, B Gyselinckx, and T Torfs. Wireless body area network for sleep staging. IEEE Biomedical Circuits and Systems Conference, BIOCAS, pages 163–166, US, 2007.

[111] O Pereira, J Caldeira, and J J Rodrigues. Body sensor network mobile solutions for biofeedback monitoring. *Mobile Networks and Applications*, 16(6):713–732, 2011.

[112] J J Rodrigues, O R Pereira, and P Neves. Biofeedback data visualization for body sensor networks. *Journal of Network and Computer Applications*, 34(1):151–158, 2011.

[113] BIOTRONIK SE & Co. Cardiomessenger, 2017. Available: https://www.biotronik.com/en-de/products/crm/transmitter.

[114] M Lipprandt, M Eichelberg, W Thronicke, J Kruger, I Druke, D Willemsen, C Busch, C Fiehe, E Zeeb, and A Hein. OSAMI-D: An open service platform for healthcare monitoring applications. 2nd Conference on Human System Interactions, HSI, pages 139–145, Italy, 2009.

[115] J Nehmer, M Becker, A Karshmer, and R Lamm. Living assistance systems: an ambient intelligence approach. 28th International Conference on Software engineering, pages 43–50, Shanghai, China, 2006.

[116] Bluetooth SIG. Specification of the bluetooth system v4.0, 2010. Available: www.Bluetooth.org.

[117] D Lewis. 802.15.6 call for applications in body area networks response summary. *15–08–0407–05-0006*, 2008.

[118] J Y Khan, M R Yuce, G Bulger, and B Harding. Wireless body area network (WBAN) design techniques and performance evaluation. *Journal of medical systems*, 36(3):1441–1457, 2012.

[119] B Zhen, M Patel, S Lee, E Won, and A Astrin. Tg6 technical requirements document (TRD) IEEE p802.15-08-0644-09-0006. *Tech. Rep.*, 2008.

[120] K S Kwak, S Ullah, and N Ullah. An overview of IEEE 802.15. 6 standard. 3rd International Symposium on Applied Sciences in Biomedical and Communication Technologies, ISABEL, pages 1–6, Italy, 2010.

[121] S Saleem, S Ullah, and Hyeong S Yoo. On the security issues in wireless body area networks. *JDCTA*, 3(3):178–184, 2009.

[122] J Mitola. The software radio architecture. *IEEE Communications Magazine*, 33(5):26–38, 1995.

[123] P Bahl, R Chandra, P A Chou, J I Ferrell, T Moscibroda, S Narlanka, and Y Wu. KNOWS: Kognitiv networking over white spaces. 2nd IEEE International Symposium on New Frontiers in Dynamic Spectrum Access Networks, DySPAN, page 32, Ireland, 2007.

[124] B A Fette. *Cognitive radio technology*. Newnes, 2006.

[125] A J Petrin. *Maximizing the utility of radio spectrum: Broadband spectrum measurements and occupancy model for use by cognitive radio*. PhD thesis, Georgia Institute of Technology, 2005.

[126] D A Roberson, C S Hood, J L LoCicero, and J T MacDonald. Spectral occupancy and interference studies in support of cognitive radio technology deployment. 1st IEEE Workshop on Networking Technologies for Software Defined Radio Networks, pages 26–35, 1st IEEE Workshop on Networking Technologies for Software Defined Radio Networks, 2006.

[127] R I C Chiang, G B Rowe, and K W Sowerby. A quantitative analysis of spectral occupancy measurements for cognitive radio. 65th IEEE Vehicular Technology Conference, VTC, pages 3016–3020, 2007.

[128] M Wellens, A de Baynast, and P Mahonen. Exploiting historical spectrum occupancy information for adaptive spectrum sensing. IEEE Wireless Communications and Networking Conference, WCNC, pages 717–722, Las Vegas, US, 2008.

[129] M Nekovee. Quantifying the availability of TV white spaces for cognitive radio operation in the uk. IEEE International Conference on Communications Workshops, ICC Workshops, pages 1–5, 2009.

[130] M J Marcus. Unlicensed cognitive sharing of TV spectrum: The controversy at the federal communications commission. *IEEE Communications Magazine*, 43(5):24–25, 2005.

[131] A M Wyglinski, M Nekovee, and T Hou. *Cognitive radio communications and networks: Principles and practice*. Academic Press, 2009.

[132] Y C Liang, K C Chen, G Y Li, and P Mahonen. Cognitive radio networking and communications: An overview. *IEEE Transactions on Vehicular Technology*, 60(7):3386–3407, 2011.

[133] M Naeem, A Anpalagan, M Jaseemuddin, and Daniel C Lee. Resource allocation techniques in cooperative cognitive radio networks. *IEEE Communications Surveys & Tutorials*, 16(2):729–744, 2014.

[134] H A B Salameh, M Krunz, and O Younis. Cooperative adaptive spectrum sharing in cognitive radio networks. *IEEE/ACM Transactions on Networking (TON)*, 18(4):1181–1194, 2010.

[135] F R Yu and H Tang. *Cognitive radio mobile ad hoc networks*. Springer, 2011.

[136] C X Wang, X Hong, H H Chen, and J Thompson. On capacity of cognitive radio networks with average interference power constraints. *IEEE Transactions on Wireless Communications*, 8(4), 2009.

[137] J R Foerster. The performance of a direct-sequence spread ultrawideband system in the presence of multipath, narrowband interference, and multiuser interference. IEEE Conference on Ultra Wideband Systems and Technologies, pages 87–91, 2002.

[138] S Ponappa. Open spectrum for development India case study. *Association for Progressive Communications*, 2011.

[139] V C Gungor and D Sahin. Cognitive radio networks for smart grid applications: A promising technology to overcome spectrum inefficiency. *IEEE Vehicular Technology Magazine*, 7(2):41–46, 2012.

[140] A Sahai, N Hoven, and R Tandra. Some fundamental limits on cognitive radio. Allerton Conference on Communication, Control, and Computing, pages 1662–1671, Illinois, 2004.

[141] A Koubaa, M Alves, and E Tovar. A comprehensive simulation study of slotted CSMA/CA for IEEE 802.15.4 wireless sensor networks. IEEE International Workshop on Factory Communication Systems, pages 183–192, Italy, 2006.

[142] T Chakraborty, I S Misra, and S K Sanyal. Design and study of VoIP model in cognitive radio network under different simulation platforms. CUBE International Information Technology Conference, pages 160–165, Pune, India, 2012.

[143] S M S Jalaleddine, C G Hutchens, R D Strattan, and W A Coberly. ECG data compression techniques: A unified approach. *IEEE Transactions on Biomedical Engineering*, 37(4):329–343, 1990.

[144] L Sörnmo and P Laguna. *Bioelectrical signal processing in cardiac and neurological applications*, volume 8. Academic Press, 2005.

[145] M L Hilton. Wavelet and wavelet packet compression of electrocardiograms. *IEEE Transactions on Biomedical Engineering*, 44(5):394–402, 1997.

[146] Z Lu, D Y Kim, and W A Pearlman. Wavelet compression of ECG signals by the set partitioning in hierarchical trees algorithm. *IEEE Transactions on Biomedical Engineering*, 47(7):849–856, 2000.

[147] J G Proakis and D G Manolakis. *Digital signal processing: principles, algorithms, and applications*. Pearson Prentice Hall, 2007.

[148] S Lam. Delay analysis of a time division multiple access (tdma) channel. *IEEE Transactions on Communications*, 25(12):1489–1494, 1977.

[149] S G Mallat. A theory for multiresolution signal decomposition: The wavelet representation. *IEEE Transactions on Pattern Analysis and Machine Intelligence*, 11(7):674–693, 1989.

[150] Texas Instruments. CC1101 low-power sub-1 ghz RF transceiver datasheet, 2018. Available: www.ti.com/lit/ds/symlink/cc1101.pdf.

[151] Interaction Design Institute. Arduino Uno, 2018. Available: www.arduino.org/products/boards/arduino-uno.

[152] Analog Devices Inc. AD8232 datasheet, 2018. Available: www.analog.com/media/en/technical-documentation/data-sheets/AD8232.pdf.

[153] panStamp. Panstamp library, 2018. Available: github.com/panStamp/panstamp/wiki.

[154] Interaction Design Institute. Arduino Mega, 2018. Available: www.arduino.cc/en/Main/ArduinoBoardMega.

[155] Y Zigel, A Cohen, and A Katz. The weighted diagnostic distortion (WDD) measure for ECG signal compression. *IEEE Transactions on Biomedical Engineering*, 47(11):1422–1430, 2000.

[156] Federal Communications Commission. Unlicensed operation in the TV broadcast bands. *FCC 10-174*, 2010.

[157] J Mitola and G Q Maguire. Cognitive radio: Making software radios more personal. *IEEE Personal Communications*, 6(4):13–18, 1999.

[158] Federal Communications Commission. Notice of proposed rulemaking, in the matter of unlicensed operation in the TV broadcast bands (docket no. 04-186), 2004.

[159] Y Zhao, L Morales, J Gaeddert, K K Bae, J S Um, and J H Reed. Applying radio environment maps to cognitive wireless regional area networks. 2nd IEEE International Symposium on New Frontiers in Dynamic Spectrum Access Networks, DySPAN, pages 115–118, 2007.

[160] N Hoven, R Tandra, and A Sahai. Some fundamental limits on cognitive radio. *Wireless Foundations EECS, Univ. of California, Berkeley*, 2005.

[161] W Lin and Q Zhang. A design of energy detector in cognitive radio under noise uncertainty. 11th IEEE Singapore International Conference on Communication Systems, ICC, pages 213–217, Guangzhou, China, 2008.

[162] E Blossom. GNU radio: Tools for exploring the radio frequency spectrum. *Linux Journal*, 2004(122):4, 2004.

[163] K Amiri, Y Sun, P Murphy, C Hunter, J R Cavallaro, and A Sabharwal. WARP: A modular testbed for configurable wireless network research at Rice. IEEE SWRIF. Citeseer, 2007.

[164] C Chang, J Wawrzynek, and R W Brodersen. BEE2: A high-end reconfigurable computing system. *IEEE Design & Test of Computers*, 22(2):114–125, 2005.

[165] M Dardaillon, K Marquet, T Risset, and A Scherrer. Software defined radio architecture survey for cognitive testbeds. 8th International Wireless Communications and Mobile Computing Conference, IWCMC, pages 189–194, Istanbul, 2012.

[166] Rice University. Wireless open access research platform, 2017. Available: warp.rice.edu.

[167] L C Wang, C W Wang, and C J Chang. Modeling and analysis for spectrum handoffs in cognitive radio networks. *IEEE Transactions on Mobile Computing*, 11(9):1499–1513, 2012.

[168] Y Saleem and M H Rehmani. Primary radio user activity models for cognitive radio networks: A survey. *Journal of Network and Computer Applications*, 43:1–16, 2014.

[169] S Geirhofer, L Tong, and BM Sadler. Interference-aware OFDMA resource allocation: A predictive approach. IEEE Military Communications Conference, pages 1–7, California, 2008.

[170] S Geirhofer, L Tong, and B M Sadler. Cognitive radios for dynamic spectrum access-dynamic spectrum access in the time domain: Modeling and exploiting white space. *IEEE Communications Magazine*, 45(5), 2007.

[171] H Urkowitz. Energy detection of unknown deterministic signals. *Proceedings of the IEEE*, 55(4):523–531, 1967.

[172] YC Liang, Y Zeng, ECY Peh, and AT Hoang. Sensing-throughput tradeoff for cognitive radio networks. *IEEE Transactions on Wireless Communications*, 7(4):1326–1337, 2008.

[173] Putty, 2017. Available: www.putty.org.

[174] M A Huq, E Dutkiewicz, G Fang, Ren P Liu, and R Vesilo. MEB mac: Improved channel access scheme for medical emergency traffic in wban. International Symposium on Communications and Information Technologies, pages 371–376, Australia, 2012.

[175] C Li, J Li, B Zhen, H B Li, and R Kohno. Hybrid unified-slot access protocol for wireless body area networks. *International Journal of Wireless Information Networks*, 17(3-4):150–161, 2010.

[176] C Li, H B Li, and R Kohno. Reservation-based dynamic TDMA protocol for medical body area networks. *IEICE Transactions on Communications*, 92(2):387–395, 2009.

[177] Sana Ullah and Kyung Sup Kwak. Throughput and delay limits of ieee 802.15. 6. Wireless Communications and Networking Conference (WCNC), pages 174–178, 2011.

[178] Sana Ullah, Min Chen, and Kyung Sup Kwak. Throughput and delay analysis of ieee 802.15. 6-based csma/ca protocol. *Journal of medical systems*, 36(6):3875–3891, 2012.

[179] B Liu, Z Yan, and Chang W Chen. Medium access control for wireless body area networks with qos provisioning and energy efficient design. *IEEE Transactions on Mobile Computing*, 16(2):422–434, 2017.

[180] W Chu and ALAN KoNHEIM. On the analysis and modeling of a class of computer communication systems. *IEEE Transactions on Communications*, 20(3):645–660, 1972.

[181] S Tasaka. *Performance analysis of multiple access protocols*. MIT press, 1986.

[182] S J Bose. An introduction to queuing systems, 2002.

[183] S Alouf, E Altman, and A P Azad. Analysis of an M/G/1 queue with repeated inhomogeneous vacations with application to IEEE 802.16 e power saving mechanism. Fifth International Conference on Quantitative Evaluation of Systems, QEST, pages 27–36, St Malo, France, 2008.

[184] I Dimitriou. A modified vacation queueing model and its application on the discontinuous reception power saving mechanism in unreliable long term evolution networks. *Performance Evaluation*, 77:37–56, 2014.

[185] S R Yang and Y B Lin. Modeling UMTS discontinuous reception mechanism. *IEEE Transactions on Wireless Communications*, 4(1):312–319, 2005.

[186] B T Doshi. Queueing systems with vacations: A survey. *Queueing Systems*, 1(1):29–66, 1986.

[187] J G Proakis. Digital communications. 1995. *McGraw-Hill, New York*.

[188] L Kleinrock. *Queueing systems*. Wiley New York, 1976.

[189] R W Wolff. Poisson arrivals see time averages. *Operations Research*, 30(2):223–231, 1982.

[190] David Dagan Feng. *Biomedical information technology*. Academic Press, 2011.

[191] Nordic. nRF24L01+, 2018. Available: www.nordicsemi.com/.

[192] A Milenković, C Otto, and E Jovanov. Wireless sensor networks for personal health monitoring: Issues and an implementation. *Computer Communications*, 29(13):2521–2533, 2006.

[193] C Otto, A Milenkovic, C Sanders, and E Jovanov. System architecture of a wireless body area sensor network for ubiquitous health monitoring. *Journal of Mobile Multimedia*, 1(4):307–326, 2006.

[194] National health expenditures 2014 highlights, 2014. Available: www.cms.gov/research-statistics-data-and-systems/statistics-trends-and-reports/nationalhealthexpenddata/downloads/highlights.pdf.

[195] R Istepanian, E Jovanov, and Y T Zhang. Guest editorial introduction to the special section on m-health: Beyond seamless mobility and global wireless health-care connectivity. *IEEE Transactions on Information Technology in Biomedicine*, 8(4):405–414, 2004.

[196] G H Crossley, A Boyle, H Vitense, Y Chang, R H Mead, and et.al. The CONNECT (clinical evaluation of remote notification to reduce time to clinical decision) trial: the value of wireless remote monitoring with automatic clinician alerts. *Journal of the American College of Cardiology*, 57(10):1181–1189, 2011.

[197] P Mabo, F Victor, P Bazin, S Ahres, D Babuty, A D Costa, D Binet, and J C Daubert. A randomized trial of long-term remote monitoring of pacemaker recipients (the COMPAS trial). *European Heart Journal*, 33(9):1105–1111, 2011.

[198] A Gupta and R K Jha. A survey of 5G network: Architecture and emerging technologies. *IEEE Access*, 3:1206–1232, 2015.

[199] A S Tanenbaum and D J Wetherall. *Computer networks*. Pearson, 2011.

[200] Part11: Wireless LAN medium access control (MAC) and physical layer (PHY) specifications. *ANSI/IEEE Std. 802.11*, 1999.

[201] Apple Inc. Apple watch, 2014. Available: https://www.apple.com/in/watch/.

[202] P Wang, L Xiao, S Zhou, and J Wang. Optimization of detection time for channel efficiency in cognitive radio systems. IEEE Wireless Communications and Networking Conference, pages 111–115, Hong Kong, 2007.

[203] H Kim and K G Shin. Efficient discovery of spectrum opportunities with MAC-layer sensing in cognitive radio networks. *IEEE Transactions on Mobile Computing*, 7(5):533–545, 2008.

[204] A Aijaz and A H Aghvami. Cognitive machine-to-machine communications for internet-of-things: A protocol stack perspective. *IEEE Internet of Things Journal*, 2(2):103–112, 2015.

[205] M R Palattella, N Accettura, X Vilajosana, T Watteyne, L A Grieco, G Boggia, and M Dohler. Standardized protocol stack for the internet of (important) things. *IEEE Communications Surveys & Tutorials*, 15(3):1389–1406, 2013.

[206] R Murty, R Chandra, T Moscibroda, and P Bahl. Senseless: A database-driven white spaces network. *IEEE Transactions on Mobile Computing*, 11(2):189–203, 2012.

[207] FCC frees up vacant tv airwaves for super wi-fi technologies and other technologies. Technical report, FCC, 2010.

[208] J Jia, Q Zhang, and Xuemin S Shen. HC-MAC: A hardware-constrained cognitive MAC for efficient spectrum management. *IEEE Journal on Selected Areas in Communications*, 26(1):106–117, 2008.

[209] B Wang and D Zhao. Scheduling for long term proportional fairness in a cognitive wireless network with spectrum underlay. *IEEE Transactions on Wireless Communications*, 9(3):1150–1158, 2010.

[210] D M Ritchie, B W Kernighan, and M E Lesk. *The C programming language*. Prentice Hall, 1988.

[211] A S Tanenbaum et al. *Computer networks*. Pearson, 1996.

[212] S S Rao. *Engineering optimization: Theory and practice*. John Wiley & Sons, 2009.

[213] B S Grewal. *Higher engineering mathematics*. Khanna Publishers, New Delhi, 2002.

[214] L Duan, J Huang, and B Shou. Investment and pricing with spectrum uncertainty: A cognitive operator's perspective. *IEEE Transactions on Mobile Computing*, 10(11):1590–1604, 2011.

[215] MATLAB. Mathworks, 2017. Available: www.mathworks.com.

[216] CESC Ltd. Tariff and associated terms and conditions, 2016-17. Available: www.cesc.co.in/wp-content/uploads/tariff/TARIFF%20AND%20ASSOCIATED%20CONDITIONS.pdf.

[217] Bharti Airtel Ltd. Basic prepaid tariff, 2017. Available: www.airtel.in/prepaid-tariff.

[218] WIZnet. Wiznet w5100, 2017. Available: www.wiznet.io/wp-content/uploads/wiznethome/Chip/W5100/Document/W5100_Datasheet_v1.2.7.pdf.

[219] M R Yuce, S W Ng, N L Myo, C K Lee, J Y Khan, and W Liu. A MICS band wireless body sensor network. IEEE Wireless Communications and Networking Conference, pages 2473–2478, Hong Kong, 2007.

[220] Arduino. Arduino ethernet shield 2, 2017. Available: //www.arduino.cc/en/Guide/ArduinoEthernetShield.

[221] Apple Inc. Apple health kit, 2017. Available: developer.apple.com/reference/healthkit.

[222] Commtunnel, 2017. Available: www.serialporttool.com.

[223] Wireshark, 2017. Available: www.wireshark.org.

[224] A Al-Fuqaha, M Guizani, M Mohammadi, Mohammed Aledhari, and Moussa A. Internet of things: A survey on enabling technologies, protocols, and applications. *IEEE Communications Surveys & Tutorials*, 17(4):2347–2376, 2015.

[225] Unlicensed operations in the TV broadcast bands. Technical Report Second memorandum opinion and order, FCC 10-174, 2010.

[226] G Wu, S Talwar, K Johnsson, N Himayat, and K D Johnson. M2M: From mobile to embedded internet. *IEEE Communications Magazine*, 49(4):36–43, 2011.

[227] T Manna, I S Misra, S K Sanyal, and T Chakraborty. A framework for implementation of wireless body area network over software defined radios. IEEE Region 10 Symposium, pages 17–20, India, 2015.

[228] J W Huang and V Krishnamurthy. Cognitive base stations in LTE/3GPP femtocells: A correlated equilibrium game-theoretic approach. *IEEE Transactions on Communications*, 59(12):3485–3493, 2011.

[229] T Manna and I S Misra. Joint optimization of detection thresholds and power allocation in ofdm based cognitive femtocell networks. IEEE International Conference on Communication, Networks and Satellite, pages 69–73, India, 2013.

[230] I F Akyildiz, B F Lo, and R Balakrishnan. Cooperative spectrum sensing in cognitive radio networks: A survey. *Physical Communication*, 4(1):40–62, 2011.

[231] C H Park, S W Kim, and M S Song. Apparatus and method for predicting channel status based on cognitive radio, June 27 2008. US Patent App. 12/674,667.

[232] J W Wang and R Adriman. Analysis of opportunistic spectrum access in cognitive radio networks using hidden markov model with state prediction. *EURASIP Journal on Wireless Communications and Networking*, 2015(1):10, 2015.

[233] C Ghosh, C Cordeiro, D P Agrawal, and M B Rao. Markov chain existence and hidden markov models in spectrum sensing. IEEE International Conference on Pervasive Computing and Communications, pages 1–6, Galveston, TX, 2009.

[234] J Baker. The DRAGON system-An overview. *IEEE Transactions on Acoustics, Speech, and Signal Processing*, 23(1):24–29, 1975.

[235] V K Tumuluru, P Wang, and D Niyato. Channel status prediction for cognitive radio networks. *Wireless Communications and Mobile Computing*, 12(10):862–874, 2012.

[236] S Wang, J Zhang, and L Tong. Delay analysis for cognitive radio networks with random access: A fluid queue view. IEEE INFOCOM, pages 1–9, Brazil, 2010.

[237] D I Kim, L B Le, and E Hossain. Joint rate and power allocation for cognitive radios in dynamic spectrum access environment. *IEEE Transactions on Wireless Communications*, 7(12), 2008.

[238] W Huang and X Wang. Capacity scaling of general cognitive networks. *IEEE/ACM Transactions on Networking*, 20(5):1501–1513, 2012.

[239] S Stotas and A Nallanathan. Enhancing the capacity of spectrum sharing cognitive radio networks. *IEEE Transactions on Vehicular Technology*, 60(8):3768–3779, 2011.

[240] C Ridders. A new algorithm for computing a single root of a real continuous function. *IEEE Transactions on Circuits and Systems*, 26(11):979–980, 1979.

[241] A Ralston and P Rabinowitz. *A first course in numerical analysis*. Dover Publications, New York, 2001.

[242] C H Papadimitriou and K Steiglitz. *Combinatorial optimization: Algorithms and complexity*. Dover Publications, 1998.

[243] H Kuhn. The hungarian method for the assignment problem. *Naval Research Logistics (NRL)*, 2(1-2):83–97, 1955.

[244] E L Lawler. *Combinatorial optimization: Networks and matroids*. Courier Corporation, 1976.

[245] Xylinx. Atlys spartan-6 fpga trainer board, 2016. Available: https://store.digilentinc.com/atlys-spartan-6-fpga-trainer-board-limited-time-see-nexys-video/.

[246] M M Freda, L Ma, S Ahmad, J L Gauvreau, A Demir, and C Ye. Silent period method and apparatus for dynamic spectrum management, November 2 2011. US Patent App. 13/287,381.

[247] M Mehrjoo, Mohamad K Awad, M Dianati, and X S Shen. Design of fair weights for heterogeneous traffic scheduling in multichannel wireless networks. *IEEE Transactions on Communications*, 58(10):2892–2902, 2010.

[248] PhysioNet. Physiotoolkit software index, 2014. Available: www.physionet.org/physiotools/matlab/ECGwaveGen/.

Appendix A

A.1 OPNET based Simulation Results of IEEE 802.15.6 SAM

The OPNET based simulation results of IEEE 802.15.6 based 1-periodic uplink SAM under ideal and non-ideal channel conditions are provided in Figures A.1, A.2 and their primary observations are summarized below.

Ideal Channel Results

The variations of average frame waiting delay, the energy consumed by the sensor node and the average throughput for TL-3 having payload size (P_{size}) of 150 bytes with respect to different Allocation Intervals (AIs) under ideal channel conditions are shown in Figure A.1. It is noted that with increase in AI the waiting delay decreases. We also observe that the energy consumption initially decreases and then gradually increases with increase in AI. Whereas, the throughput remains unchanged for changes in AI, the value being equal to the incoming data rate.

Non-Ideal Channel Results

Figure A.2 shows the variation of the same metrics with respect to payload sizes for TL-3 under non-ideal channel conditions, while keeping the AI fixed at 11slots. We note that as payload size increases, the delay initially decreases and then increases. It is also observed that, the energy consumption continues to decrease with increase in payload size, whereas the average throughput shows the reverse trend.

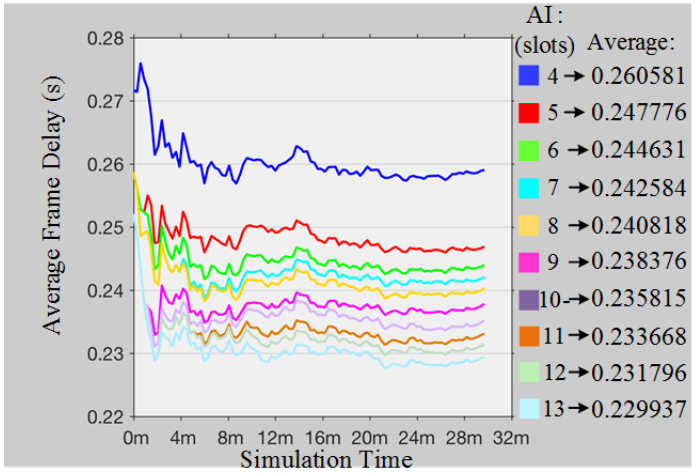

(a) Average frame delay

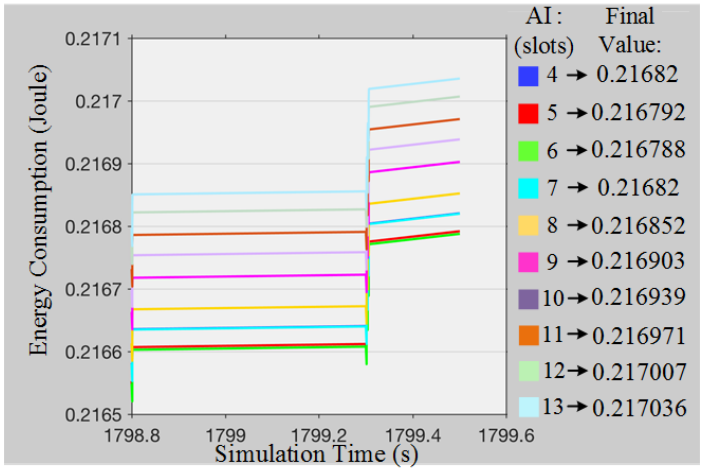

(b) Energy consumption

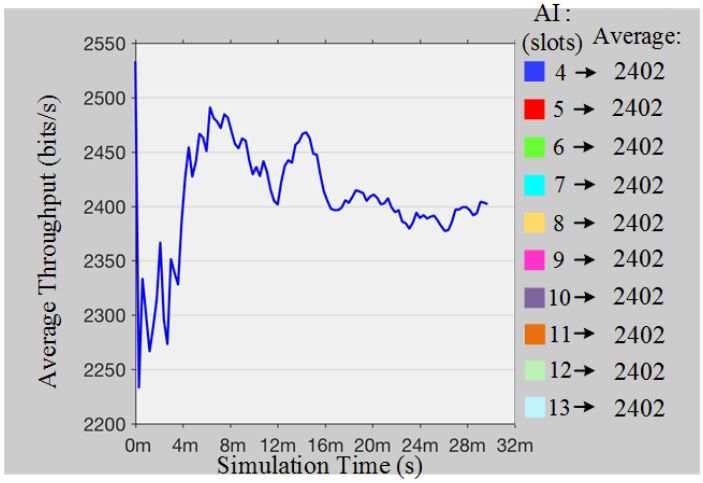

(c) Average throughput

Fig. A.1 Variation of performance with respect to allocation intervals under ideal channel condition for TL-3 with P_{size}= 150 bytes.

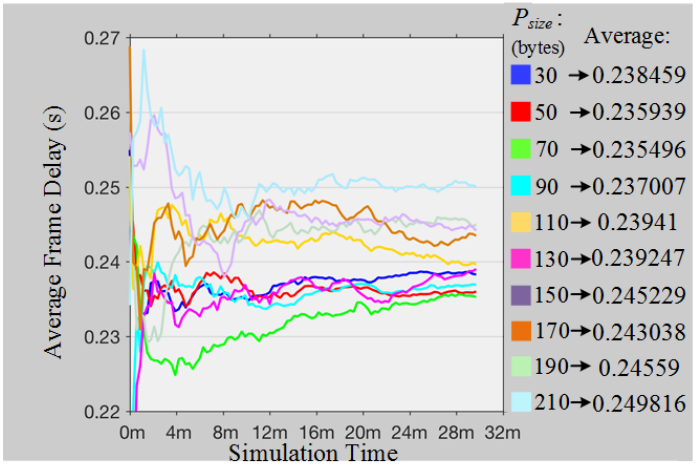

(a) Average frame delay

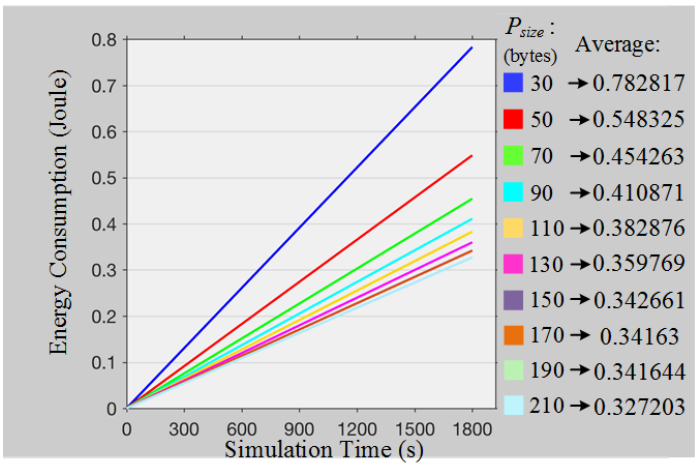

(b) Energy consumption

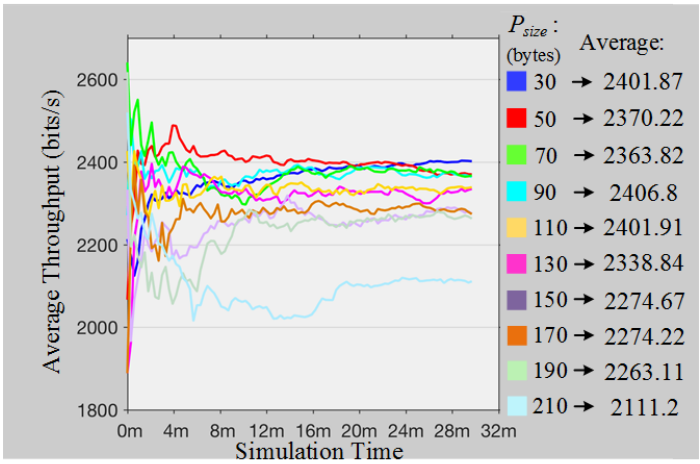

(c) Average throughput

Fig. A.2 Variation of performance metrics with respect to payload sizes (P_{size}) under non-ideal channel (SNR=18dB) for TL-3 with AI of 11 slots.

Appendix B

B.1 Proof of concavity of energy-efficiency of BodyCog-BNC for transmission over single PU channel

The energy-efficiency (η) of BodyCog-BNC for transmission over a single PU channel given by (6.5) is a strictly concave function of inter-sensing duration (T_D) since its second-order derivative

$$\begin{aligned}\frac{\mathrm{d}^2\eta}{\mathrm{d}{T_D}^2} = \frac{1}{(D+ET_D)^4}\Big[&(D+ET_D)^3\left\{A\lambda^2 e^{-\lambda T_D} - B\mu^2 e^{-\mu T_D}\right\} \\ &+2E\left\{A\left(D\lambda+E+E\lambda T_D\right)e^{-\lambda T_D} - B\left(D\mu+E+E\mu T_D\right)e^{-\mu T_D}+K\right\}\Big] < 0\end{aligned} \tag{B.1}$$

where,

$$A = \frac{P(H_1)(1-P_d)}{\lambda} \tag{B.2}$$

$$B = \frac{P(H_0)(1-P_f)}{\mu} \tag{B.3}$$

$$C = B\,\mu \tag{B.4}$$

$$D = \frac{I_r\,T_S}{P_{trans}} \tag{B.5}$$

$$E = I_t \tag{B.6}$$

$$K = (1-C)D + E(A-B) \tag{B.7}$$

Equation B.1 can be validated for different values of T_D under varied operating conditions highlighted in Section 6.8.1.

Appendix C

C.1 Derivation of Average Collision Duration, T_C

The probability that a collision due to miss-detection will occur is the same as the probability of PU being present but SU not being able to observe the PU and also predicting that the PU will be absent in the next sensing slot. It can be obtained as,

$$P\left(H_1, O^{(0)}, O_{0p}\right) = P\left(O_{0p}/O^{(0)}, H_1\right) P\left(O^{(0)}/H_1\right) P(H_1) = (1-P_{ma})(1-P_d)P(H_1) \tag{C.1}$$

where, P_{ma} is the probability of avoiding a miss-detection and is obtained as in (7.37).
The probability of correctly detecting PU absence can be obtained as,

$$P\left(H_0, O^{(0)}, O_{0p}\right) = P\left(O^{(0)}, O_{0p}\right) - P\left(H_1, O^{(0)}, O_{0p}\right) = P_{trans} - P\left(H_1, O^{(0)}, O_{0p}\right) \tag{C.2}$$

However, even after accurate detection of a white space, collision can occur due to sudden appearance of PU. Therefore, using (C.1) and (C.2) the average collision duration can be derived as,

$$\begin{aligned} T_C &= T_{bc} P\left(H_1, O^{(0)}, O_{0p}\right) + T_{ic} P\left(H_0, O^{(0)}, O_{0p}\right) \\ &= T_{bc} P\left(H_1, O^{(0)}, O_{0p}\right) + T_{ic} \left[P_{trans} - P\left(H_1, O^{(0)}, O_{0p}\right)\right] \\ &= (T_{bc} - T_{ic}) P\left(H_1, O^{(0)}, O_{0p}\right) + T_{ic} P_{trans} \\ &= (T_{bc} - T_{ic}) (1-P_{ma})(1-P_d)P(H_1) + T_{ic} P_{trans} \end{aligned} \tag{C.3}$$

Appendix D

D.1 Video Demonstration: IEEE 802.15.6 Scheduled Access MAC

This video demonstration shows the continuous simultaneous monitoring of ECG and temperature by the WBAN test-bed setup developed in Chapter 3.

LINK: https://www.dropbox.com/s/tb6guwr0ha0bsc2/SAM_Demo.mp4?dl=0

D.2 Video Demonstration: BodyCog-BNC for NRT Remote Health Monitoring

This video demonstration shows the ability of BodyCog-BNC developed in Chapter 6 in facilitating NRT transfer of WBAN captured data over backhaul CRN/licensed WAN under varied operating scenarios.

LINK: https://www.dropbox.com/s/eqa0rimo03uja4c/BodyCog_Demo.mp4?dl=0